A Bayesian Forecast Model for the Climatic Response of Unsaturated Soils

by

Austin Hunter Olaiz

A Dissertation Presented in Partial Fulfillment
of the Requirements for the Degree
Doctor of Philosophy

Approved October 2022 by the
Graduate Supervisory Committee:

Claudia E. Zapata, Chair
Sandra Houston
Edward Kavazanjian
Yasser Soltanpour

ARIZONA STATE UNIVERSITY

December 2022

ABSTRACT

The climate-driven volumetric response of unsaturated soils (shrink-swell and frost heave) frequently causes costly distresses in lightly loaded structures (pavements and shallow foundations) due to the sporadic climatic fluctuations and soil heterogeneity which is not captured during the geotechnical design. The complexity associated with the unsaturated soil mechanics combined with the high degree of variability in both the natural characteristics of soil and the empirical models which are commonly implemented tends to lead to engineering judgment outweighing the results of deterministic computations for the basis of design. Recent advances in the application of statistical techniques and Bayesian Inference in geotechnical modeling allow for the inclusion of both parameter and model uncertainty, providing a quantifiable representation of this invaluable engineering judgement.

The overall goal achieved in this study was to develop, validate, and implement a new method to evaluate climate-driven volume change of shrink-swell soils using a framework that encompasses predominantly stochastic time-series techniques and mechanistic shrink-swell volume change computations. Four valuable objectives were accomplished during this research study while on the path to complete the overall goal: 1) development of an procedure for automating the selection of the Fourier Series form of the soil suction diffusion equations used to represent the natural seasonal variations in suction at the ground surface, 2) development of an improved framework for deterministic estimation of shrink-swell soil volume change using historical climate data and the Fourier series suction model, 3) development of a Bayesian approach to randomly

generate combinations of correlated soil properties for use in stochastic simulations, and 4) development of a procedure to stochastically forecast the climatic parameters required for shrink-swell soil volume change estimations.

The models presented can be easily implemented into existing foundation and pavement design procedures or used for forensic evaluations using historical data. For pavement design, the new framework for stochastically forecasting the variability of shrink-swell soil volume change provides significant improvement over the existing empirical models that have been used for more than four decades.

DEDICATION

I would like to dedicate this work to two individuals who significantly impacted my life during my PhD studies. Firstly, to Elizabeth Rockwell, my significant other and biggest motivator. I thought I was the hardest worker around, until I met you. A full time engineering job and your own graduate schoolwork, yet you still found time each day to help where you could. I sincerely would not have been able to do it without you. You keep always working hard, but smiling the whole time, and I love you for that. Our Evelyn will be proud of what you have helped me accomplish.

Secondly, to the late Dr. Mathew Witczak, who we unfortunately lost in early 2022. Dr. Witczak was an international legend in the field of pavement engineering, most known for his technical excellence, professionalism, and ability to produce useful research for implementation into practice. I was fortunate enough to spend time learning from and working with Professor Witczak at the beginning of this study, which was invaluable and helped make me the engineer I am today, both technically and professionally. Dr. Witczak's memory, legacy, and knowledge will be carried on by his dear wife, my Ph.D. advisor Dr. Claudia Zapata, as well as all the people who were fortunate enough to work with him over the years. I know Matt would be proud of the work we've done to advance the field of civil engineering through a multi-disciplinary approach with modern statistics and computer science; however, he would absolutely have a list of recommendations already prepared for us to take the work to the next level.

ACKNOWLEDGMENTS

I would like to give special thanks to my advisor and good friend Dr. Claudia Zapata. There were many ups and downs over the past few years, but the ride was fun the whole way. Thank you to my master's advisor Dr. Sandra Houston who was willing to spend some of her retirement time serving as a committee member on this work. This whole career in geotechnical engineering started back in your undergraduate foundations course when you allowed me to join your research team.

Thank you to Dr. Edward Kavazanjian who volunteered to join my committee relatively late in the processes after the passing of Dr. Matt Witczak. Aside from this research work, thank you for all that you do for the ASU geotechnical students and community. Lastly, thank you to Dr. Yasser Soltanpour, with AECOM, who also volunteered to join my committee relatively late in the process but provided creative insight that helped me overcome a few significant hurdles that I initially could not wrap my head around. It has been an honor to work with all of you, and I hope that we can continue collaborating in the future.

Special thanks to the people who provided opportunities to gain industry experience during my graduate studies. Firstly, Dr. Jeffry Vann of Vann Engineering. I would not be where I am today without your graciousness to take me under your wing fresh out of undergraduate studies. I have adopted your passion for the field of geotechnical engineering, both practice and research, and your values of high ethics and continual mentorship. Secondly, the AECOM team: Thomas Hull, Jeff Heyman, Sandy

Gourlay, Elizabeth Stallings Young, Kendal Foster, and Miriam Woolley who were all supportive throughout the duration of this work, especially down the stretch when they would willingly take over my work responsibilities, day after day, allowing me to focus on this study.

I would also like to thank the other members of the NCHRP 01-59 research team: Dr. Xiong (Bill) Yu and Yusheng Jiang from Case Western Reserve University, and Dr. Mohammad Mosawi from ASU.

This work would not have been possible without the funding from the National Academies of Science, Engineering, and Medicine Transportation Research Board's (TRB) National Cooperative Highway Research Program (NCHRP). The opinions, conclusions, and interpretations are those of the authors and not necessarily of NCHRP.

TABLE OF CONTENTS

CHAPTER Page

LIST OF TABLES xi

LIST OF FIGURES xv

1 INTRODUCTION 1

1.1 Background 1

1.2 Motivation 3

1.2.1 Motivation by Implementation 3

1.2.2 Motivation by Advancement 3

1.3 Purpose 5

1.4 Organization 6

1.4.1 Flow 9

1.5 Development of Computer Software 9

2 SOIL SUCTION PROFILES USING A FOURIER SERIES APPROACH 11

2.1 Introduction 11

2.1.1 Objectives 12

2.2 Relevant Background 13

2.2.1 Thornthwaite Moisture Index, TMI 16

2.2.2 TMI-Suction Model 18

2.2.3 Unsaturated Soil Suction Envelopes 22

2.2.4 Suction-Based Diffusion Equation 24

CHAPTER Page

TMI-Suction Envelope Relationships (Vann and Houston, 2021) 30

2.2.5 Variation in Suction at the Ground Surface 35

2.2.6 Diffusion Parameters 36

2.3 Proposed Climate-Suction Model for Uncovered Sites 39

2.4 Validation of the NOFS Suction Profile Approach 44

2.4.1 Overview of ASU-NSF Expansive Soil Study In Situ Soil Data 44

2.4.2 Denver, CO Climate-Suction Model Exploration 46

2.4.3 San Antonio, TX Climate-Suction Model Exploration 48

2.4.4 Evaluation of Proposed Climate-Suction Model 50

2.5 Representation of Suction Profiles using Fourier Series 53

2.5.1 Overview of Fourier Series Analysis 53

2.6 Fourier Series Suction Profile 56

2.6.1 Adjustments to NOFS Suction Profiles using Measured Data 58

2.6.2 Order of the Fourier Series Fit 60

2.7 Natural Order Fourier Series (NOFS) Algorithm 62

2.7.1 Automating the Fourier Series Order Selection 62

2.8 Validation of the NOFS Suction Profile Approach 68

2.8.1 Denver, CO NOFS Suction Profile Evaluation 69

2.9 Implementation of NOFS Suction Profiles in Practice 78

2.9.1 Limitations of the Proposed NOFS Suction Profile Model 80

3 BAYESIAN CHARACTERIZATION OF COMMON SOIL PROPERTIES 82

CHAPTER Page

3.1 Introduction 82

3.1.1 Objectives 84

3.2 Relevant Background 85

3.2.1 Review of General Statistical Theory 85

3.2.2 Review of Uncertainties in Geotechnical Engineering 97

3.2.3 Review of Bayesian Inference 99

3.3 Existing Hierarchical Soil Property Statistics used in MEPDG 101

3.4 Proposed Hierarchical Soil Parameter Statistics for SSVC Analysis 104

3.4.1 Soil Property Statistics for Level 1 Analysis 105

3.4.2 Soil Property Statistics for Level 2 Analysis 106

3.4.3 Proposed Soil Property Statistics 111

3.5 Randomization of Soil Index Properties 112

3.5.1 Correlation Study using NRCS Soil Database 114

3.6 Implementation of Random Soil Properties Generator 128

3.7 Implementation of Random Soil Properties Algorithm in Practice 136

3.7.1 Limitations 137

4 STOCHASTIC CLIMATIC PARAMETER FORECAST MODEL 138

4.1 Introduction 138

4.1.1 Objectives 140

4.2 Relevant Background 140

4.2.1 Review of Time-Series Analysis 140

CHAPTER Page

4.2.2 Review of Bayesian Forecasting Techniques 144

4.2.3 Markov Chain Monte Carlo (MCMC) Simulations..... 145

4.3 Time Series Decomposition of Monthly TMI Data..... 149

4.4 MCMC Framework for Stochastic Climate Parameter Forecasting..... 151

4.4.1 Stability and Optimization of Stochastic Climate Parameter Forecasting Model 153

4.5 Validation of Stochastic TMI Forecast Model..... 155

4.5.1 Performance of the Bayesian TMI Forecast Model..... 163

4.5.2 Stability of the Bayesian TMI Forecast Model..... 169

4.6 Potential Future Improvements to the Bayesian TMI Forecast Model..... 170

4.6.1 Limitations of the Bayesian TMI Forecast Model..... 171

5 STOCHASTIC SHRINK-SWELL VOLUME CHANGE FORECAST MODEL 172

5.1 Introduction..... 172

5.1.1 Objectives 172

5.2 Deterministic Shrink-Swell Volume Change (SSVC)..... 173

5.2.1 Suction-Volume Change Relationship..... 175

5.2.2 2D SSVC Estimates for Pavements 179

5.3 Stochastic Framework for SSVC Forecasting 198

5.4 Example of the Stochastic SSVC Forecast Model..... 201

5.5 Performance of the Proposed Stochastic SSVC Model 205

CHAPTER Page

5.6 Implementation of the Proposed Stochastic SSVC Model 205

5.6.1 Limitations of the Stochastic SSVC Model 206

6 CONCLUSIONS 208

6.1 Limitations of Research 209

6.2 Future Work 211

REFERENCES 214

APPENDIX

A TMI CALCULATION FOR DENVER NOAA STATION: USW00023067 229

B SOIL AND ROCKS JOURNAL PUBLICATION 240

C GEOCONGRESS 2023 PROCEEDINGS PAPER (FORTHCOMING) 255

D HIERARCHICAL DESCRIPTIVE STATISTICS FOR GROUPS BY AASHTO CLASSIFICATION AND WPI 268

E CLIMATE MODEL FIGURES 282

F STOCHASTIC SHRINK-SWELL ANALYSIS OUTPUT 353

LIST OF TABLES

Table Page

2-1 TMI-P200 Regression Constants (Perera 2003) 20

2-2 TMI-P200/wPI Regression Coefficients (Perera et al., 2005). 21

2-3 ASU-NSF Study Sites in Texas for Development of Climate-Suction Model 40

2-4 Regression Coefficients for Proposed Climate-Suction Model for Uncovered Sites 43

2-5 Relationships Between TMI and Equilibrium Suction for ASU-NSF Study Sites (adapted from Vann, 2019) 45

2-6 Soil Properties for Upper 2 ft of Uncovered Borings at ASU-NSF Denver Site 46

2-7 Suction at ASU-NSF Denver Site using Proposed Climate-Suction Model 48

2-8 Soil Properties for Upper 2 ft of Uncovered Borings at ASU-NSF San Antonio Site 49

2-9 Suction at ASU-NSF San Antonio Site using Proposed Climate-Suction Model ... 50

2-10 Comparison of Suction Estimates to Measured Values at the Denver Study Site . 51

2-11 Relationships Between TMI and Equilibrium Suction for Denver Study Site (adapted from Vann, 2019) 69

3-1: Comparison of Bayesian vs. Frequentist Statistics (adopted from Amrhein et al., 2019)..... 99

3-2. Descriptive Statistics for In Situ Dry Unit Weight and Moisture Content 108

3-3: Descriptive Statistics for Filtered NRCS Soil Data 114

Table Page

3-4. Correlation Matrix for *PI*, *LL*, $P_{\#200}$, and P_{clay} from NRCS Soil Database Filtered with $PI > 0$ 116

3-5. Summary of Regression Analyses for *LL*, *PI*, $P_{\#200}$, and P_{clay} 117

4-1. Sites for Validation Study of the Proposed Stochastic TMI Forecast Model 156

5-1 Input Parameters Used in the Vertical Moisture Barrier Model 184

5-2 Input Parameters Used in the Vertical Moisture Barrier Model 188

5-3 Input Parameters Used in the Example Vertical Moisture Barrier Model. 194

5-4: Preliminary Plan to Estimate Volume Change Due to Swell/Shrink at Three Hierarchical Levels of Design 199

5-5: Listing of Input Variables for Hierarchical Shrink-Swell Analysis 200

D-1 A-1-a Soil Properties (Rosenbalm, 2011) 269

D-2 A-1-b Soil Properties (Rosenbalm, 2011) 269

D-3. A-2-4 Soil Properties (Rosenbalm, 2011) 269

D-4. A-2-5 Soil Properties (Rosenbalm, 2011) 270

D-5. A-2-6 Soil Properties (Rosenbalm, 2011) 270

D-6. A-2-7 Soil Properties (Rosenbalm, 2011) 270

D-7. A-3 Soil Properties (Rosenbalm, 2011) 271

D-8. A-4 Soil Properties (Rosenbalm, 2011) 271

D-9. A-5 Soil Properties (Rosenbalm, 2011) 271

D-10. A-6 Soil Properties (Rosenbalm, 2011) 272

D-11. A-7-5 Soil Properties (Rosenbalm, 2011) 272

D-12. A-7-6 Soil Properties (Rosenbalm, 2011) 272

Table Page

D-13. Granular Base Material Soil Properties (Rosenbalm, 2011) 273

D-14. Granular Subbase and Subgrade Material Soil Properties (Rosenbalm, 2011).. 273

D-15. Fine Grained Material Soil Properties (Rosenbalm, 2011) 273

D-16. “Clayey” Fine Grained Material Soil Properties (Rosenbalm, 2011) 274

D-17. “Silty” Fine Grained Material Soil Properties (Rosenbalm, 2011) 274

D-18. Level 2 A-1-a Soil Properties 274

D-19. Level 2 A-1-b Soil Properties 275

D-20. Level 2 A-2-4 Soil Properties 275

D-21. Level 2 A-2-5 Soil Properties 275

D-22. Level 2 A-2-6 Soil Properties 276

D-23. Level 2 A-2-7 Soil Properties 276

D-24. Level 2 A-3 Soil Properties 276

D-25. Level 2 A-4 Soil Properties 277

D-26. Level 2 A-5 Soil Properties 277

D-27. Level 2 A-6 Soil Properties 277

D-28. Level 2 A-7-5 Soil Properties 278

D-29. Level 2 A-7-6 Soil Properties 278

D-30. Level 2 Shrink-swell Soil with $10 < wPI < 20$ 278

D-31. Level 2 Shrink-swell Soil with $20 \leq wPI < 30$ 279

D-32. Level 2 Shrink-swell Soil with with $30 \leq wPI < 40$ 279

D-33. Level 2 Shrink-swell Soil with $40 \leq wPI < 50$ 279

D-34. Level 2 Shrink-swell Soil with $wPI \geq 50$ 280

Table Page

D-35. Level 3 Granular Material Properties (A-1, A-2 & A-3) 280

D-36. Level 3 Fine Grained Material Properties (A-4, A-5, A-6, &, A-7) 280

D-37. Level 3 “Silty” Fine Grained Material Properties (A-4 & A-5)..... 281

D-38. Level 3 “Clayey” Fine Grained Material Properties (A-6 & A-7)..... 281

D-39. Level 3 Shrink-swell Soil (A-6 & A-7 with $wPI > 10$)..... 281

LIST OF FIGURES

Figure Page

1-1 Flow of Documents Chapters 9

2-1 Sensitivity of Averaging Period on TMI (Karunarathne, 2016) 18

2-2: TMI-P200/wPI Relationship with Soil Suction (Perera et al., 2005) 22

2-3 Water Content Profile in the Active Zone (After Nelson and Miller 1992) 23

2-4 Suction Profiles, Modified from Bulut (2001) (After Amer 2016) 24

2-5 Characteristic Suction Envelopes for Humid, Semi-Arid, and Arid Climates (Aubeny & Long, 2007) 29

2-6 Suction Profile versus Depth with Adding Stabilized Layer (left) for Fort Worth North Site and Case of No Moisture Control (right) at Atlanta US 271 Site (Lytton et al., 2005) 30

2-7: Relationship Between TMI and the Depth to Equilibrium Soil Suction (Vann and Houston, 2021) 33

2-8 Soil Suction Estimation using Moisture Content and Liquid Limit (Vann et al. 2018) 34

2-9: Equilibrium Suction vs. TMI with Literature Values (Vann and Houston, 2021) .. 35

2-10: Limits of the Potential Change in Suction at the Surface vs. TMI with Literature Values (Vann and Houston, 2021) 36

2-11 Relationship between Diffusion Coefficient and TMI (Mitchell, 2008) 37

2-12: Relationship Between the Climate Parameter, *r*, and TMI (Vann and Houston, 2021) 38

Figure Page

2-13 Incremental Impact of Predictor Variables to R^2 of the Regression for the Developed Climate-Suction Model (Minitab Output) 43

2-14 Monthly Average Temperature (red), Total Rainfall (blue), and TMI at the NOAA Station (ID: USW00023066) from 07/1986 to 12/2020..... 47

2-15 Monthly Average Temperature (red), Total Rainfall (blue), and TMI at the NOAA Station (ID: USW00012921) from 01/1987 to 12/2017..... 49

2-16 Characteristic Suction Envelopes for Humid, Semi-Arid, and Arid Climate 58

2-17: 1st and 8th order Fourier fit to the Surface Suction Data for the TX 48-1068 Section for the Date Range 3/1987 to 9/1997 61

2-18 Monthly-TMI vs. Variation in Suction at the Ground Surface for the Denver Study Site..... 66

2-19 Selection Process for NOFS Fit to Climate-Drive Suction Variation at the Ground Surface for the Denver Study Site..... 67

2-20 Comparison of NOFS Fit to Minimum and Maximum Order Fourier Series Fit to the Variation in Suction at the Ground Surface for the Denver Study Site..... 68

2-21: Measured Soil Suction Data versus Depth for Three Test Borings in Denver 69

2-22 Monthly-TMI vs. Variation in Suction at the Ground Surface for the Denver Study Site from 07/1986 to 12/2020..... 70

2-23 Variation in Suction at the Ground Surface for the Denver Study Site from 09/2011 to 03/2019 with Dates of Interests 71

Figure Page

2-24 Suction Profile Estimations for Denver Study Site Validation Scenario #2.3 - Measured Magnitude and Depth of Equilibrium Suction from Vann (2019) 73

2-25 Suction Profile Estimations for Denver Study Site for Validation Scenario #2.4 - Empirically Estimated Magnitude and Depth of Equilibrium Suction from Vann and Houston (2021) 76

2-26 Suction Profile Estimations for Denver Study Site for Validation Scenario #2.5 – Adjusted Depth of Equilibrium Suction using Measured Data of Uncovered Borings 78

3-1. Percentage of Normal Distribution Represented by Number of Standard Deviations from the Mean. 87

3-2. Example of Beta Distributions Between [0,1] with Varying Shape Factors Alpha (α) and Beta (β) (Montgomery et al., 2011) 91

3-3. Example of Bivariate Normal Probability Density Function (Fenton and Griffiths, 2008)..... 96

3-4. Example Bivariate Probability Density Functions with $\mu_x = \mu_y = 5$, $\sigma_x = \sigma_y = 1.5$ and Correlation Coefficients (ρ_{xy}) Equal to (a) Zero and (b) 0.6 (Fenton and Griffiths, 2008)..... 97

3-5. Uncertainty in Soil Property Estimates (Kulhawy, 1992)..... 98

3-6: Generalized Bayesian Framework for Geotechnical Characterization (Wang, 2016) 100

Figure Page

3-7: Correlation Plots for *PI*, *LL*, $P_{\#200}$, and P_{clay} from NRCS Soil Database Filtered with $PI > 0$ 116

3-8. Normality Test and Descriptive Statistics for *PI* from NRCS Soil Database with $PI > 0$ 119

3-9. Normality Test and Descriptive Statistics for *LL* from NRCS Soil Database with $PI > 0$ 119

3-10. Normality Test and Descriptive Statistics for $_{Pclay}$ from NRCS Soil Database with $PI > 0$ 120

3-11. Normality Test and Descriptive Statistics for $P_{\#200}$ from NRCS Soil Database with $PI > 0$ 120

3-12. Normality Test and Descriptive Statistics for P_{clay} from NRCS Soil Database with $PI > 0$ 121

3-13. Minitab Summary of Linear Regression of *PI* to *LL* 122

3-14. Minitab Summary of Linear Regression of *PI* to P_{clay} 123

3-15. Minitab Summary of Linear Regression of *PI* to *wPI*Algorithm for Randomizing Correlated Soil Index Properties 124

3-16. Example of Histograms and Fitted Beta Distributions for Randomly Generated Data Points *PI*, *p200*, *pClay*, *LL*, *d_UW*, and *w*. 128

3-17 Default Descriptive Statistics for the Level 3 “Clayey FGM” Material Soil Group. 130

3-18 Default Beta Distributions for the Level 3 “Clayey FGM” Soil Group 130

Figure Page

3-19 Default and Randomized Beta Distributions for the Level 2 “Clayey FGM” Soil Group using 1000 Monte Carlo draws 131

3-20 Default Descriptive Statistics for the Level 2 A-7-6 Soil Group. 132

3-21 Default and Randomized Beta Distributions for the Level 2 A-7-6 Soil Group using 1000 Monte Carlo draws 133

3-22 Default Descriptive Statistics for the Level 2 “wPI 30-40” Soil Group 133

3-23 Default and Randomized Beta Distributions for the Level 2 “wPI 30-40” Soil Group using 1000 Monte Carlo draws 134

3-24 Example of Various User Adjusted Descriptive Statistics for the Level 3 “Clayey FGM” Soil Group 135

3-25: Example of the Randomized Beta Distributions (red) based on the various User Adjusted descriptive statistics (3-24) for the Level 3 “Clayey FGM” Soil Group 135

4-1 Autocorrelation Function Plot for Monthly TMI and Monthly Change in TMI (*dTMI*) 143

4-2 Time Series Decomposition of TMI and *dTMI* (black) using Moving Average (MA in red) with lag = 12 and 3, respectively, and the Associated Monthly Residuals (blue). 151

4-3 Procedure for Obtaining Monthly Parameterized Prior Distributions for the TMI MCMC Forecast Model 152

4-4 Framework for monthly MCMC TMI forecast model using the Metropolis-Hasting Acceptance criteria. 153

Figure Page

4-5 Prior and Forecasted Monthly TMI from 03/2017 to 03/2022 for Arlington, VA (NOAA Station USW00013743) 157

4-6 Prior and Forecasted Monthly TMI from 03/2017 to 03/2022 for Dallas, TX (NOAA Station USW00013960) 158

4-7 Prior and Forecasted Monthly TMI from 03/2017 to 03/2022 for Denver, CO (NOAA Station USW00023062) 159

4-8 Prior and Forecasted Monthly TMI from 03/2017 to 03/2022 for Salt Lake City, UT (NOAA Station USW00024127) 160

4-9 Prior and Forecasted Monthly TMI from 03/2017 to 03/2022 for Tempe, AZ (NOAA Station USW00013743) 161

4-10 Histograms of Prior and Posterior (forecasted) Monthly Change in TMI for the Arlington, VA Validation Study Site from 03/2017 to 03/2022. 165

4-11 Histograms of Prior and Posterior (forecasted) Monthly Change in TMI for the Dallas, TX Validation Study Site from 03/2017 to 03/2022. 166

4-12 Histograms of Prior and Posterior (forecasted) TMI for the Arlington, VA Validation Study Site from 03/2017 to 03/2022. 167

4-13 Histograms of Prior and Posterior (forecasted) TMI for the Dallas, TX Validation Study Site from 03/2017 to 03/2022. 168

5-1 Flow of the Deterministic SSVC Analysis Procedure 175

5-2 Volume Change Due to Change in Suction in Uncovered Area Compared to Different Locations under Covered Area 181

Figure Page

5-3 Typical Cross-Section of a Pavement with Vertical Moisture Barriers (Jayatilaka, 1999)..... 182

5-4 Normalized Vertical Movement as a Function of TMI..... 185

5-5 Normalized Vertical Movement as a Function of Depth of Vertical Moisture Barrier 186

5-6 Normalized Vertical Movement as a Function of Mean Suction..... 186

5-7 Normalized Vertical Movement at Different Thornthwaite Moisture Index at the Edge of the Pavement..... 187

5-8 Normalized Vertical Movement for Different Depths of Vertical Moisture Barriers at the Edge of the Pavement..... 187

5-9 Vertical Movement at Edge vs. Depth of Available Moisture with (d/D) = 1..... 189

5-10 Vertical Movement at Edge vs. Depth of Available Moisture with Varying Ratios of (d/D)..... 190

5-11 Vertical Movement at Edge vs. Depth of Available Moisture with (d/D) = 1..... 192

5-12 Vertical Movement at Edge vs. Depth of Available Moisture with d/D = 1 194

5-13 Volume Change Below Pavement with Vertical Moisture Barrier with Db=0 ... 195

5-14 Normalized Volume Change Below Pavement with Vertical Moisture Barrier.. 196

5-15 Volume Change Below Pavement with Vertical Moisture Barrier..... 197

5-16 Normalized Volume Change Below Pavement with Vertical Moisture Barrier.. 197

5-17 Bayesian Forecast of TMI at Denver Study, Including the True Values for Validation, from 03/2002 to 03/2022..... 202

Figure Page

5-18 Example Results of the Stochastic Shrink-Swell Analysis for the Monthly TMI and Monthly Volume Change for the Denver Study Site from 03/2002 to 03/2022 ... 203

5-19 Example Results of the Stochastic Shrink-Swell Analysis for the Monthly Difference in TMI (*dTMI*) and Monthly Difference in Volume Change for the Denver Study Site from 03/2002 to 03/2022 ... 204

D-1 NOAA Station USW00013743 Climate Data Extract and Calculated *TMI* from 03/1988 to 03/2022 ... 283

D-2 ACF and PACF for *TMI* and *dTMI* for NOAA Station USW00013743 from 03/1988 to 03/2022 ... 284

D-3 Time Series Decomposition Using 1st differenced Moving Average for NOAA Station USW00013743 from 03/1988 to 03/2022 ... 285

D-4 Histograms for Decomposed *TMI* and *dTMI* for NOAA Station USW00013743 from 03/1988 to 03/2022 ... 286

D-5 Box Plots for Monthly Parameterized *TMI* and *dTMI* for Decomposed *TMI* and *dTMI* for NOAA Station USW00013743 from 03/1988 to 03/2022 ... 287

D-6 Histograms for Monthly Parameterized *TMI* for NOAA Station USW00013743 from 03/1988 to 03/2022 ... 288

D-7 Histograms for Monthly Parameterized *dTMI* for NOAA Station USW00013743 from 03/1988 to 03/2022 ... 289

D-8 Histograms of Prior and Posterior (forecasted) *dTMI* for NOAA Station USW00013743 from 03/1988 to 03/2022 ... 290

Figure Page

D-9 Histograms of Prior and Posterior (forecasted) *TMI* for NOAA Station USW00013743 from 03/1988 to 03/2022. 291

D-10 Example of Single Simulation Results of *dTMI* and *TMI* for NOAA Station USW00013743 from 03/1988 to 03/2022. 292

D-11 NOAA Station USW00013960 Climate Data Extract and Calculated TMI from 03/1988 to 03/2022 293

D-12 ACF and PACF for *TMI* and *dTMI* for NOAA Station USW00013960 from 03/1988 to 03/2022 294

D-13 Time Series Decomposition Using 1st differenced Moving Average for NOAA Station USW00013960 from 03/1988 to 03/2022 295

D-14 Histograms for Decomposed *TMI* and *dTMI* for NOAA Station USW00013960 from 03/1988 to 03/2022 296

D-15 Box Plots for Monthly Parameterized *TMI* and *dTMI* for Decomposed TMI and dTMI for NOAA Station USW00013960 from 03/1988 to 03/2022 297

D-16 Histograms for Monthly Parameterized *TMI* for NOAA Station USW00013960 from 03/1988 to 03/2022 298

D-17 Histograms for Monthly Parameterized *dTMI* for NOAA Station USW00013960 from 03/1988 to 03/2022 299

D-18 Histograms of Prior and Posterior (forecasted) *dTMI* for NOAA Station USW00013960 from 03/1988 to 03/2022 300

Figure Page

D-19 Histograms of Prior and Posterior (forecasted) *TMI* for NOAA Station USW00013960 from 03/1988 to 03/2022. 301

D-20 Example of Single Simulation Results of *dTMI* and *TMI* for NOAA Station USW00013960 from 03/1988 to 03/2022. 302

D-21 NOAA Station USW00023062 Climate Data Extract and Calculated *TMI* from 03/1988 to 03/2022 303

D-22 ACF and PACF for *TMI* and *dTMI* for NOAA Station USW00023062 from 03/1988 to 03/2022 304

D-23 Histograms for Decomposed *TMI* and *dTMI* for NOAA Station USW00023062 from 03/1988 to 03/2022 305

D-24 Box Plots for Monthly Parameterized *TMI* and *dTMI* for Decomposed TMI and dTMI for NOAA Station USW00023062 from 03/1988 to 03/2022 306

D-25 Time Series Decomposition Using 1st differenced Moving Average for NOAA Station USW00023062 from 03/1988 to 03/2022 307

D-26 Histograms for Monthly Parameterized *TMI* for NOAA Station USW00023062 from 03/1988 to 03/2022 308

D-27 Histograms for Monthly Parameterized *dTMI* for NOAA Station USW00023062 from 03/1988 to 03/2022 309

D-28 Histograms of Prior and Posterior (forecasted) *dTMI* for NOAA Station USW00023062 from 03/1988 to 03/2022. 310

Figure Page

Figure Page

D-29 Histograms of Prior and Posterior (forecasted) *TMI* for NOAA Station USW00023062 from 03/1988 to 03/2022 311

D-30 Example of Single Simulation Results of *dTMI* and *TMI* for NOAA Station USW00023062 from 03/1988 to 03/2022. 312

D-31 NOAA Station USW00024127 Climate Data Extract and Calculated TMI from 03/1988 to 03/2022 313

D-32 ACF and PACF for *TMI* and *dTMI* for NOAA Station USW00024127 from 03/1988 to 03/2022 314

D-33 Histograms for Decomposed *TMI* and *dTMI* for NOAA Station USW00024127 from 03/1988 to 03/2022 315

D-34 Box Plots for Monthly Parameterized TMI and *dTMI* for Decomposed TMI and *dTMI* for NOAA Station USW00024127 from 03/1988 to 03/2022 316

D-35 Time Series Decomposition Using 1st differenced Moving Average for NOAA Station USW00024127 from 03/1988 to 03/2022 317

D-36 Histograms for Monthly Parameterized *dTMI* for NOAA Station USW00024127 from 03/1988 to 03/2022 318

D-37 Histograms for Monthly Parameterized *dTMI* for NOAA Station USW00024127 from 03/1988 to 03/2022 319

D-38 Histograms of Prior and Posterior (forecasted) *dTMI* for NOAA Station USW00024127 from 03/1988 to 03/2022. 320

Figure Page

D-39 Histograms of Prior and Posterior (forecasted) *TMI* for NOAA Station USW00024127 from 03/1988 to 03/2022 321

D-40 Example of Single Simulation Results of *dTMI* and *TMI* for NOAA Station USW00024127 from 03/1988 to 03/2022. 322

D-41 NOAA Station USW00023183 Climate Data Extract and Calculated TMI from 03/1988 to 03/2022 323

D-42 ACF and PACF for *TMI* and *dTMI* for NOAA Station USW00023183 from 03/1988 to 03/2022 324

D-43 Histograms for Decomposed *TMI* and *dTMI* for NOAA Station USW00023183 from 03/1988 to 03/2022 325

D-44 Time Series Decomposition Using 1st differenced Moving Average for NOAA Station USW00023183 from 03/1988 to 03/2022 326

D-45 Box Plots for Monthly Parameterized TMI and dTMI for Decomposed TMI and dTMI for NOAA Station USW00023183 from 03/1988 to 03/2022 327

D-46 Histograms for Monthly Parameterized *TMI* for NOAA Station USW00023183 from 03/1988 to 03/2022 328

D-47 Histograms for Monthly Parameterized *TMI* for NOAA Station USW00023183 from 03/1988 to 03/2022 329

D-48 Histograms of Prior and Posterior (forecasted) *dTMI* for NOAA Station USW00023183 from 03/1988 to 03/2022 330

Figure Page

D-49 Histograms of Prior and Posterior (forecasted) *TMI* for NOAA Station USW00023183 from 03/1988 to 03/2022. 331

D-50 Example of Single Simulation Results of *dTMI* and *TMI* for NOAA Station USW00023183 from 03/1988 to 03/2022. 332

D-51 NOAA Station USW00013960 Climate Data Extract and Calculated TMI from 09/1988 to 09/2022 333

D-52 ACF and PACF for *TMI* and *dTMI* for NOAA Station USW00013960 from 09/1988 to 09/2022 334

D-53 Histograms for Decomposed *TMI* and *dTMI* for NOAA Station USW00013960 from 09/1988 to 09/2022 335

D-54 Time Series Decomposition Using 1st differenced Moving Average for NOAA Station USW00013960 from 09/1988 to 09/2022 336

D-55 Box Plots for Monthly Parameterized TMI and dTMI for Decomposed TMI and dTMI for NOAA Station USW00013960 from 09/1988 to 09/2022 337

D-56 Histograms for Monthly Parameterized *TMI* for NOAA Station USW00013960 from 09/1988 to 03/2022 338

D-57 Histograms for Monthly Parameterized *dTMI* for NOAA Station USW00013960 from 09/1988 to 03/2022 339

D-58 Histograms of Prior and Posterior (forecasted) *dTMI* for NOAA Station USW00013960 from 09/1988 to 09/2022. 340

Figure Page

D-59 Histograms of Prior and Posterior (forecasted) *TMI* for NOAA Station USW00013960 from 09/1988 to 09/2022 341

D-60 Example of Single Simulation Results of *dTMI* and *TMI* for NOAA Station USW00013960 from 09/1988 to 09/2022. 342

D-61 NOAA Station USW00013960 Climate Data Extract and Calculated *TMI* from 03/1983 to 03/2022 343

D-62 ACF and PACF for *TMI* and *dTMI* for NOAA Station USW00013960 from 03/1982 to 03/2022 344

D-63 Histograms for Decomposed *TMI* and *dTMI* for NOAA Station USW00013960 from 03/1982 to 03/2022 345

D-64 Time Series Decomposition Using 1st differenced Moving Average for NOAA Station USW00013960 from 03/1982 to 03/2022 346

D-65 Box Plots for Monthly Parameterized TMI and dTMI for Decomposed TMI and dTMI for NOAA Station USW00013960 from 03/1982 to 03/2022 347

D-66 Histograms for Monthly Parameterized *TMI* for NOAA Station USW00013960 from 03/1982 to 03/2022 348

D-67 Histograms for Monthly Parameterized *dTMI* for NOAA Station USW00013960 from 03/1982 to 03/2022 349

D-68 Histograms of Prior and Posterior (forecasted) *dTMI* for NOAA Station USW00013960 from 03/1982 to 03/2022 350

Figure Page

Figure Page

D-69 Histograms of Prior and Posterior (forecasted) *TMI* for NOAA Station USW00013960 from 03/1982 to 03/2022 351

D-70 Example of Single Simulation Results of *dTMI* and *TMI* for NOAA Station USW00013960 from 03/1982 to 03/2022. 352

D-71 Example of Single Simulation Results of *dTMI* and *TMI* for NOAA Station USW00023062 from 03/1988 to 03/2022. 354

D-72 Histograms of Prior and Posterior (forecasted) dTMI for NOAA Station USW00023062 from 03/1988 to 03/2022 355

D-73 Histograms of Prior and Posterior (forecasted) TMI for NOAA Station USW00023062 from 03/1988 to 03/2022. 356

D-74 Example Results of the Stochastic Shrink-Swell Analysis for the Monthly Difference in TMI (*dTMI*) and Monthly Difference in Volume Change for the Denver Study Site from 03/2002 to 03/2022 357

D-75 Example Results of the Stochastic Shrink-Swell Analysis for the Monthly TMI and Monthly Volume Change for the Denver Study Site from 03/2002 to 03/2022 358

CHAPTER 1

1 INTRODUCTION

1.1 Background

The shrink-swell soil response to moisture changes, caused by seasonal weather variations or alterations to site drainage due to new development, is a leading cause of infrastructure damage. Puppala and Cerato (2009) reported that more than to $13 billion worth of infrastructure damage per year is caused by expansive (shrink-swell) soils in the United States, with one-third of the damage appearing in residential and commercial buildings. As such, research and improvements to design/building codes, residential and public infrastructure damage due to shrink-swell soils continue.

The fundamental mechanics of SS soils has been researched extensively in recent decades and there is a common understanding that the soil composition, environmental factors, degree of variability in each parameter, and the non-linear behavior creates a highly complex analyses which must be conservatively simplified in practical applications.

Current engineering practice for estimating the shrink-swell volume change (SSVC) primarily follows a deterministic approach of the extreme, long-term, ("worst-case") scenario. The calculation procedures are commonly empirical based using simplified laboratory tests and correlations with index properties. Occasionally one-dimensional response to wetting tests are performed, slightly improving the confidence in the estimated volume change. However, the sporadic climatic fluctuations and soil

heterogeneity are hard to capture in the deterministic approach without being highly over conservative. Such practices can lead to misleading design solutions and as a result, distresses or over-design of foundations, pavements, and other structures on SS soils are common.

The Post-Tensioning Institute's (PTI) Design of Post-Tensioned Slabs-on-Ground 3rd Edition (2008) and the American Association of State Highway and Transportation Officials (AASHTO) Mechanistic-Empirical Pavement Design Guide (MEPDG) are two existing design standards in the United States that incorporate procedures for designing foundations and pavements, respectively, on shrink-swell soils. The PTI design of slabs-on-ground encompasses a suction-based mechanistic framework for estimating time-based volume change of SS soils developed by Lytton et al. (2005) as part of a study for the Texas Department of Transportation (TxDOT). The MEPDG procedure uses an empirical approach to quantify the effect of SS soils on pavement performance. The empirical approach includes a modification to the roughness condition based upon the site's specific environmental conditions and subgrade index properties. The AASHTO MEPDG does not incorporate a mechanistic procedure to estimate soil volume change and evaluate the associated pavement distresses. Neither standard, nor any other standard of the author's knowledge, encompass stochastic techniques to estimate the expected SS soil volume change and quantify the uncertainty of the estimate based on the variability of the numerous input parameters.

1.2 Motivation

The research work presented herein was motivated by potential implementation of the work to engineering practice and by the continual strive to include in interdisciplinary frameworks, specifically statistics/data analytics, into common geotechnical engineering analyses and concepts.

1.2.1 Motivation by Implementation

The primary motivation for the research efforts was to help fulfill the requirements set in the NCHRP 01-59 which includes the development of a useful computer program which addresses the variability of the International Roughness Index (IRI) caused by climate-driven volume change of the subgrade soils. The Arizona State University research team associated with the NCHRP 01-59 project (Dr. Claudia Zapata, Dr. Sandra Houston, and Dr. Mohammad Mosawi) and the author worked to produce useful models which could be implemented into the existing Pavement Mechanical-Empirical Design (PMED), or commonly referred to as the MEPDG, which include stochastic versions of mechanistic unsaturated soil volume change analysis.

1.2.2 Motivation by Advancement

The compilation of the algorithmic procedures based on statistical theory and the stochastic simulations which produce both the expected outcome, and the associated variability is referred to herein as stochastic forecasting. The lack of quantifiable uncertainty in geotechnical analysis and the experienced-based engineering decision

making that is commonly required in practice today, is referred to herein as judgement forecasting. Although there have been considerable advancements in stochastic forecasting techniques in recent decades, implementation into geotechnical engineering practice has been minimal. Stochastic forecasting provides a formalized framework that can quantify parameter uncertainty, includes steps to estimate expected values and provides insight to the associated variability of the prediction error.

Other professional sectors such as the insurance industry, the financial investment field and the marketing industry have provided substantial evidence that stochastic forecasts are generally more efficient and representative of the actual outcomes, compared to judgement forecasts. For example, recent significant events commonly influence people to bet in the direction of short-term trends. The formalization of statistical forecast procedures and algorithms help reduce the effects of this recency bias common in judgment forecasting. Standardizing processes for generating, optimizing, and revising stochastic forecasts provide reproducible frameworks with minimal user bias.

Adopting analytical techniques for decision making does not mean that our engineering judgement goes unused. The development of analytical forecast tools requires insights and extensive knowledge of the natural mechanics of the system. One common mistake in statistical inference is the acceptance of correlation as causation. Although there may be statistical significance and/or patterns in a relationship, they may not necessarily represent the physical mechanics of that system. This interpretation error can occur during the statistical/engineering analysis stage, or by the client reviewing the work, and even by a legal team or jury.

However, these common statistical inference mistakes are avoidable. It is always recommended that the potential forecast errors are documented and relayed to all stakeholders to minimize over optimistic thinking that all potential variability, probabilities, and risks have been captured in the model. The judgement-based methods which are widely accepted in geotechnical practice today are rarely outlined in any official document. Although most clients care solely about the final products and not the path taken to get there, independent reviewers may wonder about this lack of proper documentation. Although it is likely that more time (money) will be required on the front end, the formalization of design procedures, which encompass high parameter uncertainty and engineering judgement, can improve efficiency and confidence in decision making.

The development and implementation of stochastic forecasting frameworks can eliminate the inherent inconsistencies, biases, and the "lack of enough experience" argument associated with the human-brain-led judgement forecasts. Such a statement may be discredited in many geotechnical firms in the US today; however, as the success of other professional and technological industries continue to exponentially advance due to their adoption of Bayesian Inference techniques, artificial intelligence, and modern data analytics, the civil engineering practice will be pressured to follow suit to meet client requests and maintain competitor advantages.

1.3 Purpose

The climate-driven volumetric response of shrink-swell soils frequently causes costly distresses in lightly loaded structures (pavements and shallow foundations) due to

the sporadic climatic fluctuations and soil heterogeneity which is not captured during the geotechnical design. The complexity associated with the unsaturated soil mechanics combined with the high degree of variability in both the natural characteristics of soil and the empirical models which are commonly implemented tends to lead to engineering judgment outweighing the results of deterministic computations for the basis of design. Recent advances in the application of statistical techniques and Bayesian Inference in geotechnical modeling allow for the inclusion of both parameter and model uncertainty, providing a quantifiable representation of this invaluable engineering judgement. This research study will seek to continue this trend by implementing Bayesian techniques into characterization of common soil properties, the analysis of climate-driven shrink-swell volume change using unsaturated soil moisture flow mechanics.

1.4 Organization

The proposed research is organized into seven chapters which include this introductory section, the five key studies required to reach the overall project goal, and a concluding chapter. Chapter 2 through Chapter 5, summarized below, present key accomplishments identified by the author which have potential to provide beneficial advancements to the field of geotechnical engineering. Each of the chapters for these key studies include the relevant background and literature review required to effectively complete the objectives so that the chapter could act as standalone documents if needed.

- Chapter 2 **Soil Suction Profiles using a Fourier Series Approach** presents the application of the Fourier Series for modeling monthly climate-driven soil suction

profiles. A review of existing literature pertaining to suction-based methods for modeling moisture flow within the vadose zone of unsaturated soil is summarized. An algorithmic approach was developed, referred to as the Natural-Order Fourier Series (NOFS), which uses a selection criterion for the order of the Fourier Series. An evaluation of the NOFS suction profile approach is presented using two locations within arid and temperate climate regions for time periods of 5, 15, and 30 years. The goodness of fit for increasing durations of analysis and increasing orders of the Fourier Series are evaluated.

- Chapter 3 **Bayesian Characterization of Common Soil Properties** introduces a tool to generate estimates and variability of various soil parameters for use in stochastic shrink-swell analysis analyses. A brief review of the theory of statistical moments, correlation, and Beta distributions. A review of Bayesian Inference is also included which focuses on sources of uncertainty, likelihood functions, random variable generation, and techniques for simulating random processes. A database of the necessary soil input variables was collected and used to generate updated statistical parameters for varying soil types. A Bayesian framework for randomly generating sets of each variable while accounting for high correlation between soil properties will be developed. A validation effort and discussion of potential implementation is also provided using prior data from three different soil groups.
- Chapter 4 **Stochastic Climate Forecast Model** presents a brief overview of time-series analysis techniques including autocorrelation, decomposition, forecasting, and the Fourier Series. Additional background on existing techniques for applying

Bayesian Inference to stochastically forecast time-series data is also included. A method for stochastically forecasting the climate input parameter (TMI) on a monthly basis using a component-wise, transitional, Markov Chain Monte Carlo (MCMC) approach is proposed. A discussion of the optimization and validation of the proposed model using historical climate data from the National Oceanic and Atmospheric Administration (NOAA) is also included.

- Chapter 5 Application of **Stochastic Forecast Model for Shrink-swell Volume Change** (SSVC) will bring together the deterministic shrink-swell soil volume change model and the stochastic TMI model to produce a new method for forecasting the monthly shrink-swell soil volume. A summary of the deterministic SSVC framework will be provided by the inclusion of a recent journal publication by the author and ASU research team which includes an improved framework for estimating the 1D shrink-swell volume change of soil exposed to time-varying climatic effects, as well as an evaluation of deterministic framework using the LTTP Seasonal Monitoring Program (SMP) database. The steps taken for the optimization and validation of the stochastic model are provided. The potential implementation of the proposed stochastic shrink-swell volume change forecast model to foundation and pavement performance analysis/design is discussed. The uncertainty and sensitivity of the estimations using the proposed method will be compared to those generated using current engineering practice procedures.

A concluding chapter is also included which briefly summarizes the overall research accomplishments, discusses limitations pertaining to work, and identifies aspects of the work which can be improved through additional research efforts.

1.4.1 Flow

The organization of the chapters in the report represent the various steps in the overall procedure for stochastically simulating climate-driven volume change of shrink-swell soils. Figure 1-1 provides a flow diagram for the process using the Chapter titles and sub-section titles.

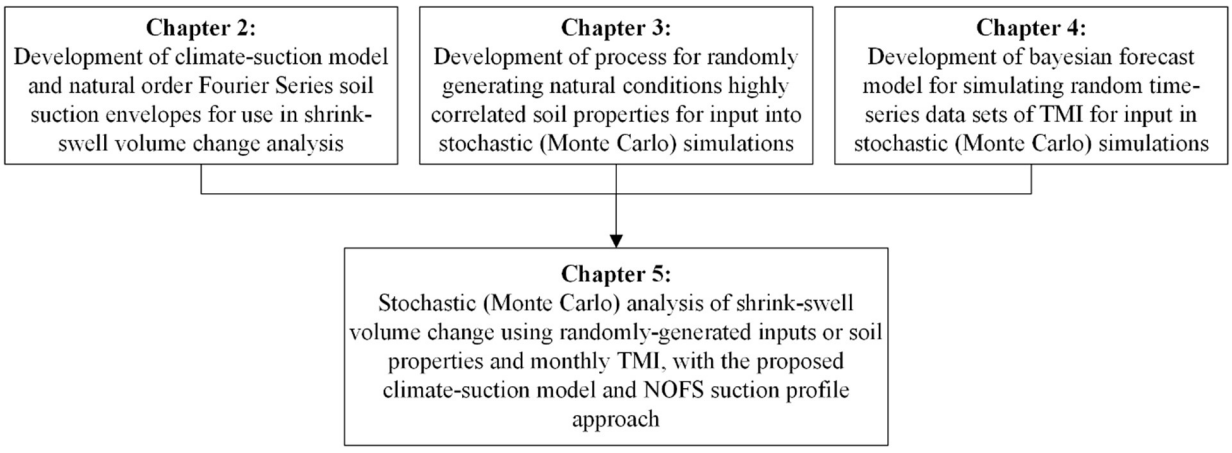

Figure 1-1 Flow of Documents Chapters

1.5 Development of Computer Software

As part of the NCHRP 01-59 requirements, the models and overall analysis procedure developed as part of the research efforts was to be programmed into a desktop application with a user interface (UI) and accompanied Manual of Practice so that the consideration

for implementation in to the existing MPED software (AASHTOware) can be efficiently evaluated by a party associated with the research team. As such, most of the algorithm procedures and resulting data/graphics were programmed using the MATLAB computing language. Unfortunately, this document precedes the review and publication of the software by NCHRP and therefore, referral to the program herein is limited to excerpts (partial screenshots) or the programs UI, and no source code is included. The author anticipates that a full report of the NCHRP 01-59 findings and final products (software) will be published by the National Academes of Sciences, Engineering, Medicine's Transportation Research Board (TRB) following the research team's final deliverable in late 2022 to early 2023.

CHAPTER 2

2 SOIL SUCTION PROFILES USING A FOURIER SERIES APPROACH

2.1 Introduction

The quantification of the moisture flux at the ground surface and the transient state of the moisture flow through the vadose zone continues to be a challenging problem for geotechnical engineers. In unsaturated soil mechanics, the near-ground-surface moisture flow is commonly evaluated using the 1-dimensional (1D) diffusion equation derived by Peter Mitchell in 1979, which is a closed form solution of the Richard's unsaturated moisture flow differential equation studied (1965). There have been several successful studies which sought to measure the parameters involved with the diffusion equation (i.e., equilibrium suction and the diffusion coefficient). Perera et al. (2005) and Vann and Houston (2021) were able to correlate the magnitude and depth of equilibrium suction to the Thornthwaite Moisture Index (TMI). Aubeny & Long (2007) found that the diffusion coefficient had high uncertainty, low reproducibility, and significant discrepancies between lab and field measurements. The seasonal fluctuations of the suction at the ground surface have been commonly applied as an average long-term trend (PTI, 2008) or as a periodic function (Lytton et al., 2005); however, Mitchell (1979) proposed the use of a Fourier Analysis to better represent the irregular patterns in climate which would allow for prolonged durations of drying or wetting to be captured.

This chapter presents the application of a Fourier Series approach for modeling monthly climate-driven soil suction profiles. Historically, the order of a Fourier Series was limited

by the increased complexity of capturing additional amplitudes which were atypical to the overall data set. To remove this limitation while maintaining computational efficiency, an algorithmic approach was developed, referred to as the Natural-Order Fourier Series (NOFS), which uses a selection criterion defined by the distribution of amplitudes of an infinite-order Fourier fit. The NOFS models the suction profiles using the diffusion equation which exhibits an exponential decay of the amplitudes with depth. The climate-induced change in soil suction at the ground surface and the long-term equilibrium state of the suction profiles are empirically estimated using the Perera et al. (2006) and Vann & Houston (2021) relationships, respectively. The knowledge of these boundary conditions allows for the back-calculation of the diffusion coefficient, removing the high uncertainty associated with measuring the parameter.

2.1.1 Objectives

The following objectives were accomplished as part of this study:

- Development of an algorithm for an automated selection of the order of a Fourier Series fit to the climate-driven variation in suction at the ground surface.
- An evaluation of the goodness of fit of the NOFS suction profile approach using two locations within arid and temperate climate regions for time periods of 5, 15, and 30 years.
- Development of a procedure for adjusting the NOFS suction profiles using measured data.
- Comparison of the adjusted NOFS suction profiles to simple periodic suction profiles.

2.2 Relevant Background

Trends in qualitative behavior of SS soils can be reasonably clear, the quantification of the magnitudes and time rate of shrink-swell can be complex. In recent years, several models have been developed that can account for some of these behaviors.

Methods for estimating shrink-swell soil volume change can be generally subdivided by empirical approaches using soil index properties such Atterberg Limits, particle size distribution, etc. and mechanistic approaches using engineering properties such as SWCCs, hydraulic conductivity, and results of 1-D oedometer tests.

Several publications reviewed as part of this study which empirically relate soil index properties to shrink-swell soil volume change potential include but are not limited to: Seed et al. (1962), van der Merve (1964), Ranganatham and Satyanarayana (1965), Nayak and Christensen (1971), Schneider and Poor (1974), O'Neil & Ghazzally (1977), Chen (1975), Johnson & Snethan (1978), Weston (1980), Picornell and Lytton (1984), Dhowian (1990a, 1990b), Basma (1993).

Direct laboratory measurements of the soil volume change potential help improve the estimation of potential volume change used for design. The 1-D oedometer "Response to Wetting Test" (ASTM D4546, 2014) is a common laboratory test for volume change determination. The following published studies include 1-D oedometer test-based relationships to unsaturated soil volume change: Jennings and Knight (1957), De Bruijn (1961, 1965), Sampson et al. (1965), Noble (1966), Sullivan and McCelland (1969), NAVFAC (1971), Wong & Yong (1973), Gibbs (1973) Jennings et al. (1973), Smith

(1973), Teng et al. (1972, 1973), Teng & Clisby (1975), Porter & Nelson (1980), Fredlund et al. (1980), Sridharan et al. (1986), Erol et al. (1987), Shanker et al. (1987), Nelson et al. (1998, 2001), Al-Shamrani & Al-Mhaidib (1999), Basma et al. (2000), Subba Rao & Tripathy (2003), Lopes (2007), Singhal (2010), and Olaiz (2017).

One key difference from the laboratory oedometer test compared to the field conditions the unsaturated soil will experience is the final degree of saturation. The response to wetting test inundates the sample, driving to saturation. However, with proper drainage, there is a reasonable probability that the soil will not reach this moisture level over the period of the pavement/structure design life. (Houston and Houston 2017). Suction-based volume change approaches can be used for the estimation of the unsaturated soil volume change at moisture levels below saturation.

Several methods which account for the moisture/suction state of the soil include the Barcelona Basic Model (Alonso et. al., 1990), the Lytton et al. (2005) approach adopted by the Texas DOT and the Post-Tensioning Institute (PTI, 2004, 2008), the Sheng, Fredlund, Gens model (Sheng. et al., 2008), the Modified State Surface Approach (MSSA) first introduced by Zhang and Lytton (Zhang 2009a, 2009b), and the Surrogate Path Method (Singhal, 2010; Houston and Houston, 2018).

The ability to estimate soil volume change as a function of time can be a valuable tool in the design of pavement structure as it allows for estimation of the cumulative International Roughness Index (IRI) impacted by environmental factors. Time-dependent estimations of shrink-swell soil volume change must quantify the changes in soil

moisture/suction due to the varying climate. For a relatively near-surface groundwater table, significant potential exists for capillary rise into subgrade soils. The conventional assumption that negative pore water pressures (i.e. soil suction) can be estimated by backward extrapolation above the groundwater table of a line of slope equal to the depth times the unit weight of water, appropriate in a thin region above the groundwater table, where soils are wetted to a degree of saturation of 85% or more (Houston et al. 2000). When the groundwater table is relatively deep, the environmental factors such as precipitation, temperature, wind speed, solar radiation, and relative humidity effect the moisture state of the soils near the surface, commonly referred to as the active zone (Nelson et al., 2001).

Given the complexity and large number of climatic parameters affecting the climate-driven flux boundary conditions, the Thornthwaite Moisture Index (TMI) (Thornthwaite, 1948; Thornthwaite and Mather, 1955, Witczak et al., 2006) is commonly used by geotechnical engineers as an index which quantifies climate variability at a given location (McKeen and Johnson 1990). The TMI represents the aridity or humidity of a soil-climate system by summing the effects of annual precipitation, evapotranspiration, storage, deficit and runoff. To a significant degree, the TMI index balances lateral infiltration and evapotranspiration for a particular region. Olaiz et al. (2017), reviewed the differing published procedures which attempt to simplify the TMI calculation from the original proposed by Thornthwaite in 1948, and concluded that the simplified equation by Witzcak et al. (2006) provides values similar to those determined by the original procedure (Thornthwaite, 1948).

The TMI has been used by geotechnical engineers to estimate soil suction envelope parameters, required for suction-based shrink-swell soil volume change estimations, such as the depth to stable (commonly referred to as equilibrium) suction, magnitude of stable suction, and total potential suction change at the surface. Published studies reviewed by the author that relate TMI to suction envelope parameters include but are not limited to: Mitchell (1979, 1980, 2008, 2013), McKeen & Johnson (1990), Fityus et al. (1998, 2004), Fityus & Smith (1998), Fox (2000), Cameron (2001), Briaud et al. (2003), McManus et al. (2004), Aubeny & Long (2007), Chan & Mostyn (2008), Fityus & Buzzi (2008), Vanapalli & Lu (2012), Karunarathne et al. (2012, 2016), Li et al. (2013, 2015), Sun (2017), the Post-Tensioning Institute 2nd and 3rd Edition (2004, 2008), Lytton et al. (2005), Cuzme (2018), Singhar (2018), Vann (2019), Vann & Houston (2021), and Olaiz et al. (2021).

2.2.1 Thornthwaite Moisture Index, TMI

Thornthwaite Moisture Index, TMI, is a parameter that represents the balance between the infiltration and evaporation in the soil, based on climatic data collected from weather stations. There have been many successful studies which have developed relationships between TMI and the climate-driven response of unsaturated soil, which will be discussed further herein.

To determine yearly TMI for each month, first the potential evapotranspiration (*PET*) for each month must be calculated

$$PET(cm) = f_1 f_2 1.6\left(\frac{10t}{I}\right)^a \quad (1)$$

Where, f_1 is the fraction of the number of days in month divided by the average number of days in month, 30; f_2 is the fraction of the number of hours in a day divided by the base of 12 h in a day; t is the mean monthly temperature in degrees Celsius; I is the annual heat index; and a is a coefficient.

$$I = \sum_{i=1}^{12}\left(\frac{t_i}{5}\right)^{1.514} \quad (2)$$

Where, t_i is the mean temperature for the i^{th} month, and

$$a = 6.75I^3x10^{-7} - 7.71I^3x10^{-5}1.792Ix10^{-2} + 0.49239 \quad (3)$$

The TMI (Witczak et al., 2006) can now be determined by

$$TMI = 75\left(\frac{P}{PET} - 1\right) + 10 \quad (4)$$

Where, P is the sum of the monthly total rainfall over the previous 12 months.

When the precipitation is greater than the evaporation, the TMI is positive, while negative TMI values represent arid and semi-arid regimes. As defined by Thornthwaite, the TMI represents an average annual condition; while the modified TMI equation can be used to represent monthly or annual conditions for any locations which weather data is available. Olaiz et al. (2017) and Singhar (2018) developed a geographic information system (GIS) tool which presented the TMI for all NOAA stations in the United States based on the 30-year monthly normal from approximately 1980 to 2010.

Karunarathne (2016) conducted a sensitivity study on the effects of the number of years of data, or averaging period, used in the calculation of the TMI. Figure 2-1 from the study illustrates how the variability in TMI significantly increases from a 25-year duration to a yearly duration.

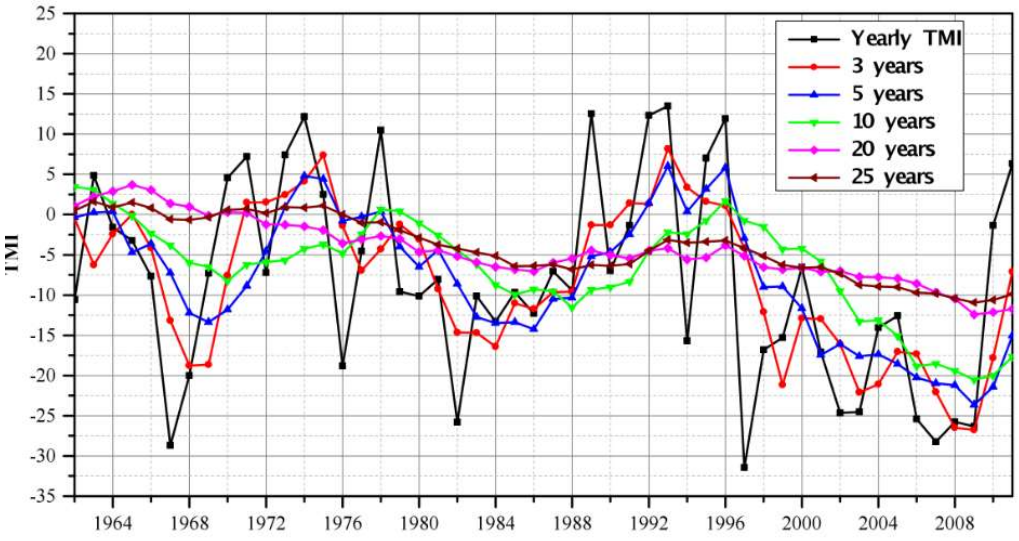

Figure 2-1 Sensitivity of Averaging Period on TMI (Karunarathne, 2016)

2.2.2 TMI-Suction Model

As part of the NCHRP 9-23 project entitled *Environmental Effects in Pavement Mix and Structural Design*, material samples were collected from beneath the highway pavement of two WesTrack cells, one MnRoad section, and 27 Long-Term Pavement Performance (LTPP) sites located throughout the United States (LTPP 2021, Houston et al. 2006). The sites were selected to represent an unbiased statistical distribution with respect to factors such as pavement type, depth to groundwater table, mean annual

temperature, precipitation, freezing conditions, soil type, and presence of cracking (Perera 2003, 2005, and Perera et al. 2004a).

Perera (2003, 2005) studied the relationship between in-situ moisture content, suction, TMI, and index soil properties. Correlations were for two models: the *TMI-P_{200}* model, which is valid for granular base materials; and the *TMI-P_{200}/wPI* model can used to estimate the equilibrium suction of subbase and subgrade materials (Rosenbalm, 2011). The two models are briefly explained in the following subsections. Note that the Perera study also included samples from sides of the pavement (uncovered) but the relationship between the in situ suction of the uncovered samples and the TMI consisted of relatively high uncertainty.

2.2.2.1 TMI-P200 Model

This model is used to find the equilibrium soil suction based on every aspect that affects water content, such as climate conditions (represented by TMI) and percent passing the #200 sieve. The following equation was presented:

$$\psi = \alpha + e^{\left[\beta+\gamma(TMI+101)\right]} \tag{5}$$

where, Ψ – the matric suction of the soil; and α, β, γ are regression constants.

The values of P_{200} range between zero and sixteen percent. If more than 16% passes sieve #200, P_{200} is limited to 16%. The regression constants can be found in Table 2-1 and interpolation between values is allowed (Perera, 2003).

Table 2-1 TMI-P200 Regression Constants (Perera 2003)

P_{200}	α	β	γ
0	3.649	3.338	-0.05046
2	4.196	2.741	-0.03824
4	5.285	3.473	-0.04004
6	6.877	4.402	-0.03726
8	8.621	5.379	-0.03836
10	12.180	6.646	-0.04688
12	15.590	7.599	-0.04904
14	20.202	8.154	-0.05164
16	23.564	8.283	-0.05218

For programming purposes, Rosenbalm developed the following equations to estimate the regression constants (Rosenbalm, 2011):

$$a = -0.00157(P_{200})^3 + 0.110566(P_{200})^2 - 0.11352(P_{200}) + 3.8218 \quad (6)$$

$$\beta = -0.0044713(P_{200})^3 + 0.112094(P_{200})^2 - 0.33636(P_{200}) + 3.2358 \quad (7)$$

$$\gamma = 2.87563x10^{(-5)}(P_{200})^3 - 0.00085(P_{200})^2 + 0.006108(P_{200}) - 0.04977 \quad (8)$$

2.2.2.2 TMI-P_{200}/*w*PI model

The *TMI-P200/wPI* model is of interest to this study. This model was developed for fine-grained material, which makes it suitable for expansive soils. For such materials, in addition to P_{200}, the weighted plasticity index, *w*PI, property was added, where:

$$wPI = \left(\frac{P_{200}}{100}\right) PI \quad (9)$$

The following equation is used to calculate suction based TMI, P_{200}, and *w*PI (Perera et al., 2005).

$$\psi = \alpha\left[e^{\left(\frac{\beta}{TMI+\gamma}\right)} + \delta\right] \tag{10}$$

where, Ψ is the matric suction of the soil; and $\alpha, \beta, \gamma, and\ \delta$ are regression constants. Table 2-2 presents the values of the regression constants for this model. In cases where the *wPI* value is less than 0.5 and P_{200} is less than 10, the *TMI-P_{200}* model should be used.

Table 2-2 TMI-P200/wPI Regression Coefficients (Perera et al., 2005).

P_{200}	*w*PI	α	β	γ	δ
10		0.3	419.07	133.45	15.0
50	0.5	0.3	521.50	137.30	16.0
	5.0	0.3	663.50	142.50	17.5
	10	0.3	801.00	147.60	25.0
	20	0.3	975.00	152.50	32.0
	50	0.3	1171.2	157.50	27.8

Equations for the regression constants were developed as part of the NCHRP 9-23 project (Rosenbalm, 2011). The regression constant for *w*PI < 0.5 are expressed as:

$$\beta = 2.56075\left(P_{200}\right) + 393.4625 \tag{11}$$

$$\gamma = 0.09625\left(P_{200}\right) + 132.4875 \tag{12}$$

$$\delta = 0.025\left(P_{200}\right) + 14.75 \tag{13}$$

The regression constant for *w*PI ≥ 0.5 are expressed as:

$$\beta = 0.006236(wPI)^3 - 0.7798334(wPI)^2 + 36.786486(wPI) + 501.9512 \quad (14)$$

$$\gamma = 0.000395(wPI)^3 - 0.04042(wPI)^2 + 1.454066(wPI) + 136.4775 \quad (15)$$

$$\delta = -0.01988(wPI)^2 + 1.27358(wPI) + 13.91244 \quad (16)$$

The Perera et al. (2006) TMI-P200/wPI Suction relationships were graphed to provide a visual representation and is provided in .

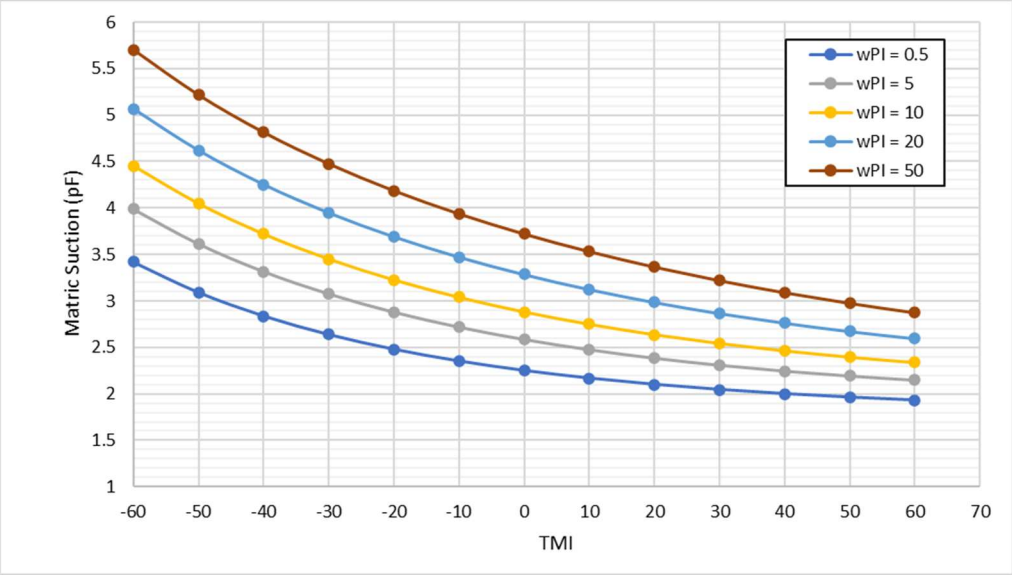

Figure 2-2: TMI-P200/wPI Relationship with Soil Suction (Perera et al., 2005)

2.2.3 Unsaturated Soil Suction Envelopes

The key aspects which affect the volume change potential of soil are the climatic conditions of the site and the soil properties. The two aspects directly affect the active zone, or depth of influence, of the soil profile, illustrated in the figure below.

The change in water content occurs in the unsaturated zone of the subsurface. However, at some depth, no dramatical change in water content occurs. In other words, the change in suction decreases with depth until reaching a point where it is almost zero, or the water content becomes nearly constant and does not change with depth (Figure 2-3 and Figure 2-4) (Nelson and Miller, 1992; Bulut, 2001). The depth to the zero-suction-change is known as the depth of influence or the active zone. Other definitions can be found in the literature for the active zone such as the zone of seasonal moisture fluctuation, the depth of wetting, or the depth to constant/equilibrium suction.

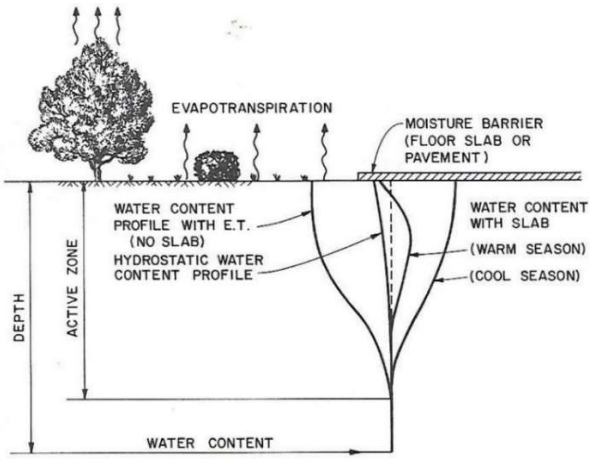

Figure 2-3 Water Content Profile in the Active Zone (After Nelson and Miller 1992)

Other factors that influence the depth of the active zone are the site cover (i.e. structure, pavement, vegetation, etc., groundwater table and soil cracking pattern, and the amount of clay minerals within the soil profile.

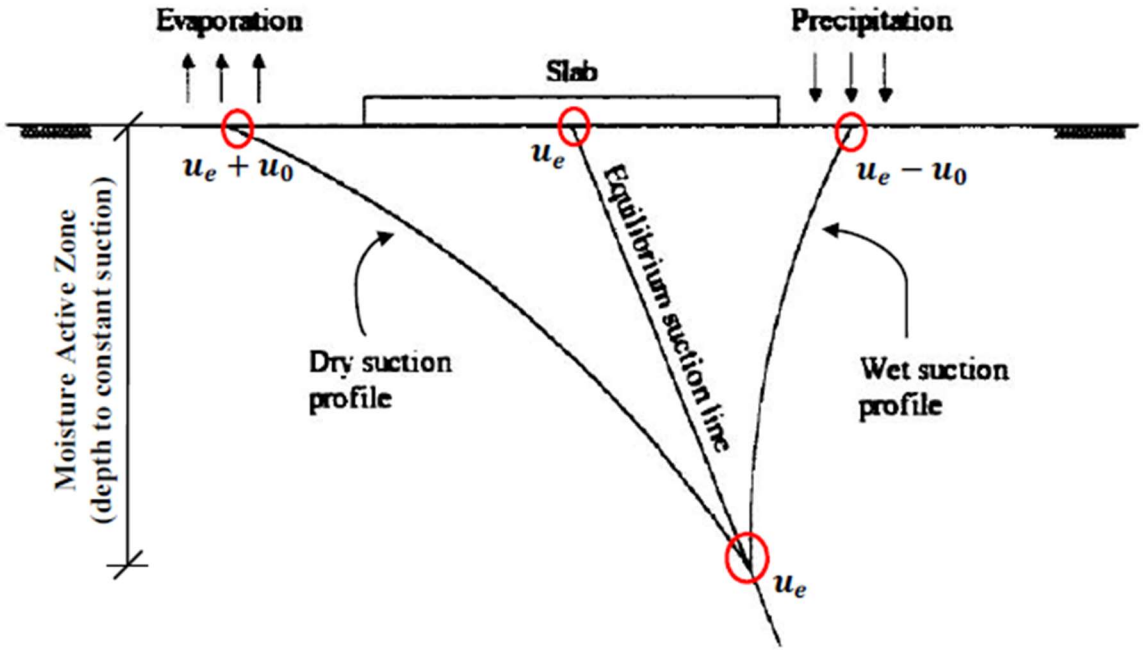

Figure 2-4 Suction Profiles, Modified from Bulut (2001) (After Amer 2016)

Based on those factors, it can be realized that activity in the active zone is in a transient state which leads to non-linear constitutive relationships. The depth of the active zone has a significant role in the estimations of potential shrink-swell soil volume change driven by seasonal climate/moisture variations.

2.2.4 Suction-Based Diffusion Equation

The diffusion of moisture through a soil proceeds from a state of low suction to a state of high suction. The moisture flow through unsaturated soil is represented as soil suction as function of location and time. The moisture flow at any location in saturated soil is represented by Darcys Law

$$v = -k_{sat} \frac{d\psi}{dx} \tag{17}$$

Where: v = velocity of flow, k = permeability, $\frac{d\psi}{dx}$ = gradient of potential in x direction, and

$$\psi = z + h_t \tag{18}$$

Where: z = elevation above the datum and h_t = total suction.

For unsaturated soil, the permeability is not constant but rather suction dependent. In 1967, LaLibere G.E. & Corey A.T. observed expressed the unsaturated soil permeability (k_{unsat}) as:

$$k_{unsat} = k_{sat} \left(\frac{h_o}{h_t} \right)^n , h_t > h_o \tag{19}$$

Where: h_o = total suction of approximately 100 cms of water (9.81 kPa), k_{sat} = saturated permeability, and n = positive constant close to 1 for clays and near 4 + for sands.

The differential equation representing the suction variation in unsaturated soils is term the diffusion equation (Mitchell, 1979) which can be solved by implementation of known or estimated boundary and initial conditions. For an unsaturated clay, the exponent n in Eq 2. is set to 1 and then substituted into Eq. 1, resulting in the expression:

$$v = -k_{sat} \left(\frac{h_o}{h_t} \right) \frac{dh_t}{dx} \tag{20}$$

Using the expression:

$$\frac{d\left(\log h\right)}{dx} = \frac{\log e}{h}\frac{dh}{dx} \tag{21}$$

And substituting into Eq. 3:

$$v = \frac{k_{sat}h_o}{0.434}\left(\frac{d}{dx}\right)\log h_t \tag{22}$$

Which can be simplified down to:

$$v = -p\frac{du}{dx} \rightarrow p = \frac{k_{sat}h_o}{0.434} \tag{23}$$

Mitchell (1979) referred to the constant p as the unsaturated permeability, which for clays with saturated permeabilities on the order of 10^{-8} to 10^{-6} cm/sec results in p ranging from $2\text{x}10^{-6}$ cm^2/sec to $2\text{x}10^{-4}$ cm^2/sec.

The suction range moves between two profiles, one is when water enters the soil with a constant velocity, low suction due to wetting, and the other is when water exits the soil with constant velocity, high suction due to drying.

Mitchell defines the constant c as the moisture characteristic which represents the change in moisture content per the change in soil suction. This term can be related to the slope of the moisture content soil water characteristic curve (SWCC) within the transition zone which is generally constant. Although the slope of the SWCC is affected by hysteresis, Mitchell assumes the hysteresis for clays is practically negligible and the value of c can be used for wetting and drying scenarios.

Mitchell derived the diffusion equation using the moisture flow in and out of a 3D incremental unit of soil. The diffusion equation defines the variation in soil suction throughout a bod of soil with respect to space and time. The diffusion equation is like the well-established relation of consolidation for saturated soils and the heat flow equation in fluid dynamics.

The general form of the diffusion equation defining moisture flow through unsaturated soil is expressed as:

$$\frac{\partial^2 u}{\partial x}+\frac{\partial^2 u}{\partial y}+\frac{\partial^2 u}{\partial z}+\frac{f\left(x,y,z,t\right)}{p}=\frac{1}{\alpha}\frac{\partial u}{\partial t} \tag{24}$$

Where α = the diffusion coefficient of the soil and is assumed constant of a small suction change. The magnitude of the diffusion coefficient represents the rate of diffusion of soil moisture under changes in suction. Based on the range of suction changes in the laboratory soaking and evaporation tests, two tests used to measure the coefficient of diffusion, the magnitude of suction change that the diffusion coefficient is applicable to is 2.75 pF (saturated) to 6.34 pF.

Using the diffusion equation, the suction at any depth (z) and time in a 1-dimensional view provided that the surface is subjected to a periodic change in suction, is expressed as:

$$u\left(z,t\right)=U_e+U_o e^{-\sqrt{\frac{n\pi}{\alpha}}z}\cos\left(2\pi nt-\sqrt{\frac{\pi n}{\alpha}}z\right) \tag{25}$$

Where, $u(z,t)$ is the suction as a function of space, y, and time, t, in pF or kPa, z is depth , U_e is the equilibrium value of suction expressed as pF, U_0 is the amplitude of pF (suction) change at the ground surface, n is the number of suction cycles per second (1 year = $31.5\times^6$ seconds), α is the soil diffusion coefficient The 1D diffusion equation indicates that the amplitude of suction at any depth decreases exponentially as a function of the diffusion coefficient. If the suction at the surface and at any depth is measured, the coefficient of diffusion can be determined by the 1D diffusion equation. Furthermore, the 1D diffusion equation captures the lag in suction change with depth and time. The suction at depth z lags the suction at the surface ($z = 0$) by time:

$$t = \frac{z}{2}\sqrt{\frac{1}{\alpha\pi n}} \tag{26}$$

If the time lag in suction at a specific depth is measured, the diffusion coefficient can be back calculated using Eq. 9.

$$\alpha = \frac{z^2}{t^2 4\pi n} \tag{27}$$

The diffusion equation method can produce a suction envelope, which is asymmetric about the magnitude of constant suction value if the surface flux boundary condition is modeled as a time-series with varying amplitudes (e.g., Fourier series). Aubeny & Long (2007) produced theoretical examples of how the skewness of a humid, semi-arid, and arid climates differ is depicted in the Figure 2-5.

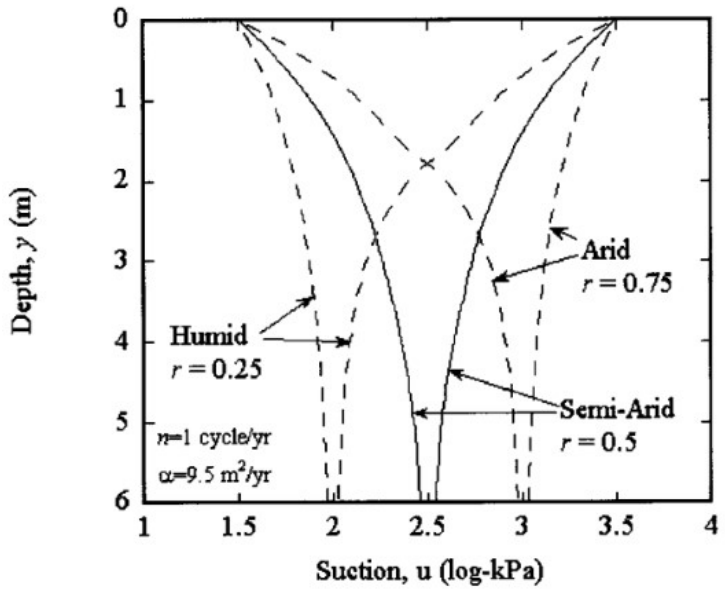

Figure 2-5 Characteristic Suction Envelopes for Humid, Semi-Arid, and Arid Climates (Aubeny & Long, 2007)

Alterations to the suction profile have also been studied and proposed. Alterations include post-construction drainage changes such as a sloping grade, replacing the native expansive soil with imported granular soil, vegetation, and natural desiccation cracking. Lytton et al. (2005) developed changes to the Mitchell (1979) suction envelope method to encompass such scenarios. Figure 2-6 presents two example profiles from Lytton et al. (2005), which the natural suction profile is altered due to the addition of granular soil and the presence of deep roots from adjacent vegetation. Efforts to simplify the development of the suction envelope have been a focus of the associated research in the past two decades. A triangular envelope, which linearly interpolates from the surface flux to the depth of equilibrium suction has been incorporated into AS2870 (2011).

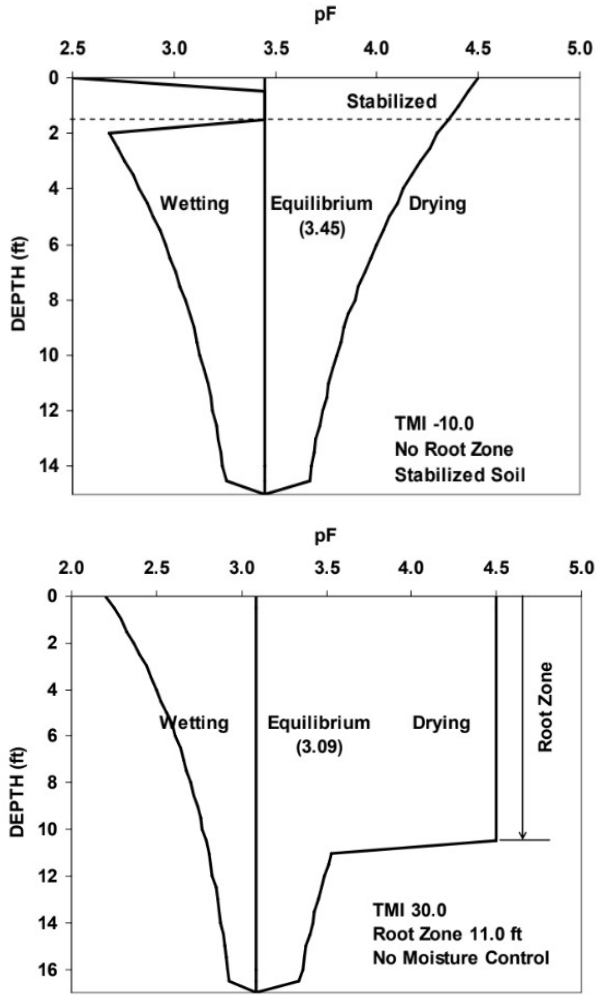

Figure 2-6 Suction Profile versus Depth with Adding Stabilized Layer (left) for Fort Worth North Site and Case of No Moisture Control (right) at Atlanta US 271 Site (Lytton et al., 2005)

TMI-Suction Envelope Relationships (Vann and Houston, 2021)

The long-term limits of the soil suction variation within the active zone are referred to as the suction envelope. This envelope can be visualized by computer simulations of the soil diffusion equation or measured in the field through instrumentation and a long-

term monitoring plan. The latter is much more expensive and no feasible for most practical situations, researchers have sought to build empirical correlations which can be used to validate or improve the input parameters required for the computer modeled soil suction diffusion analyses.

The active zone or soil suction envelope can be modeled using Mitchell's (1979) diffusion equation if the following key parameters are directly measured or empirically estimated:

1) The **variation of suction at the surface**, commonly referred to as the surface flux boundary condition, which is directly affected by the climatic conditions and can be altered due to site cover,
2) The depth which corresponds to a stable or negligible change in soil suction, referred to as the **depth to equilibrium suction**,
3) The magnitude of equilibrium suction at the depth of equilibrium,
4) The **diffusion parameters of the suction envelope** which provide the rate of diffusion and the triangular to trumpet shape of the long-term suction envelope. The diffusions parameters consist of the *frequency of cyclic variations in surface suction* and the *diffusion coefficient.*

Olaiz (2017), Cuzme (2018), Vann (2019), and Houston and Vann (2020) published on an extensive study of suction envelopes which was part of the National Science Foundation (NSF) study (#1462358) on "Soil Suction Surrogates for Advancing Complete-Stress-State Solutions to Expansive Soils" at Arizona State University.

Specifically, Vann and Houston (2021) published updates to empirical relationships between TMI and the suction envelope parameters discussed above. The Vann and Houston (2021) TMI-suction envelope relationships were developed through a compilation of historical soil suction data gathered from an extensive literature, a data mining effort of professional geotechnical investigation reports, and significant drilling effort at sites in Texas, Oklahoma, Colorado, and Arizona. As such, the methods for obtaining the suction envelope parameters in this study will follow the Vann and Houston (2021) relationships with TMI as they encompass data from the previous major studies, have been validated with measured data, and are relatively simple (i.e., based on TMI only). Published literature of related studies are continuously reviewed by the author; however, will not be included herein unless there are aspects being directly applied to this study. The author recommends Vann (2019) be referenced for additional background as it includes a very extensive and clear literature review of the soil suction envelope parameters.

The soil suction unit of pF (log to the base 10 of soil suction in centimeters of water) was used in the Vann and Houston (2021) study due to its extensive use in the geotechnical practice, with regards to unsaturated soils. Note that log of suction in kPa units is approximately equal to suction in pF units, minus 1 (i.e., 4.0 pF = 3.0 log (suction (kPa)). The pF units for soil suction will also be adopted in this document.

Vann and Houston (2021) developed an improved relationship between the depth of equilibrium suction and the 30-year TMI through a comprehensive literature review search and the additions of several new drill sites (Figure 2-7).

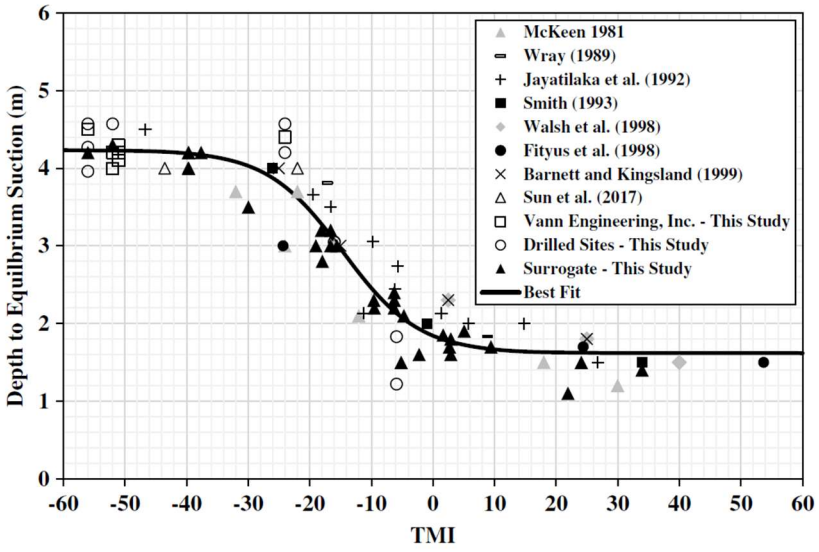

Figure 2-7: Relationship Between TMI and the Depth to Equilibrium Soil Suction (Vann and Houston, 2021)

The relationship between the Depth to Equilibrium Suction (D_{ψ_e}) [m] and 30-year TMI is expressed as:

$$D_{\psi_e} = 1.617 + \frac{2.617}{1 + e^{(2.36 + 0.1612 TMI)}} \quad (28)$$

With an $R^2 = 0.90$ and standard error = 0.315 m.

The Vann and Houston (2021) study also developed a surrogate equation which uses a ratio of the field moisture content and the Liquid Limit to estimate soil suction. The surrogate suction equation (Figure 2-8), can be used to verify the estimated depth of equilibrium suction or to estimate the full in-situ suction profile.

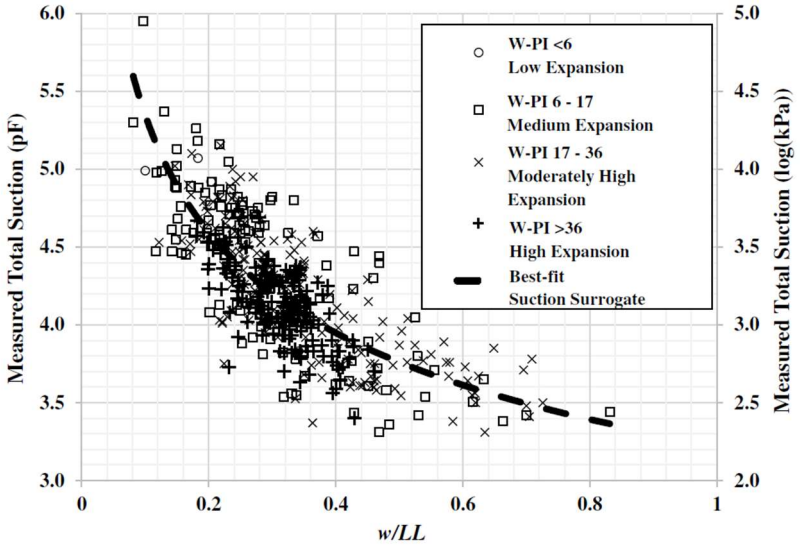

Figure 2-8 Soil Suction Estimation using Moisture Content and Liquid Limit (Vann et al. 2018)

The relationship between the soil suction [pF] and the ratio of moisture content to the Liquid Limit is expressed as:

$$\psi = 3.235\left(\frac{w}{LL}\right)^{-0.217} \tag{29}$$

With an $R^2 = 0.61$ and a standard error = 0.258 pF.

The stable, or equilibrium, suction value is determined using the Vann and Houston (2021) model (Figure 2-9).

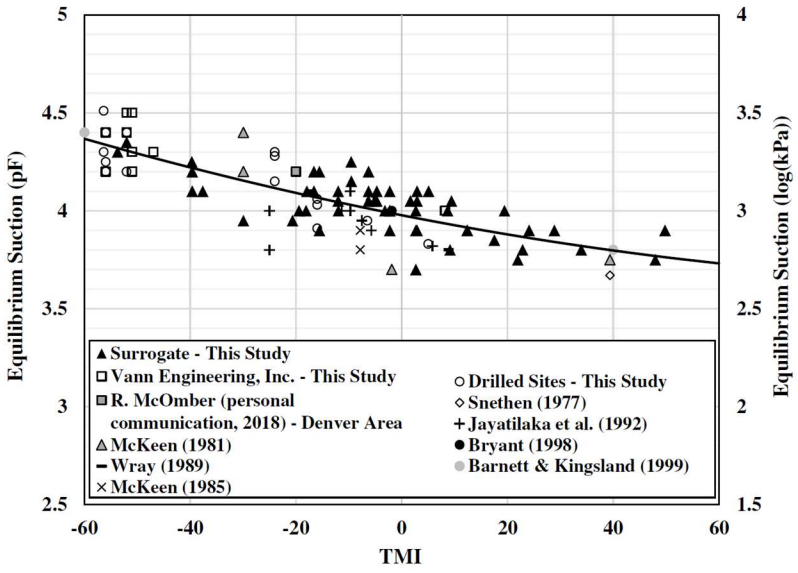

Figure 2-9: Equilibrium Suction vs. TMI with Literature Values (Vann and Houston, 2021)

The equation for the Equilibrium Suction (ψ_e) [pF] as a function of 30-year TMI is:

$$\psi_e = 0.0002TMI^2 - 0.0053TMI + 3.9771 \quad (30)$$

With an $R^2 = 0.65$ and a standard error = 0.196 pF.

2.2.5 Variation in Suction at the Ground Surface

The limits of the potential change in suction at the surface can be estimated using the Vann and Houston (2021) relationship presented in Figure 2-10. The relationship is only recommended to be used for 30-year TMI values in the range of -60 to +30. For TMI values greater than 30, which represents humid climate conditions, McManus et al. (2004) recommend the change is suction at the surface to not be less than 1 pF.

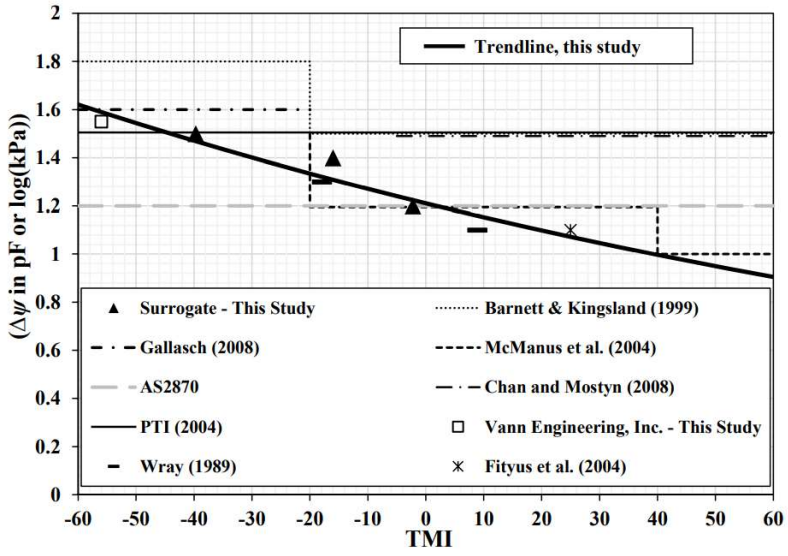

Figure 2-10: Limits of the Potential Change in Suction at the Surface vs. TMI with Literature Values (Vann and Houston, 2021)

The relationship between the potential change in suction at the surface ($\Delta\psi$) [pF] and the 30-year TMI is expressed as:

$$\Delta\psi = 1.2109e^{(-0.005TMI)} \tag{31}$$

With an $R^2 = 0.92$ and a standard error = 0.18 pF.

2.2.6 Diffusion Parameters

A key soil parameter necessary for the suction envelope computation is the soil diffusion coefficient. In 2008, Mitchell performed a study, which resulted in the following relationship between TMI and the diffusion coefficient, shown below (Figure 2-11).

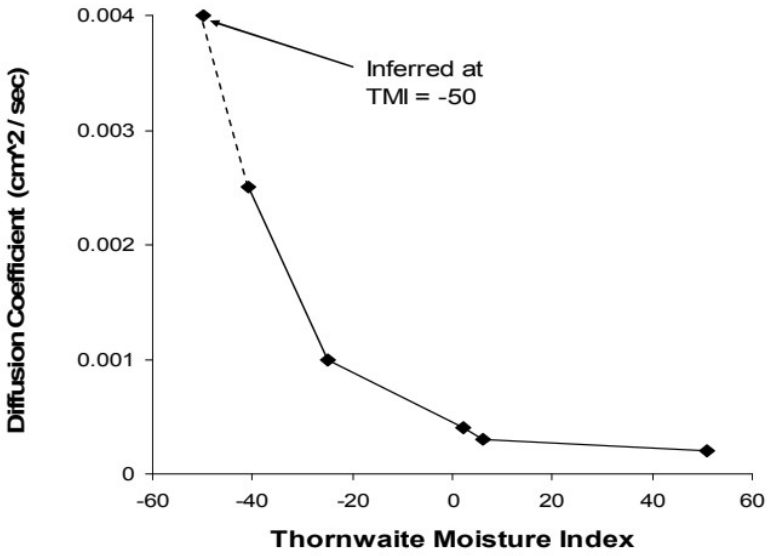

Figure 2-11 Relationship between Diffusion Coefficient and TMI (Mitchell, 2008)

The diffusion coefficient can also be back calculated for a given site if the surface flux, magnitude of equilibrium suction, depth to equilibrium suction and the variation of soil suction at the depth of equilibrium suction is assumed.

Aubeny & Long (2007) also studied the uncertainty of the key variables required in the Mitchell's equation (1979) for the change in soil suction with time. The study concluded that the diffusion coefficient (α) had significant ranges for a given soil, low reproducibility, and discrepancies between lab and field measurements, and was dependent upon the number of climatic cycles per year (*n*) when performing a back-calculation from the depth of equilibrium suction.

Aubeny & Long (2007) also presented illustrative suction envelopes, developed from the Mitchell (1980) diffusion equation to demonstrate that asymmetrical soil suction

envelopes are expected on due to variations is the climate-induced suction change at the ground surface and the hysteresis phenomena of unsaturated hydraulic conductivity. Aubeny & Long (2007) introduced a climate parameter, *r*, that is the percentage of the total anticipated change in soil suction at the surface, ($\Delta\psi$), comprising the wet side of the suction envelope. The climatic parameter can be expressed in terms of the equilibrium suction and the minimum (wet) and maximum (dry) suction at the surface (z=0):

$$r = \frac{\left(\psi_e - \psi_{wet_{z=0}}\right)}{\left(\psi_{dry_{z=0}} - \psi_{wet_{z=0}}\right)} = \frac{\left(\psi_e - \psi_{wet_{z=0}}\right)}{\Delta\psi} \tag{32}$$

Houston and Vann created a relationship between the climatic parameter (*r*) and TMI (Figure 2-12).

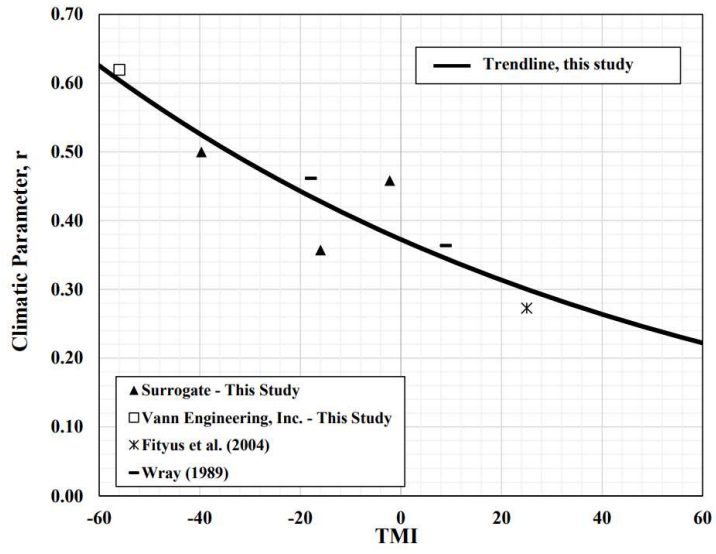

Figure 2-12: Relationship Between the Climate Parameter, *r*, and TMI (Vann and Houston, 2021)

The equation for the climatic parameter (r) as a function of TMI is expressed as:

$$r = 0.3725e^{(-0.009TMI)} \tag{33}$$

With an $R^2 = 0.80$ and a standard error = 0.11.

Depending on the approach taken, knowledge of a portion of the suction envelope parameters allows for the back calculation of the other unknown parameters. The assumption that the depth of equilibrium occurs at the location where the seasonal fluctuations fall below 0.2 pF provides an additional boundary condition to aid in back-calculation of unknown parameters (Naiser, 1997; Lytton, 1997).

2.3 Proposed Climate-Suction Model for Uncovered Sites

Perera et al. (2005) *TMI-P_{200}/wPI* provides a useful relationship between TMI, wPI, and equilibrium suction for subgrade soils beneath pavements, which was developed from extensive testing at 44 sites across the US. The model can relate the monthly variation in climate (TMI) to the variation in suction at the ground surface of a covered site by assuming that the subgrade suction will trend towards the equilibrium suction value estimated using the monthly TMI in the *TMI-P_{200}/wPI* model. The climate-driven variation of suction at the ground surface for a covered profile is not expected to be as large as an uncovered profile with the same soil properties at the same location. Although Perera (2003) also studies subgrade soils outside of the pavement edge (uncovered) and statistically significant relationship could not be developed.

A study was conducted using the ASU-NSF database to attempt to relate the monthly climate data (average temperature, precipitation, and TMI) to the in situ suction at the ground surface. The ground surface was defined as the upper two feet and the in situ suction was estimated using the Vann and Houston (2021) surrogate suction relationship with in situ moisture content and Liquid Limit. The ASU-NSF database was filtered to include only uncovered, undeveloped sites with groundwater greater than 8 feet below the surface and the average wPI in the upper 2 feet greater than 10. The filtering resulted in 75 data points from 50 different locations in Texas which had 30-year TMI values ranging from -46.68 to 36.33. Table 2-3 presents the ASU-NSF study sites in Texas used to develop the climate-suction relationship for uncovered sites.

Table 2-3 ASU-NSF Study Sites in Texas for Development of Climate-Suction Model

City (Texas)	Drill Date	NOAA Station ID	USCS	In situ Moisture Content	LL	%-200	PI	Suction* (pF)	30-year TMI	Monthly TMI (i-1)	Monthly PRCP (i-2)	Monthly PRCP (i-3)
San Antonio	2/15/13	USW00012970	SC	0.16	70	42	51	4.46	-16.6	-33.84	0.47	1.32
Killeen	3/20/14	USW00013959	CH	0.30	53	84	52	3.66	-4.99	-10.20	0.76	3.4
Killeen	3/20/14	USW00013959	CH	0.15	75	84	41	4.59	-4.99	-10.20	0.76	3.4
Killeen	3/20/14	USW00013959	CH	0.29	82	88	31	4.05	-4.99	-10.20	0.76	3.4
Breckenridge	1/15/14	USC00411042	CH	0.19	52	86	31	4.02	-9.57	-18.34	1.65	4.16
Carthage	5/1/10	USW00013972	CL	0.21	23	67	4	3.30	20.17	10.94	9.59	7.93
Carthage	5/1/10	USW00013972	CL	0.14	23	53	4	3.60	20.17	10.94	9.59	7.93
Frisco	4/16/14	USW00012917	CH	0.28	66	98	42	3.90	36.33	16.09	13.83	3.23
The Woodlands	5/1/14	USW00012960	SC	0.10	23	48	12	3.88	14.36	13.74	6.23	6.08
Fisco	4/1/14	USW00012917	CH	0.31	68	89	44	3.84	36.33	16.09	13.83	3.23
Fisco	4/1/14	USW00012917	CH	0.29	69	86	45	3.90	36.33	16.09	13.83	3.23
Fisco	4/1/14	USW00012917	CH	0.27	66	86	38	3.93	36.33	16.09	13.83	3.23
College Station	3/1/13	USW00003904	CL	0.07	32	35	16	4.56	-0.01	-22.74	12.85	9.49
College Station	3/1/13	USW00003904	CL	0.17	39	69	20	3.87	-0.01	-22.74	12.85	9.49
La Grange	3/1/12	USW00013904	CH	0.31	70	89	49	3.86	-4.43	-21.99	18.57	12.42
La Grange	3/1/12	USW00013904	CH	0.30	31	90	50	3.26	-4.43	-21.99	18.57	12.42
La Grange	3/1/12	USW00013904	CH	0.31	67	88	46	3.82	-4.43	-21.99	18.57	12.42
Abilene	1/21/14	USW00013962	CH	0.16	57	79	43	4.26	-18.09	-24.40	2.98	3.57
Abilene	1/21/14	USW00013962	CH	0.14	58	80	37	4.40	-18.09	-24.40	2.98	3.57
Hidalgo	12/5/12	USW00012959	CH	0.17	39	51	40	3.87	-37.64	-46.78	3.53	4.83

City (Texas)	Drill Date	NOAA Station ID	USCS	In situ Moisture Content	LL	%-200	PI	Suction* (pF)	30-year TMI	Monthly TMI (i-1)	Monthly PRCP (i-2)	Monthly PRCP (i-3)
Bulverde	4/20/11	USW00012921	CH	0.25	82	43	48	4.19	-13.29	-25.88	1.27	6.75
Bulverde	4/20/11	USW00012921	CH	0.20	81	43	46	4.38	-13.29	-25.88	1.27	6.75
Crowly	9/12/06	USW00013961	CH	0.20	53	78	32	4.00	-0.5	-30.30	1.07	8.01
Crowly	9/12/06	USW00013961	CH	0.21	53	77	33	3.95	-0.5	-30.30	1.07	8.01
Burleson	1/1/14	USC00411246	CH	0.25	53	90	32	3.81	5.42	-11.62	4.98	9.58
Burleson	1/1/14	USC00411246	CH	0.21	52	83	32	3.94	5.42	-11.62	4.98	9.58
Castroville	4/1/13	USW00012962	CH	0.23	64	93	46	4.04	-20.88	-31.20	0.28	4.1
Castroville	4/1/13	USW00012962	CH	0.19	57	93	39	4.11	-20.88	-31.20	0.28	4.1
Denton	12/1/12	USW00013961	SC	0.15	38	46	22	3.96	-0.5	-15.83	4.11	5.89
Segun	6/1/13	USW00012921	CH	0.31	64	80	38	3.79	-13.29	-5.42	7.04	2.41
Kyle	4/1/12	USW00013904	CH	0.22	77	94	57	4.25	-4.43	-21.64	9.82	18.57
Kyle	4/1/12	USW00013904	CH	0.22	67	94	48	4.12	-4.43	-21.64	9.82	18.57
Cedar Park	10/14/11	USW00013958	CH	0.13	67	95	38	4.62	-10.09	-47.97	0	0.13
Cedar Park	10/14/11	USW00013958	CH	0.08	51	51	35	4.84	-10.09	-47.97	0	0.13
Baytown	3/5/12	USW00012918	CH	0.50	111	96	84	3.85	21.8	-14.93	13.66	10.68
Baytown	3/5/12	USW00012918	CH	0.47	109	98	84	3.88	21.8	-14.93	13.66	10.68
Baytown	3/5/12	USW00012918	CH	0.44	94	95	71	3.81	21.8	-14.93	13.66	10.68
San Antonio	8/1/12	USW00012970	CH	0.15	58	86	42	4.34	-16.6	-27.19	0.59	12.59
Fort Worth	7/1/14	USW00013961	CH	0.12	49	64	30	4.39	-0.5	-25.09	6.02	5.99
Fort Worth	7/1/14	USW00013961	CH	0.16	48	78	29	4.11	-0.5	-25.09	6.02	5.99
Kaufman	3/1/12	USW00053911	CH	0.24	44	69	26	3.69	9.37	-12.64	11.87	11.89
Friendswood	4/1/13	USW00012975	CH	0.25	52	93	31	3.79	21.94	4.43	5.36	11.2
Red Oak	7/1/14	USW00013960	CH	0.32	81	89	51	3.96	-2.24	-23.23	10.13	4.62
Red Oak	7/1/14	USW00013960	CH	0.30	81	86	55	4.01	-2.24	-23.23	10.13	4.62
Beamount	9/1/13	USW00012917	CL	0.14	40	68	24	4.06	36.33	20.55	7.6	8.05
Beamount	9/1/13	USW00012917	CL	0.15	48	84	28	4.16	36.33	20.55	7.6	8.05
San Antonio	12/1/12	USW00012970	CH	0.33	84	93	57	3.96	-16.6	-27.75	5.77	9.29
San Antionio	12/1/12	USW00012970	CH	0.24	75	95	56	4.14	-16.6	-27.75	5.77	9.29
San Antonio	6/1/12	USW00012970	CL	0.11	36	11	18	4.18	-16.6	-35.01	0.06	6.71
San Antonio	6/1/12	USW00012970	CL	0.08	31	9	19	4.34	-16.6	-35.01	0.06	6.71
San Antonio	6/1/12	USW00012970	CL	0.13	33	10	16	3.96	-16.6	-35.01	0.06	6.71
El Paso	6/1/14	USW00023044	CL	0.03	19	14	9	4.83	-46.68	-49.04	1.14	0.46
El Paso	6/1/14	USW00023044	CL	0.02	16	15	8	5.08	-46.68	-49.04	1.14	0.46
Spring	10/1/14	USW00053910	CL	0.11	43	77	29	4.35	22.41	3.87	0.96	8.71
Killeen	12/1/14	USW00013959	CH	0.36	80	91	42	3.85	-4.99	-11.30	12.73	3.26
Converse	9/1/12	USW00012921	CH	0.17	94	87	59	4.69	-13.29	0.21	9.64	0.29
Glenn Heights	7/1/14	USW00013960	CH	0.17	63	70	42	4.30	-2.24	-23.23	10.13	4.62
Lubbock	12/1/14	USW00023042	CL	0.19	25	52	7	3.43	-45.46	-16.98	0.96	17.62
McAllen	3/1/13	USW00012959	CL	0.10	38	59	23	4.32	-37.64	-53.91	2.5	0
Weslaco	1/1/13	USW00012904	CH	0.15	63	82	42	4.42	-30.89	-46.18	0.9	1.32
Austin	3/1/13	USW00013958	CH	0.30	69	80	50	3.88	-10.09	-29.53	7.32	0.8
Tyler	6/1/13	USW00013972	SC	0.14	32	55	27	3.87	20.17	-9.17	5.62	7.4

City (Texas)	Drill Date	NOAA Station ID	USCS	In situ Moisture Content	LL	%-200	PI	Suction* (pF)	30-year TMI	Monthly TMI (i-1)	Monthly PRCP (i-2)	Monthly PRCP (i-3)
Tyler	6/1/13	USW00013972	SC	0.08	32	37	17	4.37	20.17	-9.17	5.62	7.4
Tyler	6/1/13	USW00013972	SC	0.16	32	49	17	3.76	20.17	-9.17	5.62	7.4
New Carney	9/1/13	USW00012960	ML	0.07	32	76	19	4.50	14.36	-16.19	10.4	11.33
New Carney	9/1/13	USW00012960	ML	0.05	33	79	21	4.87	14.36	-16.19	10.4	11.33
New Carney	9/1/13	USW00012960	ML	0.06	39	74	25	4.86	14.36	-16.19	10.4	11.33
McAllen	7/24/13	USW00012959	CL	0.07	30	93	16	4.44	-37.64	-54.01	2.79	3.37
Houston	7/1/13	USW00012918	CL	0.15	33	74	17	3.84	21.8	-9.42	7.52	24.27
Hewitt	10/14/13	USW00013959	CH	0.25	72	96	47	4.07	-4.99	-4.06	0.56	13.97
Princeton	2/1/14	USW00053914	CH	0.38	89	98	59	3.89	11.09	-16.02	7.26	6.05
Atascocita	11/1/13	USW00012960	CH	0.17	55	64	34	4.17	14.36	-1.14	12.94	8.46
Houston	11/19/13	USW00012918	SM	0.15	17	45	2	3.32	21.8	9.04	15.12	3.73
Texas City/ La Marque	1/31/11	USW00012918	CL	0.24	44	73	28	3.69	21.8	9.62	12.1	0.18
Dallas	11/16/09	USW00003927	CH	0.29	66	89	42	3.87	-1.87	3.45	16.56	4.16

*Estimated using in situ moisture content and Liquid Limit per Vann and Houston (2001)

The Climate-Suction model for uncovered sites was developed using a similar approach as Perera et al., (2005). The data was subdivided into groups by wPI (wPI < 15, 20, 25, 30, 35, 40, 45, 50, 50+) and an iterative multi-variate regression (linear and non-linear) using the climate data associated with site was performed using the Minitab statistical software package. The 30-year TMI, the monthly average temperature (Celsius), and the monthly rainfall (cm) were gathered using the nearest NOAA weather station and the drill date associated with the in situ moisture content measurements. The climate parameters for 12 months prior to the drill date were also gathered to explore the possibility of inherent lag in unsaturated soil moisture flow.

After numerous iterations the following model was developed relating the soil suction near the ground surface (ψ) to wPI, the 30-year TMI, the monthly TMI of the month previous to the drill date (TMI_{i-1}), and the precipitation (cm) during 2 and 3 months prior to the drill date ($PRCP_{i-2}$) and ($PRCP_{i-3}$) respectively:

$$\psi = \alpha + \beta\left(PRCP_{i-2}\right) - 0.0177\left(PRCP_{i-3}\right) - 0.00604\left(TMI_{i-1}\right) + \gamma\left(TMI_{30}\right)... \\ +0.000316\left(PRCP_{i-2}\right)\left(PRCP_{i-3}\right) + 0.000626\left(PRCP_{i-2}\right)\left(TMI_{i-1}\right) \quad (34)$$

Where, the suction (ψ) is in pF, and α, β, and γ are the regression coefficients presented in based on the wPI of the soil.

Table 2-4 Regression Coefficients for Proposed Climate-Suction Model for Uncovered Sites

wPI	<15	15-20	20-25	25-30	30-35	35-40	40-45	45-50	50+
α	4.073	4.609	4.201	3.882	4.765	4.219	3.864	4.364	3.961
β	-0.0309	0.088	-0.0362	0.0308	-0.1115	0.064	0.0172	-0.0369	-0.005
γ	-0.00466	0.00299	0.00516	0.01543	0.01538	0.00016	0.00204	0.029	-0.00776

Note that the proposed climate suction model is in units of pF, while the *TMI-P_{200}/wPI* model for covered profiles *(*Perera et al., 2006) is in units of kPa. The model fit was able to explain 84.9% of the variation in the suction data (i.e. R^2 = 84.9%). Figure 2-13 presents the incremental impact of each variable to the overall regression, indicating that the subdividing the data by wPI had the most impact, with the rainfall from 3 months prior to the drill date having the second most impact.

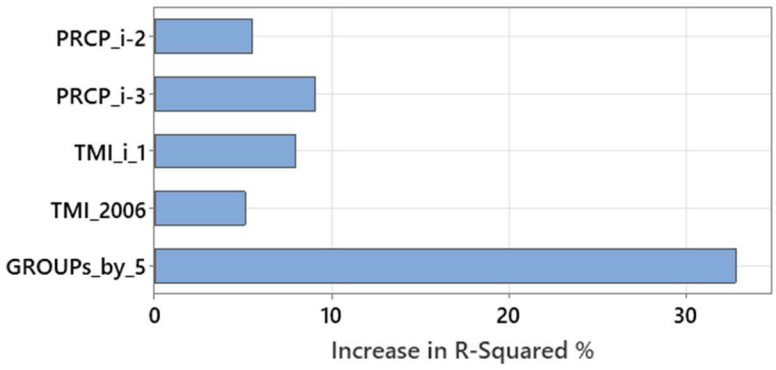

Figure 2-13 Incremental Impact of Predictor Variables to R^2 of the Regression for the Developed Climate-Suction Model (Minitab Output)

2.4 Validation of the NOFS Suction Profile Approach

Validation efforts were performed using measured suction profile data at two uncovered sites from the ASU NSF study (#1462358) on "Soil Suction Surrogates for Advancing Complete-Stress-State Solutions to Expansive Soils", which the author was a co-investigator on (Olaiz, 2017; Cuzme, 2018; Vann 2019; Vann and Houston, 2020).

2.4.1 Overview of ASU-NSF Expansive Soil Study In Situ Soil Data

As part of those research efforts involved with the NSF #1462358 study, 19 testing borings were performed at seven total locations within Arizona, Colorado, Texas, and Oklahoma extending to a depth of 30 feet below the ground surface using a CME-55 drill rig. The selected locations were representative of areas where shrink-swell soils were suspected to be prominent, based on prior experience of the local consultants. During the drilling efforts, relatively undisturbed samples were retrieved at various depths using a Modified California Split Ring Sampler consisting of 18.0" long split barrel sampler with 2.5" outer diameter, with a blunt nosed shoe (area ratio of 56%). Bulk (disturbed) samples were obtained at 1.0-foot intervals. Lab testing of the ring samples included 1D response to wetting tests (ASTM D4546), WP4-C total suction measurements (Decagon Devices, 2011), and Soil Water Characteristic Curves with strain measurements using an oedometer pressure plate device (OPPD) developed by Fredlund (GCTS, 2007). Lab testing of each bulk sample included Sieve Analysis, Atterberg Limits, moisture content, and Total Suction via the WP4-C.

Olaiz (2017) evaluated the applicability of the WP4-C as part of the same NSF study and concluded that:

- the device produces very similar results to the filter paper suction test,
- the disturbance of the sample does not significantly affect the precision of the measurement due to the relatively small sample size, and
- developed a method for converting the total suction measurement of the WP4-C to the matric suction using an oedometer pressure plate device (OPPD) to measure the suction matric suction of a natural and relatively undisturbed sample.

The extensive lab testing effort of 1-foot intervals provides a detailed picture of the field suction profile at the time of drilling. As such, data from four sites associated with covered and uncovered borings, as defined by Vann (2019), were used to explore and validate the proposed NOFS suction model. Applicable information gathered from the four of the studied sites is in summarized in Table 2-5.

Table 2-5 Relationships Between TMI and Equilibrium Suction for ASU-NSF Study Sites (adapted from Vann, 2019)

Test Boring ID	Location	TMI (30-Year)	Date Drilled	NOAA Station ID
DEN-2-U-N	Denver, CO	-20.6	9/16/16	USW00023066
DEN-3-U-N	Denver, CO	-20.6	9/16/16	USW00023066
SA-2-U-I	San Antonio, TX	-13.3	9/23/16	USW00012921
SA-4-U-I	San Antonio, TX	-13.3	9/23/16	USW00012921

At the Denver site, one test boring was advanced in a covered area where there was at least 3.048 m (10 ft) to the edge of the covering (asphalt), and two test borings were

completed in uncovered areas. At the San Antonio site, two test borings were advanced in covered areas where there was at least 3.048 m (10 ft) to the edge of the covering (asphalt), one test boring in an uncovered area that was routinely irrigated, and one test boring in an uncovered area that was not irrigated.

2.4.2 Denver, CO Climate-Suction Model Exploration

The drill date for the Denver, CO ASU-NSF study site was 09/17/2016 and the local NOAA weather station is "DENVER-STAPLETON" (ID: USW00023066). Test borings performed at this location were uncovered and included all the necessary laboratory measurements for the validation. Table 2-6 presents the Soil Properties for Upper 2 ft of Uncovered Borings at ASU-NSF Denver, CO Site (Vann, 2019) and Figure 2-14 presents the monthly climate data from 30 years prior to the drill date. Average values up the upper two feet, and an average of both boring locations combined were also explored to help smooth potentially sporadic data.

Table 2-6 Soil Properties for Upper 2 ft of Uncovered Borings at ASU-NSF Denver Site

Boring ID	Depth Interval (ft)	p200 (%)	LL	PI	w (%)	wPI	WP4-C Suction (pF)
DEN-2-U-N	0-1	71	40	24	10.9	17.0	4.59
DEN-2-U-N	1-2	71	38	23	10	16.3	4.6
DEN-3-U-N	0-1	75	39	22	9.4	16.5	4.8
DEN-3-U-N	1-2	69	38	22	9.7	15.2	4.66
DEN-2-U-N	Avg.	71	39	24	10.45	16.7	4.60
DEN-3-U-N	Avg.	72	38.5	22	9.55	15.8	4.73
Combined	Avg.	71.5	38.8	22.8	10.0	16.3	4.7

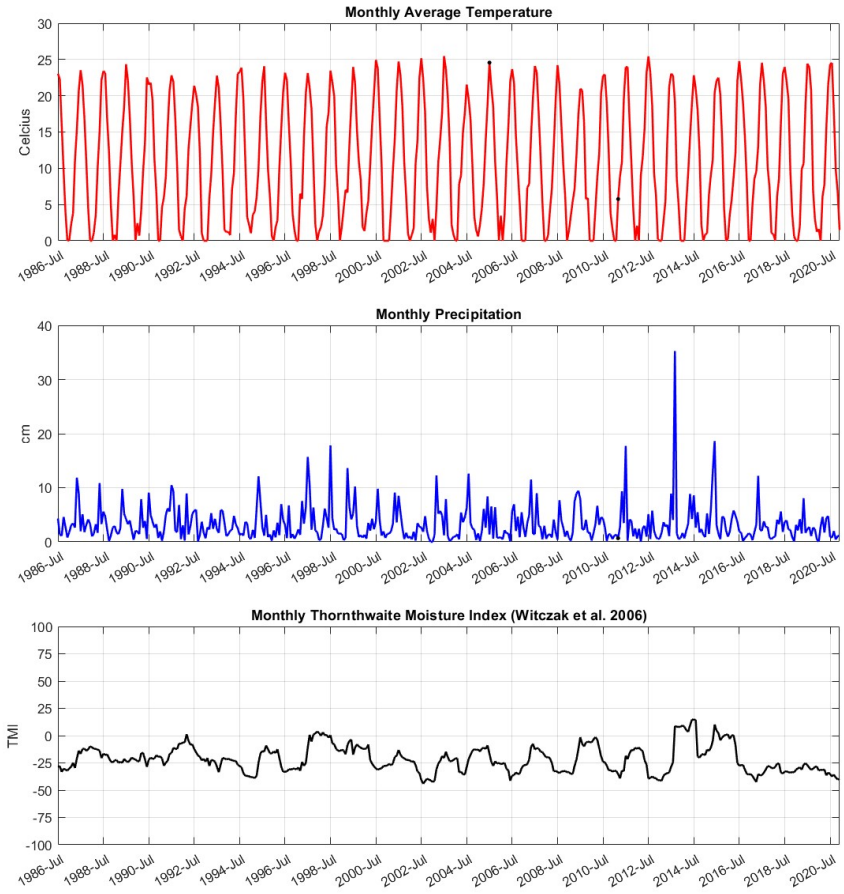

Figure 2-14 Monthly Average Temperature (red), Total Rainfall (blue), and TMI at the NOAA Station (ID: USW00023066) from 07/1986 to 12/2020

The measured soil index properties and the gathered climate data at the site, were used to estimate the suction near the ground surface during the drill date was estimated using the proposed Climate-Suction model for uncovered sites. Table 2-8 presents the estimated near the ground surface suction at the ASU-NSF Denver Site for the 7 data points summarized previously in Table 2-6

Table 2-7 Suction at ASU-NSF Denver Site using Proposed Climate-Suction Model

Boring ID	Depth Interval (ft)	Drill Month (i)	wPI	PRCP (i-2) (7/2016) (cm)	PRCP (i-3) (6/2016) (cm)	Monthly TMI (i-1) (8/2016)	30-year TMI	Estimated Suction (Proposed Uncovered Model) (pF)
DEN-2-U-N	0-1	9/2016	4.59	1.89	3.69	-27.62	-20.6	4.50
DEN-2-U-N	1-2	9/2016	4.6	1.89	3.69	-27.62	-20.6	4.50
DEN-3-U-N	0-1	9/2016	4.8	1.89	3.69	-27.62	-20.6	4.50
DEN-3-U-N	1-2	9/2016	4.66	1.89	3.69	-27.62	-20.6	4.50
DEN-2-U-N	Avg.	9/2016	4.60	1.89	3.69	-27.62	-20.6	4.50
DEN-3-U-N	Avg.	9/2016	4.73	1.89	3.69	-27.62	-20.6	4.50
Combined	Avg.	9/2016	4.7	1.89	3.69	-27.62	-20.6	4.50

2.4.3 San Antonio, TX Climate-Suction Model Exploration

The drill date for the San Antonio ASU-NSF study site was 09/23/2016 and the local NOAA weather station ID "SAN ANTONIO INTL AP" (ID: USW00012921). Only one of the test borings performed at this location was uncovered and included all the necessary laboratory measurements for the validation. Table 2-8 Soil Properties for Upper 2 ft of Uncovered Borings at ASU-NSF San Antonio Site presents the Soil Properties for Upper 2 ft of Uncovered Borings at ASU-NSF Denver, CO Site (Vann, 2019 and Figure 2-15 presents the monthly climate data from 30 years prior to the drill date. The average values up the upper two feet were also explored to help smooth potentially sporadic data.

Table 2-8 Soil Properties for Upper 2 ft of Uncovered Borings at ASU-NSF San Antonio Site

Boring ID	Depth Interval (ft)	p200 (%)	LL	PI	w (%)	wPI	WP4-C Suction (pF)
SA-4-U-I	0-1	79	58	43	18.7	34.0	4.24
SA-4-U-I	1-2	90	58	43	18.4	38.7	4.14
Combined	Avg.	84.5	58.0	43.0	18.6	36.3	4.20

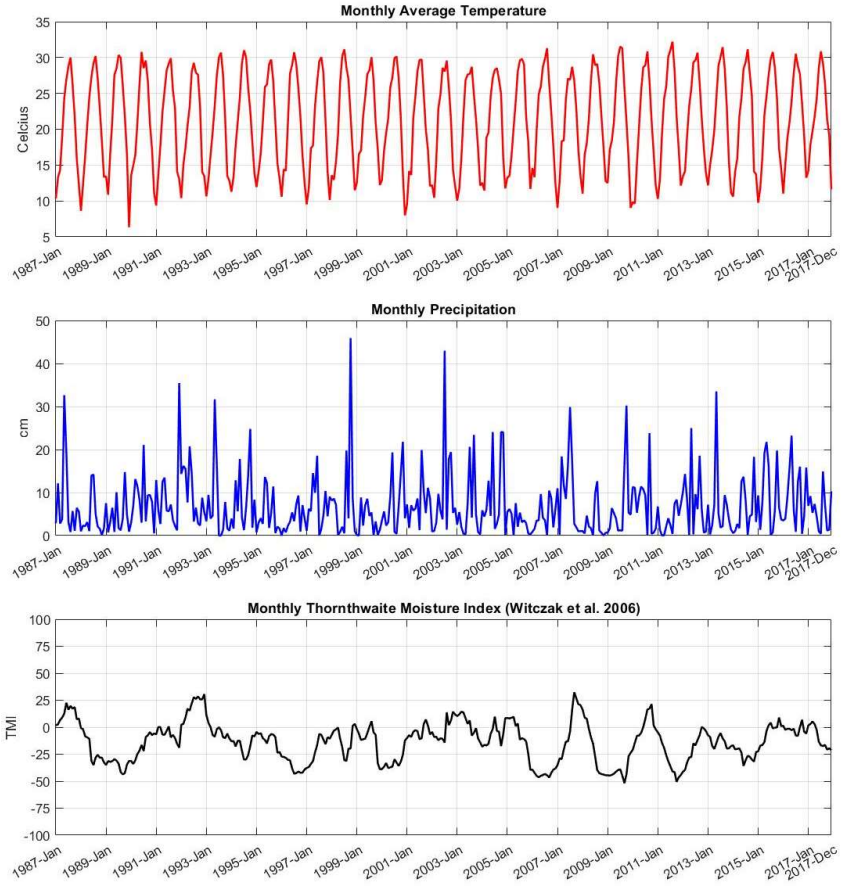

Figure 2-15 Monthly Average Temperature (red), Total Rainfall (blue), and TMI at the NOAA Station (ID: USW00012921) from 01/1987 to 12/2017

The measured soil index properties and the gathered climate data at the site, were used to estimate the suction near the ground surface during the drill date was estimated using the proposed Climate-Suction model for uncovered sites. Table 2-9 presents the estimated near the ground surface suction at the ASU-NSF Denver Site for the 7 data points summarized previously in Table 2-8

Table 2-9 Suction at ASU-NSF San Antonio Site using Proposed Climate-Suction Model

Boring ID	Depth Interval (ft)	Drill Month (i)	wPI	PRCP (i-2) (7/2016) (cm)	PRCP (i-3) (6/2016) (cm)	Monthly TMI (i-1) (8/2016)	30-year TMI	Estimated Suction (Proposed Uncovered Model) (pF)
SA-4-U-I	0-1	9/2016	34.0	6.08	0.85	-8.05	-13.29	4.26
SA-4-U-I	1-2	9/2016	38.7	6.08	0.85	-8.05	-13.29	4.29
Combined	Avg.	9/2016	36.3	6.08	0.85	-8.05	-13.29	4.29

2.4.4 Evaluation of Proposed Climate-Suction Model

The estimated suction at the ground surface at the ASU-NSF Denver site (Table 2-7) and the San Antonio site (Table 2-9) using the proposed climate-suction model for uncovered sites (ψ_{uncv}) were compared to the directly measured values form the Vann (2019) study (ψ_{WP4C}), the estimated values using the surrogate approach from Vann and Houston (2021) based on in situ moisture content and Liquid Limit (ψ_{srgt}), and the estimated values using the Perera et al. (2006) *TMI-P200/wPI* model for covered profiles (ψ_{cvrd}). The results of the comparisons for the Denver site and the San Antonio sire are presented in Table 2-10. The residual (comparison differences) mean error (RME), the residual standard error (RSE), and the mean absolute error (MAE) are also presented.

Table 2-10 Comparison of Suction Estimates to Measured Values at the Denver Study Site

Boring ID	Depth Range (ft)	ψ_{WP4C} (pF)	ψ_{srgt} (pF)	ψ_{cvrd} (pF)	ψ_{uncv} (pF)	ψ_{srgt} vs. ψ_{WP4C}	ψ_{cvrd} vs. ψ_{WP4C}	ψ_{uncv} vs. ψ_{WP4C}	ψ_{uncv} vs. ψ_{srgt}	ψ_{uncv} vs. ψ_{cvrd}
DEN-2-U-N	0-1	4.59	4.29	3.37	4.50	-0.30	-1.22	-0.09	0.21	0.83
DEN-2-U-N	1-2	4.6	4.32	3.38	4.50	-0.28	-1.22	-0.10	0.18	0.82
DEN-3-U-N	0-1	4.8	4.41	3.38	4.50	-0.39	-1.42	-0.30	0.10	0.82
DEN-3-U-N	1-2	4.66	4.35	3.40	4.50	-0.31	-1.26	-0.16	0.15	0.81
DEN-2-U-N	Avg.	4.60	4.31	3.38	4.50	-0.29	-1.22	-0.09	0.20	0.83
DEN-3-U-N	Avg.	4.73	4.38	3.39	4.50	-0.35	-1.34	-0.23	0.13	0.81
Avg.	Avg.	4.7	4.3	3.38	4.50	-0.32	-1.28	-0.16	0.16	0.82
SA-4-U-I	0-1	4.24	4.14	2.39	4.26	2.39	4.26	-0.10	-1.85	0.02
SA-4-U-I	1-2	4.14	4.15	2.24	4.29	2.24	4.29	0.01	-1.90	0.15
Avg.	Avg.	4.2	4.14	2.31	4.29	2.31	4.29	-0.05	-1.88	0.10
Residual Mean Error (RME) of Combined Data:						-0.250	-1.448	-0.099	0.113	1.023
Residual Standard Error (RSE) of Combined Data:						0.252	1.448	0.135	0.113	1.023
Mean Absolute Error (MAE) of Combined Data:						0.277	1.472	0.156	0.139	1.072

Based on the validation study using the Denver and San Antonio ASU-NSF expansive soil study site data, the proposed climate-suction model appears to provide reasonable approximations for estimating the climate-driven suction near the ground surface for uncovered sites based on the following evidence provided in Table 2-10.

- The residual standard error between ψ_{WP4C} and ψ_{uncv} (RSE = 0.135 pF) is less than that between ψ_{WP4C} and ψ_{srgt} (RSE = 0.252 pF), indicating that for the two sites explored, the proposed model which incorporates only index properties and climate data produces a more accurate estimate of the measured suction than the surrogate approach (Vann and Houston, 2021), which requires knowledge of the in situ moisture content.

- The residual standard error between ψ_{WP4C} and ψ_{uncv} (RSE = 0.135 pF) is similar to that between ψ_{srgt} and ψ_{uncv} (RSE = 0.113 pF), indicating that for the two sites explored, the proposed model produces similar suction values the surrogate approach (Vann and Houston, 2021).
- The average of the residuals between ψ_{WP4C} and ψ_{cvrd} (RME = -1.448 pF) indicate that the Perera et al. (2005) model significantly underestimates the suction at the ground surface for uncovered sites, which agrees with assumption that covered soils should experience less climate-driven variation than uncovered sites.
- The average of the residual between ψ_{uncv} and ψ_{cvrd} (RME = 1.023 pF) indicates that the proposed climate-model for uncovered sites produces values that are on average approximately 1 pF greater than the Perera et al. (2006) model for covered sites.
- For each comparison the RME and the MAE are approximately the same magnitude indicating that the model either underestimated or overestimated the measured value for all data points, the exception of the and ψ_{uncv} to ψ_{WP4C} (RME = -0.099 and MAE = 0.135) which indicates the proposed model produces an average estimate similar to the average of the measured data.

Based on this validation study, the proposed climate-suction model for uncovered sites will be implemented in this study of suction envelopes and volume change of shrink/swell soils.

2.5 Representation of Suction Profiles using Fourier Series

To model the suction changes as a function of time and depth, an equation must be developed to represent the variation of suction at the surface. Historically, a simple periodic (sinusoidal) fit has been used to represent the surface suction variation with time. However, The Mitchell (1979) formulation of the closed-form suction diffusion equation allows for a Fourier time series to be applied as the surface flux boundary conditions.

2.5.1 Overview of Fourier Series Analysis

Time series techniques like the autoregressive moving average (ARMA) or the more advanced autoregressive moving average (ARiMA) are effectives methods for modeling sporadic data. However, such methods represent the data in a discrete manner. When continuous functions of time series data are required, the Fourier Series analysis can be used to generate a representative equation. The Fourier Series (FS) decomposes, or transforms, the time series data into a summation of periodic sine and cosine terms with differing amplitudes.

The Fourier approach takes advantage of orthogonality relationships of sine and cosine which is generally defined using two functions $f(x)$ and $g(x)$ over an interval between *a* and *b*:

$$\left\langle f(x) \mid g(x) \right\rangle \equiv \int_a^b f(x)\, g(x)\, w(x)\, dx = 0 \tag{35}$$

Where $w(x)$ is a weighting function used to normalize (N_n) theorthogonal functions expressed as:

$$\int \left[f_n(x)^2 \right] w(x)\, dx = N_n \tag{36}$$

Where subscript *n* is the number of terms in the data. The computation of the Fourier series includes the following integral identities of a complete orthogonal system over the domain $[-\pi, \pi]$.

$$\int_{-\pi}^{\pi} \sin(mx) \sin(nx)\, dx = \pi \delta_{mn} \tag{37}$$

$$\int_{-\pi}^{\pi} \cos(mx) \cos(nx)\, dx = \pi \delta_{mn} \tag{38}$$

$$\int_{-\pi}^{\pi} \sin(mx) \cos(nx)\, dx = 0 \tag{39}$$

$$\int_{-\pi}^{\pi} \sin(mx) = 0 \tag{40}$$

$$\int_{-\pi}^{\pi} \cos(mx) = 0 \tag{41}$$

Where, $m \neq 0$, $n \neq 0$, and δ_{mn} is the Kronecker delta.

The general form of a Fourier Series equation $f_s(x)$ can be expressed as:

$$f_s(x) = \tfrac{1}{2} \alpha_0 + \sum_{k=1}^{\infty} a_k \cos(kx) + \sum_{k=1}^{\infty} b_k \sin(kx) \tag{42}$$

Where *k* is the order (number of cosine/sine terms) used to represent the time series data, *a* is the Fourier cosine coefficient, *b* is Fourier sine coefficient. The Fourier coefficients are expressed as:

$$a_0 = \tfrac{1}{\pi}\int_{-\pi}^{\pi} f_s(x)\,dx \tag{43}$$

$$a_k = \tfrac{1}{\pi}\int_{-\pi}^{\pi} f_s(t)\cos(kx)\,dx \tag{44}$$

$$b_k = \tfrac{1}{\pi}\int_{-\pi}^{\pi} f_s(t)\sin(kx)\,dx \tag{45}$$

For a data set defined by the domain $[-L, L]$ rather than $[-\pi, \pi]$, a change of variables such that $x' = Lx/\pi$ can be used to express the Fourier series as:

$$f_s(x') = \tfrac{1}{2}\alpha_0 + \sum_{k=1}^{\infty} a_k \cos\left(\tfrac{\pi k x'}{L}\right) + \sum_{k=1}^{\infty} b_k \sin\left(\tfrac{\pi k x'}{L}\right) \tag{46}$$

With the Fourier coefficients expressed as:

$$a_0 = \tfrac{1}{L}\int_{-L}^{L} f_s(x')\,dx' \tag{47}$$

$$a_k = \tfrac{1}{L}\int_{-L}^{L} f_s(x')\cos\left(\frac{\pi k x'}{L}\right)dx' \tag{48}$$

$$b_k = \tfrac{1}{L}\int_{-L}^{L} f_s(x')\sin\left(\frac{\pi k x'}{L}\right)dx' \tag{49}$$

The Fourier series can also be represented using complex coefficients, which provides the most effective approach for transforming discrete data into a continuous function:

$$f_s(x) = \sum_{k=-\infty}^{\infty} A_k e^{ikx} \tag{50}$$

Where, $i = \sqrt{-1}$, and,

$$A_k = \tfrac{1}{2\pi}\int_{-\pi}^{\pi} f_s(x)e^{-ikx}\,dx \tag{51}$$

Which can be simplified down to a piece-wise equation based on *k*:

$$a_0 = \begin{Bmatrix} \frac{1}{2}\left(a_k + ib_k\right) & k < 0 \\ \frac{1}{2}a_0 & k = 0 \\ \frac{1}{2}\left(a_k - ib_k\right) & k > 0 \end{Bmatrix} \tag{52}$$

For a periodic domain $\left[-L/2, L/2\right]$, the Fourier series with complex coefficients is expressed as:

$$f_s\left(x\right) = \sum_{k=-\infty}^{\infty} A_k e^{i\left(2\pi kx/L\right)} \tag{53}$$

$$A_k = \frac{1}{L}\int_{-L/2}^{L/2} f_s\left(x\right) e^{i\left(2\pi kx/L\right)} dx \tag{54}$$

The general form of a Fourier Series equation as function of time $f_s\left(t\right)$, which will be incorporated herein is expressed as:

$$f_s\left(t\right) = \frac{1}{2}\alpha_0 + \sum_{k=1}^{\infty} a_k \cos\left(\omega_k t\right) + \sum_{k=1}^{\infty} b_1 \sin\left(\omega_k t\right) \tag{55}$$

$\omega_k = fk$ represents multiples of the fundamental frequency of the time series data expressed as: $f = \frac{2\pi}{\Delta t}$. The order parameter k will represent half of the number of terms (N) in the discrete time series data minus 1 (i.e. $k = \frac{1}{2}N - 1$).

2.6 Fourier Series Suction Profile

Aubeny & Long (2007) expressed the long term suction envelopes time: $u\left(y,t\right)$ using the Fourier series expansion of the suction diffusion equation:

$$u\left(y,t\right) = U_e - \left(U_{dry} - U_{wet}\right)\sum_{k=1}^{\infty} a_k \exp\left(-\sqrt{\lambda k}\right)\cos\left(\tau k - \sqrt{\lambda k}\right) \tag{56}$$

Where: U_e is the equilibrium suction value, U_{dry} is the maximum value of the suction variation at the ground surface, U_{wet} is the maximum value of the suction variation at the ground surface, k is the order of the series (i.e. k =1, 2, 3…), a_k is the coefficients of the Fourier series expressed as:

$$a_k = \left(2/k\pi\right)\sin\left(k\pi r\right) \tag{57}$$

τ is the dimensionless time factor expressed as:

$$\tau = 2\pi t n_\lambda \tag{58}$$

λ is the dimensionless depth factor expressed as:

$$\lambda = \pi y^2 n_\lambda / \alpha \tag{59}$$

α is the soil suction diffusion coefficient, and n_λ is the lowest frequency of cyclic suction variation at the ground surface. Figure 2-16 from Aubeny & Long (2007) presents characteristic suction envelopes for humid, semi-arid, and arid climates with equilibrium suction values of 2, 2.5 and 3 log-kPa, respectively. Note that the log-kPa unit is 1.008 units less than the pF units used in this study. The variable *r* presented in the figure is the climate parameter which Aubeny & Long (2007) express as:

$$r = \frac{\left(U_e - U_{wet}\right)}{\left(U_{dry} - U_{wet}\right)} \tag{60}$$

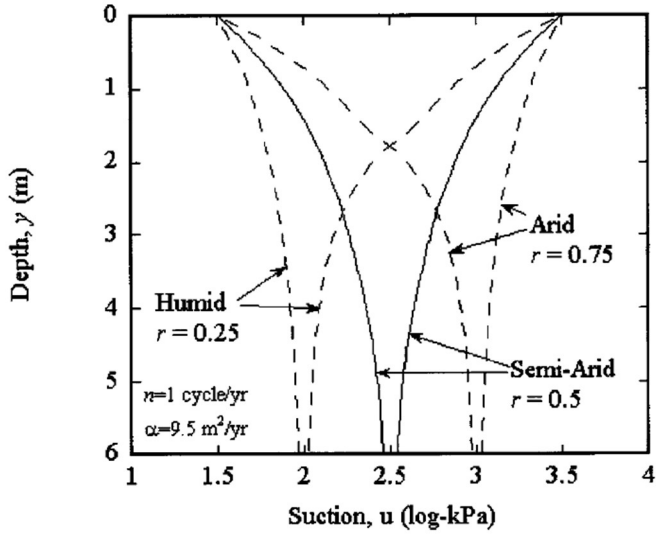

Figure 2-16 Characteristic Suction Envelopes for Humid, Semi-Arid, and Arid Climate

2.6.1 Adjustments to NOFS Suction Profiles using Measured Data

The Fourier series diffusion equation incorporates the dimensionless depth factor into an exponential decay which indicates that both the diffusion coefficient and the frequency of suction at the ground surface affect the depth of equilibrium value that is interpreted from the analysis.

The diffusion coefficient is a relatively difficult parameter to obtain as it requires in situ suction measurements up to and sometimes greater than 20 feet below the surface over a long period of time, which is generally not feasible for practicing engineers. Although it could also be measured in a laboratory, it requires a specialized procedure which most commercial geotechnical laboratories are not equipped to perform. Furthermore, Aubeny & Long (2007) performed an extensive study to evaluate the lab measured and the field

measured diffusion coefficient both separately and together. The study concluded that each method resulted in a high range of values, and that lab measured diffusion coefficients were significantly less than those calculated from in situ suction measurements in the field over a long period of time, which also had a large range of results. As such, the quantifying the diffusion coefficient continues to be a focus of research in unsaturated soil mechanics, typically with state Department of Transportation (DOT) divisions partnering with the local universities like the Oklahoma DOT with Oklahoma State University (Bulut et al., 2013) and Texas DOT with Texas A&M University (Lytton et al., 2005).

Additional uncertainty is incorporated into the dimensionless depth factor of the Fourier series diffusion equation via the selected value to represent the frequency of cyclic suction variation. Although this parameter can be calculated from the Fourier fit of the time-series suction data, the value will be governed by the timeframe of the provided suction data. If the time frame of the provided data for the variation in suction at the surface is relatively short (e.g., 1 to 10 years), the suction envelope and the depth of equilibrium suction value interpreted from the analysis may be erroneous, especially if the suction data was measured during a period of prolonged drying (drought) or prolonged wetting. To obtain a more accurate representation of the depth of equilibrium suction interpreted from the Fourier series diffusion equation, suction data for longer time frames should be incorporated. Unfortunately, such data sets of directly measured suction data are very rare.

As such, the author recommends the climate-driven change in soil suction at the ground surface and the long-term equilibrium state of the suction profiles, both magnitude and depth to equilibrium suction, be empirically estimated using models like the Perera et al. (2005) and/or Vann and Houston (2021) which relate soil suction envelope parameters to soil index properties and the Thornthwaite Moisture Index. The use of such models provides additional known boundary and initial conditions of the diffusion equation allowing for the highly variable and difficult-to-measure parameters like the diffusion coefficient and the frequency of cyclic suction variation at the surface to be back-calculated.

2.6.2 Order of the Fourier Series Fit

Generally, the goodness of fit of a Fourier equation to the discrete time series data improves as the order (number of sine and cosine terms) increases. However, for large data sets which do not have significantly different amplitudes throughout, it is generally more efficient to choose the minimum number of terms which represents the key features (large amplitudes, long periods, etc.) of the data to reduce the computation time and the complexity of applying the Fourier series fit to physical modeling.

Figure 2-17 presents the 1st and 8th order Fourier fit to the Vann and Houston (2021) adjusted surface suction for the TX 48-1068. The 1st order fit closely represents the original approach to modeling the surface suction flux by Lytton et al. (2005) using Mitchell's (1979) equation. The adjusted R^2 for the 1st order Fourier fit to the suction data is 0.2903, while the 8th order Fourier fit increases the adjusted R^2 to 0.7056.

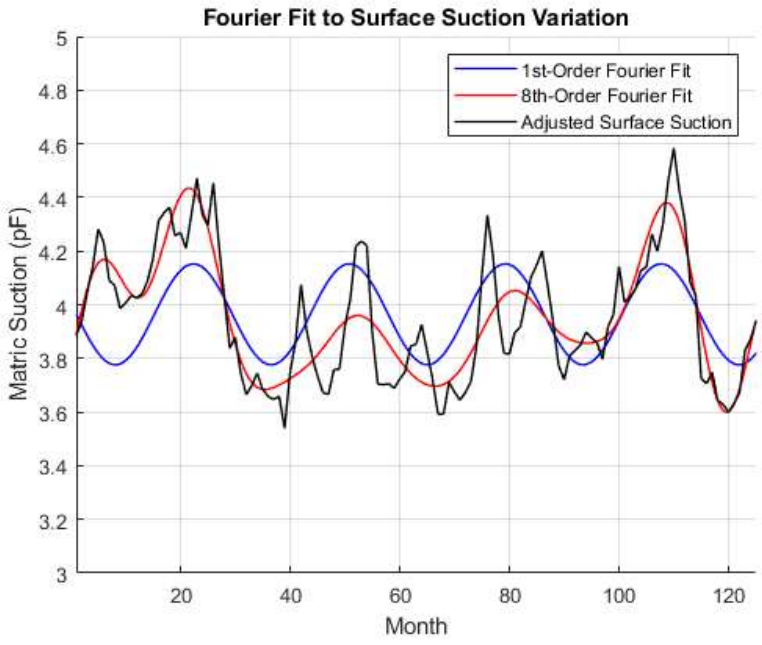

Figure 2-17: 1st and 8th order Fourier fit to the Surface Suction Data for the TX 48-1068 Section for the Date Range 3/1987 to 9/1997

Note that the initial suction is a function of the TMI value for that month. The initial suction (time = 0) can be adjusted using a phase shift of the Fourier equation. Lytton et al. (2005), provided values of phase shifts for different initial conditions of the soil (wet, dry, and equilibrium).

However, there is a significant limitation to applying a fixed order series fit to time series data; depending on the duration of the series and the number of natural frequencies significant amounts of terms may be required to encompass the extreme values (maximum and minimum) of the individual monthly data. For infrastructure build upon or with unsaturated soils, the inclusion of the peak values allows for a more accurate and conservative representation of the soil's response to extreme weather events. As such,

the Fourier series for seasonal suction variation should be adjusted to include the extreme values by one of the following techniques:

- Normalization of the Fourier series between the maximum and minimum values of the seasonal surface suction,
- Inclusion of a phase shift that improves the representation of the extreme values, or
- Improvement of the goodness of fit of the Fourier series at the extreme value data points by increasing the order of the series (i.e., number of terms).

2.7 Natural Order Fourier Series (NOFS) Algorithm

This study presents the application of a Fourier Series approach for modeling monthly climate-driven soil suction profiles. Historically, the order of a Fourier Series was limited by the increased complexity of capturing additional amplitudes which were atypical to the overall data set. To remove this limitation while maintaining computational efficiency, an algorithmic approach was developed, referred to as the Natural-Order Fourier Series (NOFS), which uses a selection criterion defined by the distribution of amplitudes of an infinite-order Fourier fit. The NOFS models the suction profiles using the diffusion equation which exhibits an exponential decay of the amplitudes with depth.

2.7.1 Automating the Fourier Series Order Selection

An algorithmic model for the Natural Order Fourier Series fit of time-varying surface suction data was developed as part of this study to improve the representation

(goodness of fit) of the quantification (equation) of the soil-climate interaction for unsaturated soils (TMI-Suction) while attempting to avoid overfitting of empirical estimated data (compounding errors) and improve computation time (increase efficiency).

A selection process for the NOFS includes the following three statistical evaluations which compared various aspects of the Fourier series fit to the time-varying suction data. After several optimization cycles using the ASU-NSF expansive soil study sites as examples, the following three selection criteria were established.

Note that, the criteria threshold presented herein were based on the evaluations performed in this study and should be taken as recommendations only by the author only. The threshold values may require a site-specific sensitivity study prior to implementation.

2.7.1.1 Natural Order Selection Criterion 1: Mean Absolute Deviation of the Fit

The first check to optimize the order of the Fourier fit to the monthly variation of suction at the ground surface uses the Mean Absolute Deviation (MAD) of the Fourier fit equation to the monthly suction data.

This threshold provides the goodness of fit of the Fourier series equation to the monthly suction data. As expected, the rate of decrease in the MAD initially starts of high as the order of the Fourier series moves away from a periodic-like function ($k < 4$) to more asymmetrical representations. Based on the iterative optimization process performed during this study, it appears that the MAD of the Fourier series fit tends to fall below 0.05 pF once the order of the series has increase past approximately 25% of the maximized fit (i.e., order = ½ total months of data). Furthermore, the order of the Fourier fit associated

with a 0.5 pF MAD threshold value did not govern the selection of the order of the fit for any of the locations explored as part of this study. As such, a MAD threshold value of 0.05 pF is adopted herein.

2.7.1.2 Natural Order Selection Criterion 2: Absolute Error at Initial Point

The first check to optimize the order of the Fourier fit to the monthly variation of suction at the ground surface uses the Absolute Error of the Fourier fit to the suction data at the initial month (t = 0).

Errors associated with the initial point of the equation representing the climate-driven variation in suction are commonly caused by high discrepancies in the initial point (t = 0). Others of sought to correct for this issue using a phase shit of the Fourier series equation. Although this correction process is not difficult to perform, it does introduce additional steps and threshold recommendations into the process. As such, a quick evaluation of the absolute error at t=0 ($AE_{t=0}$) for each order of the Fourier fit is recommended. Similar to the MAD evaluation, the absolute error at t=0 generally tends to decrease with increasing order; however, there is much more sporadic behavior of this comparison compared to the MAD. For the sites explored as part of this study, the $AE_{t=0}$ generally falls below 0.05 pF around 33% of the maximum order of the fit and falls below 0.1 pF around 20% of the overall fit. Based on the iterative optimization effort performed as part of this study, along with the recommendations from Lytton (1997), and acceptable range for establishing equilibrium soil suction in the subsurface is 0.1 pF, although error ranges up

to 0.4 pF have been used. As such, the absolute error of the Fourier fit to the suction data at the initial month (t = 0) is recommended to be less than 0.1 pF.

2.7.1.3 Natural Order Selection Criterion 3: Residual Error

The first check to optimize the order of the Fourier fit to the monthly variation of suction at the ground surface uses the residual error of the Fourier series to the estimated suction at the Extreme Values.

The difference, or residual error at the highest and lowest estimated suction data can be used to improve the representation of extreme climate values for locations associated with unsaturated soils. The residual error at the extreme values was quantified using the conservative direction which forces the Fourier equation fit to capture the extreme values (i.e. the FS fit at the maximum suction should be greater than the estimate suction for that month, and the FS fit at the minimum suction should be less than the suction for the month). This approach reduces the possibility of missing the effects of extreme weather changes in the computation model. Although the desired threshold was zero (i.e. the model either mimics or over predicts the variability in the climate, such results were not reproducible with the same size evaluated as part of this study. Therefore, a threshold value of less than 0.05 pF provides more practical solutions.

2.7.1.4 Example of Automated NOFS Selection Algorithm

The automated algorithm for the NOFS fit to the climate-driven variation in soil suction is explored using Denver ASU-NSF expansive soil study site, which contains data of soil properties with directly measured in situ moisture/suction data An average of

the two uncovered borings DEN-2-U-N and DEN-3-U-N was used to generate this example (Refer to Table 2-6). Thirty years of historical climate data (Figure 2-14) including the monthly average temperate (TAVG) and monthly rainfall (PRCP) were gathered from the nearby NOAA station (USW00023066). The yearly-TMI was calculated on a monthly (running) basis and the previously proposed climate-suction model was used to generate empirical estimates of the time-varying suction at the ground surface (Figure 2-18).

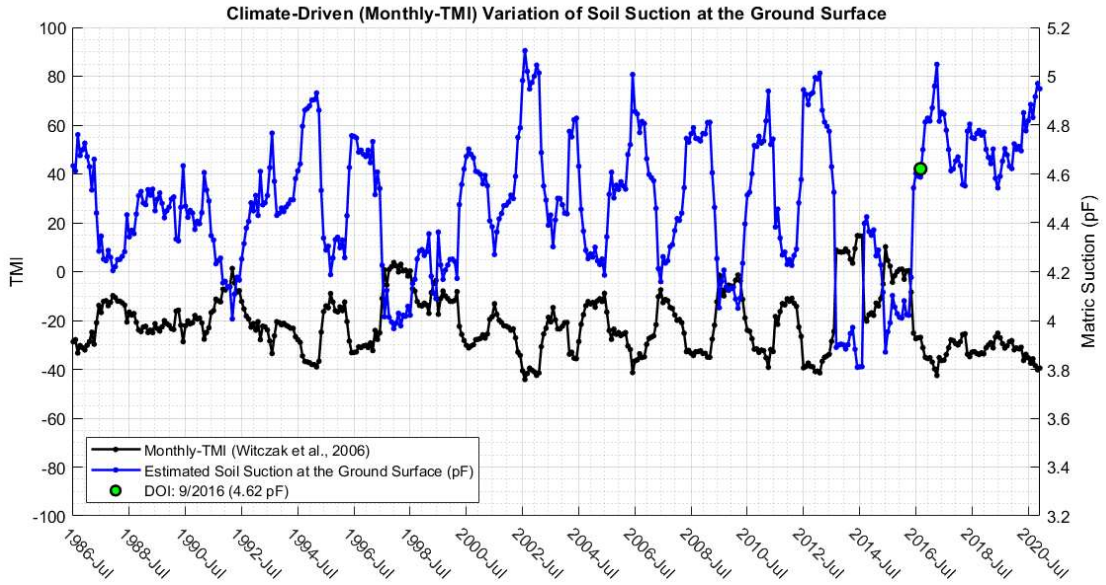

Figure 2-18 Monthly-TMI vs. Variation in Suction at the Ground Surface for the Denver Study Site.

The selection criteria for the NOFS including the following:

- Mean Absolute Deviation (MAD) of the FS fit to the suction data less 0.05 pF.
- Absolute Error at the initial month (t = 0) less than 0.1 pF.

- The residual error at the extreme values less than 0.05 in the conservative direction (i.e. the estimate of the FS fit at the greatest suction value had to be greater than or no less than 0.05 pF and the estimate of the FS fit at the minimum suction had to be less than or no greater than 0.05 pF).

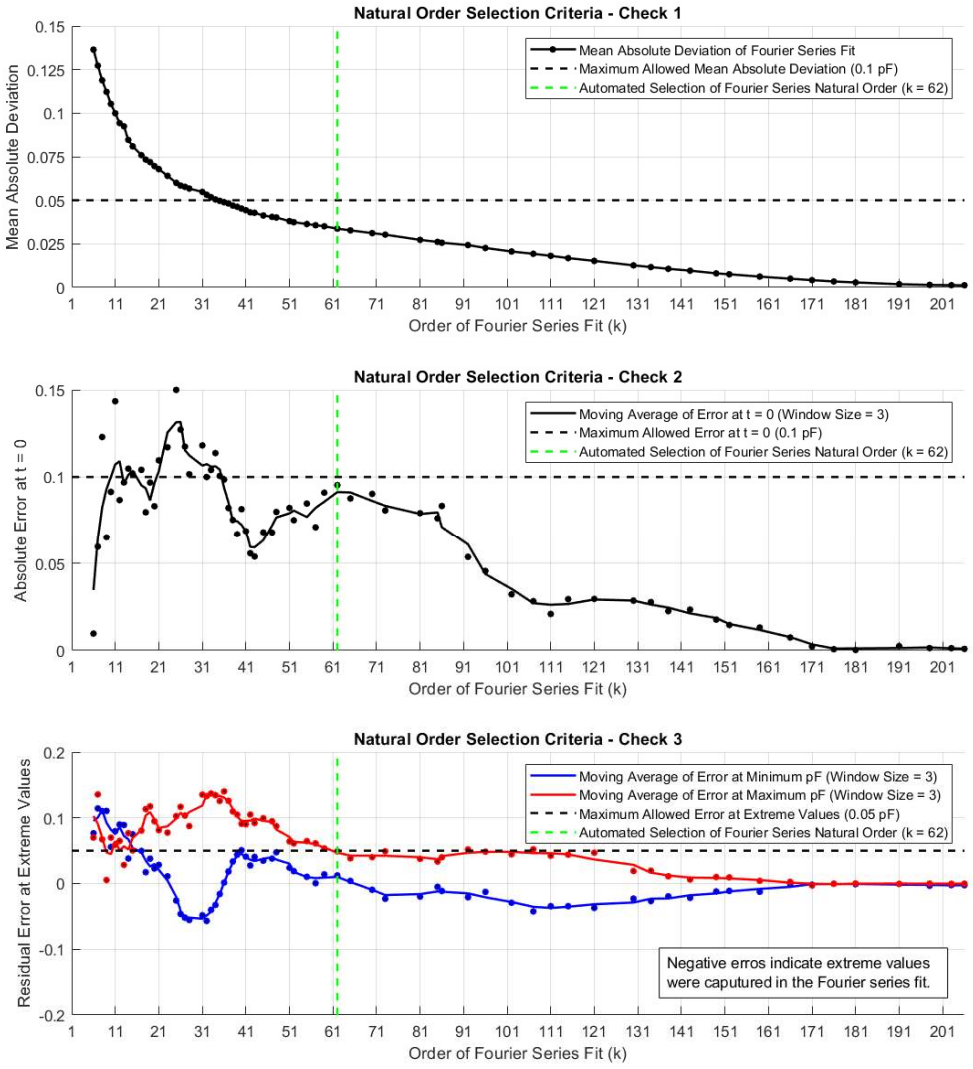

Figure 2-19 Selection Process for NOFS Fit to Climate-Drive Suction Variation at the Ground Surface for the Denver Study Site

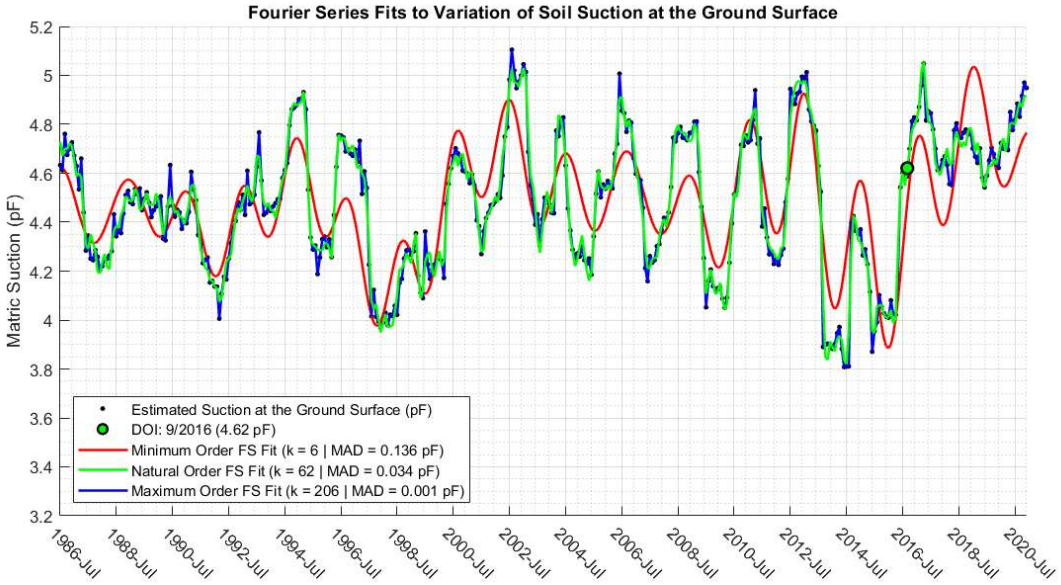

Figure 2-20 Comparison of NOFS Fit to Minimum and Maximum Order Fourier Series Fit to the Variation in Suction at the Ground Surface for the Denver Study Site.

2.8 Validation of the NOFS Suction Profile Approach

Validation efforts were performed using measured suction profile data from the Denver site from the ASU NSF Expansive Soil Study. Applicable information gathered from the four of the studied sites is in summarized in Table 2-5. Note that the 30-year TMI values presented of -20.6 slightly differs from the -24 value tabulated in Vann (2019) due to the use of a different nearby NOAA weather stations and/or different time periods of historical data used. Figure 2-21 presents the measured soil suction data using for the Denver and San Antonio sites which was measured using the WP4-C.

Table 2-11 Relationships Between TMI and Equilibrium Suction for Denver Study Site (adapted from Vann, 2019)

Test Boring ID	TMI (30-Year)	Date Drilled	NOAA Station ID	Measured Depth to Equilibrium Suction (m)	Estimated Depth to Equilibrium Suction * (2021) (m)	Measured Equilibrium Suction (pF)	Estimated Equilibrium Suction (pF)
DEN-2-U-N	-20.6	9/16/16	USW00023067	3.66 (12 ft)	3.51 (11.52 ft)	4.31	4.1
DEN-3-U-N	-20.6	9/16/16	USW00023067	3.66 (12 ft)	3.51 (11.52 ft)	4.31	4.1

* Parameters estimated per Vann and Houston (2021) relationship with the 30-year TMI

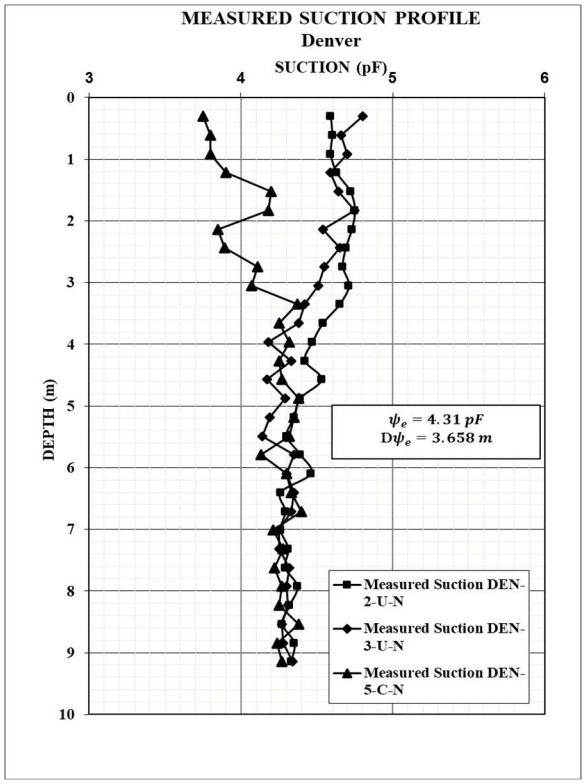

Figure 2-21: Measured Soil Suction Data versus Depth for Three Test Borings in Denver

2.8.1 Denver, CO NOFS Suction Profile Evaluation

The Denver ASU-NSF expansive soil study site with directly measured soil properties within situ moisture/suction data, and quantifications of equilibrium suction

and depth to equilibrium suction. The proposed model for NOFS suction profile estimates were compared to the in situ suction measurements of the two uncovered borings DEN-2-U-N and DEN-3-U-N. The monthly-TMI and estimate the climate-driven change in suction at the ground surface were estimated using thirty years of historical climate data gathered from the NOAA station (USW00023066). Several scenarios using the studied for validation purposes. Figure 2-22 presents the estimated climate-driven suction at the ground surface from 07/1986 to 12/2020 for the Denver study site using the proposed climate-suction relationship.

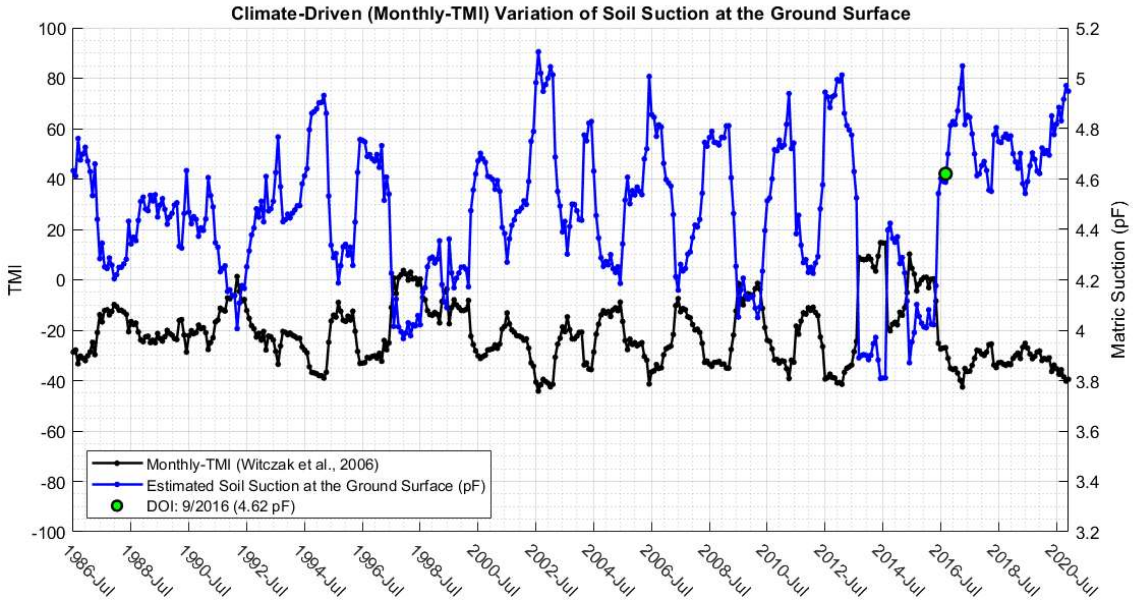

Figure 2-22 Monthly-TMI vs. Variation in Suction at the Ground Surface for the Denver Study Site from 07/1986 to 12/2020

Note the trend in climate data moving from a recent period of high TMI (wetting) from approximately 2013 to 2016, followed by a sharp transition to low TMI (drying) when

the date of interest of 09/2016 (boring drill date) occurs. Figure 2-23 presents the same estimated climate-driven suction at the ground surface with a duration "window" of analysis and three dates of interests (DOI) that will be used in the validation study: the drill date (09/2016), six months after the drill date (03/2017), and 12 months after the drill date (12/2017). The colors of the data points presented on Figure 2-23 and subsequent plots are used to visually link the estimated suction at the ground surface for a given month to the suction profiles for that same month.

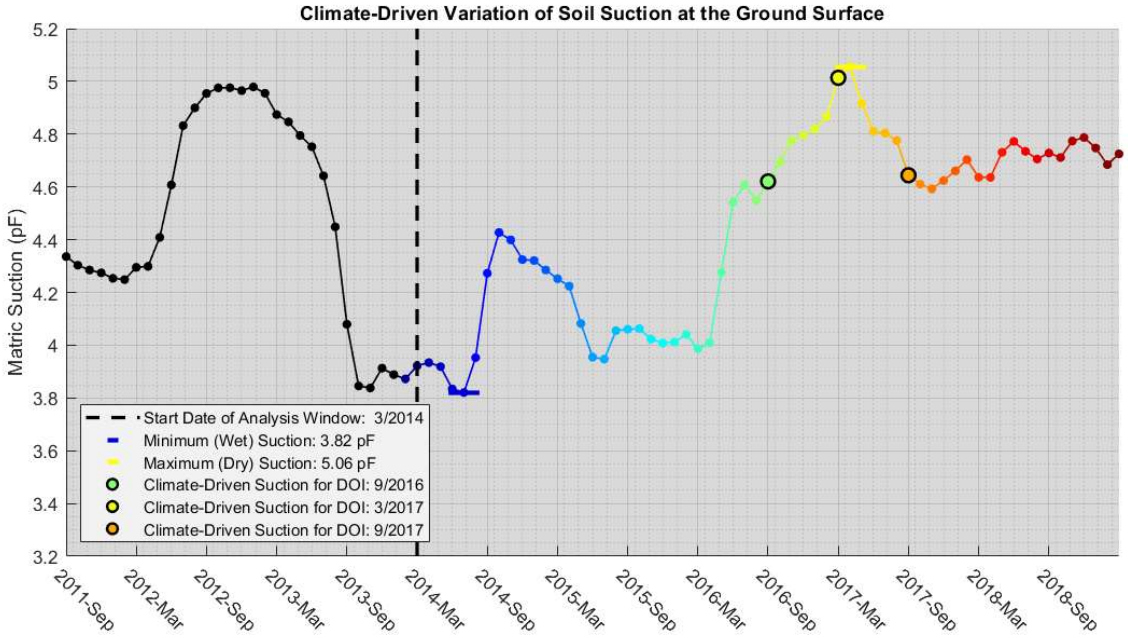

Figure 2-23 Variation in Suction at the Ground Surface for the Denver Study Site from 09/2011 to 03/2019 with Dates of Interests

2.8.1.1 Validation Scenario #2.3:

For the first validation scenario of the Denver study site, the depth of equilibrium suction of 3.66m and the magnitude of equilibrium suction of 4.31 pF of from the Vann (2019) were set as known parameters in the analysis. Figure 2-24 suction profile estimations for Denver study site using the measured magnitude and depth of equilibrium suction from Vann (2019). The two colored backgrounds in Figure 2-24 and subsequent suction profile plots are provided to help distinct the Climate-Driven suction at the surface as a function of time (sky blue background), which is essentially Figure 2-23 rotated 90 degrees clockwise, and the suction profiles as a function of time within the subsurface (tan background). The dates of interests are emphasized on the plots with using heavier line weights; however, each month within the study window can observed via the link in colors. Note that the suction envelope is plotted to a depth twice that of the depth to equilibrium suction value as the shape diffusion profile is based up the variation in the suction envelope (limits) being 0.1 pF off of the equilibrium suction value at twice the depth of equilibrium suction. This approach was based on the recommendations from Vann and Houston (2021) which provides envelopes with approximately 0.2 pF variation in suction at the depth of equilibrium.

Based on a visual evaluation of the suction envelopes for this scenario, it appears that the suction profiles generated by the NOFS diffusion equation method sufficiently model the variation in the climate-driven suction at the ground surface as a function of time. The generated profile adequately encompasses the measured depth of equilibrium value (4.31 pF) at the measured depth of equilibrium (12 ft) with approximately 0.2 pF variation.

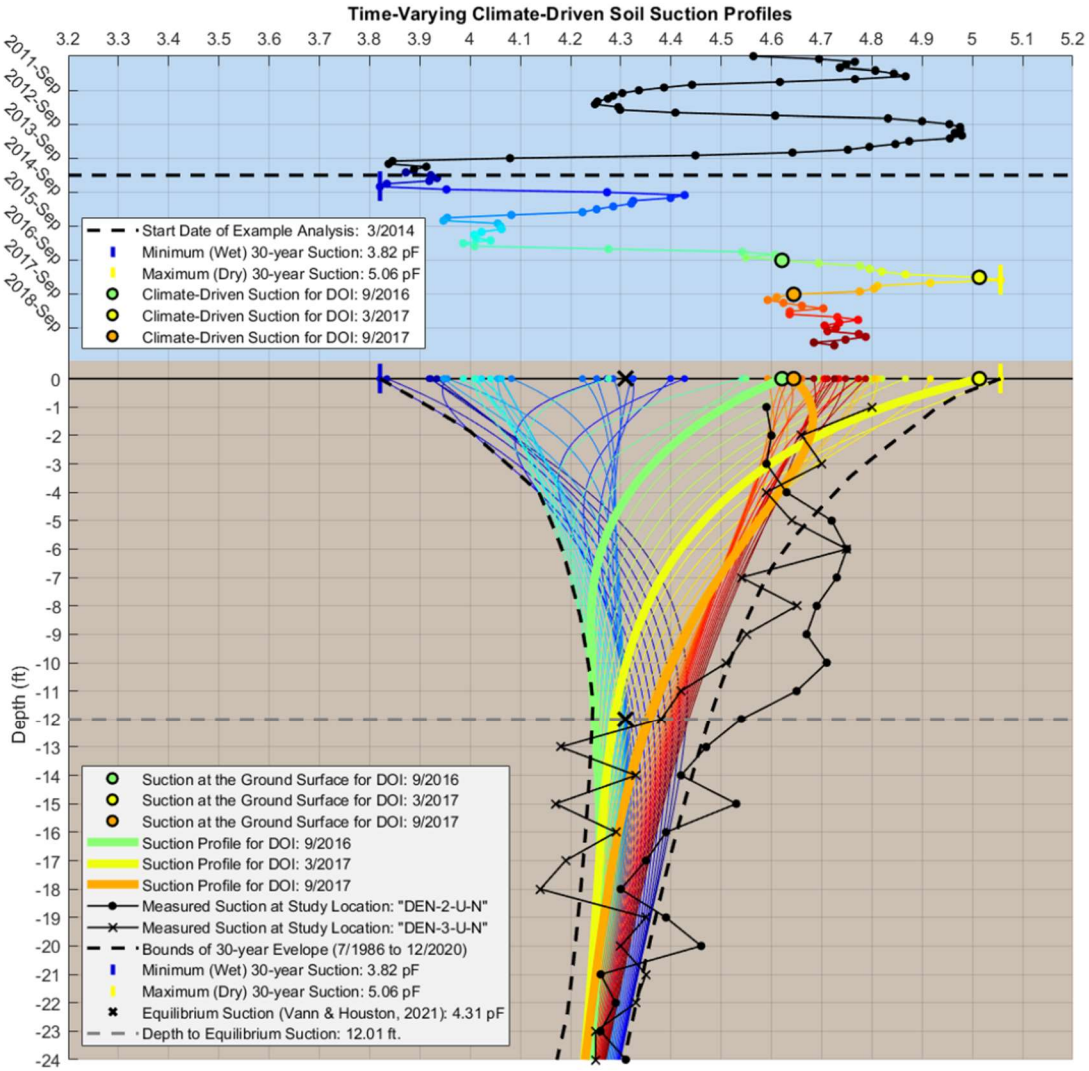

Figure 2-24 Suction Profile Estimations for Denver Study Site Validation Scenario #2.3 - Measured Magnitude and Depth of Equilibrium Suction from Vann (2019)

The relatively wet period at the start of the analysis window from 03/2014 to approximately 03/2016 (colors fading from dark blue to light blue) generates suction profiles near the low suction (wet) side of the envelope. As the drying period begins at approximately 04/2016 (light blue to green), the upper portion of the suction profiles

move towards the high suction (dry) side of the envelope, while the lower portion of the envelope lags on the transition to the dry side. This lag in suction changes within the subsurface is also apparent in the DOI 09/2017 profile which corresponds to a suction at the ground surface near the 30-year maximum value, however due to the quick transition from the wet side for the envelope just 12 months prior, there is significant decreases in the suction values with depth for that month. During the time from approximately 01/2018 to 12/2020 (light red to dark red), the suction variation at the surface is relatively stable for nearly 2 years and the corresponding profiles begin to appear linear with little variation in depth.

Based on Figure 2-24, it also appears that the suction profiles generated by the NOFS diffusion equation approach provide an adequate estimation of the measured suction profiles (DEN-2-U-N and DEN-3-U-N) below the depth of equilibrium suction but portion above the equilibrium suction appears to lag behind the transition to the dry side. The profile for the drill date (DOI: 09/2016), displayed in light green, does not appear to be a good fit; however, the profile for 12 months after the drill date (DOI: 09/2017), displayed in orange, provides a significantly better representation of the measured profiles.

2.8.1.2 Validation Scenario #2.4

The second validation scenario of the Denver study site used the 30-year TMI of the site to develop the long-term suction envelope parameters (Magnitude and depth of equilibrium suction) using the Vann and Houston (2021) relationship with the 30-year

TMI equilibrium suction of 4.31 pF of from the Vann (2019) were set as known parameters in the analysis.

Figure 2-25 presents the suction profile estimations for Denver study site using the estimated magnitude and depth of equilibrium suction from Vann and Houston (2021). Based on a visual evaluation of the suction envelopes for this scenario, it appears that the suction profiles generated by the NOFS diffusion equation method using the estimated magnitude (4.09 pF) and depth (11.5 ft) of equilibrium suction from Vann and Houston (2021) does not adequately encompass the measured depth of equilibrium value (4.31 pF) at the measured depth of equilibrium (12 ft). This error is mostly likely caused by the difference in the estimated equilibrium suction and the measured equilibrium suction of 0.22 pF. The boundary condition assumption used in the NOFS diffusion profile method that the variation in suction at the twice the depth of equilibrium suction (23 ft) must be 0.1 pF rather than 0.2 pF at the depth of equilibrium suction (11.5 ft) prohibits the profile from making drastic transitions when the input magnitude of equilibrium suction varies significantly from the 30-year average of the suction variation at the ground surface (4.44 pF). Although the 30-year average of the suction variation at the ground surface is generally not equivalent to the magnitude of equilibrium suction at depth, they are not typically that more than 0.2 pF different.

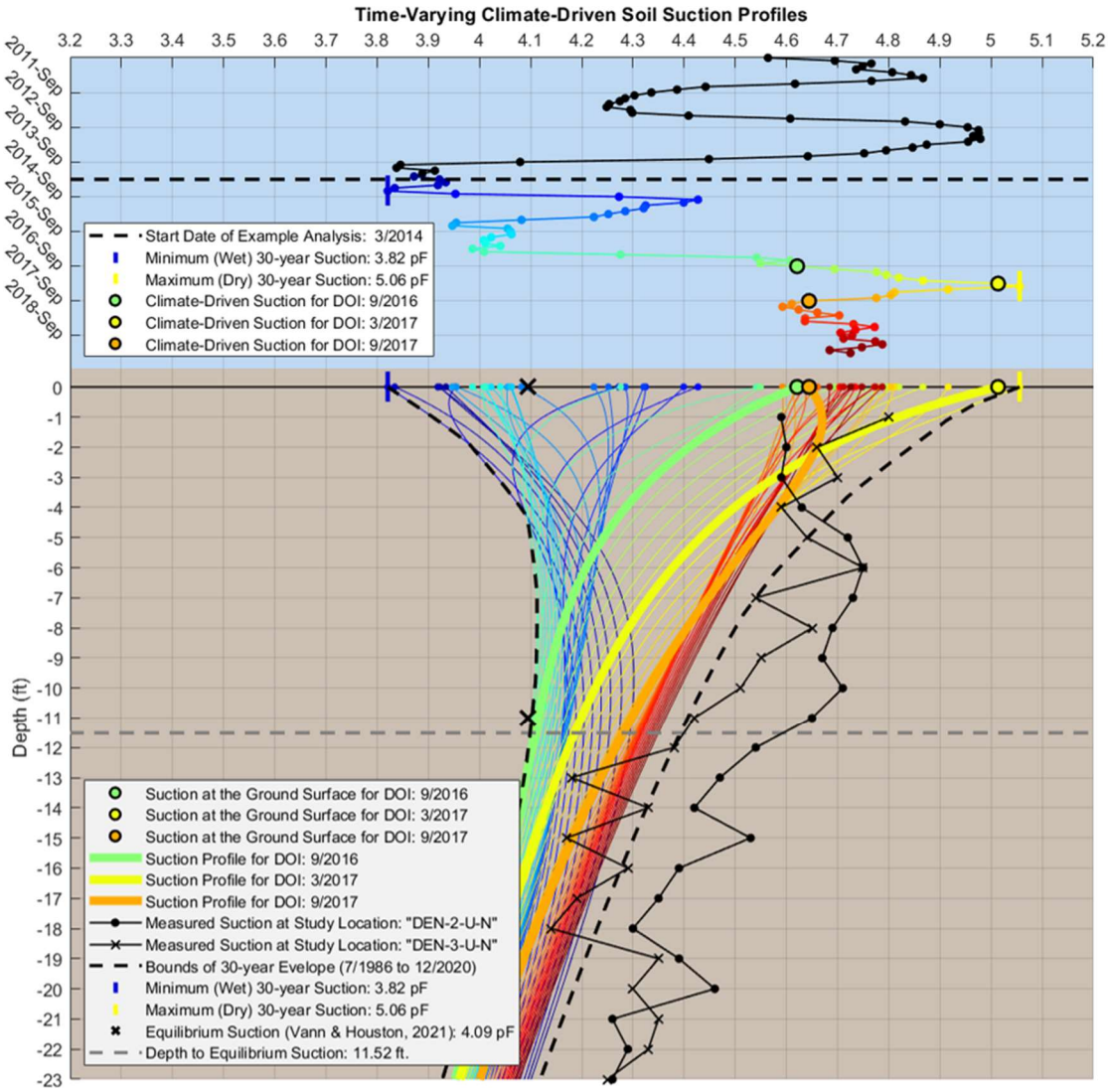

Figure 2-25 Suction Profile Estimations for Denver Study Site for Validation Scenario #2.4 - Empirically Estimated Magnitude and Depth of Equilibrium Suction from Vann and Houston (2021)

2.8.1.3 Validation Scenario #2.5

A third scenario of the compared the proposed model for NOFS suction profile estimates to the in situ suction measurements of the two uncovered borings DEN-2-U-N and DEN-3-U-N. The magnitude of equilibrium suction of 4.31 pF from Vann (2019) was set as a known parameter in the analysis. The depth of equilibrium suction of 3.66m from the Vann (2019) was adjusted to 4.57m (15 feet) to better represent the depth of equilibrium suction of the two uncovered borings only. Figure 2-26 presents the suction profile estimations for Denver study site adjusted depth of equilibrium suction using measured data of uncovered borings.

Based on a visual evaluation of the suction envelopes for this scenario, it appears that the suction profiles generated by the NOFS diffusion equation using the depth of equilibrium form the two uncovered borings improves the over model performance relative to estimating the measured suction profiles. The generated profile adequately encompasses the measured depth of equilibrium value (4.31 pF) at the adjusted depth of equilibrium (15 ft) with approximately 0.2 pF variation. The suction envelope provides nearly completely encompasses the measured suction profiles below the depth of equilibrium suction but portion above the equilibrium suction still appears to lag behind the transition to the dry side.

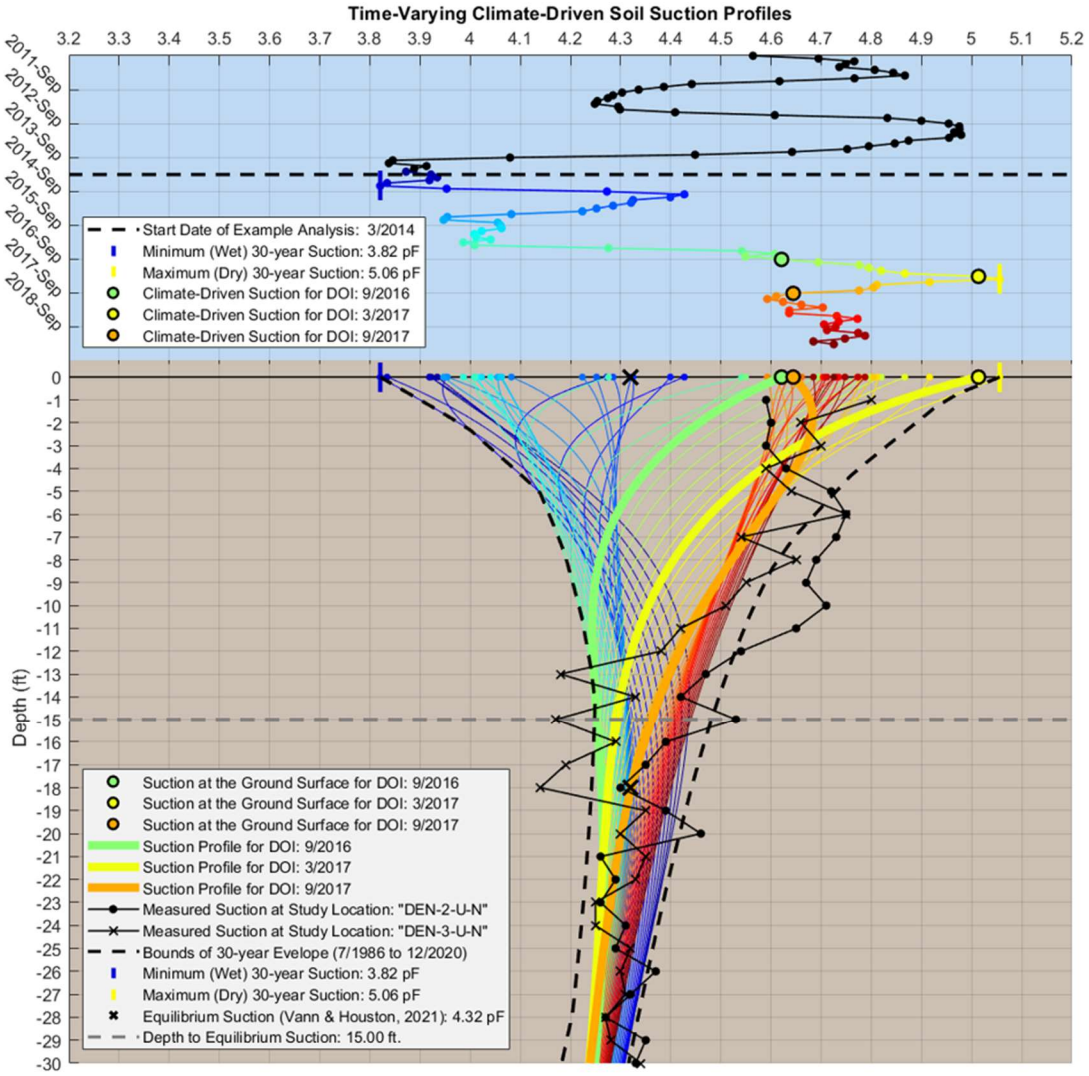

Figure 2-26 Suction Profile Estimations for Denver Study Site for Validation Scenario #2.5 – Adjusted Depth of Equilibrium Suction using Measured Data of Uncovered Borings

2.9 Implementation of NOFS Suction Profiles in Practice

An evaluation of the NOFS suction profile approach is presented using two locations from the ASU-NSF expansive soil study. The automated NOFS approach for

modeling suction envelopes provided significant increases in the goodness of fit of the suction variation at the ground surface, encompassed the extreme values, while minimizing the number Fourier series terms to do so. Significant differences in the goodness of fit between a standard periodic fit and the NOFS are observed as the duration of analysis increased to 30 years.

The suction profiles and 30-year envelopes generated by the NOFS approach sufficiently model the climate-driven variation in suction at the ground surface as a function of depth and time. The validation study using the Denver site indicated that the generated suction profiles lag approximately 12 months behind the measured profiles using directly measured inputs of the magnitude and depth of equilibrium suction. The profiles and envelope generated using the empirically estimated magnitude and depth of equilibrium suction did not compare well with the measured profiles.

The proposed procedure can effectively be implemented in geo-forensic evaluations involving problematic unsaturated soils such as slope instabilities due to moisture driven reductions in shear strength or foundation distress caused by soil volume change. The Natural-Order Fourier Series provides an improved representation of the sporadic changes in soil suction by capturing the extreme climate periods which are generally missed with the standard periodic approach. Direct measurements of the magnitude and depth of equilibrium suction at a given site will help produce the performance of the model to generate profiles of past suction data.

2.9.1 Limitations of the Proposed NOFS Suction Profile Model

Although the findings of this study may indicate that the proposed Natural Order Fourier Series suction profile framework should improve any suction-based vadose-zone transient moisture flow models, one must be aware of the associated assumptions and limitations:

- The empirical models developed by Vann and Houston (2020) used to define the equilibrium suction envelope parameters (equilibrium suction depth and magnitude) were generated using limited data from geotechnical investigation reports by various engineering firms across the United States. Furthermore, all the models which related TMI to soil suction parameters were developed from sites which the elevation of the groundwater table did not affect the moisture state within the typical depth from ground surface associated with the unsaturated soil "active zone", which is generally 5 to 20 feet. As such, the proposed model should not be used to evaluate locations which have shallow groundwater.
- The term covered is used herein when referring to pavement structures although there is still a two-dimensional lateral moisture flow movement which is not accounted for in the NOFS model. This lateral movement would be directly affected by the width of the roadway and distance/location of interest which is being analyzed (e.g. pavement edge, wheel paths, centerline).
- The Perera (2005) model which relates long-term TMI values to soil suction under pavements was produced under the assumption that the soil suction measured below the pavement at the time of the field sampling corresponded to

the equilibrium state of moisture reached sometime after construction of the roadway.

- The error of the regression fit of the empirical models were not included in this deterministic approach for modeling monthly changes in the soil suction profiles.
- The validation studies of the NOFS model presented herein indicate that there is a time-lag effect which has yet to be accounted for, although the inclusion of additional validation sites may provide contrasting observations.

CHAPTER 3

3 BAYESIAN CHARACTERIZATION OF COMMON SOIL PROPERTIES

3.1 Introduction

Geotechnical engineering analyses and designs commonly require knowledge parameters other than just soil/rock properties such as structural loads, traffic volumes, climate data, and manufactured material specifications (e.g., concrete, rebar, geosynthetics, etc.). For new designs, each of these parameters has an associated degree of uncertainty, with manufactured materials generally having minimal uncertainty and future climate data having the highest uncertainty. Such climatic inputs which are often required in geotechnical modeling can include temperature, rainfall, humidity, runoff, and solar radiation.

Historically engineers have adopted a conservative estimate of a design parameter in a deterministic approach to account for uncertainty. To better represent the performance of a design, probabilistic/stochastic approaches can be applied which include consideration of parameter uncertainties (Phoon & Kulhawy, 1999; Fenton & Griffiths 2008). There has been tremendous advancement in the application of stochastic modeling to civil engineering in the recent decades. Couple this momentum in statistical modeling with the continued advances in parameter measurement technologies, and all the ingredients are present for engineers to develop powerful and reliable tools to simulate complex geological models. Such accomplishments in this field include, but are not limited to, the use of Bayesian inference to characterize soil uncertainty (Medina-Cetina and

Esmailzadeh, 2014; Gong et al. 2021; Zhang et al. 2022) and the implementation of advanced Markov models to simulate gaps in hydrological data (Zheng & Ham, 2015; Vrugt 2016).

Randomization of the soil properties is required for the stochastic Monte Carlo volume change analyses. Random variables are generated from probability distributions. Beta distributions were generated for the required soil inputs for each hierarchal level of analysis: plasticity index (*PI*), liquid limit (*LL*), percent fines/percent passing the No. 200 sieve ($P_{\#200}$), and percent $_{clay}$/percent fine than 2 microns (P_{clay}), in situ moisture content (w), and dry unit weight (γ_d). The LTPP soil database (FHWA) and the NCHRP 9-23 (2006) soil databases were used to develop the statistical parameters for new subsets of soil types for the shrink-swell analysis.

The U.S. Department of Agriculture (USDA) Natural Resources Conservation Service (NRCS) Soil Survey Laboratory (SSL) soil database was used to explore correlations and relationships between required input soil index properties: *PI*, *LL*, $P_{\#200}$, and P_{clay}. Due to significant correlation between the input soil index properties, an algorithmic approach was developed to randomly generate each property.

General laboratory investigations for a given project provide average values of geotechnical properties which are used as input into a deterministic solution in which only a mean value is produced. To obtain a stochastic answer, the dimensionless coefficient of variation (*CV*) is used to characterize the randomness and uncertainty in the measured properties. The coefficient of variation is generated through replicates of the

test results which can require either more time and money for sampling/testing, or historical project data variance. If the coefficients of variation for the required soil properties of a project are known, sampling/testing can be reduced while increasing or maintaining the same level of confidence in the analyses and designs (provided the engineering team is experienced in statistical/stochastic analyses). As such, the coefficients of variation for the soil properties are used as key soil inputs for the stochastic volume change analyses.

This chapter introduces an updated approach to stochastically model the variability of the required soil properties. A database of the necessary soil input variables will be collected and used to generate updated statistical parameters for each variable. A Bayesian framework for randomly generating sets of each variable while accounting for high correlation between soil properties will be developed.

3.1.1 Objectives

The following objectives were accomplished as part of this study:

- Review of the existing hierarchical levels of the descriptive statistics for the soil properties using the EICM and MEPDG.
- Evaluation of the applicability of the existing models for use in the stochastic volume change models (shrink-swell).
- Adjustment of the datasets used for the hierarchical levels of the descriptive statistics to better represent the common soil types susceptible to shrink-swell potential.

- Exploration of issues pertaining to correlation and fixed ranges of soil properties which arise during the random generation of input values required for stochastic modeling.
- Development of an algorithmic process to produce random combinations of the required soil inputs within the natural ranges and correlations.
- Validation of the algorithmic approach to produce natural combinations of randomized soil properties for input into the stochastic model.

3.2 Relevant Background

A Review of statistical theory with a focus on probability distributions, correlation, stochastic analyses. The literature review also includes the existing stochastic analyses implemented in the MEPDG and explores the recent advancements in probabilistic modeling in geotechnical engineering. The overall goal of the literature review is to understand the current state of practice, explore recent research breakthroughs, and optimize the technical approach required to meet the research objectives.

3.2.1 Review of General Statistical Theory

The statistical moments, and statistical distributions used in this study are summarized herein. The descriptions of the statistical moments, hypothesis testing, and statistical distributions are referenced from Fenton and Griffiths (2008), Montgomery et al. (2009, 2011), and Benjamin and Cornell (2014).

The notation used for the mean, standard deviation, and variance depends on the sample size and how representative that sample is to the true population. In this study:

- the sample mean ($\bar{x}$) is assumed to represent the population mean (μ);
- the sample standard deviation (s) is assumed to represent the population standard deviation (σ);
- and the sample variance (s^2) is assumed to represent the population variance (σ^2);
- therefore, the notation representing the population adopted for simplicity.

Furthermore, subscripts can be added to each of the variables to further denote what population the variable is representing.

There are four statistical moments that are used to describe any distribution: mean, variance, skewness, and kurtosis. The mean and variance are heavily utilized in stochastic analyses and are defined herein. are parameters used to further define the shape of the distribution. The standard deviation and the coefficient of variation (CV) are also defined.

The first statistical moment is referred to as the expected value ($E[X]$), or the mean value (μ).

$$E[X] = \mu = \left(\frac{1}{n}\right)\sum_{i=1}^{n} x_i \tag{61}$$

Where: n = Number of point estimations and x_i = The ith observation of the random variable (x).

The second statistical moment is used to describe the scatter or dispersion in the data and is referred to as the variance ($E\left[X^2\right]$ or σ^2).

$$E\left[X^2\right]=\sigma^2=\left(\frac{1}{n}\right)\sum_{i=1}^{n}\left(x_i-\mu\right)^2 \tag{62}$$

The standard deviation (σ) is defined by the positive square root of the variance and is in the same units as the random variable.

$$\sigma=\sqrt{\sigma^2} \tag{63}$$

The standard deviation can be used to define a range of data within a distribution. For example, Figure 3-1, depicts the percentage of a normal distribution represented by number of standard deviations from the mean.

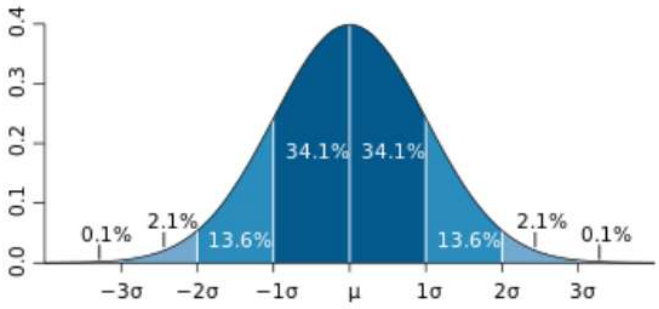

Figure 3-1. Percentage of Normal Distribution Represented by Number of Standard Deviations from the Mean.

In a normal distribution, 66.6% (2/3) of the data is represented by 1 standard deviation away from the mean (-1σ to $+1\sigma$); and 95% of the data is represented by 2 standard deviations away from the mean (-2σ to $+2\sigma$). Six standard deviations (6σ) is often

referred to as the width of the normal distribution due 99.73% of the data being represented by 3 standard deviations away from the mean (-3σ to $+3\sigma$).

The coefficient of variation (CV) is defined by the ratio of the mean to the standard deviation.

$$CV = \frac{\sigma}{\mu} \tag{64}$$

The third and fourth statistical moment are referred to as skewness and kurtosis. The skewness represents how the mean of the distribution differs from a theoretical mean representing a normal distribution. The kurtosis helps define how much data is dispersed around the mean. The skewness and kurtosis are expressed in the following equations, respectively.

$$E\left[X^3\right] = \left(\frac{1}{n}\right)\sum_{i=1}^{n}\left(\frac{x_i - \overline{x}}{\sigma}\right)^3 \tag{65}$$

$$E\left[X^4\right] = \left(\left(\frac{1}{n}\right)\sum_{i=1}^{n}\left(\frac{x_i - \overline{x}}{\sigma}\right)^4\right) - 3.0 \tag{66}$$

Continuous random numbers are most often represented using a normal distribution. The normal distribution, or the “Gaussian” distribution, follows a bell curve that is centered about the mean. The variance describes how dispersed or tight the tails of the distribution are from the mean. The probability density function (PDF) represents the shape of probability distributions. The PDF of the normal distribution is expressed as:

$$f(x) = \frac{1}{\sqrt{2\pi\sigma^2}} e^{-\frac{(x-\mu)^2}{2\sigma^2}} \quad \text{for} \quad -\infty < x < \infty \tag{67}$$

The normal distribution is not bound between any values (i.e. the left tail of the distribution will approach negative infinity and the right tail of the distribution will approach positive infinity). As such, issues can arise when generating random numbers for data sets which represent percentages or index values that must be greater than 1 because there is a possibility of producing negative values. This scenario is applicable to the required soil index properties of PI, LL, p200, and pClay as each parameter is a percentage greater than 0%. The PI and LL parameters do not have an upper bound value but p200 and pClay cannot be greater than 100%. Furthermore, PI is computed from LL and pClay is a fraction of p200 (i.e. must be less than), resulting in high correlation between the parameters, which is discussed further herein. Albeit these limitations for application in stochastic analyses with natural soil properties, the normal distribution is still used as effective tool for preliminary screening of normality for input variable and residuals of regression fits.

For scenarios where the data may be normally distributed but must be greater than zero, a lognormal distribution can effectively represent the data. If a continuous distribution is flexible and bounded on each end with a minimum and maximum value, the Beta distribution can be useful. The basic form of the Beta distribution is defined on an interval [0,1] with two shape factors, denoted as alpha (α) and beta (β), which will be referred to as the "Two-Parameter Beta Distribution" for clarity.

$$f\left(x;\alpha,\beta\right)=\frac{1}{B\left(\alpha,\beta\right)}x^{\alpha-1}\left(1-x\right)^{\beta-1}\ for\quad 0\le x\le 1\quad \&\quad \alpha,\beta>0 \tag{68}$$

Where:

$$B\left(\alpha,\beta\right)=\frac{\Gamma\left(\alpha\right)\Gamma\left(\beta\right)}{\Gamma\left(\alpha+\beta\right)} \tag{69}$$

and Γ = the Gamma function expressed as,

$$\Gamma\left(n\right)=\left(n-1\right)! \tag{70}$$

For "Two-Parameter Beta Distribution" with random variable (x), the mean and variance are expressed in terms of the shape factors alpha and beta:

$$\mu_x=\frac{\alpha}{\alpha+\beta} \tag{71}$$

$$\sigma_x^{\,2}=\frac{\alpha\beta}{\left(\alpha+\beta\right)^2\left(\alpha+\beta+1\right)} \tag{72}$$

The ability of the Beta distribution to take on many shapes while staying within the defined limits makes it ideal for practical applications. If both shape parameters are greater than one ($\alpha > 1$ & $\beta > 1$), the distribution will be bell-shaped, with the skewness to the right if alpha is less beta ($\alpha < \beta$) or to the left if alpha is greater than beta ($\alpha > \beta$), and with the *mode* representing the peak of the density expressed as:

$$mode=\frac{\alpha-1}{\alpha+\beta-2}\quad for\quad \alpha,\beta>1 \tag{73}$$

Beta distributions meeting this criterion with a left-sided skewness can resemble a lognormal, Gamma, Weibull, or Rayleigh distributions. If alpha is less than one, and beta is greater than one ($\alpha < 1$ & $\beta > 1$), the distribution will be "J-shaped" with the *mode* = 0 and the tail heading towards one. Contrary, if alpha is greater than one, and beta is less than one ($\alpha > 1$ & $\beta < 1$), the distribution will be "J-shaped" with the *mode* = 1 and the tail heading towards zero. Beta distributions that are "J-shaped" with *mode* = 0 resemble an Exponential distribution. However, recall that the Beta distributions are bounded by the specified minimum and maximum values, and the shapes can be flipped if needed the data requires it to be so. An example of this is depicted Figure 3-2 with the shape of the distribution with $\alpha = 1$ and $\beta = 3$ appearing similar the shape of an Exponential distribution, and the shape of the distribution with $\alpha = 5$ and $\beta = 1$ being very similar but in the opposite direction.

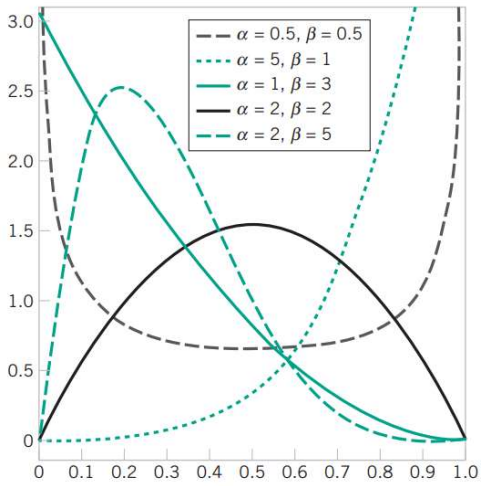

Figure 3-2. Example of Beta Distributions Between [0,1] with Varying Shape Factors Alpha (α) and Beta (β) (Montgomery et al., 2011)

The shapes that mimic the listed distributions (and the reverse of) are ideal for representing distributions of soil properties. However, the Beta distribution can also take on shapes that may not represent the natural characteristics of most geological conditions which are defined within a reasonable limit (i.e. site-specific data, data grouped by general soil type, etc.). An example of an unnatural shaped distribution, with respect to this application of this study, is depicted in Figure 3-2 by the "U-shaped" distribution with α = 0.5 and β = 0.5. The distribution starts to become "U-shaped" if alpha is less than one and beta is less than alpha ($\alpha < 1$ & $\beta < \alpha$).

As the values of the shape parameters increase, the kurtosis increases, and the distribution becomes more leptokurtic (i.e. the distribution becomes thinner and concentrates around the mode.

The Beta distribution can also be defined between defined within a range of minimum (a) and maximum (b) values, commonly referred to as the "Four Parameter Beta Distribution". In this case, the two shape factors can be expressed in terms of the mean, standard deviation, minimum and maximum values (μ, σ, a, b). The shape factors, denoted as alpha (α) and beta (β), must be greater than 0. The beta distribution pdf is expressed by:

$$f\left(y;\alpha,\beta,a,b\right)=\frac{1}{B\left(\alpha,\beta\right)}\left(\frac{y-a}{b-a}\right)^{\alpha-1}\left(\frac{y-x}{b-a}\right)^{\beta-1} \quad for \quad a\le y\le b \qquad (74)$$

A simple linear relationship exists between a random variable (X) calculated with a Beta distribution within the range [0,1] and a random variable (Y) calculated using the "Four Parameter Beta Distribution" over the range [a,b].

$$Y = a + X\left(b - a\right) \tag{75}$$

This linear relationship can be used to shift the mean and variance values between distributions with parameter space. For Beta Distributions of random variable (y) defined within the range [a,b], the mean and variance are expressed in terms of the shape factors alpha and beta:

$$\mu_y = a + \mu_x\left(b - a\right) = a + \frac{\alpha}{\alpha + \beta}\left(b - a\right) \tag{76}$$

$$\sigma_y{}^2 = \left(b - a\right)^2 \sigma_x{}^2 = \left(b - a\right)^2 \frac{\alpha\beta}{\left(\alpha + \beta\right)^2\left(\alpha + \beta + 1\right)} \tag{77}$$

The alpha shape parameter can be expressed as,

$$\alpha = \left(\frac{\mu - a}{b - a}\right)\left(\frac{\left(\frac{\mu - a}{b - a}\right)\left(1 - \left(\frac{\mu - a}{b - a}\right)\right)}{\frac{\sigma^2}{\left(b - a\right)^2}} - 1\right) \tag{78}$$

or in terms of CV as:

$$\alpha = \left(\frac{\mu - a}{b - a}\right)\left(\frac{\left(\frac{\mu - a}{b - a}\right)\left(1 - \left(\frac{\mu - a}{b - a}\right)\right)}{\frac{\left(CV\,\mu\right)^2}{\left(b - a\right)^2}} - 1\right) \tag{79}$$

and the beta shape parameters can be expressed as:

$$\beta = \left(1 - \frac{\mu - a}{b - a}\right)\left(\frac{\left(\frac{\mu - a}{b - a}\right)\left(1 - \left(\frac{\mu - a}{b - a}\right)\right)}{\frac{\sigma^2}{\left(b - a\right)^2}} - 1\right) \tag{80}$$

or in terms of CV as:

$$\beta = \left(1 - \frac{\mu - a}{b - a}\right)\left(\frac{\left(\frac{\mu - a}{b - a}\right)\left(1 - \left(\frac{\mu - a}{b - a}\right)\right)}{\frac{\left(CV\,\mu\right)^2}{\left(b - a\right)^2}} - 1\right) \tag{81}$$

Multivariate distributions can be used to represent parameters that are influenced by one another or jointly influenced by separate factor. In the simplest cast, a continues multivariate distribution of two random variables x and y is referred to a bivariate distribution and can be generally represented by $f_{xy}\left(x, y\right)$.

The influence of parameters on one another is other is referred to as covariance and can be expressed as:

$$Cov\left[x, y\right] = E\left[\left(x - \mu_x\right)\left(y - \mu_y\right)\right] \tag{82}$$

The covariance depends on the units and variability between two random variables. To obtain information about the strength and direction of a linear relationship, the normalized and nondimensional Pearson correlation coefficient (ρ_{xy}) can be used, which is expressed as:

$$\rho_{xy} = \frac{Cov[x, y]}{\sigma_x \sigma_y} \tag{83}$$

The correlation coefficient can range in value from −1 to +1. The sign of the coefficient indicates the direction of the correlation. If both variables tend to increase or decrease together, the coefficient is positive. If one variable tends to increase as the other decreases, the coefficient is negative. The larger the absolute value of the coefficient, the stronger the relationship between the variables. A correlation close to 0 indicates no correlation between the parameters. However, a correlation coefficient near zero does not always mean that no relationship exists between the variables; the variables may have a nonlinear relationship.

The correlation coefficient is also used to express multivariate distributions. Normal distributions are commonly used to represent multivariate because they need only the mean and variance of each parameter to be defined. A continues multivariate normal distribution of two random variables x and y can be expressed as:

$$f_{x,y}(x, y) = \frac{1}{2\pi\sigma_x\sigma_y\sqrt{1-\rho^2}} e^{\left\{\frac{-1}{2(1-\rho^2)}\left[\left(\frac{x-\mu_x}{\sigma_x}\right)^2 - 2\rho\frac{(x-\mu_x)(y-\mu_y)}{\sigma_x\sigma_y} + \left(\frac{y-\mu_y}{\sigma_y}\right)^2\right]\right\}} \tag{84}$$

Probability density functions of bivariate distributions can represented in a three-dimensional space as depicted in Figure 3-3 or in a two-dimensional space as depicted in Figure 3-4, which help visualize the effect of the correlation coefficient on the shape of the joint distribution.

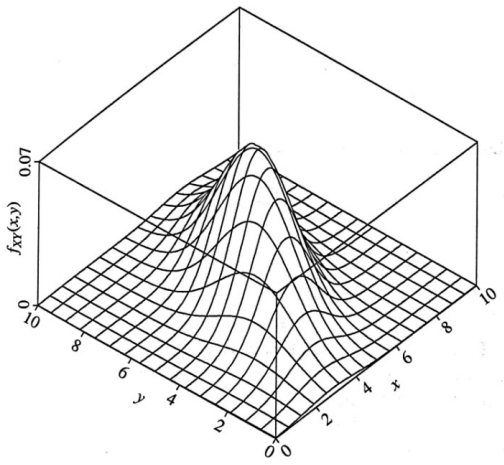

Figure 3-3. Example of Bivariate Normal Probability Density Function (Fenton and Griffiths, 2008)

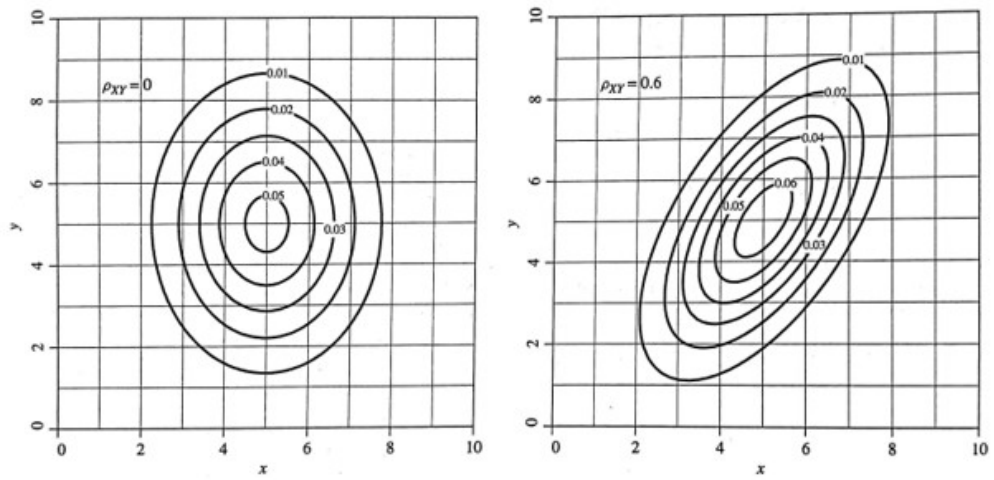

Figure 3-4. Example Bivariate Probability Density Functions with $\mu_x = \mu_y = 5$, $\sigma_x = \sigma_y$ =1.5 and Correlation Coefficients (ρ_{xy}) Equal to (a) Zero and (b) 0.6 (Fenton and Griffiths, 2008)

3.2.2 Review of Uncertainties in Geotechnical Engineering

There are two types of uncertainties that can affect the accuracy of a geotechnical analysis, i.e., (a) the uncertainty in model input parameters due to the presence of test errors, insufficient number of tests and the inherent variability of soil properties and (b) the uncertainty associated with the geotechnical model due to the inability of the model to fully represent the actual geotechnical system. Figure 3-5 present a flow chart with the different aspects of uncertainty in soil property estimates. To explicitly consider the uncertainties and to control the risk in a geotechnical design, probabilistic methods have been widely studied in the past decades. In a rigorous probabilistic analysis, both the uncertainty in model input parameters and the model uncertainty should be considered. Extensive research has been conducted on how to assess the uncertainty in model input

parameters. In general, the uncertainty in model input parameters can be assessed using such methods as geotechnical testing, engineering judgment or a combination of them.

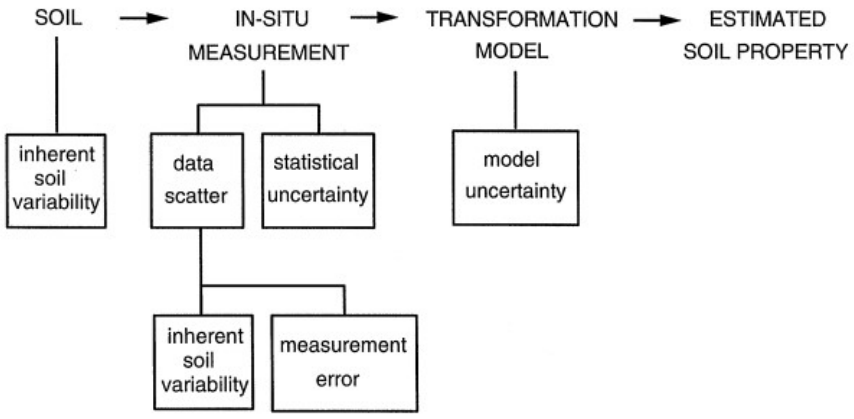

Figure 3-5. Uncertainty in Soil Property Estimates (Kulhawy, 1992)

To consider all such uncertainties systematically, the model uncertainty of a geotechnical model may be characterized using a Bayesian method. In this method, a model uncertainty factor is used to denote the magnitude of the model uncertainty, and the statistics of the model uncertainty factor are modelled as random variables. In addition, uncertain model input parameters and uncertain system performance of different geotechnical systems can also be modeled as random variables. The distributions of these uncertain variables can then be updated simultaneously with the observed system performance data using stochastic techniques such as Monte Carlo simulations.

3.2.3 Review of Bayesian Inference

Bayesian statistics is an approach to applying probability to engineering and statistical problems. It can provide mathematical tools to update how outcomes based on about random events are inferred, with or without the inclusion of new data or evidence about those events. Bayesian statistics can produce realizations, insightful estimates of models which include the variability of parameters and quantify uncertainty of the estimates without being limited by the strict rules of conventional statistics, referred to as Frequentist statistics. Table 3-1 provides a brief comparison of Bayesian vs. Frequentist statistics.

Table 3-1: Comparison of Bayesian vs. Frequentist Statistics (adopted from Amrhein et al., 2019)

	Bayesian Statistics	Frequentist Statistics
Data	Fixed - Non-random	Uncertain – Random
Parameters	Uncertain - Random	Fixed – Non-random
Inference	Uncertainty over parameter values	Uncertainty over a sampling procedure from an infinite population
Probability	Subjective	Objective (but with strong model assumptions)
Uncertainty	Credible Interval	Confidence Interval

From a Bayesian perspective, such a process can be considered as a process of updating the prior knowledge using site observation data for a given project site, as shown in Figure 3-6.

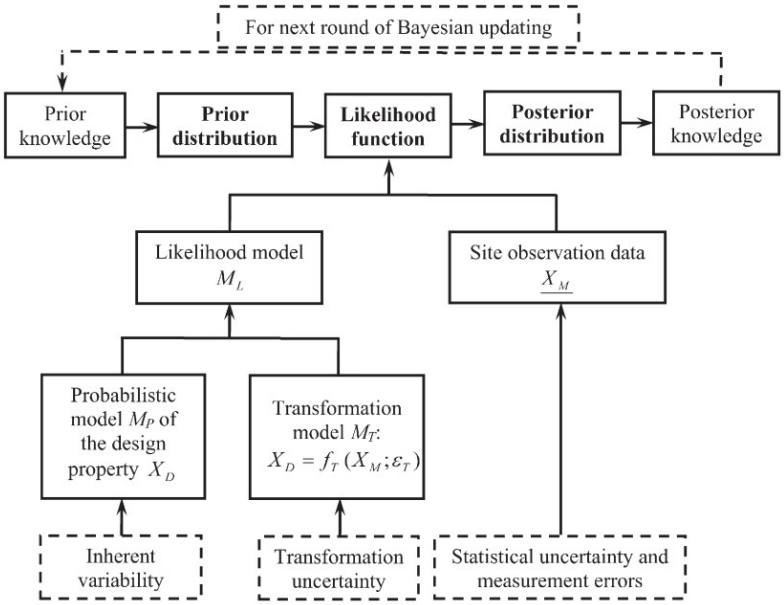

Figure 3-6: Generalized Bayesian Framework for Geotechnical Characterization (Wang, 2016)

The notation and nomenclature used by Gelman et al. (2014) is adopted throughout this document when referring to variables or expressions pertaining to Bayesian Inference. The core rule which governs Bayesian Inference is referred to as Baye's Rule and represents the probability of unobserved (posterior) data (θ) as the conditional joint probability distribution of θ and observed (prior) data (y):

$$p(\theta \mid y) = \frac{p(\theta, y)}{p(y)} = \frac{p(\theta)\, p(y \mid \theta)}{p(y)} \tag{85}$$

Where $p(y)$ and $p(\theta)$ is the marginal probability distributions of the observed and unobserved data and $p(y \mid \theta)$ is the conditional probability distribution of θ given y, also referred to as the likelihood function. In Bayesian Inference, the likelihood principle

states that probability model with the same likelihood function will result in similar inferences of θ for a given sample of data.

Bayesian methods provide useful tools for representing unobserved, or yet to be observed, data based on available data, which typically does not represent the full population of the data set. Probability functions of the prior data can be assigned using empirical data or implied based on plausible assumptions. Typically, the posterior distribution is of most interest, and is generated through a simulation of randomized draws and an acceptance criterion.

3.3 Existing Hierarchical Soil Property Statistics used in MEPDG

The approach for selecting or determining material inputs in the Pavement ME Design is a hierarchical (level) system. The hierarchical input concept or approach provides the designer engineer flexibility in obtaining the inputs for a project based on the criticality of the project, available resources, and knowledge of the input parameters. With regards to soil related properties, the Mechanistic-Empirical Pavement Design Guide (MEPDG) currently allows the engineer to design pavement cross-sections using the different hierarchical levels analyses for the unbound and subgrade material properties including resilient modulus, classification/volumetric properties, soil-water characteristic relationships, and the saturated hydraulic conductivity. The material properties are estimated by the Enhanced Integrated Climatic Model (EICM) within the program which calculates the resilient modulus at equilibrium for a given hierarchical level using various

models. Per MEPDG Manual of Practice (NCHRP, 2006; AASHTO 2008), the hierarchical level input is currently defined as:

- **Level 1** - —Input parameter is measured directly; it is site- or project-specific. This level represents the greatest knowledge about the input parameter for a specific project but has the highest testing and data collection costs to determine the input value. Level 1 should be used for pavement designs having unusual site features, materials, or traffic conditions that are outside the inference space used to develop the correlations and defaults included for input Levels 2 and 3.
- **Level 2** - Input parameter is estimated from correlations or regression equations. In other words, the input value is calculated from other site-specific data or parameters that are less costly to measure. Input Level 2 may also represent measured regional values that are not project specific. and
- **Level 3** – Input parameter is estimated from correlations or regression equations. In other words, the input value is calculated from other site-specific data or parameters that are less costly to measure. Input Level 2 may also represent measured regional values that are not project specific.

The variances of the hierarchical levels will generally increase as the hierarchical level increases from Level 1 to Level 2 to Level 3, provided that the site-specific variance of the parameters (Level 1) is not greater than the assumed variance from not-site-specific historical data (Levels 2 and 3).

The MEPDG incorporates the statistical parameters for the necessary soil parameters for each hierarchical level of analyses developed by Rosenbalm (2011) using data obtained from the LTPP DataPave library and the NCHRP 9-23A database, which was a processes version of the U.S. Department of Agriculture's (USDA) Natural Resources Conservation Service (NRCS) soil database (FHWA, 2010; Zapata et al., 2009).

Rosenbalm (2011) further defines the process for generating Level 1 parameters as site specific data consisting of the average value and the coefficient of variation measured from extensive lab or in situ testing. In essence, the design engineer performing the analysis must have a high level of confidence that the statistical distributions of measured soil properties (sample) statistically represent nearly all conditions at the site (population). Rosenbalm (2011) extracted data from the LTPP SPS-1 for 28 granular soils and 28 fine grained soils from the seven states and developed pooled coefficients of variation to represent the variability in site-specific data. The existing MEPDG provides example values for coefficient of variation for Level 1 analysis for the user.

Rosenbalm (2011) breaks down the Level 3 statistics into two subgroups, referred to as Level 3A and Level 3B. For Level 3B analyses, the descriptive statistics for each AASHTO classification, which are presented in Appendix D.

In Level 3A, the AASTO classifications are divided into 5 groups defined as: granular base material, granular subbase/subgrade material, fine grained material, "clayey" fine grained material, and "silty" fine grained material which are presented in Table D-13 through Table D-17, respectively. The granular base material is a grouping of the A-l-a

and the A-l-b soils. The granular subbase/subgrade material is a grouping of all of A-1, A-2, and A-3 soils. The fine-grained soils included all A-4, A-5, A-6, and A-7's soils. The "clayey" fine grained group included only the A-6 and the A-7 while the "silty" fine grained group included only the A-4 and A-5 soils.

Each table provides the data count (#) mean (μ), variance (σ^2), standard deviation (σ), coefficient of variation (CV), minimum value (a), maximum value (b). Note that all parameters are in units of percent, with the exceptions of specific gravity (G_s) and *wPI* which are unitless and the particle diameter corresponding to 60% passing (D_{60}) which is in millimeters (mm). The skewness ($E[X^3]$) and kurtosis ($E[X^4]$) parameters provided by Rosenbalm (2011) were not included in the summary tables as they are not applicable to the approach used in this study. The two Beta shape factors alpha (α) and beta (β) provided by Rosenbalm (2011) were also not included in the summary table for clarity because an updated method for estimating the shape factors was used in this study.

3.4 Proposed Hierarchical Soil Parameter Statistics for SSVC Analysis

The proposed hierarchical statistics groups for shrink-swell analyses were developed by:

- further defining the process to obtain project related/site-specific coefficients of variation for Level 1 statistics,
- adopting the descriptive statistics and classification groups defined by Rosenbalm (2011) for Level 2 and Level 3 statistics,

- updating Beta shape factors from Rosenbalm (2011) which do not represent natural distribution of the soil properties,
- and by defining new groups of soil types which better represent the variations of shrink-swell susceptible soils.

The soil parameters required as input for the shrink-swell analyses over the three hierarchical levels include the index properties of Plasticity Index (*PI*), Liquid Limit (*LL*), percent fines or passing the No. 200 sieve ($P_{\#200}$), percent $_{clay}$ (P_{clay}), the in situ properties of dry density (γ_d) and moisture content (w), and the engineering property used to relate soil suction changes to volumetric strain, referred to in this report as the suction compression index (*SCI*).

3.4.1 Soil Property Statistics for Level 1 Analysis

Although the existing MEPDG provides example values for coefficient of variation for Level 1 analyses, such values will not be provided for the proposed shrink-swell analyses. There have been tremendous advancements in the recent decade on quantifying site-specific geotechnical uncertainty (Phoon and Kulhawy, 1999; Fenton and Griffiths 2008, Medina-Cetina and Esmailzadeh, 2014; Gong et al. 2021; Zhang et al. 2022). As such, Level 1 analyses will be reserved for projects which have sufficient site-specific information for the design engineer to produce representative distribution of the soil input parameters.

3.4.2 Soil Property Statistics for Level 2 Analysis

If the design engineer does not have a high level of confidence that the project data adequately represents the site-specific variability, they may choose to apply the Level 2 or Level 3 coefficients of variation to their site-specific average values. If the site-specific coefficient of variation is greater than the provided Level 2 or Level 3 values, it will be up to the design engineer's judgement on which coefficient of variation to apply. Such scenarios should warrant additional field and lab investigations as the site conditions have higher variability than the pooled LTTP data from across the US, most likely indicating a complex geology at project site with a potentially substantial mix of coarse and fine-grained soils.

A new set of groups of data were used to define the descriptive statistics for the Level 2 and Level 3 shrink-swell analyses. Soils with a propensity to exhibit shrink-swell behavior, defined by A-6 and A-7 soils with a $wPI > 10$, were extracted from the LTTP database and used as the dataset to represent the Level 3 analyses. This group of soils is similar to the "clayey" fine grained soil group defined by Rosenbalm (2011), but does not include A-6 and A-7 soils that may have a low PI and $P_{\#200}$; for example, a lean $_{clay}$ (CL) which is classified as an A-6 with 40% fines and a PI of 12 (i.e. $wPI = 4.8$) typically exhibits very low expansion potential. The grouping of material for the Level 2 analysis followed a similar idea of the Level 3A groups defined by Rosenbalm (2011) but instead of grouping by AASHTO classification, the soils were grouped by *wPI* in intervals of 10. Although this may result in a very similar arrangement of the data, the *wPI* criteria will

tend to group soils together that have similar expansion potentials, as *wPI* is considered to be an adequate correlation for expansion potential.

The dry unit weight and the in situ moisture content statistical parameters had to be determined using the Perera (2003) soil database. Due to the lack of data points with high expansion potential, the data was with $wPI > 10$ was used for all Level 2 subgroups regardless of the *wPI* limits.

The soil parameters required as input for the shrink-swell analysis for Level 2 and Level 3 include the index properties of percent fines or passing the No. 200 sieve ($P_{\#200}$), percent clay (P_{clay}), the in situ properties of dry density (γ_d) and moisture content (w). The mean, variance, standard deviation, coefficient of variation, minimum, maximum, and the Beta distribution shape factors for the required index properties were calculated for Level 2 and Level 3. The statistical parameters for the maximum dry density and the optimum moisture content were referenced from the Perera (2003) data.

3.4.2.1 In situ dry density and moisture content for Level 2 and Level 3 analyses

Unfortunately, the LTTP database lacks sufficient data to generate representative statistics for in situ dry unit weight and moisture content. This is issue is not new and was addressed in the EICM update summarized in the NCHRP 1-40D report (Witczak, 2006) by producing models that related in situ moisture and density to Proctor Compaction results and index properties using the Perera (2003) dataset which consisted of 30 sites corresponding to 143 soils. This database was used in this study to be used to represent the variance of the in situ dry density and moisture content parameters for Level 2 and

Level 3 inputs. The Perera (2003) dataset was divided into the same Level 3B groups as defined by Rosenbalm (2011) and the descriptive statistics for in situ dry density and the moisture content were calculated, which are presented in Table 3-2.

Table 3-2. Descriptive Statistics for In Situ Dry Unit Weight and Moisture Content

	A-1		A-1, A-2, & A-3		A-4, A-5, A-6 & A-7		A-4 & A-5		A-6 & A-7	
	w	γ_d	w	γ_d	w	γ_d	w	γ_d	w	γ_d
#	14		23		120		34		86	
μ	14	14	7.99	119.18	19.53	106.03	17.57	106.11	20.30	106.00
σ^2	6.62	127.60	7.88	604.59	27.47	83.82	32.11	95.80	23.86	80.15
σ	1.22	75.59	2.81	24.59	5.24	9.16	5.67	9.79	4.88	8.95
CV	1.10	8.69	35.13	20.63	26.84	8.63	32.24	9.22	24.06	8.45
a	16.68	6.81	5.33	14.52	8.84	82.24	8.84	83.00	10.13	82.24
b	5.33	108.46	14.87	141.14	35.21	126.11	31.76	124.36	35.21	126.11
α	22.26	88.66	5.56	3.25	7.85	60.85	5.57	51.30	9.86	63.72
β	37.79	62.73	14.38	0.68	11.51	51.37	9.05	40.51	14.45	53.95

For Level 3 analyses, if the average (input) value of the in situ moisture content of the subgrade is unknown the user must assume that it is equivalent to the optimum moisture content, which is generally true for new construction. If the user is running an exploratory or preliminary analysis and the optimum moisture content of the subgrade is also unknown, the program will estimate an optimum moisture content using index property and correlation models from the EICM.

3.4.2.1.1 Compaction *Model for Granular Materials (wPI = 0)*

The maximum dry unit weight for compacted materials is expressed as:

$$\gamma_{\text{d max comp mod}} = \frac{G_s \gamma_{water}}{1 + \frac{w_{opt} G_s}{S_{opt}}} \tag{86}$$

Where: $\gamma_{d\ max\ comp\ mod}$ = Maximum dry density by Modified proctor (pcf), G_s = Specific gravity, γ_{water} = Unit weight of water (pcf), w_{opt} = Optimum gravimetric moisture content by Modified proctor (%), and S_{opt} = Degree of saturation at optimum conditions (%).

The relationship between optimum gravimetric moisture content and gradation data for granular materials is expressed as:

$$w_{opt} = -120.14 - 0.06766P_{1.5"} + 3.7269D_{60} - 0.167P_{40} + 0.117P_{60} + 142.53e^{(-0.0389*D_{60})} \quad (87)$$

Where: $P_{1.5"}$ = Percent passing 1.5" (%), P_{40} = Percent passing #40 US sieve (%), P_{60} = Percent passing #60 US sieve (%), and D_{60} = Diameter corresponding to 60% passing material (mm).

The relationship for saturation at optimum conditions given gradation data for granular materials is expressed as:

$$S_{opt} = -100.17 + 1.4991P_{2"} + 0.56155P_{1"} - 0.36755P_{0.5"} \quad (88)$$

Where: $P_{2"}$ = Percent passing 2" (%), $P_{1"}$ = Percent passing 1" (%), and $P_{0.5"}$ = Percent passing 0.5" (%).

For compacted materials, the dry unit weight is assumed to be equal to the maximum dry unit weight found above.

$$\gamma_d = \gamma_{d\ maxcomp\ mod} \quad (89)$$

3.4.2.1.2 Compaction Model for Plastic Materials (wPI > 0)

The relationship between the gravimetric optimum water content and soil index properties is expressed as:

$$w_{opt} = 8.3932 wPI_{adj}^{0.3075} \tag{90}$$

Where: wPI_{adj} = an adjusted PI value applicable only to the empirical correlations for the optimum water content and the maximum dry unit weight for plastic soils presented in this section.

The adjusted *wPI* is expressed as:

$$wPI_{adj} = \frac{PI_{adj} P_{200}}{100} \tag{91}$$

Where: PI_{adj} = an adjusted PI value. If $wPI_{adj} < 1$ then $wPI_{adj} = 1$

The adjusted PI value is expressed as:

$$PI_{adj} = e^{\frac{P_{200} + 42.13}{33.94}} \tag{92}$$

If $PI > PI_{adj}$, then use PI_{adj} and if $PI \leq PI_{adj}$, then $PI_{adj} = PI$.

For wPI_{adj} values that are equal to 1, both the predicted optimum water content for low-plasticity materials (equation above) and the water content predicted for non-plastic materials should be calculated and an average value used. The maximum dry density for fine grained materials can be expressed in terms of the optimum moisture content as:

$$\gamma_{d\max\_comp\_std} = 142.115 - 1.959 w_{opt} \quad (93)$$

Where: $\gamma_{d\ max\ comp\ std}$ = maximum dry density by Standard proctor (pcf).

For uncompacted materials, the dry unit weight was related to the maximum dry unit weight from the the Standard proctor:

$$\gamma_d = 1.0156\gamma_{d\ maxcomp\ std} - 2.464 \quad (94)$$

Note that user input is required for the expected value and coefficient of variation (or standard deviation) for the Level 1 analyses based on the site-specific data.

The following tables summarize the statistics for the AASHTO soil classifications based on the LTTP and NCHRP database. To eliminate unnatural "U-shaped" distribution, the beta shape factor was corrected to 1 if both shape factors were initially less than 1, and the alpha shape factor was less than the beta shape factor.

3.4.3 Proposed Soil Property Statistics

To eliminate unnatural "U-shaped" distribution, the beta shape factor was corrected to 1 if both shape factors were initially less than 1, and the alpha shape factor was less than the beta shape factor. For Level 3 analyses, if the average (input) value of the in situ moisture content of the subgrade is unknown the user must assume that it is equivalent to the optimum moisture content, which is generally true for new construction. If the user is running an exploratory or preliminary analysis and the optimum moisture content of the subgrade is also unknown, the program will estimate an optimum moisture content using index property and correlation models from the EICM.

Appendix D presents the descriptive statistics and the Beta distribution shape factors of the Level 2 and Level 3 soil groups defined by AASTHO soil classification and wPI ranges.

3.5 Randomization of Soil Index Properties

General laboratory investigations for a given project provide average values of geotechnical properties which are used as input into a deterministic solution in which only a mean value is produced. To obtain a stochastic answer, the dimensionless coefficient of variation (*CV*) is used to characterize the randomness and uncertainty in the measured properties. The coefficient of variation is generated through replicates of the test results which can require either more time and money for sampling/testing, or historical project data variance. If the coefficients of variation for the required soil properties of a project are known, sampling/testing can be reduced while increasing or maintaining the same level of confidence in the analyses and designs (provided the engineering team is experienced in statistical/stochastic analyses). As such, the coefficients of variation for the soil properties are used as key soil inputs for the stochastic volume change analyses.

Randomization of the soil properties is required for the stochastic Monte Carlo volume change analyses. Random variables are to be generated from probability distributions. Beta distributions will be used for the required soil inputs for each hierarchal level of analysis: plasticity index (*PI*), liquid limit (*LL*), percent fines/percent passing the No. 200 sieve ($P_{\#200}$), and percent $_{clay}$/percent fine than 2 microns (P_{clay}), in situ moisture content

(w), and dry unit weight (γ_d). The LTPP soil database (FHWA) and the NCHRP 9-23 (2006) soil databases will be used to develop the statistical parameters for new subsets of soil types for the shrink-swell analysis.

It is well known that soil properties tend to be correlated within one another. Due to this high correlation between the soil properties, the random generation of each property cannot be performed individ*ually on* one another because there is a high potential that non-realistic soils will be generated. For example, the random generations of *PI*, *LL*, $P_{\#200}$, and P_{clay} separately can result in values of 55, 50, 10, and 20, respectively. It is impossible for *PI* to be greater than *LL*, and it is impossible for P_{clay} to be greater than $P_{\#200}$. Although constraints can be placed to limit these scenarios, there will s*till* be a potential for non-realistic soils to be generated. For example, the random generations of *PI*, *LL*, $P_{\#200}$, and P_{clay} can result in values of 85, 50, 10, and 5, respectively. Although these values meet the constraints of *LL* greater than *PI*, and $P_{\#200}$ greater than P_{clay}, it is highly unlikely that a natural soil with a *PI* of 50 to only have 10% fines and 5% $_{clay}$. More realistic soils can be randomly generated using regression equations for the correlated properties.

The U.S. Department of Agriculture (USDA) Natural Resources Conservation Service (NRCS) Soil Survey Laboratory (SSL) soil database was used to explore correlations and relationships between required input soil index properties: *PI*, *LL*, $P_{\#200}$, and P_{clay}. Due to significant correlation between the input soil index properties, an algorithmic approach was developed to randomly generate each property.

3.5.1 Correlation Study using NRCS Soil Database

The NRCS soil database was used to test for general correlations between the required soil index properties for the stochastic SS analysis: plasticity index (*PI*), liquid limit (*LL*), percent fines ($P_{\#200}$), and percent clay (P_{clay}). The *wPI* for each soil entry was also calculated per Zapata et al. (1999, 2000) and was included in the regression analyses. Correlations between index properties and in situ properties (density and moisture) were not explored. The NRCS soil database filtered using the following criteria in order:

- Filtered out entries with missing $P_{\#200}$ (could not classify it)
- Filtered out entries with $P_{clay} > P_{\#200}$ (non-realistic entry)
- Filtered out entries with $LL < PI$, resulted in 0 entries (non-realistic entry)
- Filtered out entries with all values the same (non-realistic entry)
- Determined AASHTO classification for each entry based on $P_{\#200}$, *PI*, and *LL*.

The total entry count after the filtering 28,323 soils.

The software Minitab (2021), version 20, was used to perform the statistical analyses described herein. Table 3-3 presents the descriptive statistics of the explored parameters from the NRCS database.

Table 3-3: Descriptive Statistics for Filtered NRCS Soil Data

Variable	N	N*	Mean	StdDev	Variance	CV	Minimum	Median	Maximum	Mode
p200	28323	0	56.085	25.788	665.029	45.98	0.000	57.500	100.000	85
pClay	28013	310	22.128	13.698	187.638	61.90	0.0000	21.000	85.000	22.5
pSilt	28013	310	34.084	19.746	389.902	57.93	0.000	32.500	95.500	35

LL	25264	3059	32.817	12.407	153.942	37.81	0.0000	30.000	200.000	30
PI	28274	49	10.899	9.947	98.934	91.26	0.0000	7.500	70.000	0
wPI	28274	49	7.7596	8.8222	77.8312	113.69	0.0000	4.6000	62.3000	0

The correlation coefficient was to examine relationship between the soil properties *PI*, *LL*, $P_{\#200}$, and P_{clay}. Correlations between *LL* and *PI* are expected as *PI* is determined from the difference of the *LL* and the Plastic Limit (*PL*), however, *PI* was included in the correlation evaluation, as PL is not included in the input parameters for the stochastic soil volume change analyses. The *wPI* parameter was excluded from the correlation test as it is directly calculated from *PI* and $P_{\#200}$.The Pearson correlation coefficient (*r*) was used to examine relationship between the soil properties *PI*, *LL*, $P_{\#200}$, and P_{clay}. Figure 3-7 illustrates the different patterns in the strength and direction of the relationships between the soil properties *PI*, *LL*, $P_{\#200}$, and P_{clay} from the NRCS soil database filtered with $PI > 0$.

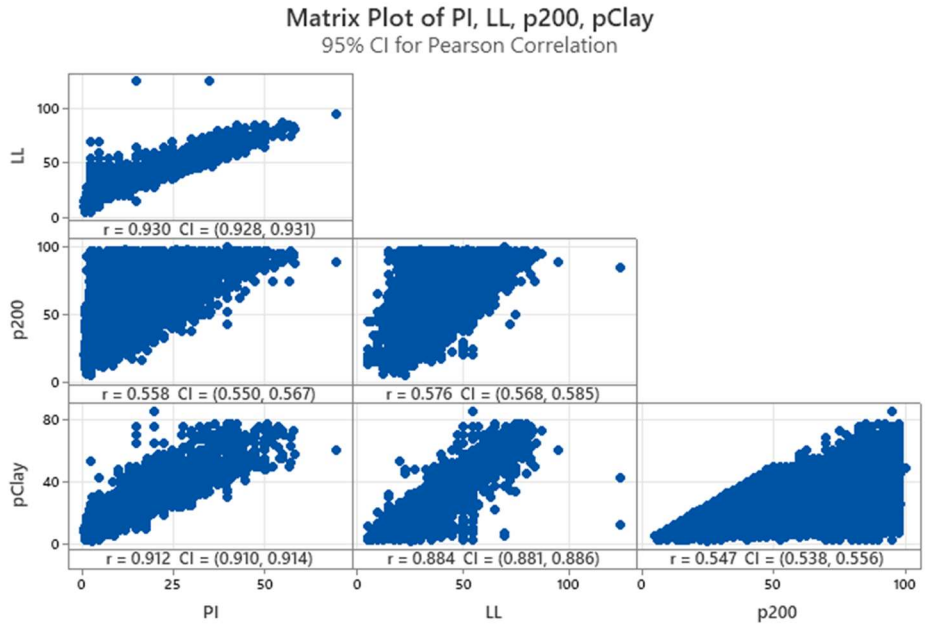

Figure 3-7: Correlation Plots for *PI*, *LL*, $P_{\#200}$, and P_{clay} from NRCS Soil Database Filtered with $PI > 0$

Table 3-4 presents the Minitab output of the correlation coefficients matrix. The Pearson (linear) correlation coefficients indicate that the *PI*, *LL*, and P_{clay} properties are highly correlated, which is expected based on the nature of the geotechnical index properties. The $P_{\#200}$ parameter resulted in a low linear correlation. The *PI* resulted in the strongest correlation to *LL* and P_{clay}, which was used as the basis of the regression study summarized in the following section.

Table 3-4. Correlation Matrix for *PI*, *LL*, $P_{\#200}$, and P_{clay} from NRCS Soil Database Filtered with $PI > 0$

	PI	LL	$P_{\#200}$
LL	0.930		
$P_{\#200}$	0.558	0.576	
P_{clay}	0.912	0.884	0.547

Nine regression trails have been performed with the goal of building statistically significant relationships. (p-value < 0.1). A summary of the adjusted r-square and standard deviation of the residuals of the regression fit is presented in Table 3-5 All of the regression relationships were determined to be statistically significant with all p-values < 0.01.

Table 3-5. Summary of Regression Analyses for *LL*, *PI*, $P_{\#200}$, and P_{clay}

Trial No	Dependent Variable	Independent Variables			Linear		Quadratic (Q)/Multiple (M) [1]	
		1	2	3	R-squared (adjusted)	Residual Standard Deviation	R-squared (adjusted)	Residual Standard Deviation
1	LL	PI			86.42	4.429	86.43 (Q)	4.427
2	PI	LL			86.42	3.569	86.52 (Q)	3.556
3	P_{clay}	PI			83.15	5.310	84.17 (Q)	5.148
4	P_{200}	PI			31.18	18.693	34.71 (Q)	18.207
5	P_{200}	PI	P_{clay}				35.04 (M)	
6	P_{200}	PI	P_{clay}	LL			37.93 (M)	
7	wPI	PI			93.38	2.289	93.95 (Q)	2.187
8	wPI	PI	P_{clay}				94.07 (M)	
9	wPI	PI	P_{clay}	LL			94.25 (M)	

[1] Alternate quadratic model regression fits are automatically generated by Minitab when using the linear regression tool.

Based on the correlation and regression study, the regression models for *PI* to *LL*, *PI* to P_{clay}, and *PI* to *wPI* explained a high percentage of the variation. There was not a significant difference in the adjusted R-squared values between the linear and quadratic/multiple regression models; therefore, thelinear regression models were chosen for implementation due to simplicity.

As portrayed in the correlation study, the regression models to estimate $P_{\#200}$ explained only 31.18% to 37.79% of the variation in $P_{\#200}$. Although the regressions to estimate $P_{\#200}$ indicated a statistically significant relationship (P < 0.001), the high scatter of

residuals and relatively low r-squared does not provide high enough confidence to implement the regression models into the stochastic analyses.

3.5.1.1 Graphical Summary and Normality tests

The Anderson-Darling (AD) statistic is used by Minitab to measure how well the data follows a particular distribution. The null hypotheses (H_0) for the Anderson-Darling test when testing normality is that the data follows a normal distribution.

If the p-value for the Anderson-Darling test is lower than the chosen significance level of 0.05, it is concluded that the data does not follow a normal distribution (i.e. reject the null hypothesis). The graphical summaries and normality tests for each parameter are provided in Figure 3-8 through Figure 3-12.

Based on the results of the normality test presented in Figure 3-8 through Figure 3-12, the five soil properties from the NRCS soil database filtered with $PI > 0$ are not normally distributed. Based on a visual evaluation of each property histogram, Beta distributions were chosen to represent the soil properties, following the existing approach of the MEPDG.

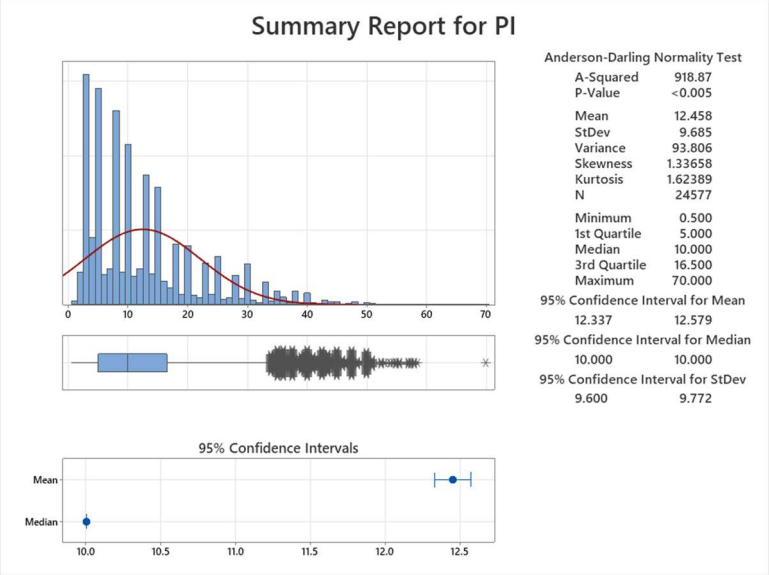

Figure 3-8. Normality Test and Descriptive Statistics for *PI* from NRCS Soil Database with $PI > 0$

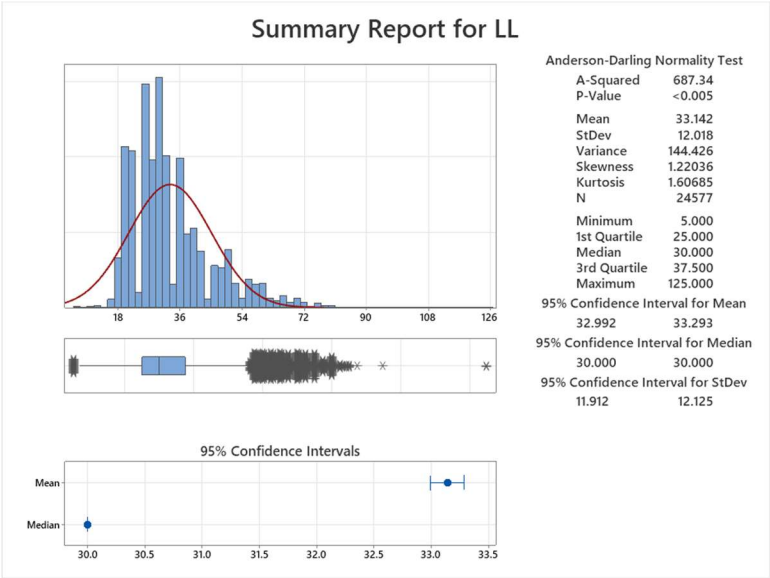

Figure 3-9. Normality Test and Descriptive Statistics for *LL* from NRCS Soil Database with $PI > 0$

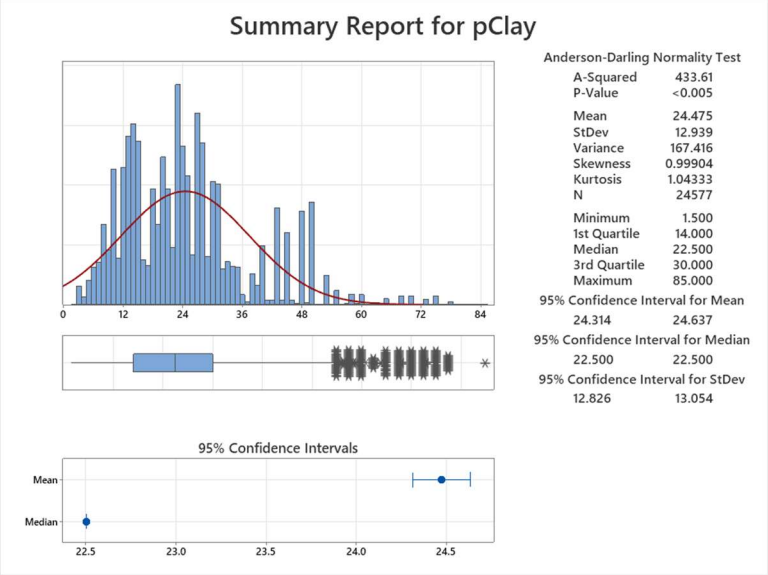

Figure 3-10. Normality Test and Descriptive Statistics for P_{clay} from NRCS Soil Database with $PI > 0$

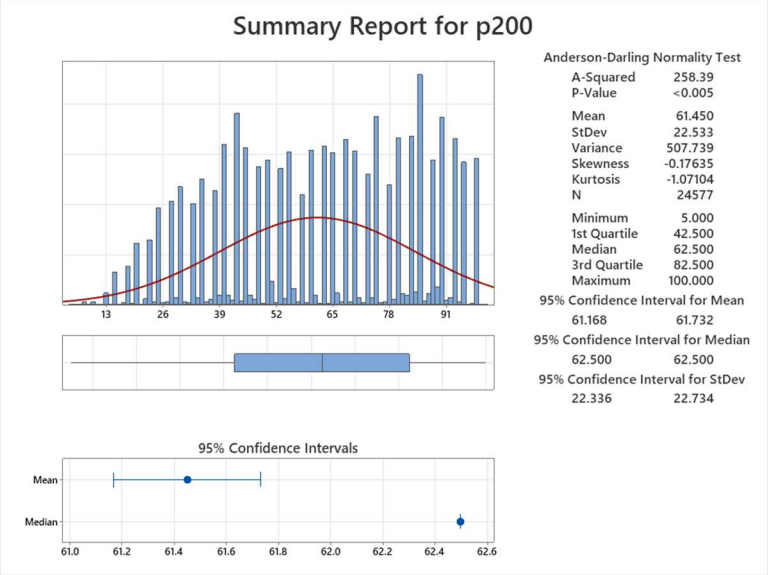

Figure 3-11. Normality Test and Descriptive Statistics for $P_{\#200}$ from NRCS Soil Database with $PI > 0$

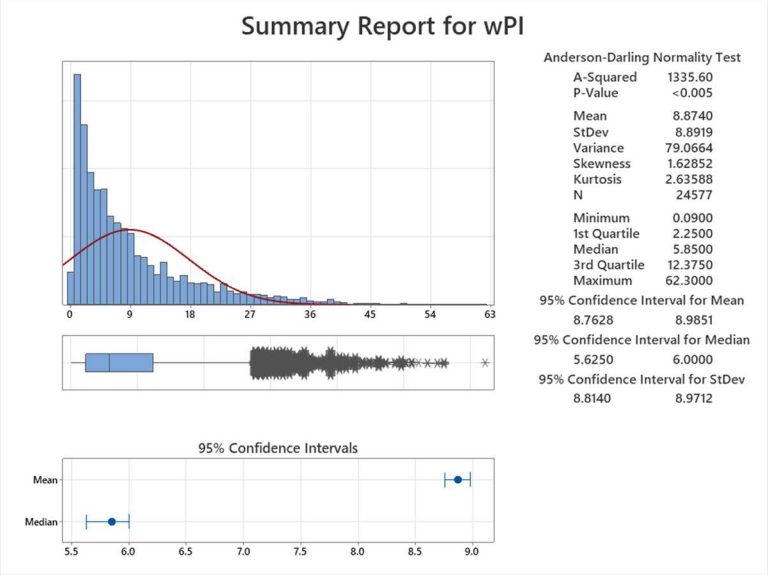

Figure 3-12. Normality Test and Descriptive Statistics for P_{clay} from NRCS Soil Database with PI >0

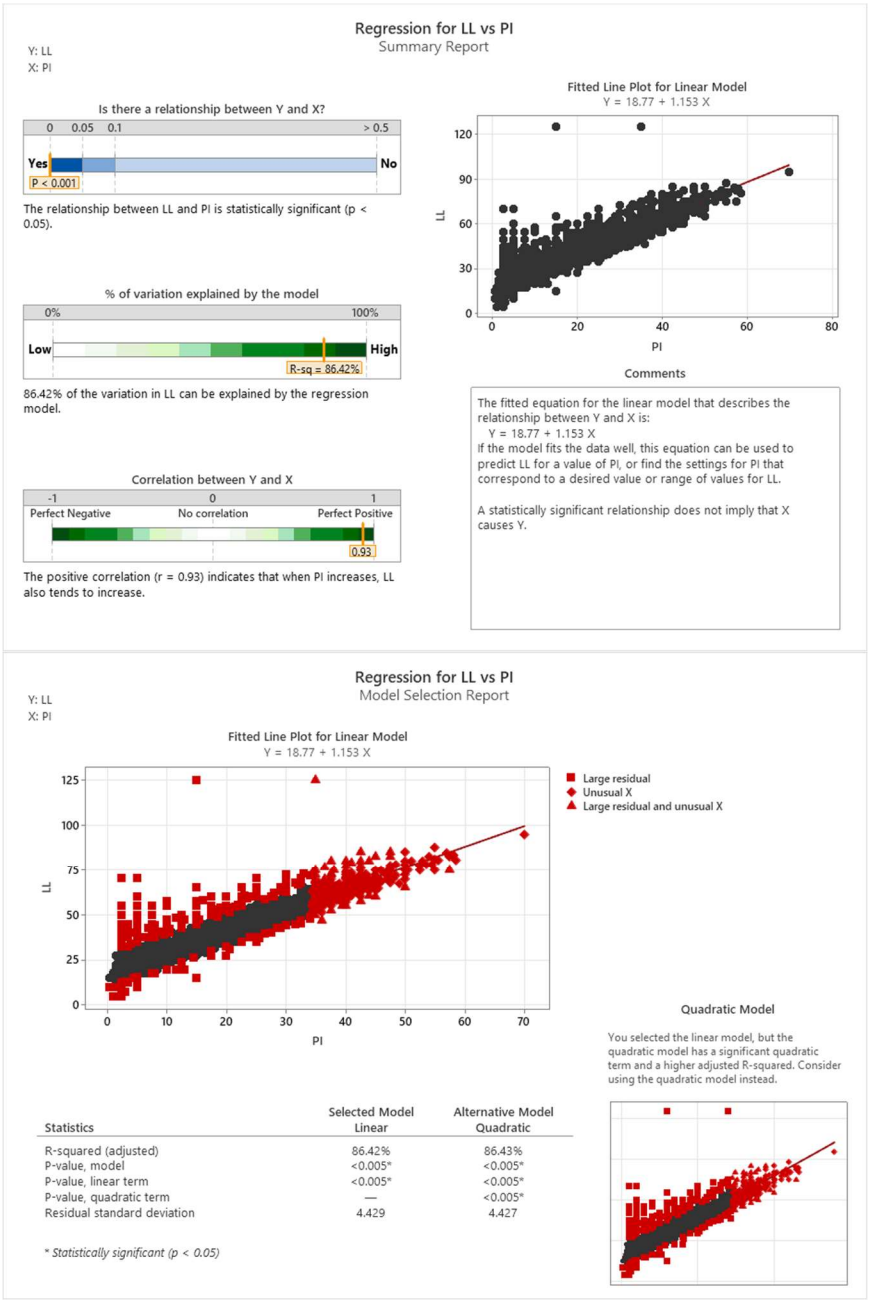

Figure 3-13. Minitab Summary of Linear Regression of *PI* to *LL*

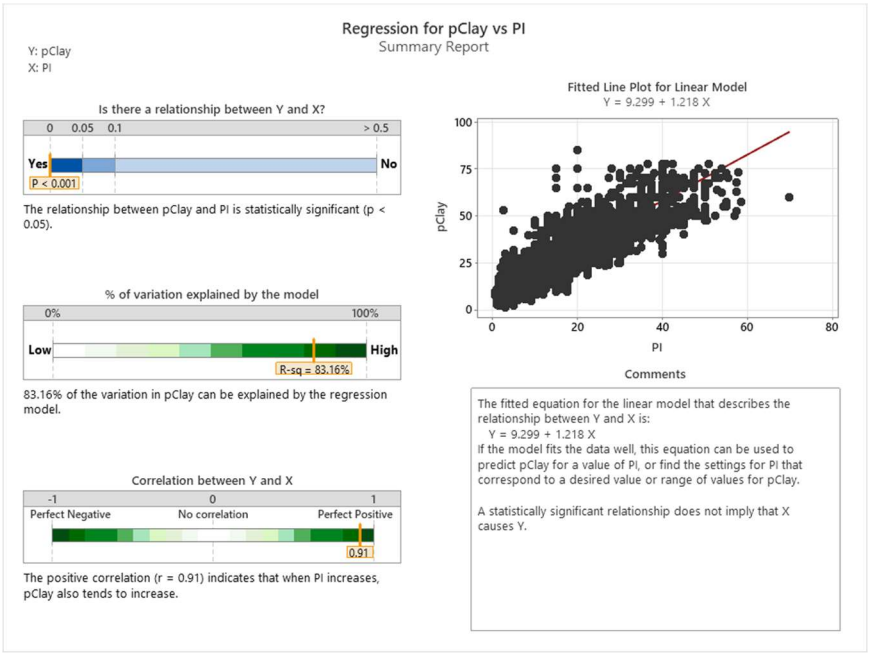

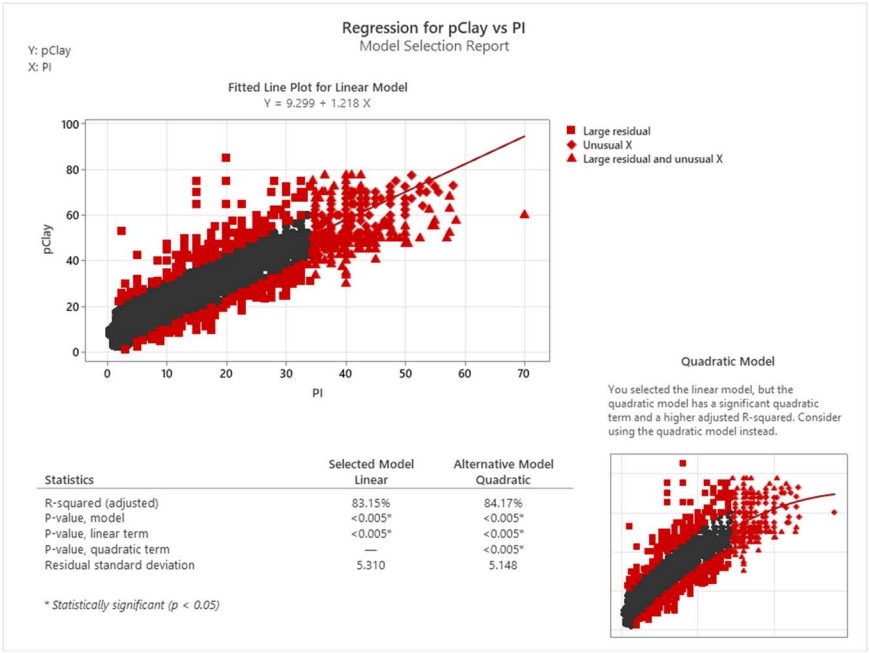

Figure 3-14. Minitab Summary of Linear Regression of *PI* to P_{clay}

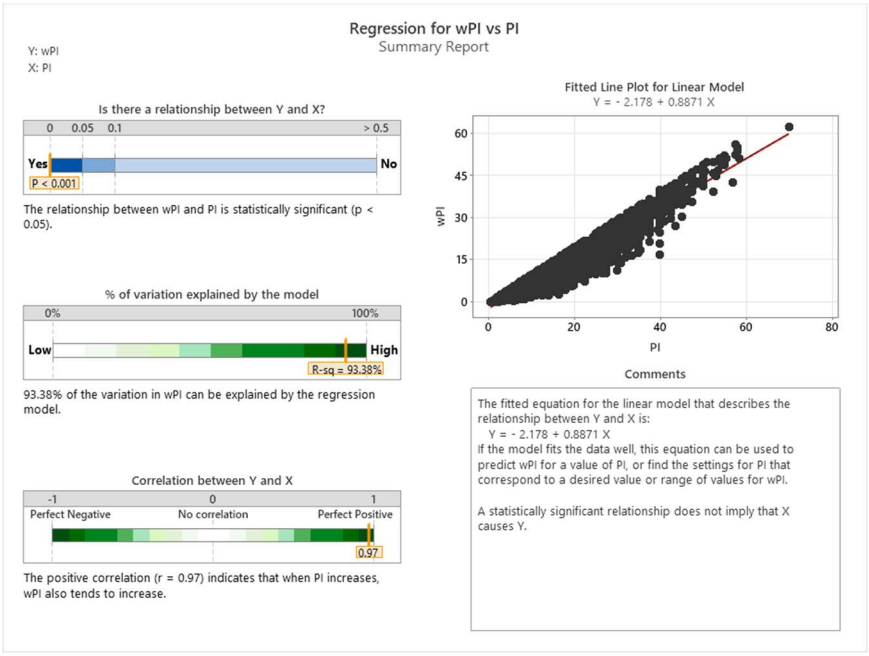

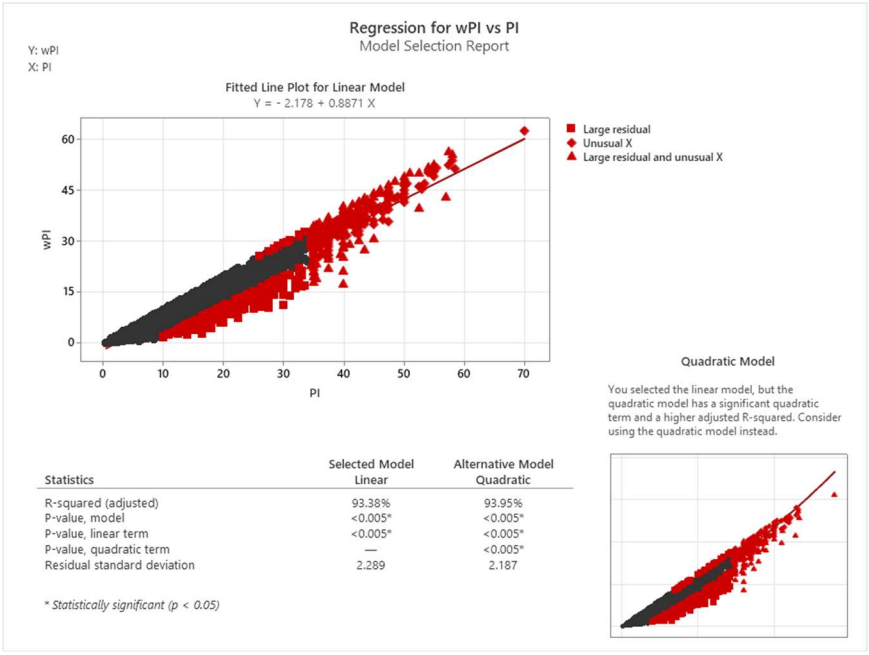

Figure 3-15. Minitab Summary of Linear Regression of *PI* to *wPI*Algorithm for Randomizing Correlated Soil Index Properties

To improve the randomization process to produce more natural results, an algorithmic approach was developed to randomly generate the *PI*, *LL*, $P_{\#200}$, and P_{clay} inputs for the stochastic volume change analyses using beta distributions, linear regression equations for properties correlated to *PI*, standard deviations of the residuals of the regression models, and criteria for the minimum and maximum bounds of the beta distributions based on the nature of the soil properties.

1) Randomly generated *PI* based on the beta distributions for the hierarchical level.
2) Randomly generated p200 based on the beta distributions for the hierarchical level.
3) Randomly generate *LL* based on regression model with *PI*
    a) Use linear regression model to estimate expected value of *LL* using *PI* (Eq. 8-25).
    b) Randomly generate *LL* using a beta distribution with:
        i) the mean equal to the expected value from the regression fit with *PI*,
        ii) the standard deviation equal to the standard deviation of the residuals of the regression fit,
        iii) the maximum equal to the expected value plus 3 times the standard deviation of the residuals from the regression fit, and
        iv) the minimum equal to the greater of the *PI* or the expected value minus 3 times the standard deviation of the residuals from the regression fit
4) Randomly generate P_{clay} based of regression model with *PI*
    a) Use linear regression model to estimate expected value of P_{clay} with *PI* (Eq. 8-26),
    b) Randomly generate P_{clay} using a beta distribution with:
        i) the mean equal to the expected value from the regression fit with *PI*,

ii) the standard deviation equal to the standard deviation of the residuals of the regression fit,

iii) the maximum equal to the expected value plus 3 times the standard deviation of the residuals from the regression fit, and

iv) the minimum equal to the greater of zero or the expected value minus 3 times the standard deviation of the residuals from the regression fit

Note that the engineering soil properties of in situ moisture content and dry unit weight are also required as inputs for the stochastic analyses but it assumed that these engineering properties act independently and are not correlated to any of the of the soil index properties or to one another. As such, the moisture content and dry unit weight can be randomly generated from the beta distributions without correlation concerns, described further herein.

The normal distribution is not bound between any values (i.e., the left tail of the distribution will approach negative infinity and the right tail of the distribution will approach positive infinity). As such, issues can arise when generating random numbers for data sets which represent percentages or index values that must be greater than 1 because there is a possibility of producing negative values. This scenario is applicable to the required soil index properties of PI, LL, p200, and pClay as each parameter is a percentage greater than 0%. The PI and LL parameters do not have an upper bound value but p200 and pClay cannot be greater than 100%. Furthermore, PI is computed from LL and pClay is a fraction of p200 (i.e., must be less than), resulting in high correlation between the parameters, which is discussed further herein. Albeit these limitations for

application in stochastic analyses with natural soil properties, the normal distribution is still used as effective tool for preliminary screening of normality for input variable and residuals of regression fits.

Randomization of the soil properties is required for the stochastic Monte Carlo volume change analyses. To validate that the Beta random number generator function in MATLAB, histograms with increasing numbers of Monte Carlo simulations (*nMC*) can be generated and the predetermined Beta distributions for each input parameter can be visually checked for fit to the distribution, as shown in the example in Figure 3-16.

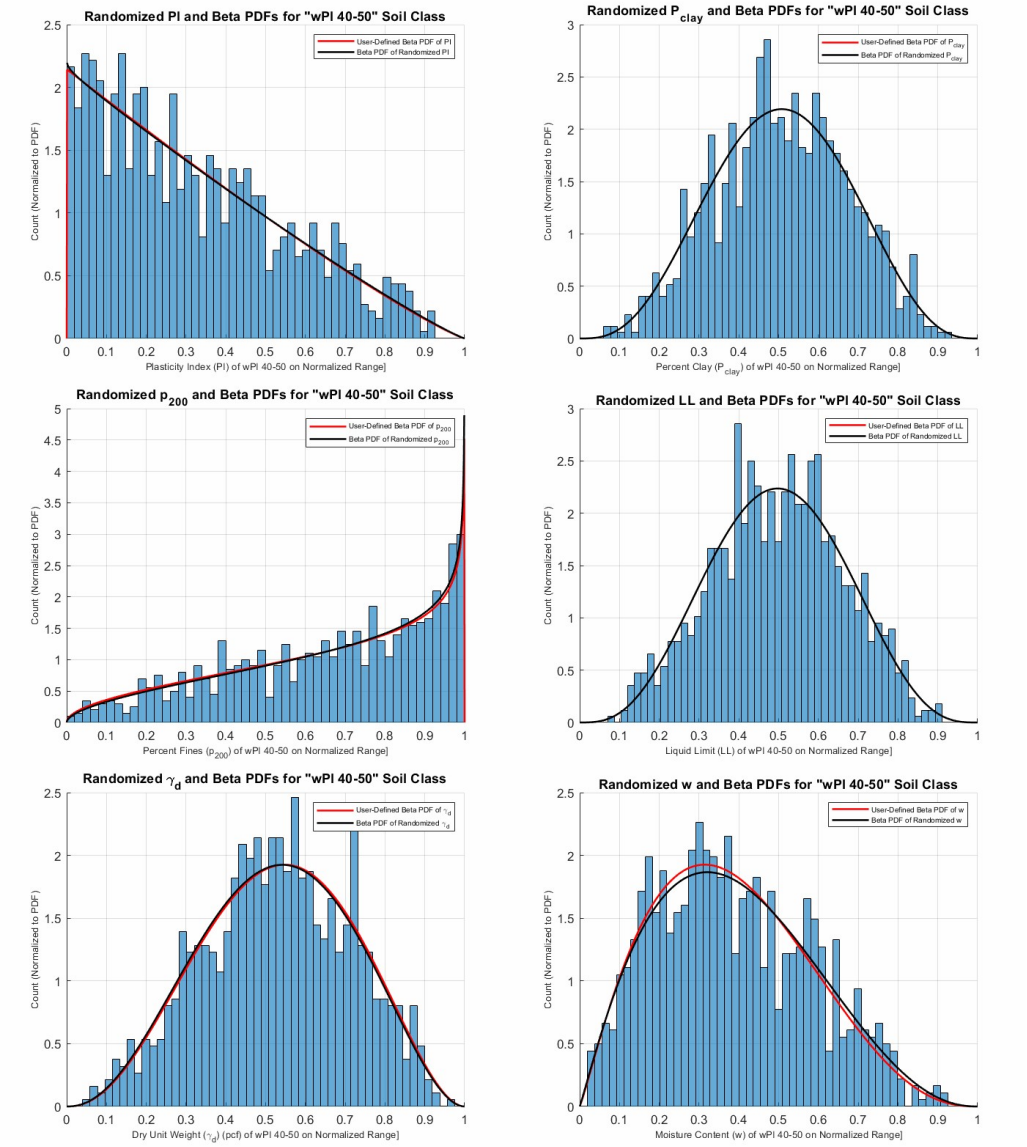

Figure 3-16. Example of Histograms and Fitted Beta Distributions for Randomly Generated Data Points *PI*, *p200*, *pClay*, *LL*, *d_UW*, and *w*.

3.6 Implementation of Random Soil Properties Generator

The hierarchical descriptive statistics with Beta distributions and the random soil properties algorithm are being considered for implementation in the Pavement

Mechanistic-Empirical Design (PMED) guide, also referred to as MEPDG, as part of the NCHRP Project 01-59. As part of the work on that project, the author developed a computer program with a graphical user interface which allows users to perform most of the stochastic analyses presented herein. Figure 3-17 through Figure 3-25 present excerpts (screenshots) from the developed software program which provide an example of the random soil index property model using a few different scenarios.

Figure 3-17 presents the default descriptive statistics for the Level 3 "Clayey FGM" material soil group. Note that only the Mean, coefficient of variation (*CV*), minimum (Min), and maximum (Max) are displayed. The standard deviation and variance parameters are not necessary as they can be represented using *CV*, and the Beta shape factors were deemed by the author and the NCHRP 01-59 research group to not be allowed for direct user updating. Calculations of Beta shape factors are generally based on known statistical moments (mean and variance) and known/desired limits of the distribution (min and max). It is uncommon for the beta shape factors to be the known parameters requiring the statistical moments and limits of the distributions to be back calculated. As such, the program automates the calculation of the updated Beta shape factors/distributions based on the user input of either Mean, *CV*, Min, or Max. Not that the work "either" is not a mistake in the previous statement, as the develop random soil properties model uses a Bayesian type framework to update the default Beta Distribution based on any known (user-input) parameters and does not need all four to be input.

Design Level 3 SS/FH FH Soil Type Clayey FGM

	Mean	CV	Min	Max
p200	75.7493	0.2103	36.1000	100.0000
PI	21.2993	0.4277	10.5000	75.0000
wc	20.3036	0.2406	10.1300	35.2100
d_UW	105.9969	0.0845	82.2400	126.1100

Figure 3-17 Default Descriptive Statistics for the Level 3 “Clayey FGM” Material Soil Group.

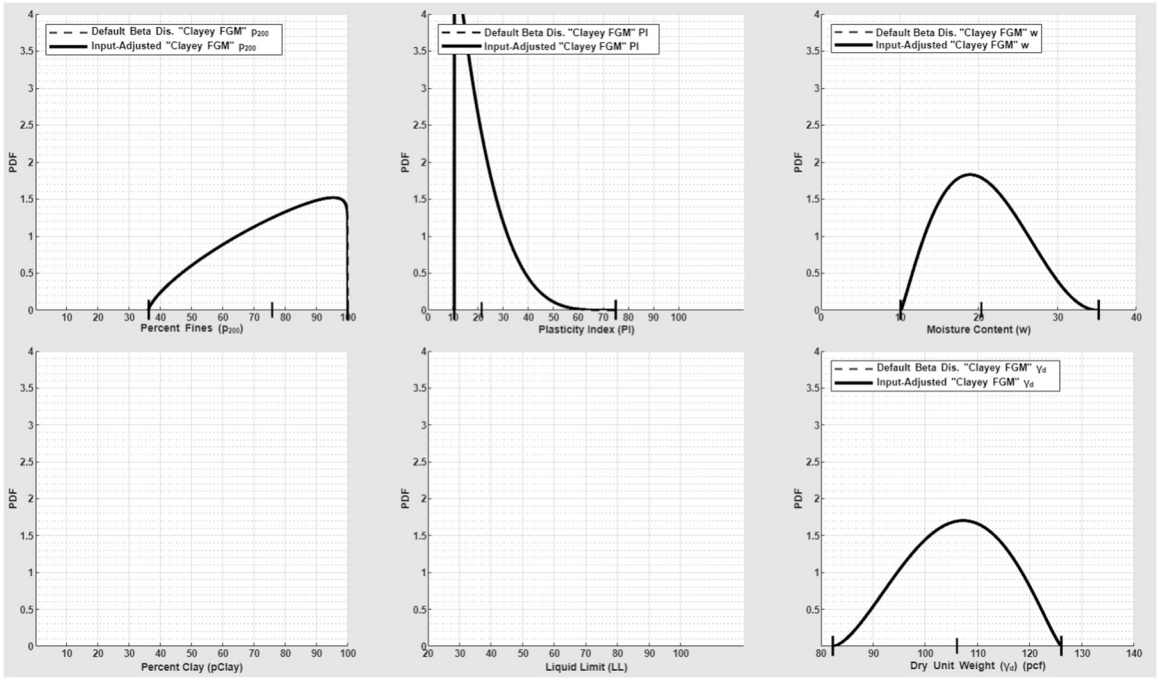

Figure 3-18 Default Beta Distributions for the Level 3 “Clayey FGM” Soil Group

The Beta distribution for the input soil properties percent fines (*p200*), *Plasticity Index* (*PI*), moisture content (*w*), and dry unit weight (*d_UW*) are displayed in Figure 3-18. Note that units for the dry unit weight is in pounds per cubic foot (pcf), and the other

three variables are in percent (%). The Beta Distributions of the additional parameters *LL* and *pClay,* are not defined by user input due to the high correlation with *p200* and *PI,* but rather produced using the regression equations and algorithmic process proposed herein. Figure 3-19 presents the Beta Distributions for *LL* and *pClay* generated by fitting the histograms of the data produced using the randomized regression-based algorithm (although the actual histogram is not displayed on this portion of the interface). The number of randomized draws used to produce the distributions in Figure 3-19 was 1000.

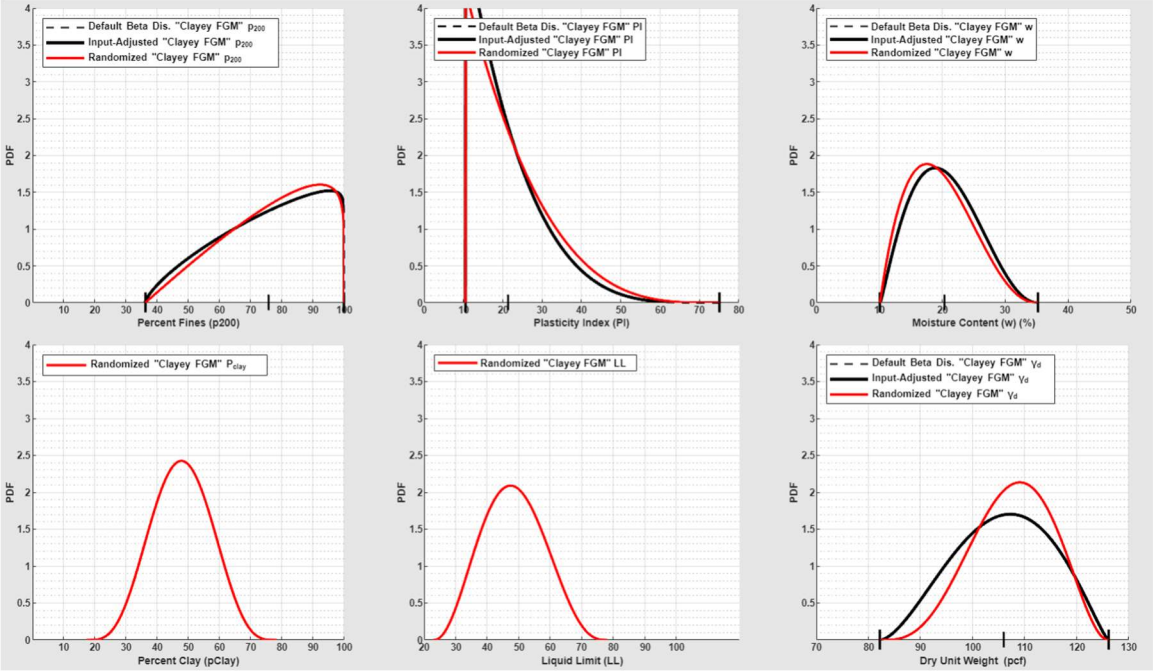

Figure 3-19 Default and Randomized Beta Distributions for the Level 2 "Clayey FGM" Soil Group using 1000 Monte Carlo draws

This number of draws was chosen to present these examples as it generally provides a relatively good fit to the default distributions but not the most ideal fit. One can expect

visually noticeable differences between the default distributions and the distributions fit to the randomly generated data when the number of draws is at or below 1000. Generally the number of draws is governed by the stability of the produced variance of the complete Monte Carlo analysis, which for the full shrink-swell volume change model presented in this study, the required number of simulations (draws) will need to be 10,000 at minimum, which is discussed further herein. As such, the randomized soil property algorithm will generally produce stable representations of the variability of the soil input properties.

The difference between the variability of the default hierarchical soil groups can be visually evaluated using Figure 3-20 and Figure 3-21 which present the default descriptive statistics and randomized distributions for the Level 2 A-7-6 soil which encompasses clayey soils as presented in the previous example of Level 3 "Clayey FGM" in Figure 3-19. Note that there is a difference in the x-axis scale for the Beta distributions for the different soil groups. An example of the randomly generate Beta Distributions for the proposed soil groups for Shrink-Swell soils is presented in Figure 3-21 and Figure 3-23.

Design Level 1 or 2 ▼ SS/FH FH ▼ Soil Type A-7-6 ▼

	Mean	CV	Min	Max
p200	81.7784	0.1565	37.5000	98.0000
PI	28.7988	0.2722	14.0000	75.0000
wc	20.3036	0.2406	10.1300	35.2100
d_UW	105.9969	0.0845	82.2400	126.1100

Figure 3-20 Default Descriptive Statistics for the Level 2 A-7-6 Soil Group.

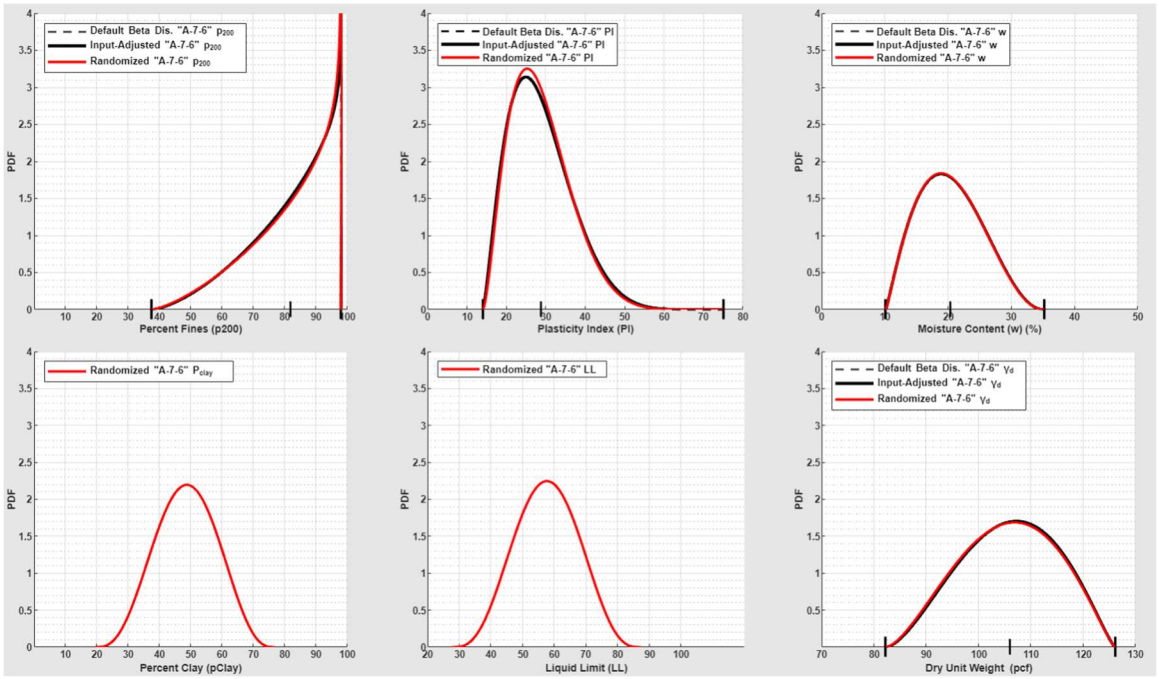

Figure 3-21 Default and Randomized Beta Distributions for the Level 2 A-7-6 Soil Group using 1000 Monte Carlo draws

Design Level 1 or 2 ▼ SS/FH SS ▼ Soil Type wPI 30-40 ▼

	Mean	CV	Min	Max
p200	88.7400	0.1077	60.6000	99.0000
PI	39.1100	0.1561	31.0000	61.0000
wc	22.1800	0.1786	14.1900	35.2100
d_UW	103.0900	0.0703	82.2400	121.3900

Figure 3-22 Default Descriptive Statistics for the Level 2 “wPI 30-40” Soil Group

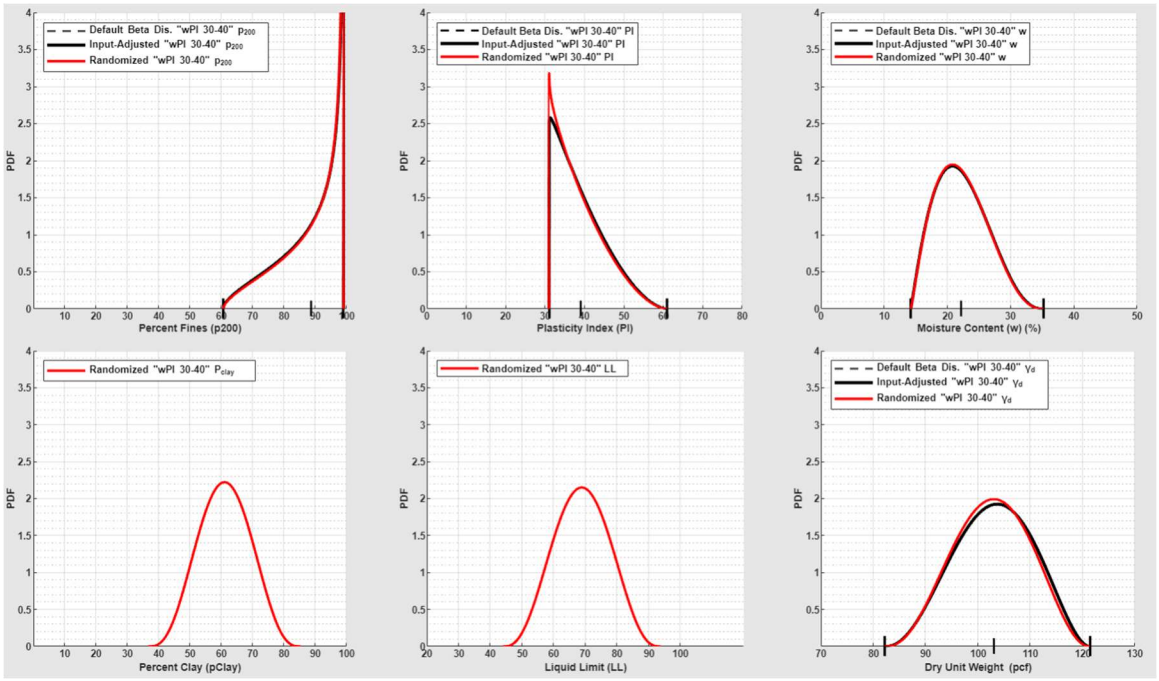

Figure 3-23 Default and Randomized Beta Distributions for the Level 2 "wPI 30-40" Soil Group using 1000 Monte Carlo draws

The computer program developed by the author allows for the user to adjust any of the input descriptive statistics for the four input soil properties. This allows for the user to include any site-specific knowledge into the generation of the Beta distribution, which can either decrease or increase the overall variability of the parameter compared to the default soil group values. Figure 3-24 presents an example of user adjusted parameters (highlighted cells) for various, but not all, of the descriptive statistics of the input variables.

Design Level 3 SS/FH FH Soil Type Clayey FGM

	Mean	CV	Min	Max
p200	80	0.2103	55	100.0000
PI	25	0.4277	15	35
wc	20.3036	0.1000	10.1300	35.2100
d_UW	90	0.0845	82.2400	126.1100

Figure 3-24 Example of Various User Adjusted Descriptive Statistics for the Level 3 "Clayey FGM" Soil Group

The program displays the default Beta Distribution along with the user defined Beta distribution and the randomized beta distribution based on the user adjusted descriptive statistics to allow for a visual comparison, as shown in the Figure 3-25 example.

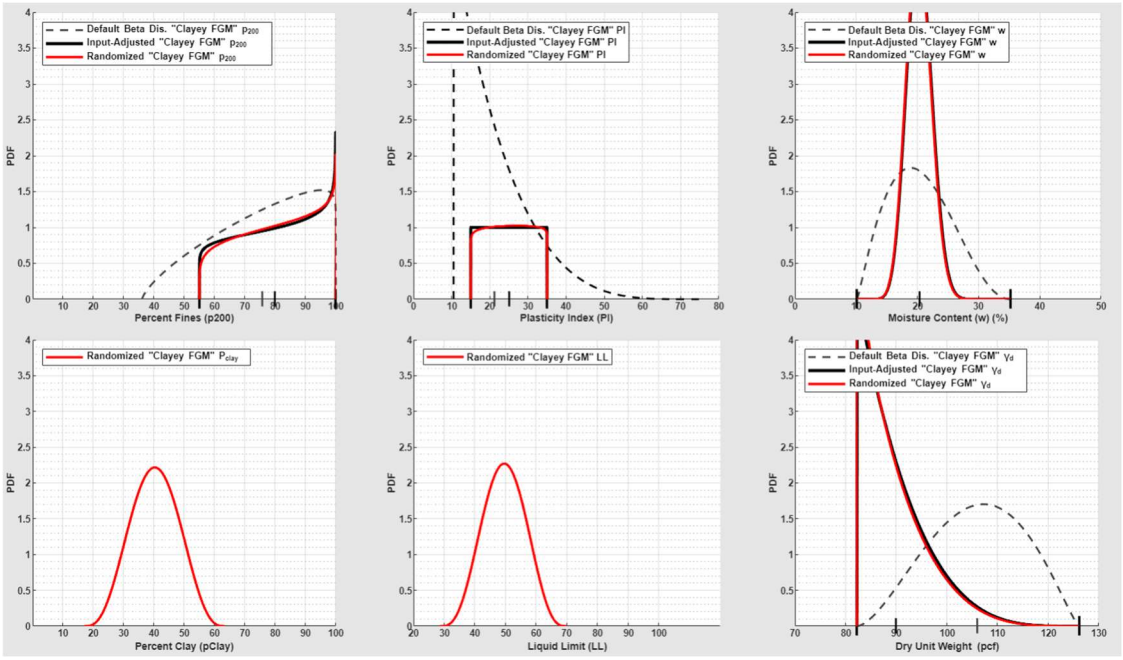

Figure 3-25: Example of the Randomized Beta Distributions (red) based on the various User Adjusted descriptive statistics (Figure 3-24) for the Level 3 "Clayey FGM" Soil Group

3.7 Implementation of Random Soil Properties Algorithm in Practice

Randomization of the soil properties is required for the stochastic Monte Carlo volume change analyses. Random variables are generated from probability distributions. Beta distributions were generated for the required soil inputs for each hierarchal level of analysis: plasticity index (*PI*), liquid limit (*LL*), percent fines/percent passing the No. 200 sieve ($P_{\#200}$), and percent $_{clay}$/percent fine than 2 microns (P_{clay}), in situ moisture content (w), and dry unit weight (γ_d). The LTPP soil database (FHWA) and the NCHRP 9-23 (2006) soil databases were used to develop the statistical parameters for new subsets of soil types for the shrink-swell analysis.

This study introduced an updated approach to stochastically model the variability of the required soil properties. A database of updated statistical parameters for common soil index properties has been compiled for the AASHTO soil groups and for soils groups differentiated by wPI. A Bayesian framework for randomly generating natural combinations of highly correlated variables was developed. Adjustment of the datasets used for the hierarchical levels of the descriptive statistics to better represent the common soil types susceptible to shrink-swell potential. The ability for the engineer to use historical/prior data as a starting point to represent the variability of common soil properties provides a tool which can be used for preliminary sensitivity analyses prior to a site visit, which can provide insight to which soil properties need additional measurements via sampling and testing. Improvement to the overall level of confidence in the geotechnical produced output, and associated variability, can be increased using any site-specific adjustment to the default Beta distributions.

3.7.1 Limitations

The limitations pertaining to the Bayesian characterization model for generating randomized inputs of common soil properties should be understood prior to consideration of implementation into engineering practice:

- The NRCS and LTTP databases were used to generate descriptive statistics for the default variability characterization for the defined soil groups. Although these databases are considered by the field to adequately represent most soil types, there is always a chance for a location to consist of soils which exhibit characteristics away from the norm. It is always recommended that some site-specific data be obtained to gain an understanding of the material types at hand and rule out any potential unusual scenarios.
- The proposed approach for characterizing the variability of common soil properties uses the general variability of the measured properties for a given soil type to represent the 2D variability at the subject site. As such, the proposed framework can be considered a pseudo-2D approach for characterizing soil variability but does not include the modern techniques of quantifying spatial variability.

CHAPTER 4

4 STOCHASTIC CLIMATIC PARAMETER FORECAST MODEL

4.1 Introduction

Geotechnical engineering analyses and designs commonly require knowledge parameters other than just soil/rock properties such as structural loads, traffic volumes, climate data, and manufactured material specifications (e.g., concrete, rebar, geosynthetics, etc.). For new designs, each of these parameters has an associated degree of uncertainty, with manufactured materials generally having minimal uncertainty and future climate data having the highest uncertainty. Such climatic inputs which are often required in geotechnical modeling can include temperature, rainfall, humidity, runoff, and solar radiation.

For geotechnical engineers designing with soil parameters that are subjected to moisture-driven changes, rainfall and temperature data is crucial information. Although such data is readily available, forecasting rainfall events over the design life of common civil engineering structures is difficult due to the extremely random and nonstationary nature of the events. As such, the Thornthwaite Moisture Index (TMI) is commonly adopted by geotechnical engineers as a climatic parameter as it provides a quantitative representation of the historical monthly rainfall and temperature (Thornthwaite, 1948). More specifically in unsaturated soil applications, researchers have successfully related the TMI to geotechnical design parameters used to estimate seasonal moisture variations

within the subgrade (Mckeen and Johnson, 1990; Perera, 2003, Witczak et al. 2006; Australian Standard, 2011; Vann and Houston, 2021, and Olaiz et al. 2021).

Understanding soil-climate interaction is crucial for geo-civil analysis due to the moisture-dependency of the soil shear strength, storage capacity, and volume change potential. The Thornthwaite Moisture Index (TMI) is commonly used by geotechnical engineers to represent both short- and long-term trends of the climate-driven soil-moisture balance within the vadose zone. The long-term average TMI (20+ years) has correlated well with unsaturated soil moisture flow parameters but fails to characterize the extreme climate events which are crucial to the performance of civil infrastructure that have relatively short-term design lives (e.g., pavements). However, the highly variable and the nonstationary nature of the short-term TMI hinders its usefulness in civil design. This study presents a Bayesian framework for stochastically forecasting a short-term TMI using time-series analysis techniques and a component-wise transitional Markov Chain Monte Carlo (MCMC) approach. A validation of the proposed framework is presented for three locations within different climate zones: arid, temperate, and alpine.

This study presents a new Bayesian framework for stochastically forecasting monthly TMI values using time-series analysis techniques and a component wise transitional Markov Chain Monte Carlo (MCMC) approach (Hastings, 1970; Tierney, 1994). The proposed framework for stochastically forecasting monthly TMI is optimized and validated by comparing the forecasted monthly TMI to historic monthly TMI data. An example of the implementation of the proposed framework is also presented which correlates the forecasted monthly TMI to a time-varying soil suction surface boundary

condition used for simulations of seasonal soil moisture variations and shrink-swell volume change estimates.

4.1.1 Objectives

The following objectives were accomplished as part of this study:

- Optimize time-series decomposition of monthly TMI data
- Develop Markov Chain Monte Carlo process for stochastically forecasting monthly TMI
- Optimize and Validate monthly TMI forecast model using historical climate data.
- Perform sensitivity analyses for the stochastic forecast model

4.2 Relevant Background

A review of time-series analysis including stationarity, autocorrelation, trend analysis, regression, and forecasting was conducted and is summarized below. Recent advancements in Bayesian Inference techniques such as Markov-Chains Monte Carlo (MCMC) methods for forecasting random time-series processes were also reviewed.

4.2.1 Review of Time-Series Analysis

The initial time series analysis gathered from the deterministic model must be decomposed into long-term/seasonal trends and the monthly deviations from those trends, referred to as *noise* (Montgomery et al. 2016). The time series decomposition includes stationarity tests, autocorrelation tests, determination of lag, and normality tests of the

residual values to determine the most efficient model to fit the data. The stochastic model proposed herein utilizes a second-order moving average (MA(2)) of the monthly change in TMI (difference) to fit the historic data.

The first step of time series decomposition is to vary the stationarity of the data. Stationarity implies that the time series data moves around a relatively stable equilibrium or mean value. On the extreme side, strict stationarity indicates that the joint probability distribution at any time range within the series is equivalent to a different time range within the series. General stationarity can be judged visually using a time series plot. The stationarity can also be judged mathematically using an autocorrelation approach. It is common to study both the raw time series data as well as the smoothed/transformed time series data when determining stationarity, autocorrelation, and lag (time period associated with autocorrelated data).

Time series data is often transformed or adjusted to remove seasonal/long-term trends and to obtain a more stationary data set. A common form of transformation, used in the proposed forecasting model is differencing. Differencing is simply calculating the change between time steps, which can be represented using TMI as follows:

$$\Delta TMI_t = TMI_t - TMI_{t-1} \tag{95}$$

A second common transformation technique is to smooth the data using a moving average (M_T). The moving average represents the mean of the time series of a specified span (N). The moving average of the TMI at time period (T) is represented as:

$$M_T = \frac{TMI_T + TMI_{T-1} + ...TMI_{T-N+1}}{N} = \frac{1}{N}\sum_{t=T-N+1}^{T} TMI_t \tag{96}$$

The span of the moving average which provides the best fit to the data represents the lag term. The lag can be determined from a study of the autocorrelation functions. The covariance between the TMI at a given time (t) and the TMI a different time ($t+k$) is the autocovariance at lag (k), expressed as:

$$\gamma_k = Cov\left(TMI_t, TMI_{t+k}\right) = E\left[\left(TMI_t - \mu\right)\left(TMI_{t+k} - \mu\right)\right] \tag{97}$$

Where E represents the expected value of the expression. The autocovariance at zero lag ($k = 0$) represents the variance of the time series: $Var(TMI_t) = \gamma_0$.

Stationarity and lag can be visually interpreted from the ACF plot. Time series data, which exhibit stationary behavior, will have ACFs that decrease initially from 1 to approximately zero, and then will oscillate around zero, as both TMI and *dTMI* show, with minimal spikes above a specified significance level (not shown above). The lag for both TMI and *dTMI* were determined by selecting were the ACFs just passed the zero value (TMI lag = 12, *dTMI* lag = 3). Note that the developed ACF values and plots were validated by the authors using the commercial statistical software Minitab.

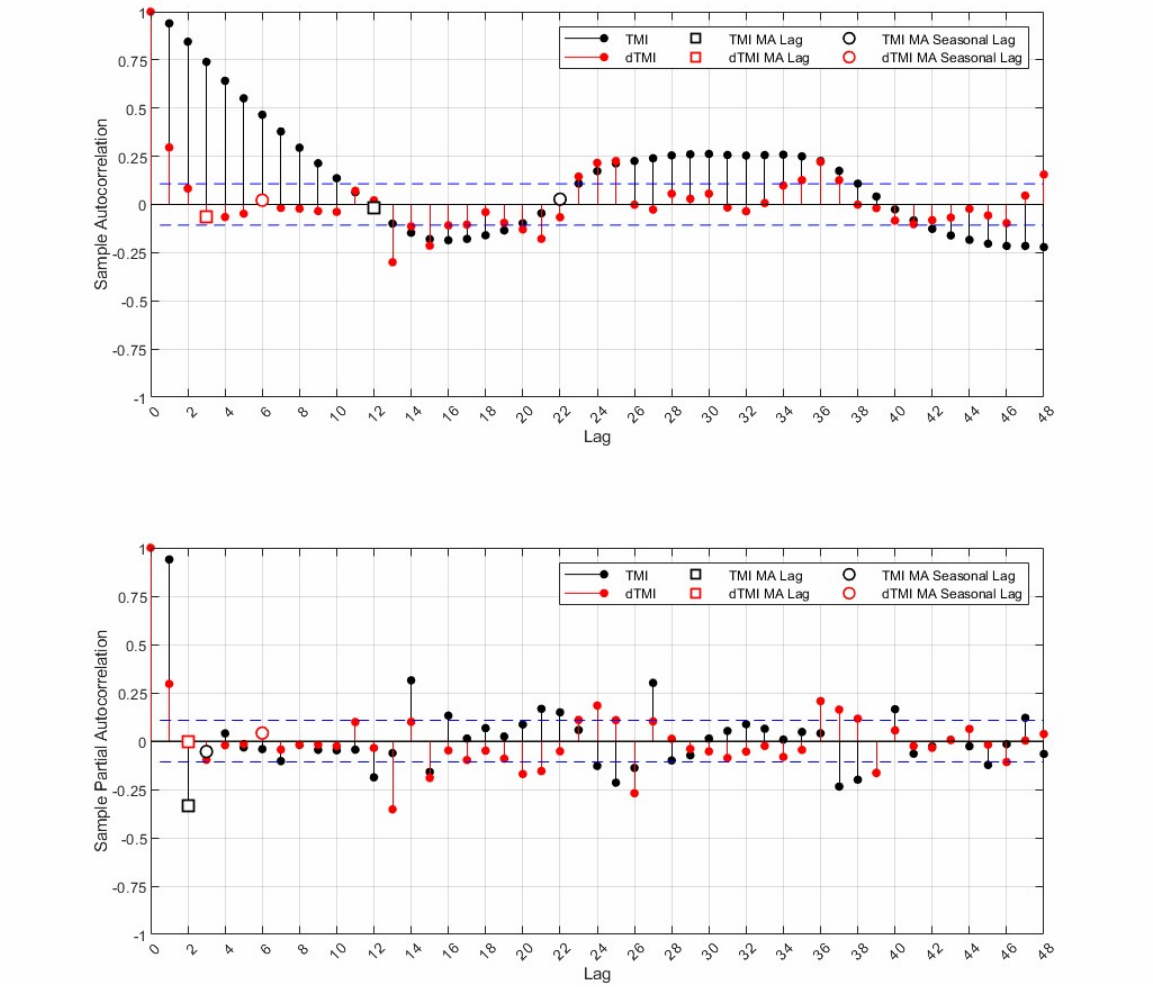

Figure 4-1 Autocorrelation Function Plot for Monthly TMI and Monthly Change in TMI (*dTMI*)

Once stationarity of the time series data has been verified and the lag has been determined, the proper data transformation can be completed. Although there are several sophisticated time series data transformations (Montgomery et al., 2016), the TMI data has an inherent lag of 12 months due to its annual heat index, which allows a 12-span moving average to provide a reasonably good fit for most occasions. This phenomenon is

evident in the previously presented ACF plot. However, an algorithmic approach was include into the climate model which selected the lag associated with *dTMI* and TMI based on the calculated autocorrelation function. The lag was automated to be set at the point at which correlation to previous time-steps became negative.

4.2.2 Review of Bayesian Forecasting Techniques

Bayesian frameworks are a recent focus of study and implementation in geotechnical engineering (Zhang et al., 2004; Najjar and Gilbert, 2009; Ching et al., 2010; Chiu et al., 2012; Juang et al., 2013; Medina-Cetina and Esmailzadeh, 2014; Wang et al., 2016). However, the mathematical and computational complexity have limited the speed of adoption by the overall field (e.g., Zhang et al., 2009).

Prior knowledge and site/project specific data are used during geotechnical site characterization to estimate subsurface properties. The prior knowledge, or prior distribution, represents the estimation of the PDFs for the model parameters based on historical data/experience of similar parameters (e.g. the expansion potential of a fat clay at a new site is likely to be similar to other fat clays in the area or even around the world). The likelihood function is a key step in the Bayesian framework. The likelihood function is the PDF of site observation data for a given set of model parameters.

Bayesian framework are already being studied and implemented in in geotechnical engineering (Najjar and Gilbert, 2009; Ching et al., 2010; Chiu et al., 2012; Juang et al., 2013; Medina-Cetina & Esmailzadeh, 2014; Wang et al., 2016, Soltanpour, 2017).

However, the mathematical and computational complexity have limited the speed of adoption by the overall field (e.g., Zhang et al., 2009).

It has been common practice to force normal distributions on prior and likelihood functions for the sole reason of convenience and simplicity. Although many geotechnical model parameters can pass a normality test, many will night and being able to represent the true variability of the model parameters (i.e. reflect the physical characteristics of the parameter) can have a significant effect of the model outcome.

4.2.3 Markov Chain Monte Carlo (MCMC) Simulations

One powerful tool in stochastic analyses and Bayesian Inference is the Markov-Chain Monte Carlo (MCMC) simulation, which can produce forecast estimates of highly correlated, multi-parameter, time-series data. MCMC forecasts data based on the conditional probability of observed (prior) data. Several recent publications which applied MCMC techniques to analysis of time series data and/or analysis of engineering related problems were reviewed as part of this study: Valdivieso (2009), Chen and Liu (2011), Sengupta et al. (2016), Bentancourt (2018), Koch et al. (2020), and Li et al. (2021).

A series of data is referred to as a Markov Chain is the conditional distribution of each time step is dependent or correlated to the previous time step. The general MCMC analysis approach involves a drawing proposal values unobserved data (θ^t) which is dependent upon or corrected by the previous draws (θ^{t-1}) so that a better representation of the target distribution is produced. Markov Chains can be represented by the joint

distributions of the given/observed data, referred to as the marginal distribution. Transition probabilities, or jumping distributions express the joint probability of the proposed variable at the current time step (θ^*) and the accepted variable at the previous time step (θ^{t-1}):

$$J^t\left(\theta^b \mid \theta^a\right) \equiv J^t\left(\theta^* \mid \theta^{t-1}\right) \tag{98}$$

Two common approaches are used in Bayesian inference to produce proposal variables and define criteria for acceptance and rejection of the proposed variables. One main goal of MCMC simulations are to create stationary Markov processes which results in the proposed variables falling within the distributions of the prior data for each sequential draw. The variance of a Markov Chain differs from the typical Monte Carlo simulation, or the good old-fashioned Monte Carlo (GOFMC) as defined by Geyer (). Due to the dependency on the previous data, the variance (σ^2) of a MCMC simulation, lets say $g\left(X\right)$, can be expressed as:

$$\sigma^2 = \operatorname{var}\left\{g\left(X_i\right)\right\} + 2\sum_{k=1}^{\infty} \operatorname{cov}\left\{g\left(X_i\right), g\left(X_{i+k}\right)\right\} \tag{99}$$

Where, *i* refers to the previous time current time step and k refers to either the previous or the future time steps (if the MCMC chain is reversible). Markov chains are not limited to representation of one variable at a time, but the general framework can apply to vectors and array variables as well. Furthermore, MCMC frameworks do not need to have stationary transition distributions; the variance and/or jumping distributions can be adaptive over time (Rosenthal, 2010).

4.2.3.1 Time-Series MCMC

Transitional probabilities for MCMC can also be defined by the autocovariance function, which is a common explanatory technique for time series analysis. The covariance function at any lag (k) can be expressed as:

$$\gamma_k = \operatorname{cov}\left\{g\left(X_i\right), g\left(X_{i+k}\right)\right\} = \frac{1}{n}\sum_{i=1}^{n-k}\left[g\left(X_i\right)-\hat{\mu}_n\right]\left[g\left(X_{i+k}\right)-\hat{\mu}_n\right] \qquad (100)$$

Where n represent the total number of observations, $\hat{\mu}_n$ is the mean of the Markov Chain for an assumed normally distributed prior data set:

$$\hat{\mu}_n \approx \text{Normal}\left(\mu, \frac{\sigma^2}{n}\right) \qquad (101)$$

4.2.3.2 Metropolis-Hastings

The key to performance of an MCMC simulation is the proposal mechanism and the acceptance/rejection process for the proposed sample. A common method to the acceptance/rejection process is the Metropolis-Hasting (MH) approach. The MH techniques can be and are commonly combined with Gibbs sampling techniques to improve efficiency, usefulness, and computation time of the MCMC simulation. Originally, the Metropolis algorithm was as follows:

- Propose an unobserved data point (θ^*) given the conditional probability between either the prior or the accepted posterior distributions.

  $p(\theta \mid y) \quad or \quad p\left(\theta^* \mid \theta^{t-1}\right)$

- Calculate the Hastings Ratio:

$$r(y \mid \theta) \equiv r\left(\theta^{t-1} \mid \theta^{*}\right) = \frac{p(\theta)\, p(\theta \mid y)}{p(y)\, p(y \mid \theta)} \equiv \frac{p\left(\theta^{*}\right) p\left(\theta^{*} \mid \theta^{t-1}\right)}{p\left(\theta^{t-1}\right) p\left(\theta^{t-1} \mid \theta^{*}\right)} \tag{102}$$

- Accept the proposed move to the variable (θ^{*}) if the $\min\left(1, r\left(\theta^{t-1} \mid \theta^{*}\right)\right) > u$.

The Metropolis-Hasting algorithm provided an update to the rejection aspect of the process and included the generation of a uniform random variable (u) between [0,1] following the calculation of the Hasting ratio.

4.2.3.3 Variance Estimation

The approach to represent the variance in MCMC simulations is a key factor which affects the performance of the model, and can be represented/estimated in several ways. A batch sampling approach can be used which simply accounts for a finite amount of samples, less than the total amount of samples, and assumes stationarity within the batch sample. Similar to a moving average approach, the variance within the batch sample is calculated and assumed to represent the posterior data at that time step. Batch sampling can include overlapping or not overlapping ranges of the sample data.

A second approach for defining the variance of time series data for MCM simulations is referred as the Initial Sequence Method and uses the autocorrelation function to represent dependency of the next time step on not only the typical lag data points, but also the period after the typical lag effect is negligible, and the period as the autocorrelation reverses to be opposite trend of the initial relationship.

4.2.3.4 Initiating a MCMC Simulation

One unfortunate aspect of MCMC models is that most useful models are developed and optimized to provide insight for a specific scenario and the application of each MCMC framework to other applications is difficult.

Generally, a "Burn-in" or "warm-up" period is implemented into a MCMC model to allow for the posterior distributions to stabilize at or near the target distributions. Common practice when developing MCMC models is to start with a warm-up period that is 50% of the total number of simulations (Gelman et al., 2014).

This initial starting proposal point of an MCMC simulation can be chosen through a variety of approaches. The initial point can be a random draw from the prior distribution, or even the mean of the prior distribution can be used. The random draw of the posterior distribution can also be used, provided a warm-up period has been complete and the variance of the posterior distribution has stabilized. It there is a decent level of confidence in the prior distribution, or the prior data is highly correlated as with time-series data, a Gibbs sampling approach can be used to generate an approximation of the first proposal point.

4.3 Time Series Decomposition of Monthly TMI Data

The initial time series analysis gathered from the deterministic model must be decomposed into long-term/seasonal trends and the monthly deviations from those trends, referred to as *noise* (Montgomery et al. 2016). The time series decomposition includes

stationarity tests, autocorrelation tests, determination of lag, and normality tests of the residual values to determine the most efficient model to fit the data. The stochastic model proposed herein, utilizes a second-order moving average (MA(2)) of the monthly TMI (moving average of the monthly change in TMI) to fit the historic data.

The second order moving average (MA(2)) model of the differenced TMI (*dTMI*) is expressed as:

$$dTMI_t = \mu_{TMI} + \varepsilon_t - \theta_1 \varepsilon_{t-1} - \theta_2 \varepsilon_{t-2} \tag{103}$$

Where μ_{dTMI} is the average value of the sampled *dTMI* and represents the ACF parameters for *dTMI* at the lag identified by the subscripts. To improve the fit, the average value of the sample can be replaced by the moving average of the terms prior with lag = 3, as presented in the figure below. Note that once the *dTMI* value is estimated, the TMI term for a given month is calculated adding the change to the previous term. The *dTMI* model expressed in Eq. 104 will serve as the basis for the stochastic forecasting solution. However, the stochastic approach will incorporate the monthly statistics associated with each of the parameters in the equation (i.e., monthly means of *dTMI*, and autocorrelated monthly residual values). A visual example of the time series decomposition for using the MA(2) model of the monthly *dTMI* values is presented in Figure 4-2.

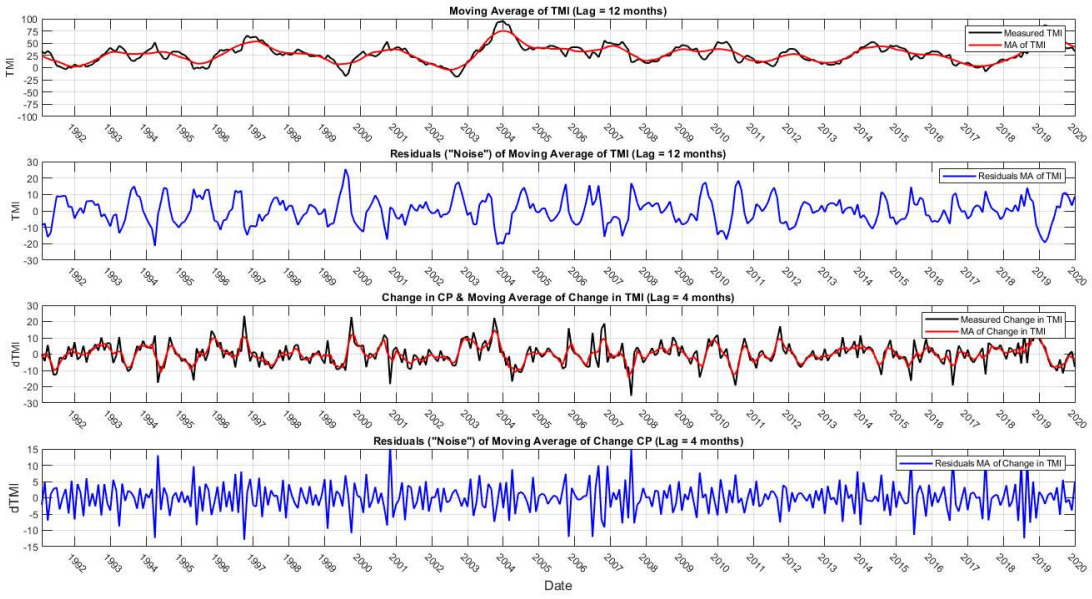

Figure 4-2 Time Series Decomposition of TMI and *dTMI* (black) using Moving Average (MA in red) with lag = 12 and 3, respectively, and the Associated Monthly Residuals (blue).

4.4 MCMC Framework for Stochastic Climate Parameter Forecasting

The monthly parameterized prior distributions for the MCMC TMI forecast model are obtained using the procedures presented in the diagram in Figure 4-3.

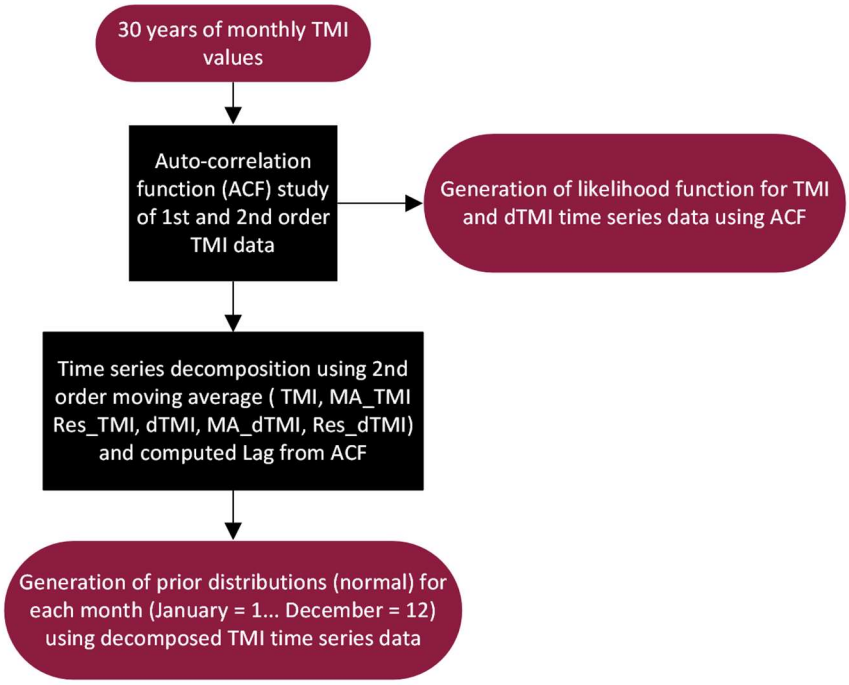

Figure 4-3 Procedure for Obtaining Monthly Parameterized Prior Distributions for the TMI MCMC Forecast Model

The overall framework of the MCMC algorithm using a Metropolis-Hastings acceptance criteria is presented in Figure 4-4.

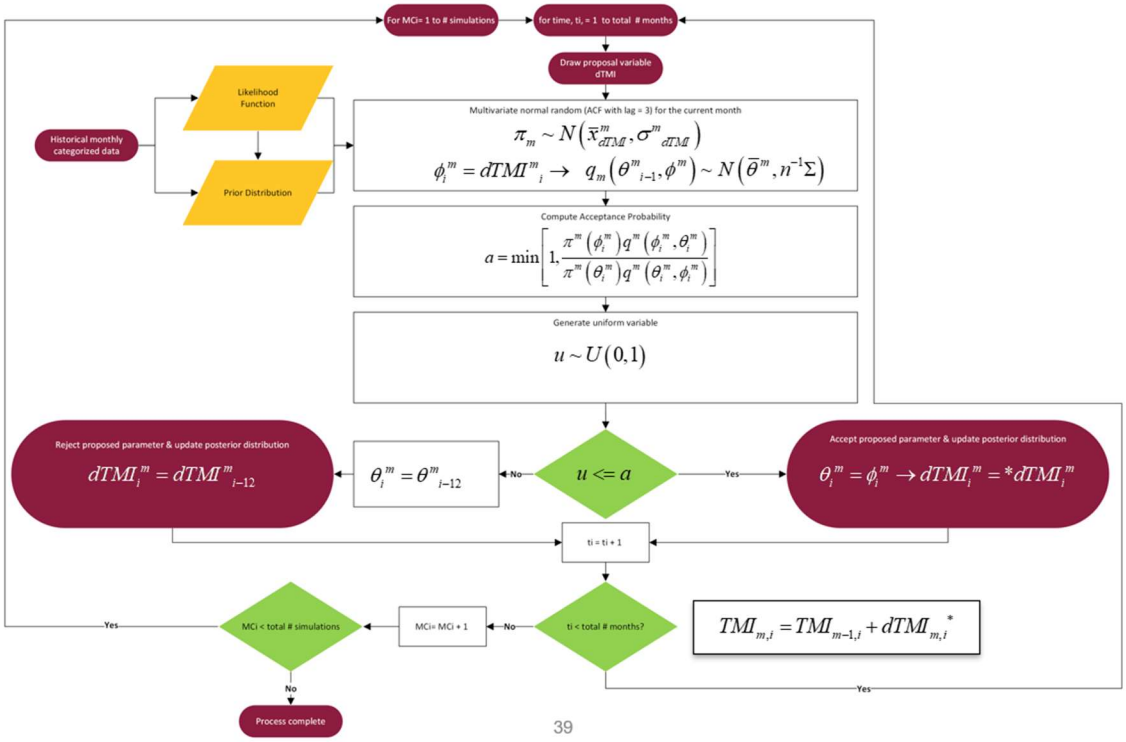

Figure 4-4 Framework for monthly MCMC TMI forecast model using the Metropolis-Hasting Acceptance criteria.

4.4.1 Stability and Optimization of Stochastic Climate Parameter Forecasting Model

The MCMC framework for stochastically forecasting the Thornthwaite Moisture Index went through numerous was optimized through numerous adaptations through iterations of trial and error until a useful model was obtained which could be efficiently applied to just about all locations in the US. The following concepts were incorporated into the analysis to help evaluate the stability and optimize the performance of the climate model.

- The generation of the proposal point initially began with a randomly generated value from the monthly parameterized prior distributions. To improve the efficiency and acceptance rate of the MCMC algorithm, a multivariate random

number based on the posterior distributions within the lag period for *dTMI* is included final model. Frameworks which use Gaussian noise randomly generated number and the autocorrelation with the data points within the lag period was also explored but no benefit to the model performance was observed.

- The acceptance rate of Metropolis Hasting algorithm was calculated and evaluated to see if it fell within the typically accepted value for multidimensional models of 24%.
- A warm-up period was included in the algorithm which was set at 50% of the total simulations per recommendations by Gelman et al. (2014).
- An adaptive Metropolis-Hastings algorithm was developed which updated the target variance after a user-defined number of iterations to help drive and maintain the acceptance criteria around 24%. The adjustment factor and the update period were initially chosen to be 0.2 and 50 simulations based on recommendations by Vrugt (2016), however, after a few
- Bounds of the posterior forecasted data were implemented on the TMI values, the moving average of the TMI, and the moving average of the change in TMI. The bounds were defined as three standards deviations on each side of the mean for the monthly parameterized prior data. The bound checks occur at each sequential time step and include a "step-back" process if the current proposal point falls outside of the bounds. On the time scale, the step-back period was set to be the lag of *dTMI* or *TMI* depending on which parameter had failed the bound checks. The implementation of the bound check and the step-back process is a rough approach

to adding the benefit of a Hamilton Monte Carlo type algorithm without the direct inclusion of the energy expressions or the leapfrog algorithm.

- The Metropolis-Hasting algorithm was updated to include the conditional probability of the proposal TMI to help drive the posterior distribution of TMI closer to the target distribution and help improve stability of the model by reducing the variance of the posterior distribution of TMI.

4.5 Validation of Stochastic TMI Forecast Model

Five locations within differing climate regions were used to evaluate the performance of the TMI forecast model. The simulated time period was from March 2017 to March 2022 (5 years). By using a forecast window of historical data, a comparison can be made between the forecasted TMI and the actual TMI during that period. Note that the historical data during the comparison period was not included in the prior distributions. Thirty years of prior climate data from NOAA was collected and used to develop monthly distributions for *TMI*, *dTMI*, *TMI_MA*, and *dTMI_MA*. Using a monthly-based component-wise setup allows for the qualitative knowledge that weather data is typically similar in each month year after year; however, the monthly component-wise setup limits the number of data points for each component distribution to the number of years of historical data available at the site. The five locations used for evaluation of the proposed TMI forecast model are presented in Table 4-1 along with the NOAA weather station ID, the 30-year TMI, and the climate region as defined by AS2870 (2011).

Table 4-1. Sites for Validation Study of the Proposed Stochastic TMI Forecast Model

Location	NOAA Weather Station (ID#)	30-Year TMI	Climate Region*
Arlington, VA	Washington Reagan Airport (USW00013743)	24	Wet Coastal / Alpine
Dallas, TX	Dallas FAA Airport (USW00013960)	-5	Wet Temperate to Temperate
Denver, CO	Denver Central Park (USW00023062)	-19	Dry Temperate
Salt Lake City, UT	Salt Lake City International Airport (USW00024127)	-26	Semi-Arid
Tempe, AZ	Phoenix Sky Harbor International Airport (USW00013743)	-58	Arid

* As defined by AS2870 (2011) based on TMI

The autocorrelation functions, histograms and boxplots of the parameterized data of the monthly TMI time-series decomposition and the MCMC forecasted TMI for the five locations are presented in Appendix E. The results of the TMI forecast for Arlington, VA, categorized as a wet coastal/alpine climatic region, are presented in Figure 4-5. The results of the TMI forecast for Dallas, TX, categorized as a Temperate to Wet Temperate climatic region, are presented in Figure 4-6. The results of the TMI forecast for Denver, CO, categorized as a dry temperate climatic region, are presented in Figure 4-7 . The results of the TMI forecast for Salt Lake City, UT, categorized as a Semi-Arid climatic region, are presented in Figure 4-8. The results of the TMI forecast for Tempe, AZ, categorized as an arid climatic region, are presented in Figure 4-9. The figures present the prior data, the forecasted data, and the true data within the forecast period for comparisons and validation purposes.

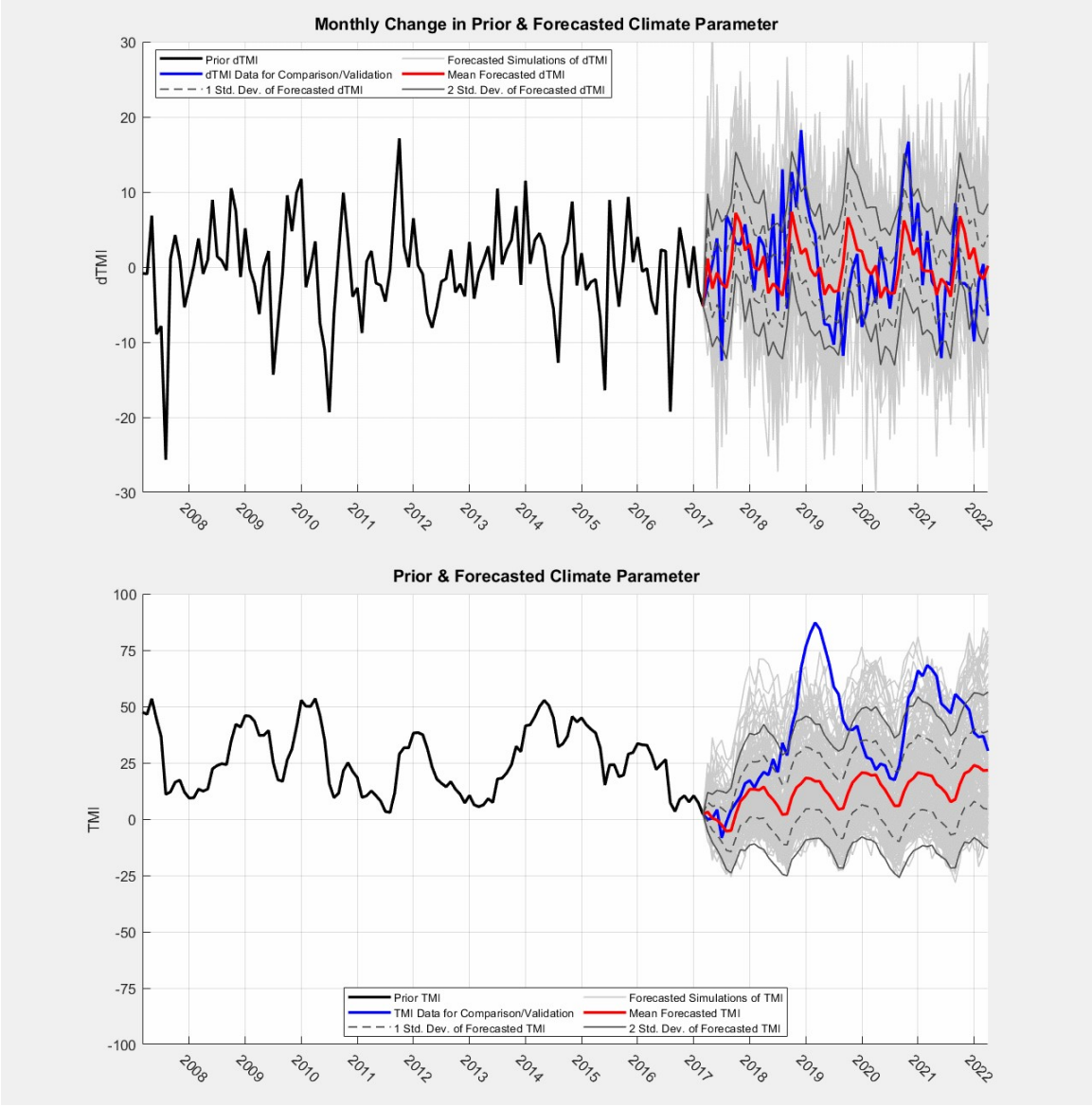

Figure 4-5 Prior and Forecasted Monthly TMI from 03/2017 to 03/2022 for Arlington, VA (NOAA Station USW00013743)

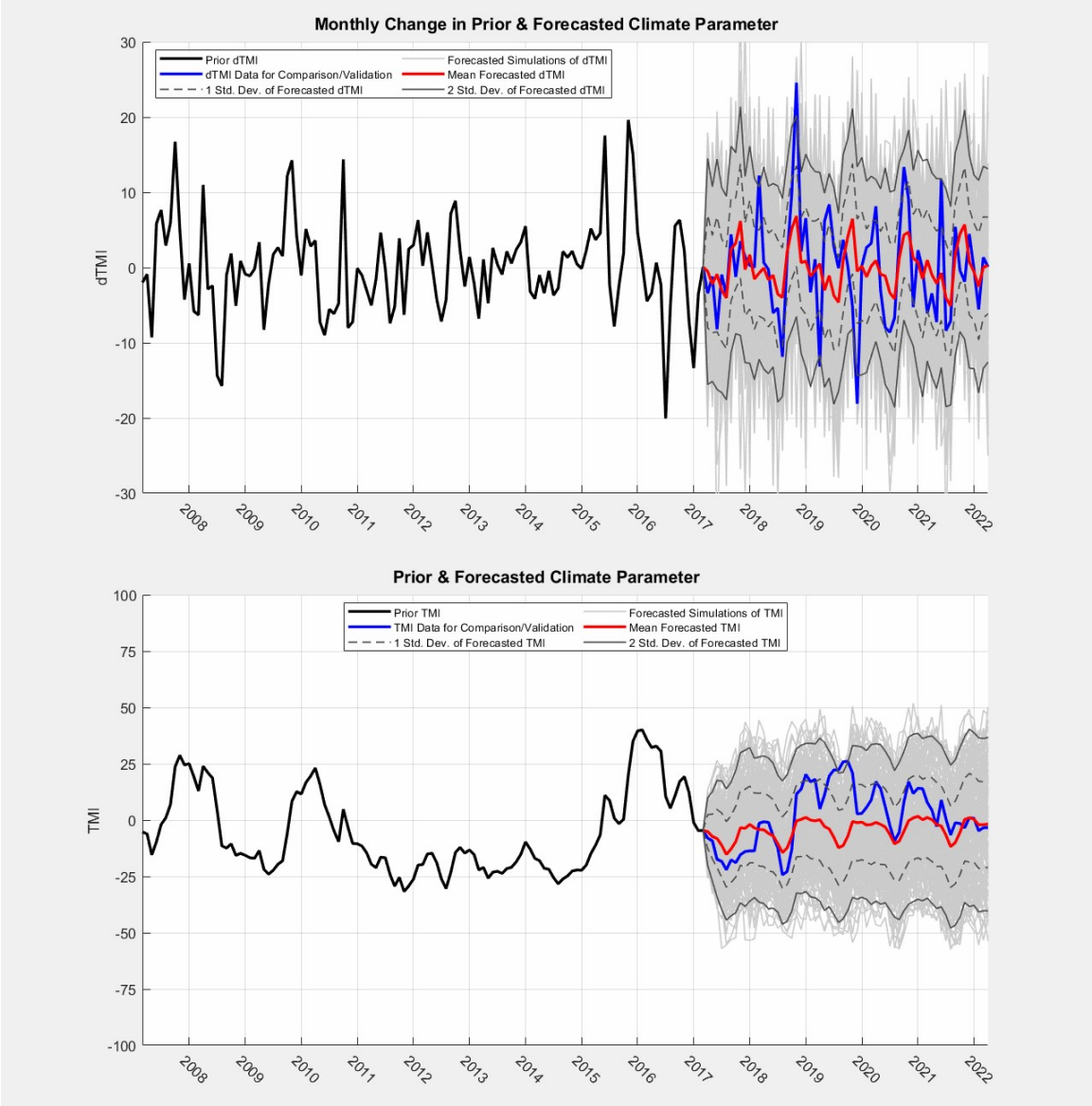

Figure 4-6 Prior and Forecasted Monthly TMI from 03/2017 to 03/2022 for Dallas, TX (NOAA Station USW00013960)

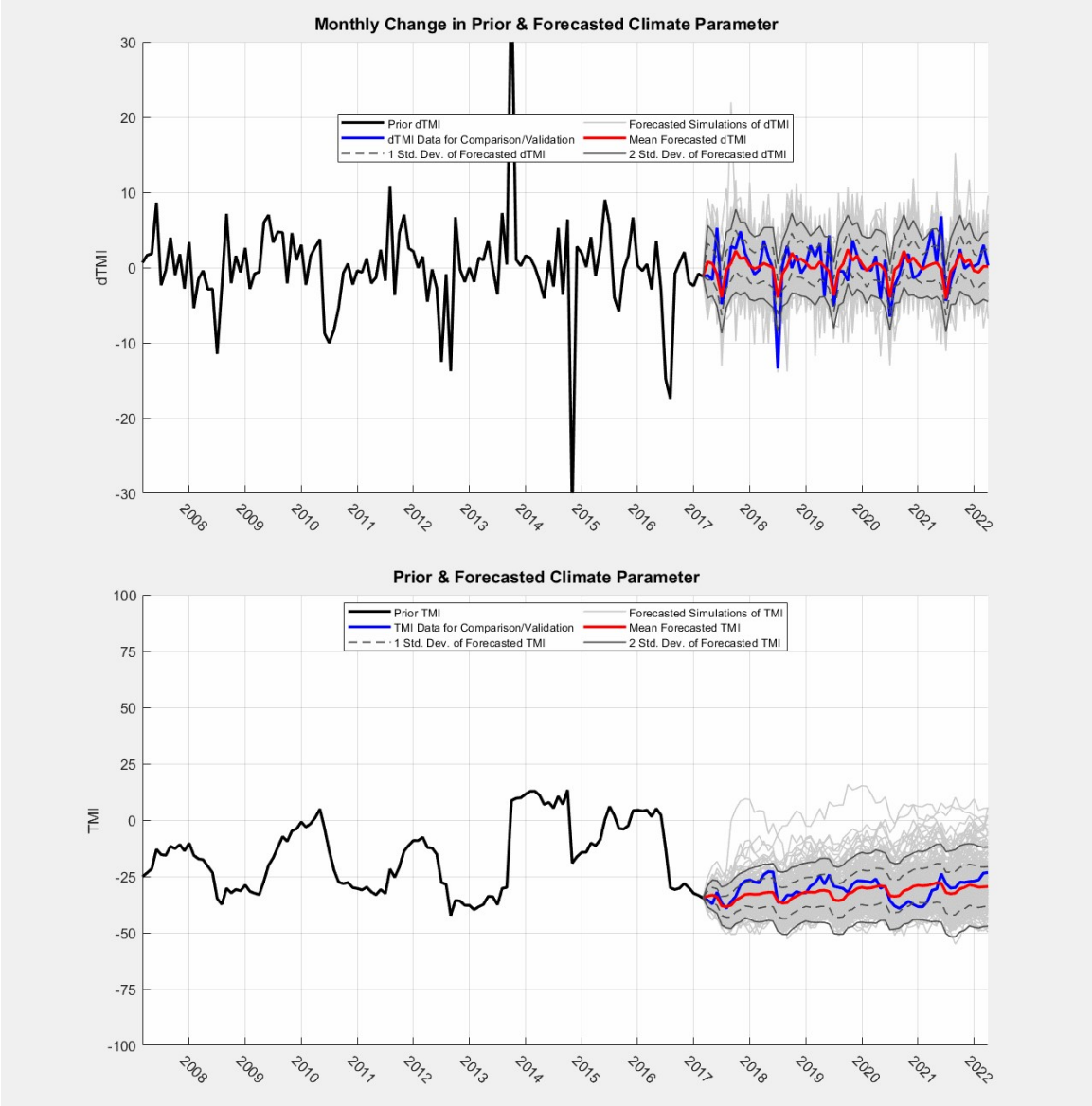

Figure 4-7 Prior and Forecasted Monthly TMI from 03/2017 to 03/2022 for Denver, CO (NOAA Station USW00023062)

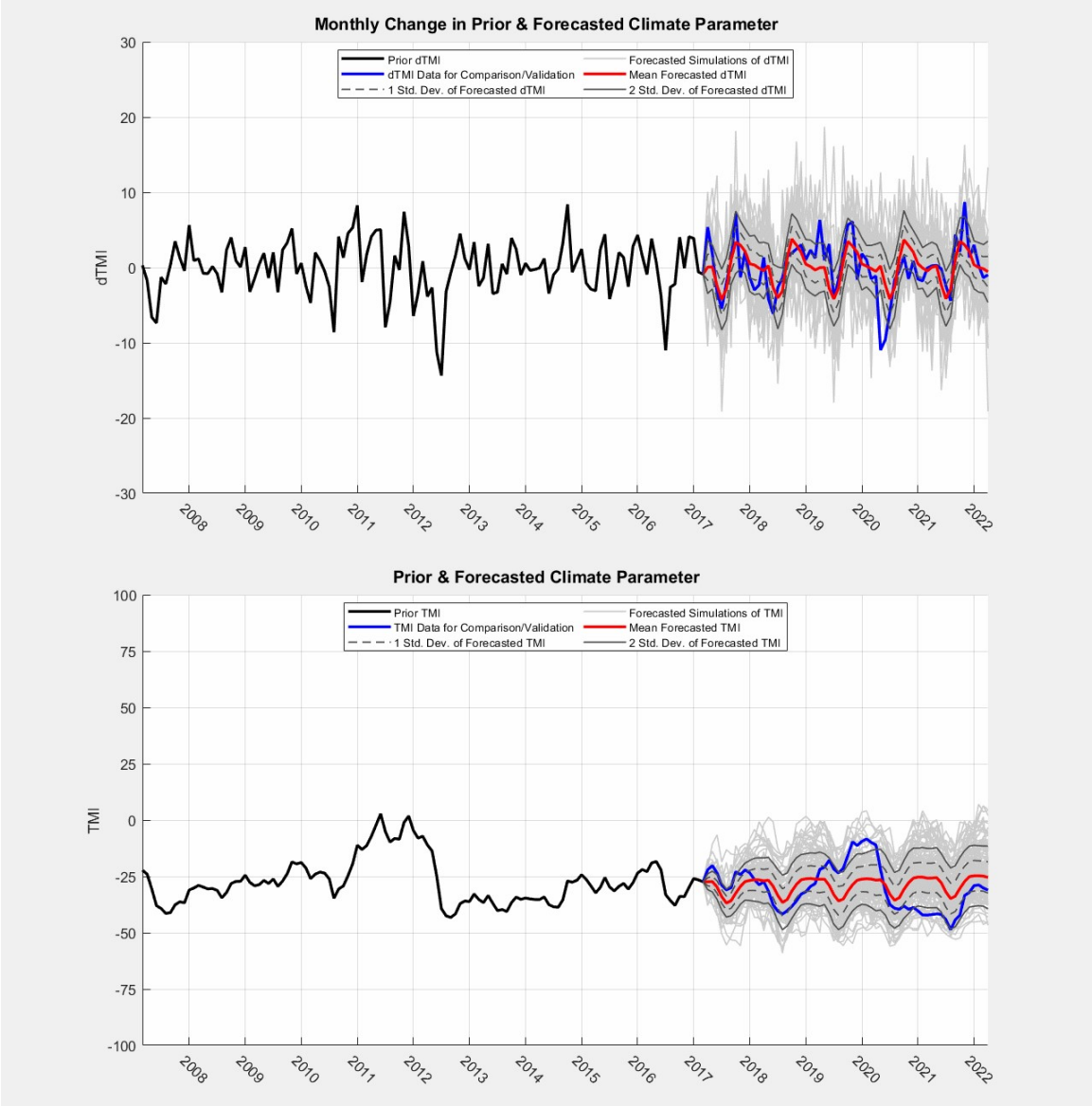

Figure 4-8 Prior and Forecasted Monthly TMI from 03/2017 to 03/2022 for Salt Lake City, UT (NOAA Station USW00024127)

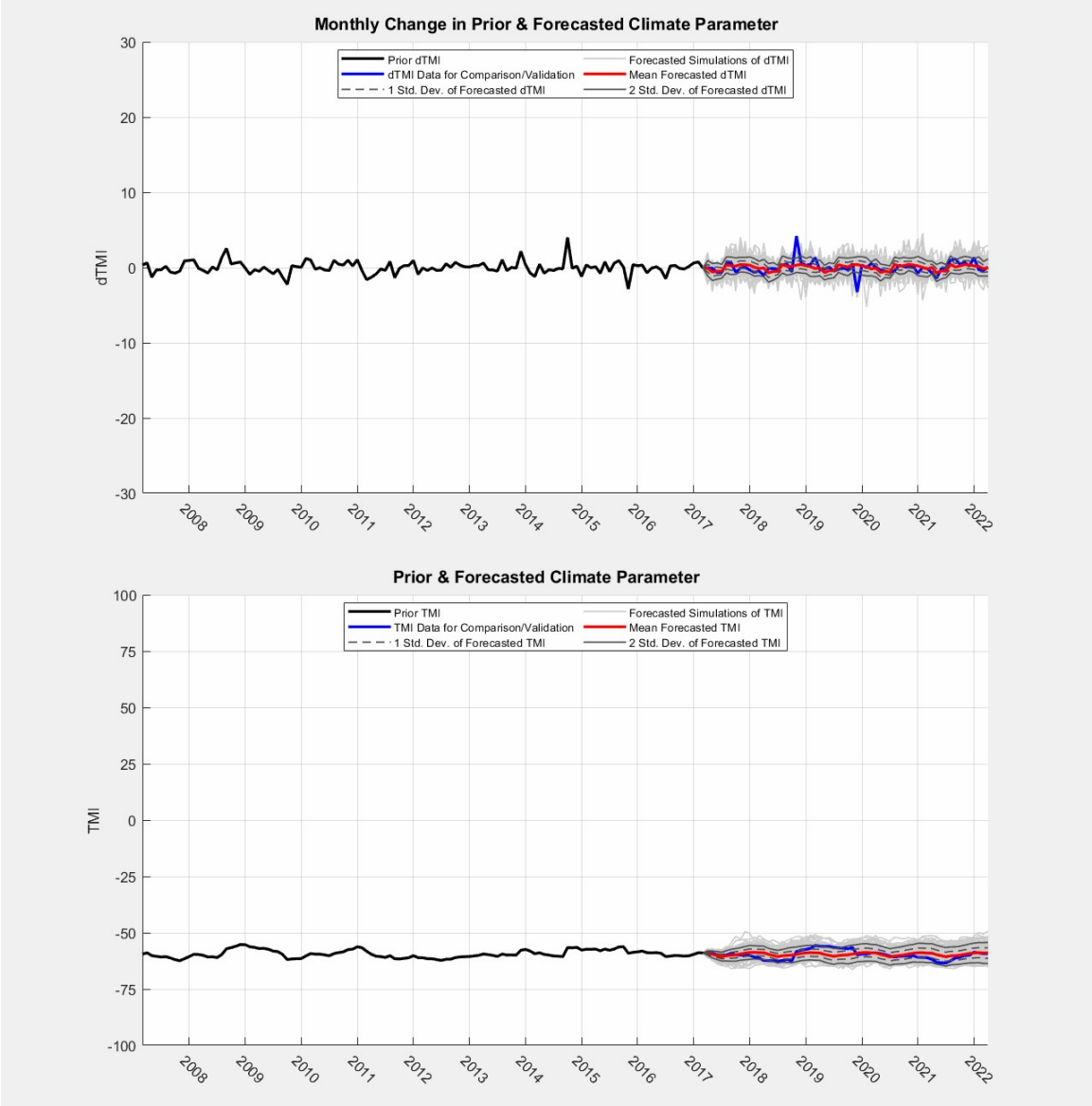

Figure 4-9 Prior and Forecasted Monthly TMI from 03/2017 to 03/2022 for Tempe, AZ (NOAA Station USW00013743)

Based on a visual evaluation of the forecasted TMI and monthly change in TMI of the five locations presented in Table 4-1, the following conclusions cans be made regarding the validation of proposed model.

- The prior TMI data (30 years) of the wet coastal/alpine location in Arlington, VA exhibited relatively high seasonal variation. The forecasted *dTMI* captures most of the true data within one standard deviation from the forecasted mean and nearly all of the extreme values of the true data are captured within two standard deviations from the forecasted mean. The individual forecasted chains of *dTMI* resulted in show that there were several forecasted chains which consisted of extreme values greater than both the prior data and the true data within the forecast period. Although the *dTMI* forecast provides adequate representation of the true data and the variability of the prior data, the TMI forecast fails to encompass the extreme wetting period between 2017 and 2020 within two standard deviations of the mean, which is most likely caused by this period exhibiting TMI values higher than data from the 30 years of prior data.
- The example forecast for the wet temperate to temperate location in Dallas, TX resulted in a relatively better fit to the true data. Although the *dTMI* forecast does not fully capture all extreme values within two standard deviations from the mean, the corresponding TMI forecast data does encompass the extreme events within 2 standard deviations. This improvement may be due to the four years of relatively dry (low) TMI values followed by a two-year period of wetter (increased) TMI values just before the start of the forecast period. Additionally, the period of wetting prior to the forecast period consists of higher TMI values that the true data within the forecast period. Overall, the Bayesian TMI forecast model for this example location in a wet temperate to temperate climate region

produces forecasted values which adequately represent the variability of the prior data and encompassed the potential extreme events

- The example forecasts for the dry temperate and semi-arid locations of Denver, CO and Salt Lake City, UT, respectively, produced promising results for the forecasted *dTMI* and TMI data. The moving of the forecasted *dTMI* is similar to the true values within the forecast period with the exception of a few extreme values. The standard deviations of the forecasted *dTMI* data are much closer to the mean values, compared to the wet coastal/alpine and wet temperate to temperate examples. This reduction in forecasted variability is also observed on the forecasted TMI plots, without a noticeable reduction in the over forecast performance. Most of the true TMI data for both the dry temperate and the semi-arid example are encompassed within one standard deviation from the forecasted mean with the exception of one extreme period in the Salt Lake City example from 2019 to 2020, which falls just outside two standard deviations from the forecasted mean.
- The example forecast for the arid location of Tempe, AZ also produced a relatively good fit to the true data, although the variability and volatility in both TMI data for this climate region was minimal.

4.5.1 Performance of the Bayesian TMI Forecast Model

Overall, the visual evaluation of the Bayesian TMI forecast model for the five locations explored herein provide an adequate job of producing forecasted data which exhibit near the same seasonal averages and monthly variation as the prior and the true

data within the forecast period. The forecast model appeared to perform best for the dry temperate and semi-arid locations which is a promising outcome for the potential implementation for unsaturated soil shrink-swell volume change analysis as these climate regions are commonly associated with expansive soil related issues to infrastructure. The performance of the model in the arid region is tough to evaluate using the Tempe, AZ example as the variability of the prior data was minimal. It appears that the climate within this region is relatively stable which would indicate that the issues with shrink-swell soils would be governed by extreme events and not the natural seasonal moisture variations.

To further evaluate the performance of the Bayesian TMI forecast model, the histograms of the monthly parameterized priors and posterior (forecasted) *dTMI* and TMI values were generated and are presented in Appendix E for each of the five locations used in the validation study. Figure 4-10 and Figure 4-12 present the *dTMI* and TMI prior and posterior histograms, fitted with normal distributions, for the Arlington, VA validation study location, respectively. Figure 4-11 and Figure 4-13 present similar data for the Dallas, TX validation study location.

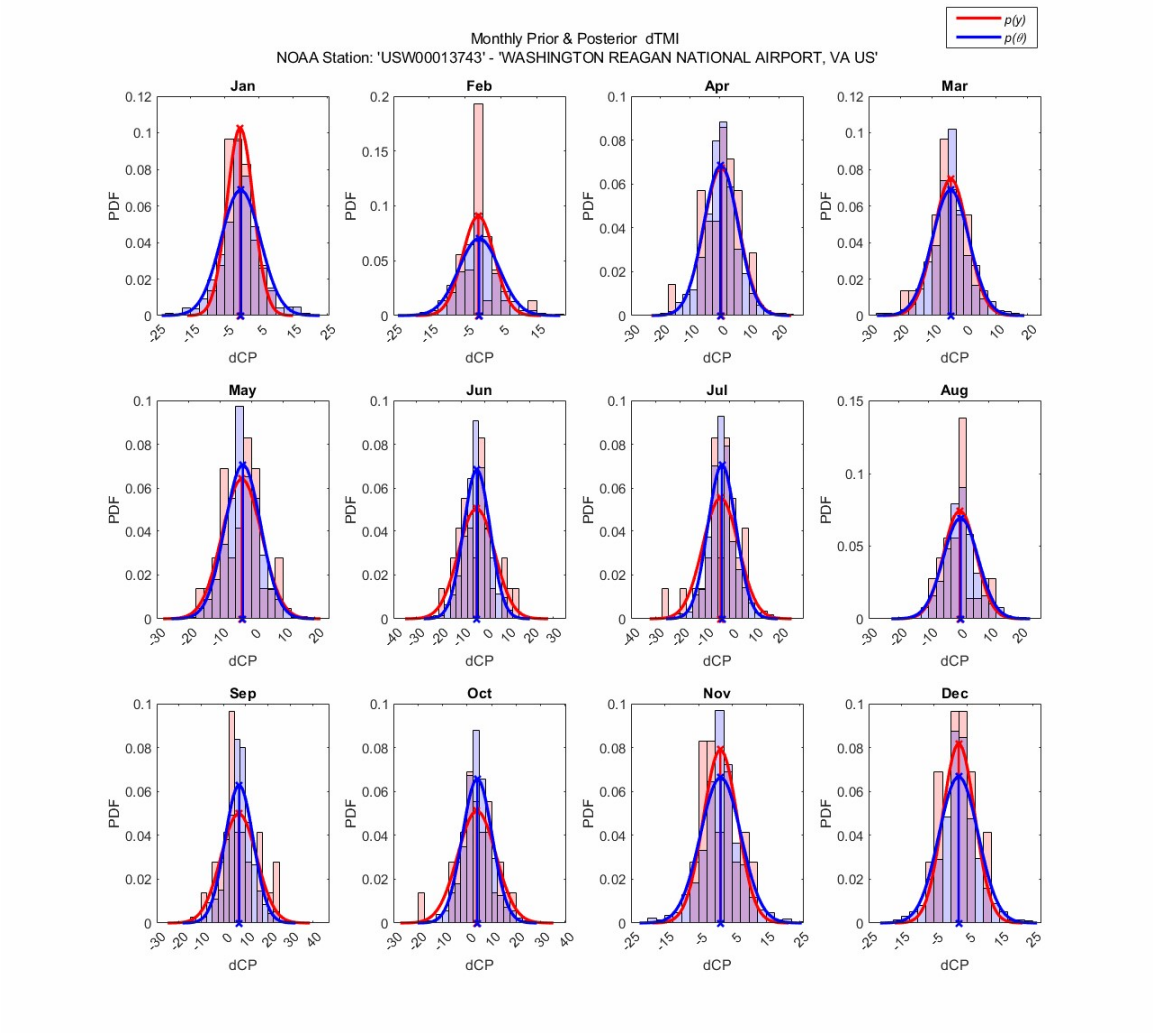

Figure 4-10 Histograms of Prior and Posterior (forecasted) Monthly Change in TMI for the Arlington, VA Validation Study Site from 03/2017 to 03/2022.

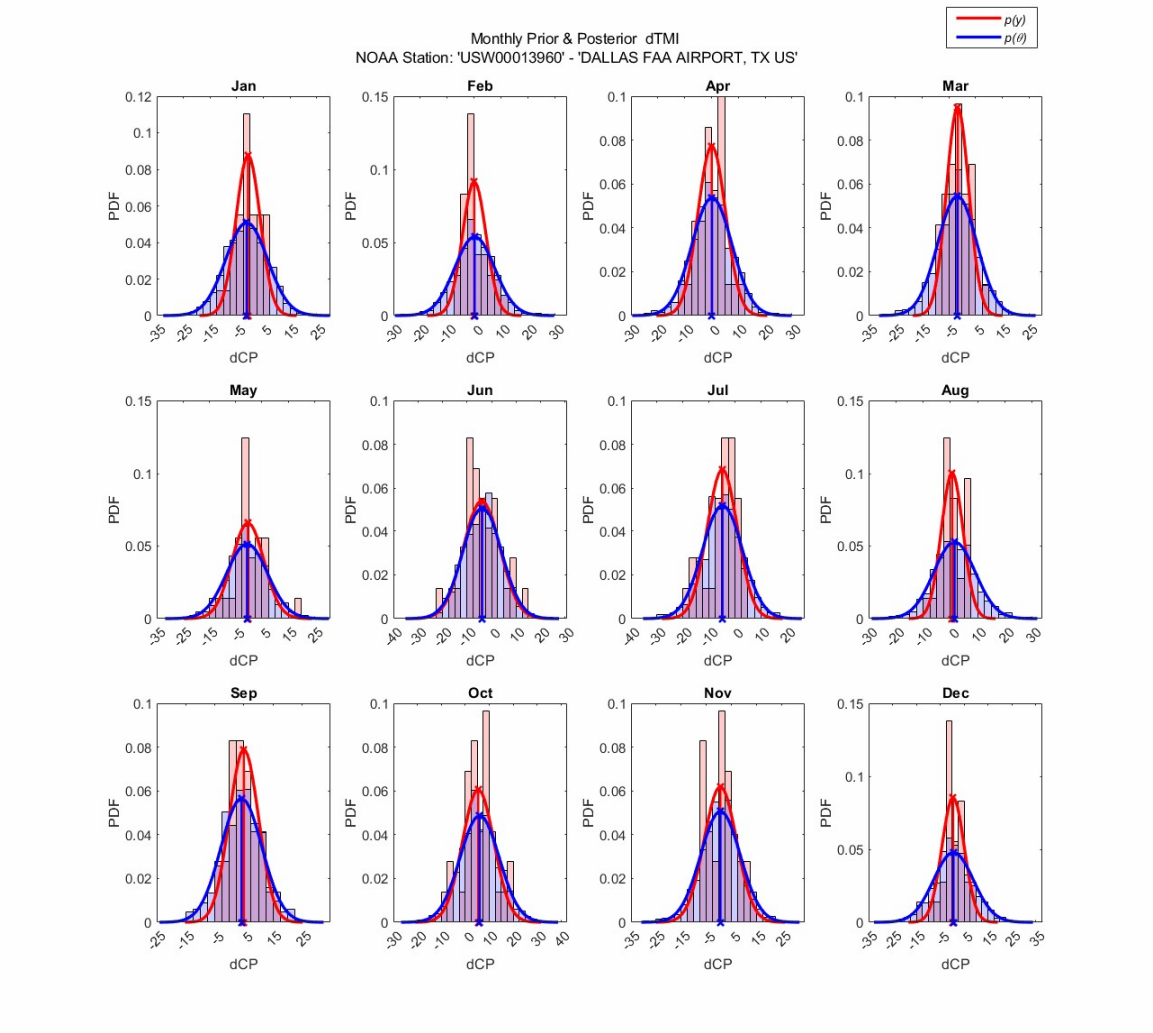

Figure 4-11 Histograms of Prior and Posterior (forecasted) Monthly Change in TMI for the Dallas, TX Validation Study Site from 03/2017 to 03/2022.

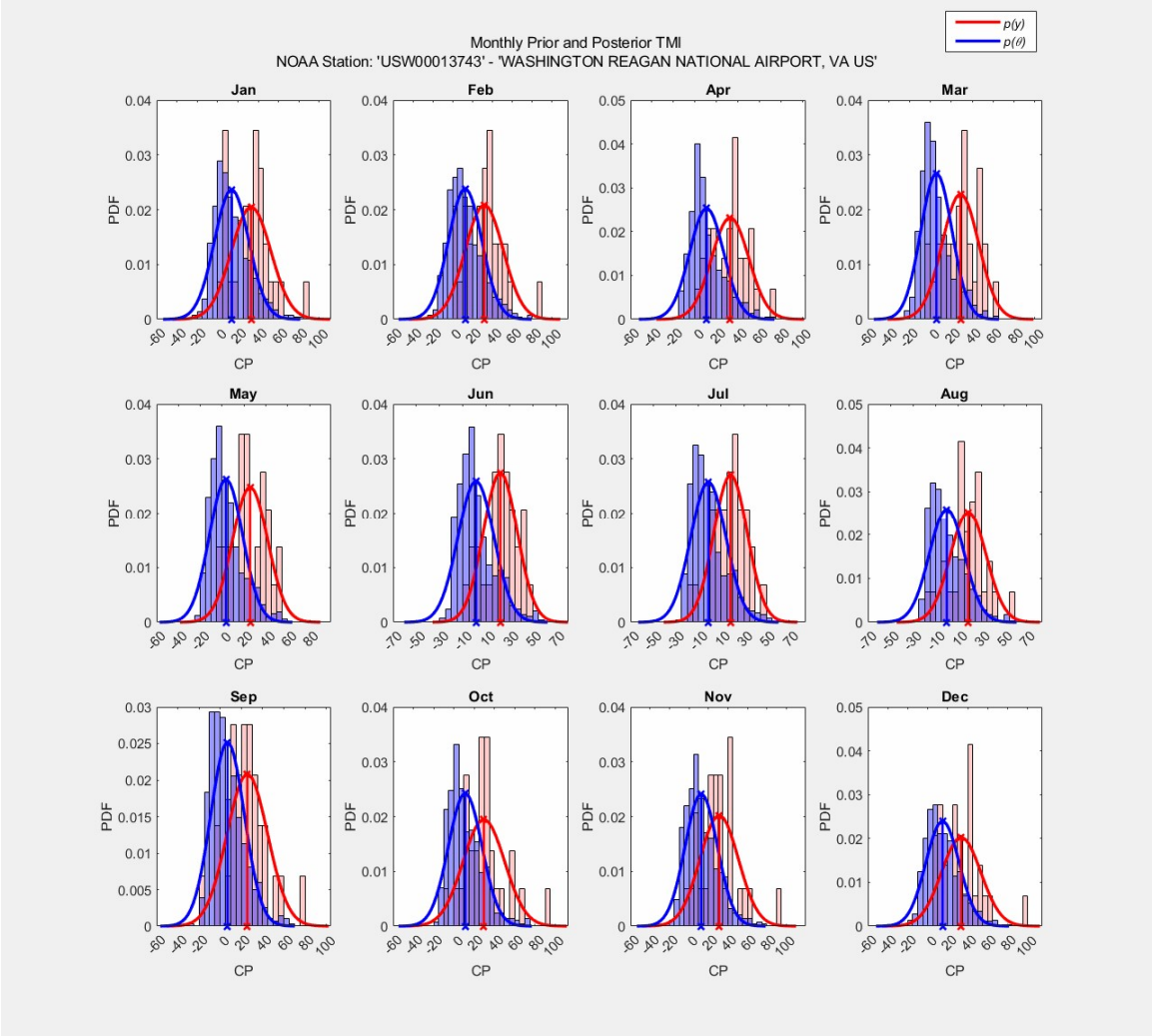

Figure 4-12 Histograms of Prior and Posterior (forecasted) TMI for the Arlington, VA Validation Study Site from 03/2017 to 03/2022.

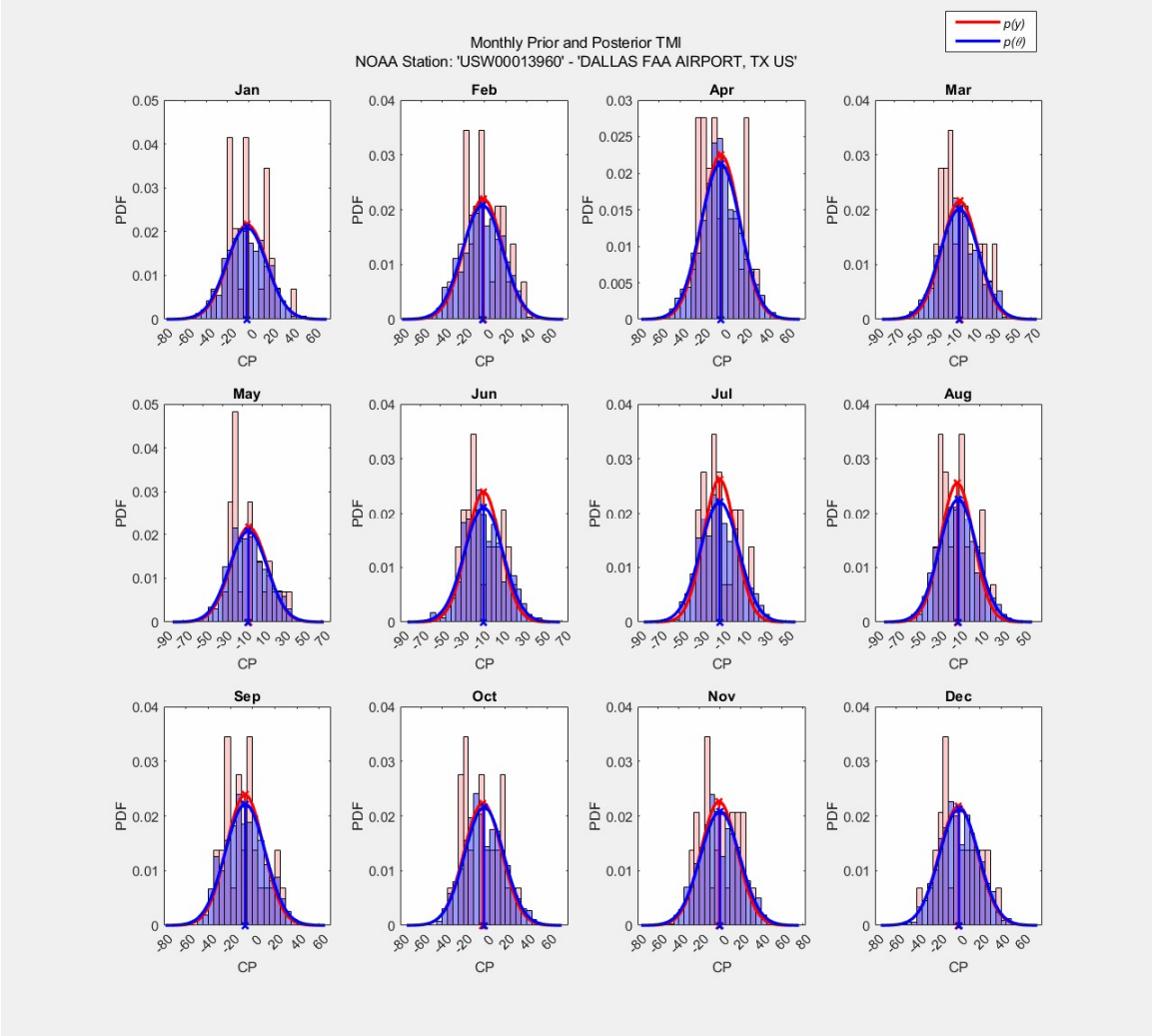

Figure 4-13 Histograms of Prior and Posterior (forecasted) TMI for the Dallas, TX Validation Study Site from 03/2017 to 03/2022.

The *dTMI* histograms for the Arlington study location indicate that posterior data produced by the Bayesian TMI forecast model resulted in a reduction of variability of the monthly data compared to the priors, which can be observed by the narrower distribution fit and increased frequency of values near the mean (i.e., increased kurtosis). This is not a favorable result as the forecast model under predicts the variability of the historical data. The TMI histograms for the Arlington study site display another unfavorable outcome of

the forecasted data as the average of each monthly posterior distribution noticeably differs (more positive) than the average of the prior distributions. This indicates that the forecast model is not producing data which follows the mean of the historical prior data. These two lack of fits between the forecasted posterior data and the historical prior data may be what caused the lack of fit of the extreme event shown previously in Figure 4-5.

In contrast, the prior and posterior histograms for the *dTMI* values for the Dallas, TX study location indicate that the Bayesian TMI forecast model is over predicting the variability of the prior data (decreased kurtosis) for most of the months; and the distruibtuions of the TMI prior and posterior data show that the model is producing nearly equivalent means for each of the monthly priors.

4.5.2 Stability of the Bayesian TMI Forecast Model

The stability of the Bayesian TMI Forecast Model was tested by performing forecast simulations for differing starting seasons/dates, over varying forecast durations (2 to 20 years), for the five locations used in the validation study. The graphical results of the stability analyses are presented in Appendix F. In summary, the forecast model performed sufficiently and efficiently regardless of the initial conditions and the duration of the forecast period. However, the stability of the model was not tested using priors with limited or missing data, or at locations were the average TMI is near the limits of either -100 or 100.

4.6 Potential Future Improvements to the Bayesian TMI Forecast Model

The research efforts produced useful frameworks for the stochastic forecast of the climatic parameter TMI using time-series and Bayesian Inference techniques Although the proposed model produced promising results for the sites explored in the validation study, which has potential for several further improvements.

- The inclusion of multiple weather station data should be incorporated into both the deterministic and the stochastic models. For the deterministic model, a decision would have to be made to use the average monthly data, or another statistically representative monthly value. Although it is not a straightforward analysis, the most conservative approach would be to use the monthly data which results in the greatest monthly changes and/or seasonal variations, regardless of the location of the weather station (assuming only weather stations near the site that are chosen).
- Improvement and optimization of the Bayesian forecast model for the climatic parameter TMI to include an adaptive Langevin Markov Chain (LMC) or a Hamiltonian Markov Chain (HMC) which incorporates a physics-based approach to control the stability and limit the random walk potential of the simulated time-series by representing the MCMC framework as energy equations (potential and kinetic). The HMC framework also includes a leap-frog step which can significantly optimize the computation time of the MCMC simulation.
- Evaluation of extreme climate events (in perspective of TMI) with the potential development of a Bayesian probability model which can force the forecasted TMI

values to include some percentage and probability of extreme events into the forecasted data.

4.6.1 Limitations of the Bayesian TMI Forecast Model

The author recommends that the models be treated as preliminary framework which needs further optimization, validation, and sensitivity analyses, the following efforts should be performed as part of future research work:

- As displayed in the outcome of the Arlington, VA validation study, the proposed Bayesian TMI forecast model has potential to miss extreme events which were not characterized by the 30 years of prior climate data.
- The Bayesian TMI forecast model presented herein is programmed to produce forecasts which sufficiently represent the variability and volatility of the prior data without "walking" too far from the prior distributions. If a more conservative approach is warranted which encompasses some pre-defined increase in the variability/volatility of the forecasted data, the tuning criteria can be increased by either increasing the initial tuning factor to be greater than 2.4. An additional stability study should be performed in such a case.

CHAPTER 5

5 STOCHASTIC SHRINK-SWELL VOLUME CHANGE FORECAST MODEL

5.1 Introduction

This chapter brings together the deterministic shrink-swell soil volume change model and the stochastic TMI model to produce a new method for forecasting the monthly shrink-swell soil volume. A discussion of potential implementation of the proposed stochastic shrink-swell soil volume change model to foundation and pavement performance analysis/design will also be included. The uncertainty and sensitivity of the estimations using the proposed method will be compared to those generated from current practice.

5.1.1 Objectives

The following objectives were accomplished as part of this study:

- Review and choose the deterministic SSVC framework which is to be incorporated into the stochastic analysis.
- Development of a framework for stochastically estimating the volume change on shrink-swell soils using the previously developed models for random soil property generation and monthly TMI forecasting.
- Exploration of the stability and sensitivity of the proposed shrink-swell forecast model.
- A comparison of the proposed models to the existing engineering practice including the differences in the uncertainty and sensitivity of the estimates.

- Exploration of the potential implementation of the proposed stochastic shrink-swell soil volume change model to foundation and pavement performance analysis/design.

5.2 Deterministic Shrink-Swell Volume Change (SSVC)

The ability to estimate soil volume change as a function of time is a valuable tool in the design of shallow foundations of pavement structures. Specifically pertaining to pavement design, estimating soil volume change as a function of time allows for the prediction of the potential cumulative International Roughness Index (IRI). The time-varying volume change can also be a valuable tool in the forensic analysis of existing foundation movement of a lightly loaded structure on shallow footings.

The author and members of the ASU research team (Zapata and Mosawi) published a paper in 2021 in the Soil and Rocks International Journal of Geotechnical and Geoenviromental Engineering titled “An Improved Framework for Volume Change of Shrink/Swell Soils Subjected to Time-Varying Climatic Effects”. The paper presents an improved framework for estimating the volume change of shrink-swell soils due to time-varying climatic effects using the Lytton et al. (2005) approach with the suction envelope models created by Vann and Houston (2021). The proposed framework for estimating soil volume change of shrink-swell soils as a function of time is presented with an example calculation with data from an AASHTO Long-Term Pavement Performance (LTPP) Seasonal Monitoring Program (SMP) section TX 48-1068 (FHWA, 1995), which is located approximately 80 miles northeast of Dallas, Texas. The framework presented is applicable to uncovered sites where the groundwater table effects are negligible, but it

has been calibrated to account for covered areas and for the spatial variation between the pavement center and edges.

Refer to Appendix B for the full paper which includes a detailed background, evaluation, and recommendations regarding suction-volume change analysis of Shrink-Swell soils. The following outline summarizes the steps of the improved framework for estimating the volume change of shrink-swell soils due to time-varying (monthly) climatic effects:

1. Weather station identification and data extraction
2. 30-year and monthly Thornthwaite Moisture Index per Witczak et al. (2006)
3. Determination of equilibrium suction envelope parameters per Vann and Houston (2021): depth to equilibrium suction and magnitude of equilibrium suction
4. Back-calculation of variables for Mitchell's (1979) equation
5. Development of long-term wet and dry suction profiles
6. Initial estimation of monthly changes in suction at the surface per Perera (2003)
7. Fourier equation fit to the monthly suction change at the surface
8. Generation of monthly suction profile
9. Suction profile adjustments for varying surface boundary conditions
10. Calculation of net normal stress profile
11. Estimation of suction compression index (assuming value is not directly measured)
12. Calculation of strain on a monthly basis
13. Calculation of volume change on a monthly basis

The above deterministic framework is used in the stochastic analysis presented herein. Figure 5-1 presents a flow chart for the deterministic SSVC procedure.

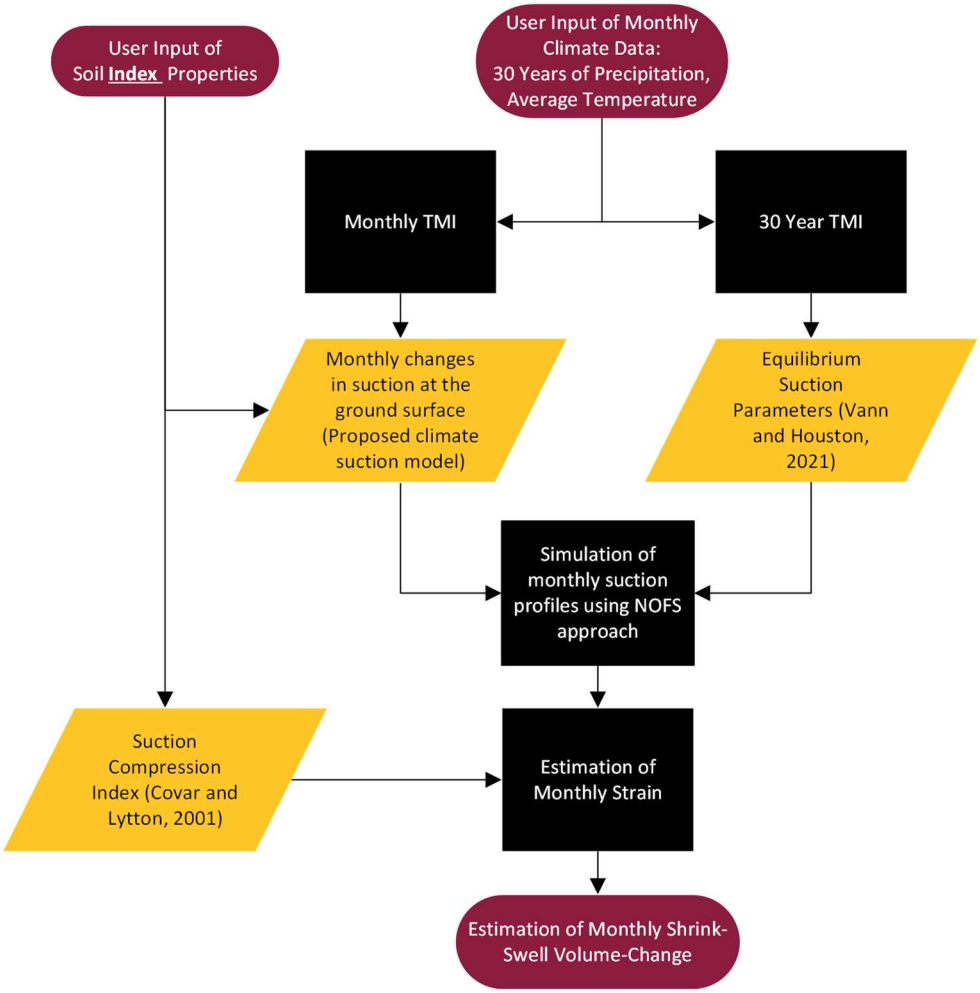

Figure 5-1 Flow of the Deterministic SSVC Analysis Procedure

5.2.1 Suction-Volume Change Relationship

Direct laboratory measurements of the volume change potential of a soil help improve the estimation of potential volume change in the field. The 1-D oedometer

"Response to Wetting Test" as described in ASTM D4546 is the common type of laboratory test for volume change determination. One key difference from the laboratory oedometer test compared to the field conditions the soil will experience is the final degree of saturation. The response to wetting test inundates the sample, driving to almost full saturation. However, it is the probability that the soil will reach this moisture level over the period of the structure/pavements design life is very low (Houston and Houston 2017).

A common method for volume change estimation is the Potential Vertical Rise published by the Texas Department of Transportation (TxDOT-12-E, 1978), which includes both empirical-based relationships and result from an oedometer test. In 2005, the Texas DOT updated the approach to determining the volume change of expansive soils using the work by Lytton et al. (2005), which encompassed a suction-based approach. The study concluded that the previous empirical-based approach significantly over-estimated the soil heave and did not account for the shrinkage of the soil during dry climatic periods.

A thorough literature review of volume change estimates of unsaturated soil (odometer-based, or suction-based) was performed by Vann (2019). The authors of this paper have carefully reviewed this relative literature summary as part of the research leading up to this paper.

The evaluation of moisture-driven volume change of unsaturated clay soil requires consideration of the net normal (p) and the matric suction (s) stress states. For clays under relatively light confinement, increases in s during drying will typically cause clays to

decrease in volume (compress or shrink) and reductions in *s* during wetting will cause increases in volume (expansion or swell). Clay soils at high net normal stress states can also reduce in volume (collapse) during wetting (Houston and Zhang, 2021; Nooray, 2017). The volumetric response is commonly expressed in terms of changes in void ratio (*e*), and the general relationship between *e*, *p* and *s* for clay soils is represented using three-dimensional (3D) state surfaces (Alonso et al., 1994, 1999; Delage & Graham, 1996; Fredlund & Morgernstern, 1976; Gens & Alonso, 1993; Gens et al., 2016; Wheeler & Sivakumar, 1995; Vu & Fredlund, 2004; Wray et al., 2005; Zhang & Lytton, 2009a, 2009b). For many foundation and pavement applications in engineering practice, vertical deformations govern the design which allow for the *e-p-s* relationship to be analyzed using one-dimensional (1D) at-rest (K_0) conditions - or at least the 1-D analyses provide adequate information for decision making (Adem & Vanapalli, 2013; Fredlund et al., 1980; Houston & Houston, 2018; Lytton, 1997; Nelson & Miller, 1992; Nelson et al., 2015; Overton et al., 2006).

The author and research team (Zapata, Houston, and Mosawi) have produced a publication regarding this topic, titled “Suction-Volume Change Indices for Natural and Recompacted Clay Soils”, which will be published in the proceedings of the 2023 American Society of Civil Engineer’s (ASCE) Geo-Institute’s (GI) annual national conference, GeoCongress 2023. The paper draft is included in Appendix C and should be considered the opinions of the authors only, until the expected publication by ASCE in 2023. To minimize repetition, only a summary of the study is included herein.

The study presents a comparison of the matric suction-volume change indices (for 1-D monotonic loading by wetting or drying) of intact clays (natural soil stress states) using relatively undisturbed specimens tested by Olaiz (2017), to those of reconstituted/compacted specimens measured by Singhal (2010) and Mosawi (2022) using OPPDs, including the Fredlund SWCC (SWC-150) developed by GCTS in Tempe, AZ. Singhal (2010) created a unique database from laboratory measurement of the mechanical response of clay soils under imposed conditions of both stress state variables using the OPPD, with attention on evaluation of a substantial portion of the void ratio state surface for clay soils. Olaiz (2017) and Mosawi (2022) continued the exploration of testing relatively intact and reconstituted soil specimens in the OPPD, respectively. The materials tested by Olaiz and Mosawi were obtained from locations associated with expansive soil areas in San Antonio, TX, and Denver, CO (same study sites previously analyzed in this document). The compilation of data from these extensive laboratory efforts was used to provide qualitative and quantitative comparisons of the mechanical response of reconstituted to relatively intact specimens.

Refer to Appendix C for the full (draft) document which includes a detailed background, evaluation, and recommendations regarding suction-volume change analysis of Shrink-Swell soils.

The comparison of the matric suction-volume change indices of the intact samples from Olaiz (2017) resulted in significantly lower magnitude volume change than those of the remolded samples tested by Singhal (2010) and Mosawi (2022) for similar range of *wPI* specimens and suction range. A brief statistical analysis using descriptive statistics,

box plots, and 1:1 comparison indicated that for the compiled dataset, *wPI* provides a useful indicator for volumetric response for remolded specimens under relatively light confining stress. The data also demonstrated the critical role of stress history in shrink/swell response of clays to changes in moisture state. The data from the two-stress state controlled OPPD results provides a substantial start for development of *e-p-s* relationships and correlations for expansive clay soils.

5.2.2 2D SSVC Estimates for Pavements

To account for covered areas, pavement or moisture barriers, a regression model was developed by Jayatilaka (1999) to estimate the vc movement using two programs developed by Gay (1994), MOPREC and FLODEF. The idea is to estimate the relationship between 1-D and 2-D vertical movement. Such analysis can be used to adjust suction profiles to consider boundary conditions, such as comparing the suction change at the edge of a covered area and the middle of the covered area, Figure 5-2, or using moisture barriers, Figure 5-3. Calibrated using data collected from ten sites located in Texas within three different climatic regions, the model is as follows:

$$\frac{VM_{2D}}{VM_{1D}} = \xi_1 \exp\left(\left(\xi_2 \frac{d}{D}\right)^{\xi_3}\right) \tag{104}$$

Where, VM_{2D} is the two-dimensional vertical movement from the FLODEF program, VM_{1D} is the one-dimensional vertical movement from the MOPREC program, d is the distance from the center of the pavement to the point where the vertical movement needs to be calculated in m, D is half width of the pavement in m, and ξ_1, ξ_2 ,ξ_3 are regression coefficients.

For pavement width less than 18.0 m:

$$\begin{aligned}\xi_1 &= 0.0561 + 1.5872\left(d_{am}\right) + 0.1244\left(S_m\right) - 0.1936\ln\left(D\right) \\ &-0.0007139\left(VM_{1D}S_m\right) - 0.1443\left(D_b d_{am}\right)\end{aligned} \tag{105}$$

$$\begin{aligned}\xi_2 &= -0.068 + 0.09134\left(S_m\right) - 0.101\left(D_b\right) - 0.000188\left(TMI^2\right) + 0.321\ln\left(D\right) \\ &+0.000153\left(VM_{1D}S_m\right) + 0.000706\left(VM_{1D}D_b\right)\end{aligned} \tag{106}$$

$$\xi_3 = \exp\begin{bmatrix}1.8061 - 0.4397\left(S_m\right) + 0.4711\ln\left(D\right) + 0.08855\left(D_b^{\,2}\right) \\ -0.000143\left(VM_{1D}TMI\right) + 0.003022\left(VM_{1D}D_b\right) - 1.2592\left(D_b d_{am}\right)\end{bmatrix} \tag{107}$$

For pavement width greater than 22.0 m:

$$\begin{aligned}\xi_1 &= 0.376 + 0.4141\left(d_{am}\right) + 0.04078\left(S_m\right) - 0.0924\left(D_b\right) \\ &-0.00426\left(VM_{1D}S_m\right) - 0.02584\left(D_b d_{am}\right)\end{aligned} \tag{108}$$

$$\begin{aligned}\xi_2 &= -0.068 + 0.09134\left(S_m\right) - 0.101\left(D_b\right) - 0.000188\left(TMI^2\right) + 0.321\ln\left(D\right) \\ &+0.000153\left(VM_{1D}S_m\right) + 0.000706\left(VM_{1D}D_b\right)\end{aligned} \tag{109}$$

$$\xi_3 = \exp\begin{bmatrix}3.5562 - 0.8125\left(S_m\right) + 0.3707\ln\left(D\right) + 0.05649\left(D_b^{\,2}\right) \\ -0.000306\left(VM_{1D}TMI\right) - 1.6175\left(VM_{1D}D_b\right) - 0.4207\left(D_b d_{am}\right)\end{bmatrix} \tag{110}$$

Where, VM_{1D} is the vertical movement from 1-D program in mm, D_b is the depth of barrier in m, d_{am} is the depth of available moisture in m, D is half width of the pavement in m, S_m is the mean suction at site in pF, and TMI is the Thornthwaite Moisture Index.

For pavement widths between 18.0 m and 22.0 m:

$$\xi = \frac{\left[\xi_{18}\left(22 - D\right) + \xi_{22}\left(D - 18\right)\right]}{4} \tag{111}$$

Where, ξ is the parameter ξ_1 ,ξ_2 or ξ_3 for a pavement width of D, ξ_{18} is the parameter ξ_1 ,ξ_2 or ξ_3 estimated from the equations for the pavement widths less than 18.0 m, and ξ_{22} is the parameter ξ_1 ,ξ_2 or ξ_3 estimated from the equations for the pavement widths less than 22.0 m.

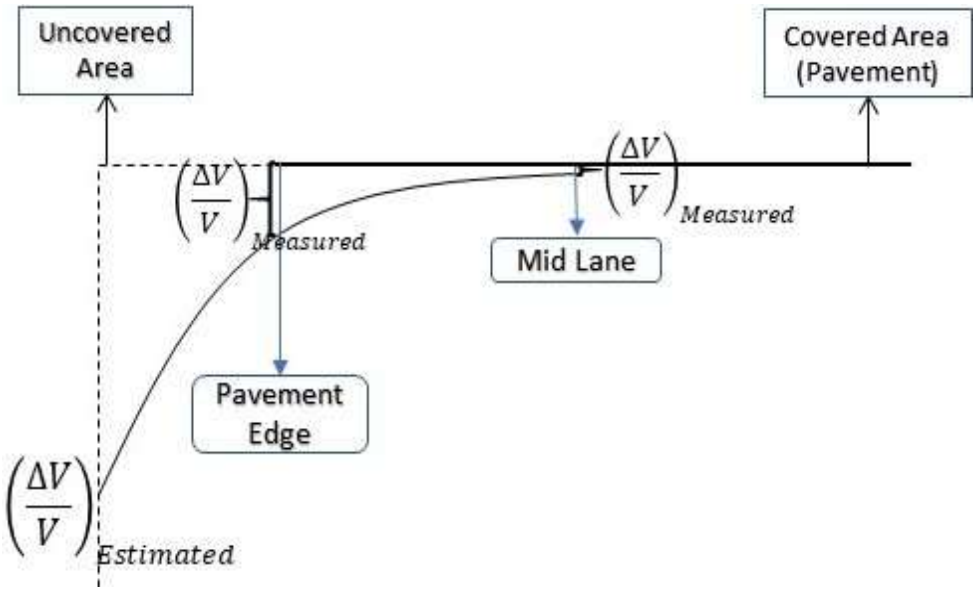

Figure 5-2 Volume Change Due to Change in Suction in Uncovered Area Compared to Different Locations under Covered Area

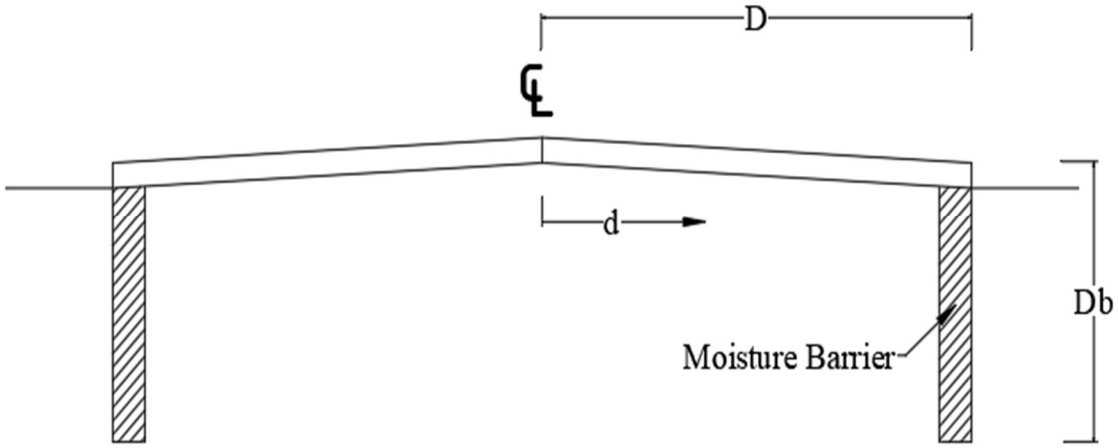

Figure 5-3 Typical Cross-Section of a Pavement with Vertical Moisture Barriers (Jayatilaka, 1999)

Lytton describes the depth of available moisture as the "maximum depth of the moisture that may be stored within the rooting depth of the soil profile." (Jayatilaka, 1992). This definition was expanded upon by Gay in 1994:

> "The depth of available moisture is the maximum depth of moisture available for use by transpiring vegetation, which is assumed to be stored within the rooting depth of the soil profile. This depth is dependent on the type and texture of the soil and the rooting depth; it is not dependent on the type of vegetation. It therefore represents the maximum depth of moisture that is lost from a soil during a transition from its wet state at field capacity to its dry state at the root potential (pF 4.2 - 4.5) of resident vegetation. Typical values for this depth have been reported to be between 5 cm and 20 cm (Thornthwaite 1948, Penman 1963); however, values as high as 27 cm have been reported for heavy clays at sites in Texas (Richardson and Ritchie 1973) and the Netherlands (Bouma and de Laat

1981)."

Gay (1994) also states that the depth of available moisture can be determined numerically by integrating a soil water characteristic curve (SWCC), over the root depth zone, between the saturation moisture content and the residual moisture content. Jayatilaka (1999) expresses the simplified triangular integration used to determine the depth of available moisture.

Gay (1994) and Jayatilaka (1999) state that if the soil-specific residual moisture content is unknown, the wilting point of vegetation (4.2 pF) or the air-dried state (5.7 pF) can be used depending on the general field conditions.

5.2.2.1 Effect of Moisture Barriers on SSVC Estimations

The depth of available moisture is a parameter used to determine the effect of vertical moisture barriers used in pavement design. In order to determine the sensitivity of the depth of available moisture parameter with regards to vertical moisture barriers, the empirical relationship between 1D volume change and 2D (lateral) volume change must first be understood.

The prediction of the vertical movement on expansive soils with the inclusion of vertical moisture barriers as a special provision will be based on previous studies reported in the literature. Jayatilaka (1999) suggested a regression model to estimate the relationship between one-dimensional and two-dimensional vertical movement including the effect of vertical moisture barrier depth, using the two programs MOPREC and FLODEF developed by Gay (1994). The one-dimensional model was based on the soil deformation

model proposed by Lytton (1977). The regression model was calibrated using data collected from ten sites located in Texas within three different climatic regions.

A brief description of the required input parameters used in this model are shown in Table 5-1. All the needed parameters are available either as part of the AASHTOWare ME Pavement design procedure (i.e., pavement geometry) or from the one-dimensional model results from this project. Therefore, no additional parameters will be needed to implement the model.

Table 5-1 Input Parameters Used in the Vertical Moisture Barrier Model

Input Parameter	Description
VM_{1D} (mm)	Maximum vertical movement (sum of swell and shrink)
D_b (m)	Depth of vertical moisture barrier
d_{am} (m)	Depth of available moisture
S_m (pF)	Mean suction
TMI	Thornthwaite moisture index
2D (m)	Pavement width
d (m)	Horizontal distance from the center of pavement to point of interest

5.2.2.2 Sensitivity Analysis of 2D SSVC Estimation

A sensitivity analysis was conducted to recognize the most critical parameters of the 2D moisture barrier model. Fixed input values of 100 mm of maximum vertical movement, 0.3 m of depth of available moisture, 3.5 pF of mean suction and 12 m of pavement width were used. Input varied in the analysis included TMI from -40 to 40; the depth of the vertical moisture barrier from 0 to 4 meters; and the mean suction value from 0 to 4 pF. These variables were compared and plotted against a normalized vertical movement.

Note that the pavement edge is located at a normalized distance of one (d/D =1). The results are presented in Figure 5-4 through Figure 5-6 below, show high sensitivity of the model to the three variables analyzed: TMI, moisture barrier depth and to the mean suction value.

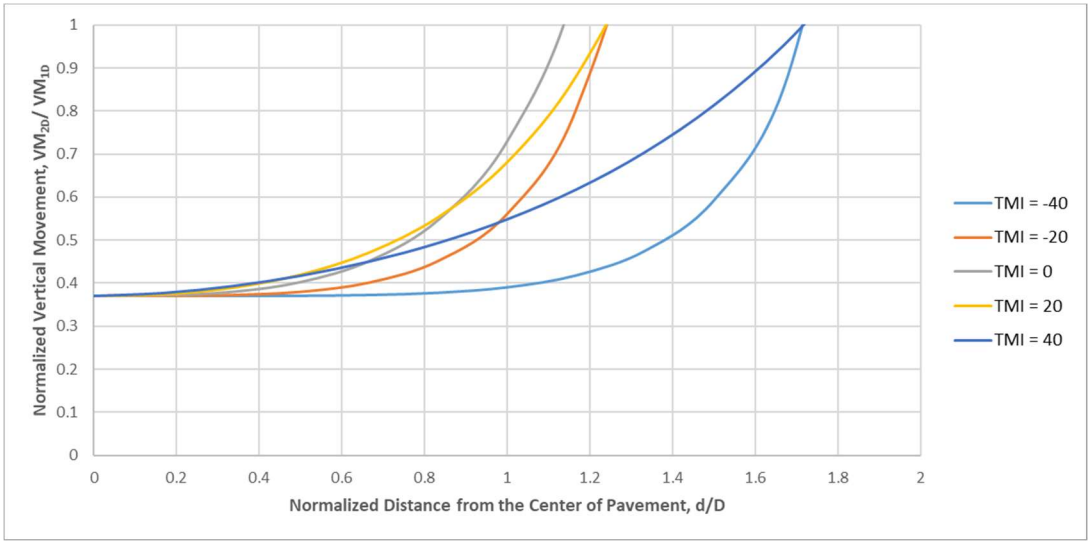

Figure 5-4 Normalized Vertical Movement as a Function of TMI

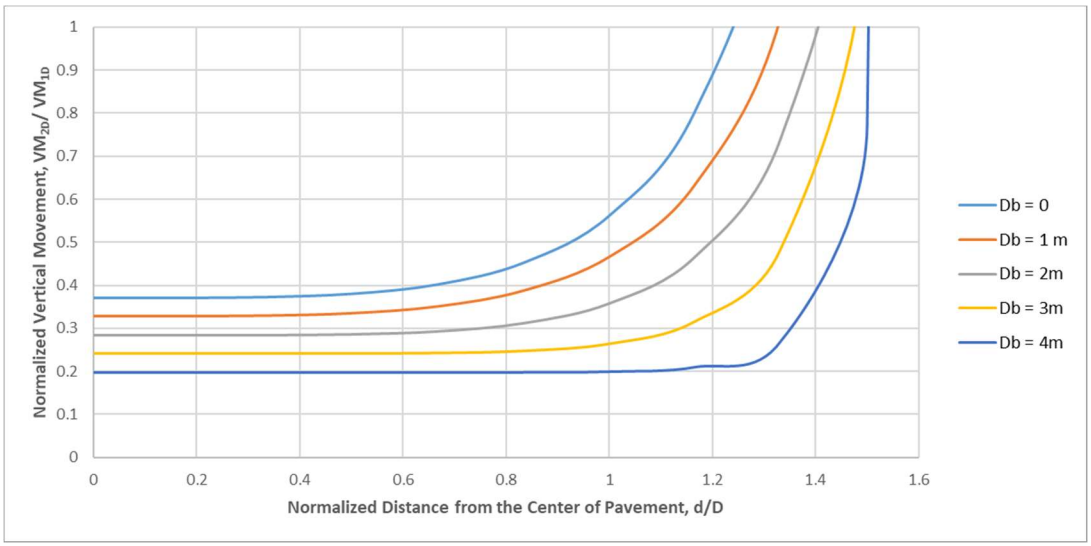

Figure 5-5 Normalized Vertical Movement as a Function of Depth of Vertical Moisture Barrier

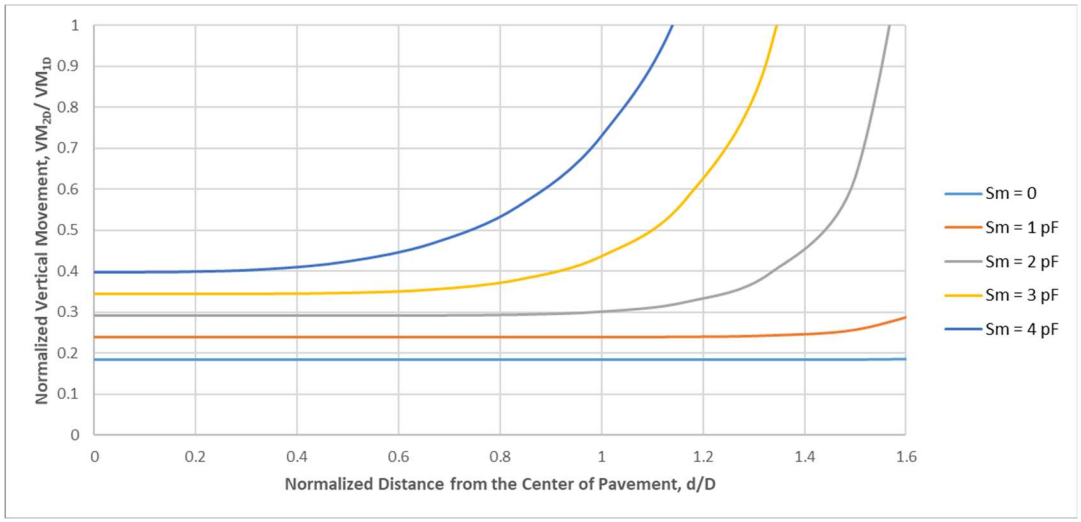

Figure 5-6 Normalized Vertical Movement as a Function of Mean Suction

The normalized vertical movement at the edge of the pavement is shown in Figure 5-7 and Figure 5-8 for different TMIs and Moisture barrier depths, respectively.

The research team is confident that this model will be extremely useful to 1) assess the vertical movement prediction away from the edge and towards the center of the pavement with and without moisture barriers; 2) as a surrogate path to calibration of the 1-D swelling predictions; and 3) to optimize design parameters.

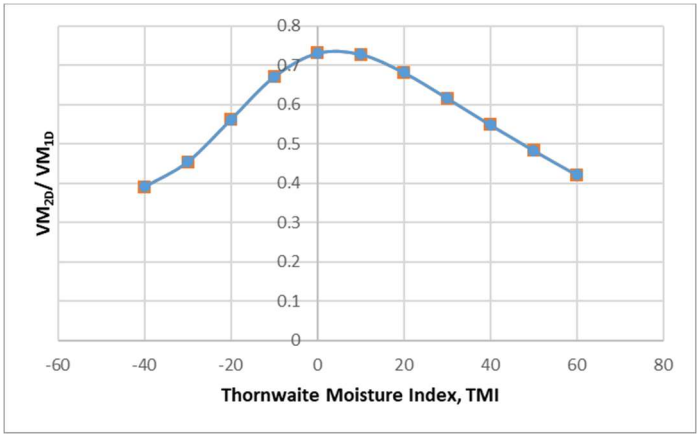

Figure 5-7 Normalized Vertical Movement at Different Thornthwaite Moisture Index at the Edge of the Pavement

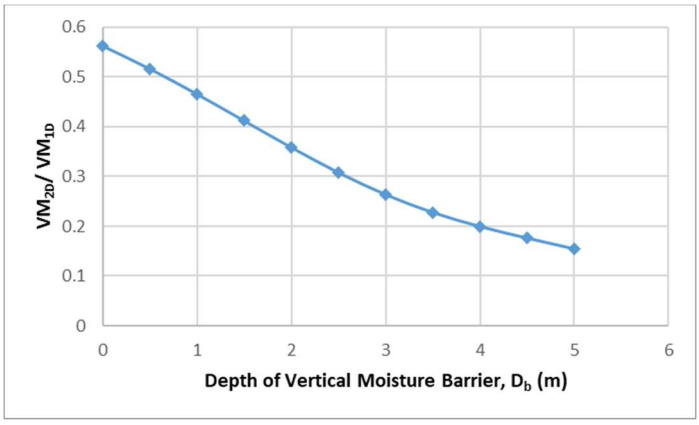

Figure 5-8 Normalized Vertical Movement for Different Depths of Vertical Moisture Barriers at the Edge of the Pavement

5.2.2.3 Sensitivity of the Depth of Available Moisture Parameter

Note that Gay (1994) and Jayatilaka (1992, 1999) observed that the depth of available moisture typically does not exceed 30 cm. Therefore, the first analysis performed varied the depth of available moisture from 5 cm to 50 cm. The following table, Table 5-2, summarizes the necessary parameters used in the model. Note that only the depth of available moisture was varied; all other parameters were kept constant.

Table 5-2 Input Parameters Used in the Vertical Moisture Barrier Model

Input Parameter	Value
VM_{1D} (mm)	50 mm
D_b (m)	0.9 m
d_{am} (m)	variable
S_m (pF)	4.45 pF
TMI	-46.5
2D (m)	18 m
d (m)	9 m (pavement edge)

The following figure, Figure 5-9, represents the sensitivity of the volume change at the edge of the pavement (d/D = 1) to the depth of available moisture parameter within the range of 5 to 50 cm.

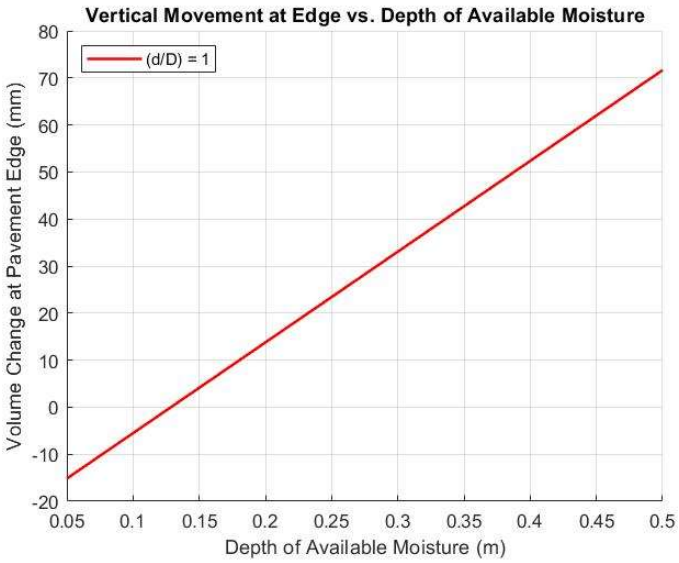

Figure 5-9 Vertical Movement at Edge vs. Depth of Available Moisture with (d/D) = 1

Note that empirical relationship results in negative volume change values (i.e. shrinkage) when the depth of available moisture is below approximately 12 cm (for this specific scenario). It is also important to note that the maximum vertical movement (VM_{1D}) of 50 mm is exceeded at the pavements edge once the depth of available moisture reaches approximately 39 cm. Based on the work on Jayatilaka (1999) and previous sensitivity analyses performed as part of this study, the lateral location of the maximum vertical movement (VM_{1D}) is typically outside the edge of the pavement and is affected by the TMI, mean suction, and depth of the vertical moisture barrier. Therefore, the volume change at the edge of the pavement is expected to be less than the maximum potential vertical movement value which would require the depth of available moisture to be less than 39 cm (for this specific scenario). This outcome agrees with observed depths of available moisture by Lytton (Jayatilaka 1992, 1999; Gay, 1994).

To ensure that the lateral location chosen for the sensitivity analysis above (pavement edge) did not affect the results, the same sensitivity analysis was performed with the location varying from the center of the pavement (d/D = 0) to a distance equal to half the width of the pavement away from the edge (d/D = 2).

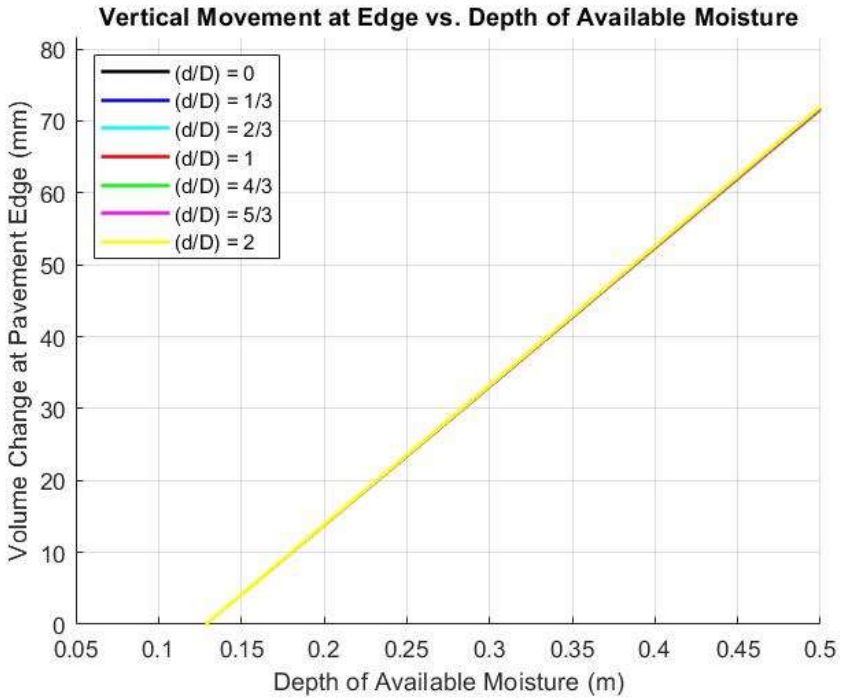

Figure 5-10 Vertical Movement at Edge vs. Depth of Available Moisture with Varying Ratios of (d/D)

It is clear from Figure 5-10 that the location chosen had no effect on the sensitivity analyses of the depth of available moisture. The effect of the depth of available moisture on the estimation of the volume change is insensitive to the lateral location within pavement profile.

The concept of the depth of available moisture can be confused with the depth of the active zone and the depth to equilibrium/stable suction. It is important to note that the depth of available moisture, as defined by Gay (1994) and Jayatilaka (1992, 1999), is not equivalent to the depth of stable suction, as defined by Vann (2019). To determine if the result of using the depth to stable suction (Vann, 2019) in place of depth of available moisture in the empirical estimation of the lateral heave reduction due to the presence of vertical moisture barriers, the previous analysis was performed a second time with an increased range of the depth of available moisture from 0.05 m (5 cm) to 4.5 m. The 4.5 m value represents an upper limit of the depth to stable suction observed by Cuzme (2018) and Vann (2019). Figure 5-11 represents the sensitivity of the Depth of Available Moisture parameter within the range of 0.05 m to 4.5 m.

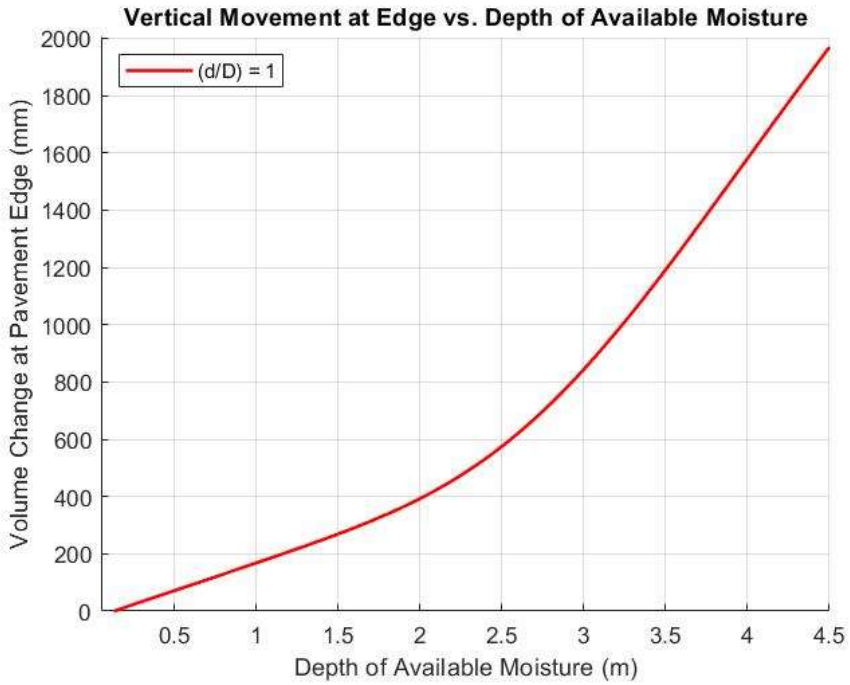

Figure 5-11 Vertical Movement at Edge vs. Depth of Available Moisture with (d/D) = 1

Once again, the results indicate that the magnitude of the volume change at the pavements edge is highly sensitive to the depth of available moisture parameter. If the depth to stable suction is used in-place of the depth of available moisture parameter in the analysis, the estimated volume change at the edge of the pavement will be significantly greater than the initial input of the maximum vertical movement (VM_{1D} = 50 mm was used in the analysis).

In summary, it has been observed that the location of the maximum vertical movement is directly affected by the depth of available moisture, provided all other parameters remain constant.

5.2.2.4 Back Calculation of the Depth of Available Moisture

As previously discussed, the depth of available moisture is determined from the SWCC of the soil within the root zone and knowledge of the depth of the root zone. SWCC data from all soil types is readily available and is already incorporated in the current AASHTOware software. However, data on the depth of the root zone if not readily available and may require site specific knowledge of the landscape adjacent to the roadway, which is subject to change as part of the roadway construction.

In order to eliminate the uncertainty associated with the root depth, the depth of available moisture parameter can be determined numerically if the location of the maximum vertical movement is known or estimated during the design stage. For example, a conservative assumption can be made that the maximum vertical movement will occur at the pavement edge regardless of when no vertical moisture barrier is present.

Once the location of the maximum vertical movement is assumed, an iterative calculation equivalent to the sensitivity analysis performed previously can be conducted in order to determine the depth of available moisture required for that scenario.

Table 5-3 summarizes an example scenario of a two-lane roadway with high-volume change soil, in a semi-arid climate, and variable vertical moisture barrier depth.

Table 5-3 Input Parameters Used in the Example Vertical Moisture Barrier Model.

Input Parameter	Value	Comments
VM_{1D} (mm)	140 mm	approximately 5.5 inches
D_b (m)	(0, 0.5, 1, 1.5, 2, 2.5, 3) m	Typical range or depths
d_{am} (m)	Back calculated	Based on selected location of VM_1D
S_m (pF)	4 pF	Per Vann (2019) with TMI = 10
TMI	10	semi-arid climate
2D (m)	19 m	two-lane road

Figure 5-12 presents the results of the volume change at the pavement edge based on the depth of available moisture with no vertical moisture barrier.

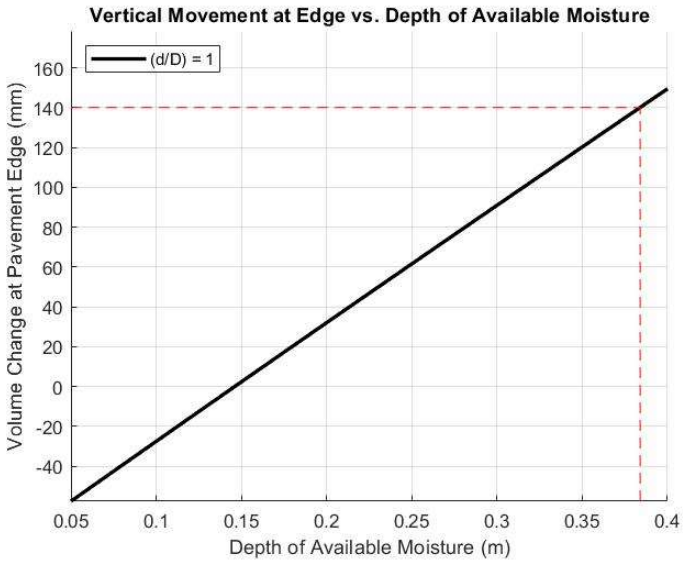

Figure 5-12 Vertical Movement at Edge vs. Depth of Available Moisture with d/D = 1

The red dashed lines on Figure 5-12 indicate the expected maximum vertical movement at the pavement edge when there is no moisture barrier (VM_{1D}) and the corresponding depth of available moisture.

The reduction in soil volume change due only to the pavement cover (no moisture barrier) can now be modeled using the moisture barrier factor (MBF) approach. Figure 5-13 represents the soil volume change due to the pavement covering alone.

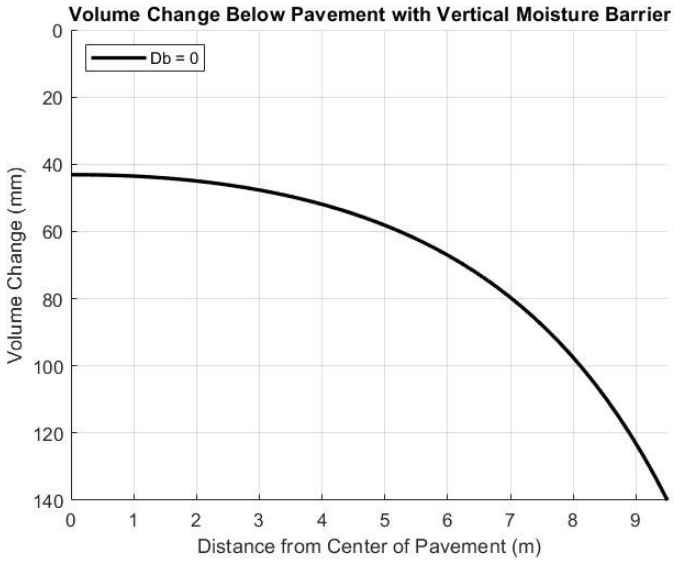

Figure 5-13 Volume Change Below Pavement with Vertical Moisture Barrier with Db=0

Note that volume changed is still estimated to occur at the center of the pavement for the given scenario.

The results above are commonly normalized by the maximum vertical movement and the pavement width as shown in Figure 5-14.

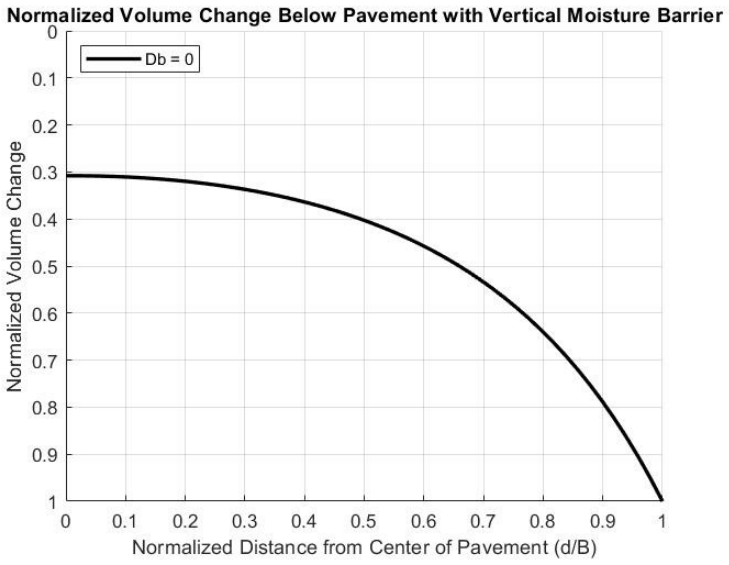

Figure 5-14 Normalized Volume Change Below Pavement with Vertical Moisture Barrier

By presenting the results in this manner, the percentage of the volume change reduction due to the pavement covering can be obtained from Figure 5-14. For this example, the covering from the pavement, without the presence of a vertical moisture barrier, results in approximately 30% of the maximum vertical movement occur at the edge of the pavement.

The effect of the depth of the vertical moisture barrier can now be determined using the back-calculated depth of available moisture and the parameters summarized in the table above. Figure 5-15 and Figure 5-16 present the raw and normalized results of the analysis.

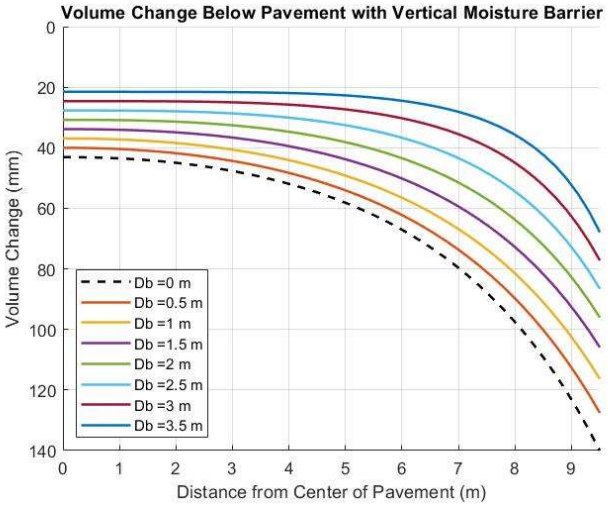

Figure 5-15 Volume Change Below Pavement with Vertical Moisture Barrier

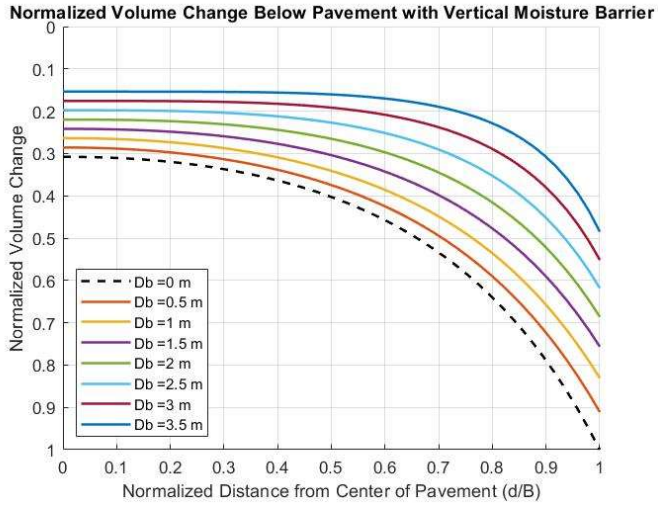

Figure 5-16 Normalized Volume Change Below Pavement with Vertical Moisture Barrier

Note that the estimated depth of stable suction (seasonal moisture fluctuation), for a site with a long term TMI = 10, is approximately 1.7 m (Vann, 2019). The results above

indicate that a moisture barrier depth greater than the depth of stable suction (2 m) still results in vertical movements near the center of the pavement that are approximately 20% of the expected maximum vertical movement at the edge of the pavement when no barrier exists.

5.3 Stochastic Framework for SSVC Forecasting

This study presents an example calculation for a Level III analysis for the determination of volume change (shrink/swell) as a function of time. A computer program was developed in order to explain the calculation due to the multiple algorithmic processes contained within. Refer to Table 5-4, which summarizes the models used in the Level III analysis, along with the Level 1 and Level 2 analysis (not presented in this document). Table 5-5 indicates the necessary variables associated with the hierarchical level of analysis.

Table 5-4: Preliminary Plan to Estimate Volume Change Due to Swell/Shrink at Three Hierarchical Levels of Design

Hierarchical Level	Climatic Parameters	Depth to Equilibrium Suction	Equilibrium Suction	Time-Based Change in Suction on the Surface	Suction-Strain Model
1	30-year average and yearly TMI per Witczak et al. (2006)	User input of suction profile *			Direct Measurement using OPPD (Olaiz 2017)
2		Vann and Houston (2020) with lab measurements of soil index properties		NOFS Mitchell (1979) Diffusion Equation	Surrogate Path Method (SPM) (Houston & Houston 2017) or similar oedometer-based methods
3		Vann (2019) using TMI			Covar and Lytton (2001) or similar empirical relationships with soil index properties

*User input of depth of equilibrium suction and magnitude of equilibrium suction indicates that the user knows these values (with a high level of confidence) by direct suction measurements or through significant experience of suction profile measurements in the area.

Table 5-5: Listing of Input Variables for Hierarchical Shrink-Swell Analysis

		Levels		
	Parameter	1	2	3
Pavement Structure Parameters	Pavement type and layer thicknesses	Needed	Needed	Needed
Parameters Related to Boundary Conditions (Environmental)	NOAA Weather Station ID (Longitude & Latitude)	Needed	Needed	Needed
	Groundwater Table Depth	Needed	Needed	Needed
Soil Index Properties	Plasticity Index (PI)	-	Needed	Needed
	Liquid Limit (LL)	-	Needed	Needed
	Percent Passing No. 200 Sieve (P200)	-	-	Needed
	Percent Passing 2-Micron (P02)	-	-	Needed
In Situ Soil Properties	Water Content (w)	-	Needed	Needed
	Density (γ)	Needed	Needed	Needed
	Soil Suction (pF)	Needed	-	-
Strain Parameters	Wetted Oedometer strain (ε_{ob})	-	Needed	-
	Swell Pressure (σ_{cv})	-	Needed	-
	Final Suction Profile	Needed	-	-
	Suction Compression Index	Needed	-	-

The stochastic forecast of shrink-swell soil volume change is accomplished by:

1) Obtaining sufficient historical monthly climate data (minimum of 5 years, recommended 30 years)
2) Obtains site-specific soil data and/or use the best representation based on the historical/prior Beta distributions
3) Perform 10,000 Monte Carlo simulations with each including:
    a. Randomization of input soil parameters using the proposed framework

b. Estimating the monthly TMI over the structure/pavement design life using the proposed MCMC monthly TMI forecast model
c. Estimating the monthly volume-change for the given simulation using the proposed deterministic framework
d. Repeating process for each simulation

4) Calculating monthly and overall statistics for all the simulations combined.

5.4 Example of the Stochastic SSVC Forecast Model

The Denver study site previously presented herein was used to present an example of the performance of the stochastic SSVS Forecast Model. The results of the randomized input soil property variability and additional output from MCMC TMI climate model are presented in Appendix F. The example analysis was performed for 20 years to provide insight into the stability of the analyses for typical pavement design life periods. The Bayesian forecast for TMI and monthly change in TMI are presented in Figure 5-17. The stochastically prodiced estimates and variability of the monthly SSVC and monthly change in SSVC are presented in Figure 5-18 and Figure 5-19, respectfully.

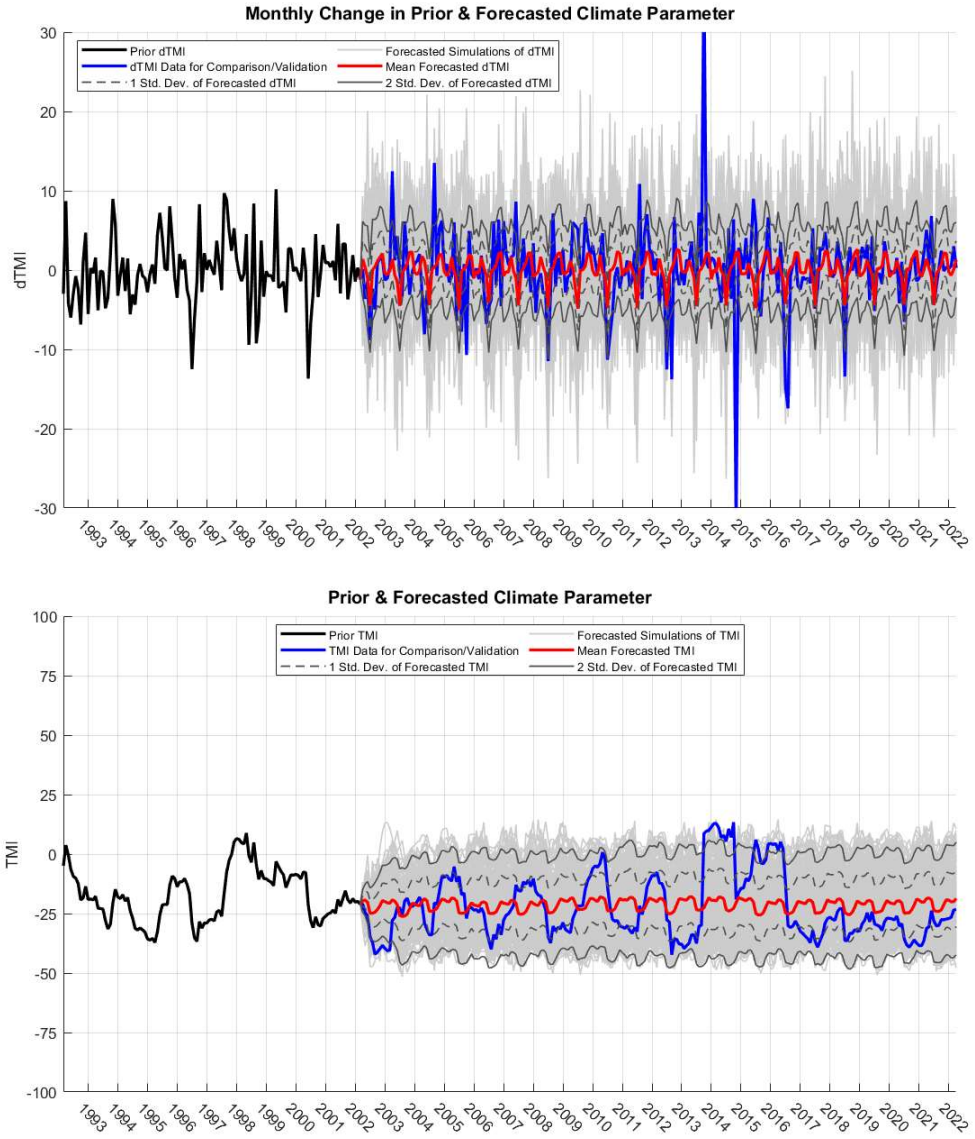

Figure 5-17 Bayesian Forecast of TMI at Denver Study, Including the True Values for Validation, from 03/2002 to 03/2022

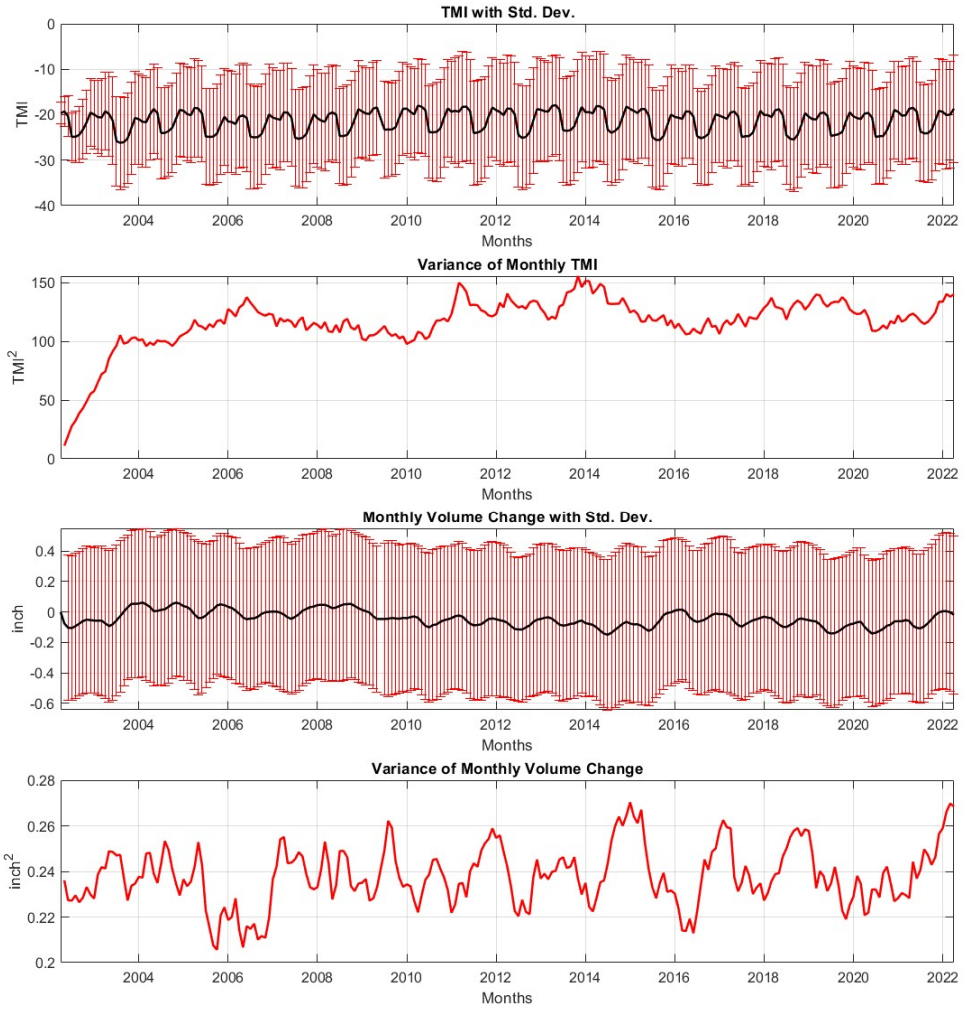

Figure 5-18 Example Results of the Stochastic Shrink-Swell Analysis for the Monthly TMI and Monthly Volume Change for the Denver Study Site from 03/2002 to 03/2022

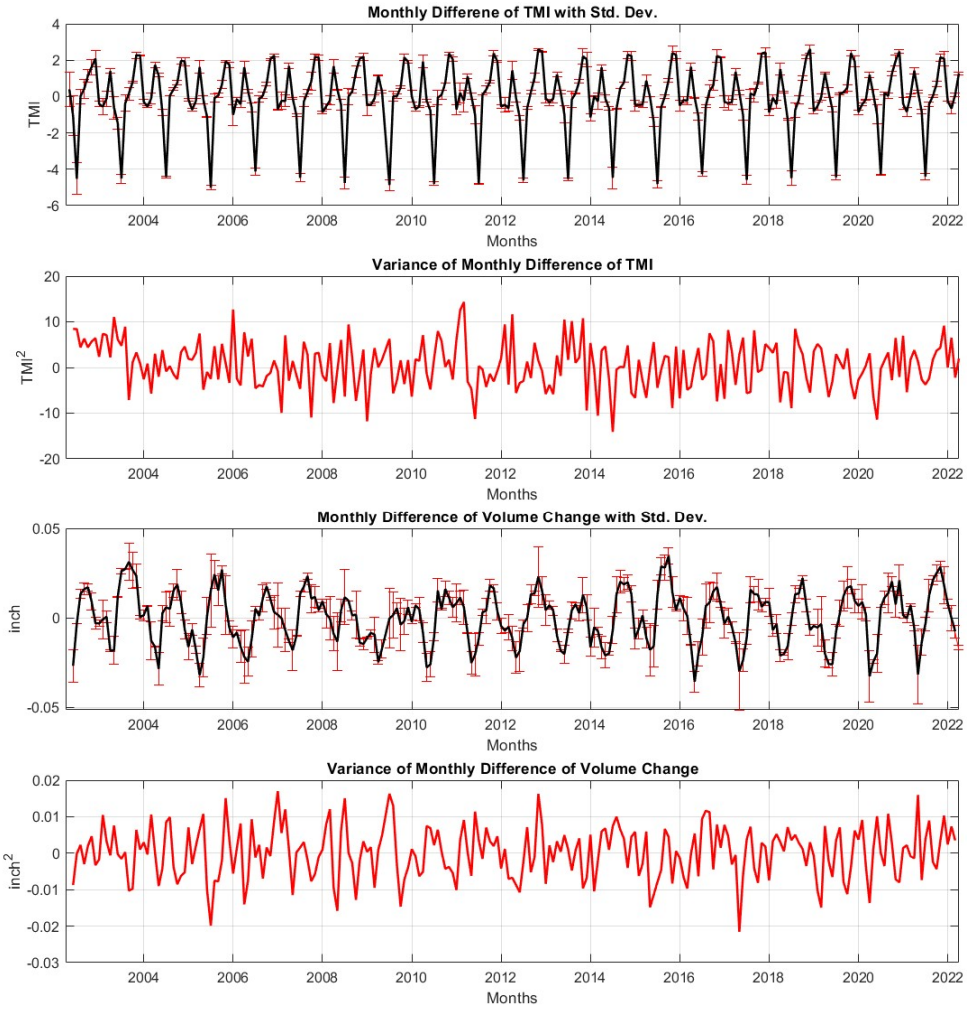

Figure 5-19 Example Results of the Stochastic Shrink-Swell Analysis for the Monthly Difference in TMI (*dTMI*) and Monthly Difference in Volume Change for the Denver Study Site from 03/2002 to 03/2022

5.5 Performance of the Proposed Stochastic SSVC Model

The stochastic SSVC analyses presented herein provides a method for quantifying the potential volume change and its associated variability monthly based on the variability of the randomized model inputs: soil index properties and forecasted monthly TMI values. As the example output in Figure 5-18 and Figure 5-19 display, the variance of the estimated monthly values continued to oscillate on a seasonal basis as expected, but the overall average of the variance visually appears to stabilize after two to three years. This indicates that the optimal analysis period for scenarios where the model is being used as an indicator for potential shrink-swell issues would be approximately 4 years. However, the results of the example calculation show that the proposed model provides useful insights for analysis periods greater than 4 years, up to 20 years. Generally, the analysis would not cover the full pavement design life as analyses of shorter durations would provide a useful representation of the volume change susceptibility which would typically result in a redesign of the pavement section or possibly a soil improvement effort. Note that this model included 250 Markov chains over the 20-year period (i.e. 60,000 MCMC simulations) with a burn in period of 25% that resulted in an Metropolis-Hastings acceptance rate of approximately 24%.

5.6 Implementation of the Proposed Stochastic SSVC Model

The proposed framework for stochastically forecasting the SSVC on a monthly basis is being review and considered for implementation into the Pavement Mechanistic-Empirical Design (PMED) design procedures and associated software as part of the

NCHRP 01-59 project which this research was funded by. A detailed report was generated by the author and the research team for NCHRP which includes a detailed performance evaluation and implantation examples of the stochastic Shrink-Swell forecast model using the computer program developed by the author. It is anticipated that report will be published by NCHRP in 2023; no drafts or excerpts of the report have been included herein.

Note that the example analysis presented herein included a scenario which forecasted the potential climate-driven volume change. A forecast scenario will typically always result in the largest amount of variability in the resulting estimate. If new site-specific data is obtained (measured soil or climate parameters), they can be used to adjust and improve the forecast performance of the model. Furthermore, the model can be used in a forensic scenario if the variability of past SSVC needs to be understood.

5.6.1 Limitations of the Stochastic SSVC Model

Although the proposed Stochastic SSVC model displays preliminary indications that the stability and performance is sufficient for implementation in geotechnical engineering practice, there are several limitations that must be understood, including but not limited to:

- The proposed stochastic SSVC model, and all of its contributing models (Bayesian characterization of general soil properties model and the MCMC TMI forecast model) should be considered preliminary frameworks with have

promising initial performance but lack an exhaustive sensitivity and stability evaluation.

- The examples of the model use presented in this document were focused on just 2 sites in the United States which the author and ASU research team had significant measured data at, which provided opportunities for model validation. The two study sites in Denver, CO and San Antonio, TX are located in dry temperate to semi-arid climate zones and the site soils exhibit relatively high susceptibility of SSVC, which make the study sites nearly ideal for the application of the proposed models. However, the study sites were also used to produce several of the empirical unsaturated soil parameter models used in the stochastic analysis. It is recommended that additional site-specific data from sites in differing climate regions be obtained for further validation studies of full stochastic SSVC model proposed herein.

CHAPTER 6

6 CONCLUSIONS

This research study focused on developing Bayesian techniques for the characterization of common soil properties, and the analysis of climate-driven shrink-swell volume change using an unsaturated soil moisture flow mechanics. The overall goal achieved in this study was to develop, validate, and implement a new method to evaluate climate-driven volume change of shrink-swell soils using a framework that encompasses predominantly stochastic time-series techniques and mechanistic shrink-swell volume change computations. Three valuable objectives were also accomplished on the path to complete the overall goal: 1) development of an procedure for automating the selection of the Fourier Series form of the soil suction diffusion equation used to represent the climate-driven variation in suction, 2) development of a Bayesian approach to randomly generate combinations of correlated soil properties for input in stochastic simulations, and 3) development of a Bayesian forecast model for the Thornthwaite Moisture Index climate parameter. The models presented can be easily implemented into existing foundation and pavement design procedures or used for forensic evaluations using historical data. For pavement design, the new framework for stochastically forecasting the variability of shrink-swell soil volume change provides significant improvement over the existing empirical models that have been used for more than four decades.

6.1 Limitations of Research

The limitations pertaining to each research achievement should be understood prior to consideration of implementation into engineering practice. Refer to the concluding subsections in each chapter of this document for an extensive list of limitations for each specific research achievement. The main limitations associated with the research findings presented in this document are, but not limited to, the following:

- The empirical models developed by Vann and Houston (2020) used to define the equilibrium parameters (equilibrium suction depth and magnitude) for the NOFS suction envelope model were generated using limited data from geotechnical investigation reports by various engineering firms across the United States. Furthermore, all the models which related TMI to soil suction parameters were developed from sites which the elevation of the groundwater table did not affect the moisture state within the typical depth from ground surface associated with the unsaturated soil "active zone", which is generally 5 to 20 feet. As such, the proposed model should not be used to evaluate locations which have shallow groundwater.
- The NRCS and LTTP databases were used to generate descriptive statistics for the default variability characterization for the defined soil groups. Although these databases are considered by the field to adequately represent most soil types, there is always a chance for a location to consist of soils which exhibit characteristics away from the norm. It is always recommended that some site-specific data be

obtained to gain an understanding of the material types at hand and rule out any potential unusual scenarios.

- The proposed approach for characterizing the variability of common soil properties uses the general variability of the measured properties for a given soil type to represent the 2D variability at the subject site. As such, the proposed framework can be considered a pseudo-2D approach for characterizing soil variability but does not include the modern techniques of quantifying spatial variability.
- As displayed in the outcome of the Arlington, VA validation study, the proposed Bayesian TMI forecast model has potential to miss extreme events which were not characterized by the 30 years of prior climate data.
- The Bayesian TMI forecast model presented herein is programmed to produce forecasts which sufficiently represent the variability and volatility of the prior data without "walking" too far from the prior distributions. If a more conservative approach is warranted which encompasses some pre-defined increase in the variability/volatility of the forecasted data, the tuning criteria can be increased by either increasing the initial tuning factor to be greater than 2.4. An additional stability study should be performed in such a case.
- The examples of the model use presented in this document were focused on just 2 sites in the United States which the author and ASU research team had significant measured data at, which provided opportunities for model validation. The two study sites in Denver, CO and San Antonio, TX are located in dry temperate to

semi-arid climate zones and the site soils exhibit relatively high susceptibility of SSVC, which make the study sites nearly ideal for the application of the proposed models. However, the study sites were also used to produce several of the empirical unsaturated soil parameter models used in the stochastic analysis. It is recommended that additional site-specific data from sites in differing climate regions be obtained for further validation studies of full stochastic SSVC model proposed herein.

6.2 Future Work

The research efforts produced useful frameworks for the stochastic characterization of common soil properties, the forecast of the climatic parameter TMI, and the stochastic analysis of SSVC. Although these models produced promising results for the study sites, the author recommends that the models be treated as preliminary frameworks only which needs further optimization, validation, and sensitivity analyses. Specifically, the following efforts should be performed as part of future research work:

- Validation of the Bayesian characterization model through an extensive field sampling and laboratory testing program at sites associated with soil types ranging from coarse to fine-grained.
- The inclusion of multiple weather station data should be incorporated into both the deterministic and the stochastic models. For the deterministic model, a decision would have to be made to use the average monthly data, or another statistically representative monthly value. Although it is not a straightforward

analysis, the most conservative approach would be to use the monthly data which results in the greatest monthly changes and/or seasonal variations, regardless of the location of the weather station (assuming only weather stations near the site that are chosen).

- Improvement and optimization of the Bayesian forecast model for the climatic parameter TMI to include an adaptive Langevin Markov Chain (LMC) or a Hamiltonian Markov Chain (HMC) which incorporates a physics-based approach to control the stability and limit the random walk potential of the simulated time-series by representing the MCMC framework as energy equations (potential and kinetic). The HMC framework also includes a leap-frog step which can significantly optimize the computation time of the MCMC simulation.
- An updated calibration effort of the both the deterministic SSVC model and the stochastic SSVC model using the LTTP Seasonal Monitoring Program (SMP) sites should be performed. The initial calibration efforts presented by Mosawi (2022) resulted in improvements of the goodness of fit (R^2) for prediction of IRI when the site factor parameter in the IRI equation was replaced with the variability of forecasted volume change for a given month.
- Further evaluations of the use of the proposed SSVC framework to estimate the variability of the volume change in two dimensional should be studied using the empirical approach proposed by Lytton et al. (2005) as a starting point which could be improved with the inclusion of additional measured data.

- The stochastic soil and climate characterization should be used with the complete (not simplified) version of the unsaturated moisture flow partial differential equation. Although the performing Monte Carlo simulations on finite element model with randomized input parameters can be computationally slow, advancements in computer performance continues to exponentially improve, which may eliminate computation time as a limitation in the near future. The use of the full unsaturated moisture flow equation will allow for the inclusion of shallow groundwater sites, as the simplified Mitchell's equation used in this study is based on the assumption of a steady suction boundary at depth.

REFERENCES

Aitchison, G. D. & Richards, B. G. (1965). A Broad scale Study of Moisture Conditions in Pavement Subgrades throughout Australia. Part 1 - 4. Butterworths, Sydney.

Adem, H.H., & Vanapalli, S.K. (2013). Constitutive modeling approach for estimating 1-D heave with respect to time for expansive soils. *International Journal of Geotechnical Engineering,* 7(2), 199-204. http://dx.doi.org/10.1179/1938636213Z.00000000024.

Al-Shamrani, M.A. & Al-Mhaidib, A.I. (1999) Prediction of potential vertical swell of expansive soils using a triaxial stress path cell. *Quarterly Journal of Engineering Geology & Hydrogeology,* 32(1). 45-54.

Alonso, E. E. (1993). Constitutive modelling of unsaturated soils, Unsaturated soils: *Recent Developments and Applications, Civil Engineering European Courses*. Universitat Polit`ecnica de Catalunya, Barcelona, Spain.

Alonso, E. E., Lloret, A., Gens, A., and Yang, D. Q. 1995. Experimental behaviour of highly expansive double-structure clay, *Proceedings of the First International Conference on Unsaturated Soils* (UNSAT-95), Paris, pp. 11–16.

Alonso, E.E, Gens, A., & Gehling, W.Y.Y. (1994). Elastoplastic model for unsaturated expansive soils. *Proceedings of the 3rd European Conference on Numerical Models in Geotechnical Engineering*. 11-18, Rotterdam.

Alonso, E.E., Gens, A., & Josa, A. (1990). A constitutive model for partially saturated soils. *Geotechnique*, 40(3), 405-430. http://dx.doi.org/10.1680/geot.1990.40.3.405.

Alonso, E.E., Vaunat, J., & Gens, A. (1999). Modelling the mechanical behaviour of expansive clays. Engineering Geology, 54(1-2), 173-183. http://dx.doi.org/10.1016/S0013-7952(99)00079-4.

Amer, O. M. I. (2016). Determining Suction Compression Index of Expansive Soils Based on non-linear suction-volumetric strain relationship. PhD Dissertation. Oklahoma State University.

American Association of State Highway and Transportation Officials (AASHTO). (2008). Mechanistic-Empirical Pavement Design Guide.

American Society for Testing and Materials (ASTM). (2014) Standard test methods for one-dimensional swell or collapse of soils. ASTM International, West Conshohocken, ASTM International, West Conshohocken, PA.

Amrhein, V., Trafimow, D. & Greenland, S. Am. Stat. (2019) Inferential Statistics as Descriptive Statistics: There Is No Replication Crisis if We Don’t Expect Replication.

The American Statistician. Vol. 73. Pg. 262-270. DOI:10.1080/00031305.2018.1543137

AS2870-2011 *Residential Slabs & Footings.* (2011). Construction Standards Australia. Homebush, NSW, Australia.

Aubeny, C., & Long, X. (2007). Moisture Diffusion in Shallow Clay Masses. Journal of Geotechnical and Geoenviromental Engineering, ASCE. 133(10), 1241-1248.

Barnett, I.C., & Kingsland, R.I. (1999). Assignment of AS2870 Soil Suction Change Profile Parameters to TMI Derived Climatic Zones for NSW. *8th Australia - New Zealand Conference on Geomechanics.* Australian Geomechanics Society.

Basma, A. A., Al-Homoud, A. S. & Malkawi, A. I. (2000). Swelling-shrinkage behaviour of natural expansive clays. Appl. Clay Sci., 11: 211-227.

Basma. A. A. T I. Al-Suleiman (1991) Climatic Consideration in New AASHTO Flexible Pavement Design. Journal of Transportation Engineering. Volume 117. No 2. pp 210-223.

Benjamin, J., & Cornell, C.A. (2018). Probabiltiy, Statistics, and Decision for Civil Engineers. Dover Publications. Mineola, NY.

Betancourt, M. (2017) A Conceptual Introduction to Hamiltonian Monte Carlo. Computer and Information Sciences. arXiv. DIO: 10.48550/ARXIV.1701.02434

Briaud, J., Zhang, X., & Moon, S. (2003). Shrink Test–Water Content Method for Shrink & Swell Predictions. *Journal of Geotechnical & Geoenvironmental Engineering, ASCE, Vol. 129, No.7*, 590–600.

Bulut, R. (2001). "Finite Element Method Analysis of Slabs on Elastic Half Space Expansive Soil Foundations", Ph.D. Dissertation, Texas A&M University, College Station.

Bulut, R., Zaman, M., Amer, O., Mantri, S., Chen, L., Tian, Y., Taghichian, A. (2013). Drying Shrinkage Problems in High-Plastic Clay Soils in Oklahoma. Oklahoma Transportation Center. OTCREOS11.1-09-F Midwest City. OK.

Cameron, D. (2001). The extent of soil desiccation near trees in a semi-arid environment. *Geotechnical & Geological Engineering*, 19(3), 357-370.

Chan, I. & Mostyn, G. (2009) Climatic factors for AS2870 for New South Wales. *Australian Geomechanics. Vol. 44, No. 2,* (pp 41- 46).

Chen, F. H. (1975). Foundations on Expansive Soils. Elsevier Scientific Pub. Co., Amsterdam, New York, NY.

Chen, C.W.S., Liu, F.C., Gerlach., R. (2011). Bayesian subset selection for threshold autoregressive moving-average models. *Comput Stat*. 26:1-30. DOI: 10.1007/s00180-010-0198-0.

Covar, A., and Lytton, R. (2001). Estimating soil swelling behavior using soil classification properties. *Proceedings of Geo-Institute Shallow Foundation and Soil Properties Committee Sessions at the ASCE 2001 Civil Engineering Conference*. 44-63. Houston, Texas: ASCE.

Cuzme, Alan J. (2018). "Estimating Expansive Soil Field Suction Profiles Using a Soil Suction Surrogate." *Arizona State University*.

De Bruijin, C. M. A. (1961). Swelling characteristics of a transported soil profile at Leeuh of Vereeniging (Transvaal). Proc. 5th Int. Conf. Soil Mech. Found. Eng. 1: 43-49.

De Bruijin, C. M. A. (1965). Some observations on soil moisture conditions beneath & adjacent to tarred roads & other surface treatments in South Africa. Moisture Equilibrium & Moisture Changes Beneath Covered Areas. (pp. 135-142). Butterworths, Australia.

Decagon Devices, Inc. (2011). Effects of sample disturbance on soil water potential. Pullman, WA: Decagon Devices, Inc.

Delage P. & Graham J. 1996. Mechanical behaviour of unsaturated soils. *Proceedings of the 1st International Conference on Unsaturated Soils* (UNSAT), 3, 1223-1256, Paris: Balkema.

Dhowian, A. W. (1990). Field performance of expansive shale formation, Journal of King Abdulaziz University (Engineering Sciences), 2: 165-82.

Dhowian, A.W., Erol, A.0. & Youssef, A. (1990). Evaluation of Expansive Soils & Foundation Methodology in the Kingdom Saudi Arabia.

Erol, A. O., Dhowian A. & Youssef, A. (1987). Assessment of oedometer methods for heave prediction. *Proceedings of 6th International Conference on Expansive Soils, Technical Session III*. (pp. 99-105).

Federal Highway Administration (FHWA). (1994). LTTP Seasonal Monitoring Program: Instrumentation Installation and Data collection Guidelines. FHWA-FD-94-110

Federal Highway Administration (FHWA). (1994). Long-Term Pavement Performance Information Management System User Guide. FHWA-HRT-21-038.

Fenton, G.A., & Griffiths, D.V. (2008). Risk Assessment in Geotechnical Engineering. John Wiley & Sons, Inc. Hoboken, NJ.

Fityus, S.G., P.F. Walsh, & P.W. Kleeman. (1998). The influence of climate as expressed by the Thornthwaite index on the design of depth of moisture change of clay soils in the Hunter Valley. Conference on Geotechnical Engineering & Engineering Geology in the Hunter Valley. (pp. 251-265) Springwood, Australia.

Fityus, S., & Buzzi, O. (2008). On the use of the Thornthwaite moisture index to infer depths of seasonal moisture change. Australian Geomechanics 43 (4): 69-76.

Fityus, S. & Smith, D. W. (1998). A simple model for the prediction of free surface movements in swelling clay profiles. Proceedings of the 2nd International Conference on Unsaturated Soils. (pp. 473-478). Beijing, China.

Fityus, S., Smith, D.W., & Allman, M.A. (2004). Expansive Soil Test Site Near Newcastle. Journal of Geotechnical and Geoenvironmental Engineering, ASCE, 130(7): 686-695.

Fox, E. (2000). A Climate-Based Design Depth of Moisture Change Map of Queensland and the Use of Such Maps to Classify Sites Under AS2870-1996. *Australian Geomechanics Journal*. 52(2): 61-75.

Fredlund, D. G., Hasan, J. U., & Filson, H. (1980). The prediction of total heave. *Proceedings 4th International Conference on Expansive Soils*. (pp. 1-11) Denver, Colorado.

Fredlund, D. G. and Pham, H., (2006). A volume-mass constitutive model for unsaturated soils in terms of two independent stress state variables. *Proceeedings of the Fourth International Conference on Unsaturated Soils.* 105-134. Carefree, AZ. ASCE.

Fredlund, D. G., Rahardjo, H, and Fredlund, M. D. (2012). Unsaturated Soil Mechanics in Engineering Practice. John Wiley & Sons, Inc. Hoboken, NJ.

Fredlund, D.G., & Morgenstern, N.R. (1976). Constitutive relations for volume change in unsaturated soils. *Canadian Geotechnical Journal*, 13(3), 261-276. http://dx.doi.org/10.1139/t76-029.

Gamerman, D., & Lopes, H.F. (2006). Markov Chain Monte Carlo: Stochastic Simulation for Bayesian Inference. 2nd Edition. Taylor & Francis Group, LLC. Chapman & Hall/CRC press. Boca Raton, FL.

Gelman, A., Carlin, J.B., Stern, H.S., Dunson, D.B., Vehtari, A., Rubin, D.B. (2014). Bayesian Data Analysis. 3rd Edition. CRC Press, Taylor & Francis Group. Boca Raton, FL.

Gens, A., & Alonso, E.E. (1992). A framework for the behaviour of unsaturated expansive clays. *Canadian Geotechnical Journal*, 29(6), 1013-1032. http://dx.doi.org/10.1139/t92-120.

Gens, A., Alonso, E. E., Suriol, J., and Lloret, A. (1995). Effect of structure on the volumetric behaviour of a compacted soil, *Proceedings of the First International Conference Unsaturated Soils*, UNSAT-95, Paris, Vol. 1, pp. 83–88.

Gens, A., Alonso, E.E., & Delage, A. (1996). Constitutive modelling: application to compacted soils. *Proceedings of the 1st International Conference on Unsaturated Soils* (UNSAT). 3, 1179-1200. Paris: Balkema.

Geotechnical Consulting and Testing Services (GCTS). (2007). SWC-150: Fredlund Soil Water Characteristic Device. 1.3. Tempe, AZ.

Gibbs, H.J. (1973) Use of a consolidometer for measuring expansion potential of soils. Proc. Workshop Expansive Clays & Shales in Highway Design & Construction. Univ. Wyoming, Laramie, May 1: 206-213.

Gong, W.P., Zhao, C., Juang, C.H., Zhang, Y.J., Tang, H.M., Lu, Y.C. (2021). Coupled Characterization of Stratigraphic and Geo-Properties Uncertainties-A Conditional Random Field Approach. *Engineering Geology*. 106348.

Houston, S. and Zhang, X. (2021) Review of expansive and collapsible soil volume change models within a unified elastoplastic framework. (F. M. T.M.P. Campos, Ed.) *Soil and Rocks,* 44(3). doi:10.28927/SR.2021.064321

Houston, S., and Houston, W. (2018). Suction-Oedometer Method for Computation of Heave and Remaining Heave. *Proceedings of the 2nd Pan-American Conference on Unsaturated Soils*. 93-116. Dallas, TX: ASCE. http://dx.doi.org/10.1061/9780784481677.005.

Jayatilaka, R., Gay, D., Lytton, R., &Wray, W. (1992). Effectiveness of controlling pavement roughness due to expansive clays with vertical moisture barriers. *Research Study No. 2/11-8-88-1165.* Texas Depart of Transportation, Texas Transportation Institute, & Texas Tech University/

Jayatilaka, R. (1999) A model to predict expansive clay roughness in pavements with vertical moisture barriers. Doctoral dissertation. Texas A&M University, College Station, TX

Jennings, J.E., & Knight, K. (1957). The prediction of total heave from double oedometer test, *In Proceedings of Symposium on Expansive Clays*. South African Institution of Civil Engineers, Johannesburg, 13-19.

Jennings, J. E. B., Firtu, R. A., Ralph, T. K. & Nagar, N. (1973). An improved method for predicting heave using the oedometer test. Proc. 3rd Int. Conf. Expansive Soils, Haifa, Israel, 2: 149-154.

Johnson, L. D. & Snethen, D. R. 1978. Prediction of potential heave of swelling soils. *Geotechnical Testing Journal*, 1(3): 117-124.

Karunarathne, A., Gad, E., Sivanerupan, S. & Wilson, J. (2012). Review of Residential Footing Design on Expansive Soil in Australia. *Swinburne University of Technology, Hawthorn, Victoria, 3122,* 7 p.

Karunarathne, A.M.A.N., E.F. Gad, S. Sivanerupan, & J.L. Wilson. (2016). Review of Calculation Procedures of Thornthwaite Moisture Index & Its Impact on Footing Design. *Australian Geomechanics 51* (1): 85-95.

Koch, M.C., Osugi, M., Fujisawa, K., Murakami, A. (2020) HamiltonianMonte Carlo for Simultaneous Interface and Spatial Field Detection (HMCSISFD) and its application to a piping zone interface detection problem. *Int J. Numer Anal Methods Geomech*. *45:2602-2626.* John Wiley & Sons, Inc. DOI: 10.1002/nag.3279

LaLibere G.E. & Corey A.T. (1967). Hydraulic properties of disturbed and undisturbed soils". American Society of Testing and Materials (ASTM) Special Technical Publication No. 417. Permeability and Capillarity of Soils.

Li, J, Cameron, D and Ren, G (2013). Case study and back analysis of a residential building damaged by expansive soils, *Computers and Geotechnics*, vol. 56, pp. 89-99.

Li, J. & Sun, X. (2015). Evaluation of changes of Thornthwaite Moisture Index in Victoria. Journal of *Australian Geomechanics, Vol.50.* No. 3, pp. 39-49.

Li, Z., Gong, W., Li, T., Juang, C.H., Chen, J., Wang (2021) Probabilistic back analysis for improved reliability of geotechnical predictions considering parameters uncertainty, model bias, and observation error. *Tunneling and Underground Space Technology*. 115. DOI: 10.1016/j.tust.2021.104051

Lopes, D. (2007). A modified shrink/swell test to calculate the instability indices of clays. *Australian Journal of Civil Engineering, Vol. 3,* pp 67-74.

Lytton, R.L. (1977). *Foundations in Expansive Soils, in Numerical Methods in Geotechnical Engineering*, Chapter 13. (pp. 427-458). C. S. Desai & J. T. Christian (Eds.), New York: McGraw-Hill.

Lytton, R., Aubeny, C., and Bulut, R. (2005). Design procedure for pavements on expansive soils. Austin, TX: Texas Department of Transportation (TxDOT).

McKeen, R. G. and Johnson, L. D. (1990). "Climate-Controlled Soil Design Parameters for Mat Foundations". J. of Geotechnical Eng., 116(7), pp. 1073-1094.

McManus, K., Lopes, D., & Osman, N.Y. (2004). The effect of Thornthwaite moisture index changes on ground movement predictions in Australian soils. *9th Australia New Zeal& Conference on Geomechanics, Proceedings Volume 2*. Auckland.

Medina-Cetina, Z., Esmailzadeh, S., (2014). Joint states of information from different probabilistic geo-profile reconstruction methods. Georisk 8 (3), 171–191.

Mitchell, P.W. (1979). The Structural Analysis of Footings on Expansive Soil. Newton: Kenneth W.G. Smith& Associates.

Mitchell, P.W. (1980). The Concepts Defining the Rate of Swell of Expansive Soils. *Proceedings of the 4th International Conference on Expansive Soils*. Denver, USA. Volume 1, pp 106-116.

Mitchell, P.W. (2008). Footing Design for Residential Type Structures in Arid Climates. *Australian Geomechanics Vol. 41*, No 4. pp 51-68.

Mitchell, P.W. (2013). Climate Change Effects on Expansive Soil Movements. *Proceedings of the 18th International Conference on Soil Mechanics and Geotechnical Engineering*. Paris, 1159-1162.

Montgomery, D., Jennings C., Kulahci, M. (2016). Time Series Analysis and Forecasting. John Wiley & Sons, Inc. Hoboken, NJ.

Naiser, D. (1997). *Procedures to predict vertical differential soil movement for expansive soil*, MS Thesis, Texas A&M University, College Station, TX, 156 p.

Navy, Dept. of, Naval Facilities Engineering Command. (1971). Design Manual-Soil Mechanics, Foundations & Earth Structures. U. S. Naval Publications & Forms Center, NAVFAC DM-7.

Nayak, N. V. & Christensen, R. W. 1971. Swell characteristics of compacted expansive soils. Clay & Clay Minerals. 19(4): 251-261.

Nelson, J.D., & Miller, D.J. (1992). *Expansive Soils: Problems & Practice in Foundation & Pavement Engineering*. New York: John Wiley & Sons, Inc.

Nelson, J.D., Overton, D.D., & Durkee, D.B. (2001). Depth of Wetting & the Active Zone. *Proceedings of Expansive Clay Soils & Vegetative Influence on Shallow Foundations, October 10-13, 2001, Houston, Texas*, USA, ASCE, 95-109.

Nelson, J., Reichler, D., & Cumbers, J. (2006). Parameters for heave prediction by oedometer tests. *Proc. 4th International Conference on Unsaturated Soils, ASCE*. (pp. 951-961). Carefree, AZ

Nelson, J.D., Chao, K.C., Overton, D.D., & Nelson, E.J. (2015). *Foundation Engineering for Expansive Aoils*. New York: Wiley Press. http://dx.doi.org/10.1002/9781118996096.

Nobel, C. A. (1966). Swelling measurements & prediction of heave for a lacustrine clay. *Canadian Geotechnical Journal,* 3(1): 32-41.

Olaiz, A.H. (2017). Evaluation of testing methods for suction-volume change of natural clay soils. Doctoral dissertation. Arizona State University. Tempe, AZ.

Olaiz, A.H.; Singhar, S.H.; Vann, J.D. & Houston, S.L. (2017). Comparison & applications of the Thornthwaite moisture index using GIS. *Proc. of the 2nd PanAm Conf. on Unsaturated Soil*s, Dallas, TX, Vol. 1, ASCE.

Olaiz, A.H., Mosawi, M., Zapata, C. (2021) An Improved Framework for Volume Change of Shrink/Swell Soils Subjected to Time-Varying Climatic Effects. (F. M. T.M.P. Campos, Ed.) *Soil and Rocks*, 44(3). doi:0.28927/SR.2021.065621

Olaiz, A.H., Mosawi, M., Zapata, C. (2023 – forthcoming) Suction Compression Indices for Natural and Recompacted Clay Soil. *Proc. of GeoCongress 2023*, Los Angeles, CA. ASCE.

O'Neill, K., & Miller, R. D. (1985). Exploration of a rigid ice model of frost heave. *Water Resources Research*, 21(3), 281-296.

Overton, D.D., Chao, K.C., & Nelson, J.D. (2006). Time rate of heave prediction for expansive soils. *GeoCongress 2006: Geotechnical Engineering in the Information Technology Age*. 1-6. Atlanta: ASCE. http://dx.doi.org/10.1061/40803(187)162.

Picornell, M. & Lytton, R. L. (1984). Modeling the heave of a heavily loaded foundation. Proceeding of 5th International Conference on Expansive Soils. (pp. 104-108). Adelaide, Australia.

Perera, Y. Y. (2003). Moisture Equilibria beneath Paved Areas. Ph.D. Dissertation, Arizona State University, Arizona, U.S.A.

Perera, Y.Y., Zapata, C.E., Houston, W.N., and Houston, S.L. (2004a). Long-Term Moisture Conditions under Highway Pavements. In M.K. Yegian & E. Kavazanjian, (eds.), Geotechnical Special Publication No. 126, Geotechnical Engineering for Transportation Projects, ASCE Geo-Institute. Los Angeles, CA, Vol. 1, pp. 1132-1143. Also Proceedings of Geo-Trans 2004, July 27-31.

Perera, Y.Y., Zapata, C.E., Houston, W.N. and Houston, S.L. (2005). Prediction of the Soil-Water Characteristic Curve Based on Grain-Size Distribution and Index Properties. In E.M. Rathje (ed.), GSPs 130-142 & GRI-18; ASCE Geo-Institute and

Geosynthetic Materials Association of the Industrial Fabrics Association International Geosynthetic Institute.

Phoon, K.K., Kulhawy, F.H., (1999). Characterization of geotechnical variability. Canadian Geotechnical Journal. 36 (4), 612–639.

Porter, A. A. & Nelson, J. D. (1980). Strain controlled testing of soils. *Proc. 4th Int. Conf Expansive Soils, ASCE & Int. Soc. Soil Mech. Found. Eng.* (pp. 34-44). Denver, CO.

Post-Tensioning Institute (PTI). (2004). Design & construction of post-tensioned slabs-on-ground, 2nd edition. Post Tensioning Institute, Phoenix.

Post-Tensioning Institute (PTI). (2008). Design & construction of post-tensioned slabs-on-ground, 3rd edition. Post Tensioning Institute, Phoenix.

Puppala, A. & Cerato, A. (2009). Heave distress problems in chemically treated sulfate-laden materials. Geo-Strata, 10 (2), 28-30, 32.

Richards, S. J. (1965). Soil Suction Measurements with Tensiometers. In Black, C. A. (Ed.). Methods of Soil Analysis, Part 1: Physical and Mineralogical Properties, Including Statistics of Measurement and Sampling (pp. 153-163).

Rosenbalm D.C. and Zapata C.E. (2013). Incorporation of the Soil-Water Characteristic Curve Hysteresis in Pavement Design. Advances in Unsaturated Soils. Caycedo et al. (eds). Proc. of the First Pan-American Conf. on Unsaturated Soils, ASCE, Cartagena, Colombia, Taylor & Francis Group, 461-467.

Roy, M., Crispin, J., Konrad, J. M., & Larose, G. (1992). Field study of two road sections during a freeze-thaw cycle. Transportation Research Record: Journal of the Transportation Research Board, (1362), 71-78

Russam, K. and J. D. Coleman. (1961) The Effect of Climatic factors on Subgrade Moisture Conditions. Geotechnique. Volume XI, No. 1, pp 22 to 28.

Salour F. Erlingsson S. and Zapata C.E. (2014). Modelling Resilient Modulus Seasonal Variation of Silty Sand Subgrade Soils with Matric Suction Control. Canadian Geotech. J. 51(12), 1413-1422.

Salour F. Erlingsson S. and Zapata C.E. (2015). Model for Seasonal Variation of Resilient Modulus in Silty Sand Subgrade Soil: Evaluation with Falling Weight Deflectometer. Transportation Research Record: J. of the Transportation Research Board, No. 2510. Transportation Research Board of the National Academies, Washington, D.C, 65-73.

Sampson, E., Schuster, R. L. & Budge, W. D. (1965). A method of determining swell potential of an expansive clay. Proc. Engineering Effects of Moisture Changes in

Soils. Int. Res. Eng. Conf Expansive Clay Soils. Texas A & M Univ. Press, College Station, TX, pp. 255-275.

Sandra, Amarendra Kumar, and Ashoke Kumar Sarkar. (2013). "Development of a Model for Estimating International Roughness Index from Pavement Distresses." International Journal of Pavement Engineering, vol. 14, no. 8, pp. 715–724.

Schneider, G.L. & Poor, A.R. (1974). The prediction of soil heave & swell pressures developed by an expansive clay. Research Report, No: TR-9-74. Construction Research Center, Univ. of Texas.

Schofield, R.K. (1935). "The pF of Water in Soil" Trans, 3rd Int. Congr. Soil Sci. (Oxford), 2, pp. 37-48.

Seed, H. B., Woodward, R.J., & Lundgren, R. (1962). Prediction of Swelling Potential for Compacted Clays. Journal of the Soil Mech. Found. Div., ASCE, vol. 88, no. SM4, 57-59.

Sengupta, B., Fristion, K.J., Penny, W.D. (2016) Gradient-based MCMCM samplers for dynamic casual modelling. *Nuerolmage* 125: 1107-1118.

Shanker, N. B., Ratnam M. V. & Rao A. S. (1987). Multi-dimensional swell behaviour of expansive clays. Proc. 6th Int. Conf. Expansive Soils. New Delhi, India.

Sheng D. Fredlund D.G. and Gens A. 2008. A new modelling approach for unsaturated soils using independent stress variables. Canadian Geotechnical Journal, 45(4): 511–534. doi:10. 1139/T07-112.

Sheng, D., Fredlund, D.G., & Gens, A. (2008a). A new modelling approach for unsaturated soils using independent stress variables. *Canadian Geotechnical Journal*, 45(4), 511-534. http://dx.doi.org/10.1139/T07-112.

Singhal, S. (2010). Expansive soil behavior: property measurement techniques and heave prediction methods. PhD Dissertation, Arizona State University, Tempe, AZ.

Singhar (2018). Evaluation of Climate Parameter with regards to Unsaturated Clay Soil Suction Profiles. MS Thesis. Arizona State University. Tempe, AZ.

Smith, A. W. (1973). Method for determining the potential vertical rise, PVR. Proc. Workshop Expansive Clays & Shales in Highway Design & Construction. Univ. of Wyoming, Denver, CO, pp. 245-249.

Snethen, D. (1980). Proceedings of the Fourth International Conference on Expansive Soils: Stouffer's Inn, Denver, Colorado, Vol 1, June 16-18, ASCE New York, N.Y.

Soltanpour, Y. (2017) A Bayesian Assessment of Regional Oil and Gas Production. PhD Dissertation. Texas A&M University. College Station, TX.

Spaans, E. J., & Baker, J. M. (1996). The soil freezing characteristic: Its measurement and similarity to the soil moisture characteristic. Soil Science Society of America Journal, 60(1), 13-19.

Sridharan, A., Sreepada Rao, A. & SivapuUaiah, P.V. (1986). Swelling pressure of clays. Geotechnical Testing Journal, GTJODJ, 9(1): 24-33.

Stallings Young E. Zapata C.E. and van Paassen L. (2020). Unsaturated Fluid Flow through Granular Soils Treated with Microbial Induced Desaturation and Precipitation. E3S Web of Conferences. 195. 05003. 10.1051/e3sconf/202019505003.

Station, Texas, USA.Covar, A. and Lytton, R. (2001). "Estimating Soil Swelling Behavior Using Soil Classification Properties", ASCE Civil Engineering Conference, GSP 115, pp. 44-63.

Style, R. W., Peppin, S. S., Cocks, A. C., & Wettlaufer, J. S. (2011). Ice-lens formation and geometrical supercooling in soils and other colloidal materials. Physical Review E, 84(4), 041402.

Su Y. Cui Y-J. 2022. Modelling the suction-dependent plastic shakedown limit of unsaturated fine/coarse soil mixture with consideration of soil-water retention curve. Transportation Geotechnics, 32, art. no. 100698

Subba Rao, K. S. & Tripathy, S. (2003). Effect of aging on swelling & swell-shrink behavior of a compacted expansive soil. ASTM Geotechnical Testing Journal, 26(1): 36-46.

Sullivan, R. A. & McClelland, B. (1969). Predicting heave of buildings on unsaturated clay. Proc. 2nd Int. Res. Eng. Conf. Expansive Soils. Texas A & M Univ. Press, College Station, TX, pp. 404-420.

Sun, Xi, et al. (July 2017). "Evaluation and Comparison of Methods for Calculating Thornthwaite Moisture Index." Australian Geomechanics Journal.

Taylor, G. S., & Luthin, J. N. (1978). A model for coupled heat and moisture transfer during soil freezing. Canadian Geotechnical Journal, 15(4), 548-555.

Teng, T. C. P. & Clisby, M. B. (1975). Experimental work for active clays in Mississippi. Transport. Eng. J. ASCE 101 (TEI): 77-95.

Teng, T. C. P., Mattox, R. M. & Clisby, M. B. (1972). A study of active clays as related to highway design. Research & Development Division, Mississippi State Highway

Dept., Engineering & Industrial Research Station, Mississippi State University, MSHD-RD-72-045, pp: 134.

Teng, T. C. P., Mattox, R. M. & Clisby, M. B. (1973). Mississippi's experimental work on active clays. Proc. Workshop on Expansive Clays & Shales in Highway design & Construction. (pp 1-17). Univ. of Wyoming, Laramie.

Thornthwaite, C. (1948). "An Approach Toward A Rational Classification of Climate", Geographical Review, Vol. 38, No. 1, pp. 55-94.

Thornthwaite, C. and Mather, J. (1955). "The Water Balance", Publications in Climatology, Vol. 8, No. 1.

Torres-Hernandez G. (2011). Estimating the Soil–Water Characteristic Curve using Grain Size Analysis and Plasticity Index. Master's Thesis. Arizona State University, Tempe, AZ.

Tu, H. & Vanapalli, S.K. (2016). Prediction of the variation of swelling pressure & one-dimensional heave of expansive soils with respect to suction using the soil-water retention curve as a tool. Canadian Geotechnical Journal, 53, NRC Research Press, 1213-1234

Tu, H. (2015). Prediction of the variation of swelling pressure & 1-d heave of expansive soils with respect to suction. (M.S. Thesis). Department of Civil Engineering, Faculty of Engineering, University of Ottawa, Ottawa, Ontario, Canada, 191 p.

Tu, H. (2015). Prediction of the variation of swelling pressure and 1-D heave of expansive soils with respect to suction. Thesis, University of Ottawa, Ottawa, Canada.

TxDOT-124-E (1978). Method for Determining the Potential Vertical Rise, PVR. Texas Department of Transportation.

U.S. Department of Agriculture, Natural Resources Conservation Service (USDA-NRCS). (1999). Soil taxonomy. 2nd ed., Gov. Print. Office, Washington, DC.

U.S. Department of Agriculture, Natural Resources Conservation Service (USDA-NRCS). (2020). Web Soil Survey. (Version 3.4.0). Lincoln, Nebraska, USA. Retrieved 2020, from http://websoilsurvey.nrcs.usda.gov

USA Army Corps of Engineers. (1948). Field Moisture Content Investigation. T.M. 3-401, Interim Report No. 1, Waterways Experiment Station

USA Army Corps of Engineers. (1955). Field Moisture Content Investigation. T. M. 3-401, Report No. 2, October 1945 -November 1952 Phase, Waterways Experiment Station

Valdivieso, L., Schoutens, W., Tuerlinckx. (2009). Maximum Likelihood estimation processes of Ornstein-Uhlenbeck type. *Stat Infer Stoch Process*. 12:1-19. DOI: 10.1007/s11203-008-9021-8

Van Der Merwe, D.H. (1964). The prediction of heave from the plasticity index & percentage clay fraction of soils. Civil Engineers in South Africa, 6: 337-42.

Vanapalli, S. and Lu, L. (2012). A State-of-the Art Review of 1-D Heave Prediction Methods for Expansive Soils. International Journal of Geotechnical Engineering, 6(1), 15-41.

Vanapalli, S. K. (1994). Simple Test Procedures and their Interpretation in Evaluating the Shear Strength of an Unsaturated Soil (Doctoral thesis, University of Saskatchewan, Canada, 1994).

Vann, J. (2019) "A soil suction-oedometer method and design soil suction profile recommendations for estimation of volume change of expansive soils." Ph.D. dissertation. State University. Tempe, AZ.

Vann, J., Houston, S., Houston, W., Singhar, S., Cuzme, A. and Olaiz, A. (2018). A soil suction surrogate & its use in the suction-oedometer method for computation of volume change of expansive soils. Proc. of the 7th International Conference on Unsaturated Soil. (pp 1205-1210). Hong Kong.

Vann, J.D., & Houston, S. (2021). Field Suction Profiles for Expansive Soil. Journal of Geotechnical and Geoenvironmental Engineering, 147(9), 04021080. https://doi.org/10.1061/(ASCE)GT.1943-5606.0002570.

Vrugt, J.A. (2016). Markov Chain Monte Carlo simulation using DREAM software package: Theory, concepts, and MATLAB implementation. *Environmental Modelling & Software,* 75:273-316.

Vu, H. Q. and Fredlund, D. G. (2004) The prediction of one-, two-, three-dimensional heave in expansive soils. *Canadian Geotechnical Journal*, 41, 713-737. Ottawa, Canada. doi: 10.1139/T04-023

Vu, H. Q., Fredlund, D. G. 2000. Volume change predictions in expansive soils using a two-dimensional finite element method, *Proceedings of the Asian Conference in Unsaturated Soils*, UNSAT ASIA 2000, Singapore, pp. 231–236.

Ward Wilson, G. (1990). Soil Evaporative Fluxes for Geotechnical Engineering Problems. PhD Thesis.

Wang, X.R., Li, Z., Wang, H., Rong, Q.G., Liang, R.Y., (2016). Probabilistic analysis of shield-driven tunnel in multiple strata considering stratigraphic uncertainty. Struct. Saf. 62:88-100.

Weston, D. J. (1980). Expansive roadbed, treatment for Southern Africa. Proceeding of the 4th International Conference on Expansive Soils, 1: 339-360.

Wheeler, S. J., and Sivakumar, V. 1995. An elasto-plastic critical state framework for unsaturated soil, *Geotechnique*, Vol. 45, No. 1, pp. 35–53.

Witczak, M.W., Zapata, C.E. and Houston, W.N. (2006). Models Incorporated into the Current Enhanced Integrated Climatic Model: NCHRP 9-23 Project Findings and Additional Changes after Version 0.7. Final Report. Project NCHRP 1-40D.

Wong, H. Y and Yong, R.M. (1973). A study of swelling & swelling force during unsaturated flow in expansive soils. Proc. 3rd Int. Conf. Expansive Soils, Haifa, Israel, 1: 143-151.

Wray, W.K. (1989). Mitigation of damage to structures supported on expansive soils. Final Report, National Science Foundation. Vol. 1.

Wray, W.K. and Meyer, K.T. (2004). Expansive Clay Soil- A Widespread & Costly GeoHazard. GeoStrata, ASCE Geo-Institute, Vol. 5, No.4. (pp 24-28).

Wray, W.K., El-Garhy, B.M., & Youssef, A.A. (2005). Three-dimensional model for moisture and volume changes prediction in expansive soils. *Journal of Geotechnical and Geoenvironmental Engineering*, 131(3), 311-324. http://dx.doi.org/10.1061/(ASCE)1090-0241(2005)131:3(311).

Yue, Er, et al. (2014). “Climatic Parameter TMI in Subgrade Soils.” Climatic Parameter TMI in Subgrade Soils | Climatic Effects on Pavement and Geotechnical Infrastructure.

Zapata C. E. (1999) “Uncertainty in Soil-Water-Characteristic Curve and Impacts on Unsaturated Shear Strength Predictions.” PhD Dissertation, Arizona State University, Arizona, USA.

Zapata C.E. Perera Y.Y. and Houston W.N. (2009). Matric Suction Prediction Model Used in the New AASHTO Mechanistic-Empirical Pavement Design Guide. Transportation Research Record: J. of the Transportation Research Board, No. 2101, Geology and Properties of Earth Materials, 53-62.

Zapata, C. (2018). Empirical approach for the use of unsaturated soil mechanics in pavement design. Geotechnical Special Publication, 2017-November (GSP 300), 149-173. https://doi.org/10.1061/9780784481677.008

Zapata, C., Houston, S., Houston, W., and Dye, H. (2006). Expansion Index and Its Relationship with Other Index Properties. *Proceeedings of the Fourth International Conference on Unsaturated Soils.* 2133-2137. Carefree, AZ. ASCE.

Zapata, C., Houston, W., Houston, S., and Walsh, K. (2000). Soil-water characteristic curve variability. Advances in Unsaturated Geotechnics, 99, 84-124.

Zapata, C.E. (2018). Empirical Approach for the Use of Unsaturated Soil Mechanics in Pavement Design. Geotechnical Special Publication, Proceedings of the Second Pan-American Conference on Unsaturated Soils. Nov. 11-14, 2017, Dallas, Texas. DOI: 10.1061/9780784481677.008, GSP 300, pp. 149-173.

Zapata, C.E., and Houston, W.N. (2009). Application of Unsaturated Soil Mechanics to Pavement Subgrade Design, Geo-Strata, Geo-Institute, American Society of Civil Engineers, May/June Issue. 3 pgs.

Zapata, C.E., Houston, W.N., Houston, S.L., and Walsh, K.D. (2000). Soil-Water Characteristic Curve Variability. In C.D. Shackelford, S.L. Houston, & N-Y Chang (eds), Advances in Unsaturated Geotechnics. Geotechnical Special Publication No. 99. Also Proceedings of Sessions of Geo-Denver 2000, August 5-8, 2000, Denver: ASCE Geo-Institute. pp. 84-124.

Zhang, X., & Lytton, R.L. (2009a). Modified state-surface approach to the study of unsaturated soil behavior. Part I: basic concept. *Canadian Geotechnical Journal*, 46(5), 536-552. http://dx.doi.org/10.1139/T08-136.

Zhang, X., & Lytton, R.L. (2009b). Modified state-surface approach to the study of unsaturated soil behavior. Part II: general formulation. *Canadian Geotechnical Journal*, 46(5), 553-570. http://dx.doi.org/10.1139/T08-137.

Zhang, J., Liu, Z., Zhang D., Haung, H., Phoon, K., Xue, Y. (2022). Improved coupled Markov Chain Method for Simulating Geological Uncertainty. *Engineering Geology*. 298.

Zheng, Y., & Ham. F. (2015). Markov Chain Monte Carlo (MCMC) uncertainty analysis for watershed quality modeling and management. *Stoch Environ Res Risk Assess,* 20:293-308. DOI: 10.1007/s00477-015-1091-8

APPENDIX A

TMI CALCULATION FOR DENVER NOAA STATION: USW00023067

Date	PRCP	TAVG	hy i	Hy	Py	alpha	pe i	N i	d i	PE i	PEy	Monthly-TMI (2006)
Jul-86	4.29	23.03	10.10	47.73	33.57	1.25	11.36	31	1.27	14.88	69.34	-28.69
Aug-86	1.36	22.29	9.61	47.65	34.22	1.24	10.91	31	1.18	13.30	69.18	-27.90
Sep-86	1.1	15.91	5.77	48.19	29.39	1.25	7.14	30	1.04	7.43	69.58	-33.32
Oct-86	4.58	9.61	2.69	47.86	32.01	1.25	3.82	31	0.96	3.79	69.11	-30.26
Nov-86	2.72	3.86	0.68	48.53	31.66	1.26	1.20	30	0.83	1.00	70.10	-31.13
Dec-86	0.79	0	0.00	48.53	30.77	1.26	0.00	31	0.81	0.00	70.10	-32.08
Jan-87	1.76	0.08	0.00	47.65	31.97	1.24	0.01	31	0.84	0.01	68.73	-30.11
Feb-87	3.08	2.28	0.30	47.65	33.39	1.24	0.64	28	0.83	0.50	68.71	-28.56
Mar-87	3.4	3.8	0.66	46.13	35.69	1.22	1.26	31	1.03	1.34	66.65	-24.84
Apr-87	2.62	11.02	3.31	46.68	31.74	1.23	4.60	30	1.11	5.11	67.42	-29.69
May-87	11.81	15.35	5.46	47.53	40.23	1.24	6.87	31	1.16	8.24	68.43	-20.91
Jun-87	8.89	20.64	8.56	47.14	46.40	1.24	9.93	30	1.25	12.40	67.99	-13.81
Jul-87	1.94	23.53	10.43	47.47	44.05	1.24	11.68	31	1.27	15.29	68.40	-16.70
Aug-87	5.08	21.49	9.09	46.95	47.77	1.23	10.45	31	1.18	12.74	67.84	-12.18
Sep-87	1.79	16.87	6.30	47.49	48.46	1.24	7.72	30	1.04	8.03	68.44	-11.90
Oct-87	3.15	10.9	3.25	48.06	47.03	1.25	4.46	31	0.96	4.42	69.07	-13.93
Nov-87	4.13	4.4	0.82	48.20	48.44	1.25	1.43	30	0.83	1.19	69.26	-12.55
Dec-87	3.3	0	0.00	48.20	50.95	1.25	0.00	31	0.81	0.00	69.26	-9.83
Jan-88	1.01	0	0.00	48.20	50.20	1.25	0.00	31	0.84	0.00	69.25	-10.63
Feb-88	1.54	1.16	0.11	48.01	48.66	1.25	0.27	28	0.83	0.21	68.97	-12.08
Mar-88	3.25	3.63	0.62	47.96	48.51	1.25	1.13	31	1.03	1.20	68.83	-12.14
Apr-88	1.65	10.13	2.91	47.57	47.54	1.24	4.09	30	1.11	4.55	68.26	-12.77
May-88	10.82	14.98	5.27	47.37	46.55	1.24	6.67	31	1.16	8.00	68.03	-13.68
Jun-88	3.26	22.13	9.51	48.32	40.92	1.25	10.79	30	1.25	13.47	69.10	-20.59
Jul-88	5.57	23.41	10.35	48.24	44.55	1.25	11.58	31	1.27	15.17	68.98	-16.56
Aug-88	4.67	23.12	10.16	49.30	44.14	1.27	11.38	31	1.18	13.87	70.11	-17.78
Sep-88	2.29	16.83	6.28	49.28	44.64	1.27	7.60	30	1.04	7.91	69.99	-17.16
Oct-88	0.16	12.23	3.87	49.90	41.65	1.28	5.03	31	0.96	4.99	70.56	-20.73
Nov-88	1.2	4.78	0.93	50.01	38.72	1.28	1.51	30	0.83	1.26	70.63	-23.89
Dec-88	2.65	0	0.00	50.01	38.07	1.28	0.00	31	0.81	0.00	70.63	-24.58
Jan-89	2.9	0.82	0.06	50.08	39.96	1.28	0.16	31	0.84	0.14	70.77	-22.65
Feb-89	1.69	0	0.00	49.97	40.11	1.28	0.00	28	0.83	0.00	70.56	-22.37
Mar-89	1.43	6.26	1.41	50.76	38.29	1.29	2.10	31	1.03	2.23	71.59	-24.89
Apr-89	2.53	10.57	3.11	50.95	39.17	1.29	4.12	30	1.11	4.57	71.61	-23.98
May-89	9.74	15.02	5.29	50.97	38.09	1.29	6.48	31	1.16	7.78	71.39	-24.98
Jun-89	5.19	18.56	7.28	48.75	40.02	1.26	8.64	30	1.25	10.77	68.70	-21.31
Jul-89	4.17	24.35	10.99	49.38	38.62	1.27	12.15	31	1.27	15.92	69.44	-23.29
Aug-89	3.26	22.03	9.44	48.67	37.21	1.26	10.72	31	1.18	13.07	68.64	-24.34
Sep-89	3.93	16.9	6.32	48.71	38.85	1.26	7.68	30	1.04	7.98	68.71	-22.59
Oct-89	2.06	10.69	3.16	47.99	40.75	1.25	4.35	31	0.96	4.32	68.04	-20.08
Nov-89	0.38	6	1.32	48.38	39.93	1.26	2.10	30	0.83	1.75	68.52	-21.30
Dec-89	2.06	0	0.00	48.38	39.34	1.26	0.00	31	0.81	0.00	68.52	-21.94
Jan-90	1.89	2.43	0.34	48.65	38.33	1.26	0.67	31	0.84	0.58	68.97	-23.32

Date	PRCP	TAVG	hy i	Hy	Py	alpha	pe i	N i	d i	PE i	PEy	Monthly-TMI (2006)
Feb-90	1.42	0.7	0.05	48.70	38.06	1.26	0.14	28	0.83	0.11	69.08	-23.68
Mar-90	7.86	4.16	0.76	48.05	44.49	1.25	1.34	31	1.03	1.42	68.26	-16.12
Apr-90	2.58	9.49	2.64	47.58	44.54	1.24	3.77	30	1.11	4.19	67.89	-15.79
May-90	3.85	13.62	4.56	46.85	38.65	1.23	5.96	31	1.16	7.15	67.26	-21.90
Jun-90	0.53	22.54	9.78	49.35	33.99	1.27	11.02	30	1.25	13.74	70.23	-28.70
Jul-90	9.06	21.54	9.13	47.48	38.88	1.24	10.46	31	1.27	13.70	68.01	-22.13
Aug-90	4.97	21.8	9.29	47.33	40.59	1.24	10.62	31	1.18	12.95	67.89	-20.16
Sep-90	3.71	19.39	7.78	48.80	40.37	1.26	9.12	30	1.04	9.49	69.40	-21.37
Oct-90	2.61	11.23	3.40	49.04	40.92	1.27	4.57	31	0.96	4.53	69.61	-20.91
Nov-90	3.25	6.67	1.55	49.27	43.79	1.27	2.35	30	0.83	1.96	69.82	-17.96
Dec-90	0.7	0	0.00	49.27	42.43	1.27	0.00	31	0.81	0.00	69.82	-19.42
Jan-91	1.93	0	0.00	48.94	42.47	1.26	0.00	31	0.84	0.00	69.24	-19.00
Feb-91	0.2	4.63	0.89	49.77	41.25	1.28	1.46	28	0.83	1.13	70.27	-20.97
Mar-91	1.96	5.99	1.31	50.33	35.35	1.29	2.00	31	1.03	2.13	70.97	-27.64
Apr-91	4.93	8.75	2.33	50.03	37.70	1.28	3.27	30	1.11	3.63	70.42	-24.85
May-91	6.18	15.7	5.65	51.12	40.03	1.30	6.86	31	1.16	8.23	71.50	-23.01
Jun-91	5.57	20.77	8.64	49.98	45.07	1.28	9.90	30	1.25	12.36	70.11	-16.79
Jul-91	10.43	22.82	9.96	50.82	46.44	1.29	11.15	31	1.27	14.61	71.01	-15.95
Aug-91	9.38	21.91	9.36	50.89	50.85	1.29	10.58	31	1.18	12.90	70.96	-11.25
Sep-91	2	16.93	6.34	49.44	49.14	1.27	7.65	30	1.04	7.96	69.43	-11.92
Oct-91	1.78	10.17	2.93	48.97	48.31	1.26	4.03	31	0.96	4.00	68.90	-12.41
Nov-91	6.79	1.5	0.16	47.58	51.85	1.24	0.38	30	0.83	0.32	67.26	-7.18
Dec-91	0.49	0.6	0.04	47.62	51.64	1.24	0.12	31	0.81	0.10	67.36	-7.50
Jan-92	3.04	0	0.00	47.62	52.75	1.24	0.00	31	0.84	0.00	67.36	-6.27
Feb-92	0.23	4.48	0.85	47.58	52.78	1.24	1.48	28	0.83	1.15	67.38	-6.25
Mar-92	8.9	6.11	1.35	47.62	59.72	1.24	2.18	31	1.03	2.32	67.57	1.28
Apr-92	1.36	12.66	4.08	49.37	56.15	1.27	5.29	30	1.11	5.88	69.81	-4.68
May-92	2.87	15.87	5.75	49.46	52.84	1.27	7.05	31	1.16	8.46	70.04	-8.42
Jun-92	5.14	18.92	7.50	48.32	52.41	1.25	8.87	30	1.25	11.06	68.75	-7.82
Jul-92	5.69	21.39	9.03	47.39	47.67	1.24	10.37	31	1.27	13.59	67.73	-12.21
Aug-92	5.92	20.21	8.29	46.32	44.21	1.22	9.71	31	1.18	11.84	66.68	-15.27
Sep-92	0.03	18.44	7.21	47.19	42.24	1.24	8.64	30	1.04	8.99	67.70	-18.21
Oct-92	1.3	12.02	3.77	48.03	41.76	1.25	5.04	31	0.96	5.00	68.70	-19.41
Nov-92	3.71	1.04	0.09	47.97	38.68	1.25	0.24	30	0.83	0.20	68.58	-22.70
Dec-92	1.71	0	0.00	47.93	39.90	1.25	0.00	31	0.81	0.00	68.48	-21.30
Jan-93	0.64	0	0.00	47.93	37.50	1.25	0.00	31	0.84	0.00	68.48	-23.93
Feb-93	2.69	0	0.00	47.08	39.96	1.24	0.00	28	0.83	0.00	67.33	-20.49
Mar-93	2.27	5.84	1.27	46.99	33.33	1.23	2.09	31	1.03	2.23	67.23	-27.82
Apr-93	5.29	9.15	2.50	45.40	37.26	1.21	3.74	30	1.11	4.15	65.50	-22.34
May-93	2.39	14.9	5.22	44.88	36.78	1.20	6.77	31	1.16	8.12	65.17	-22.67
Jun-93	4.25	19.14	7.63	45.01	35.89	1.20	9.15	30	1.25	11.41	65.52	-23.92
Jul-93	2.32	22.78	9.93	45.92	32.52	1.22	11.26	31	1.27	14.74	66.68	-28.42
Aug-93	1.65	21.11	8.85	46.48	28.25	1.23	10.24	31	1.18	12.48	67.32	-33.53

Date	PRCP	TAVG	hy i	Hy	Py	alpha	pe i	N i	d i	PE i	PEy	Monthly-TMI (2006)
Sep-93	5.83	15.9	5.76	45.03	34.05	1.20	7.31	30	1.04	7.61	65.94	-26.27
Oct-93	5.76	9.51	2.65	43.91	38.51	1.19	4.01	31	0.96	3.97	64.92	-20.51
Nov-93	3.51	1.51	0.16	43.98	38.31	1.19	0.45	30	0.83	0.37	65.09	-20.86
Dec-93	1.06	1.18	0.11	44.09	37.66	1.19	0.33	31	0.81	0.28	65.37	-21.79
Jan-94	1.37	1.25	0.12	44.21	38.39	1.19	0.35	31	0.84	0.31	65.68	-21.16
Feb-94	2.07	0.77	0.06	44.27	37.77	1.19	0.20	28	0.83	0.15	65.84	-21.97
Mar-94	2.21	7.1	1.70	44.70	37.71	1.20	2.79	31	1.03	2.97	66.58	-22.52
Apr-94	4.79	9.34	2.58	44.78	37.21	1.20	3.87	30	1.11	4.29	66.72	-23.17
May-94	3.22	17.35	6.58	46.14	38.04	1.22	8.07	31	1.16	9.68	68.27	-23.21
Jun-94	2.51	23.04	10.11	48.61	36.30	1.26	11.35	30	1.25	14.16	71.02	-26.67
Jul-94	1.28	23.26	10.25	48.93	35.26	1.26	11.47	31	1.27	15.03	71.31	-27.91
Aug-94	1.55	23.87	10.66	50.74	35.16	1.29	11.82	31	1.18	14.41	73.23	-28.99
Sep-94	1.15	19.53	7.87	52.84	30.48	1.32	9.03	30	1.04	9.39	75.01	-34.53
Oct-94	3.66	11.1	3.34	53.54	28.38	1.33	4.23	31	0.96	4.20	75.24	-36.71
Nov-94	3.4	3.28	0.53	53.91	28.27	1.34	0.82	30	0.83	0.68	75.55	-36.94
Dec-94	0.76	2.19	0.29	54.08	27.97	1.34	0.48	31	0.81	0.40	75.67	-37.28
Jan-95	0.53	1.03	0.09	54.05	27.13	1.34	0.17	31	0.84	0.15	75.51	-38.05
Feb-95	2.22	3.6	0.61	54.60	27.28	1.35	0.91	28	0.83	0.71	76.06	-38.10
Mar-95	0.71	4.04	0.72	53.62	25.78	1.34	1.10	31	1.03	1.17	74.26	-38.96
Apr-95	6.22	6.04	1.33	52.38	27.21	1.32	1.93	30	1.11	2.14	72.11	-36.70
May-95	12.06	10	2.86	48.66	36.05	1.26	3.96	31	1.16	4.76	67.19	-24.76
Jun-95	7.4	17.26	6.53	45.08	40.94	1.21	8.07	30	1.25	10.07	63.11	-16.34
Jul-95	2.66	21.97	9.40	44.23	42.32	1.19	10.82	31	1.27	14.18	62.25	-14.01
Aug-95	1.12	24.08	10.80	44.37	41.89	1.19	12.07	31	1.18	14.72	62.56	-14.78
Sep-95	4.97	16.4	6.04	42.54	45.71	1.17	7.73	30	1.04	8.04	61.21	-8.99
Oct-95	0.89	9.86	2.80	41.99	42.94	1.16	4.30	31	0.96	4.27	61.28	-12.44
Nov-95	1.36	6.15	1.37	42.83	40.90	1.17	2.44	30	0.83	2.03	62.63	-16.02
Dec-95	0.21	0.66	0.05	42.59	40.35	1.17	0.18	31	0.81	0.15	62.38	-16.49
Jan-96	2.11	0	0.00	42.50	41.93	1.17	0.00	31	0.84	0.00	62.23	-14.47
Feb-96	0.82	1.84	0.22	42.12	40.53	1.16	0.61	28	0.83	0.48	62.00	-15.97
Mar-96	3.53	2.84	0.42	41.82	43.35	1.16	1.02	31	1.03	1.09	61.92	-12.49
Apr-96	1.23	10.01	2.86	43.34	38.36	1.18	4.29	30	1.11	4.77	64.54	-20.43
May-96	6.95	15.47	5.53	46.02	33.25	1.22	7.02	31	1.16	8.42	68.21	-28.44
Jun-96	4.02	20.49	8.46	47.95	29.87	1.25	9.81	30	1.25	12.24	70.38	-33.17
Jul-96	3.1	23.18	10.20	48.75	30.31	1.26	11.43	31	1.27	14.97	71.18	-33.06
Aug-96	0.67	22.11	9.49	47.44	29.86	1.24	10.81	31	1.18	13.18	69.64	-32.84
Sep-96	6.7	16.17	5.91	47.31	31.59	1.24	7.34	30	1.04	7.63	69.23	-30.78
Oct-96	0.69	10.84	3.23	47.74	31.39	1.25	4.44	31	0.96	4.41	69.37	-31.06
Nov-96	1.44	3.72	0.64	47.01	31.47	1.23	1.20	30	0.83	1.00	68.33	-30.46
Dec-96	0.58	1.43	0.15	47.12	31.84	1.24	0.37	31	0.81	0.31	68.49	-30.13
Jan-97	1.27	0	0.00	47.12	31.00	1.24	0.00	31	0.84	0.00	68.49	-31.05
Feb-97	2.3	0	0.00	46.90	32.48	1.23	0.00	28	0.83	0.00	68.01	-29.18
Mar-97	1.29	6.5	1.49	47.96	30.24	1.25	2.34	31	1.03	2.49	69.41	-32.33

Date	PRCP	TAVG	hy i	Hy	Py	alpha	pe i	N i	d i	PE i	PEy	Monthly-TMI (2006)
Apr-97	7.52	5.76	1.24	46.34	36.53	1.22	2.09	30	1.11	2.32	66.97	-24.09
May-97	3.33	14.31	4.91	45.72	32.91	1.22	6.40	31	1.16	7.68	66.22	-27.73
Jun-97	6.37	20.36	8.38	45.64	35.26	1.21	9.83	30	1.25	12.26	66.24	-25.08
Jul-97	15.63	23.14	10.17	45.62	47.79	1.21	11.48	31	1.27	15.04	66.31	-10.95
Aug-97	10.45	21.13	8.86	44.99	57.57	1.20	10.30	31	1.18	12.56	65.69	0.73
Sep-97	2.22	18.14	7.04	46.11	53.09	1.22	8.52	30	1.04	8.86	66.92	-5.50
Oct-97	6.32	10.46	3.06	45.94	58.72	1.22	4.36	31	0.96	4.33	66.84	0.89
Nov-97	2.07	2.21	0.29	45.59	59.35	1.21	0.66	30	0.83	0.55	66.40	2.04
Dec-97	1.81	0	0.00	45.44	60.58	1.21	0.00	31	0.81	0.00	66.09	3.75
Jan-98	0.3	1.27	0.13	45.57	59.61	1.21	0.34	31	0.84	0.30	66.38	2.35
Feb-98	0.48	1.9	0.23	45.80	57.79	1.22	0.55	28	0.83	0.43	66.81	-0.13
Mar-98	2.98	3.49	0.58	44.89	59.48	1.20	1.18	31	1.03	1.26	65.58	3.02
Apr-98	6.12	7.8	1.96	45.61	58.08	1.21	3.07	30	1.11	3.41	66.67	0.34
May-98	4.4	15.81	5.71	46.41	59.15	1.23	7.19	31	1.16	8.62	67.61	0.62
Jun-98	2.59	17.65	6.75	44.78	55.37	1.20	8.31	30	1.25	10.36	65.71	-1.80
Jul-98	17.75	23.47	10.39	45.00	57.49	1.20	11.69	31	1.27	15.32	65.99	0.34
Aug-98	4.35	21.84	9.32	45.46	51.39	1.21	10.71	31	1.18	13.06	66.48	-7.02
Sep-98	2.21	19.91	8.10	46.52	51.38	1.23	9.53	30	1.04	9.91	67.53	-7.94
Oct-98	2.42	10.4	3.03	46.50	47.48	1.23	4.30	31	0.96	4.26	67.47	-12.22
Nov-98	1.52	6.14	1.36	47.57	46.93	1.24	2.20	30	0.83	1.83	68.74	-13.80
Dec-98	1.53	0	0.00	47.57	46.65	1.24	0.00	31	0.81	0.00	68.74	-14.10
Jan-99	1.46	1.94	0.24	47.68	47.81	1.24	0.52	31	0.84	0.45	68.90	-12.96
Feb-99	0.31	4.53	0.86	48.31	47.64	1.25	1.48	28	0.83	1.15	69.62	-13.68
Mar-99	0.69	7.04	1.68	49.41	45.35	1.27	2.51	31	1.03	2.67	71.03	-17.12
Apr-99	13.58	6.64	1.54	48.99	52.81	1.26	2.35	30	1.11	2.61	70.24	-8.61
May-99	6.47	13.22	4.36	47.63	54.88	1.24	5.70	31	1.16	6.83	68.45	-4.87
Jun-99	4.12	18.64	7.33	48.21	56.41	1.25	8.71	30	1.25	10.86	68.95	-3.64
Jul-99	5.24	23.98	10.74	48.56	43.90	1.26	11.93	31	1.27	15.63	69.26	-17.46
Aug-99	10.18	21.75	9.26	48.50	49.73	1.26	10.56	31	1.18	12.87	69.08	-11.01
Sep-99	2.96	15.27	5.42	45.82	50.48	1.22	6.92	30	1.04	7.20	66.37	-7.95
Oct-99	0.9	10.95	3.28	46.06	48.96	1.22	4.60	31	0.96	4.57	66.67	-9.92
Nov-99	1.22	8.37	2.18	46.88	48.66	1.23	3.27	30	0.83	2.72	67.56	-10.98
Dec-99	0.79	1.88	0.23	47.11	47.92	1.24	0.51	31	0.81	0.43	67.99	-12.14
Jan-00	1.3	1.35	0.14	47.01	47.76	1.23	0.34	31	0.84	0.30	67.84	-12.20
Feb-00	0.58	3.79	0.66	46.80	48.03	1.23	1.23	28	0.83	0.96	67.65	-11.75
Mar-00	3.49	5.5	1.16	46.28	50.83	1.22	1.98	31	1.03	2.10	67.08	-8.17
Apr-00	2.06	10.44	3.05	47.79	39.31	1.25	4.24	30	1.11	4.70	69.18	-22.38
May-00	4.27	15.94	5.79	49.22	37.11	1.27	7.10	31	1.16	8.52	70.86	-25.72
Jun-00	2.32	20.28	8.33	50.22	35.31	1.28	9.60	30	1.25	11.97	71.97	-28.20
Jul-00	3.73	24.94	11.39	50.88	33.80	1.29	12.51	31	1.27	16.38	72.72	-30.14
Aug-00	9.77	23.78	10.60	52.22	33.39	1.31	11.73	31	1.18	14.30	74.16	-31.23
Sep-00	3.99	16.97	6.36	53.16	34.42	1.33	7.48	30	1.04	7.78	74.74	-30.46
Oct-00	1.15	10.58	3.11	52.99	34.67	1.33	4.00	31	0.96	3.97	74.14	-29.93

Date	PRCP	TAVG	hy i	Hy	Py	alpha	pe i	N i	d i	PE i	PEy	Monthly-TMI (2006)
Nov-00	1.92	0	0.00	50.81	35.37	1.29	0.00	30	0.83	0.00	71.42	-27.86
Dec-00	0.72	0	0.00	50.58	35.30	1.29	0.00	31	0.81	0.00	70.99	-27.71
Jan-01	1.47	0	0.00	50.44	35.47	1.29	0.00	31	0.84	0.00	70.69	-27.37
Feb-01	1.51	0	0.00	49.78	36.40	1.28	0.00	28	0.83	0.00	69.73	-25.85
Mar-01	1.93	4.51	0.86	49.49	34.84	1.27	1.42	31	1.03	1.51	69.14	-27.21
Apr-01	3.35	9.66	2.71	49.15	36.13	1.27	3.77	30	1.11	4.18	68.62	-25.51
May-01	9.07	14.13	4.82	48.18	40.93	1.25	6.16	31	1.16	7.38	67.49	-19.51
Jun-01	3.56	20.78	8.64	48.49	42.17	1.26	9.97	30	1.25	12.44	67.95	-18.45
Jul-01	8.48	24.73	11.25	48.35	46.92	1.25	12.41	31	1.27	16.25	67.82	-13.11
Aug-01	5.41	22.79	9.94	47.69	42.56	1.24	11.22	31	1.18	13.68	67.19	-17.49
Sep-01	2.57	18.54	7.27	48.60	41.14	1.26	8.63	30	1.04	8.98	68.39	-19.88
Oct-01	0.5	10.76	3.19	48.68	40.49	1.26	4.35	31	0.96	4.31	68.73	-20.82
Nov-01	1.66	6.16	1.37	50.05	40.23	1.28	2.09	30	0.83	1.74	70.47	-22.18
Dec-01	0.69	0.9	0.07	50.13	40.20	1.28	0.18	31	0.81	0.15	70.61	-22.30
Jan-02	1	0	0.00	50.13	39.73	1.28	0.00	31	0.84	0.00	70.61	-22.80
Feb-02	0.46	0.8	0.06	50.19	38.68	1.28	0.15	28	0.83	0.12	70.73	-23.99
Mar-02	1.88	1.78	0.21	49.54	38.63	1.27	0.43	31	1.03	0.46	69.68	-23.42
Apr-02	0.23	10.69	3.16	49.99	35.51	1.28	4.23	30	1.11	4.70	70.20	-27.06
May-02	3.44	13.83	4.67	49.84	29.88	1.28	5.89	31	1.16	7.07	69.88	-32.93
Jun-02	2.8	22.49	9.74	50.94	29.12	1.29	10.94	30	1.25	13.65	71.10	-34.28
Jul-02	2.64	25.18	11.56	51.25	23.28	1.30	12.66	31	1.27	16.58	71.42	-40.55
Aug-02	1.84	22.31	9.62	50.93	19.71	1.29	10.83	31	1.18	13.20	70.95	-44.16
Sep-02	4.73	17.74	6.80	50.46	21.87	1.29	8.07	30	1.04	8.39	70.37	-41.69
Oct-02	2.02	7.49	1.84	49.12	23.39	1.27	2.73	31	0.96	2.71	68.76	-39.49
Nov-02	0.59	3.02	0.47	48.21	22.32	1.25	0.89	30	0.83	0.74	67.77	-40.30
Dec-02	0	1.1	0.10	48.24	21.63	1.25	0.25	31	0.81	0.21	67.83	-41.08
Jan-03	0	3.02	0.47	48.70	20.63	1.26	0.88	31	0.84	0.76	68.59	-42.44
Feb-03	1.29	0	0.00	48.64	21.46	1.26	0.00	28	0.83	0.00	68.47	-41.49
Mar-03	12.22	4.55	0.87	49.30	31.80	1.27	1.45	31	1.03	1.54	69.55	-30.71
Apr-03	5.16	10.95	3.28	49.42	36.73	1.27	4.40	30	1.11	4.88	69.73	-25.50
May-03	5.69	14.01	4.76	49.51	38.98	1.27	6.01	31	1.16	7.21	69.88	-23.16
Jun-03	4.85	17.68	6.77	46.53	41.03	1.23	8.23	30	1.25	10.27	66.50	-18.73
Jul-03	1.19	25.48	11.77	46.74	39.58	1.23	12.89	31	1.27	16.89	66.81	-20.57
Aug-03	7.87	23.69	10.54	47.66	45.61	1.24	11.77	31	1.18	14.35	67.96	-14.67
Sep-03	1	19.8168	8.04	48.90	41.88	1.26	9.37	30	1.04	9.75	69.32	-19.69
Oct-03	0.15	13.54	4.52	51.58	40.01	1.30	5.63	31	0.96	5.59	72.20	-23.44
Nov-03	0.46	2.21	0.29	51.40	39.88	1.30	0.53	30	0.83	0.44	71.90	-23.40
Dec-03	0.95	0.85	0.07	51.37	40.83	1.30	0.15	31	0.81	0.13	71.82	-22.36
Jan-04	0.97	0.07	0.00	50.90	41.80	1.29	0.01	31	0.84	0.01	71.06	-20.88
Feb-04	1.4	0	0.00	50.90	41.91	1.29	0.00	28	0.83	0.00	71.06	-20.77
Mar-04	0.46	7.85	1.98	52.02	30.15	1.31	2.74	31	1.03	2.92	72.45	-33.79
Apr-04	5.41	9.03	2.45	51.19	30.40	1.30	3.34	30	1.11	3.71	71.28	-33.01
May-04	3.59	14.92	5.23	51.66	28.30	1.31	6.39	31	1.16	7.66	71.73	-35.41

Date	PRCP	TAVG	hy i	Hy	Py	alpha	pe i	N i	d i	PE i	PEy	Monthly-TMI (2006)
Jun-04	4.51	17.64	6.74	51.64	27.96	1.31	7.95	30	1.25	9.92	71.37	-35.62
Jul-04	6.27	21.55	9.13	49.00	33.04	1.26	10.42	31	1.27	13.64	68.13	-28.63
Aug-04	12.56	19.58	7.90	46.36	37.73	1.22	9.34	31	1.18	11.39	65.17	-21.58
Sep-04	3.41	16.81	6.27	44.59	40.14	1.20	7.85	30	1.04	8.16	63.58	-17.65
Oct-04	2.5	10.39	3.03	43.09	42.49	1.18	4.50	31	0.96	4.47	62.46	-13.98
Nov-04	2.23	3.33	0.54	43.34	44.26	1.18	1.17	30	0.83	0.98	62.99	-12.30
Dec-04	0.33	1.45	0.15	43.43	43.64	1.18	0.44	31	0.81	0.37	63.23	-13.23
Jan-05	1.57	0.59	0.04	43.47	44.24	1.18	0.15	31	0.84	0.13	63.35	-12.63
Feb-05	0.13	2.2	0.29	43.76	42.97	1.19	0.71	28	0.83	0.55	63.90	-14.57
Mar-05	1.96	4.45	0.84	42.61	44.47	1.17	1.68	31	1.03	1.79	62.77	-11.87
Apr-05	6.06	7.98	2.03	42.20	45.12	1.16	3.35	30	1.11	3.72	62.79	-11.10
May-05	2.6	13.7	4.60	41.56	44.13	1.15	6.33	31	1.16	7.59	62.71	-12.22
Jun-05	8.36	18.79	7.42	42.24	47.98	1.16	9.07	30	1.25	11.32	64.11	-8.87
Jul-05	1.35	24.56	11.13	44.24	43.06	1.19	12.36	31	1.27	16.19	66.66	-16.55
Aug-05	6.53	21.26	8.95	45.29	37.03	1.21	10.37	31	1.18	12.64	67.91	-24.10
Sep-05	0.59	18.46	7.22	46.24	34.21	1.22	8.70	30	1.04	9.04	68.80	-27.71
Oct-05	6.38	10.94	3.27	46.49	38.09	1.23	4.57	31	0.96	4.53	68.87	-23.52
Nov-05	0.74	6.12	1.36	47.30	36.60	1.24	2.20	30	0.83	1.83	69.72	-25.63
Dec-05	0.77	0	0.00	47.15	37.04	1.24	0.00	31	0.81	0.00	69.35	-24.94
Jan-06	0.84	3.46	0.57	47.68	36.31	1.24	1.07	31	0.84	0.93	70.16	-26.18
Feb-06	0.46	0	0.00	47.40	36.64	1.24	0.00	28	0.83	0.00	69.61	-25.52
Mar-06	2.15	3.59	0.61	47.16	36.83	1.24	1.14	31	1.03	1.22	69.03	-24.99
Apr-06	1.58	10.79	3.20	48.34	32.35	1.25	4.38	30	1.11	4.86	70.17	-30.42
May-06	1.56	15.69	5.65	49.39	31.31	1.27	6.95	31	1.16	8.34	70.92	-31.89
Jun-06	0.08	22.04	9.45	51.41	23.03	1.30	10.64	30	1.25	13.28	72.88	-41.30
Jul-06	5.65	23.68	10.53	50.82	27.33	1.29	11.70	31	1.27	15.32	72.00	-36.53
Aug-06	6.91	21.76	9.27	51.14	27.71	1.30	10.47	31	1.18	12.77	72.13	-36.19
Sep-06	2	14.4	4.96	48.87	29.12	1.26	6.26	30	1.04	6.51	69.60	-33.62
Oct-06	4.63	9.65	2.71	48.31	27.37	1.25	3.81	31	0.96	3.78	68.85	-35.18
Nov-06	0.84	5.15	1.05	47.99	27.47	1.25	1.75	30	0.83	1.45	68.47	-34.91
Dec-06	5.45	0.02	0.00	47.99	32.15	1.25	0.00	31	0.81	0.00	68.47	-29.78
Jan-07	2.6	0	0.00	47.42	33.91	1.24	0.00	31	0.84	0.00	67.54	-27.34
Feb-07	0.91	0	0.00	47.42	34.36	1.24	0.00	28	0.83	0.00	67.54	-26.84
Mar-07	3.45	7.32	1.78	48.60	35.66	1.26	2.68	31	1.03	2.85	69.17	-26.34
Apr-07	4.94	7.83	1.97	47.36	39.02	1.24	2.98	30	1.11	3.31	67.62	-21.72
May-07	11.47	14.51	5.02	46.73	48.93	1.23	6.45	31	1.16	7.74	67.02	-10.24
Jun-07	1.47	19.75	8.00	45.29	50.32	1.21	9.49	30	1.25	11.84	65.58	-7.45
Jul-07	1.42	24.11	10.82	45.58	46.09	1.21	12.07	31	1.27	15.81	66.07	-12.68
Aug-07	8.95	23.23	10.23	46.54	48.13	1.23	11.51	31	1.18	14.04	67.33	-11.39
Sep-07	3	17.78	6.83	48.41	49.13	1.26	8.20	30	1.04	8.53	69.34	-11.86
Oct-07	2.71	11.8	3.67	49.37	47.21	1.27	4.84	31	0.96	4.80	70.36	-14.68
Nov-07	0.46	5.3	1.09	49.42	46.83	1.27	1.75	30	0.83	1.46	70.37	-15.09
Dec-07	2.96	0	0.00	49.42	44.34	1.27	0.00	31	0.81	0.00	70.36	-17.74

Date	PRCP	TAVG	hy i	Hy	Py	alpha	pe i	N i	d i	PE i	PEy	Monthly-TMI (2006)
Jan-08	0.54	0	0.00	49.42	42.28	1.27	0.00	31	0.84	0.00	70.36	-19.93
Feb-08	1.29	0.76	0.06	49.48	42.66	1.27	0.15	28	0.83	0.11	70.48	-19.60
Mar-08	1.4	4.27	0.79	48.48	40.61	1.26	1.36	31	1.03	1.45	69.08	-20.91
Apr-08	0.79	7.27	1.76	48.27	36.46	1.25	2.67	30	1.11	2.97	68.73	-25.22
May-08	4.1	13.04	4.27	47.52	29.09	1.24	5.61	31	1.16	6.73	67.72	-32.78
Jun-08	1.8	19.46	7.83	47.35	29.42	1.24	9.23	30	1.25	11.51	67.40	-32.26
Jul-08	0.38	24.23	10.91	47.43	28.38	1.24	12.11	31	1.27	15.86	67.46	-33.45
Aug-08	7.67	21.54	9.13	46.32	27.10	1.22	10.50	31	1.18	12.80	66.22	-34.31
Sep-08	3.97	16.03	5.83	45.33	28.07	1.21	7.37	30	1.04	7.66	65.36	-32.79
Oct-08	2.62	10.5	3.07	44.74	27.98	1.20	4.45	31	0.96	4.42	64.98	-32.70
Nov-08	0.94	6.27	1.41	45.05	28.46	1.21	2.38	30	0.83	1.98	65.51	-32.42
Dec-08	2.03	0	0.00	45.05	27.53	1.21	0.00	31	0.81	0.00	65.51	-33.48
Jan-09	0.71	1.33	0.13	45.19	27.70	1.21	0.37	31	0.84	0.32	65.82	-33.44
Feb-09	0.21	3.45	0.57	45.70	26.62	1.21	1.14	28	0.83	0.88	66.59	-35.02
Mar-09	1.62	5.45	1.14	46.05	26.84	1.22	1.97	31	1.03	2.09	67.23	-35.06
Apr-09	7.5	7.16	1.72	46.01	33.55	1.22	2.74	30	1.11	3.05	67.31	-27.62
May-09	8.8876	11.8296	3.68	45.43	38.34	1.21	5.10	31	1.16	6.11	66.70	-21.89
Jun-09	9.39	17.36	6.58	44.18	45.93	1.19	8.17	30	1.25	10.20	65.38	-12.32
Jul-09	7.85	20.97	8.76	42.04	53.40	1.16	10.32	31	1.27	13.51	63.04	-1.47
Aug-09	2.34	20.74	8.62	41.53	48.07	1.15	10.20	31	1.18	12.44	62.67	-7.48
Sep-09	2.21	16.38	6.03	41.73	46.31	1.15	7.76	30	1.04	8.07	63.08	-9.94
Oct-09	4.07	5.73	1.23	39.88	47.76	1.13	2.41	31	0.96	2.39	61.05	-6.33
Nov-09	1.67	5.91	1.29	39.76	48.49	1.13	2.50	30	0.83	2.08	61.15	-5.53
Dec-09	1.73	0	0.00	39.76	48.19	1.13	0.00	31	0.81	0.00	61.15	-5.90
Jan-10	0.23	0	0.00	39.63	47.71	1.12	0.00	31	0.84	0.00	60.83	-6.18
Feb-10	1.64	0	0.00	39.06	49.14	1.11	0.00	28	0.83	0.00	59.95	-3.52
Mar-10	3.25	4.41	0.83	38.74	50.77	1.11	1.85	31	1.03	1.97	59.82	-1.35
Apr-10	6.65	8.8	2.35	39.37	49.92	1.12	3.94	30	1.11	4.37	61.15	-3.77
May-10	3.12	12.02	3.77	39.46	44.15	1.12	5.58	31	1.16	6.69	61.72	-11.35
Jun-10	4.52	20.35	8.37	41.25	39.28	1.15	9.99	30	1.25	12.47	63.99	-18.96
Jul-10	4.28	22.75	9.91	42.41	35.71	1.17	11.33	31	1.27	14.84	65.32	-24.00
Aug-10	2.74	22.93	10.03	43.82	36.11	1.19	11.40	31	1.18	13.90	66.78	-24.44
Sep-10	0.18	18.97	7.53	45.32	34.08	1.21	9.03	30	1.04	9.40	68.10	-27.47
Oct-10	1.43	12.46	3.98	48.08	31.44	1.25	5.27	31	0.96	5.22	70.93	-31.76
Nov-10	1.33	3.76	0.65	47.44	31.10	1.24	1.20	30	0.83	1.00	69.85	-31.61
Dec-10	0.51	1.63	0.18	47.62	29.88	1.24	0.42	31	0.81	0.35	70.20	-33.08
Jan-11	1.14	0	0.00	47.62	30.79	1.24	0.00	31	0.84	0.00	70.20	-32.11
Feb-11	1.35	0	0.00	47.62	30.50	1.24	0.00	28	0.83	0.00	70.20	-32.42
Mar-11	0.66	5.75	1.24	48.03	27.91	1.25	2.00	31	1.03	2.13	70.37	-35.25
Apr-11	2.77	8.93	2.41	48.08	24.03	1.25	3.47	30	1.11	3.85	69.85	-39.20
May-11	9.31	10.84	3.23	47.54	30.22	1.24	4.46	31	1.16	5.35	68.51	-31.92
Jun-11	3.45	19.57	7.89	47.05	29.15	1.24	9.31	30	1.25	11.61	67.65	-32.68
Jul-11	17.65	23.94	10.71	47.85	42.52	1.25	11.92	31	1.27	15.62	68.43	-18.39

Date	PRCP	TAVG	hy i	Hy	Py	alpha	pe i	N i	d i	PE i	PEy	Monthly-TMI (2006)
Aug-11	0.18	23.97	10.73	48.55	39.96	1.26	11.93	31	1.18	14.54	69.07	-21.61
Sep-11	4.11	16.75	6.24	47.25	43.89	1.24	7.67	30	1.04	7.97	67.65	-16.34
Oct-11	3.86	10.77	3.20	46.46	46.32	1.23	4.49	31	0.96	4.45	66.87	-13.05
Nov-11	1	4.38	0.82	46.63	45.99	1.23	1.48	30	0.83	1.23	67.11	-13.60
Dec-11	2.49	0	0.00	46.45	47.97	1.23	0.00	31	0.81	0.00	66.76	-11.11
Jan-12	0.6	2.09	0.27	46.72	47.43	1.23	0.59	31	0.84	0.52	67.27	-12.12
Feb-12	2.42	0	0.00	46.72	48.50	1.23	0.00	28	0.83	0.00	67.27	-10.93
Mar-12	0	9.02	2.44	47.92	47.84	1.25	3.52	31	1.03	3.75	68.89	-12.92
Apr-12	2.54	11.55	3.55	49.07	47.61	1.27	4.73	30	1.11	5.25	70.29	-14.20
May-12	2.95	15.62	5.61	51.45	41.25	1.30	6.79	31	1.16	8.15	73.09	-22.67
Jun-12	0.95	23.14	10.17	53.73	38.75	1.34	11.28	30	1.25	14.07	75.55	-26.53
Jul-12	5.1	25.44	11.74	54.77	26.20	1.35	12.79	31	1.27	16.76	76.69	-39.38
Aug-12	0.51	23.22	10.23	54.26	26.53	1.35	11.32	31	1.18	13.80	75.95	-38.80
Sep-12	5.75	18.6	7.31	55.33	28.17	1.36	8.34	30	1.04	8.68	76.65	-37.44
Oct-12	2.06	9.32	2.57	54.70	26.37	1.35	3.29	31	0.96	3.26	75.47	-38.79
Nov-12	0.91	6.26	1.41	55.29	26.28	1.36	1.89	30	0.83	1.58	75.81	-39.00
Dec-12	0.55	0.21	0.01	55.30	24.34	1.36	0.02	31	0.81	0.02	75.83	-40.93
Jan-13	0.61	0	0.00	55.03	24.35	1.36	0.00	31	0.84	0.00	75.31	-40.75
Feb-13	1.7	0	0.00	55.03	23.63	1.36	0.00	28	0.83	0.00	75.31	-41.47
Mar-13	3.64	2.75	0.40	52.99	27.27	1.33	0.67	31	1.03	0.71	72.27	-36.70
Apr-13	2.79	5.48	1.15	50.59	27.52	1.29	1.77	30	1.11	1.97	68.99	-35.08
May-13	3.14	14.12	4.82	49.80	27.71	1.28	6.06	31	1.16	7.26	68.11	-34.48
Jun-13	1.05	21.28	8.96	48.58	27.81	1.26	10.27	30	1.25	12.81	66.84	-33.80
Jul-13	8.87	23.04	10.11	46.95	31.58	1.23	11.39	31	1.27	14.92	65.00	-28.56
Aug-13	4.02	22.81	9.95	46.68	35.09	1.23	11.25	31	1.18	13.72	64.93	-24.47
Sep-13	35.28	19.11	7.61	46.98	64.62	1.23	9.04	30	1.04	9.40	65.65	8.82
Oct-13	1.57	8.52	2.24	46.66	64.13	1.23	3.35	31	0.96	3.33	65.71	8.19
Nov-13	0.51	4.76	0.93	46.18	63.73	1.22	1.66	30	0.83	1.38	65.52	7.95
Dec-13	0.69	0	0.00	46.17	63.87	1.22	0.00	31	0.81	0.00	65.50	8.13
Jan-14	1.63	0	0.00	46.17	64.89	1.22	0.00	31	0.84	0.00	65.50	9.30
Feb-14	0.66	0	0.00	46.17	63.85	1.22	0.00	28	0.83	0.00	65.50	8.11
Mar-14	2.06	5.02	1.01	46.77	62.27	1.23	1.75	31	1.03	1.86	66.65	5.07
Apr-14	3.28	9.33	2.57	48.19	62.76	1.25	3.66	30	1.11	4.06	68.74	3.47
May-14	8.82	14.32	4.92	48.30	68.44	1.25	6.25	31	1.16	7.50	68.98	9.41
Jun-14	4.19	18.93	7.51	46.84	71.58	1.23	8.94	30	1.25	11.16	67.33	14.74
Jul-14	8.56	22.83	9.97	46.70	71.27	1.23	11.27	31	1.27	14.76	67.17	14.58
Aug-14	2.6	20.98	8.77	45.52	69.85	1.21	10.20	31	1.18	12.43	65.88	14.52
Sep-14	5.45	18.02	6.97	44.87	40.02	1.20	8.51	30	1.04	8.85	65.33	-19.06
Oct-14	1.7	12.38	3.95	46.58	40.15	1.23	5.31	31	0.96	5.27	67.27	-20.24
Nov-14	2.37	2.18	0.28	45.93	42.01	1.22	0.65	30	0.83	0.54	66.43	-17.57
Dec-14	1.3	0	0.00	45.93	42.62	1.22	0.00	31	0.81	0.00	66.43	-16.88
Jan-15	0.88	0.87	0.07	46.00	41.87	1.22	0.21	31	0.84	0.18	66.61	-17.86
Feb-15	5.24	1.01	0.09	46.09	46.45	1.22	0.25	28	0.83	0.19	66.81	-12.85

Date	PRCP	TAVG	hy i	Hy	Py	alpha	pe i	N i	d i	PE i	PEy	Monthly-TMI (2006)
Mar-15	1.45	6.36	1.44	46.53	45.84	1.23	2.35	31	1.03	2.50	67.45	-14.03
Apr-15	5.96	9.09	2.47	46.43	48.52	1.23	3.65	30	1.11	4.05	67.43	-11.03
May-15	12.77	11.17	3.38	44.89	52.47	1.20	4.79	31	1.16	5.75	65.68	-5.08
Jun-15	18.73	20.46	8.44	45.82	67.01	1.22	9.88	30	1.25	12.33	66.85	10.18
Jul-15	3.07	22.07	9.47	45.32	61.52	1.21	10.85	31	1.27	14.21	66.30	4.59
Aug-15	1.48	22.5	9.75	46.30	60.40	1.22	11.08	31	1.18	13.51	67.37	2.24
Sep-15	0.49	20.15	8.25	47.59	55.44	1.24	9.63	30	1.04	10.01	68.53	-4.33
Oct-15	4.66	13.71	4.61	48.25	58.40	1.25	5.92	31	0.96	5.88	69.14	-1.65
Nov-15	4.42	4.4	0.82	48.79	60.45	1.26	1.40	30	0.83	1.17	69.77	-0.02
Dec-15	2.11	0	0.00	48.79	61.26	1.26	0.00	31	0.81	0.00	69.77	0.85
Jan-16	0.94	0.24	0.01	48.73	61.32	1.26	0.04	31	0.84	0.03	69.62	1.06
Feb-16	1.9	3.62	0.61	49.25	57.98	1.27	1.08	28	0.83	0.84	70.26	-3.11
Mar-16	4.18	5.67	1.21	49.02	60.71	1.27	1.92	31	1.03	2.05	69.81	0.22
Apr-16	5.79	8.75	2.33	48.88	60.54	1.26	3.34	30	1.11	3.71	69.47	0.36
May-16	4.83	12.05	3.79	49.29	52.60	1.27	4.98	31	1.16	5.97	69.69	-8.39
Jun-16	3.69	22.09	9.48	50.33	37.56	1.29	10.71	30	1.25	13.36	70.72	-25.17
Jul-16	1.89	24.79	11.29	52.15	36.38	1.31	12.39	31	1.27	16.23	72.74	-27.49
Aug-16	1.69	22.21	9.56	51.96	36.59	1.31	10.73	31	1.18	13.08	72.32	-27.05
Sep-16	0.16	19	7.55	51.26	36.26	1.30	8.78	30	1.04	9.13	71.44	-26.93
Oct-16	0.69	14.26	4.89	51.54	32.29	1.30	6.03	31	0.96	5.98	71.55	-31.15
Nov-16	1.12	8.03	2.05	52.77	28.99	1.32	2.79	30	0.83	2.32	72.70	-35.09
Dec-16	1.59	0	0.00	52.77	28.47	1.32	0.00	31	0.81	0.00	72.70	-35.63
Jan-17	1.31	0	0.00	52.76	28.84	1.32	0.00	31	0.84	0.00	72.67	-35.23
Feb-17	0.29	5.07	1.02	53.17	27.23	1.33	1.50	28	0.83	1.17	72.99	-37.02
Mar-17	1.79	8.56	2.26	54.21	24.84	1.34	2.96	31	1.03	3.15	74.09	-39.86
Apr-17	3.17	9.55	2.66	54.54	22.22	1.35	3.41	30	1.11	3.78	74.17	-42.53
May-17	12.15	13	4.25	55.01	29.54	1.36	5.14	31	1.16	6.17	74.37	-35.21
Jun-17	2.22	21.48	9.09	54.61	28.07	1.35	10.18	30	1.25	12.70	73.71	-36.44
Jul-17	2.03	24.56	11.13	54.45	28.21	1.35	12.20	31	1.27	15.98	73.46	-36.20
Aug-17	3.79	22	9.42	54.32	30.31	1.35	10.52	31	1.18	12.83	73.21	-33.95
Sep-17	2.68	18.49	7.24	54.01	32.83	1.34	8.34	30	1.04	8.67	72.75	-31.16
Oct-17	2.75	10.16	2.93	52.05	34.89	1.31	3.85	31	0.96	3.82	70.59	-27.93
Nov-17	0.72	7.34	1.79	51.79	34.49	1.31	2.52	30	0.83	2.10	70.37	-28.24
Dec-17	0.51	1.04	0.09	51.88	33.41	1.31	0.20	31	0.81	0.16	70.53	-29.47
Jan-18	0.84	0.93	0.08	51.96	32.94	1.31	0.17	31	0.84	0.15	70.68	-30.05
Feb-18	0.98	0	0.00	50.94	33.63	1.29	0.00	28	0.83	0.00	69.51	-28.71
Mar-18	4.07	6.09	1.35	50.03	35.91	1.28	2.06	31	1.03	2.19	68.55	-25.71
Apr-18	3.25	8.6	2.27	49.64	35.99	1.27	3.22	30	1.11	3.58	68.35	-25.51
May-18	5.59	16.27	5.97	51.36	29.43	1.30	7.17	31	1.16	8.60	70.78	-33.82
Jun-18	1.82	23.01	10.09	52.36	29.03	1.32	11.23	30	1.25	14.01	72.10	-34.80
Jul-18	3.66	23.97	10.73	51.95	30.66	1.31	11.86	31	1.27	15.53	71.65	-32.91
Aug-18	3.96	21.98	9.41	51.94	30.83	1.31	10.59	31	1.18	12.91	71.72	-32.76
Sep-18	2.29	19.53	7.87	52.57	30.44	1.32	9.04	30	1.04	9.40	72.45	-33.49

Date	PRCP	TAVG	hy i	Hy	Py	alpha	pe i	N i	d i	PE i	PEy	Monthly-TMI (2006)
Oct-18	2.2	9.57	2.67	52.31	29.89	1.32	3.54	31	0.96	3.51	72.15	-33.93
Nov-18	0.84	3.69	0.63	51.16	30.01	1.30	1.05	30	0.83	0.87	70.92	-33.26
Dec-18	0.08	0.58	0.04	51.10	29.58	1.30	0.10	31	0.81	0.08	70.84	-33.68
Jan-19	3.13	0	0.00	51.02	31.87	1.30	0.00	31	0.84	0.00	70.69	-31.19
Feb-19	2.1	0	0.00	51.02	32.99	1.30	0.00	28	0.83	0.00	70.69	-30.00
Mar-19	4.18	1.98	0.25	49.92	33.10	1.28	0.49	31	1.03	0.52	69.02	-29.03
Apr-19	1.53	9.9	2.81	50.46	31.38	1.29	3.81	30	1.11	4.23	69.67	-31.22
May-19	8.03	10.62	3.13	47.62	33.82	1.24	4.34	31	1.16	5.21	66.27	-26.73
Jun-19	1.65	18.72	7.38	44.92	33.65	1.20	8.91	30	1.25	11.12	63.38	-25.18
Jul-19	2.34	24.43	11.04	45.23	32.33	1.21	12.27	31	1.27	16.07	63.91	-27.06
Aug-19	2.74	23.95	10.72	46.54	31.11	1.23	11.95	31	1.18	14.57	65.58	-29.42
Sep-19	1.07	20.65	8.56	47.23	29.89	1.24	9.94	30	1.04	10.33	66.51	-31.30
Oct-19	2.63	7	1.66	46.22	30.32	1.22	2.66	31	0.96	2.64	65.64	-30.35
Nov-19	2.3	2.95	0.45	46.04	31.78	1.22	0.93	30	0.83	0.77	65.54	-28.63
Dec-19	0.49	1.24	0.12	46.12	32.19	1.22	0.32	31	0.81	0.27	65.73	-28.27
Jan-20	0.03	1.61	0.18	46.30	29.09	1.22	0.44	31	0.84	0.38	66.11	-32.00
Feb-20	2.8	0	0.00	46.30	29.79	1.22	0.00	28	0.83	0.00	66.11	-31.20
Mar-20	4.61	6.09	1.35	47.40	30.22	1.24	2.18	31	1.03	2.32	67.91	-31.63
Apr-20	1.71	7.77	1.95	46.54	30.40	1.23	3.00	30	1.11	3.33	67.02	-30.98
May-20	4.37	15.46	5.52	48.94	26.74	1.26	6.85	31	1.16	8.21	70.03	-36.36
Jun-20	4.74	21.56	9.14	50.70	29.83	1.29	10.36	30	1.25	12.93	71.84	-33.86
Jul-20	0.92	24.34	10.98	50.63	28.41	1.29	12.12	31	1.27	15.88	71.65	-35.26
Aug-20	0.77	24.53	11.11	51.03	26.44	1.30	12.24	31	1.18	14.92	72.00	-37.46
Sep-20	1.99	17.67	6.76	49.23	27.36	1.27	8.09	30	1.04	8.42	70.08	-35.72
Oct-20	0.43	9.77	2.76	50.32	25.16	1.28	3.75	31	0.96	3.72	71.17	-38.48
Nov-20	1.06	6.73	1.57	51.44	23.92	1.30	2.27	30	0.83	1.89	72.28	-40.18
Dec-20	1.14	1.5	0.16	51.48	24.57	1.30	0.32	31	0.81	0.27	72.28	-39.51
Dec-20	1.14	1.5	0.16	51.48	24.57	1.30	0.32	31	0.81	0.27	72.28	-39.51

APPENDIX B

SOIL AND ROCKS JOURNAL PUBLICATION

Soils and Rocks
An International Journal of Geotechnical and Geoenvironmental Engineering
www.soilsandrocks.com
ISSN 1980-9743
ISSN-e 2675-5475

An improved framework for volume change of shrink/swell soils subjected to time-varying climatic effects

Austin H. Olaiz[1#], Mohammad Mosawi[1], Claudia E. Zapata[1]

Article

Keywords
Shrink/swell volume change
Time-varying climatic effects
Soil-climate interaction
Mitchell's closed-form solution
Soil suction envelopes
Unsaturated soil moisture flow

Abstract

The ability to estimate soil volume change as a function of time is a valuable tool in the design or forensic analysis of shallow foundations and pavement structures. This paper presents an improved framework for estimating the volume change of shrink/swell soils due to time-varying climatic effects using the Lytton et al. (2005) approach with the suction envelope models created by Vann & Houston (2021) and updated considerations of short-term varying climate. The procedure can be easily implemented in any country due to its mechanistic-empirical nature. The authors present an example calculation of the proposed framework using the data from an American Association of State Highway and Transportation Officials (AASHTO) Long-Term Pavement Performance (LTPP) Seasonal Monitoring Program (SMP) section, located approximately 80 miles northeast of Dallas, Texas. The volume change estimated from the proposed framework was compared to 70 measured data points from sections from the SMP study and the results look promising. The models are universal and can be used in any part of the world provided measured data is available to calibrate for local conditions. Ongoing calibration effort with the remaining LTPP SMP sections will allow obtaining calibration factors for the proposed framework that will improve the estimation of the volume change predictions under pavements and facilitate the implementation into current design procedures.

1. Introduction

The ability to estimate soil volume change as a function of time is a valuable tool in the design of shallow foundations of pavement structures. Specifically pertaining to pavement design, estimating soil volume change as a function of time allows for the prediction of the potential cumulative International Roughness Index (IRI). The time-varying volume change can also be a valuable tool in the forensic analysis of existing foundation movement of a lightly loaded structure on shallow footings.

This paper presents an improved framework for estimating the volume change of shrink/swell soils due to time-varying climatic effects using the Lytton et al. (2005) approach with the suction envelope models created by Vann & Houston (2021). The proposed framework for estimating soil volume change of shrink/swell soils as a function of time is presented as an example calculation with data from an AASHTO Long-Term Pavement Performance (LTPP) Seasonal Monitoring Program (SMP) section TX 48-1068 (FHWA, 1995), which is located approximately 80 miles northeast of Dallas, Texas. The SMP study includes measured data from 1/1994 to 9/1997 for the TX 48-1068 section. The construction date of the TX48-1068 section is 3/1987. As such, the example calculation will use the time frame of 3/1987 to 9/1997 so that a comparison of predicted and measured volume change can be performed.

2. Volume change of shrink/swell soils

The determination of the magnitude of potential soil volume change is a key focus of geotechnical engineering as it causes significant infrastructure damage each year. Studies have been published, which empirically relate soil index properties (Atterberg limits, gradation, mineralogy, etc.), along with soil engineering properties (density, moisture content, swell pressure, etc.), to volume change.

Direct laboratory measurements of the volume change potential of a soil helps improve the estimation of potential volume change in the field. The 1-D oedometer "Response to Wetting Test" as described in ASTM D4546 (ASTM, 2021) is the common type of laboratory test for volume

#Corresponding author. E-mail address: Austin.Olaiz@asu.edu
[1]Arizona State University, School of Sustainable Engineering and The Built Environment, Tempe, AZ, USA.

Submitted on April 10, 2021; Final Acceptance on July 14, 2021; Discussion open until November 30, 2021.
https://doi.org/10.28927/SR.2021.065621

change determination. One key difference from the laboratory oedometer test compared to the field conditions the soil will experience is the final degree of saturation. The response to wetting test inundates the sample, driving to almost full saturation. However, it is the probability that the soil will reach this moisture level over the period of the structure/pavements design life is very low (Houston & Houston, 2017).

A common method for volume change estimation is the Potential Vertical Rise published by the Texas Department of Transportation (TxDOT, 1978), which includes both empirical-based relationships and result from an oedometer test. In 2005, the Texas DOT updated the approach to determining the volume change of expansive soils using the work by Lytton et al. (2005), which encompassed a suction-based approach. The study concluded that the previous empirical-based approach significantly over-estimated the soil heave and did not account for the shrinkage of the soil during dry climatic periods.

A thorough literature review of volume change estimates of unsaturated soil (oedometer-based, or suction-based) was performed by Vann (2019). The authors of this paper have carefully reviewed this relative literature summary as part of the research leading up to this paper.

The suction-based approach by Lytton et al. (2005) for estimating the volume change of shrink/swell soils which was adopted by the Texas DOT and the Post-Tensioning Institute for the design of slabs on ground (PTI, 2004, 2008), was the compilation of efforts of several related studies including: Lytton (1977), McKeen & Hamberg (1981), Holtz & Gibbs (1956), Covar & Lytton (2001), Lytton et al. (2004). The approach encompasses the volumetric strain caused by changes in both stress states of the soil (matric suction and net normal stress) and uses the closed-form solution of the Richard's unsaturated moisture flow equation (Bear, 1972) developed by Mitchell (1979) to estimate the soil volume-change as a function of time when no groundwater table is present. The relationship between the change in each stress state and the volumetric strain, referred to as the compression indices, must be directly measured or empirically determined.

One limitation of the Mitchell equation (1979) used in the Lytton et al. (2005) framework is that the climate boundary condition is assumed and modelled to be a sinusoidal pattern. Aubeny & Long (2007) proposed an improvement to this limitation by fitting a Fourier equation to the climate data. The Fourier fit to the climate data allows for the irregularities of climate data to be captured and allows for the development of asymmetrical suction profiles. Aubeny & Long (2007) also studied the uncertainty of the key variables required in the Mitchell's equation (1979) for the change in soil suction with time. The study concluded that the diffusion coefficient (α) had significant ranges for a given soil, low reproducibility, and discrepancies between lab and field measurements, and was dependent upon the number of climatic cycles per year (n) when performing a back-calculation from the depth of equilibrium suction.

Vann & Houston (2021) developed correlations between the 30-year Thornthwaite Moisture Index (Thornthwaite, 1948; Witczak et al., 2006) and soil suction envelopes using measured data from over 40 geotechnical studies (Vann, 2019). The suction envelope correlations to the *TMI* allow for key aspects of the Aubeny & Long (2007) approach to estimating volume change of shrink/swell soils as function of time to be determined without the need to measure or estimate the diffusion coefficient or number of climatic cycles per year.

This paper presents an improved framework for estimating the volume change of shrink/swell soils due to time-varying climatic effects. This framework builds upon the work presented by Lytton et al. (2005) and incorporates the latest suction envelope models proposed by Vann & Houston (2021). The framework presented is applicable to uncovered sites where the groundwater table effects are negligible, but it has been calibrated to account for covered areas and for the spatial variation between the pavement center and edges.

3. Framework outline

The following outline summarizes the steps of the improved framework for estimating the volume change of shrink/swell soils due to time-varying (monthly) climatic effects:

1. Weather station identification and data extraction
2. 30-year and monthly Thornthwaite Moisture Index per Witczak et al. (2006)
3. Determination of suction envelope parameters per Vann & Houston (2021)
    a. Depth to stable suction
    b. Magnitude of stable suction
    c. Limits of suction variation at the surface
    d. Climatic parameter (r)
4. Back-calculation of variables for Mitchell (1979) equation
5. Development of long-term wet and dry suction profiles
6. Initial estimation of monthly changes in suction at the surface per Perera (2003)
7. Adjustment to estimation of monthly changes in suction using limits of suction variation at the surface from Vann & Houston (2021)
8. Fourier equation fit to the monthly suction change at the surface per Aubeny & Long (2007)
9. Generation of monthly suction profile per Aubeny & Long (2007)
10. Suction profile adjustments for varying surface boundary conditions
11. Determination of net normal stress profile
12. Estimation of suction compression index (assuming value is not directly measured)
13. Calculation of strain monthly
14. Calculation of volume change monthly

3.1 Step 1: climate data

A Season Monitoring Program (SMP) pavement section approximately 80 miles northwest of Dallas, Texas (TX 48-1068) is used to provide an example for the proposed framework (FHWA, 2021). For the purposes of this example calculation, the climate data was gathered from the weather station nearest to the site and identified using the open-access Thornthwaite Moisture Index (*TMI*) GIS map developed by Olaiz (2017), which uses the National Oceanic and Atmospheric Administration's (NOAA) 30-year climate normal database for the United States. Figure 1 presents an excerpt for the GIS map, which has the Paris, TX weather station selected.

The "Station ID" shown in the pop-up window in Figure 1 (USC00416794) is the only data needed for the purposes of this study. However, the remaining data shown may be helpful to get an understanding of the general climatic conditions at the site.

The NOAA climate data associated with each station in the country can be extracted from the online NOAA FTP site. It is recommended that the extracted weather data be filtered to contain the necessary variables for computation of the Thornthwaite Moisture Index (Witczak et al., 2006):

- Year
- Month
- Monthly Precipitation (cm)
- Monthly Average Temperature (Celsius)

Note that the Vann & Houston (2021) models used in the proposed analysis correlate the suction envelope parameters to a 30-year *TMI* value. As such, the climate data from the NOAA database for station USC00416794 was extracted for the date range of 9/1967 to 9/1997 (the last date of measured data from the SMP study for the TX 48-1068 section).

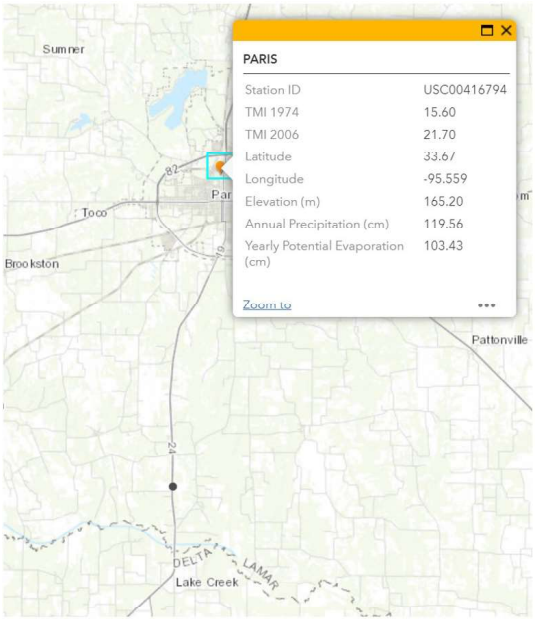

Figure 1. Paris (Texas) weather station (NOAA ID USC00416794) data from online *TMI* GIS map (Olaiz, 2017).

3.2 Step 2: monthly and 30-year Thornthwaite Moisture Index (TMI) (Witczak et al., 2006)

To determine yearly *TMI* for each month, first the potential evapotranspiration (*PET*) for each month must be calculated:

$$PET(cm) = f_1 f_2 1.6\left(\frac{10t}{I}\right)^a \quad (1)$$

where, f_1 is the fraction of the number of days in month divided by the average number of days in month, 30; f_2 is the fraction of the number of hours in a day divided by the base of 12 h in a day; t is the mean monthly temperature in degrees Celsius; I is the annual heat index; and a is a coefficient.

$$I = \sum_{i=1}^{12}\left(\frac{t_i}{5}\right)^{1.514} \quad (2)$$

where, t_i is the mean temperature for the ith month, and

$$a = 6.75I^3x10^{-7} - 7.71I^3x10^{-5} \\ 1.792Ix10^{-2} + 0.49239 \quad (3)$$

The *TMI* (Witczak et al., 2006) can now be determined by:

$$TMI = 75\left(\frac{P}{PET} - 1\right) + 10 \quad (4)$$

where, P is the precipitation for the given month.

To visualize the climate data over time, the monthly average temperature, monthly rainfall, and the calculated *TMI* can be plotted (Figure 2). For the example calculation at the TX 48-1068 SMP section, the 30-year weather data was analyzed (9/1967 to 9/1997). For the comparison of measured *versus* predicted data, measured elevation change data was also extracted from the LTPP-SMP database between 3/1987 and 9/1997.

The 30-year *TMI* value (Witczak et al., 2006) calculated from the NOAA data set for the USC00416794 station is +29.6. This value does differ slightly from the +21.7 value previously shown on the *TMI* GIS map (Figure 1) due to the difference in date ranges used in the Olaiz (2017) study.

3.3 Step 3: suction envelope parameters (Vann & Houston, 2021)

The suction envelope defines the maximum and minimum suction values at the surface and within the subsurface to a depth of stable suction. The suction envelopes are established using the following parameters: (1) equilibrium suction, ψ_e,

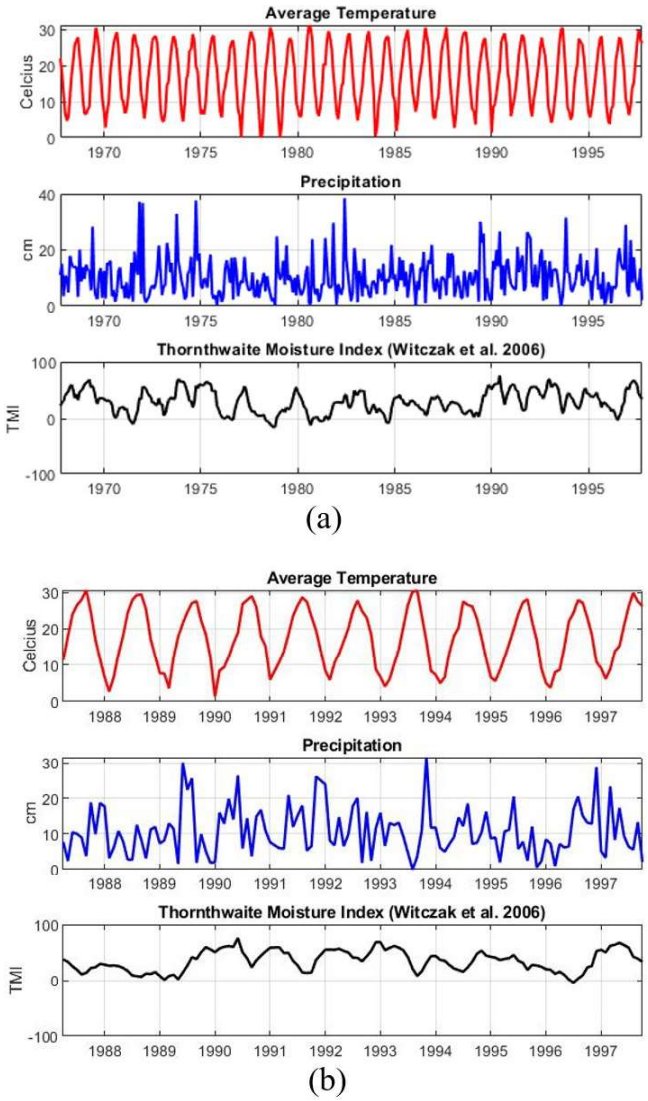

Figure 2. Monthly average temperature and rainfall data for NOAA weather station USC00416794 with the calculated yearly *TMI* (Witczak et al., 2006) between (a) 9/1967 and 9/1997 and (b) 3/1987 and 9/1997.

(2) depth to equilibrium suction, D_{ψ_e}, (3) change in suction at the ground surface, $\Delta\psi$, and (4) climate parameter, r.

The depth at which the climate-driven fluctuations in soil suction begins to stabilize, or equilibrate is determined using the Vann & Houston (2021) model (Figure 3) relatively flat uncovered sites subjected to natural climate surface flux conditions:

The equation for the Depth to Equilibrium Suction (D_{ψ_e}) *versus TMI* regression shown above is:

$$D_{\psi_e} = 1.617 + \frac{2.617}{1 + e^{(2.36 + 0.1612 TMI)}} \quad (5)$$

With an $R^2 = 0.9045$ and standard error = 0.3147 m.

The stable, or equilibrium, suction value is determined using the Vann & Houston (2021) model (Figure 4). The soil suction unit of pF (log to the base 10 of soil suction in centimeters of water) was used in the Vann & Houston (2021) study due to its extensive

use in the geotechnical practice, with regards to unsaturated soils. Note that log of suction in kPa units is approximately equal to suction in pF units, minus 1 (i.e., 4.0 pF = 3.0 log (suction (kPa))).

The equation for the Equilibrium Suction (ψ_e) as a function of *TMI* is:

$$\psi_e\left(pF\right) = 0.0002TMI^2 - 0.0053TMI + 3.9771 \quad (6)$$

With an $R^2 = 0.6539$ and a standard error = 0.1959 pF.

The limits of the potential surface flux, or potential change in suction at the surface, is determined using the Vann & Houston (2021) model (Figure 5).

The equation for the potential change in suction at the surface ($\Delta\psi$) as a function of *TMI*, as shown above is:

$$\Delta\psi\left(pF\right) = 1.2109e^{(-0.005TMI)} \quad (7)$$

With an $R^2 = 0.9184$ and a standard error = 0.1835 pF.

Aubeny & Long (2007) presented illustrative suction envelopes, developed from unsaturated flow analyses (Mitchell, 1980), to demonstrate that asymmetrical soil suction envelopes are expected, depending on the climate (*TMI*). Aubeny & Long introduced a climate parameter, *r*, that is the percentage of the total anticipated change in soil suction at the surface, ($\Delta\psi$), comprising the wet side of the suction envelope. The climatic parameter can be expressed in terms of the equilibrium suction (Ψ_e) and the minimum (Ψ_{wet}) and maximum (Ψ_{dry}) suction at the surface ($z = 0$):

$$r = \frac{\left(\psi_e - \psi_{wet_{z=0}}\right)}{\left(\psi_{dry_{z=0}} - \psi_{wet_{z=0}}\right)} = \frac{\left(\psi_e - \psi_{wet_{z=0}}\right)}{\Delta\psi} \quad (8)$$

Houston & Vann created a relationship between the climatic parameter and *TMI* (Figure 6).

The equation for the climatic parameter (*r*) as a function of *TMI* as shown above is:

$$r = 0.3725e^{(-0.009TMI)} \quad (9)$$

With an $R^2 = 0.7998$ and a standard error = 0.1132.

Table 1 presents the suction envelope parameters for the SMP TX 48-1068 section which had 30-year *TMI* of 29.6.

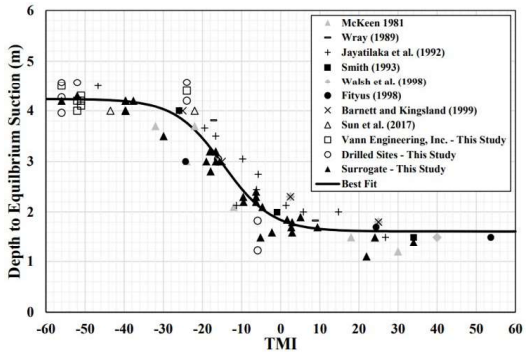

Figure 3. Relationship between *TMI* and the depth to constant soil suction for uncovered and non-irrigated sites (Vann & Houston, 2021).

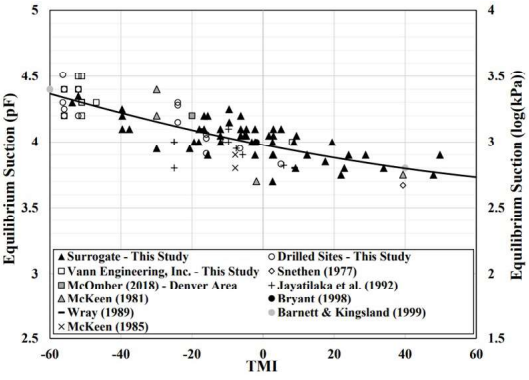

Figure 4. Equilibrium Suction vs. *TMI* with Literature Values (Vann & Houston, 2021).

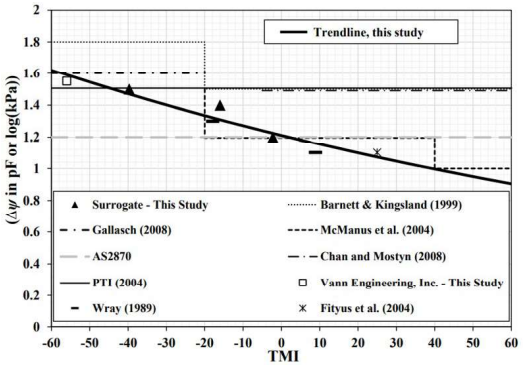

Figure 5. Limits of the potential change in suction at the surface vs. *TMI* with literature values (Vann & Houston, 2021).

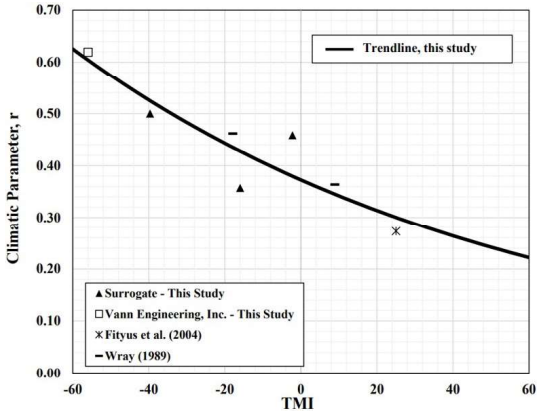

Figure 6. Relationship between the Climate Parameter, *r*, and *TMI* (Vann & Houston, 2021).

Table 1. Suction envelope parameters for the SMP TX 48-1068 per Vann & Houston (2021) with a *TMI* = 29.6.

Suction Envelope Parameter	Value
Depth to Equilibrium Suction ($D_{\emptyset_e}$)	1.62 m
Equilibrium Suction (Ψ_e)	3.84 pF
Change in suction at the surface ($\Delta\psi$)	1.044 pF
Climatic parameter (r)	0.2854

3.4 Step 4: back calculation of variables for Mitchell's equation (1980)

The suction envelope can now be generated using the simplified unsaturated flow equation derived by Mitchell in 1980. The adjustment to the equation by Aubeny & Long (2007) for asymmetrical suction envelopes has also been incorporated into this study.

The Mitchell (1979) equation for change in suction with depth and time, simplified by (Naiser, 1997) to consider only the extreme suction cases (wet and dry), by taking the time variable to infinity, is used to obtain the shape of the envelopes.

$$\psi(z) = \psi_e + \Delta\psi e^{\left(-z\sqrt{\frac{n\pi}{\alpha}}\right)} \tag{10}$$

where, ψ is units of pF and z, n and α are in consistent units, ψ (z) is the suction value at any depth z, n is the frequency of suction cycles, and α is the diffusion coefficient.

The suction change with depth is a function of change in suction at the surface ($\Delta\psi$ *in pF units*) and the equilibrium suction (ψ_e).

Once the key parameters of the profiles are established for any given *TMI*, all information required for the Mitchell (1980) flow computations (such as the ratio of the diffusion coefficient to the number of seasonal cycles per year) can be back-calculated (Vann, 2019). The n, α, π terms in the Mitchell (1980) equation, are back-calculated using the known equilibrium depth, D_{ψ_e}, change in suction at surface, $\Delta\psi$, and the 0.2 pF difference (Lytton et al., 2005; Vann, 2019), wet to dry, at the depth of equilibrium.

$$\frac{n\pi}{\alpha} = \left(\frac{\ln\left(\frac{0.2pF}{\Delta\psi}\right)}{-D_{\psi_e}} \right)^2 \tag{11}$$

The suction profile can now be generated using Equations 10 and 11 and the previously computed components of the surrogate suction, where suction is in pF units and depth is in meters.

3.5 Step 5: development of the wet and dry suction envelope

The suction envelope defines the boundary conditions for the suction value at any depth within the soil profile. At the ground surface, the minimum (wet) and maximum (dry) suction values can be determined using the following expressions:

$$\psi_{wet_{z=0}} = \psi_e - r\Delta\psi \tag{12}$$

$$\psi_{dry_{z=0}} = \psi_{wet_{z=0}} + \Delta\psi \tag{13}$$

The minimum (wet) and maximum (dry) suctions for the TX 48-1068 section are 3.54 and 4.58, respectively.

The step size, or thickness of depth intervals (dz) must be determined. A sensitivity analysis should be performed to determine the number of steps (n_s) needed for the analysis; however, a value of 20 steps has been found to be sufficient for the volume change calculation performed in this study. The step size is computed by:

$$dz = \frac{D_{\psi_e}}{(n_z - 1)} \tag{14}$$

The step size for the SMP TX 48-1068 section is 8.526 cm using 20 steps with a depth of equilibrium suction of 1.62 m.

The wet and dry limit suction curves are iteratively calculated as the depth (z) is increased from 0 (ground surface) to the depth of equilibrium suction.

$$\psi(z_i)_{wet} = \psi_e - r\Delta\psi e^{\left(-z_i\sqrt{\frac{n\pi}{\alpha}}\right)} \tag{15}$$

$$\psi(z_i)_{dry} = \psi_e + (1-r)\Delta\psi e^{\left(-z_i\sqrt{\frac{n\pi}{\alpha}}\right)} \tag{16}$$

The suction for the SMP TX 48-1068 section is shown in Figure 7.

3.6 Step 6: initial estimate of monthly changes in suction at the surface (Perera, 2003)

It is important to note that the following steps for determining the suction at the surface over time are specific to a deterministic approach for estimating historic ground movements. Such approach can be used for a case study, forensic analysis, or calibration efforts based on measured data. The suction at the surface over time can also be modeled using a stochastic analysis with randomly generated monthly *TMI* values based on the historic averages and standard deviations. The second type of analysis can be used for designs of future structures; however, an example of such analysis is not presented in this paper.

In 2003, Perera studied the relationship between in-situ moisture content, suction, *TMI*, and index soil properties. He developed correlations for two models: the *TMI*-P_{200} model, which is valid for granular base materials; and the *TMI*-P_{200}/*wPI* model, used to estimate the equilibrium suction of subbase and subgrade materials (Rosenbalm, 2011). The two models are briefly explained in the following paragraphs.

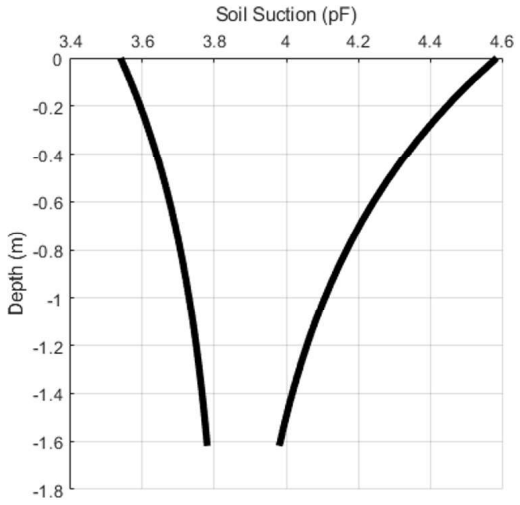

Figure 7. Suction envelope for the SMP TX 48-1068 section using the Vann & Houston (2021) models.

The *TMI-P200/wPI* model is of interest to this study. This model was developed for fine-grained material, which makes it suitable for expansive soils. For such materials, in addition to P_{200}, the weighted plasticity index, *wPI*, property was added, where:

$$wPI = \left(\frac{P_{200}}{100}\right) PI \tag{17}$$

The *wPI* for the example in Paris, TX site is 18.4 based on the percent passing the #200 sieve of 74% and a *PI* of 20.

The following equation is used to calculate suction based *TMI*, P_{200}, and *wPI* (Perera 2003).

$$\Psi = 0.3\left[e^{-\left[\frac{\beta}{TMI+\gamma}\right]} + \delta\right] \tag{18}$$

where, Ψ is the matric suction of the soil; and $\beta, \gamma, and\ \delta$ are regression constants.

Rosenbalm developed equations for each regression constant. These equations are used when *wPI* is less than 0.5 (Rosenbalm, 2011):

$$\beta = 2.56075\left(P_{200}\right) + 393.4625 \tag{19}$$

$$\gamma = 0.09625\left(P_{200}\right) + 132.4875 \tag{20}$$

$$\delta = 0.025\left(P_{200}\right) + 14.75 \tag{21}$$

The following equations are used when $wPI \geq 0.5$:

$$\beta = 0.006236\left(wPI\right)^3 - 0.7798334\left(wPI\right)^2 + 36.786486\left(wPI\right) + 501.9512 \tag{22}$$

$$\gamma = 0.00395\left(wPI\right)^3 - 0.04042\left(wPI\right)^2 + 1.454066\left(wPI\right) + 136.4775 \tag{23}$$

$$\delta = -0.01988\left(wPI\right)^2 + 1.27358\left(wPI\right) + 13.91244 \tag{24}$$

3.7 Step 7: adjustment to the estimation of monthly changes in suction at the surface (Vann & Houston, 2021)

It has been observed by the authors that the suction at the surface calculated using the Perera (2003) model typically will not reach the long-term minimum and maximum suction values observed by Vann & Houston (2021). This may not cause a significant issue if the analysis period is relatively short (e.g., less than ten years), however; for the purpose of pavement design, which typically incorporates a design life of 20+ years, it is recommended that the surface suction values determined from the Perera model be adjusted so that they will reach the limits observed by Vann & Houston (2021). This can be conducted by normalizing the maximum and minimum suction values from the Perera model to the previously computed potential change in suction at the surface (Δ^{ψ}).

$$\left(\psi_i\right)_{norm} = \left(\psi_{wet}\right)_{z=0} + \Delta\psi\left(\frac{\left(\psi_i\right)_{z=o} - \left(\psi_{Perra}\right)_{\min}}{\left(\psi_{Perra}\right)_{\max} - \left(\psi_{Perra}\right)_{\min}}\right) \tag{25}$$

After iterating the process for each month, the adjusted surface suction values can be plotted to help visualize adjustment (Figure 8).

3.8 Step 8: fourier equation fit to the monthly surface suction (Aubeny & Long, 2007)

In order to model the suction changes as a function of time and depth, an equation must be developed to represent the variation of suction at the surface. Typically, a simple sinusoidal fit has been used to represent the surface suction variation with time. However, Aubeny & Long (2007), proposed that a Fourier transform can be used to improve the goodness of fit. As such, an 8th degree Fourier series is used in this analysis to fit an equation to the highly variable surface suction data.

In general, the Fourier series is a sum of sine and cosine functions that describes a periodic signal. It is represented in either the trigonometric form or the exponential form.

$$y = a_0 + \sum_{i=1}^{n} a_i \cos(iwx) + b_i \sin\left(iwx\right) \tag{26}$$

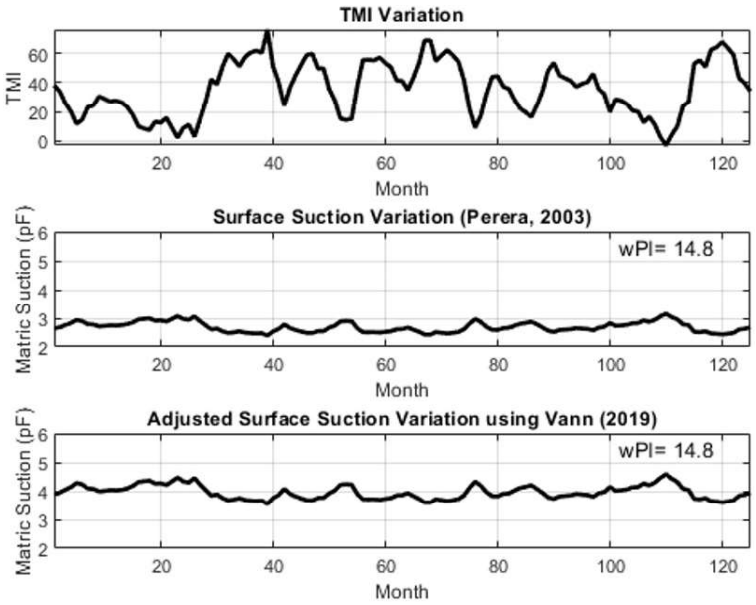

Figure 8. Monthly *TMI*, Perera (2003) surface suction, and the Vann (2019) adjusted surface suction for the TX 48-1068 section for the date range 3/1987 to 9/1997.

where, x represents time (for this analysis), a_0 models a constant (intercept) term in the data and is associated with the $i = 0$ cosine term, w is the fundamental frequency of the signal, n is the number of terms (harmonics) in the series, and $1 \leq n \leq 8$, and a_i and b_i are the fitting parameters. Additional background information on the Fourier series can be found on MathWorks help center (MathWorks, 2021).

Figure 9 presents the 1st and 8th order Fourier fit to the Vann & Houston (2021) adjusted surface suction for the TX 48-1068. The 1st order fit closely represents the original approach to modeling the surface suction flux by Lytton et al. (2005) using Mitchell (1979) equation. The adjusted R^2 for the 1st order Fourier fit to the suction data is 0.2903, while the 8th order Fourier fit increases the adjusted R^2 to 0.7056.

One limitation of requiring an equation to represent the surface suction, is that generally the equation fit will not be able to encompass the maximum and minimum values of the individual monthly data. For purposes of the shrink/swell volume change analysis, the inclusion of the peaks of the surface suction can provide more accurate and conservative representation of extreme events. As such, the Fourier surface suction equation can be normalized between the maximum and minimum values of the surface suction; however, this additional step was not performed as part of the example analysis presented in this paper.

Note that the initial suction is a function of the *TMI* value for that month. The initial suction (time = 0) can be adjusted using a phase shift of the Fourier equation. Lytton et al. (2005), provided values of phase shifts for different initial conditions of the soil (wet, dry, and equilibrium). The example calculation in this report does not include the phase shift for the initial conditions.

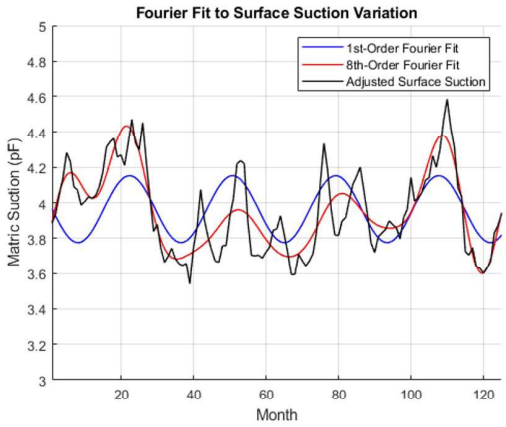

Figure 9. 1st and 8th order Fourier fit to the surface suction data for the TX 48-1068 section for the date range 3/1987 to 9/1997.

3.9 Step 9: monthly suction profile (Aubeny & Long, 2007)

The next step is to model the suction profile change with time using Aubeny & Long's (2007) adjusted 1979 Mitchell equation.

$$u(y,t) = U_e - \left(U_{dry} - U_{wet}\right) \sum_{k=1}^{\infty} \alpha_k \exp\left(-\sqrt{\lambda k}\right) \cos\left(\tau k - \sqrt{\lambda k}\right) \quad (27)$$

where, y is the depth, $\lambda = \pi y^2 n_\lambda / \alpha_k$, $\tau = 2\pi t n_\lambda$, n_λ = lowest frequency of cyclic suction variation, and $\alpha_k = (2/k\pi) sin(k\pi r)$ with k = 1,2,3…

For a given point in time, the suction profile can be estimated using the Aubeny & Long approach. Figure 10 presents the estimated suction at time = 1 month for the TX 48-1068 SMP site. Note that the long-term or extreme boundaries of the suction profile are known from the Vann (2019) correlations with the 30-year *TMI* value previously presented herein.

The monthly change in suction at each depth can be determined by calculating the following months suction profile and taking the difference of the two values at each depth. It is this ongoing change in soil suction with time that drives the volume change of shrink/swell soils. Figure 11 shows the suction profiles for t = 1 month, and t = 2 months, for the TX 48-1068 SMP site. Figure 12 shows the suction profiles for month 1 through month 12.

Figure 13 presents the monthly suction profiles over the date range 3/1987 to 9/1997 life for TX 48-1068 SMP section. From the figure, the significant swings of the suction profile from wet to dry, over the date range 3/1987 to 9/1997, can be observed. The monthly change in suction at each depth in the soil profile can be determined from this model.

To account for hysteresis effects associated with the wetting and drying of soil, it is important to record if the

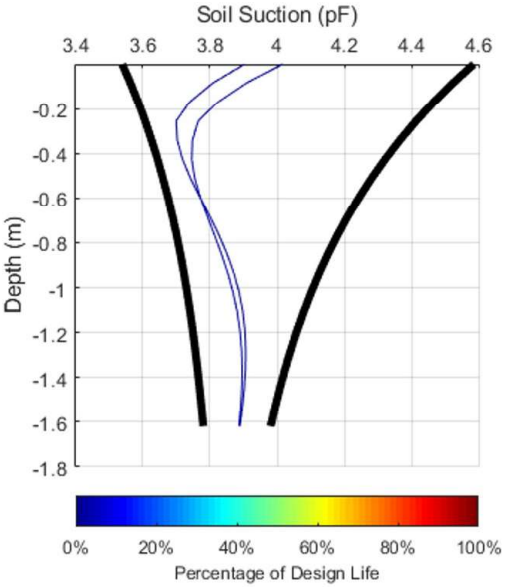

Figure 11. The estimated initial suction profiles (time = 2 months) for TX 48-1068 section.

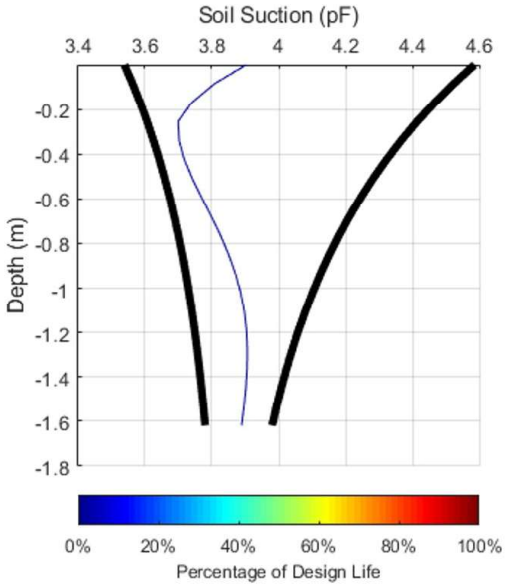

Figure 10. The estimated initial suction profile (time = 1 month) for TX 48-1068 section.

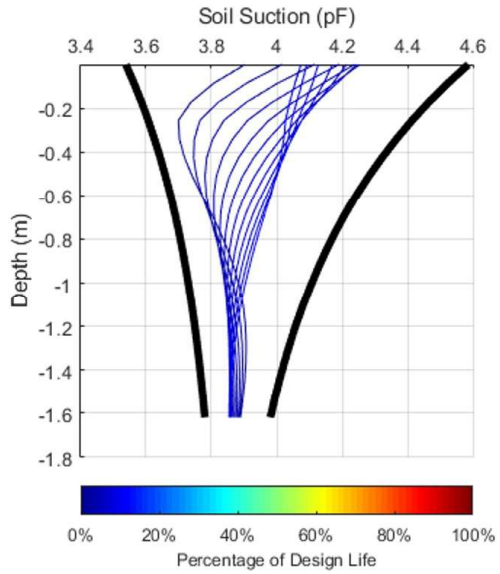

Figure 12. The estimated initial suction profiles (time = 12 months) for TX 48-1068 SMP section.

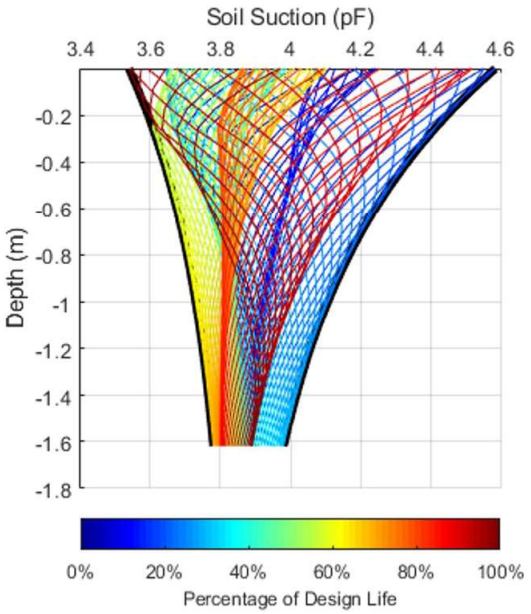

Figure 13. Monthly suction profiles over the date range 3/1987 to 9/1997.

soil is wetting or drying at each depth and time during the iterative analysis. This information will be used during the strain calculation discussed later in this report.

3.10 Step 10: suction profile adjustments due to varying boundary conditions

It is possible that the project site has a variable groundwater table, nearby vegetation, or is constructed using a moisture barrier. If any of these boundary conditions are present, the suction envelope and profile must be adjusted. (e.g. the suction profile will reach osmotic suction at the groundwater table depth). No variable boundary conditions were included in this example calculation.

3.11 Step 11: net normal stress profile

The net normal, or overburden stress, is a key component of shrink/swell volume change determination as it will help reduce potential soil swelling and can increase soil shrinkage. The overburden stress profile is determined using the conventional total stress approach.

$$\sigma_z = \sum(\gamma_{soil} z) \tag{28}$$

Note that the water content is subject to change over time as the soil suction changes, which will affect the magnitude of the net normal stress. However, for purposes of this example calculation, the effect of the changing water content on the net normal stress is negligible and is not included in the analysis.

If there are foundation loads or increases overburden stresses due to pavement layers above the subject soil profile, an increase of stress will be applied throughout the net normal stress profile.

3.12 Step 12: suction compression index (Covar & Lytton, 2001)

The most widely accepted method for estimating volumetric strain is the one developed for the Texas DOT and the Federal Highway Administration, FHWA, by Lytton et al. (2005), which is as follows:

$$\frac{\Delta V}{V} = -\gamma_h \log\left(\frac{h_f}{h_i}\right) - \gamma_\sigma \log\left(\frac{\sigma_f}{\sigma_i}\right) - \gamma_\pi \log\left(\frac{\pi_f}{\pi_i}\right) \tag{29}$$

where, $\frac{\Delta V}{V}$ is the volumetric strain (volume change with respect to initial volume); γ_h is the the matric suction compression index; γ_σ is the mean principal stress compression index; γ_π is the osmotic suction compression index; h_i is the initial matric suction; h_f is the final matric suction; σ_i is the initial mean principal stress; σ_f is the final mean principal stress; π_i is the initial osmotic suction; and π_f is the final osmotic suction.

Although, total suction is the sum of matric suction and osmotic suction, Fredlund wrote "Matric suction in a soil mass change is a result of moisture infiltration and evaporation at the ground surface. Osmotic suction in the soil does not appear to be highly sensitive to modest changes in the water content of the soil. As a result, a change in the total suction is quite representative of a change in the matric suction." (Fredlund et al., 2012). Also, Lytton wrote: "It is the change of matric suction that generates the heave and shrinkage, while osmotic suction rarely changes appreciably." (Lytton et al., 2005). Thus, the change in matric suction is responsible to shrinkage and heave and osmotic suction does not affect enough to be concerned (Lytton et al., 2005; Fredlund et al., 2012). Thus, the equation can be rewritten as:

$$\frac{\Delta V}{V} = -\gamma_h \log\left(\frac{h_f}{h_i}\right) - \gamma_\sigma \log\left(\frac{\sigma_f}{\sigma_i}\right) \tag{30}$$

Note that the net normal stress portion of the equation is added if the soil is wetting (swelling) and subtracted if the soil is drying (shrinking).

The Suction compression index, γ_h, is a parameter used to relate total suction to volume change to predict heave or shrinkage in expansive soils. This value can either be measured or estimated using soil index properties (Atterberg limits and gradation) as described in Covar & Lytton (2001).

First, the mineralogical zone is determined using Figure 14 with soils plasticity index (*PI*) and liquid limit (*LL*).

The zone for the TX 48-1068 SMP section site is Zone 2, using a *LL* = 60% and a *PI* = 40%.

The percent fine clay *(%fc*) is then calculated using the percent passing #200 sieve (P_{200}) and the percent clay (*%clay*) obtained via hydrometer testing.

$$\%fc = \left(\frac{\%clay}{P_{200}} \right) \tag{31}$$

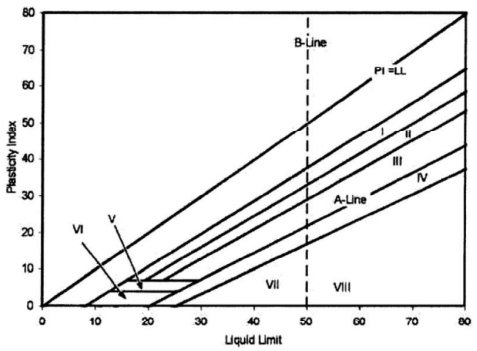

Figure 14. Mineralogical zones for soil (Covar & Lytton, 2001), units in %.

The *%fc* for the example site is 21.05%, using a *%clay* = 20% and P_{200} = 95%.

The average suction compression index (γ_0) can now be determined using the charts developed by Covar & Lytton (2001), which are separated by mineralogical zones (Figure 15).

The average suction compression index for the TX 48-1098 SMP section is 0.051 using Zone 1, *%fc* = 43.78%, *LL* = 38%, and *PI* = 20%.

The adjusted suction compression index (γ_h) is now determined by:

$$\gamma_h = \gamma_0 \left(\%fc \right) \tag{32}$$

The adjusted suction compression index for TX 48-1098 SMP section site is 0.0223.

The hysteresis effects of the soil are now accounted for using the equations from the PTI (2008) Manual. The wetting and dying suction compression indices must be calculated for each depth and time of the analysis using the recorded wetting/drying information from Step 9.

$$\gamma_{swell} = \gamma_h e^{(\gamma_h)} \tag{33}$$

$$\gamma_{shrink} = \gamma_h e^{(-\gamma_h)} \tag{34}$$

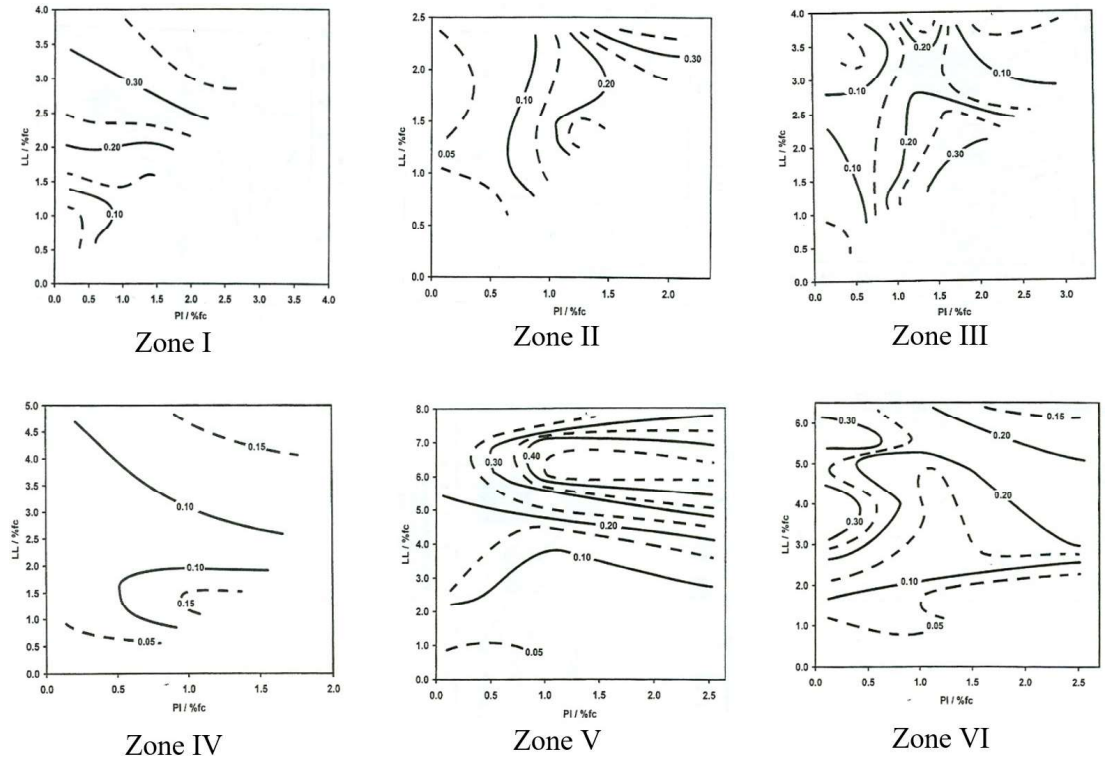

Figure 15. Suction Compression Index based on Mineralogical Classification and Soil Index Properties (Covar & Lytton, 2001).

3.13 Step 13: monthly strain calculation

The mean principal stress compression index, γ_σ, can be calculated using its relation to the compression index, C_c, and void ratio, e, as follows (Lytton et al., 2005):

$$\gamma_\sigma = \frac{C_c}{1+e_0} \tag{35}$$

where, C_c is the compression index; and e_0 is the void ratio. For purposes of this example calculation, the mean principal stress compression index was assumed to be 10% of the suction compression index as recommended by Lytton et al. (2005).

The mean principal stress must be iteratively determined at each depth and time step, as it is a function of the net normal stress and the wetting/drying condition.

$$\sigma = \frac{1+2K_0}{3}\sigma_z \tag{36}$$

where, σ_z is the previously calculated vertical stress at a point below the surface in the soil mass; and K_0 is the 1-D at-rest lateral earth pressure coefficient.

$$K_0 = e\left(\frac{1-\sin(\phi')}{1+\sin(\phi')}\right)\left(\frac{1+d\sin(\phi')}{1-k\sin(\phi')}\right)^n \tag{37}$$

Values of coefficients *e, d, k, and n* for different soil conditions are given in Table 2.

The angle of internal friction, ϕ', can be estimated from its empirical correlation with plasticity index, PI, based on triaxial compression tests.

$$\phi' = 0.0016PI^2 - 0.3021PI + 36.208 \tag{38}$$

The internal angle of friction for the TX 48-1068 SMP site is 30.8° using a $PI = 20$.

Using the data developed from the iterative steps discussed above, and the suction-overburden-strain relationships, the volume change over time can be estimated. Figure 16 presents the volume change estimation for the Paris, TX site.

4. Estimated volume change comparison to measured data

The estimated volume change from the proposed framework for the TX 48-1068 site was compared to the measured data gathered from the LTPP SMP database. The estimated data was normalized to the value of the first measurement. Figure 17 presents the measured and estimated volume change for the TX 48-1068 SMP section.

Table 2. Lateral earth pressure parameter coefficients.

Conditions	K_0	e	d	k	n
Cracked	0	0	0	0	1
Drying (Active)	1/3	1	0	0	1
Equilibrium (at rest)	1/2	1	1	0	1
Wetting (within movement active zone)	2/3	1	1	0.5	1
Wetting (below movement active zone)	1	1	1	1	1
Swelling near surface (passive earth pressure)	3	1	1	1	2

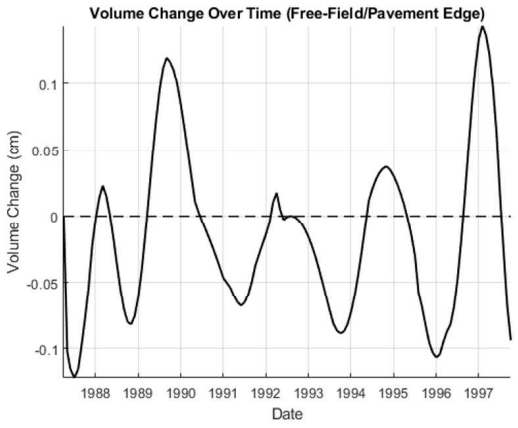

Figure 16. Volume change over time for the TX 48-1068 site.

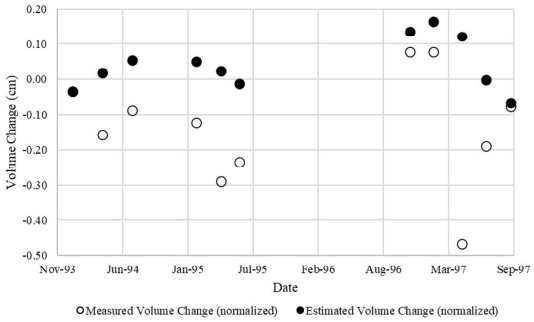

Figure 17. Measured *vs.* estimated volume change normalized to the initial measurement for the TX 48-1068 SMP Section.

A preliminary analysis of the proposed framework presented in this paper was performed on eight more sections from Alabama, Colorado, Montana, Nebraska, South Dakota and Texas from the LTPP SMP program. The resulting comparison, presented in Figure 18, of the estimated volume change and the measured field data for 70 data points yielded a coefficient of correlation of 0.45. This result is promising, and the data allows for a calibration of the model to the field conditions once all the parameters have been defined.

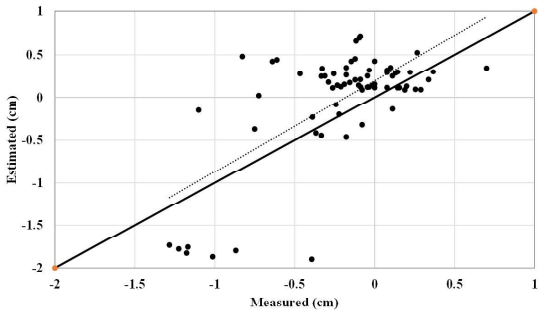

Figure 18. Measured *vs.* estimated volume change normalized to the initial measurement for the eight SMP sections.

5. Conclusions

This paper presented a preliminary mechanistic-empirical framework for the estimation of volume change. The models are universal and can be used in any part of the world provided measured data is available to calibrate for local conditions. Ongoing calibration effort with the remaining LTPP SMP sections will allow obtaining calibration factors for the proposed framework that will improve the estimation of the volume change predictions under pavements and facilitate the implementation into current design procedures.

Acknowledgements

This work is based on part of research funded by the National Academies of Science, Engineering, and Medicine Transportation Research Board's (TRB) National Cooperative Highway Research Program (NCHRP) 01-59. The opinions, conclusions, and interpretations are those of the authors and not necessarily of NCHRP.

Declaration of interest

The authors have no conflict of interests pertaining to the material included in this paper.

Authors' contributions

Austin Olaiz: conceptualization, formal analysis, methodology, writing – original draft. Mohammad Mosawi: data curation, formal analysis, writing – original draft. Claudia Zapata: conceptualization, funding acquisition, project administration, supervision, writing – review & editing.

List of symbols

a	a coefficient
a_0	constant (intercept) term, associated with the i=0 cosine term
a_i	fitting parameter
b_i	fitting parameter
C_c	compression index
D_{ψ_e}	depth to equilibrium suction
dz	thickness of depth intervals
e	void ratio
f_1	fraction of the number of days in month divided by the average number of days in month, 30
f_2	fraction of the number of hours in a day divided by the base of 12 h in a day
h_i	initial matric suction
h_f	final matric suction
I	annual heat index
K_0	lateral earth pressure coefficient
n	frequency of suction cycles
n_λ	lowest frequency of cyclic suction variation
n_z	number of steps needed for the analysis
P	precipitation for the given month
P_{200}	percent passing #200 sieve
PI	plasticity index
t	mean monthly temperature in degrees Celsius
t_i	mean temperature for the ith month
r	climate parameter
w	fundamental frequency of the signal
wPI	weighted plasticity index
x	time of the analysis
z	depth
α	diffusion coefficient
β,γ,δ	regression constants
$\Delta V / V$	volumetric strain
γ_h	matric suction compression index
γ_{soil}	unit weight of the soil
γ_σ	mean principal stress compression index
γ_π	osmotic suction compression index
$\varnothing'$	angle of internal friction
π_i	initial osmotic suction
π_f	final osmotic suction
σ_f	final mean principal stress
σ_i	initial mean principal stress
σ_z	net normal, or overburden, stress
$\Delta\psi$	change in suction at the ground surface
Ψ	matric suction
ψ_e	equilibrium suction
$\psi_{wet_{z=0}}$	minimum (wet) suction at the surface (z = 0)
$\psi_{dry_{z=0}}$	maximum (dry) suction at the surface (z = 0)
$\psi(z)$	suction value at any depth z
$\%fc$	percent of fine clay

References

ASTM D4546. (2021). *Standard Test Methods for One-Dimensional Swell or Collapse of Soils*. ASTM International, West Conshohocken, PA. https://doi.org/10.1520/D4546-21

Aubeny, C., & Long, X. (2007). Moisture diffusion in shallow clay masses. *Journal of Geotechnical and Geoenvironmental Engineering*, 133(10), 1241-1248.

Bear, J. (1972). *Dynamics of fluids in porous media*. American Elsevier.

Covar, A.P., & Lytton, R.L. (2001). *Estimating soil swelling behavior using soil classification properties*. ASCE.

Federal Highway Administration – FHWA (1995) *LTPP seasonal monitoring program site installation and initial data collection section 481068*. FHWA, Paris, TX.

Federal Highway Administration – FHWA (2021). *LTPP InfoPave*. Retrieved in July 21, 2021, from https://infopave.fhwa.dot.gov/

Fredlund, D.G., Rahardjo, H., & Fredlund, M.D. (2012). *Unsaturated soil mechanics in engineering practice*. Wiley.

Holtz, R.D., & Gibbs, H. (1956). Engineering properties of expansive clays. *Transactions of the American Society of Civil Engineers*, 121(1), 641-677.

Houston, S., & Houston, W. (2017). A suction-oedometer method for computation of heave and remaining heave. In *Proceedings of the 2nd PanAm Conference on Unsaturated Soils,* Dallas. https://doi.org/10.1061/9780784481677.005

Lytton, R., Aubeny, C., & Bulut, R. (2004). *Design procedure for pavements on expansive soils: volume 1 - Report 0-4518-1/0-4518*. Texas Department of Transportation, Austin, TX.

Lytton, R., Aubeny, C., & Bulut, R. (2005). *Design procedures for soils on expansive soils: volume 1 - Report FHWA/TX-05/0-4518*. Texas Department of Transportation, Austin, TX.

Lytton, R.L. (1977). Foundations in expansive soils. In C.S. Desai & J.T. Christian (Eds.), *Numerical methods in Geotechnical Engineering* (pp. 427-458). McGraw-Hill.

MathWorks (2021). *Help center - Fourier series*. Retrieved in July 21, 2021, from https://www.mathworks.com/help/curvefit/fourier.html

McKeen, R.G., & Hamberg, D.J. (1981). Characterization of expansive soils. *Transportation Research Record: Journal of the Transportation Research Board*, (790), 73-78.

Mitchell, P.W. (1979). *The structural analysis of footings on expansive soil*. Kenneth W.G. Smith & Associates.

Mitchell, P.W. (1980). The concepts defining the rate of swell of expansive soils. In *Proceedings of the 4th International Conference on Expansive Soils*, Denver.

Naiser, D. (1997). *Procedures to predict vertical differential soil movement for expansive soil* [Master's thesis]. Texas A&M University, College Station, TX.

Olaiz, A. H., Singhar, S. H., Vann, J. D., & Houston, S. L. (2017). Comparison and applications of the Thornthwaite moisture index using GIS. In L. R. Hoyos, J. S. McCartney, S. L. Houston, & W. J. Likos (Eds.), *PanAm Unsaturated Soils 2017: Applications, Geotechnical Special Publication 302* (pp. 280–289). Reston, VA: ASCE

Perera, Y.Y. (2003). *Moisture equilibria beneath paved areas* [Unpublished doctoral dissertation]. Arizona State University.

Post-Tensioning Institute – PTI (2004). *Design of post-tensioned slabs-on-ground* (3rd ed.). PTI.

Post-Tensioning Institute – PTI (2008). *Design & construction of post-tensioned slabs-on-ground* (3rd ed.). PTI.

Rosenbalm, D. (2011). *Reliability associated with the estimation of soil resilient modulus at different hierarchical levels of pavement design* [Master's thesis]. Arizona State University. Retrieved in July 21, 2021, from http://hdl.handle.net/2286/R.I.14453

Texas Department of Transportation – TxDOT (1978). *Method for determining the potential vertical rise, PVR - TxDOT-124-E*. TxDOT, Austin, TX.

Thornthwaite, C. (1948). An approach toward a rational classification of climate. *Geographical Review*, 38(1), 55-94.

Vann, J.D. (2019). *A soil suction-oedometer method and design soil suction profile recommendations for estimation of volume change of expansive soils* [Doctoral dissertation]. Arizona State University. Retrieved in July 21, 2021, from http://hdl.handle.net/2286/R.A.216886

Vann, J.D., & Houston, S. (2021). Field Suction Profiles for Expansive Soil. *Journal of Geotechnical and Geoenvironmental Engineering*, 147(9), 04021080. https://doi.org/10.1061/(ASCE)GT.1943-5606.0002570.

Witczak, M.W., Zapata, C.E., & Houston, W.N. (2006). *Models incorporated into the current enhanced integrated climatic model: NCHRP 9-23 Project findings and additional changes after version 0.7 - Final report, Project NCHRP 1-40D.* AASTHO & FHWA, Washington, DC.

APPENDIX C

GEOCONGRESS 2023 PROCEEDINGS PAPER (FORTHCOMING)

Suction-Volume Change Indices for Natural and Recompacted Clay Soils

Austin H. Olaiz, Ph.D., P.E.[1], Sandra Houston, Ph.D., P.E.[2]
Claudia E. Zapata, Ph.D.[3], Mohammad Mosawi, Ph.D.[4]

[1] Arizona State University, School of Sustainable Engineering and the Built Environment, Tempe, AZ, USA. Austin.Olaiz@asu.edu ORCID: 0000-0003-2194-4011

[2] Arizona State University, School of Sustainable Engineering and the Built Environment, Tempe, AZ, USA. Sandra.Houston@asu.edu ORCID: 0000-0002-5615-0986

[3] Arizona State University, School of Sustainable Engineering and the Built Environment, Tempe, AZ, USA. Claudia.Zapata@asu.edu ORCID: 0000-0002-2940-9841

[4] Arizona State University, School of Sustainable Engineering and the Built Environment, Tempe, AZ, USA. Mohammad.Mosawi@asu.edu ORCID: 0000-0001-6347-990X

ABSTRACT

The mechanical response of unsaturated soil is controlled by the two stress state variables of matric suction and net normal stress. Modern geotechnical laboratory devices allow for the direct measurement of unsaturated soil volumetric response under controlled conditions of both stress state variables. The oedometer pressure plate device (OPPD) is one apparatus that can impose suction-induced partial wetting conditions under constant or varying vertical stress conditions while measuring vertical deformations. This study brings together three extensive laboratory investigations of the mechanical response of fine-grained soil specimens to variations in both matric suction and net normal stress: Singhal (2010), Olaiz (2017), and Mosawi (2022), which were conducted using a series of OPPDs located at Arizona State University's Geotechnical Laboratory. The effects of differing soil index properties, sample preparation, and stress path history on the moisture-driven volumetric response is evaluated. A comparison between the suction-volume change indices of reconstituted clay specimens measured by Singhal (2010) and Mosawi (2022) and those of relatively intact clay specimens measured by Olaiz (2017) is also included.

INTRODUCTION

Evaluation of moisture-driven volume change of unsaturated clay soil requires consideration of the net normal (p) and the matric suction (s) stress states. For clays under relatively light confinement, increases in s during drying will typically cause clays to decrease in volume (compress or shrink) and reductions in s during wetting will cause increases in volume (expansion or swell). Clay soils at high net normal stress states can also reduce in volume (collapse) during wetting (Houston and Zhang, 2021; Nooray, 2017). The volumetric response is commonly expressed in terms of changes in void ratio (e), and the general relationship between e, p and s for clay soils is represented using three-dimensional (3D) state surfaces (Alonso et al., 1994, 1999; Delage & Graham, 1996; Fredlund & Morgernstern, 1976; Gens & Alonso, 1992; Gens et al., 2016; Wheeler & Sivakumar, 1995; Vu & Fredlund, 2004; Wray et al., 2005; Zhang & Lytton,

2009a, 2009b). For many foundation and pavement applications in engineering practice, vertical deformations govern the design which allow for the *e-p-s* relationship to be analyzed using one-dimensional (1D) at-rest (K_0) conditions - or at least the 1-D analyses provide adequate information for decision making (Adem & Vanapalli, 2013; Fredlund et al., 1980; Houston & Houston, 2018; Lytton, 1997; Nelson & Miller, 1992; Overton et al., 2006).

Modern laboratory testing equipment like oedometer pressure plate device (OPPD) allows for the direct measurement of the unsaturated soil volume change at controlled matric suction and net normal stress conditions (Gens et al. 1995; Romero et al., 1995; Lins & Schanz, 2004; Pham et al., 2005, and Perez-Garcia et al., 2007). The OPPD merges the performance of oedometer-type apparatus for 1D volume change measurements with a suction-controlled pressure chamber using the axis translation technique Hilf (1956) and is thus limited to maximum matric suction values of 1500 kPa. Delage, et al. (2008) discuss the use of salt solution to control suction in oedometer devices, thus extending the suction range, although equilibration times tend to be very long using salt solution suction control methods. There are currently no standardized procedures for the OPPD that the authors are aware of. The testing procedures associated with the OPPD are governed by the engineering property/constitutive relationship that needs to be explored, the soil type (coarse vs. fine-grained), and the stress history of the soil specimens to be tested (reconstituted or intact). Perez-Garcia et al (2007), Singhal (2010), Fredlund & Houston (2013), and Olaiz (2017), provide excellent summaries of the laboratory procedures and limitations associated with testing remolded soil samples in the OPPD.

This study presents a comparison of the matric suction-volume change indices (for 1-D monotonic loading by wetting or drying) of intact clays (natural soil stress states) using relatively undisturbed specimens tested by Olaiz (2017), to those of reconstituted/compacted specimens measured by Singhal (2010) and Mosawi (2022) using OPPDs, including the Fredlund SWCC (SWC-150) developed by GCTS in Tempe, AZ. Singhal (2010) created a unique database from laboratory measurement of the mechanical response of clay soils under imposed conditions of both stress state variables using the OPPD, with attention on evaluation of a substantial portion of the void ratio state surface for clay soils. Olaiz (2017) and Mosawi (2022) continued the exploration of testing relatively intact and reconstituted soil specimens in the OPPD, respectively. The materials tested by Olaiz and Mosawi were obtained from locations associated with expansive soil areas in San Antonio, TX, and Denver, CO. The compilation of data from these extensive laboratory efforts is provided herein and is used to provide qualitative and quantitative comparisons of the mechanical response of reconstituted to relatively intact specimens.

UNSATURATED SOIL VOLUMETRIC RESPONSE TO VARYING STRESS STATES

Numerous breakthroughs in constitutive modeling have allowed geotechnical engineers to represent all volume change mechanisms of unsaturated soils (shrink-swell and collapse) due to changes in both stress state variables. However, typical practice of estimating shrink-swell soil volume change due to seasonal moisture changes encompasses simplified approaches using soil index with empirical correlations, significant engineering judgment, and 1D response to wetting tests (ASTM D4546). Many of the existing practical approaches for estimating unsaturated soil

volume change assumed a fully saturated final stress state. However, with proper control of water, the probability that a soil in an arid environment can reach a fully saturated (s = 0) state over the period of the structure/pavement design life is relatively low in the absence of groundwater table rise (Houston & Houston 2018). As such, knowledge of the suction-driven changes in volume (void ratio change) is necessary to adequately estimate the magnitude of potential volume change of shrink-swell soils.

A shrink-swell soil's volumetric response to increases in s (drying) and decreases in s (wetting) at any constant state of p is referred herein as the suction-volume change indices. For 1D K_0 conditions, the suction-volume change indices C_m and C_{ms} represent the change in e per change in s at a constant p due to drying and wetting, respectively (Vu & Fredlund, 2004):

$$C_m = \frac{\partial e}{\partial \log(s)} = \frac{(e_f - e_i)}{\log\left(\frac{s_f}{s_i}\right)} \quad \text{for} \quad s_f > s_i \quad \text{or} \quad C_{ms} = \frac{\partial e}{\partial \log(s)} = \frac{(e_f - e_i)}{\log\left(\frac{s_f}{s_i}\right)} \quad \text{for} \quad s_f < s_i \qquad (1)$$

Where the subscripts i and f represent the initial and final states of stress.

Figure 1 illustrates two different approaches to interpreting the suction-volume change index from the e-log(s) plot for a given p, which represents one plane within the void ratio constitutive surface with log(s) and log(p). The C_m or C_{ms} can be interpreted from the e-log(s) plot in an incremental manner (Figure 1a) which helps adequately capture the nonlinearity of the relationship and can be implemented into numerical modeling. The e-log(s) plot generally experiences a distinct change in slope, likely around the air entry value (AEV), which is also depicted on Figure 1 and referred to herein as the inflection point of the *e-log(s)* plot.

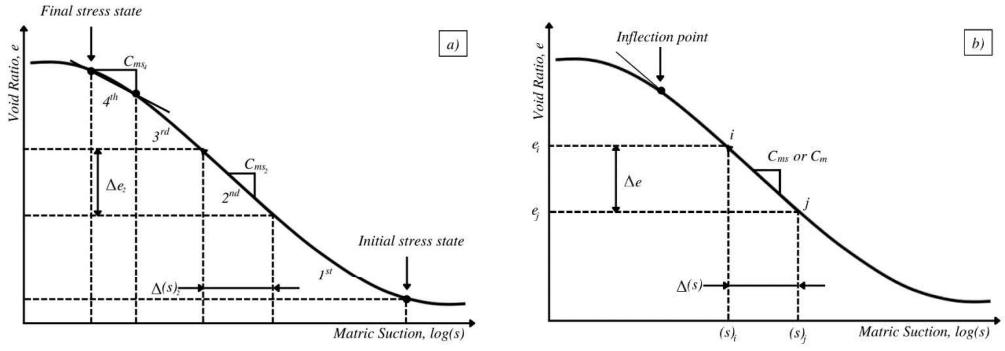

Figure 1: Interpretation of suction-volume change parameters using a) an incremental approach of *e*-log(*s*), and b) a representative value of the linear portion *e*-log(*s*)

The volumetric response of an unsaturated clay soils to changes in stress state will be dependent on the stress path history, as observed by many laboratory studies (Justo et al., 1984; Alonso, 1993; Pham & Fredlund, (2011). For reconstituted lab specimens, the effects of the natural stress path history are essentially lost as the soil structure is broken down. The stress path history prior to testing is from the sample preparation process, which for most specimens of this study likely reduced the maximum past stress compared to field conditions for both p and s. The reconstituted soils evaluated in this study were prepared using a common process which starts with

breaking down dried clay material from a bulk sample, mixing in an amount of water required to reach the targeted moisture content (e.g., optimum moisture conditions), and then recompacting in the testing mold (brass ring for oedometer testing) to the target dry density.

In geotechnical practice associated with pavement and shallow foundation design, which are highly susceptible to distresses caused by shrink-swell soils, driven ring samplers or pushed Shelby tubes are commonly used to obtain relatively undisturbed samples which are used to help improve the representation of the natural soil conditions in the laboratory. For relatively undisturbed clay specimens, the natural stress state can be sufficiently maintained using proper sampling techniques, sealing the sample to minimize potential moisture changes during transport and storage, and allowing the specimen to equilibrate under an imposed p corresponding to the estimated in situ stress state prior to any additional loading (Houston, 2014). This process is an attempt to return the soil, as close as possible, to in situ state of p-s after one p unload-reload cycle, assuming negligible changes in s and negligible effects of transport-related vibrations on the soil structure; however, there will always be irreversible effects from the sampling process (Fredlund et al., 2012; Nelson et al., 2015).

The imposed stress path followed in the three laboratory investigations evaluated herein was to initially induce a net normal stress through application of vertical load under K_0 conditions, then wet or dry the sample via induced matric suction into the OPPD chamber while maintaining the net normal vertical stress constant. As such, the e-s relationship of the complied OPPD dataset presented herein differ from the suction compression indices (SCI, γ_h) obtained from: the unconfined (p = 0) Coefficient of Linear Extensibility (COLE) tests documented by the United State Department of Agriculture National Resources Conservation Service (USDA-NRCS) Soil Survey Laboratory, which were used by Covar and Lytton (2001) to develop the empirical shrink-swell volume change models for the Texas Department of Transportation (Lytton et al., 2005) and the Post-Tensioning Institute Design of Slabs-on-Ground (PTI, 2008).

OPPD TESTING OF RECONSTITUTED SPECIMENS

In 2010, Singhal conducted an experimental laboratory investigation on a highly plastic expansive soil from Prescott, Arizona, referred to as "*PL clay*". Sample preparation included air-drying the soil and then breaking down with a mortar and pestle prior to compacting in a mold to 10% below optimum moisture content (35%) and 118% of the theoretical maximum dry density (12.82 kN/m^3) obtained from the Standard Proctor test (ASTM D689A). The specimens were exposed to several drying and wetting cycles (between 20% and 28%) over several weeks to reduce the effects from (the lack of) stress history. At the start of the OPPD testing, the moisture content and matric suction (measured using the filter paper method) was approximately 20% and 13,000 kPa, respectively.

Hysteresis effects on e-s were explored by conducting adsorption (wetting) and desorption (drying) OPPD tests at three p stages of 1 kPa, 25 kPa, and 150. The concept of "twinned" samples was used to test the response at varying normal stress states. The wetting tests were performed first by decreasing s on the OPPD apparatus from 1200 kPa, to 500 kPa, 100 kPa, and ending at a nearly saturated state of the sample (referred to as 1 kPa) when there was no additional detectable absorption of water by the specimen. The desorption portion of the test followed immediately after

the sample equilibrated at the fully wetted (near saturated) stage using *s* stages of 300 kPa, 600 kPa, and 1200 kPa. The stress path for the samples tested by Singhal can be characterized as loading then wetting from an initially dry state, followed by drying with no additional changes in vertical load. Singhal's 2010 measured *e-s* relationships for the reconstituted clay soil using the OPPD are presented on Figure 2.

The "weighted plasticity index" (*wPI*), defined by Zapata et al. (2000) as a product of the percent passing the #200 sieve (in decimal form) and the Plasticity Index, is identified in Figure 2 for the "Prescott Clay" material (*wPI* = 50.6). Mosawi (2022) used *wPI* as a categorical variable to represent the expansion potential of the material being tested. Mosawi (2022) targeted fine-grained soils with three different *wPI* values (approximately 10, 30, and 50) to explore how the suction-volume change indices change with increasing expansion potential. The soils used in the study were the same as those used by Olaiz (2017) and Vann (2019). Sample preparation included air-drying the soil and then breaking down with a mortar and pestle prior to compacting in a mold to neat the optimum moisture content and 90% of the theoretical maximum dry density obtained from the Standard Proctor test (ASTM D698A). Sample molds were then placed on porous stones and partially submerged to induce a saturated state ($s = 0$) as the initial conditions for the OPPD testing. Drying tests were performed at five different *p* stages: 1, 10, 20, 40, and 60 kPa. The concept of "twinned" samples was used to test the response at varying normal stress states. The stress path for the samples tested by Mosawi can be characterized as loading then drying from an initially saturated state with no additional changes in vertical load. Mosawi's 2022 measured *e-s* relationships for the reconstituted clay soil using the OPPD are also presented on Figure 2.

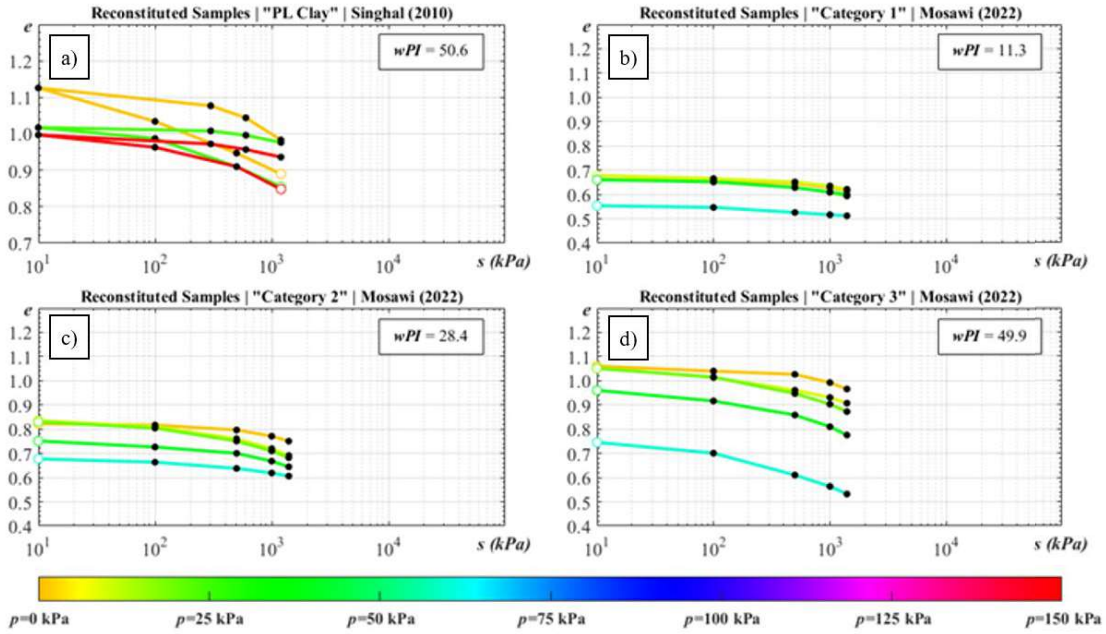

Figure 2: *e-s* plots from OPPD testing on Reconstituted Samples at various constant *s*

Note that both Singhal (2010) and Mosawi (2022) indicate that the final wetting stage of the OPPD testing corresponded to s=1 kPa. In this data set, the saturated state of the OPPD testing is considered to be the state at which the sample no longer absorbs additional water and there are no further changes in volume when the induced s in the pressure cell is turned off. Based on additional experience using the OPPD apparatus to test highly plastic clays, Olaiz (2017) noted that is extremely difficult to fully saturate a fine-grained soil using only the axis-translation technique associated with the OPPD. Hence, it is almost certain that the actual s value associated with the saturated stage of the OPPD testing on fine-grained material are greater than 1 kPa, although still quite low. In this study, a matric suction of 10 kPA was considered to be fully wetted and was used as the matric suction corresponding to the saturated stages of Singhal and Mosawi's OPPD data.

OPPD TESTING OF NATURAL CLAY SPECIMENS

In 2017, Olaiz tested the volumetric response of clay specimens to changes in s under field p using OPPDs. The study included 21 relatively intact clay specimens (10 from Denver, CO and 11 from San Antonio, TX) extracted from boreholes using a modified California Ring Sampler. Olaiz (2017) provides an extensive discussion regarding potential sample disturbance of intact unsaturated fine-grained soils. The soil index properties, and in situ moisture content, were measured for each specimen using trimmings from the ring samples. The in situ soil suction was also estimated using the WP4-C (Meter Group, Pullman, Washington). The specimens were transferred from the sealed tubes to the OPPD chamber as quickly as possible to reduce potential moisture changes, then vertically loaded to the estimated field p state. After allowing for equilibrium to be reached, a matric suction was imposed into the OPPD chamber corresponding the initial total suction measured by the WP4-C (if less than 1450 kPa). A tedious technique was used to find the matric suction state corresponding to zero changes in volume under the field p state, which was considered to be the best approach to returning the soil to the in situ field conditions. For samples which had initial total suctions greater than 1450 kPa, the initial field conditions were assumed to be when the specimen equilibrated under the field p load, prior to any imposed changes in suction. This in situ suction was assumed to correspond to the initial void ratio of the samples and is included as a data point in the OPPD results. The wetting tests were performed initially on each specimen using various intervals of suction depending on the initial stress states. Four of the 21 tests included a drying cycle and additional wetting cycle to explore the effects of hysteresis on the intact specimens. Olaiz's 2017 OPPD results of e-log(s) on intact clay soils are presented on Figure 3.

INDEX PROPERTIES, STRESS PATH HISTORY, AND HYSTERESIS EFFECTS

The effect of stress history on the volumetric response of unsaturated soils to changes in s under constant p can be further explored through a comparison of the reconstituted samples from Singhal (2010) and Mosawi (2022) to the relatively intact samples from Olaiz (2017). This stress history effect is visually evident when comparing the e-log(s) plot of the reconstituted samples from Singhal (2010) and Mosawi (2022) in Figure 2 to the e-log(s) plot of the intact samples from Olaiz (2017) in Figure 3.

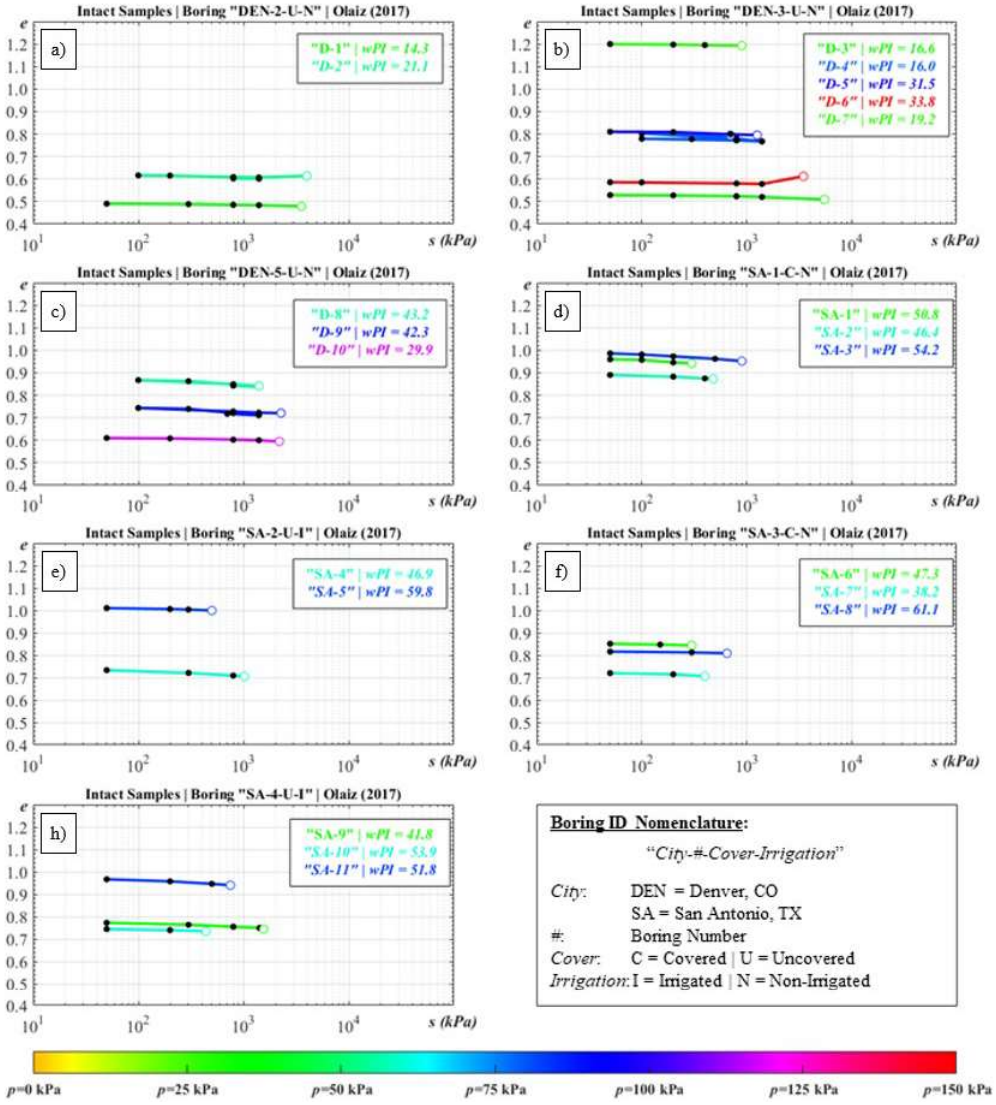

Figure 3: *e-s* Plots from OPPD Testing on Intact Samples at Various Constant *s*

The slopes of *e*-log(*s*) for intact samples appear to be relatively flat when plotted on the same scale as the *e*-log(*s*) for reconstituted samples, indicating that the suction-volume change indices of the intact samples are significantly less than the reconstituted samples, which consistent with reduced swell with added cycles of wetting and drying effects observed by Alonso & Gens (1999) and Rosenbalm (2013), and likely related to intact specimens remaining primarily in the elastic (rather than elastoplastic) range of soil response. However, when comparing Singhal's results (Figure 2a) to Mosawi's sample with nearly the same *wPI* (Figure 2c), the laboratory wetting and drying cycles imposed by Singhal prior to testing do not appear to noticeably reduce the volumetric response. This may be due to the relatively high initial density and low moisture content targeted during the sample preparation in Singhal's work.

In general, for both intact and reconstituted specimens, the volumetric response during drying for a given soil specimen was less than the wetting-induced response. For the remolded samples by Mosawi (2022), the magnitude of the suction-volume change indices tended to increase with increasing *wPI*, which provides additional evidence that *wPI* provides a useful quantitative relationship between soil index properties and volume change potential (Zapata et al., 2006). This trend is not as apparent for the intact specimens, which have reduced slopes (C_m or C_{ms}) compared to similar *wPI* reconstituted specimens.

To further evaluate the effects of index properties and the net normal stress states, the suction-volume change indices were calculated for each test in the dataset using the 2 points corresponding to the highest suction range, targeting the steeper log-linear portion of the plot beyond the infection point. This approach generally provides the most conservative calculation of the suction-volume change indices for clay soils as the slope of *e*-log(*s*) generally continues to increase up until it approaches the residual suction range, although it may appear more or less linear on the semi-log plot. This two-point interpretation approach generally results in higher indices than when using an average of the data it reduces the potential for inclusion of data points past the inflection point on the log-linear portion of *e*-log(*s*) (Figure 1). For the remolded samples in this data set, the apparent inflection point, based on the visual analysis of the change in slope of *e*-log(*s*), is relatively low, perhaps in the range of 300 to 500 kPa. The inflection point may be significantly higher in very fat clays due to the larger *AEVs* related to the tendency of fat clays to remain near saturation at substantial suction levels.

Figure 4 presents categorized box plots of the interpreted suction-volume change indices categorized by intact or remolded specimens, *p* ranges (0 to 10 kPa, 10 to 50 kPa, 50 to 100 kPa, and 100 to 150 kPa), and *wPI* ranges (10 to 20, 20 to 40, and 40 to 55). The box plots indicate that the volumetric response of the intact samples at low ranges of *p* (10 kPa or approximately 2 ft of overburden pressure and 50 kPa or approximately 10 ft of overburden pressure), is still less than the remolded samples at much higher overburden pressures of 100 to 150 kPa. This observation is supportive of the thought that the remolded specimens are more likely to exhibit elastoplastic swell response compared to intact specimen due to differences in stress history.

Although, the trend that increasing *wPI* tends to increase the suction-volume change indices appears to apply to the intact samples when grouped together. However, the overall magnitude of the indices for the intact samples at high *wPI* range (40≤wPI<55) is approximately one-third of the magnitude of the mean indices for the reconstituted samples at the low *wPI* range (10≤wPI<20), demonstrating that an undisturbed fat clay may experience significantly less volume change upon wetting than a sandy clay (SC) or lean clay (CL) which has been disturbed and recompacted. These results demonstrate the dramatic impact of specimen stress history and brings into question the use, beyond empirical, of remolded specimens in laboratory response-to-wetting tests for estimation of natural (intact) soil response. Although this dataset is limited and each field circumstance if different, this stark discrepancy between the volume change potential of undisturbed fat clays to remolded lean clays shows that it is at least plausible that recompaction of near-surface soils prior to construction could cause greater expansive soil-related stress on pavement and shallow foundations compared to leaving soils in their undisturbed state.

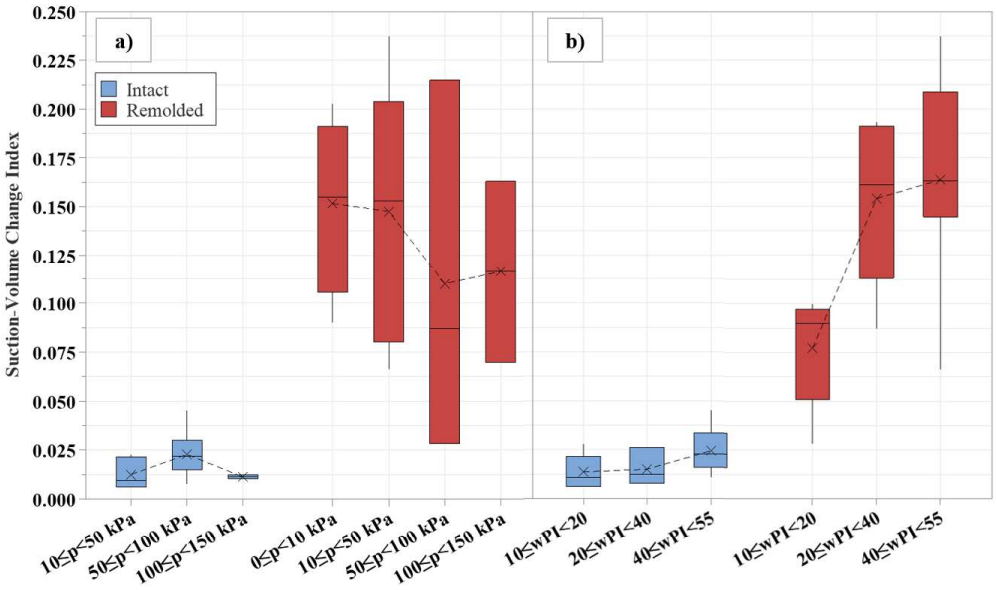

Figure 4: Box plots of suction-volume change indices for intact (blue) and remolded (red) specimens categorized by a) *p* and b) *wPI*

CONCLUSIONS

This study presents a complied data set for oedometer pressure plate device testing for the volumetric response of unsaturated reconstituted and intact samples due to changes in matric suction under constant net normal stresses. The comparison of the matric suction-volume change indices of the intact samples from Olaiz (2017) resulted in significantly lower magnitude volume change than those of the remolded samples tested by Singhal (2010) and Mosawi (2022) for similar range of *wPI* specimens and suction range. A brief statistical analysis using descriptive statistics, box plots, and 1:1 comparison indicate that for the compiled dataset, *wPI* provides a useful indicator for volumetric response for remolded specimens under relatively light confining stress. The data also demonstrate the critical role of stress history in shrink/swell response of clays to changes in moisture state. The data from the two-stress state controlled OPPD results provides a substantial start for development of *e-p-s* relationships and correlations for expansive clay soils. With the addition of similar data in the future, empirical relationships may emerge that will improve and simplify current procedures for estimation of shrink/swell volume change of clays.

DATA AVAILABILITY STATEMENT

The raw OPPD laboratory data from Singhal (2010), Olaiz (2017), and Mosawi (2022) is currently available from the first author by request and has been submitted for publication in the Arizona State University Research Data Repository and available for future access, pending current review.

ACKNOWLEDGEMENT

This work is based in part of research funded by the National Science Foundation (NSF) under Award No. 1462358, and the National Academies of Science, Engineering, and Medicine Transportation Research Board's (TRB) National Cooperative Highway Research Program (NCHRP) Project 01-59. The opinions, conclusions, and interpretations are those of the authors and not necessarily of NSF or NCHRP.

REFERENCES

Adem, H.H., & Vanapalli, S.K. (2013). Constitutive modeling approach for estimating 1-D heave with respect to time for expansive soils. *International Journal of Geotechnical Engineering,* 7(2), 199-204. http://dx.doi.org/10.1179/1938636213Z.00000000024.

Alonso, E. E. (1993). Constitutive modelling of unsaturated soils, Unsaturated soils: *Recent Developments and Applications, Civil Engineering European Courses*. Universitat Polit`ecnica de Catalunya, Barcelona, Spain.

Alonso, E.E, Gens, A., & Gehling, W.Y.Y. (1994). Elastoplastic model for unsaturated expansive soils. *Proceedings of the 3rd European Conference on Numerical Models in Geotechnical Engineering*. 11-18, Rotterdam.

Alonso, E. E., Lloret, A., Gens, A., and Yang, D. Q. 1995. Experimental behaviour of highly expansive double-structure clay, *Proceedings of the First International Conference on Unsaturated Soils* (UNSAT-95), Paris, pp. 11–16.

Alonso, E.E., Vaunat, J., & Gens, A. (1999). Modelling the mechanical behaviour of expansive clays. Engineering Geology, 54(1-2), 173-183. http://dx.doi.org/10.1016/S0013-7952(99)00079-4.

Amer, O. M. I. (2016). Determining Suction Compression Index of Expansive Soils Based on non-linear suction-volumetric strain relationship. PhD Dissertation. Oklahoma State University.

American Society for Testing and Materials (ASTM). (2007) Standard Test Methods for Laboratory Compaction Characteristics of Soil Using Standard Effort. ASTM International, West Conshohocken, ASTM International, West Conshohocken, PA.

American Society for Testing and Materials (ASTM). (2014) Standard test methods for one-dimensional swell or collapse of soils. ASTM International, West Conshohocken, ASTM International, West Conshohocken, PA.

Covar, A., and Lytton, R. (2001). Estimating soil swelling behavior using soil classification properties. *Proceedings of Geo-Institute Shallow Foundation and Soil Properties Committee Sessions at the ASCE 2001 Civil Engineering Conference*. 44-63. Houston, Texas: ASCE.

Delage P. & Graham J. 1996. Mechanical behaviour of unsaturated soils. *Proceedings of the 1st International Conference on Unsaturated Soils* (UNSAT), 3, 1223-1256, Paris: Balkema.

Delage, P., Romero, E., Tarantino, A. (2008) Recent developments in the techniques of controlling and measuring suction in unsaturated soils. *Proceeedings of the First European Conference on Unsaturated Soils*. 33-52. Durham. CRC Press. https://doi.org/10.48550/arXiv.0810.3221

Fredlund, D., and Houston. (2013). Interpretation of SWCCs when volume change occurs as soil suction is changed. *1st Pan-American Conference on Unsaturated Soils, PanAmUNSAT* 2013, (pp. 15-31). Cartegena de Indias, Colombia.

Fredlund, D.G., & Morgenstern, N.R. (1976). Constitutive relations for volume change in unsaturated soils. *Canadian Geotechnical Journal*, 13(3), 261-276. http://dx.doi.org/10.1139/t76-029.

Fredlund, D. G., Rahardjo, H, and Fredlund, M. D. (2012). Unsaturated Soil Mechanics in Engineering Practice. John Wiley & Sons, Inc. Hoboken, NJ.

Fredlund, D. G. and Pham, H., (2006). A volume-mass constitutive model for unsaturated soils in terms of two independent stress state variables. *Proceeedings of the Fourth International Conference on Unsaturated Soils.* 105-134. Carefree, AZ. ASCE.

Gens, A., & Alonso, E.E. (1992). A framework for the behaviour of unsaturated expansive clays. *Canadian Geotechnical Journal*, 29(6), 1013-1032. http://dx.doi.org/10.1139/t92-120.

Gens, A., Alonso, E. E., Suriol, J., and Lloret, A. (1995). Effect of structure on the volumetric behaviour of a compacted soil, *Proceedings of the First International Conference Unsaturated Soils*, UNSAT-95, Paris, Vol. 1, pp. 83–88.

Gens, A., Alonso, E.E., & Delage, A. (1996). Constitutive modelling: application to compacted soils. *Proceedings of the 1st International Conference on Unsaturated Soils* (UNSAT). 3, 1179-1200. Paris: Balkema.

Geotechnical Consulting and Testing Services (GCTS). (2007). SWC-150: Fredlund Soil Water Characteristic Device. 1.3. Tempe, AZ.

Hilf, J. W. (1956). An investigation of pore-water pressure in compacted cohesive soils, PhD thesis, Technical Memorandum. No. 654, U.S. Department of the Interior, Bureau of Reclamation, Design and Construction Division, Denver, CO.

Houston, S., and Houston, W. (2018). Suction-Oedometer Method for Computation of Heave and Remaining Heave. *Proceedings of the 2nd Pan-American Conference on Unsaturated Soils*. 93-116. Dallas, TX: ASCE. http://dx.doi.org/10.1061/9780784481677.005.

Houston, S. and Zhang, X. (2021) Review of expansive and collapsible soil volume change models within a unified elastoplastic framework. (F. M. T.M.P. Campos, Ed.) *Soil and Rocks,* 44(3). doi:10.28927/SR.2021.064321

Justo, J.L., Delgado, A., & Ruiz, J. (1984). The influence of stress-path in the collapse-swelling of soils at the laboratory. *Proceedings of the 5th International Conference on Expansive Soils.* 67-71. Adelaide: Institution of Engineers.

Lins, Y., and Schanz, T. (2004). Determination of hydro-mechanical properties of sand. *Proceedings from the International Conference "From Experimental Evidence towards Numerical Modeling of Unsaturated Soils,".* 15–31. Weimar, Germany.

Lytton, R., Aubeny, C., and Bulut, R. (2005). Design procedure for pavements on expansive soils. Austin, TX: Texas Department of Transportation (TxDOT).

Nelson, J.D., Chao, K.C., Overton, D.D., & Nelson, E.J. (2015). *Foundation Engineering for Expansive Aoils*. New York: Wiley Press. http://dx.doi.org/10.1002/9781118996096.

Noorany, I. (2017). Soil tests for prediction of one-dimensional heave and settlement of compacted fills. *Proceedings of the 2nd Pan-American Conference on Unsaturated Soils*. 90-99. Dallas: ASCE. https://doi. org/10.1061/9780784481707.010.

Olaiz, A.H. (2017). Evaluation of testing methods for suction-volume change of natural clay soils. Doctoral dissertation. Arizona State University. Tempe, AZ.

Overton, D.D., Chao, K.C., & Nelson, J.D. (2006). Time rate of heave prediction for expansive soils. *GeoCongress 2006: Geotechnical Engineering in the Information Technology Age*. 1-6. Atlanta: ASCE. http://dx.doi.org/10.1061/40803(187)162.

Perez-Garcia, N. Houston, S.L., Houston, W.N., Padilla, J.M. (2007). An Oedometer-Type Pressure Plate SWCC Apparatus. *Geotechnical Testing Journal*. 31(2). ASTM.

Pham, H., & Frendlund, D. (2011). A volume-mass volume–mass unsaturated soil constitutive model for drying-wetting under isotropic loading-unloading conditions. *Canadian Geotechnical Journal*, 48, 280-313. Ottawa, Canada.

Post-Tensioning Institute, (2008). Design & construction of post-tensioned slabs-on-ground, 3rd edition. Post Tensioning Institute, Phoenix.

Rosenbalm, D. C. (2013). "Volume change behavior of compacted expansive soil due to wetting and drying cycles." Ph.D. Dissertation, Arizona State Univ., Tempe, AZ.

Sheng, D., Fredlund, D.G., & Gens, A. (2008a). A new modelling approach for unsaturated soils using independent stress variables. *Canadian Geotechnical Journal*, 45(4), 511-534. http://dx.doi.org/10.1139/T07-112.

Singhal, S. (2010). Expansive soil behavior: property measurement techniques and heave prediction methods. PhD Dissertation, Arizona State University, Tempe, AZ.

Tu, H. (2015). Prediction of the variation of swelling pressure and 1-D heave of expansive soils with respect to suction. Thesis, University of Ottawa, Ottawa, Canada.

U.S. Department of Agriculture, Natural Resources Conservation Service (USDA-NRCS). (1999). Soil taxonomy. 2nd ed., Gov. Print. Office, Washington, DC.

Vann, J. (2019) "A soil suction-oedometer method and design soil suction profile recommendations for estimation of volume change of expansive soils." Ph.D. dissertation. State University. Tempe, AZ.

Vu, H. Q., Fredlund, D. G. 2000. Volume change predictions in expansive soils using a two-dimensional finite element method, *Proceedings of the Asian Conference in Unsaturated Soils*, UNSAT ASIA 2000, Singapore, pp. 231–236.

Vu, H. Q. and Fredlund, D. G. (2004) The prediction of one-, two-, three-dimensional heave in expansive soils. *Canadian Geotechnical Journal*, 41, 713-737. Ottawa, Canada. doi: 10.1139/T04-023

Wray, W.K., El-Garhy, B.M., & Youssef, A.A. (2005). Three-dimensional model for moisture and volume changes prediction in expansive soils. *Journal of Geotechnical and Geoenvironmental Engineering*, 131(3), 311-324. http://dx.doi.org/10.1061/(ASCE)1090-0241(2005)131:3(311).

Wheeler, S. J., and Sivakumar, V. 1995. An elasto-plastic critical state framework for unsaturated soil, *Geotechnique*, Vol. 45, No. 1, pp. 35–53.

Zapata, C., Houston, W., Houston, S., and Walsh, K. (2000). Soil-water characteristic curve variability. Advances in Unsaturated Geotechnics, 99, 84-124.

Zapata, C., Houston, S., Houston, W., and Dye, H. (2006). Expansion Index and Its Relationship with Other Index Properties. *Proceeedings of the Fourth International Conference on Unsaturated Soils.* 2133-2137. Carefree, AZ. ASCE.

Zhang, X., & Lytton, R.L. (2009a). Modified state-surface approach to the study of unsaturated soil behavior. Part I: basic concept. *Canadian Geotechnical Journal*, 46(5), 536-552. http://dx.doi.org/10.1139/T08-136.

Zhang, X., & Lytton, R.L. (2009b). Modified state-surface approach to the study of unsaturated soil behavior. Part II: general formulation. *Canadian Geotechnical Journal*, 46(5), 553-570. http://dx.doi.org/10.1139/T08-137.

APPENDIX D

HIERARCHICAL DESCRIPTIVE STATISTICS FOR GROUPS BY AASHTO CLASSIFICATION AND WPI

Table D-1 A-1-a Soil Properties (Rosenbalm, 2011)

	$P_{2.0"}$	$P_{1.5"}$	$P_{1.0"}$	$P_{0.5"}$	$P_{\#40}$	$P_{\#60}$	$P_{\#200}$	PI	G_s	D_{60}	*wPI*
#	1213	1213	1213	1213	2175	2175	2175	2175	489	1271	2175
μ	97.9	96.0	90.91	71.34	19.6	15.5	8.72	0.75	2.702	9.15	0.08
σ^2	43.8	80.5	144.40	188.82	38.72	26.05	14.14	2.19	0.01	42.34	0.03
σ	6.62	8.97	12.02	13.74	6.22	5.10	3.76	1.48	0.11	6.51	0.17
CV	6.8	9.3	13.2	19.3	31.7	32.9	43.1	195	4.0	71.1	206.4
a	30.0	28.0	25.0	8.0	0.0	0.0	0.0	0.0	2.243	2.4	0.000
b	100	100	100	99.0	30.0	25.9	15.0	6.0	3.152	72.2	0.894

Table D-2 A-1-b Soil Properties (Rosenbalm, 2011)

	$P_{2.0"}$	$P_{1.5"}$	$P_{1.0"}$	$P_{0.5"}$	$P_{\#40}$	$P_{\#60}$	$P_{\#200}$	PI	G_s	D_{60}	*wPI*
#	1033	1033	1033	1033	2610	2610	2610	2610	472	1939	2610
μ	99.1	98.1	95.1	83.99	35.50	28.51	16.52	1.492	2.661	2.824	0.308
σ^2	7.17	13.39	32.90	80.26	59.61	46.47	39.35	3.59	0.01	4.70	0.17
σ	2.68	3.66	5.74	8.96	7.72	6.82	6.27	1.89	0.10	2.17	0.41
CV	2.7	3.7	6.0	10.7	21.8	23.9	38.0	127	3.7	76.8	132
a	74.0	73.0	69.0	57.0	7.5	5.6	0.2	0.0	2.243	0.6	0.000
b	100.0	100.0	100.0	100.0	50.0	44.2	25.0	6.0	3.025	13.9	1.500

Table D-3. A-2-4 Soil Properties (Rosenbalm, 2011)

	$P_{2.0"}$	$P_{1.5"}$	$P_{1.0"}$	$P_{0.5"}$	$P_{\#40}$	$P_{\#60}$	$P_{\#200}$	PI	G_s	D_{60}	*wPI*
#	1683	1683	1683	1683	4218	4218	4218	4218	691	3282	4218
μ	99.5	99.1	98.0	93.9	56.08	46.03	26.7	4.24	2.677	1.34	1.16
σ^2	8.81	13.2	24.9	94.5	401	195.40	46.64	10.48	0.00	6.53	0.84
Σ	2.97	3.64	4.99	9.72	20.03	13.98	6.83	3.24	0.07	2.56	0.92
CV	3.0	3.7	5.1	10.4	35.7	30.4	25.6	76.4	2.6	191	78.9
a	54.0	44.0	36.0	31.0	8.0	6.6	2.8	0.0	2.445	0.1	0.000
B	100.0	100.0	100.0	100.0	99.0	98.3	35.4	10.0	2.975	54.9	3.500

Table D-4. A-2-5 Soil Properties (Rosenbalm, 2011)

	$P_{2.0"}$	$P_{1.5"}$	$P_{1.0"}$	$P_{0.5"}$	$P_{\#40}$	$P_{\#60}$	$P_{\#200}$	PI	G_s	D_{60}	*wPI*
#	561	561	561	561	1219	1219	1219	1219	5	1186	1219
μ	100	100	99.9	99.8	69.0	55.0	22.06	0.075	2.835	0.431	0.021
σ^2	0.00	0.00	0.50	3.07	189.9	85.85	39.76	0.39	0.00	0.34	0.03
σ	0.00	0.00	0.71	1.75	13.78	9.27	6.31	0.62	0.05	0.58	0.18
CV	0.0	0.0	0.7	1.8	20.0	16.8	28.6	828	1.8	135	848
a	100	100	92.0	81.0	30.0	27.8	10.5	0.0	2.781	0.2	0.000
b	100	100	100.0	100.0	97.5	74.8	35.0	10.0	2.877	4.8	3.250

Table D-5. A-2-6 Soil Properties (Rosenbalm, 2011)

	$P_{2.0"}$	$P_{1.5"}$	$P_{1.0"}$	$P_{0.5"}$	$P_{\#40}$	$P_{\#60}$	$P_{\#200}$	PI	G_s	D_{60}	*wPI*
#	209	209	209	209	729	729	729	729	77	330	729
μ	99.6	98.4	95.6	85.2	41.1	36.16	26.99	14.15	2.653	3.003	3.839
σ^2	2.76	11.29	36.79	173.7	256.9	139.46	44.63	6.42	0.00	12.41	1.60
σ	1.66	3.36	6.07	13.18	16.03	11.81	6.68	2.53	0.05	3.52	1.26
CV	1.7	3.4	6.3	15.5	39.0	32.7	24.8	17.9	2.0	117	32.9
a	90.0	78.0	67.0	45.0	10.0	9.3	2.8	10.5	2.507	0.1	0.448
b	100	100	100.0	100.0	99.0	78.8	35.4	25.0	2.780	19.4	8.073

Table D-6. A-2-7 Soil Properties (Rosenbalm, 2011)

	$P_{2.0"}$	$P_{1.5"}$	$P_{1.0"}$	$P_{0.5"}$	$P_{\#40}$	$P_{\#60}$	$P_{\#200}$	PI	G_s	D_{60}	*wPI*
#	28	28	28	28	174	174	174	174	1	46	174
μ	96.8	94.9	89.25	76.89	35.7	33.4	28.4	24.66	2.767	5.758	7.026
σ^2	22.54	43.83	124	254	52.08	40.91	31.21	47.11	N/A	23.36	6.28
σ	4.75	6.62	11.12	15.95	7.22	6.40	5.59	6.86	N/A	4.83	2.51
CV	4.9	7.0	12.5	20.7	20.2	19.2	19.6	27.8	N/A	83.9	35.7
a	86.0	82.0	70.0	50.0	15.0	13.2	8.6	12.5	2.767	0.4	1.892
b	100	100.0	100.0	100.0	60.0	51.0	35.3	50.0	2.767	18.4	16.95

Table D-7. A-3 Soil Properties (Rosenbalm, 2011)

	$P_{2.0"}$	$P_{1.5"}$	$P_{1.0"}$	$P_{0.5"}$	$P_{\#40}$	$P_{\#60}$	$P_{\#200}$	PI	G_s	D_{60}	*wPI*
#	508	508	508	508	689	689	689	689	92	689	689
μ	99.96	99.90	99.68	98.94	75.40	50.67	6.75	0.0	2.665	0.351	0.0
σ^2	0.31	0.61	1.70	8.66	237.25	200.87	5.41	0.0	0.00	0.03	0.0
σ	0.56	0.78	1.30	2.94	15.40	14.17	2.33	0.0	0.06	0.17	0.0
CV	0.6	0.8	1.3	3.0	20.4	28.0	34.5	0.0	0.02	49.2	0.0
a	88.0	85.0	84.0	75.0	51.0	22.0	0.3	0.0	2.445	0.1	0.0
b	100.0	100.0	100.0	100.0	100.0	96.2	10.4	0.0	2.884	2.0	0.0

Table D-8. A-4 Soil Properties (Rosenbalm, 2011)

	$P_{2.0"}$	$P_{1.5"}$	$P_{1.0"}$	$P_{0.5"}$	$P_{\#40}$	$P_{\#60}$	$P_{\#200}$	PI	G_s	D_{60}	*wPI*
#	1211				11002				465	11002	
μ	99.6	99.4	98.6	95.96	78.46	73.00	60.17	5.99	2.677	0.30	3.704
σ^2	2.81	3.98	8.30	32.4	215	215	295	7.96	0.00	0.51	4.85
σ	1.68	1.99	2.88	5.69	14.65	14.67	17.18	2.82	0.07	0.71	2.20
CV	1.7	2.0	2.9	5.9	18.7	20.1	28.6	47.1	0.03	239	59.5
a	86.0	83.0	79.0	64.0	36.0	36.0	35.5	0.0	2.494	0.0	0.00
b	100	100	100	100	100	99.3	99.0	10.0	2.935	10.8	9.76

Table D-9. A-5 Soil Properties (Rosenbalm, 2011)

	$P_{2.0"}$	$P_{1.5"}$	$P_{1.0"}$	$P_{0.5"}$	$P_{\#40}$	$P_{\#60}$	$P_{\#200}$	PI	G_s	D_{60}	*wPI*
#	31	31	31	31	332	332	332	332	14	330	332
μ	99.5	99.1	98.1	94.8	78.3	71.5	55.23	2.054	2.749	0.260	1.302
σ^2	2.92	8.69	17.66	48.47	184	179	278	8.42	0.00	0.26	3.68
σ	1.71	2.95	4.20	6.96	13.6	13.38	16.68	2.90	0.07	0.51	1.92
CV	1.7	3.0	4.3	7.3	17.3	18.7	30.2	141	0.03	195	147
a	92.0	87.0	81.0	69.0	40.0	39.3	36.3	0.0	2.620	0.0	0.000
b	100	100	100	100	100	99.3	97.5	10.0	2.869	4.8	9.250

Table D-10. A-6 Soil Properties (Rosenbalm, 2011)

	$P_{2.0"}$	$P_{1.5"}$	$P_{1.0"}$	$P_{0.5"}$	$P_{\#40}$	$P_{\#60}$	$P_{\#200}$	PI	G_s	D_{60}	*wPI*
#	926	926	926	926	6860	6860	6860	6860	251	6740	6860
μ	99.83	99.59	99.06	97.26	84.69	79.94	69.06	14.81	2.686	0.171	10.29
σ^2	0.89	1.94	4.81	19.0	167	178	269	8.83	0.00	0.32	11.50
σ	0.94	1.39	2.19	4.36	12.92	13.35	16.39	2.97	0.06	0.57	3.39
CV	0.9	1.4	2.2	4.5	15.3	16.7	23.7	20.1	0.02	331	33.0
a	91.0	89.0	85.0	71.0	37.5	37.5	35.6	10.5	2.507	0.0	3.885
b	100	100	100	100	100	99.4	98.2	29.0	3.089	8.8	24.36

Table D-11. A-7-5 Soil Properties (Rosenbalm, 2011)

	$P_{2.0"}$	$P_{1.5"}$	$P_{1.0"}$	$P_{0.5"}$	$P_{\#40}$	$P_{\#60}$	$P_{\#200}$	PI	G_s	D_{60}	*wPI*
#	58	58	58	58	683	683	683	683	17	487	683
μ	99.2	98.8	98.2	96.4	91.2	88.83	83.37	28.92	2.666	0.08	24.60
σ^2	15.41	25.29	37.47	53.15	109	122	176	83.33	0.00	0.17	95.71
σ	3.93	5.03	6.12	7.29	10.44	11.05	13.26	9.13	0.07	0.41	9.78
CV	4.0	5.1	6.2	7.6	11.5	12.4	15.9	31.6	0.03	517	39.8
a	79.0	73.0	67.0	63.0	40.0	39.3	37.0	10.5	2.605	0.0	5.52
b	100	100	100	100	100	100	100	55.0	2.875	4.8	52.25

Table D-12. A-7-6 Soil Properties (Rosenbalm, 2011)

	$P_{2.0"}$	$P_{1.5"}$	$P_{1.0"}$	$P_{0.5"}$	$P_{\#40}$	$P_{\#60}$	$P_{\#200}$	PI	G_s	D_{60}	*wPI*
#	618	618	618	618	4935	4935	4935	4935	141	4617	4935
μ	99.6	99.2	98.7	97.3	88.75	86.18	80.09	28.496	2.676	0.086	23.06
σ^2	3.81	7.91	14.75	31.46	138	146	193	63.06	0.00	0.20	69.70
σ	1.95	2.81	3.84	5.61	11.75	12.09	13.88	7.94	0.06	0.44	8.35
CV	2.0	2.8	3.9	5.8	13.2	14.0	17.3	27.9	0.02	516	36.2
a	83.0	75.0	70.0	66.0	40.0	39.3	36.4	14.0	2.550	0.0	6.630
b	100	100	100	100	100	99.4	99.0	75.0	2.884	8.7	66.24

Table D-13. Granular Base Material Soil Properties (Rosenbalm, 2011)

	$P_{2.0"}$	$P_{1.5"}$	$P_{1.0"}$	$P_{0.5"}$	$P_{\#40}$	$P_{\#60}$	$P_{\#200}$	PI	G_s	D_{60}	*wPI*
#	2272				4785				961	3210	4785
μ	98.5	97.0	92.9	77.4	28.3	22.59	12.97	1.159	2.682	5.330	0.206
σ^2	27.0	50.24	96.9	182	1123	79.2	42.98	3.08	0.01	29.18	0.12
σ	5.20	7.09	9.85	13.51	10.62	8.90	6.56	1.76	0.10	5.40	0.34
CV	5.3	7.3	10.6	17.4	37.6	39.4	50.5	152	0.04	101	166
a	30.0	28.0	25.0	8.0	0.0	0.0	0.0	0.0	2.243	0.6	0.00
b	100	100	100	100	50.0	44.2	25.0	6.0	3.152	72.2	1.50

Table D-14. Granular Subbase and Subgrade Material Soil Properties (Rosenbalm, 2011)

	$P_{2.0"}$	$P_{1.5"}$	$P_{1.0"}$	$P_{0.5"}$	$P_{\#40}$	$P_{\#60}$	$P_{\#200}$	PI	G_s	D_{60}	*wPI*
#	3062				7029				866	5533	7029
μ	99.7	99.4	98.4	95.2	58.16	46.70	24.00	4.632	2.675	1.158	1.272
σ^2	5.41	8.96	19.82	85.62	420	197	76.38	33.30	0.00	5.47	2.77
σ	2.33	2.99	4.45	9.25	20.49	14.03	8.74	5.77	0.07	2.34	1.66
CV	2.3	3.0	4.5	9.7	35.2	30.0	36.4	125	0.03	202	131
a	54.0	44.0	36.0	31.0	8.0	6.6	0.3	0.0	2.445	0.1	0.00
b	100	100	100	100	100	98.3	35.4	50.0	2.975	54.9	16.95

Table D-15. Fine Grained Material Soil Properties (Rosenbalm, 2011)

	$P_{2.0"}$	$P_{1.5"}$	$P_{1.0"}$	$P_{0.5"}$	$P_{\#40}$	$P_{\#60}$	$P_{\#200}$	PI	G_s	D_{60}	*wPI*
#	11206						23814		888		23814
μ	99.9	99.9	99.7	99.2	82.75	78.16	67.45	13.80	2.680	0.214	10.18
σ^2	0.78	1.38	2.84	9.64	201	218	330	104	0.00	0.39	83.61
σ	0.88	1.17	1.68	3.11	14.17	14.75	18.17	10.18	0.07	0.63	9.14
CV	0.9	1.2	1.7	3.1	17.1	18.9	26.9	73.7	0.02	292	89.8
a	79.0	73.0	67.0	63.0	10.0	36.0	35.5	0.0	2.494	0.0	0.000
b	100	100	100	100	100	100	100	75.0	3.089	10.8	66.24

Table D-16. “Clayey” Fine Grained Material Soil Properties (Rosenbalm, 2011)

	$P_{2.0"}$	**$P_{1.5"}$**	**$P_{1.0"}$**	**$P_{0.5"}$**	**$P_{\#40}$**	**$P_{\#60}$**	***$P_{\#200}$***	**PI**	**G_s**	**D_{60}**	***wPI***
#	1604				12480				409	12480	
μ	99.7	99.4	98.9	97.3	86.65	82.89	74.21	21.0	2.682	0.134	16.12
σ^2	2.55	5.11	9.84	25.0	157	173	266	81.07	0.00	0.27	80.84
σ	1.60	2.26	3.14	5.00	12.54	13.17	16.32	9.00	0.06	0.52	8.99
CV	1.6	2.3	3.2	5.1	14.5	15.9	22.0	42.9	0.02	386	55.8
a	79.0	73.0	67.0	63.0	37.5	37.5	35.6	10.5	2.507	0.0	3.885
b	100	100	100	100	100	100	100	75.0	3.089	8.8	66.24

Table D-17. “Silty” Fine Grained Material Soil Properties (Rosenbalm, 2011)

	$P_{2.0"}$	**$P_{1.5"}$**	**$P_{1.0"}$**	**$P_{0.5"}$**	**$P_{\#40}$**	**$P_{\#60}$**	***$P_{\#200}$***	**PI**	**G_s**	**D_{60}**	***wPI***
#	4606				11334				479	11334	
μ	99.9	99.8	99.6	98.9	78.46	72.95	60.02	5.873	2.679	0.298	3.63
σ^2	0.79	1.17	2.68	12.11	214	214	295	8.41	0.01	0.50	4.98
σ	0.89	1.08	1.64	3.48	14.62	14.64	17.19	2.90	0.07	0.71	2.23
CV	0.9	1.1	1.6	3.5	18.6	20.1	28.6	49.4	0.03	238	61.4
a	86.0	83.0	79.0	64.0	10.0	36.0	35.5	0.0	2.494	0.0	0.00
b	100	100	100	100	100	99.3	99.0	10.0	2.935	10.8	9.76

Table D-18. Level 2 A-1-a Soil Properties

	PI	*$P_{\#200}$*	*w*	γ_d
#	2175		23	
μ	0.75	8.72	7.99	123.33
σ^2	2.19	14.14	7.88	92.54
σ	1.48	3.76	2.81	9.62
CV	197.33	43.12	35.13	7.80
a	0	0	5.33	108.46
b	6	15	14.87	141.14
α	0.10	1.67	5.56	89.12
β	1*	1.20	14.38	106.74

Table D-19. Level 2 A-1-b Soil Properties

	PI	$P_{\#200}$	*w*	γ_d
#	2610		23	
μ	1.492	16.52	7.99	123.33
σ^2	3.57	39.31	7.88	92.54
σ	1.89	6.27	2.81	9.62
CV	126.68	37.95	35.13	7.80
a	0	0.2	5.33	108.46
b	6	25	14.87	141.14
α	0.22	1.72	5.56	89.12
β	1*	0.89	14.38	106.74

Table D-20. Level 2 A-2-4 Soil Properties

	PI	$P_{\#200}$	*w*	γ_d
#	4218		23	
μ	4.24	26.7	7.99	123.33
σ^2	10.50	46.65	7.88	92.54
Σ	3.24	6.83	2.81	9.62
CV	76.42	25.58	35.13	7.80
a	0	2.8	5.33	108.46
B	10	35.4	14.87	141.14
α	0.56	3.35	5.56	89.12
β	1*	1.22	14.38	106.74

Table D-21. Level 2 A-2-5 Soil Properties

	PI	$P_{\#200}$	*w*	γ_d
#	1219		23	
μ	0.08	22.06	7.99	123.33
σ^2	0.38	39.82	7.88	92.54
σ	0.62	6.31	2.81	9.62
CV	828.00	28.60	35.13	7.80
a	0.00	10.50	5.33	108.46
b	10.00	35.00	14.87	141.14
α	0.01	5.99	5.56	89.12
β	1.00	6.70	14.38	106.74

Table D-22. Level 2 A-2-6 Soil Properties

	PI	$P_{\#200}$	*w*	γ_d
#	729		23	
μ	14.15	26.99	7.99	123.33
σ^2	6.40	44.62	7.88	92.54
σ	2.53	6.68	2.81	9.62
CV	17.90	24.80	35.13	7.80
a	10.50	2.80	5.33	108.46
b	25.00	35.40	14.87	141.14
α	23.10	3.45	5.56	89.12
β	68.67	1.20	14.38	106.74

Table D-23. Level 2 A-2-7 Soil Properties

	PI	$P_{\#200}$	*w*	γ_d
#	174		23	
μ	24.66	28.40	7.99	123.33
σ^2	47.06	31.25	7.88	92.54
σ	6.86	5.59	2.81	9.62
CV	27.80	19.60	35.13	7.80
a	12.50	8.60	5.33	108.46
b	50.00	35.30	14.87	141.14
α	8.42	5.99	5.56	89.12
β	17.54	2.09	14.38	106.74

Table D-24. Level 2 A-3 Soil Properties

	PI	$P_{\#200}$	*w*	γ_d
#	689		23	
μ	0.00	6.75	7.99	123.33
σ^2	0.00	5.43	7.88	92.54
σ	0.00	2.33	2.81	9.62
CV	0.00	34.50	35.13	7.80
a	0.00	0.30	5.33	108.46
b	0.00	10.40	14.87	141.14
α	0.00	2.40	5.56	89.12
β	0.00	1.36	14.38	106.74

Table D-25. Level 2 A-4 Soil Properties

	PI	$P_{\#200}$	*w*	γ_d
#	11002		34	
μ	5.99	60.17	17.57	106.11
σ^2	7.95	295.15	32.11	95.80
σ	2.82	17.18	5.67	9.79
CV	47.08	28.55	17.86	7.03
a	0.00	35.50	8.84	83.00
b	10.00	99.00	31.76	124.36
α	1.21	7.11	19.02	88.72
β	0.81	11.19	30.90	70.06

Table D-26. Level 2 A-5 Soil Properties

	PI	$P_{\#200}$	*w*	γ_d
#	332		34	
μ	2.05	55.23	17.57	106.11
σ^2	8.41	278.22	32.11	95.80
σ	2.90	16.68	5.67	9.79
CV	141.00	30.20	17.86	7.03
a	0.00	36.30	8.84	83.00
b	10.00	97.50	31.76	124.36
α	0.19	7.26	19.02	88.72
β	1*	16.22	30.90	70.06

Table D-27. Level 2 A-6 Soil Properties

	PI	$P_{\#200}$	*w*	γ_d
#	6860		86	
μ	14.81	69.06	20.30	106.00
σ^2	8.82	268.63	23.86	80.15
σ	2.97	16.39	4.88	8.95
CV	20.05	23.73	24.06	8.45
a	10.50	35.60	10.13	82.24
b	29.00	98.20	35.21	126.11
α	18.84	7.73	9.86	63.72
β	62.03	6.73	14.45	53.95

Table D-28. Level 2 A-7-5 Soil Properties

	PI	$P_{\#200}$	*w*	γ_d
#	683		86	
μ	28.92	83.37	20.30	106.00
σ^2	83.36	175.83	23.86	80.15
σ	9.13	13.26	4.88	8.95
CV	31.57	15.91	24.06	8.45
a	10.50	37.00	10.13	82.24
b	55.00	100.00	35.21	126.11
α	5.47	9.70	9.86	63.72
β	7.74	3.48	14.45	53.95

Table D-29. Level 2 A-7-6 Soil Properties

	PI	$P_{\#200}$	*w*	γ_d
#	4935		86	
μ	28.50	80.09	20.30	106.00
σ^2	63.04	192.65	23.86	80.15
σ	7.94	13.88	4.88	8.95
CV	27.86	17.33	24.06	8.45
a	14.00	36.40	10.13	82.24
b	75.00	99.00	35.21	126.11
α	9.58	9.36	9.86	63.72
β	30.74	4.05	14.45	53.95

Table D-30. Level 2 Shrink-swell Soil with $10 < wPI < 20$

	LL	*PI*	$P_{\#200}$	P_{clay}	*w*	γ_d
#					55	
μ	46.49	23.48	66.31	30.92	22.18	103.09
σ^2	25.60	17.81	184.14	73.79	15.68	52.56
σ	5.06	4.22	13.57	8.59	3.96	7.25
CV	10.89	17.96	20.47	27.77	17.86	7.03
a	41.00	14.00	36.40	10.00	14.19	82.24
b	64.00	35.00	98.00	52.60	35.21	121.39
α	63.96	16.56	11.79	6.11	19.05	94.05
β	203.99	20.12	12.49	6.33	31.07	82.55

Table D-31. Level 2 Shrink-swell Soil with $20 \leq wPI < 30$

	LL	*PI*	$P_{\#200}$	P_{clay}	*w*	γ_d
#	101				55	
μ	52.17	29.61	76.98	36.58	22.18	103.09
σ^2	105.68	102.21	281.57	152.52	15.68	52.56
σ	10.28	10.11	16.78	12.35	3.96	7.25
CV	19.71	34.13	21.80	33.76	17.86	7.03
a	25.00	11.00	30.20	5.70	14.19	82.24
b	102.00	75.00	99.00	75.50	35.21	121.39
α	16.31	5.80	6.05	4.45	19.05	94.05
β	29.90	14.14	2.85	5.61	31.07	82.55

Table D-32. Level 2 Shrink-swell Soil with with $30 \leq wPI < 40$

	LL	*PI*	$P_{\#200}$	P_{clay}	*w*	γ_d
#					55	
μ	61.13	39.11	88.74	46.41	22.18	103.09
σ^2	67.24	37.33	91.39	114.28	15.68	52.56
σ	8.20	6.11	9.56	10.69	3.96	7.25
CV	13.41	15.61	10.77	23.03	17.86	7.03
a	50.00	31.00	60.60	15.50	14.19	82.24
b	85.00	61.00	99.00	75.50	35.21	121.39
α	37.61	29.67	22.30	8.63	19.05	94.05
β	80.65	80.09	8.13	8.12	31.07	82.55

Table D-33. Level 2 Shrink-swell Soil with $40 \leq wPI < 50$

	LL	*PI*	$P_{\#200}$	P_{clay}	*w*	γ_d
#					55	
μ	70.50	47.36	92.86	58.98	22.18	103.09
σ^2	69.89	27.46	29.05	87.42	15.68	52.56
σ	8.36	5.24	5.39	9.35	3.96	7.25
CV	11.85	11.07	5.80	15.85	17.86	7.03
a	57.00	41.00	79.40	40.70	14.19	82.24
b	83.00	61.00	98.90	68.80	35.21	121.39
α	33.72	55.34	91.39	13.26	19.05	94.05
β	31.22	118.67	41.01	7.12	31.07	82.55

Table D-34. Level 2 Shrink-swell Soil with $wPI \geq 50$

	LL	*PI*	$P_{\#200}$	P_{clay}	*w*	γ_d
#					55	
μ	87.20	65.40	89.48	57.52	22.18	103.09
σ^2	89.68	50.84	16.89	31.92	15.68	52.56
σ	9.47	7.13	4.11	5.65	3.96	7.25
CV	10.86	10.90	4.59	9.81	17.86	7.03
a	77.00	59.00	82.40	51.00	14.19	82.24
b	102.00	75.00	92.60	64.00	35.21	121.39
α	49.79	50.10	144.49	51.29	19.05	94.05
β	72.24	75.15	63.68	50.98	31.07	82.55

Table D-35. Level 3 Granular Material Properties (A-1, A-2 & A-3)

	PI	$P_{\#200}$	*w*	γ_d
#	7029		23	
μ	4.632	24.00	7.99	123.33
σ^2	33.29	76.39	7.88	92.56
σ	5.77	8.74	2.81	9.62
CV	124.57	36.42	35.13	7.80
a	0	0.3	5.33	108.46
b	50	35.4	14.87	141.14
α	0.49	1.77	5.56	89.10
β	4.82	0.85	14.38	106.74

Table D-36. Level 3 Fine Grained Material Properties (A-4, A-5, A-6, &, A-7)

	PI	$P_{\#200}$	*w*	γ_d
#	23814		120	
μ	13.8	67.45	19.53	106.03
σ^2	103.63	330.15	27.47	83.82
σ	10.18	18.17	5.24	9.16
CV	73.77	26.94	26.84	8.63
a	0	35.5	8.84	82.24
b	75	100	35.21	126.11
α	1.32	6.46	7.85	60.85
β	5.83	6.58	11.51	51.37

Table D-37. Level 3 “Silty” Fine Grained Material Properties (A-4 & A-5)

	PI	$P_{\#200}$	*w*	γ_d
#	11334		34	
μ	5.873	60.02	17.57	106.11
σ^2	8.41	295.50	32.11	95.80
σ	2.9	17.19	5.67	9.79
CV	49.38	28.64	32.24	9.22
a	0	35.5	8.84	83.00
b	10	99	31.76	124.36
α	1.11	7.10	5.57	51.30
β	0.78	11.28	9.05	40.51

Table D-38. Level 3 “Clayey” Fine Grained Material Properties (A-6 & A-7)

	PI	$P_{\#200}$	*w*	γ_d
#	12480		86	
μ	21	74.21	20.30	106.00
σ^2	81.00	266.34	23.86	80.15
σ	9	16.32	4.88	8.95
CV	42.86	21.99	24.06	8.45
a	10.5	35.6	10.13	82.24
b	75	100	35.21	126.11
α	4.40	7.68	9.86	63.72
β	22.60	5.13	14.45	53.95

Table D-39. Level 3 Shrink-swell Soil (A-6 & A-7 with $wPI > 10$)

	LL	*PI*	$P_{\#200}$	P_{clay}	*w*	γ_d
#					55	
μ	45.68	25.53	77.16	33.50	22.18	103.09
σ^2	151.04	105.27	239.94	124.10	15.69	52.53
σ	12.29	10.26	15.49	11.14	3.96	7.25
CV	26.92	40.17	20.07	33.25	17.86	7.03
a	25.00	11.00	30.20	0.00	14.19	82.24
b	102.00	75.00	99.00	75.50	35.21	121.39
α	9.82	4.56	7.20	4.59	19.05	94.05
β	26.76	15.54	3.35	5.75	31.07	82.55

APPENDIX E

CLIMATE MODEL FIGURES

CLIMATE MODEL OUTPUT FOR ARLINGTON, VA FROM 03/2017 TO 03/2022

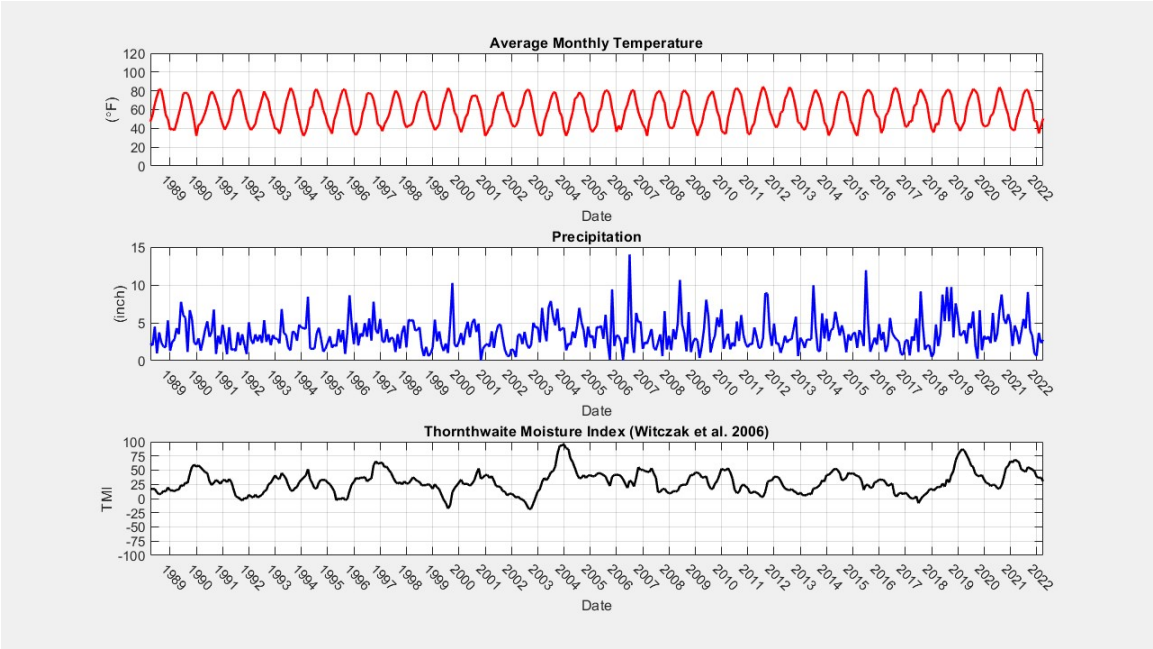

Figure D-1 NOAA Station USW00013743 Climate Data Extract and Calculated *TMI* from 03/1988 to 03/2022

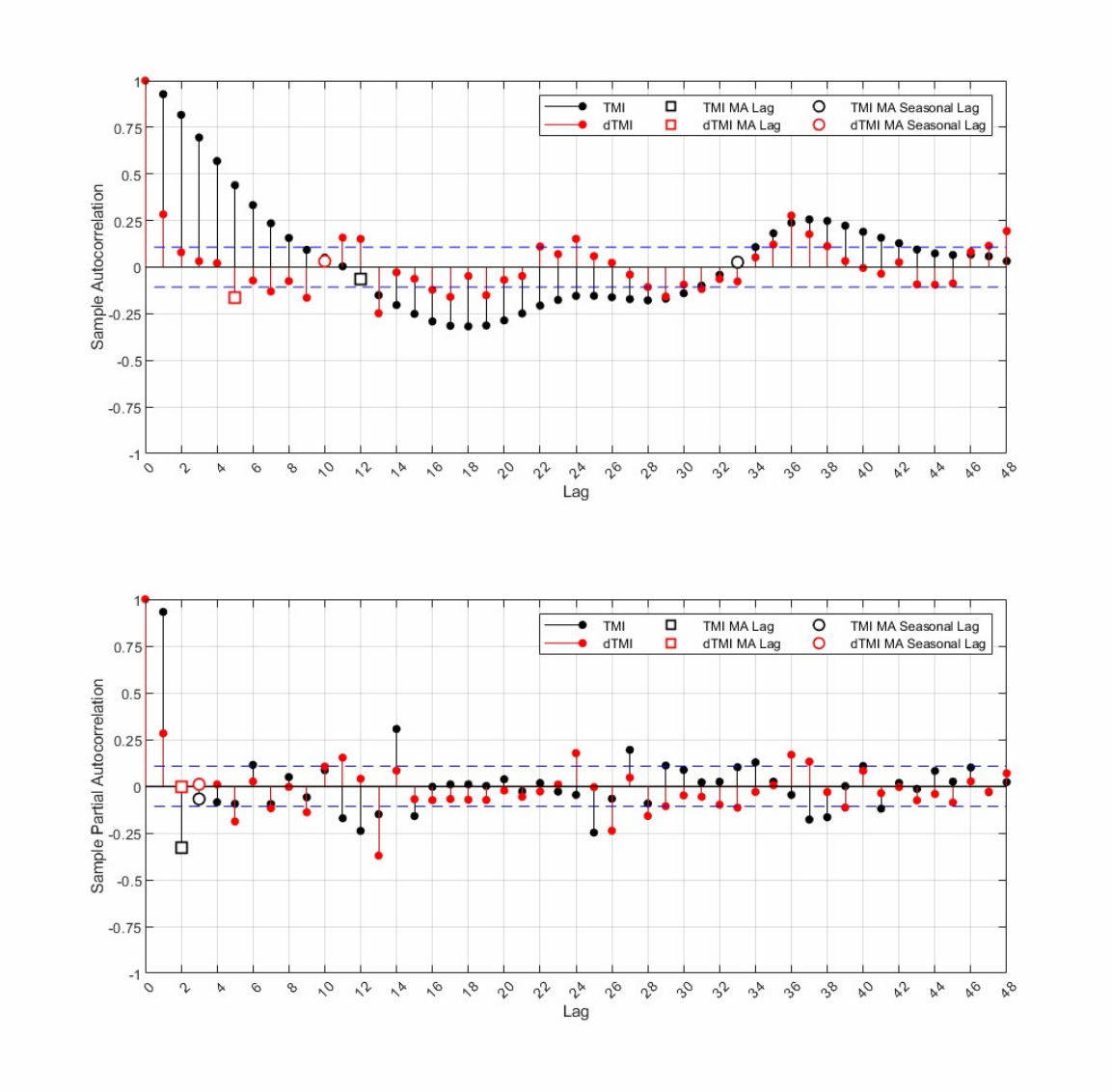

Figure D-2 ACF and PACF for *TMI* and *dTMI* for NOAA Station USW00013743 from 03/1988 to 03/2022

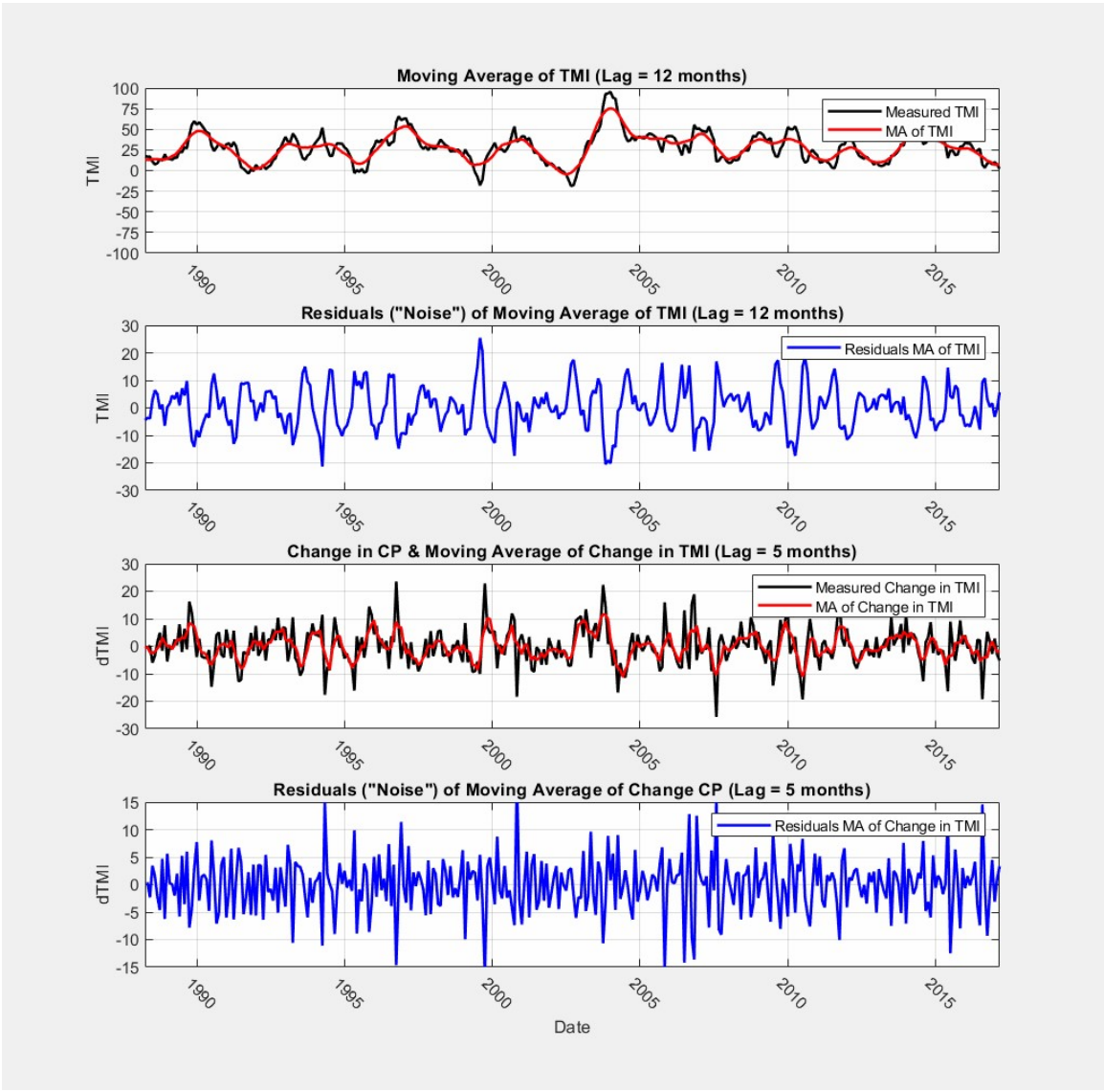

Figure D-3 Time Series Decomposition Using 1st differenced Moving Average for NOAA Station USW00013743 from 03/1988 to 03/2022

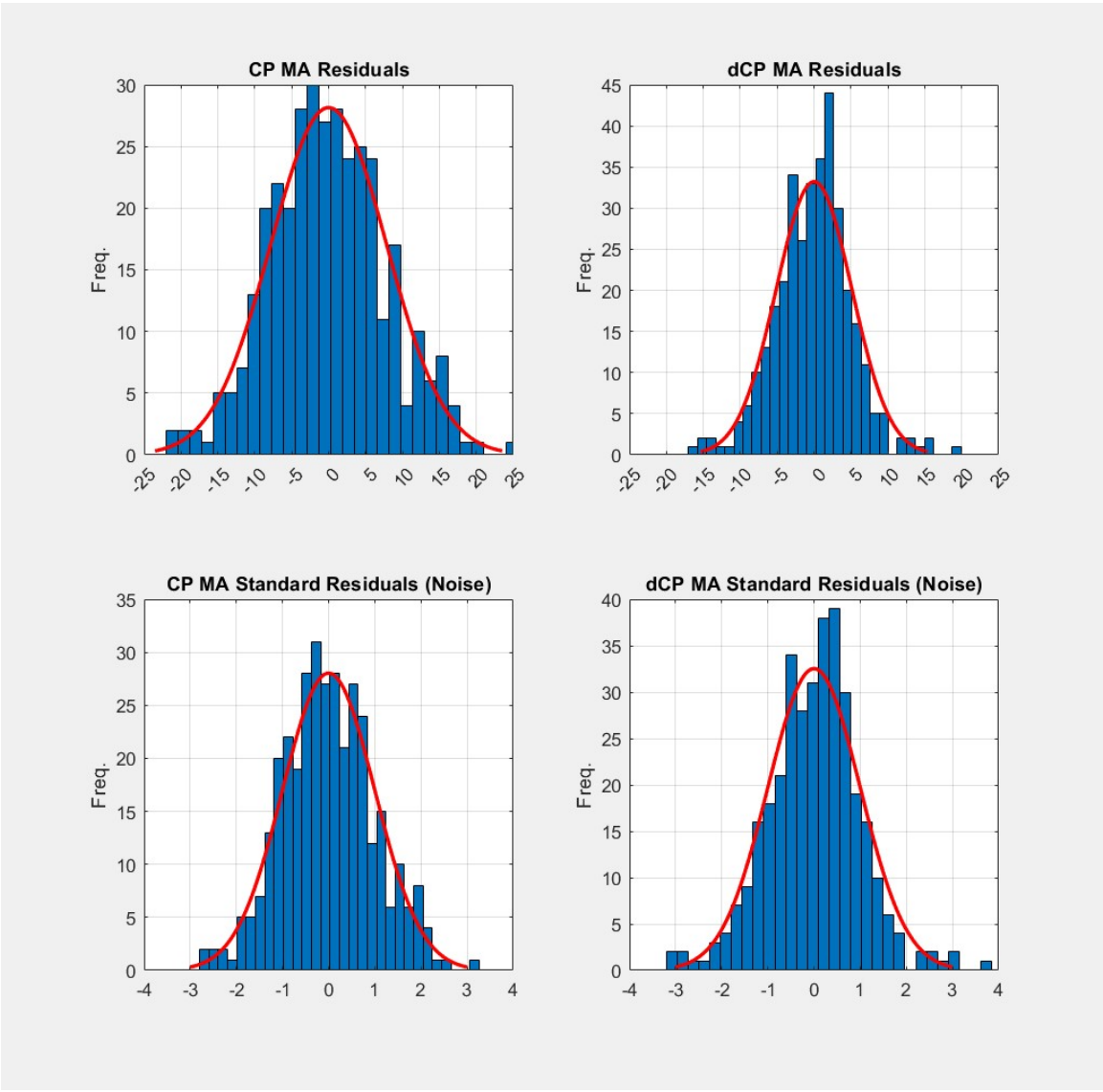

Figure D-4 Histograms for Decomposed *TMI* and *dTMI* for NOAA Station USW00013743 from 03/1988 to 03/2022

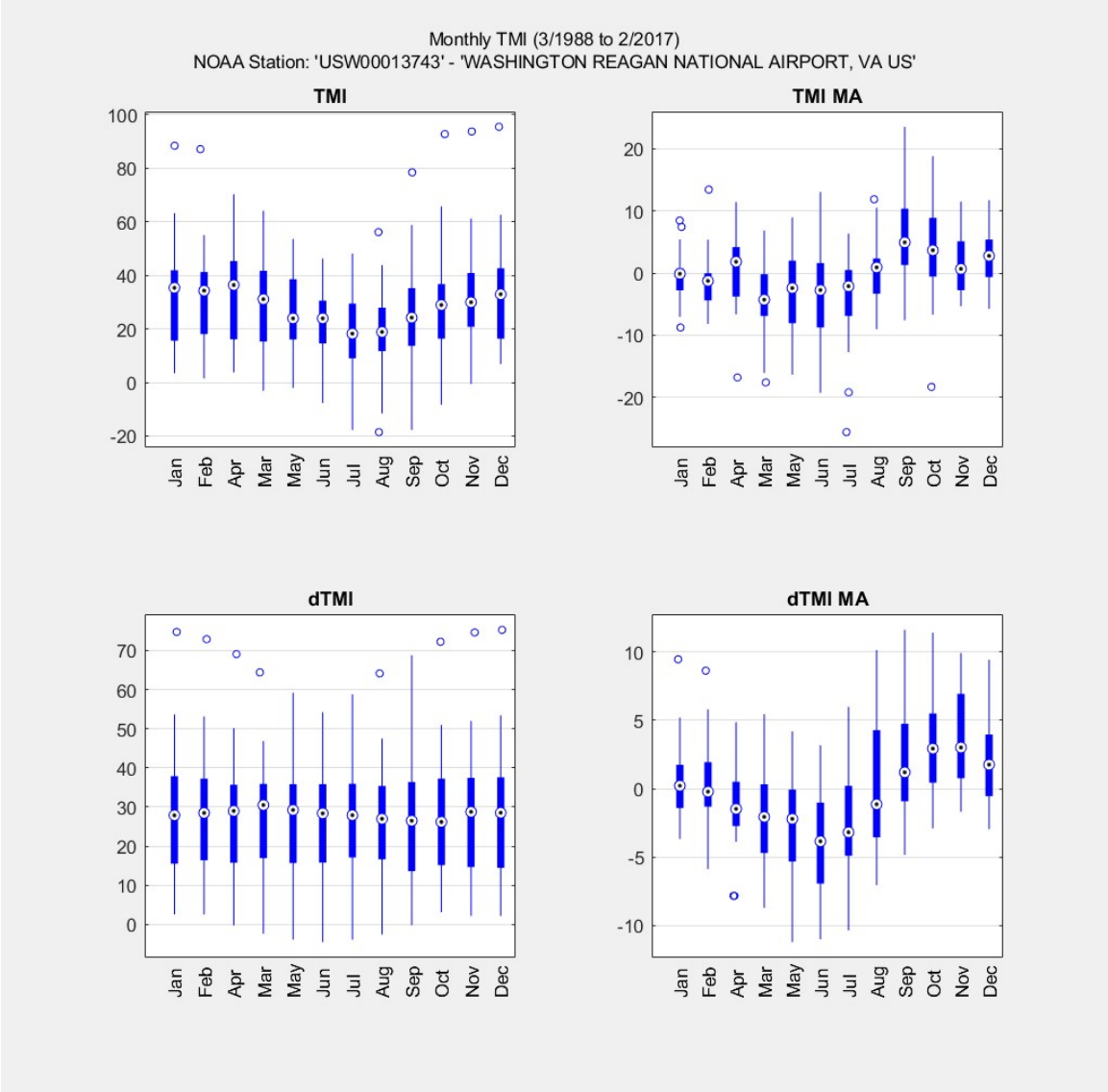

Figure D-5 Box Plots for Monthly Parameterized *TMI* and *dTMI* for Decomposed *TMI* and *dTMI* for NOAA Station USW00013743 from 03/1988 to 03/2022

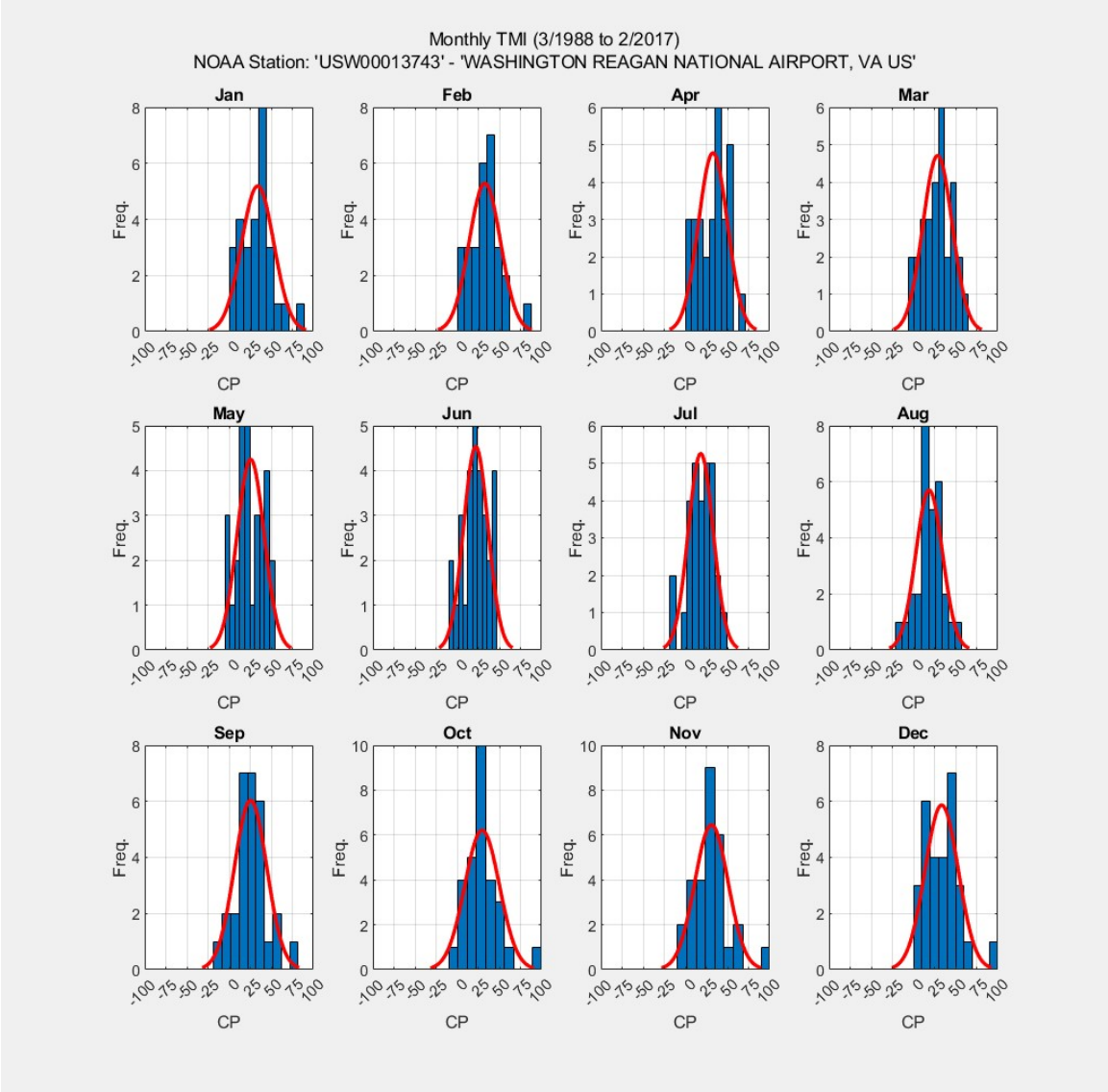

Figure D-6 Histograms for Monthly Parameterized *TMI* for NOAA Station USW00013743 from 03/1988 to 03/2022

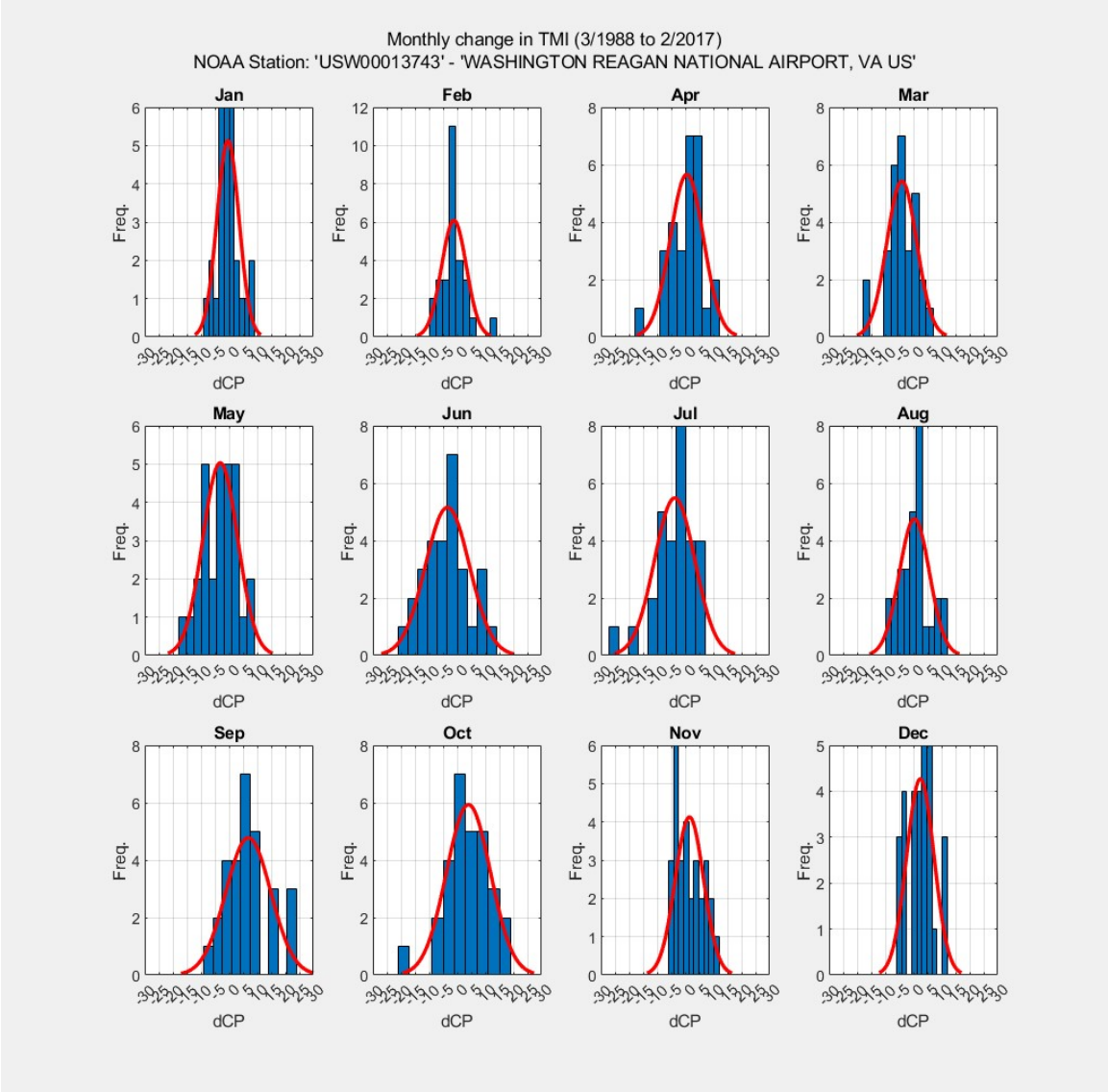

Figure D-7 Histograms for Monthly Parameterized *dTMI* for NOAA Station USW00013743 from 03/1988 to 03/2022

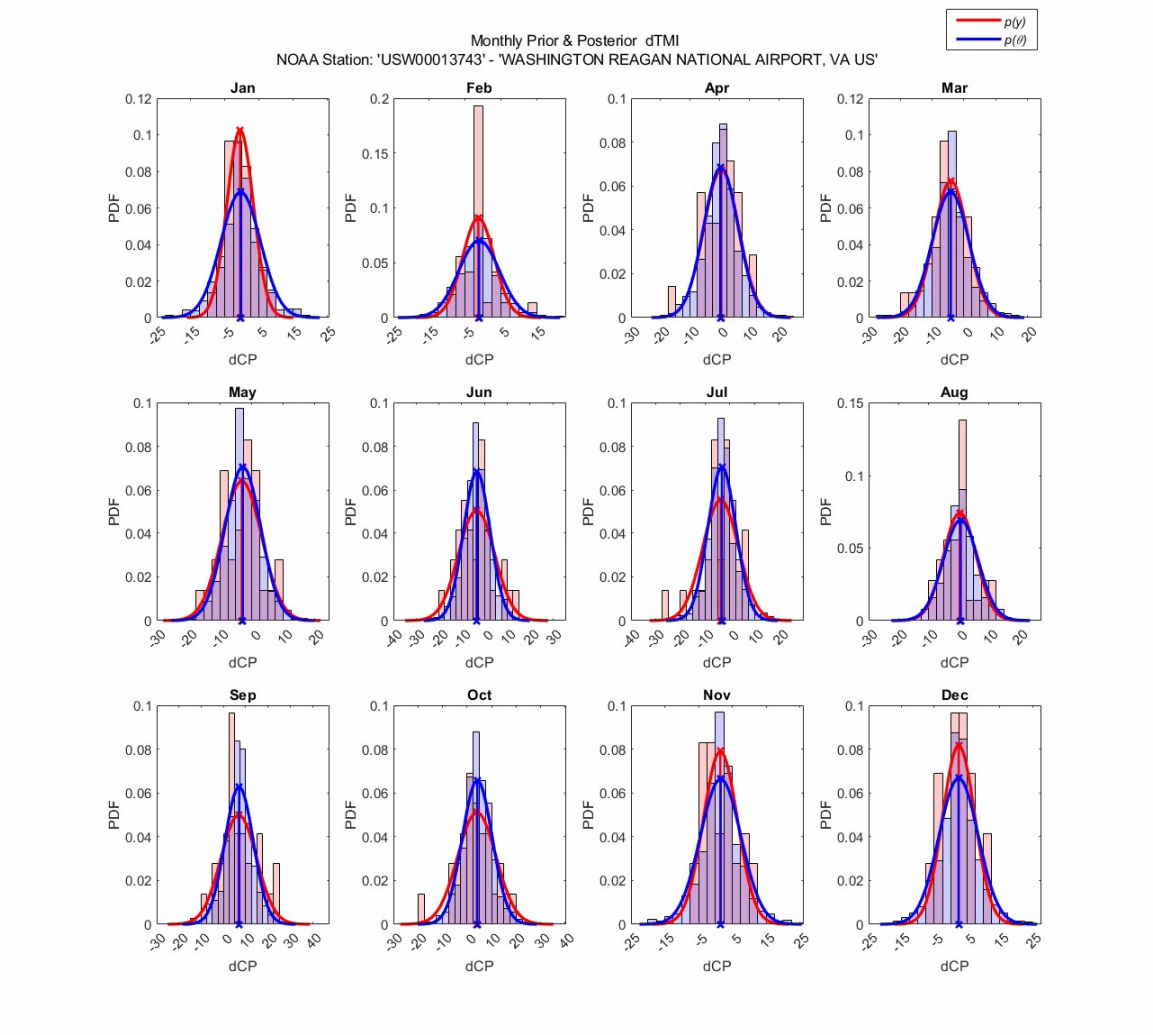

Figure D-8 Histograms of Prior and Posterior (forecasted) *dTMI* for NOAA Station USW00013743 from 03/1988 to 03/2022

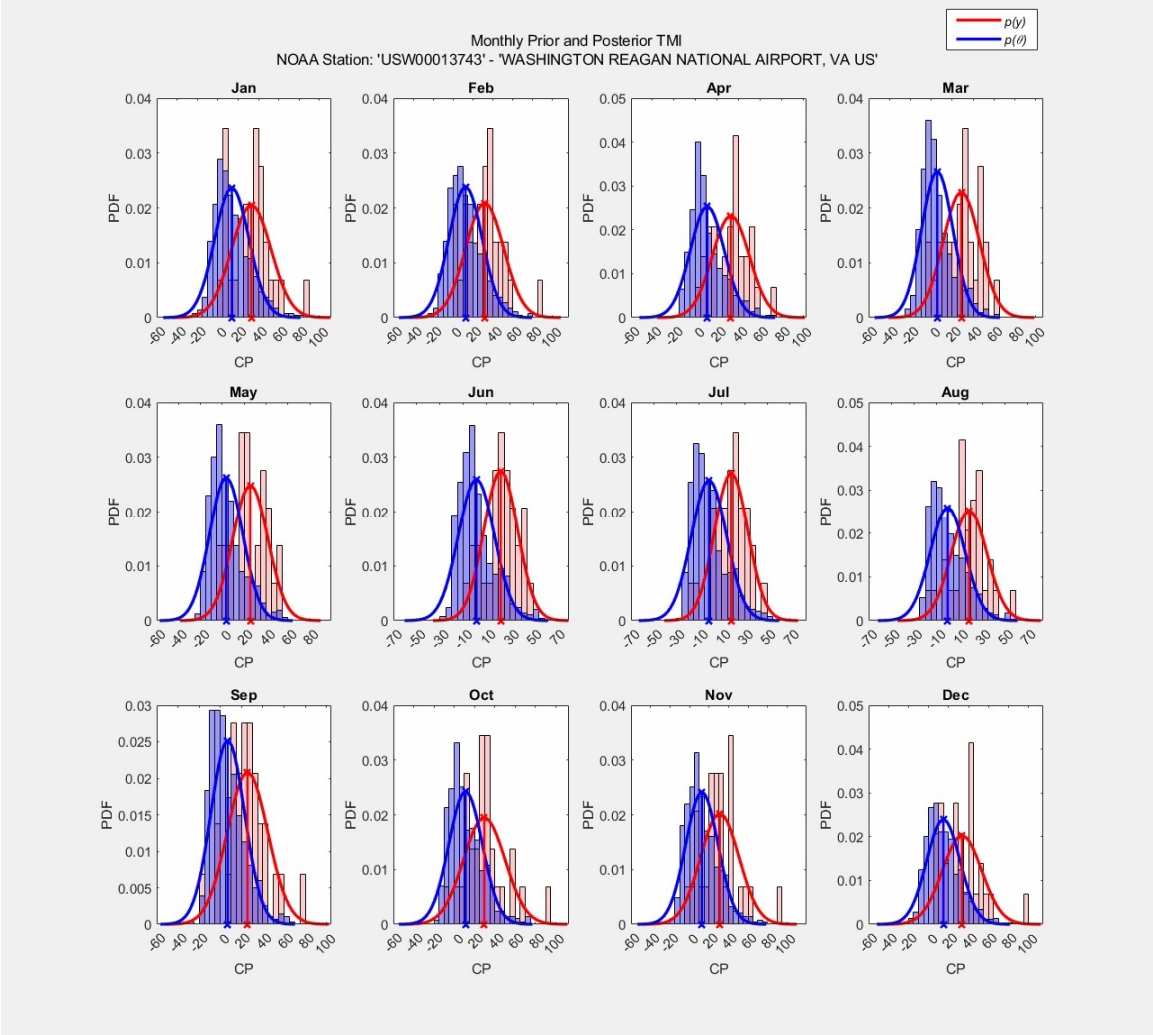

Figure D-9 Histograms of Prior and Posterior (forecasted) *TMI* for NOAA Station USW00013743 from 03/1988 to 03/2022.

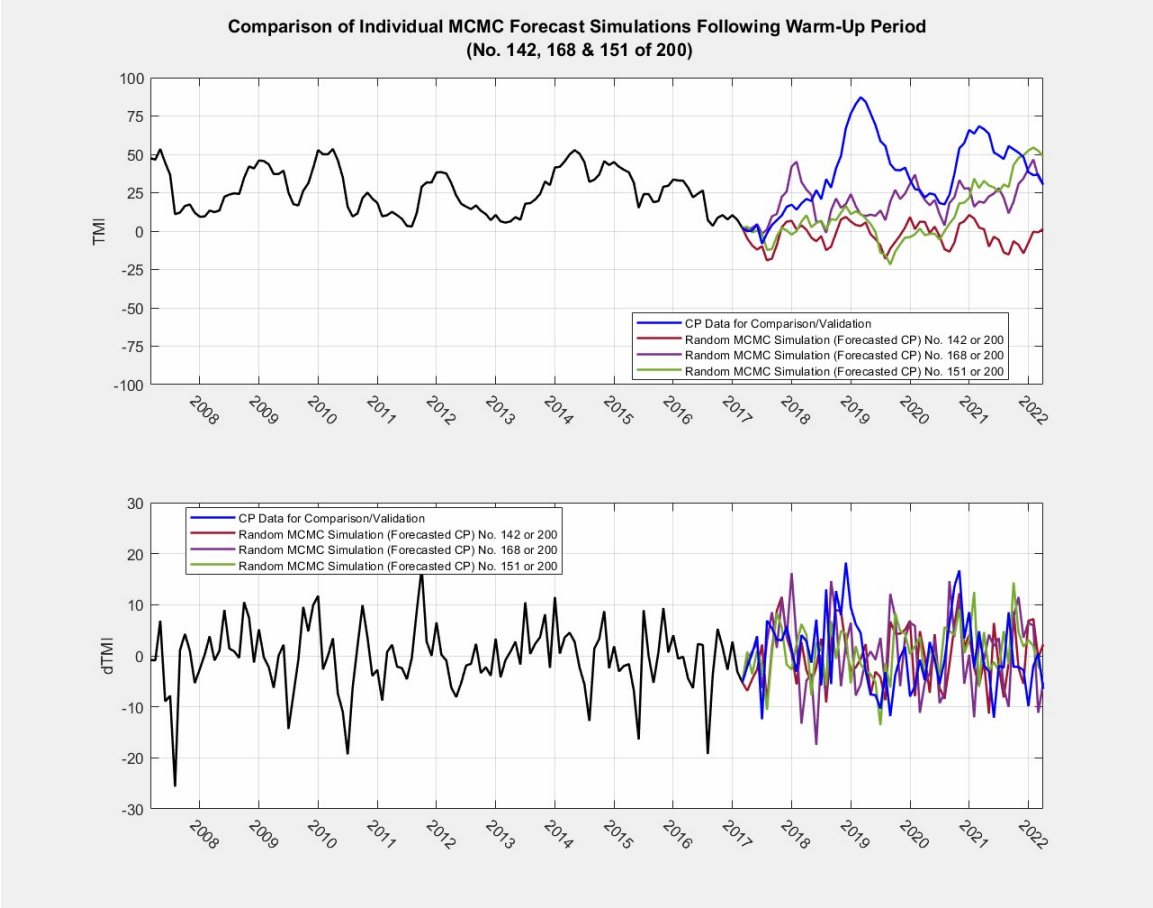

Figure D-10 Example of Single Simulation Results of *dTMI* and *TMI* for NOAA Station USW00013743 from 03/1988 to 03/2022.

CLIMATE MODEL OUTPUT FOR DALLAS, TX FROM 03/2017 TO 03/2022

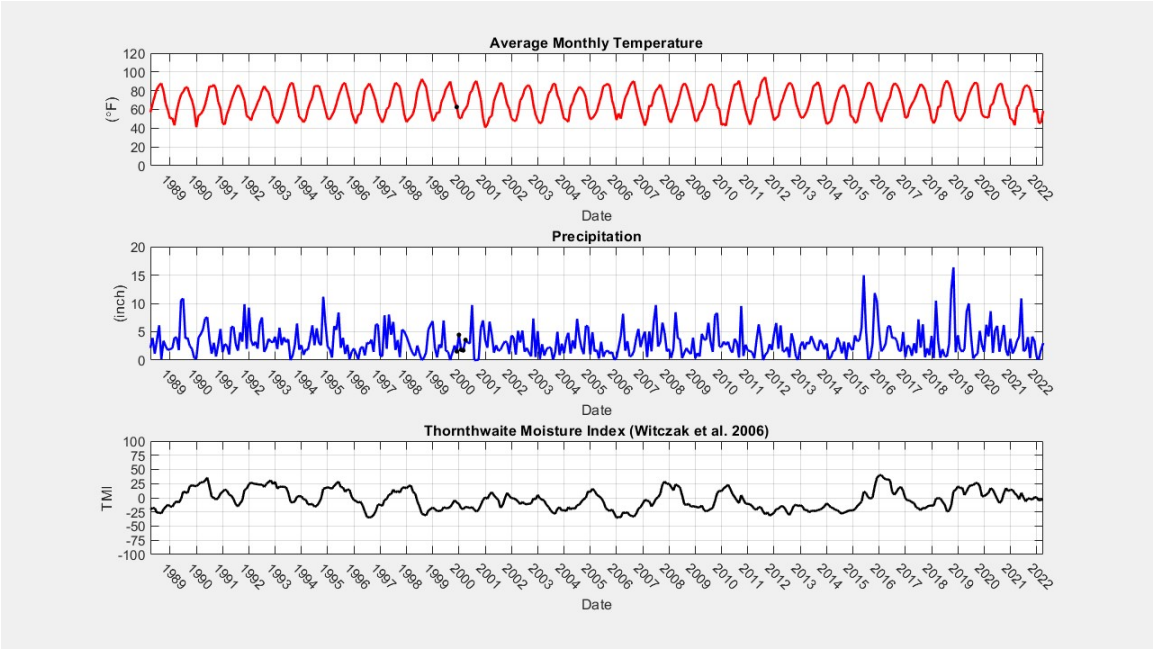

Figure D-11 NOAA Station USW00013960 Climate Data Extract and Calculated TMI from 03/1988 to 03/2022

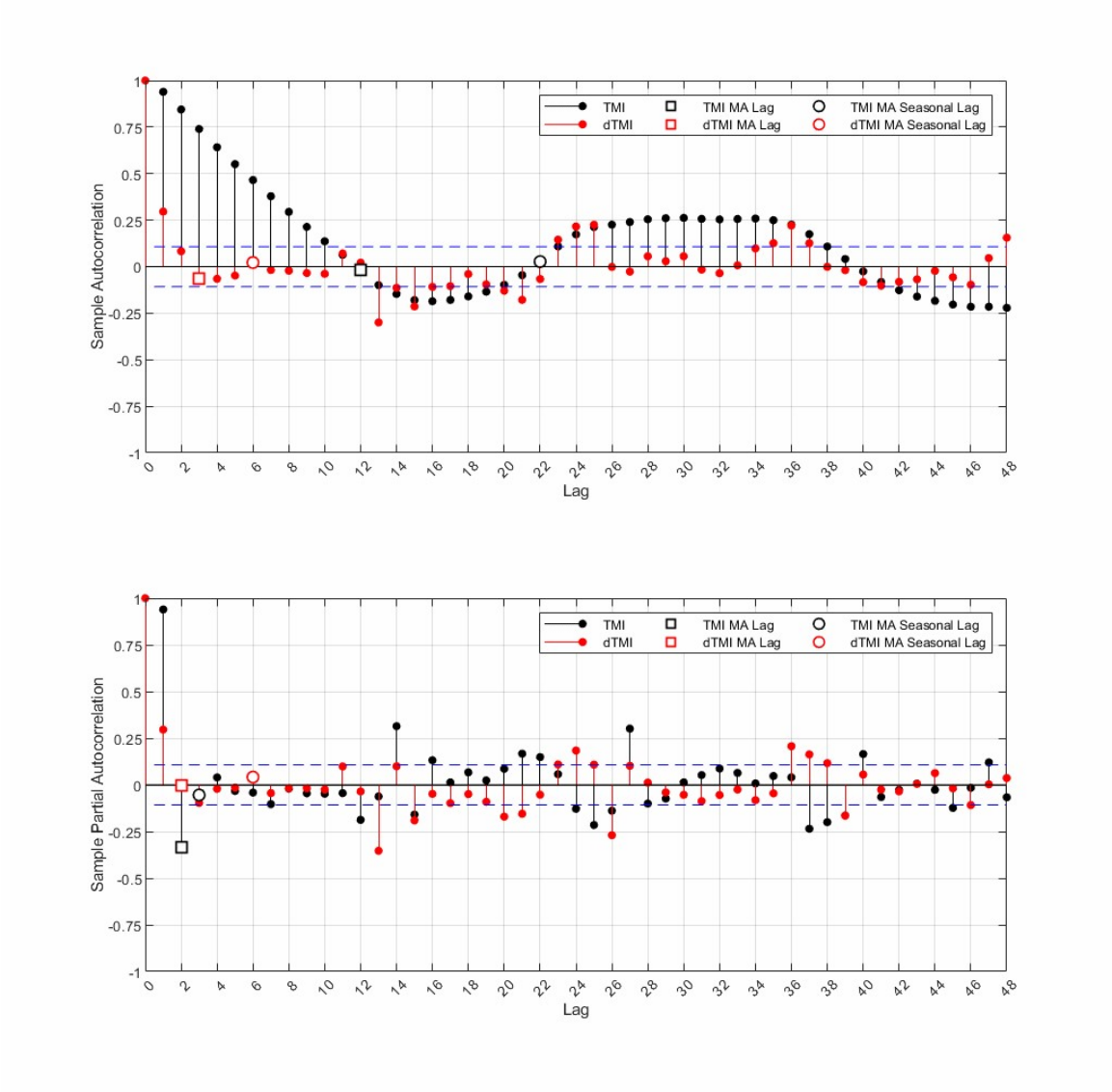

Figure D-12 ACF and PACF for *TMI* and *dTMI* for NOAA Station USW00013960 from 03/1988 to 03/2022

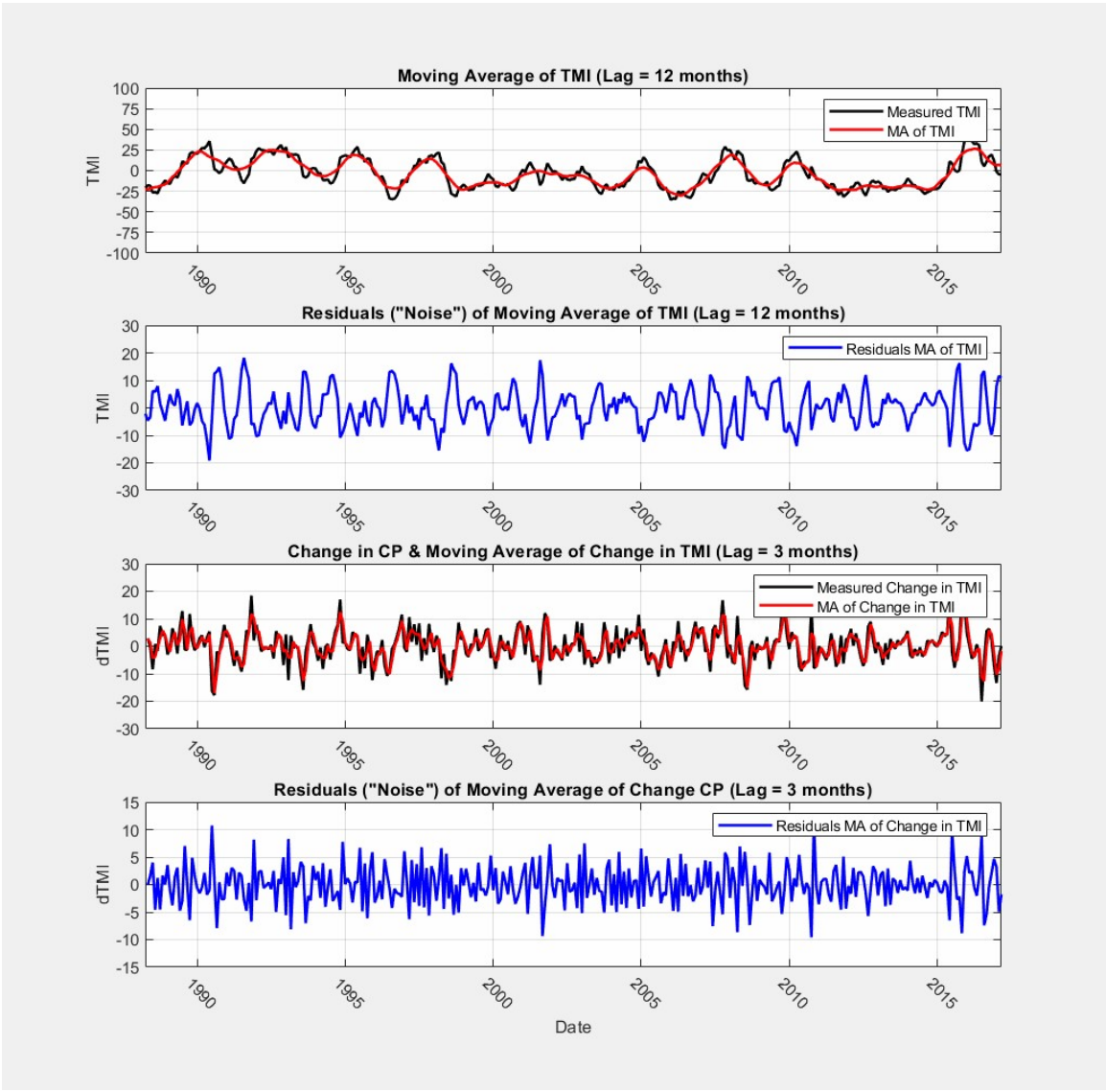

Figure D-13 Time Series Decomposition Using 1st differenced Moving Average for NOAA Station USW00013960 from 03/1988 to 03/2022

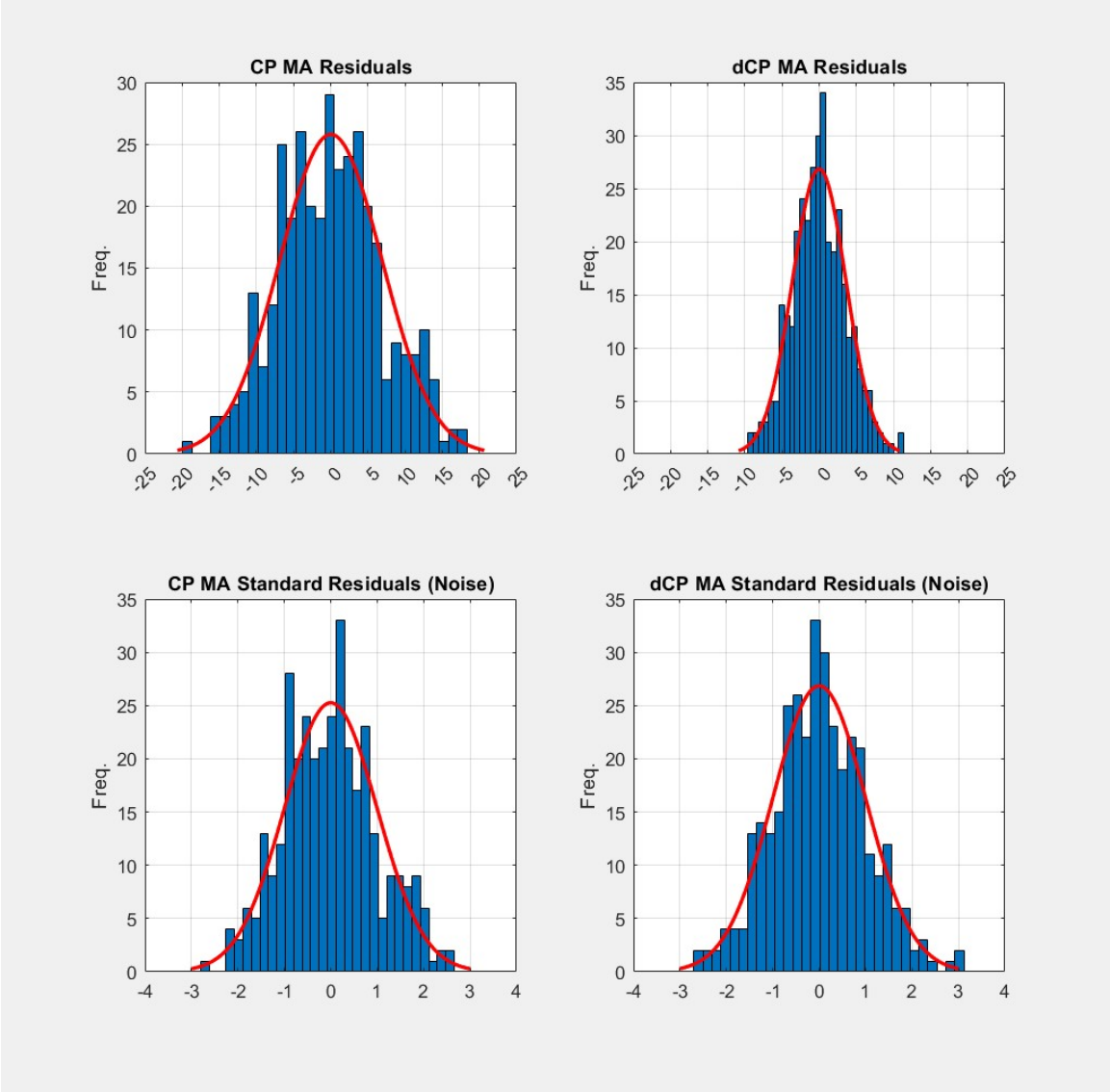

Figure D-14 Histograms for Decomposed *TMI* and *dTMI* for NOAA Station USW00013960 from 03/1988 to 03/2022

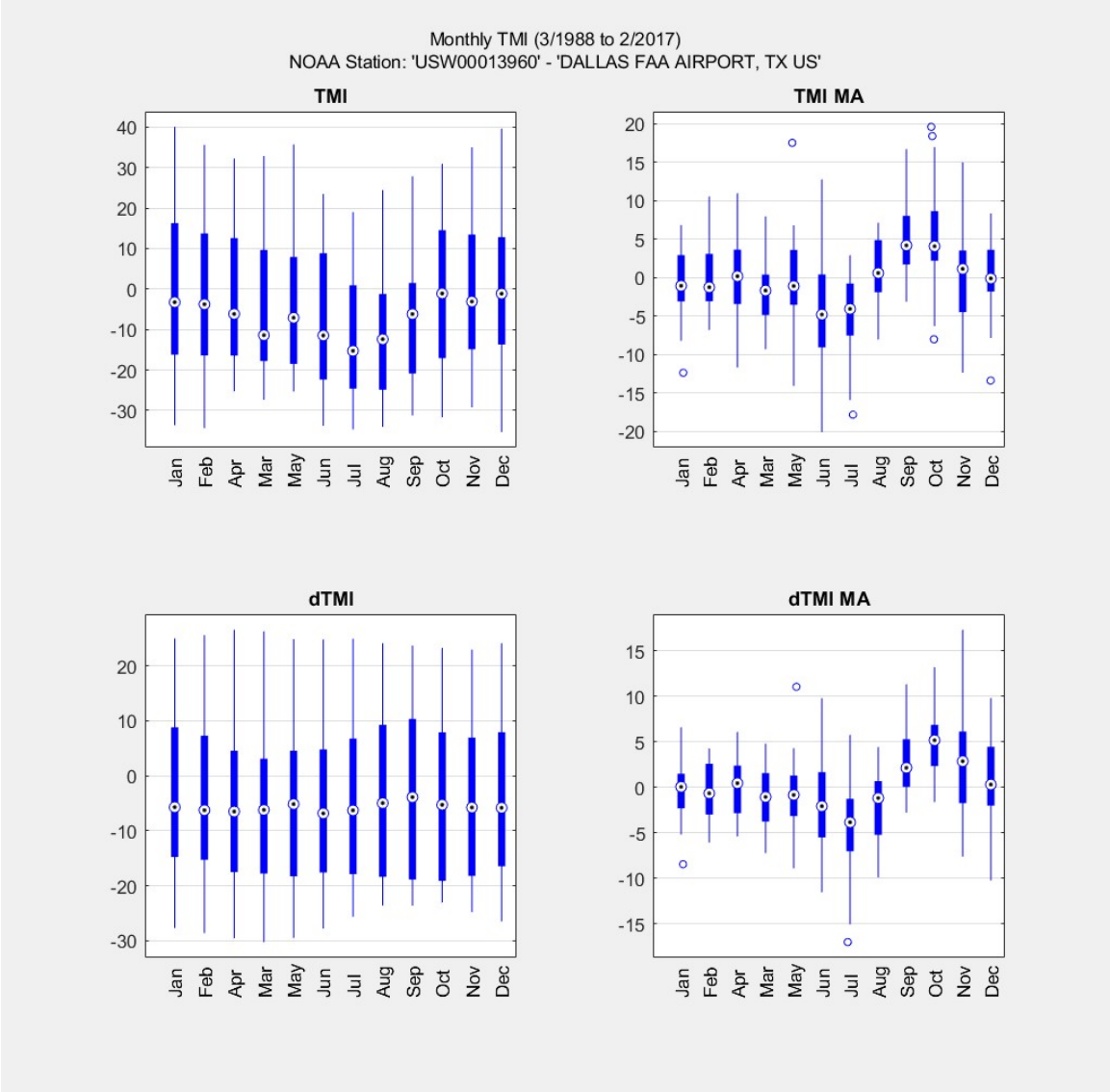

Figure D-15 Box Plots for Monthly Parameterized *TMI* and *dTMI* for Decomposed TMI and dTMI for NOAA Station USW00013960 from 03/1988 to 03/2022

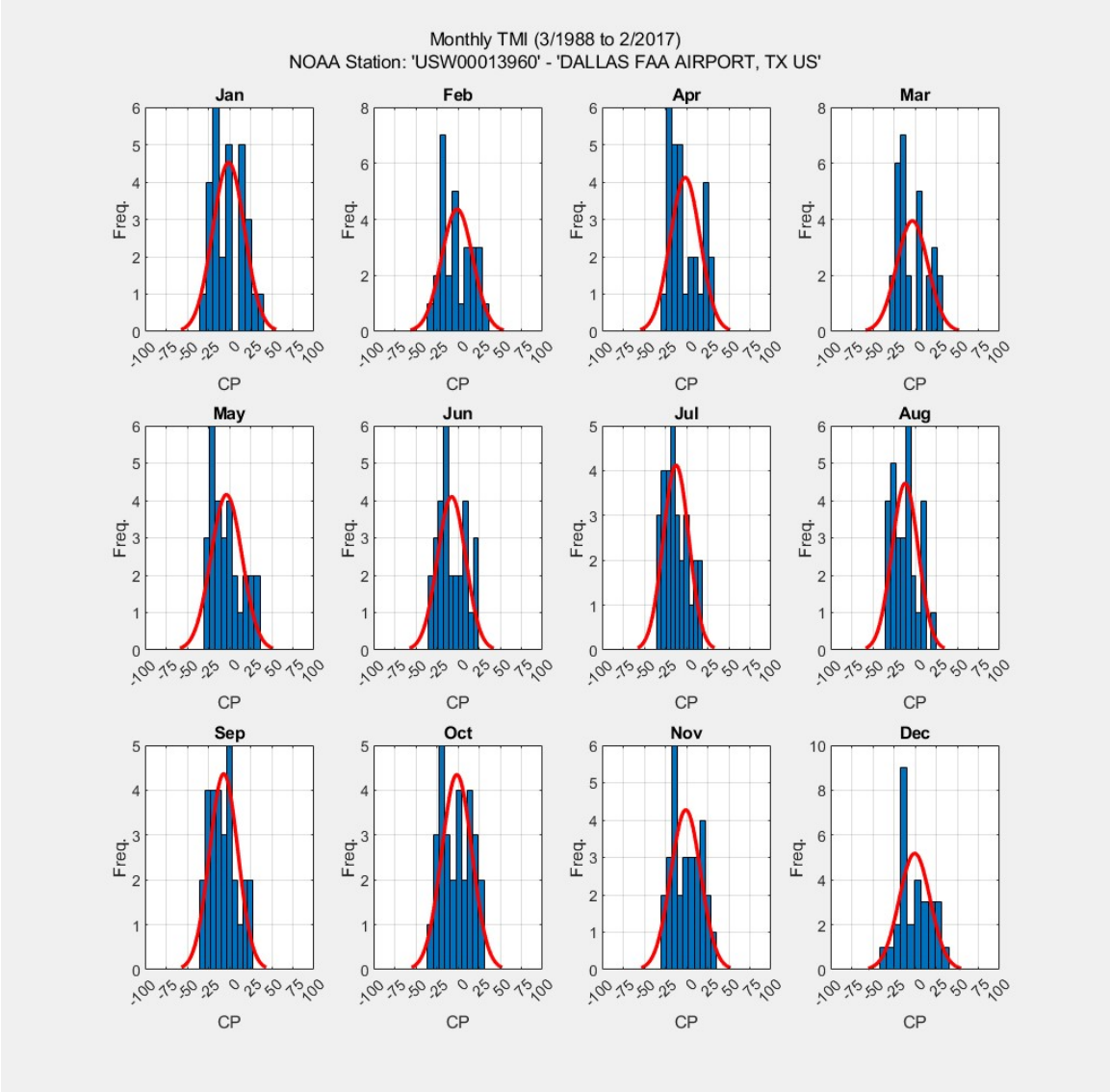

Figure D-16 Histograms for Monthly Parameterized *TMI* for NOAA Station USW00013960 from 03/1988 to 03/2022

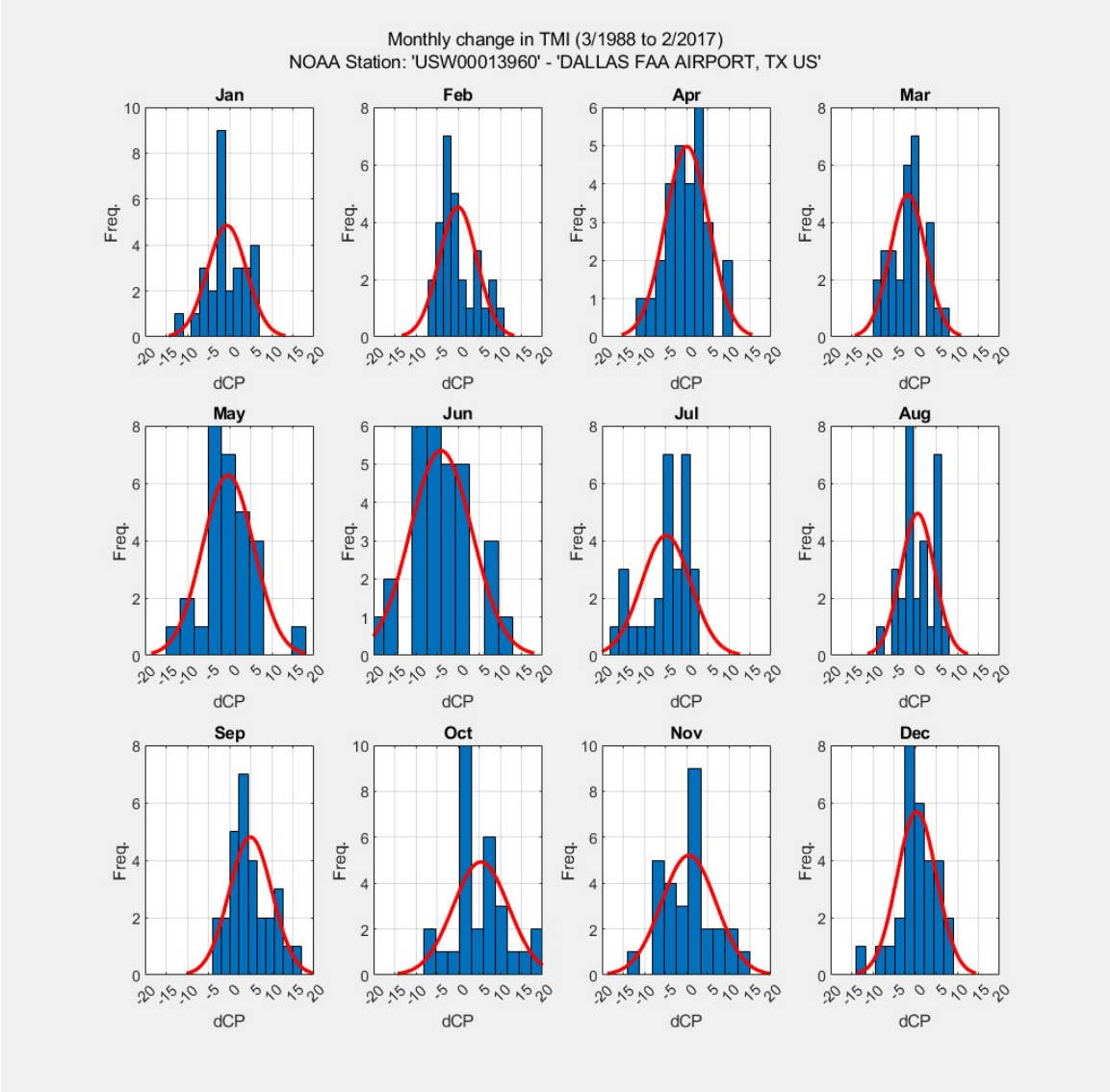

Figure D-17 Histograms for Monthly Parameterized *dTMI* for NOAA Station USW00013960 from 03/1988 to 03/2022

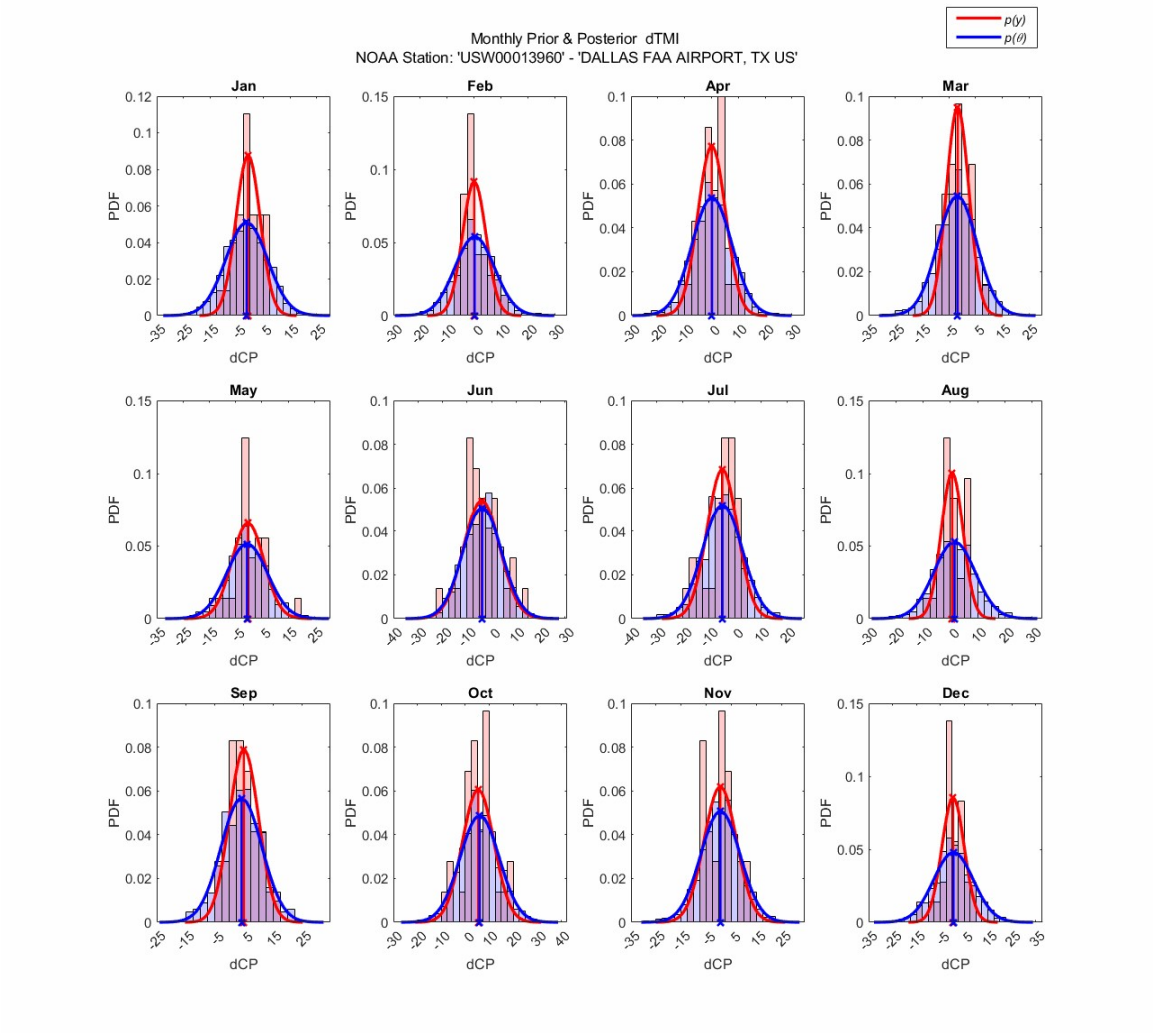

Figure D-18 Histograms of Prior and Posterior (forecasted) *dTMI* for NOAA Station USW00013960 from 03/1988 to 03/2022

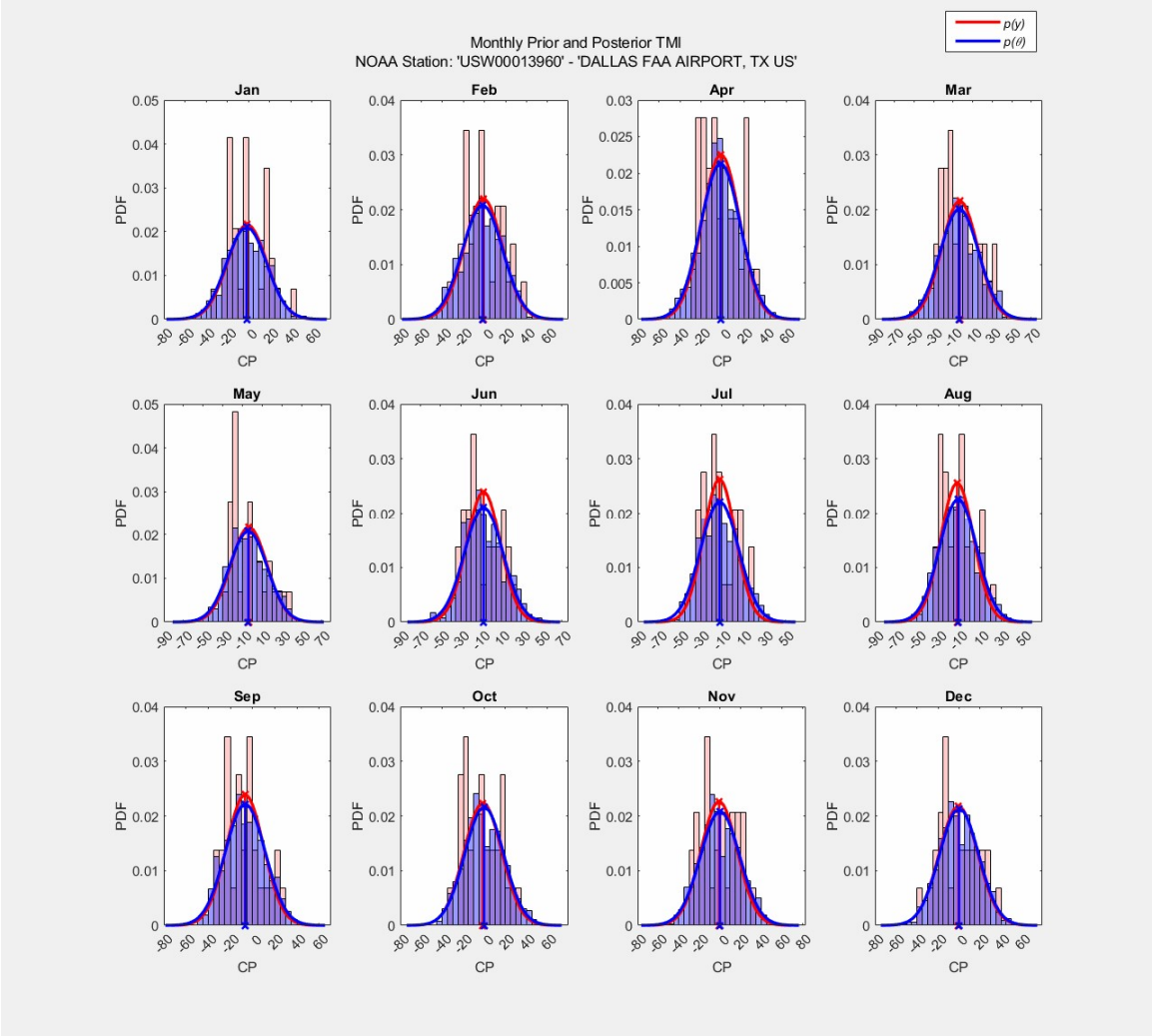

Figure D-19 Histograms of Prior and Posterior (forecasted) *TMI* for NOAA Station USW00013960 from 03/1988 to 03/2022.

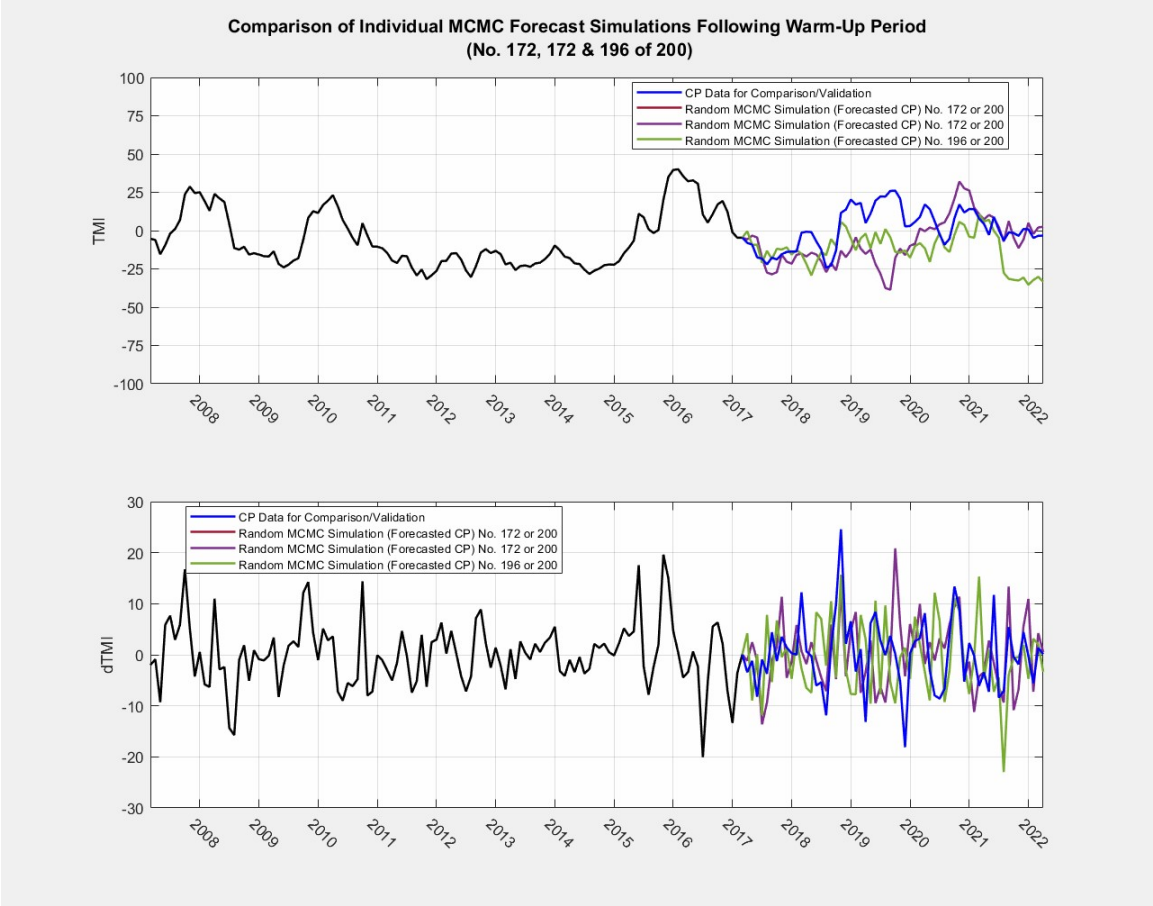

Figure D-20 Example of Single Simulation Results of *dTMI* and *TMI* for NOAA Station USW00013960 from 03/1988 to 03/2022.

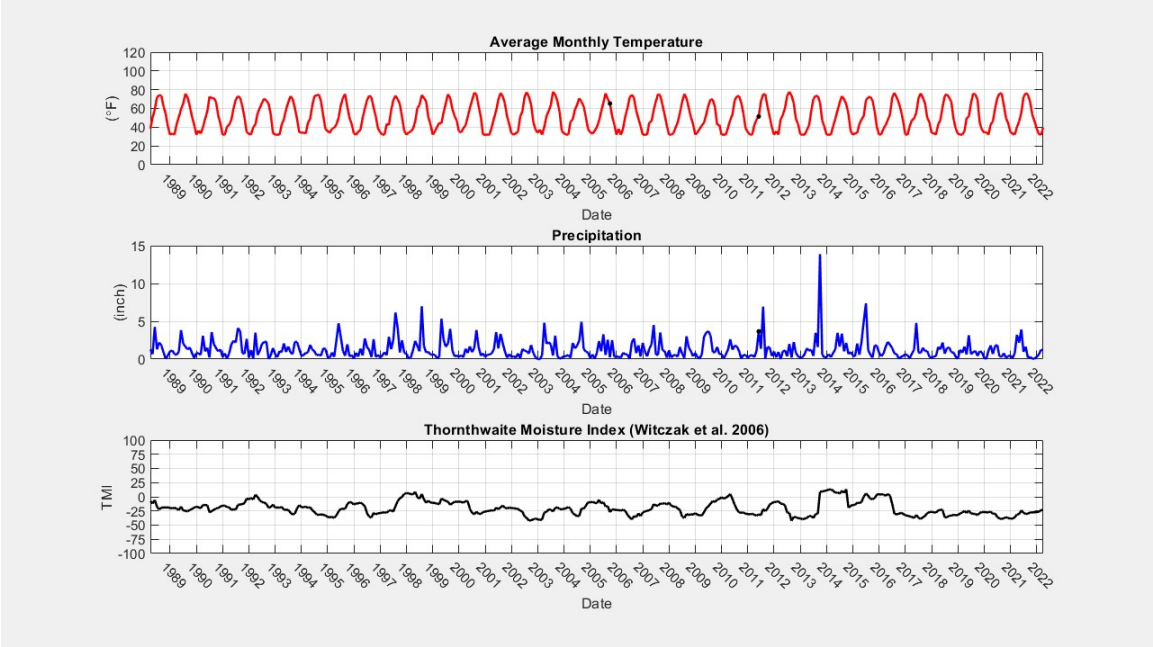

Figure D-21 NOAA Station USW00023062 Climate Data Extract and Calculated *TMI* from 03/1988 to 03/2022

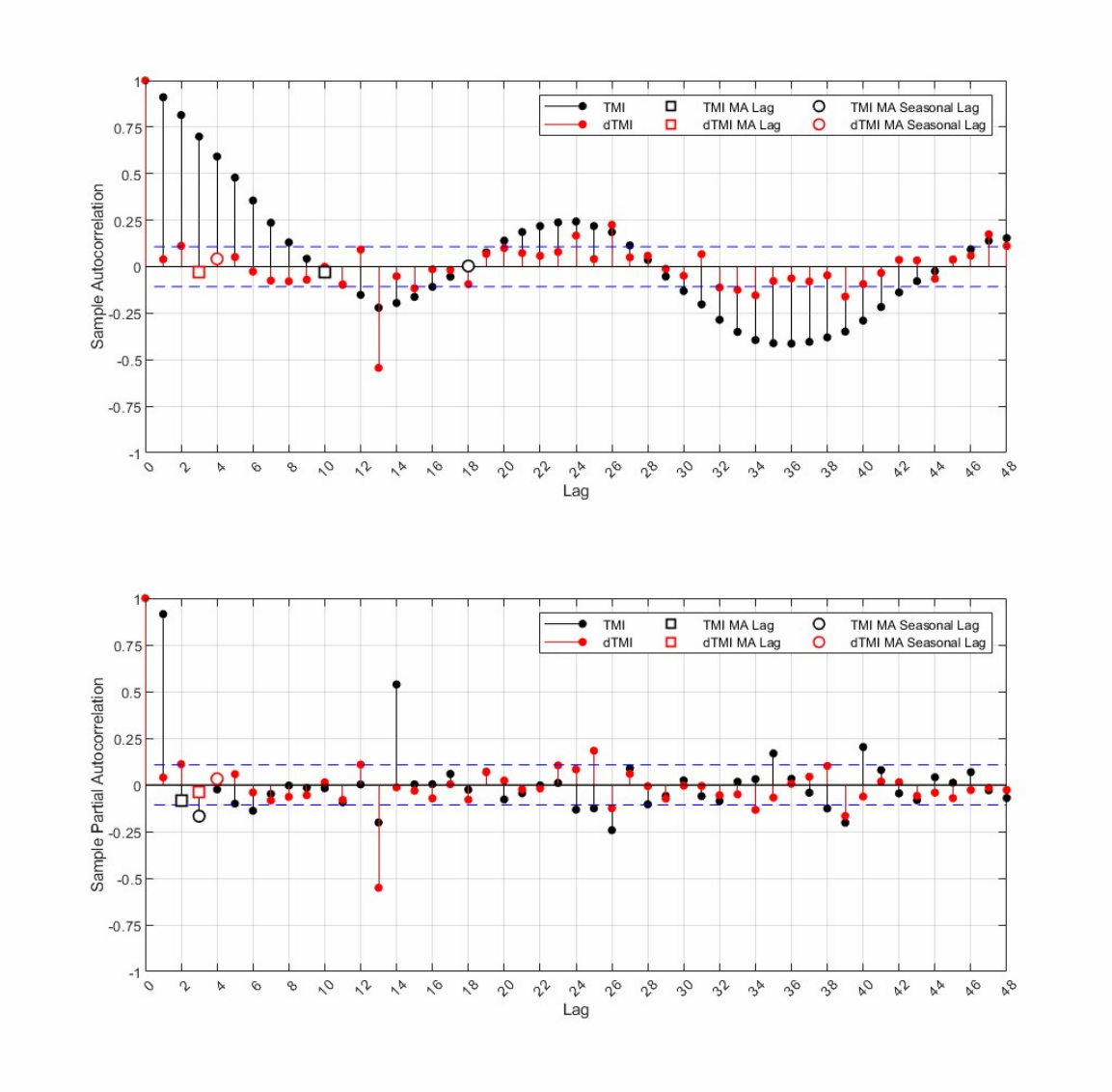

Figure D-22 ACF and PACF for *TMI* and *dTMI* for NOAA Station USW00023062 from 03/1988 to 03/2022

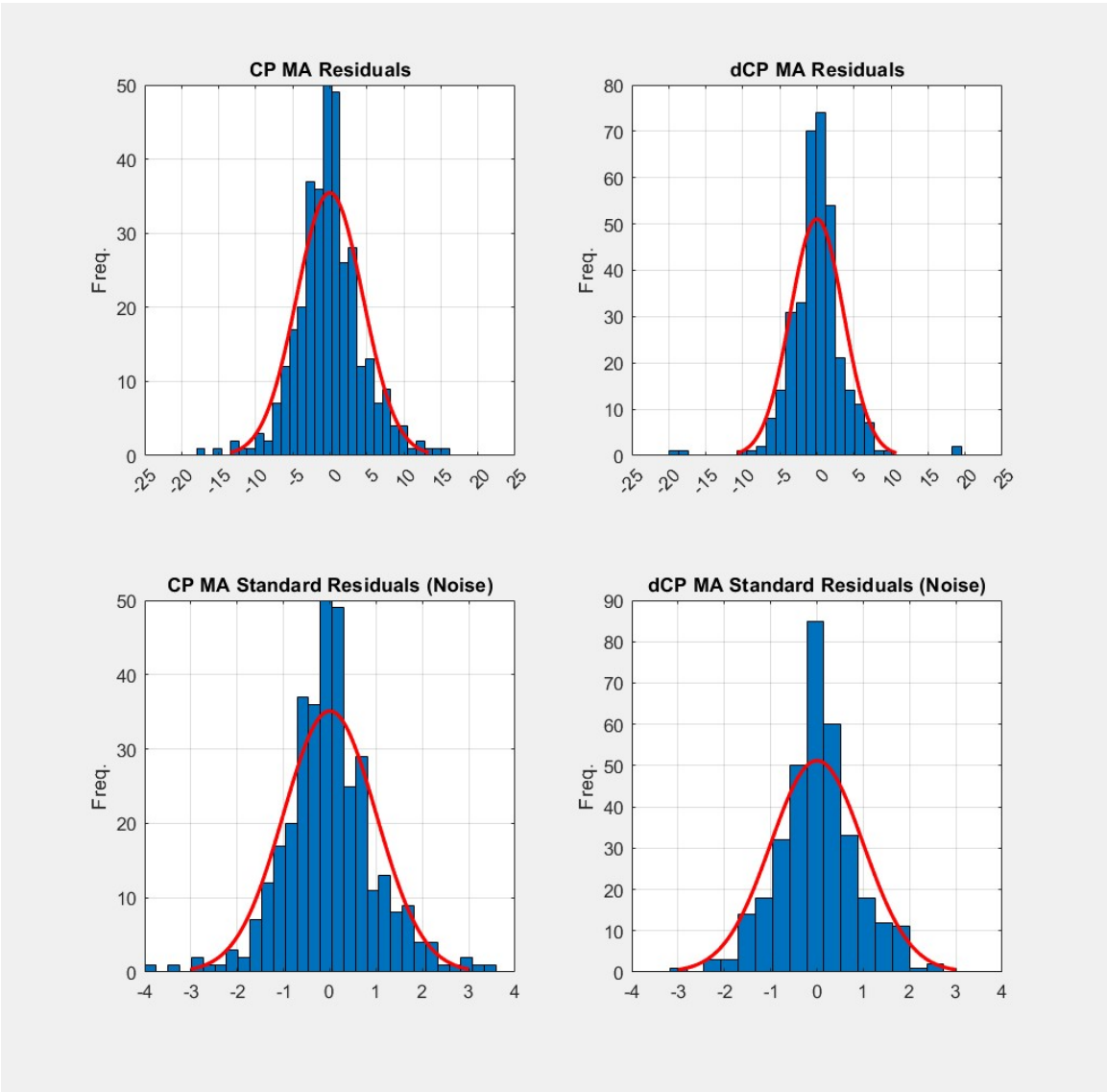

Figure D-23 Histograms for Decomposed *TMI* and *dTMI* for NOAA Station USW00023062 from 03/1988 to 03/2022

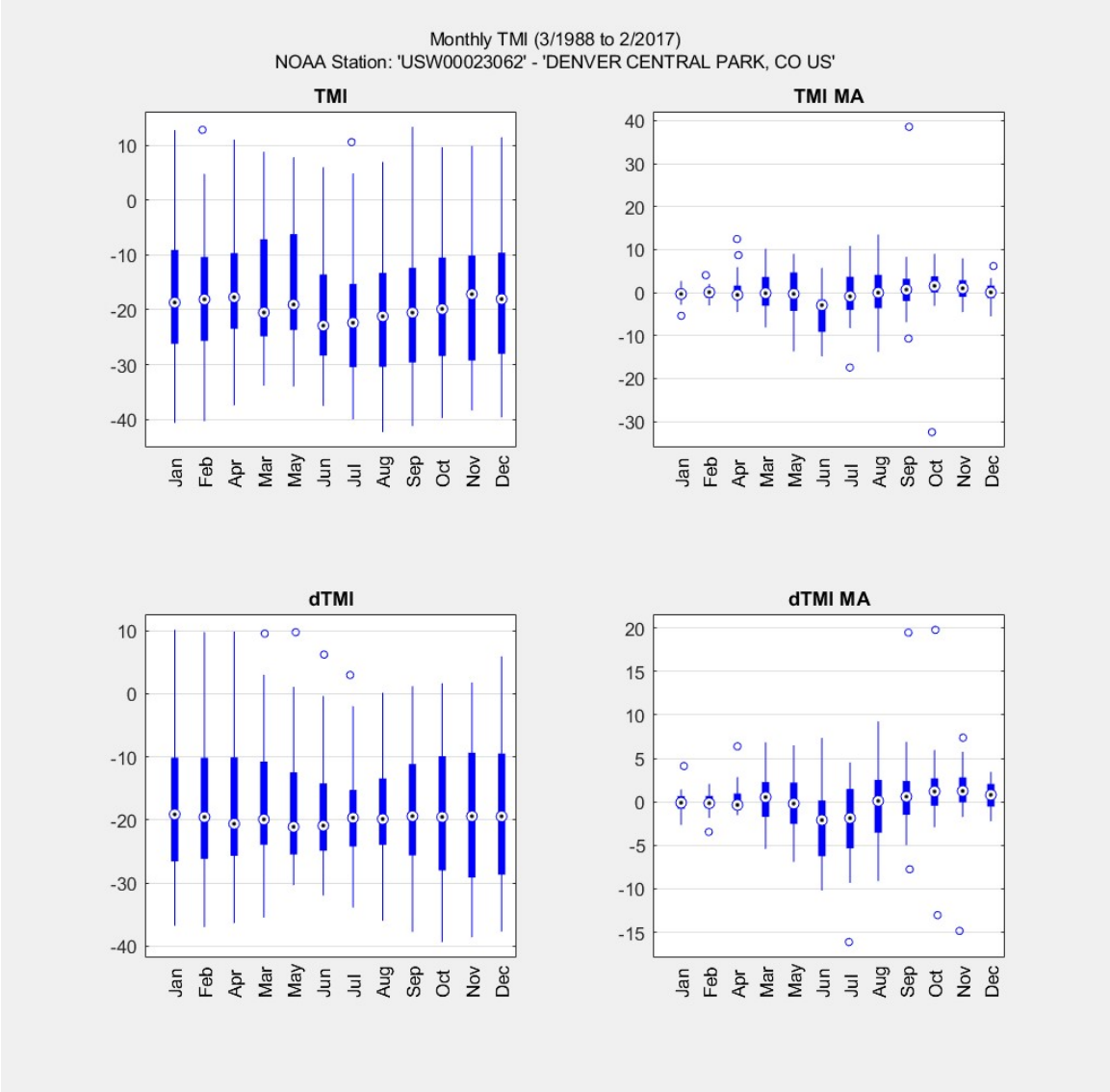

Figure D-24 Box Plots for Monthly Parameterized *TMI* and *dTMI* for Decomposed TMI and dTMI for NOAA Station USW00023062 from 03/1988 to 03/2022

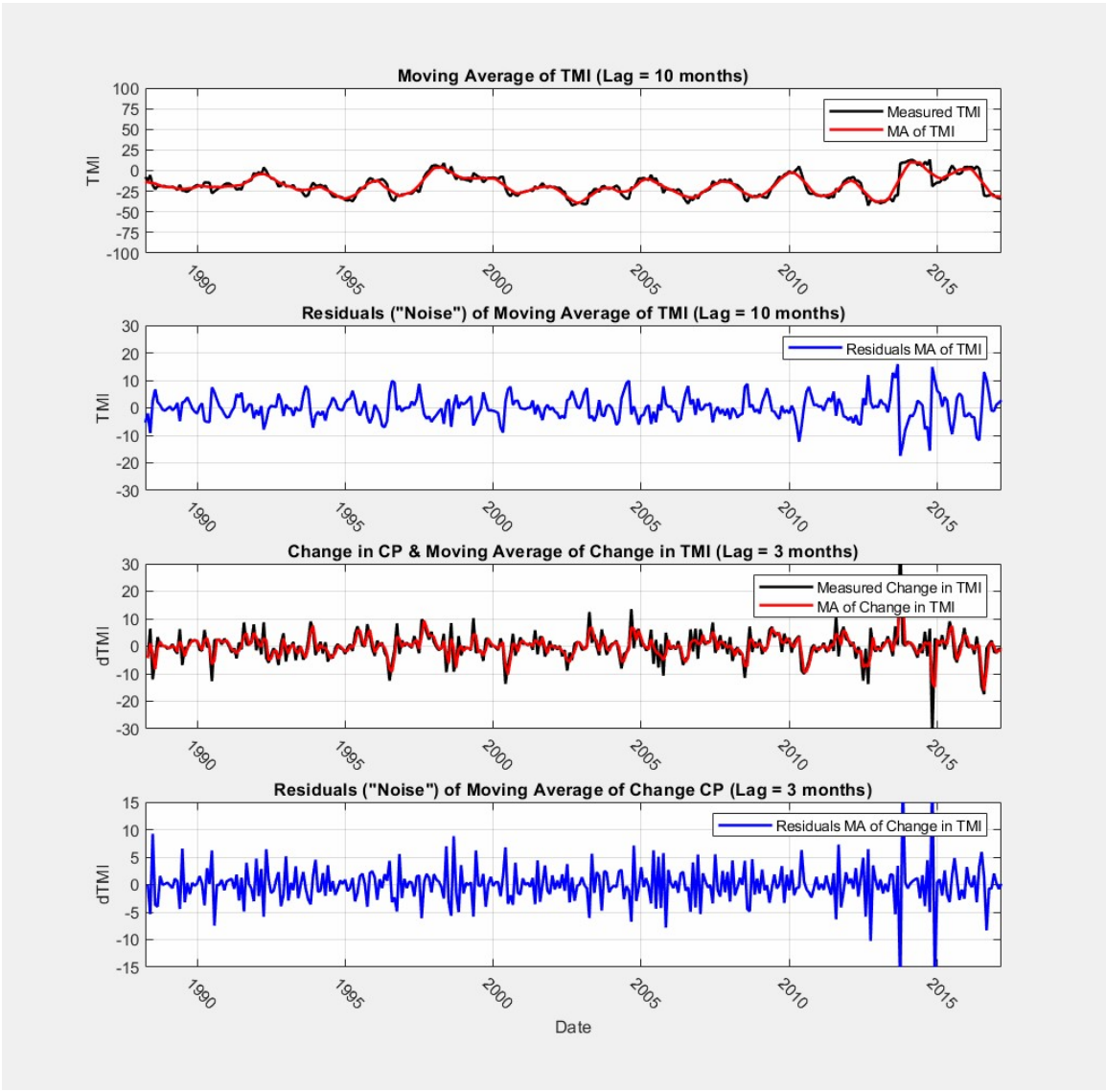

Figure D-25 Time Series Decomposition Using 1st differenced Moving Average for NOAA Station USW00023062 from 03/1988 to 03/2022

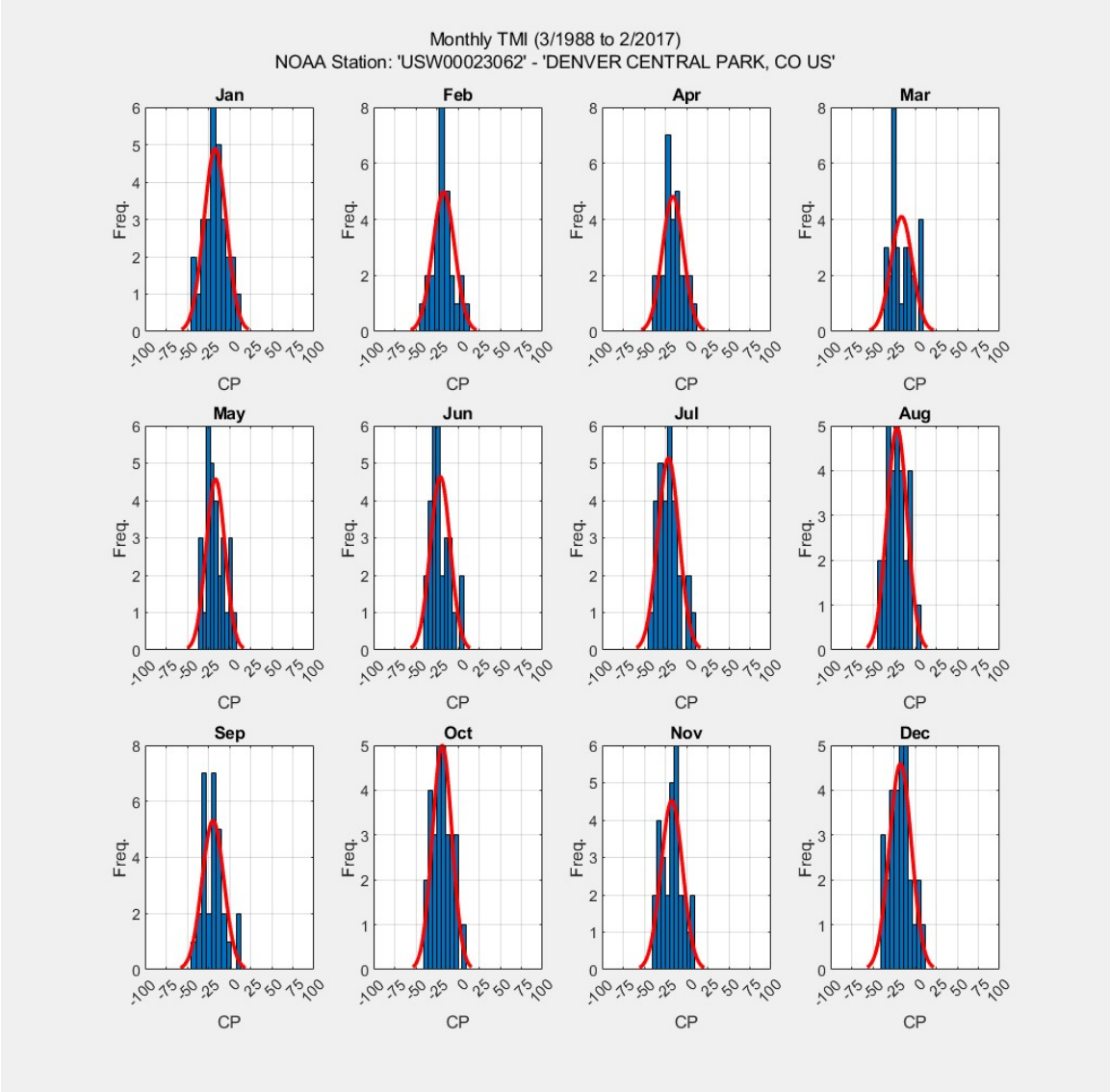

Figure D-26 Histograms for Monthly Parameterized *TMI* for NOAA Station USW00023062 from 03/1988 to 03/2022

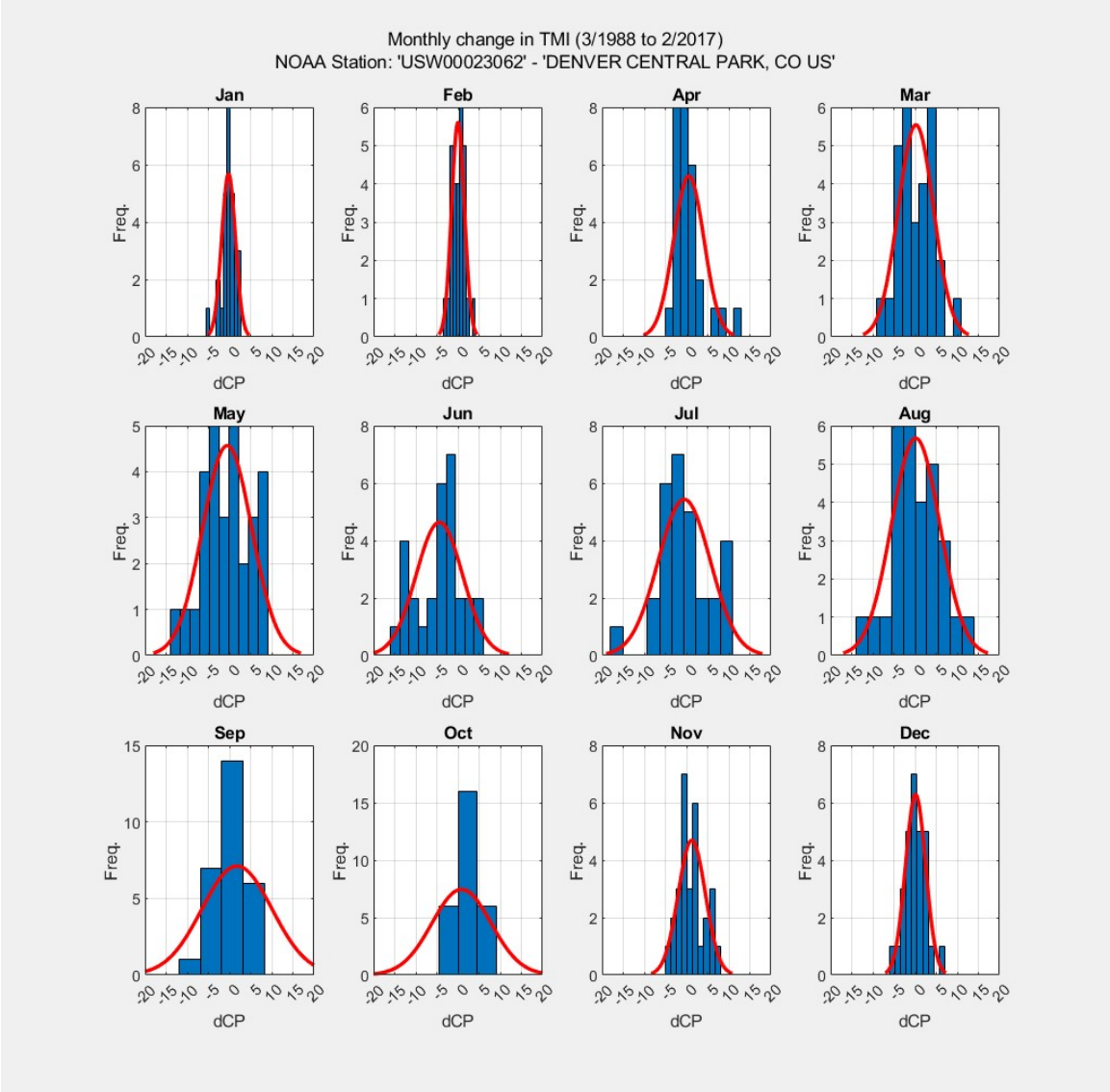

Figure D-27 Histograms for Monthly Parameterized *dTMI* for NOAA Station USW00023062 from 03/1988 to 03/2022

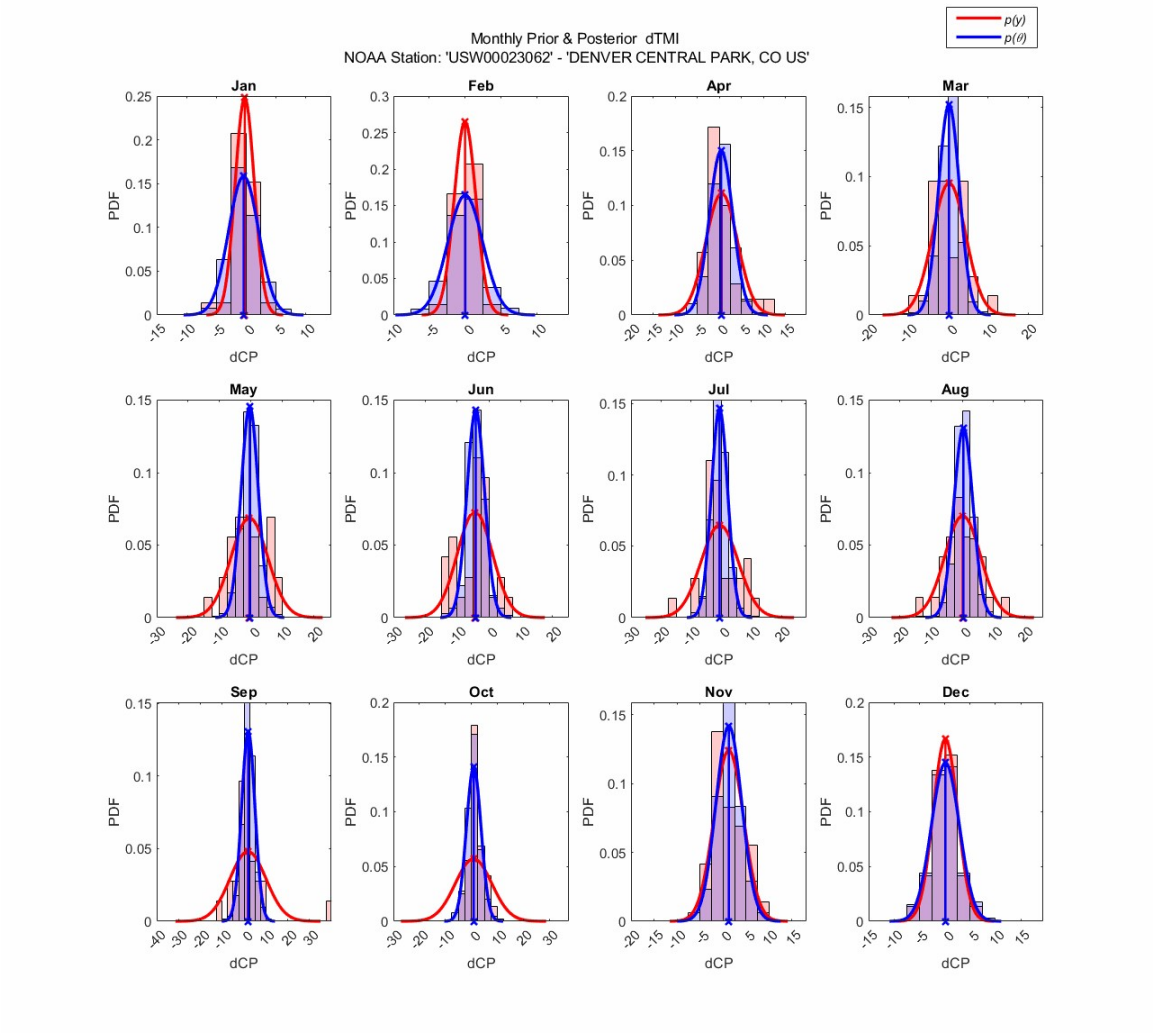

Figure D-28 Histograms of Prior and Posterior (forecasted) *dTMI* for NOAA Station USW00023062 from 03/1988 to 03/2022.

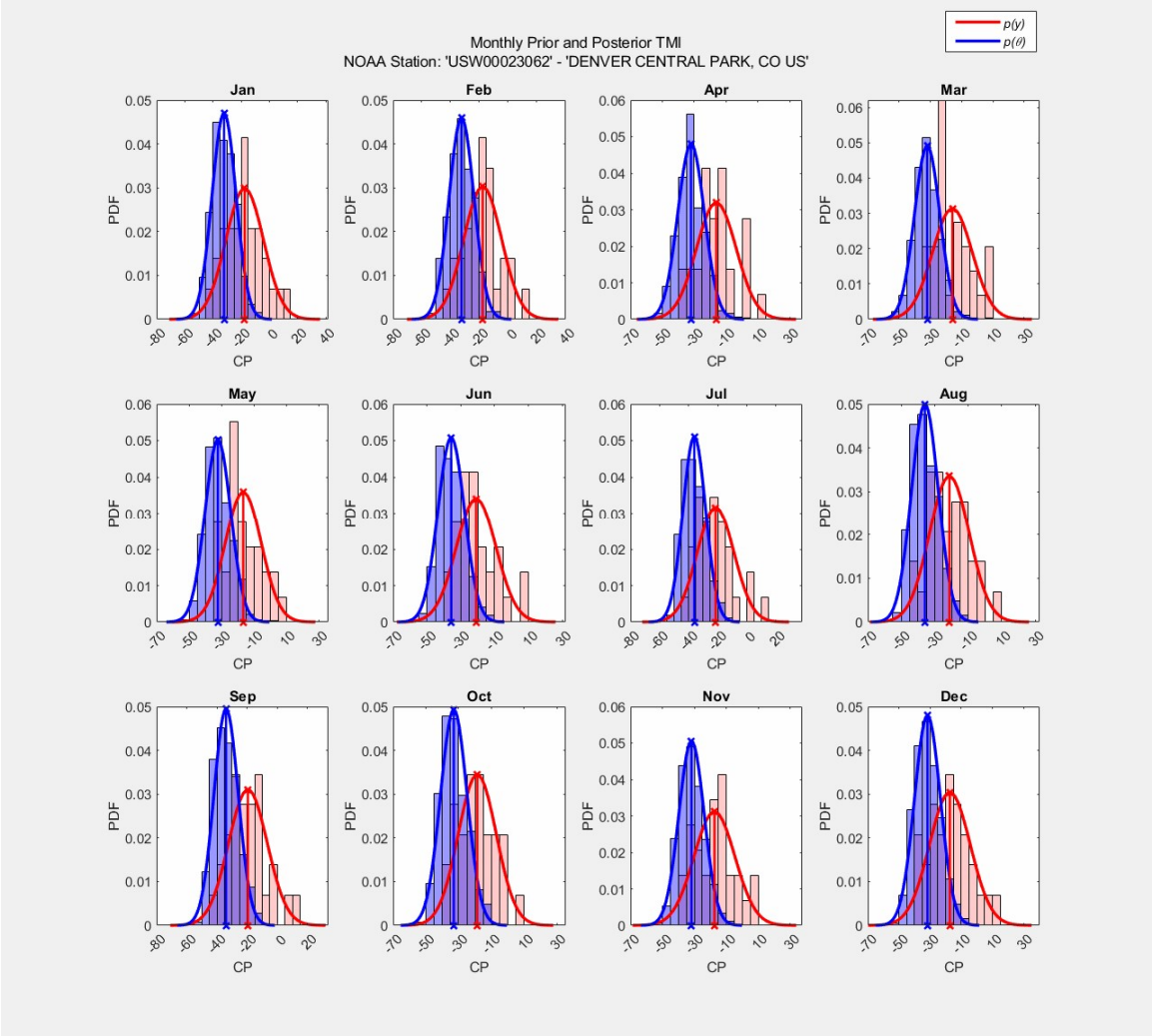

Figure D-29 Histograms of Prior and Posterior (forecasted) *TMI* for NOAA Station USW00023062 from 03/1988 to 03/2022

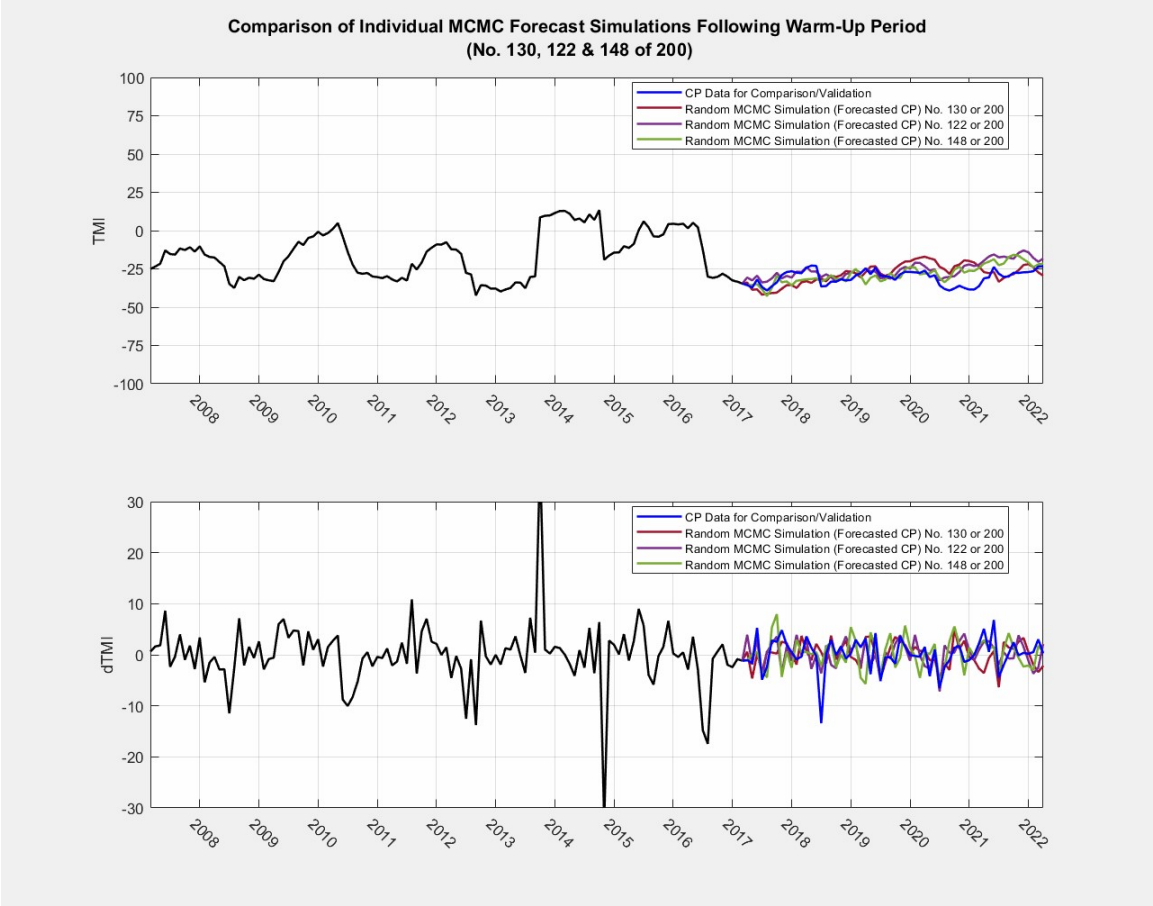

Figure D-30 Example of Single Simulation Results of *dTMI* and *TMI* for NOAA Station USW00023062 from 03/1988 to 03/2022.

CLIMATE MODEL OUTPUT FOR SALT LAKE CITY, UT FROM 03/2017 TO 03/2022

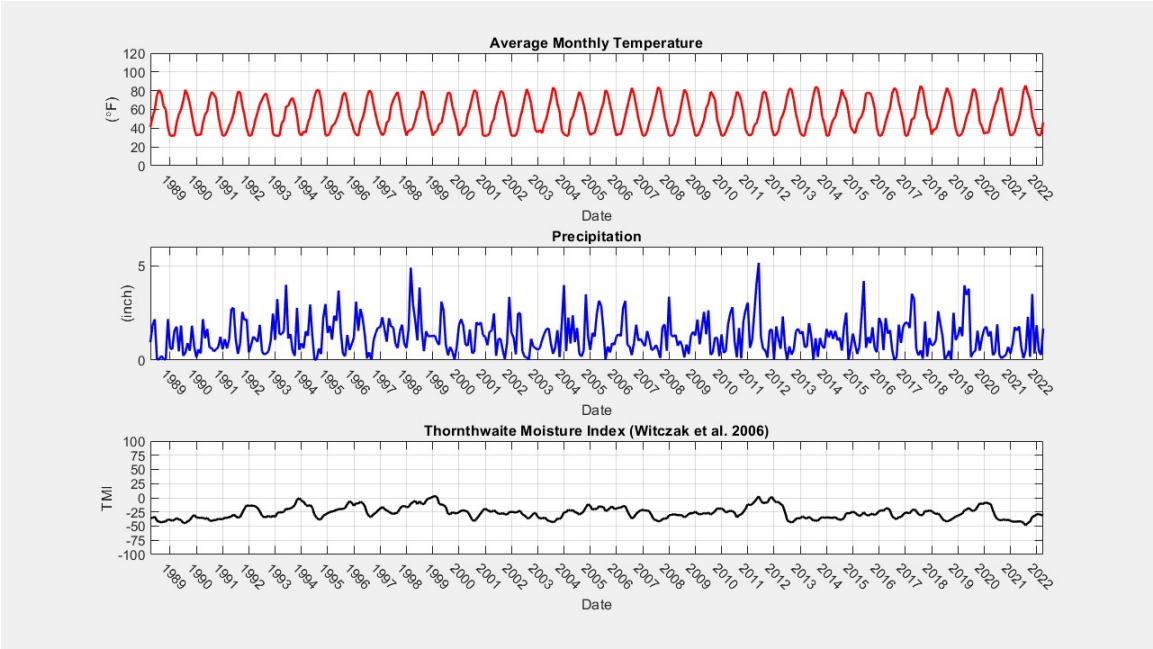

Figure D-31 NOAA Station USW00024127 Climate Data Extract and Calculated TMI from 03/1988 to 03/2022

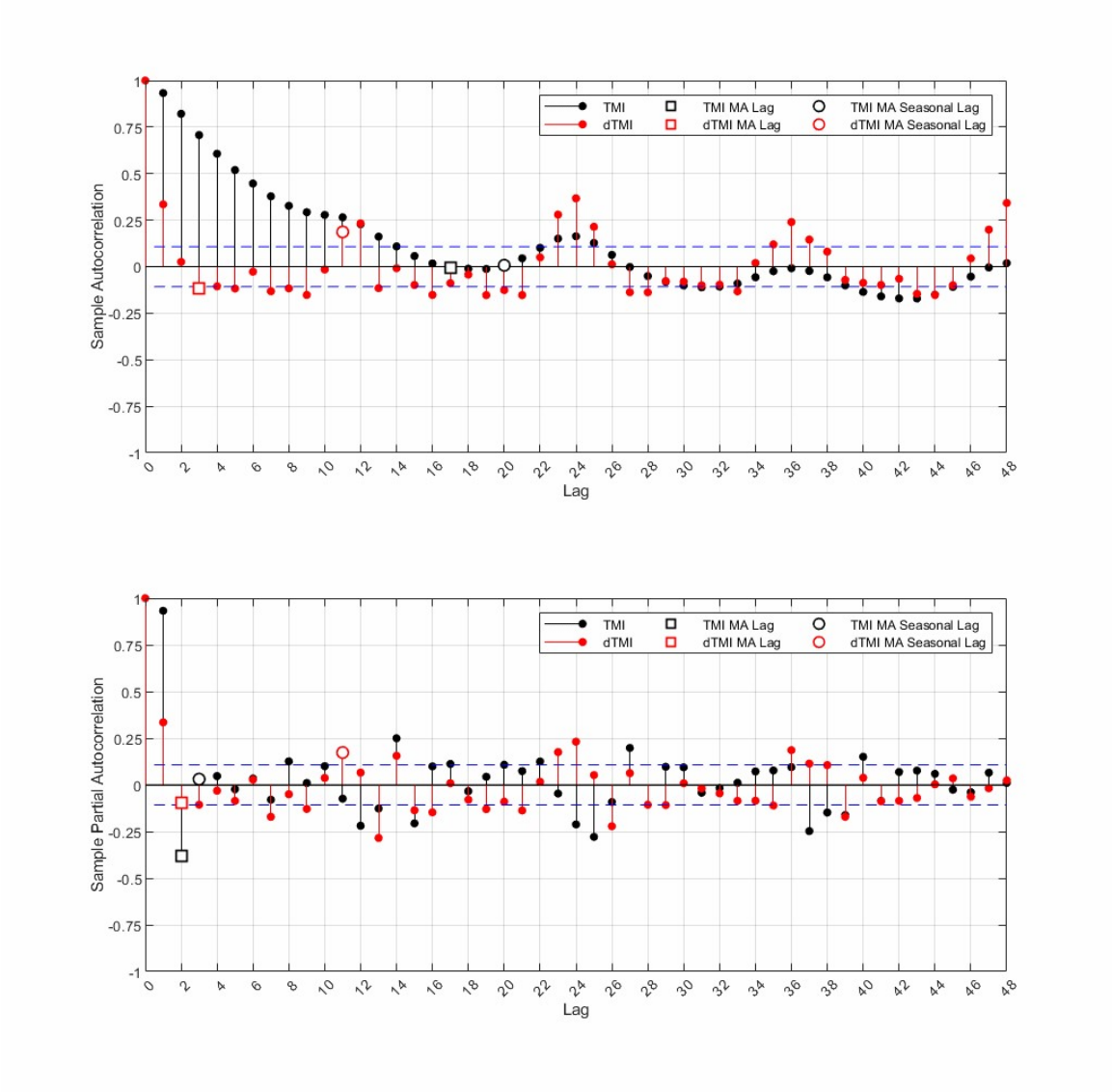

Figure D-32 ACF and PACF for *TMI* and *dTMI* for NOAA Station USW00024127 from 03/1988 to 03/2022

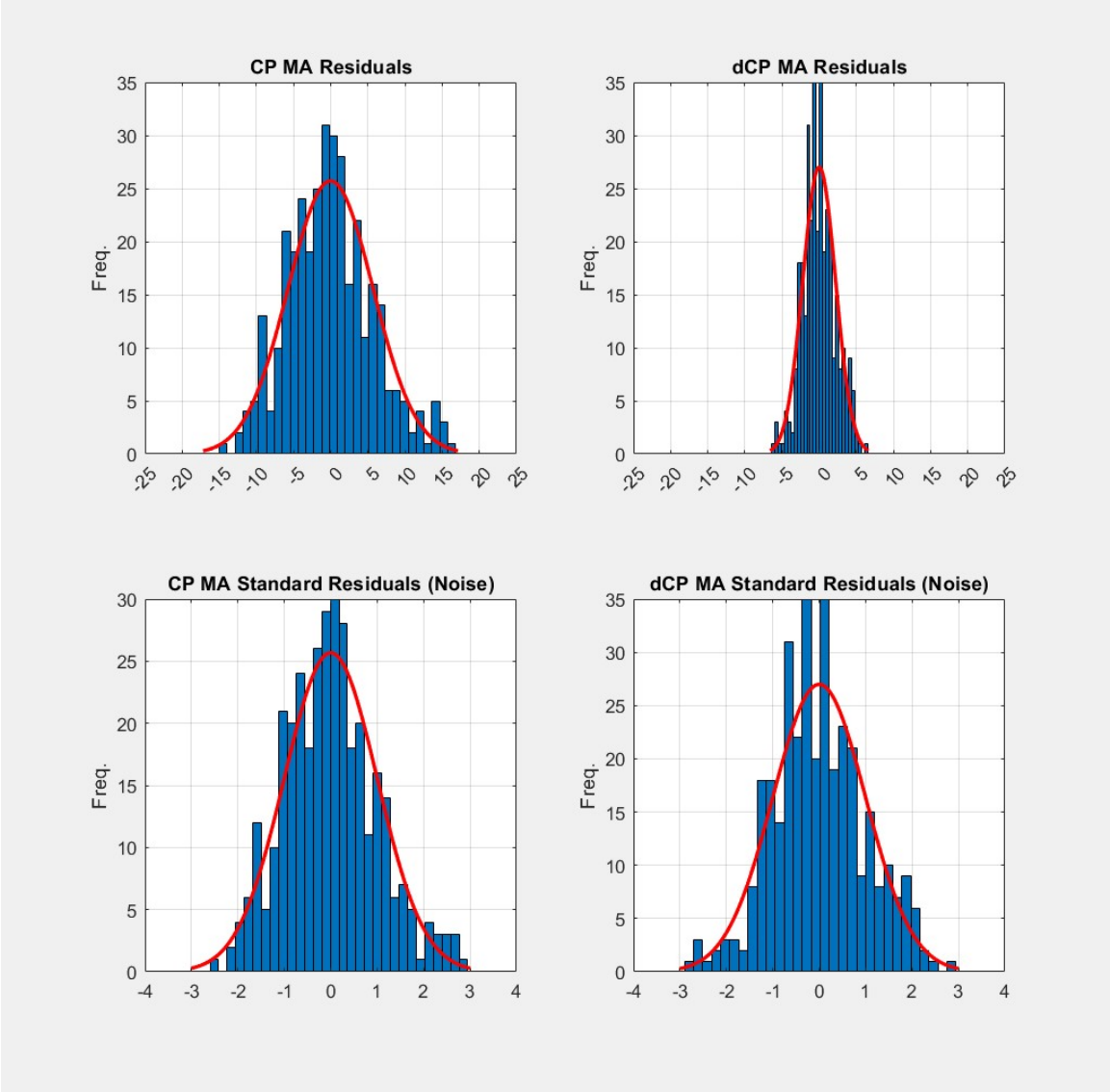

Figure D-33 Histograms for Decomposed *TMI* and *dTMI* for NOAA Station USW00024127 from 03/1988 to 03/2022

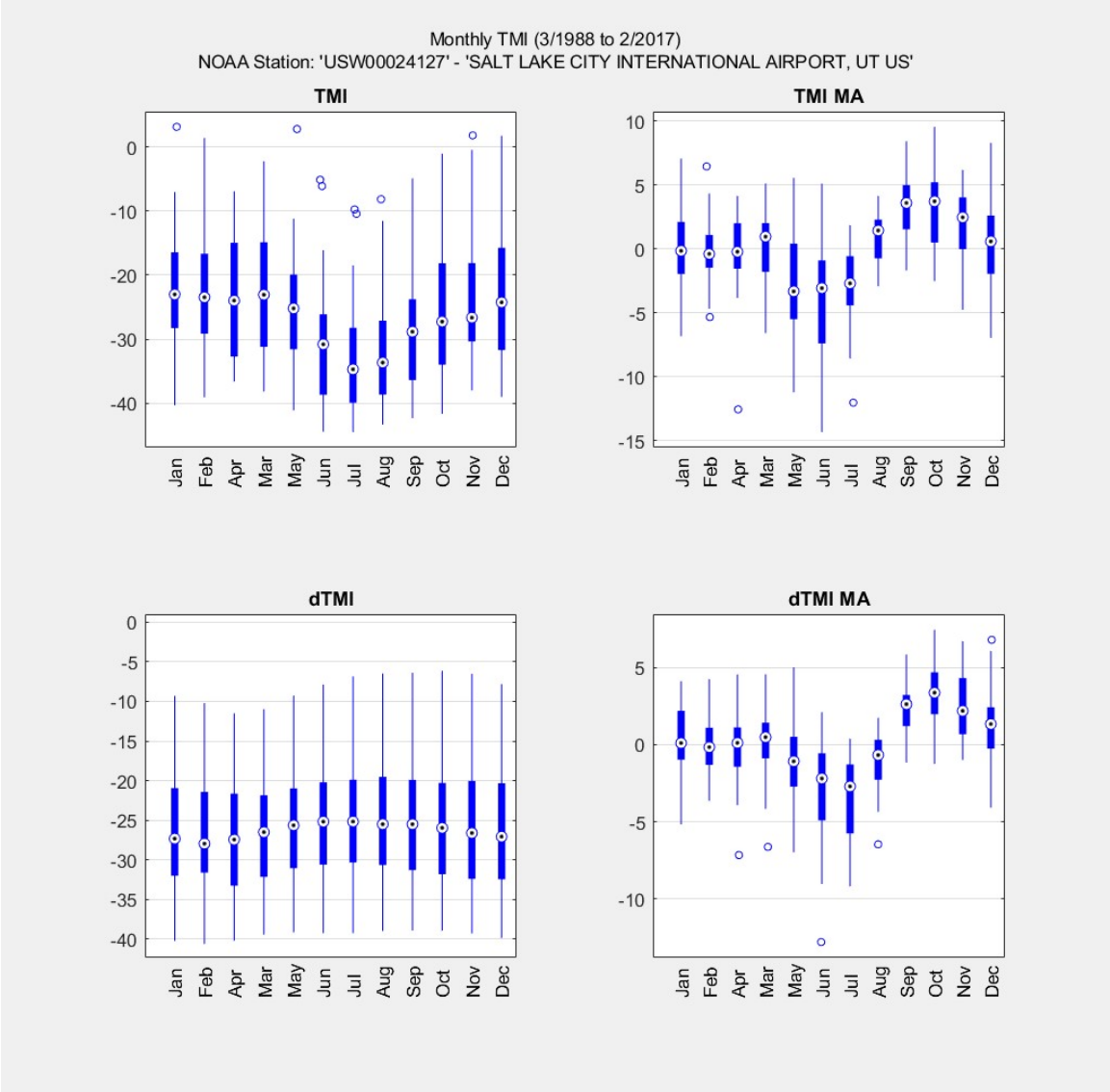

Figure D-34 Box Plots for Monthly Parameterized TMI and *dTMI* for Decomposed TMI and *dTMI* for NOAA Station USW00024127 from 03/1988 to 03/2022

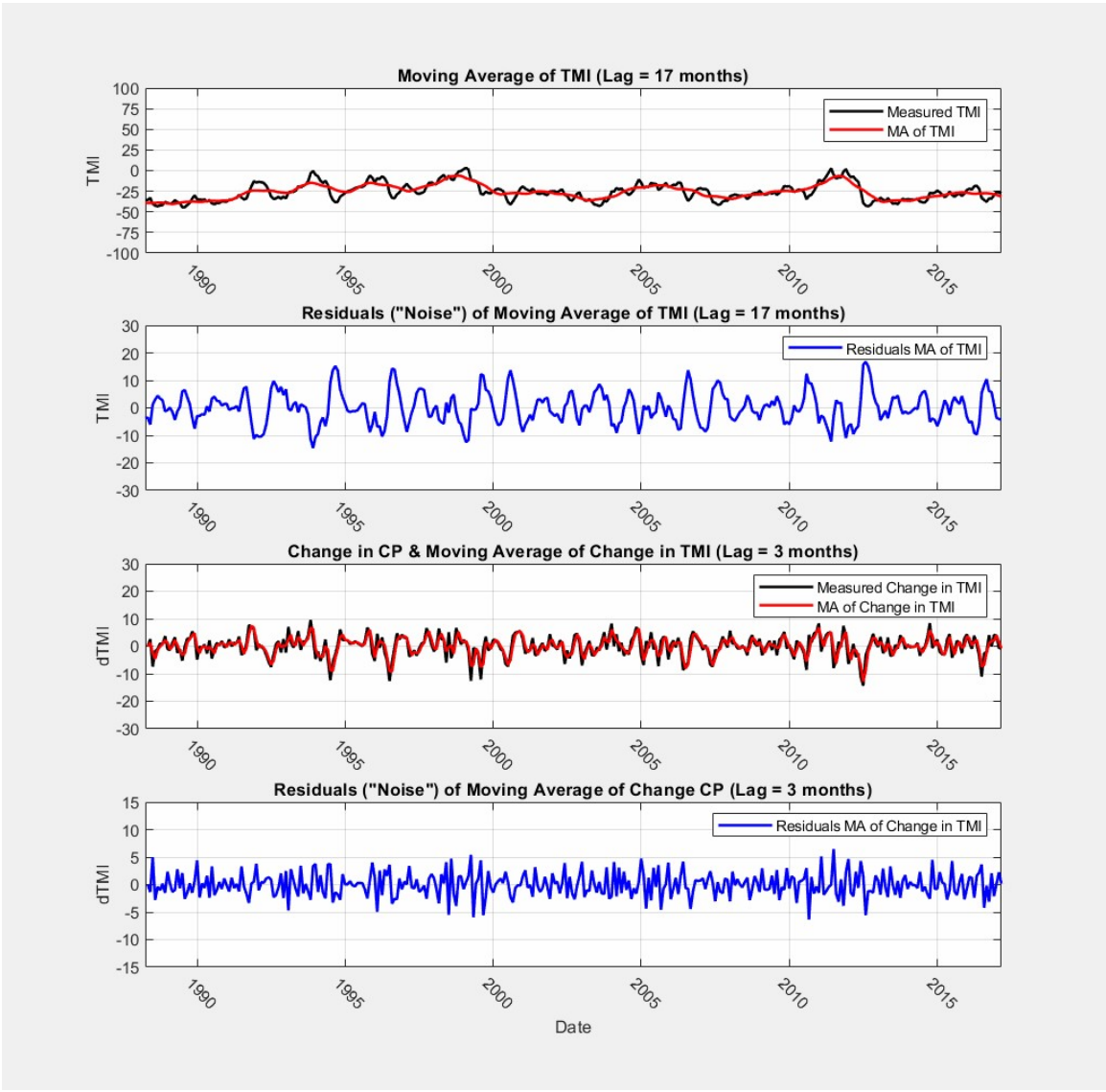

Figure D-35 Time Series Decomposition Using 1st differenced Moving Average for NOAA Station USW00024127 from 03/1988 to 03/2022

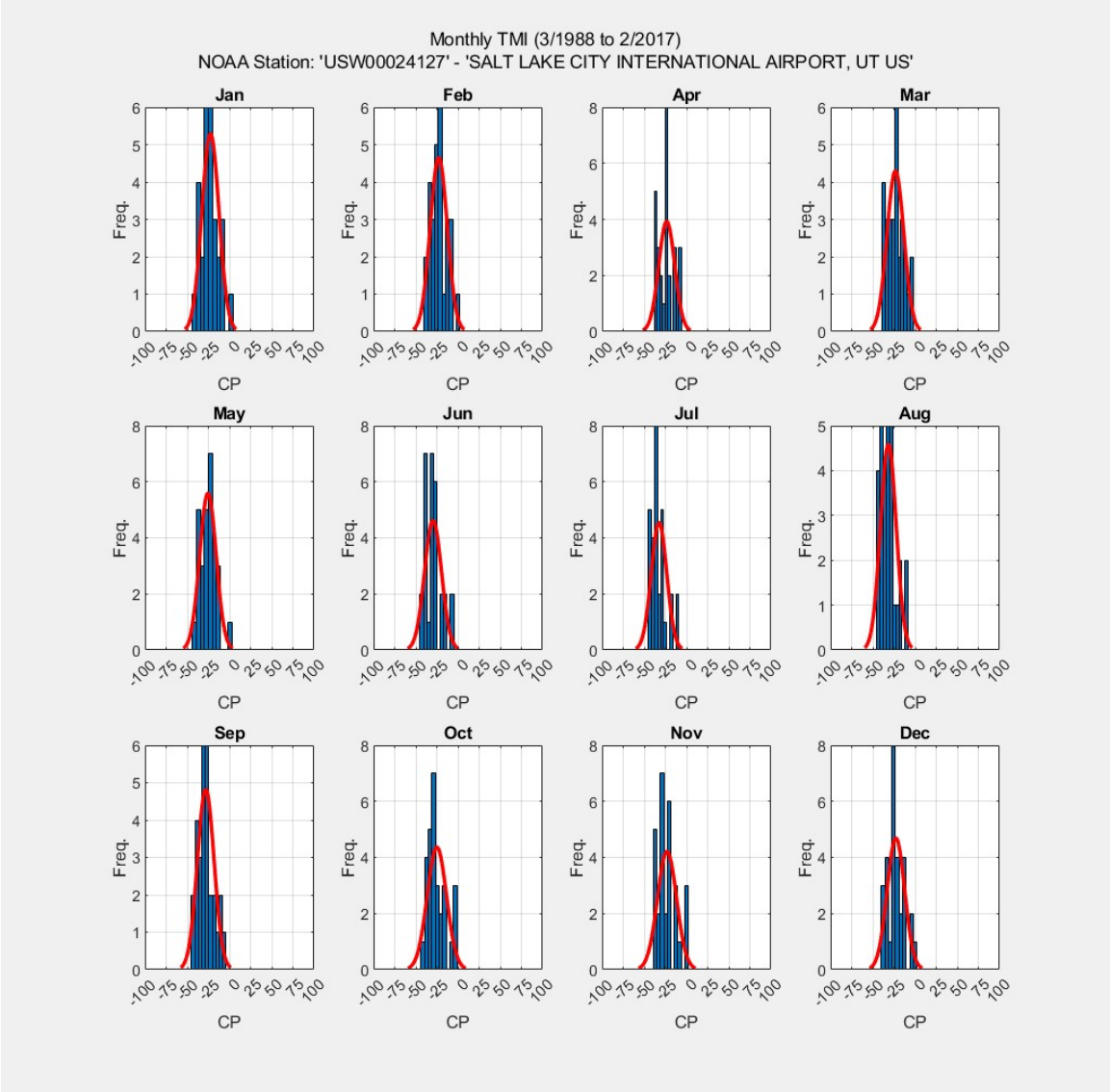

Figure D-36 Histograms for Monthly Parameterized *dTMI* for NOAA Station USW00024127 from 03/1988 to 03/2022

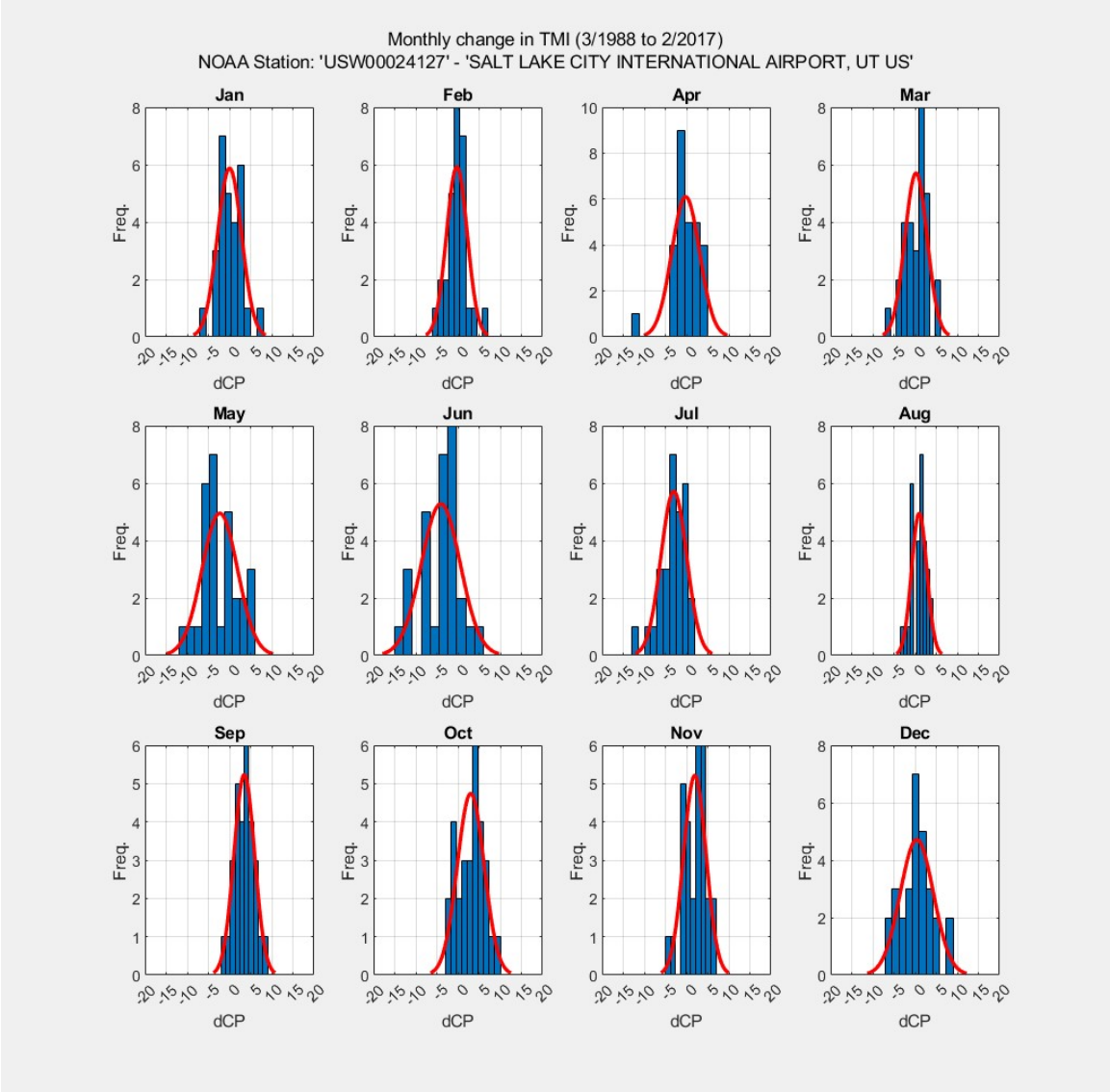

Figure D-37 Histograms for Monthly Parameterized *dTMI* for NOAA Station USW00024127 from 03/1988 to 03/2022

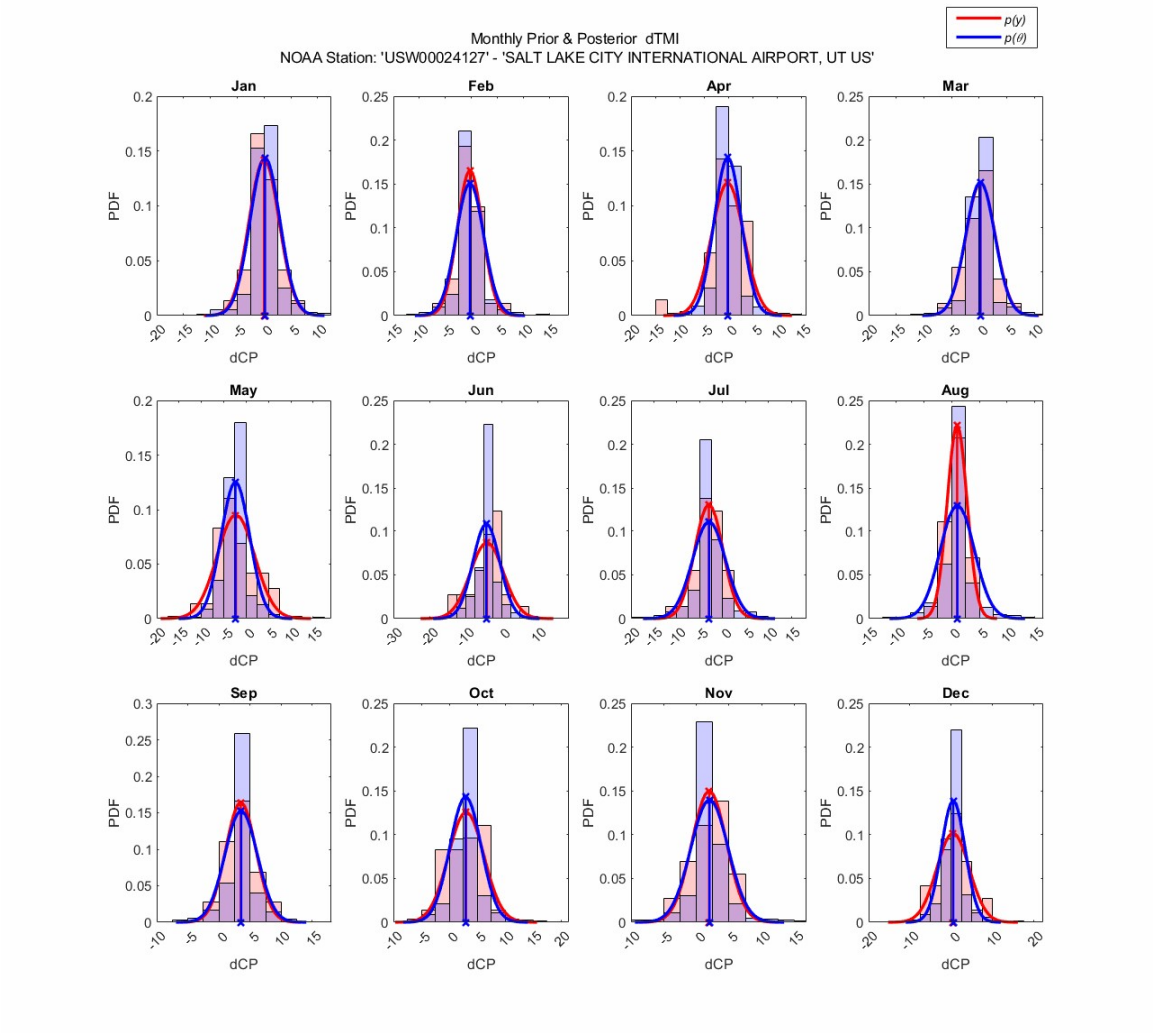

Figure D-38 Histograms of Prior and Posterior (forecasted) *dTMI* for NOAA Station USW00024127 from 03/1988 to 03/2022.

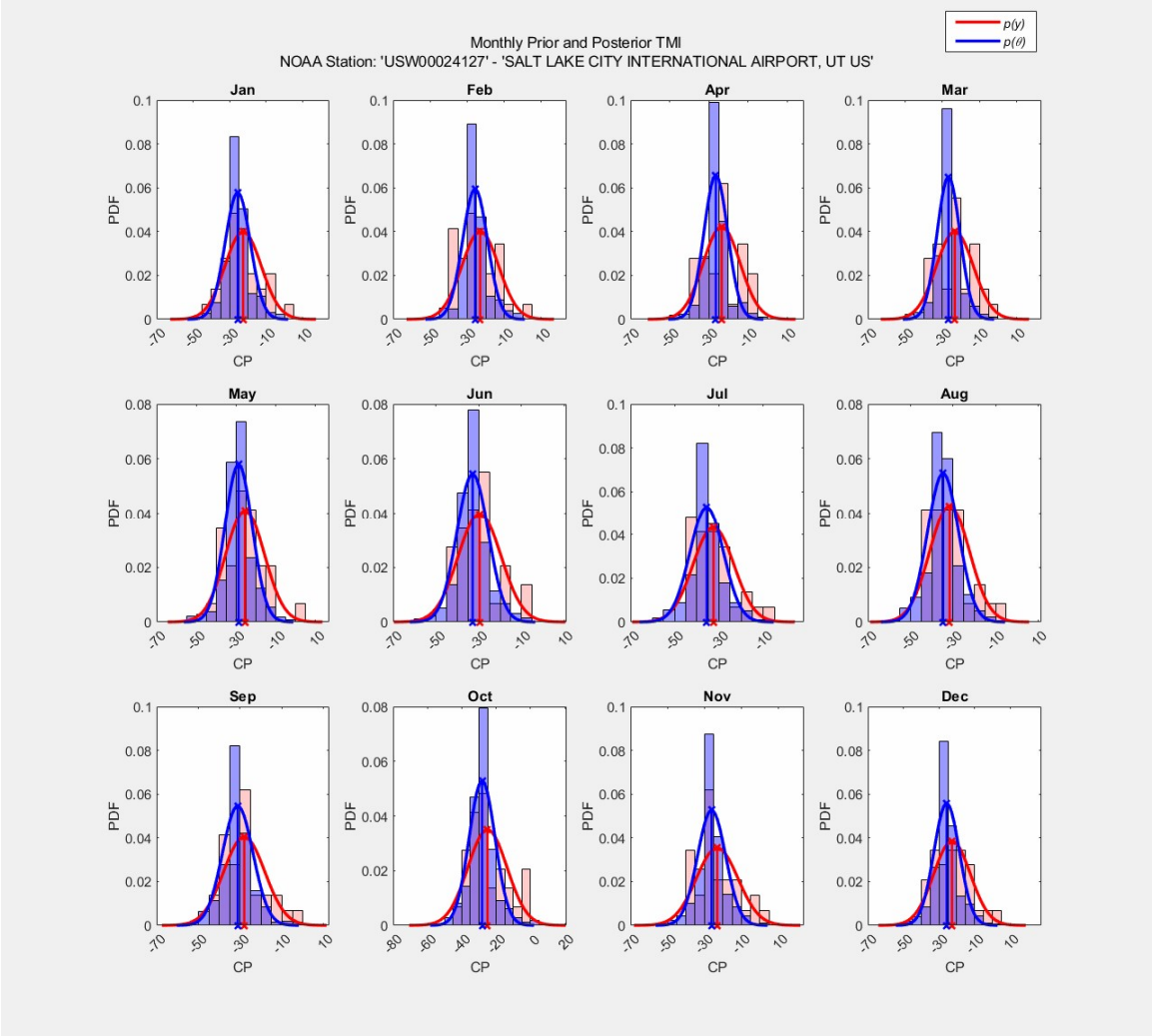

Figure D-39 Histograms of Prior and Posterior (forecasted) *TMI* for NOAA Station USW00024127 from 03/1988 to 03/2022

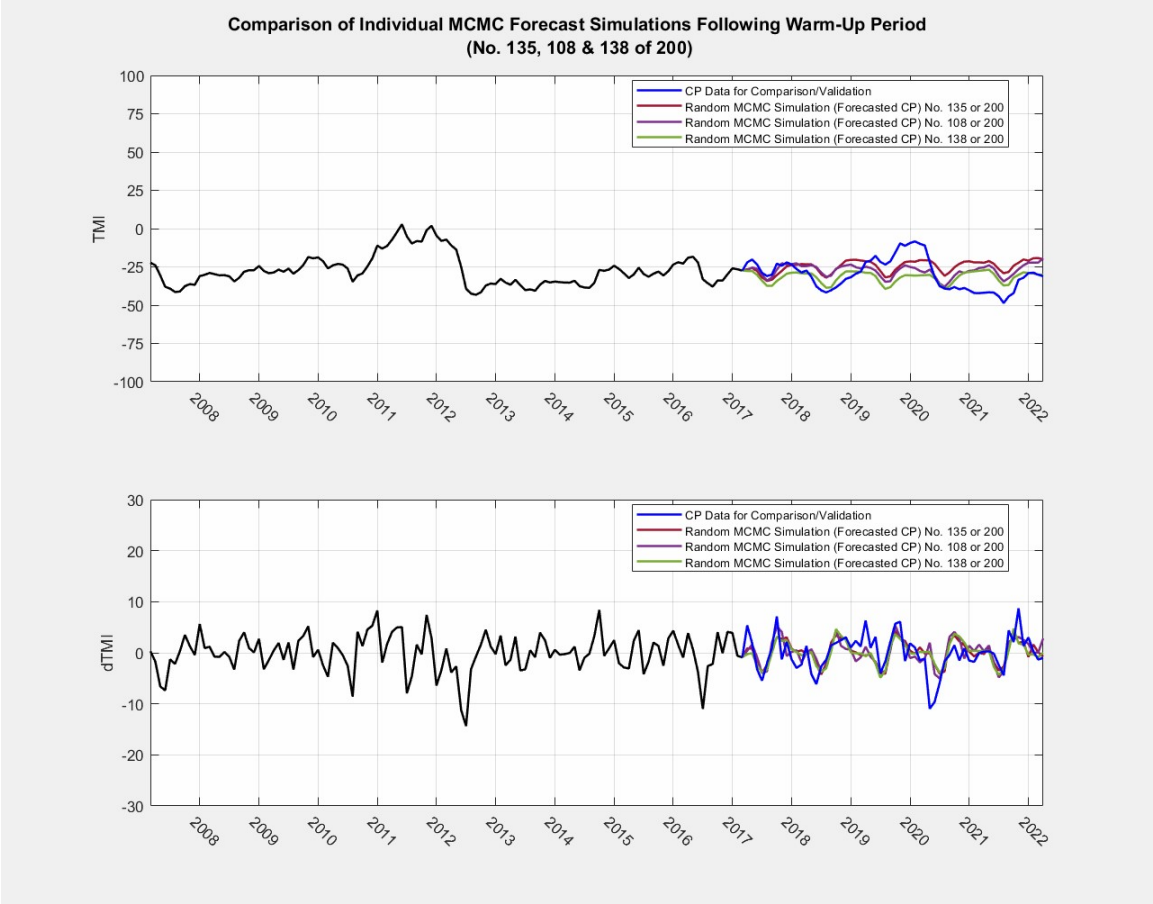

Figure D-40 Example of Single Simulation Results of *dTMI* and *TMI* for NOAA Station USW00024127 from 03/1988 to 03/2022.

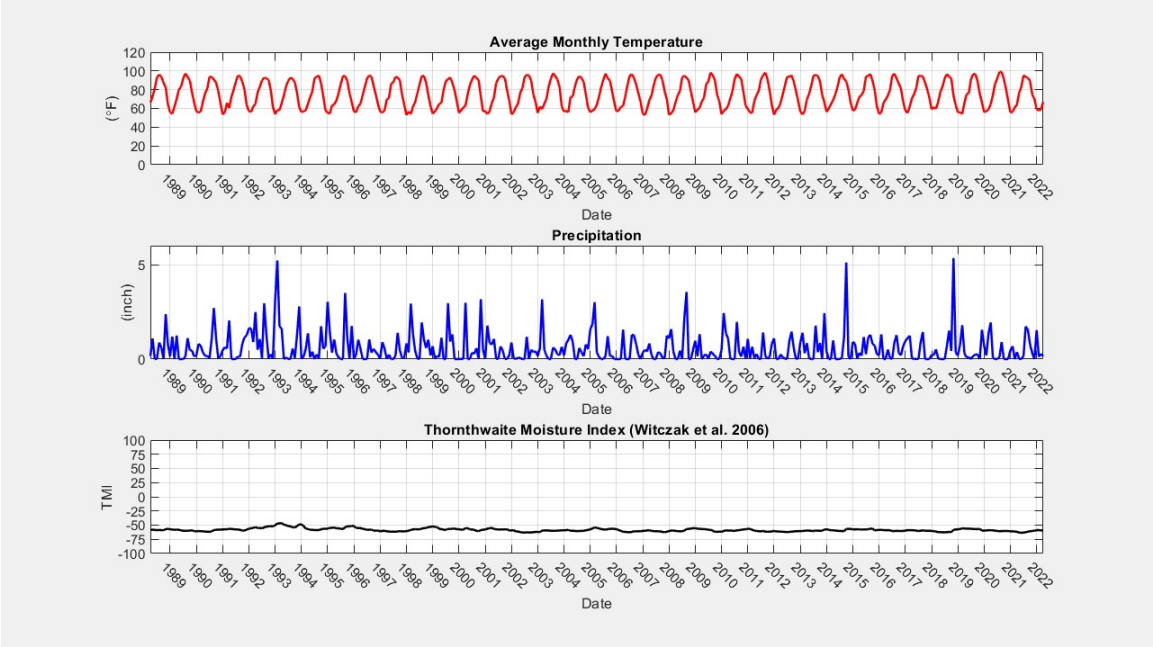

Figure D-41 NOAA Station USW00023183 Climate Data Extract and Calculated TMI from 03/1988 to 03/2022

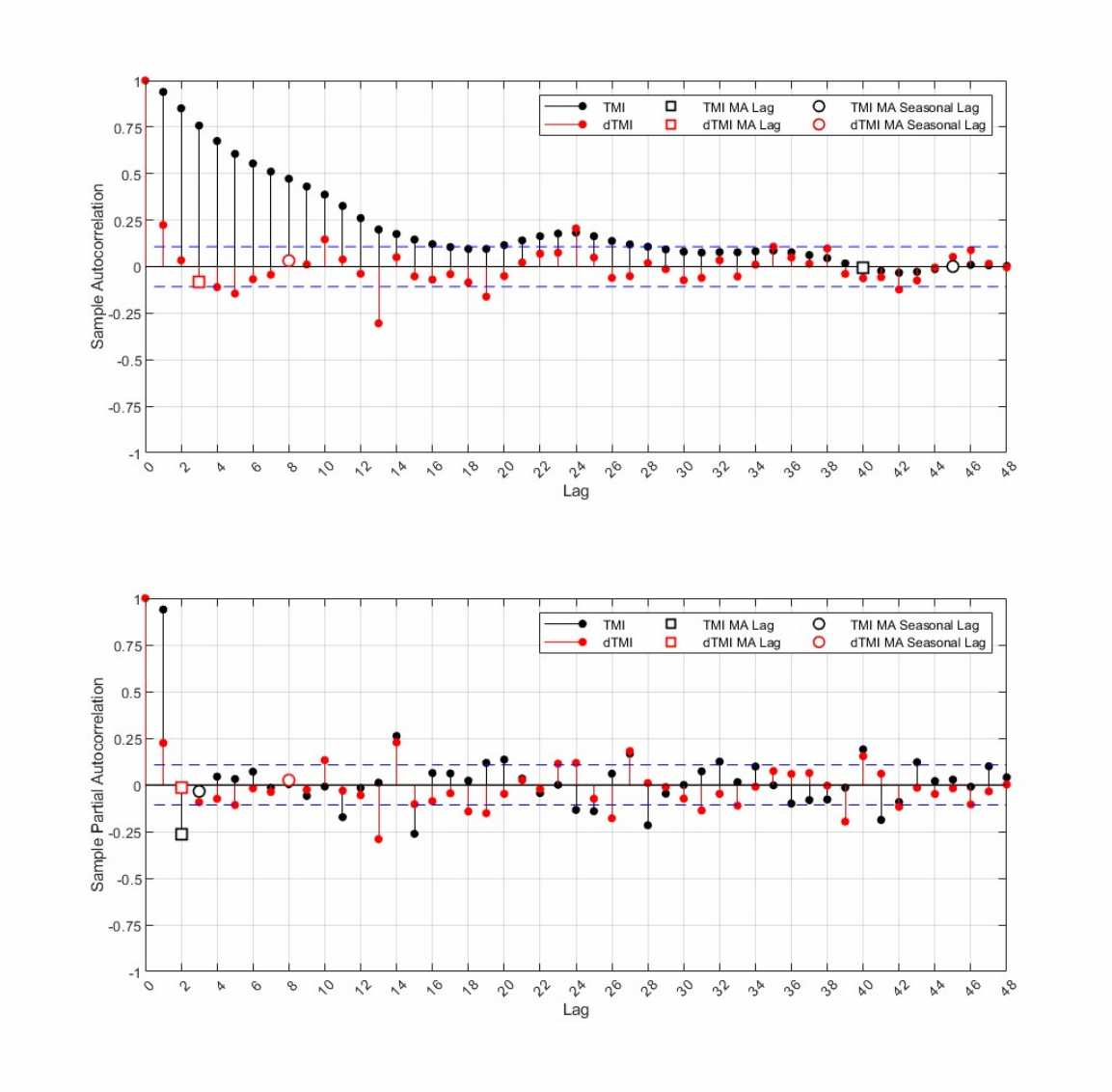

Figure D-42 ACF and PACF for *TMI* and *dTMI* for NOAA Station USW00023183 from 03/1988 to 03/2022

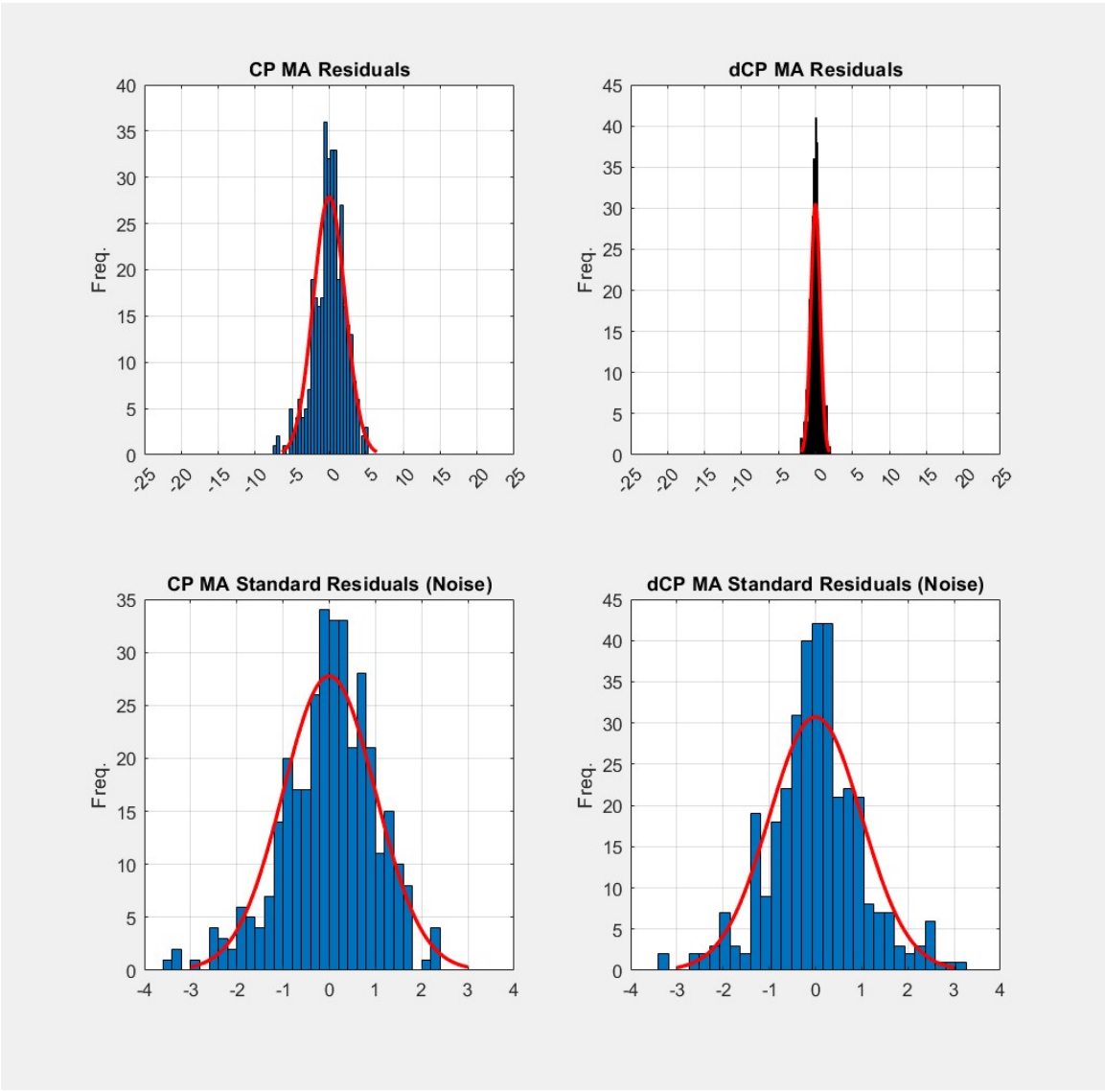

Figure D-43 Histograms for Decomposed *TMI* and *dTMI* for NOAA Station USW00023183 from 03/1988 to 03/2022

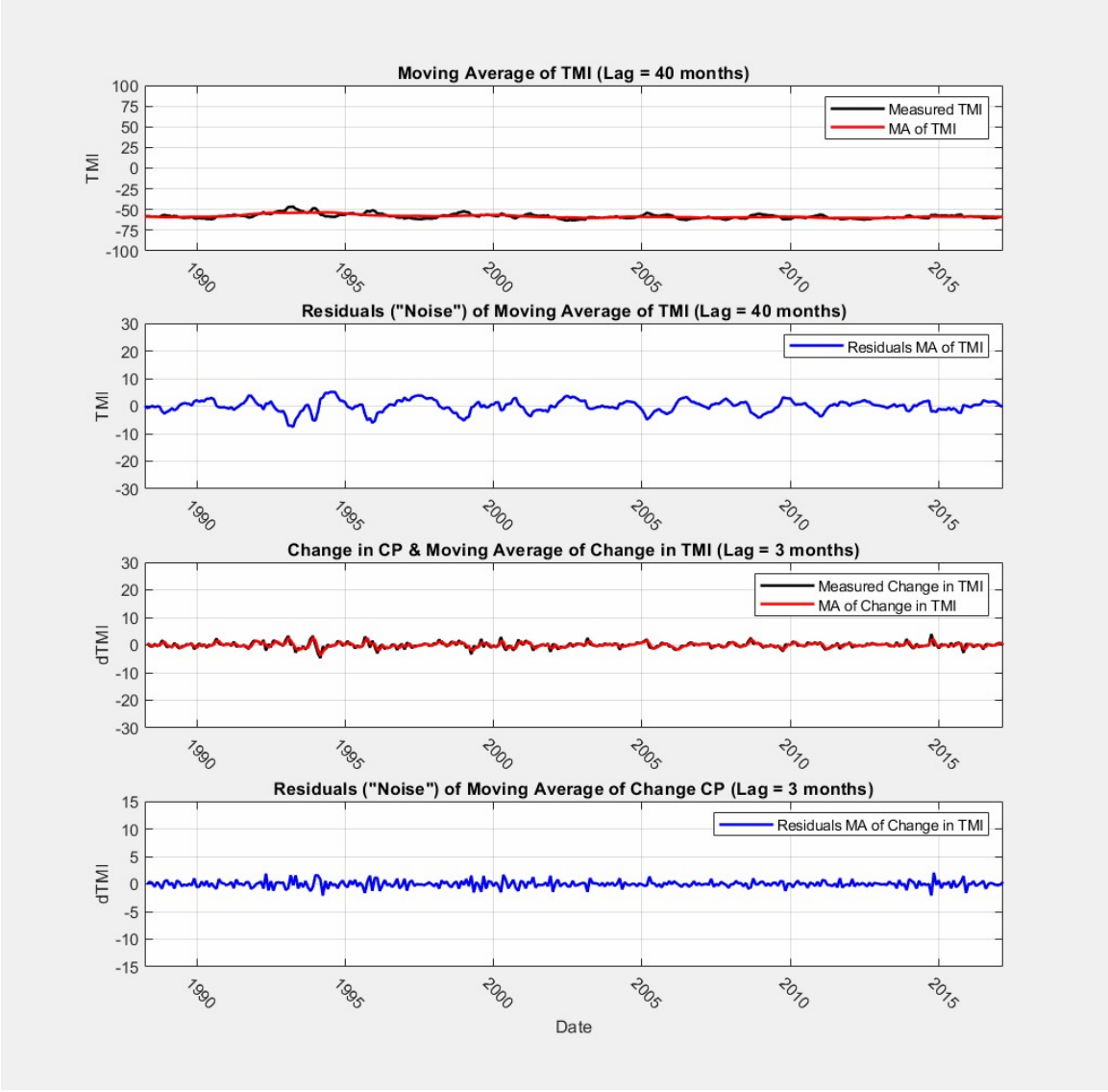

Figure D-44 Time Series Decomposition Using 1st differenced Moving Average for NOAA Station USW00023183 from 03/1988 to 03/2022

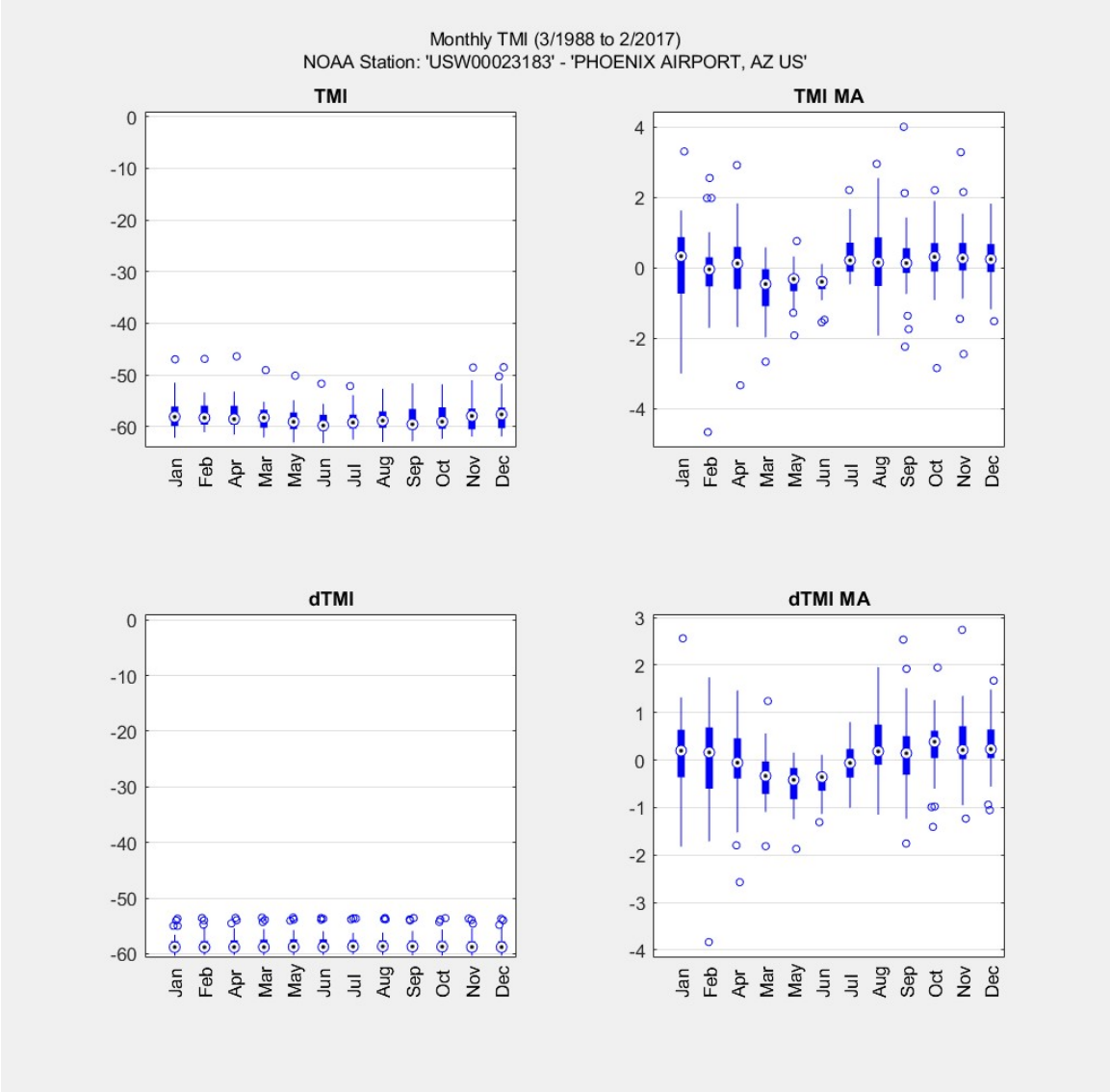

Figure D-45 Box Plots for Monthly Parameterized TMI and dTMI for Decomposed TMI and dTMI for NOAA Station USW00023183 from 03/1988 to 03/2022

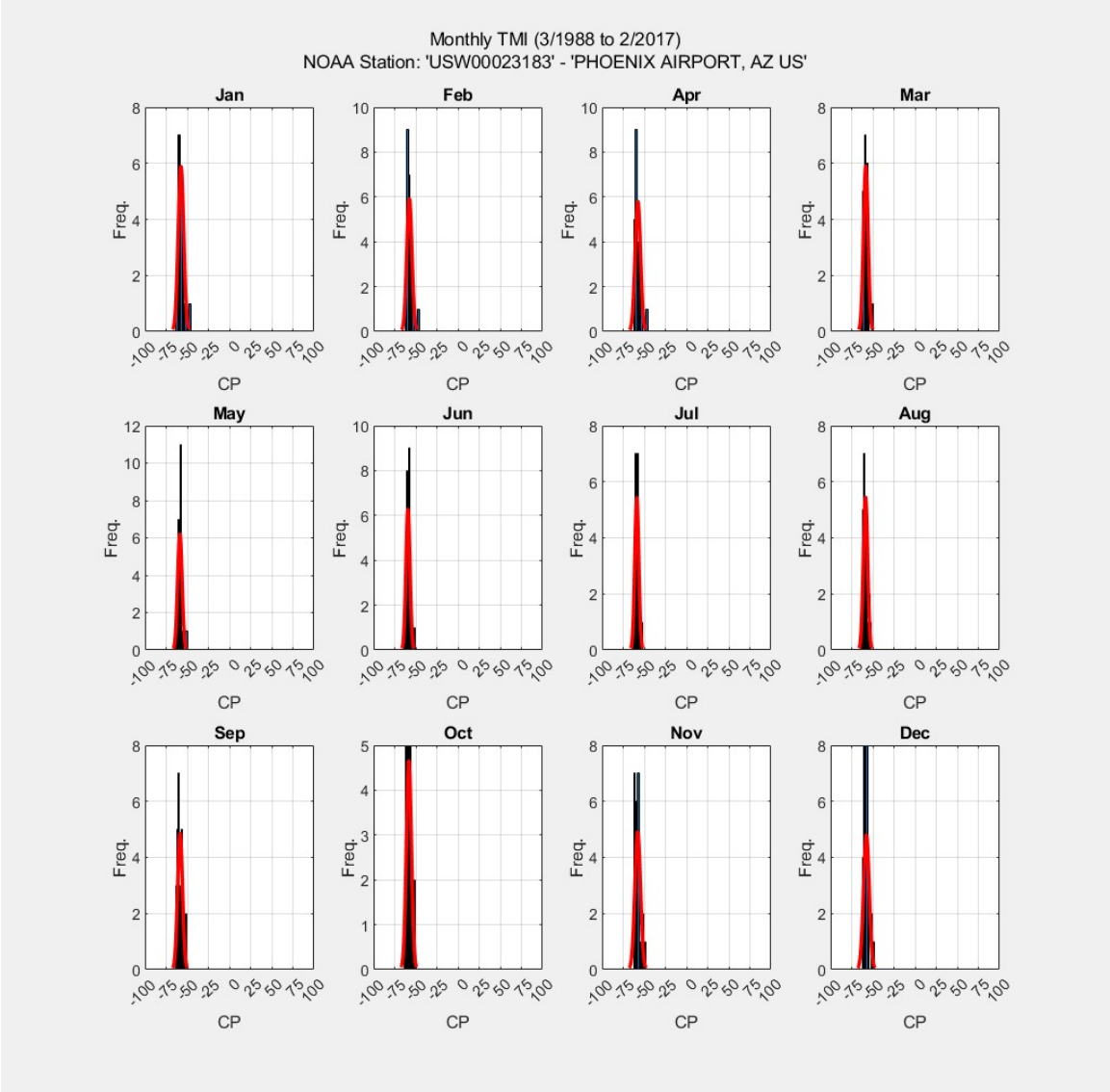

Figure D-46 Histograms for Monthly Parameterized *TMI* for NOAA Station USW00023183 from 03/1988 to 03/2022

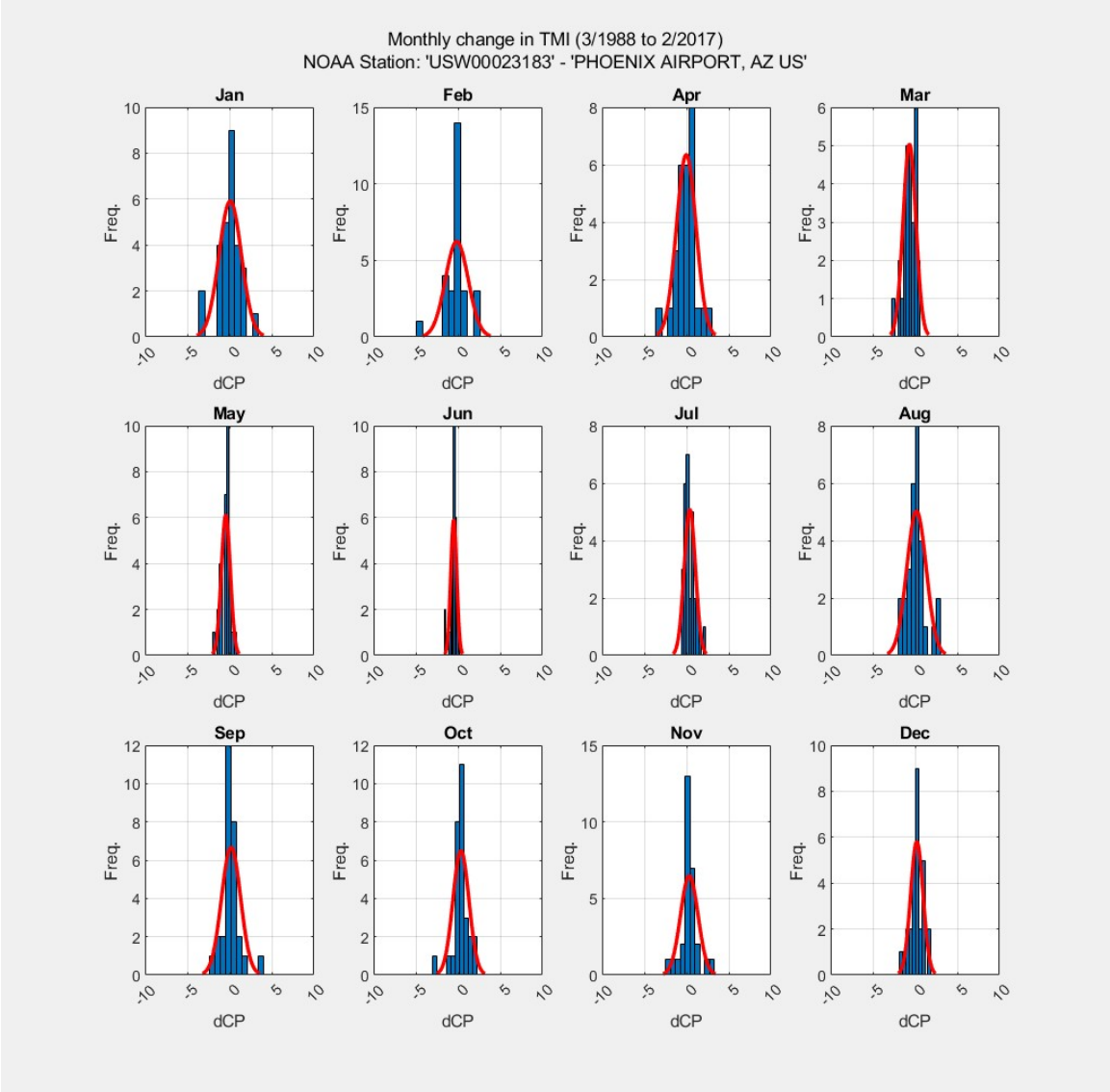

Figure D-47 Histograms for Monthly Parameterized *TMI* for NOAA Station USW00023183 from 03/1988 to 03/2022

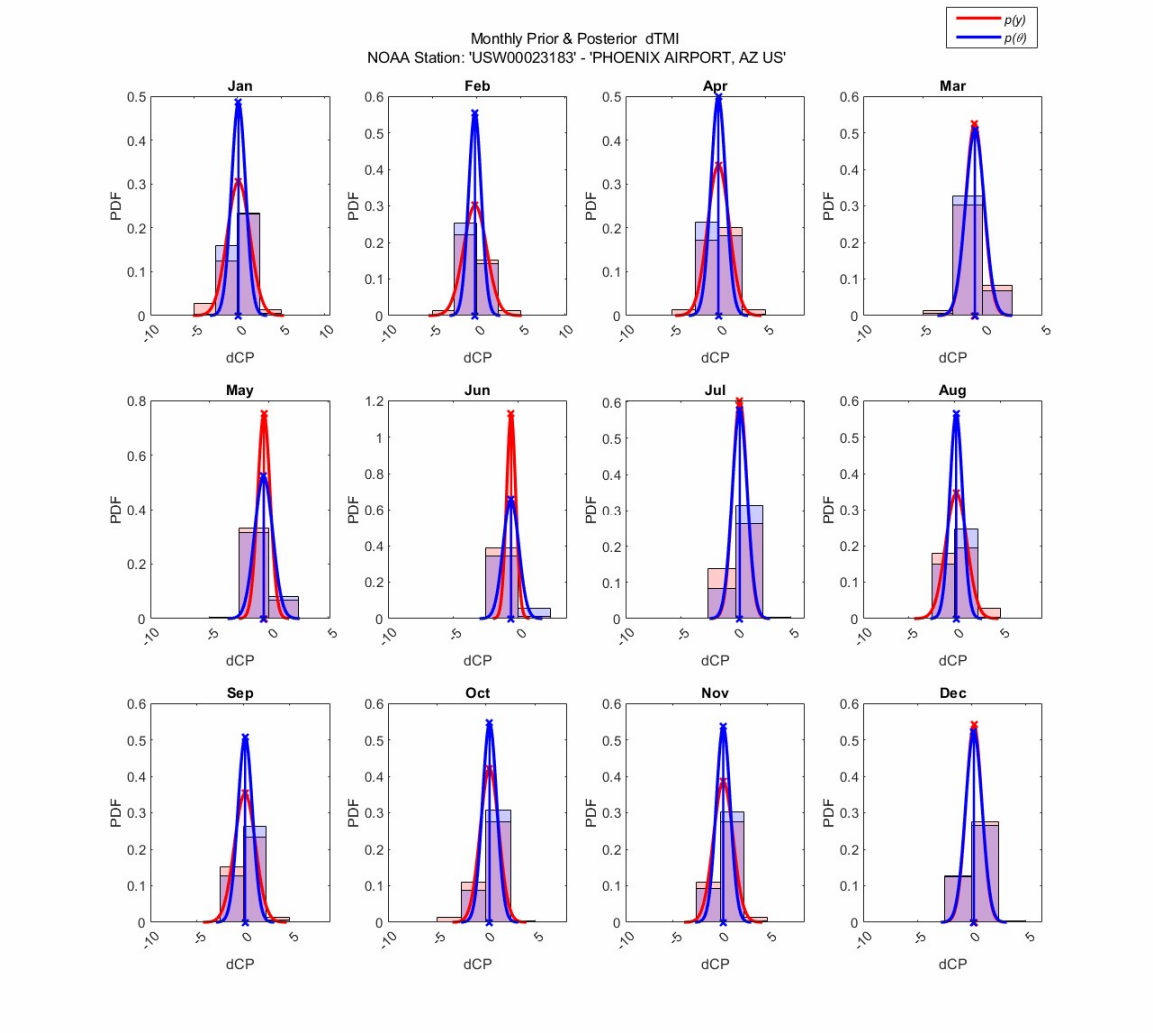

Figure D-48 Histograms of Prior and Posterior (forecasted) *dTMI* for NOAA Station USW00023183 from 03/1988 to 03/2022

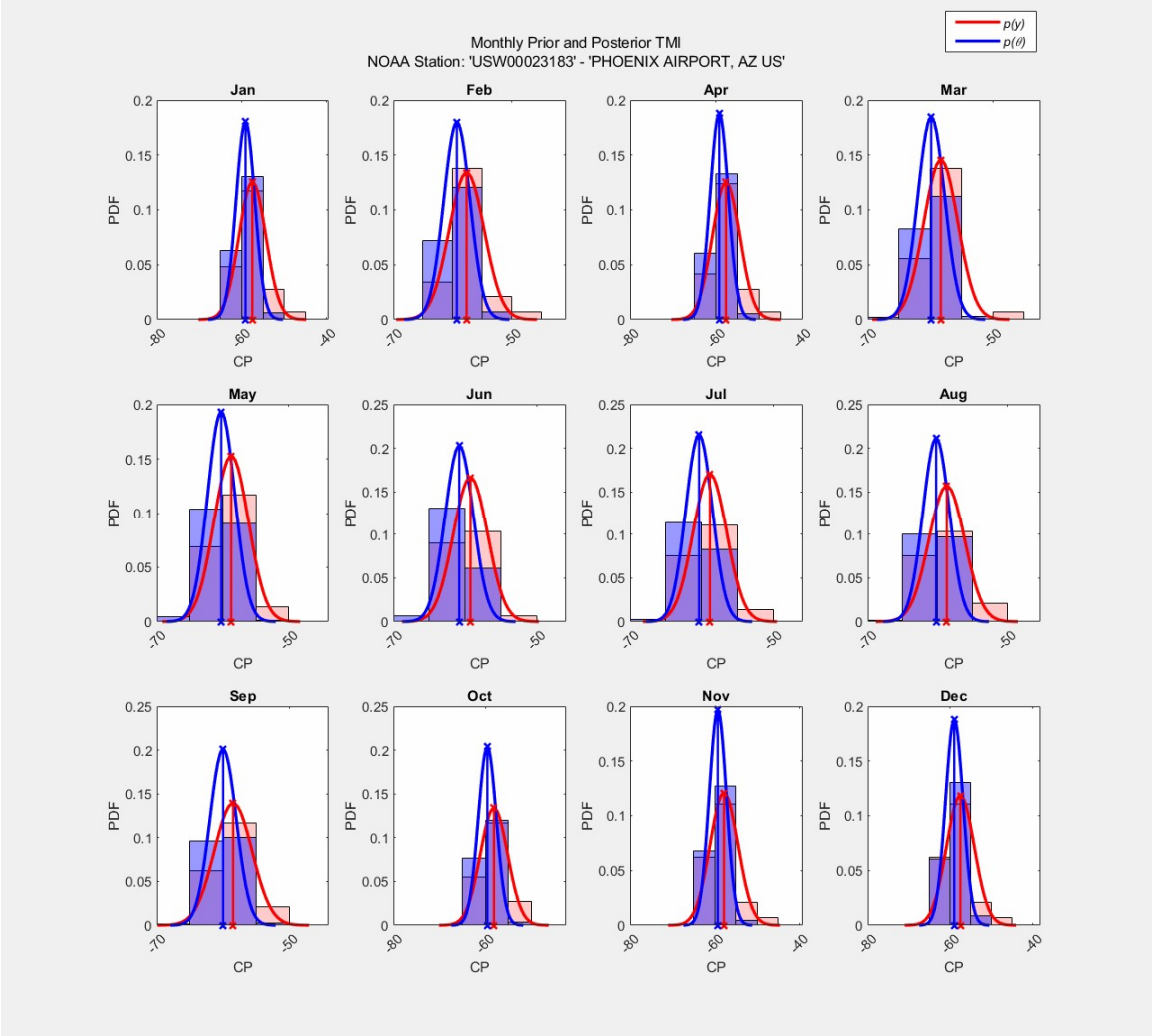

Figure D-49 Histograms of Prior and Posterior (forecasted) *TMI* for NOAA Station USW00023183 from 03/1988 to 03/2022.

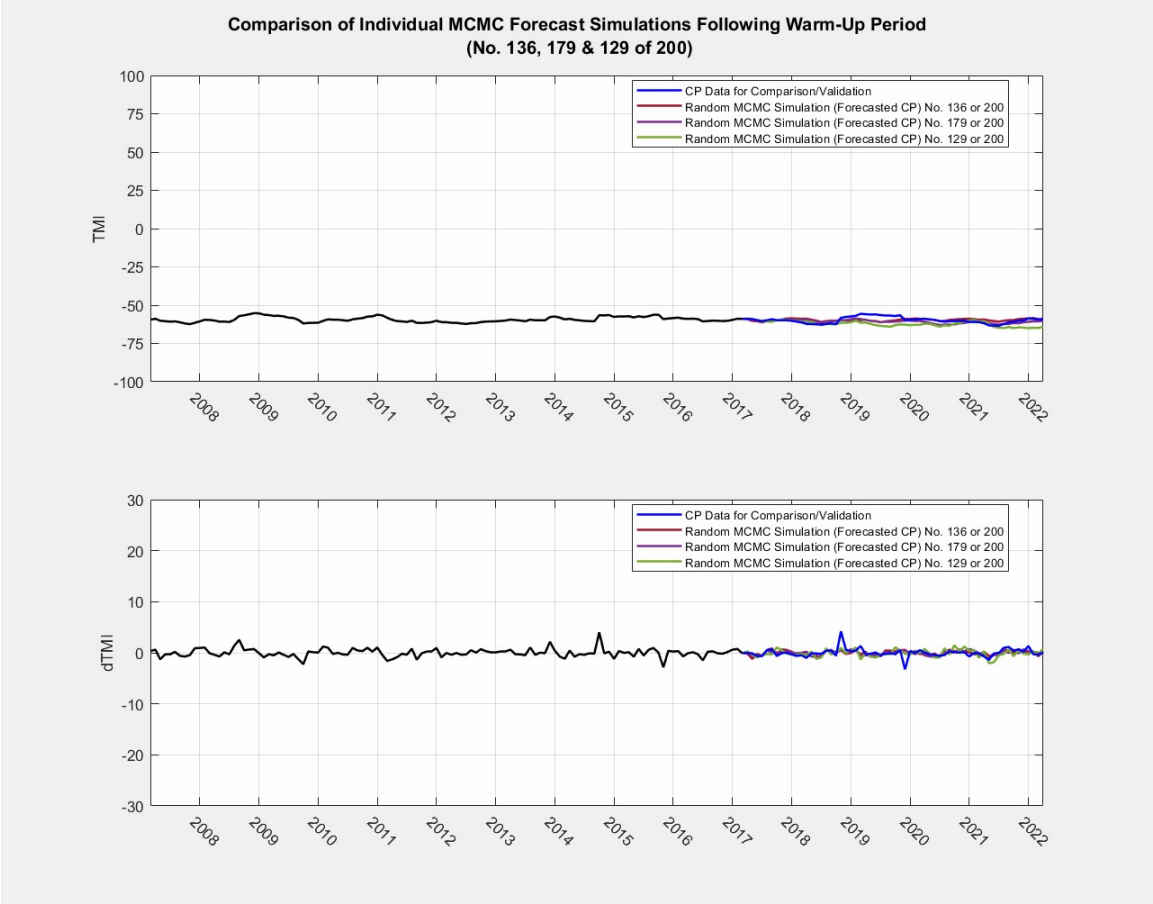

Figure D-50 Example of Single Simulation Results of *dTMI* and *TMI* for NOAA Station USW00023183 from 03/1988 to 03/2022.

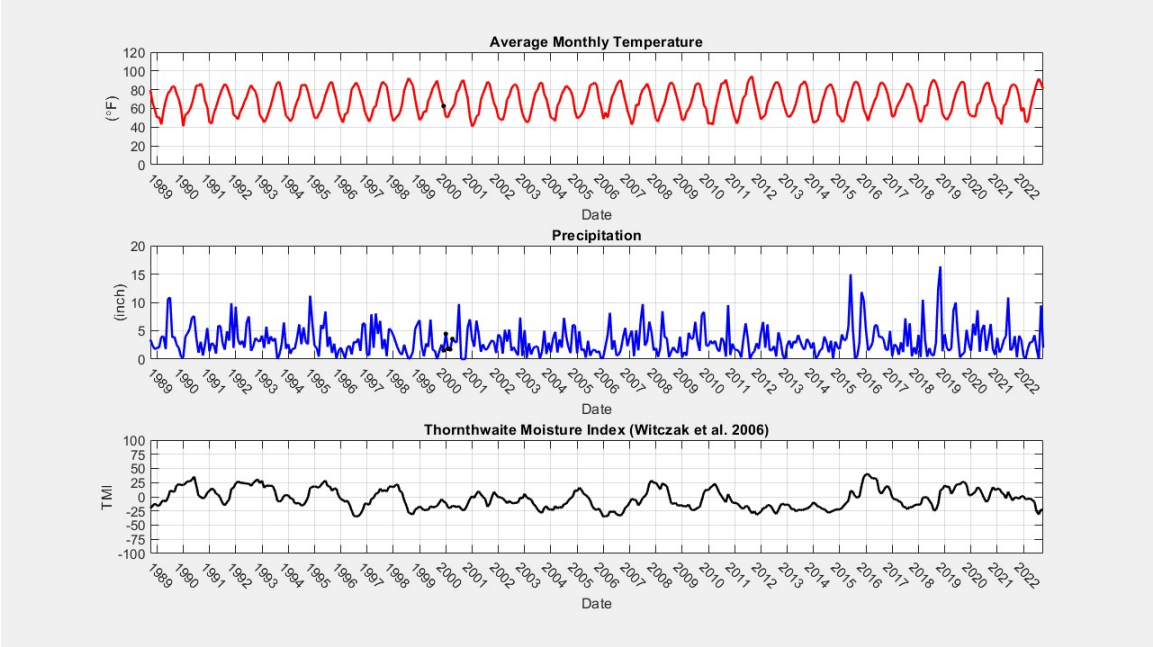

Figure D-51 NOAA Station USW00013960 Climate Data Extract and Calculated TMI from 09/1988 to 09/2022

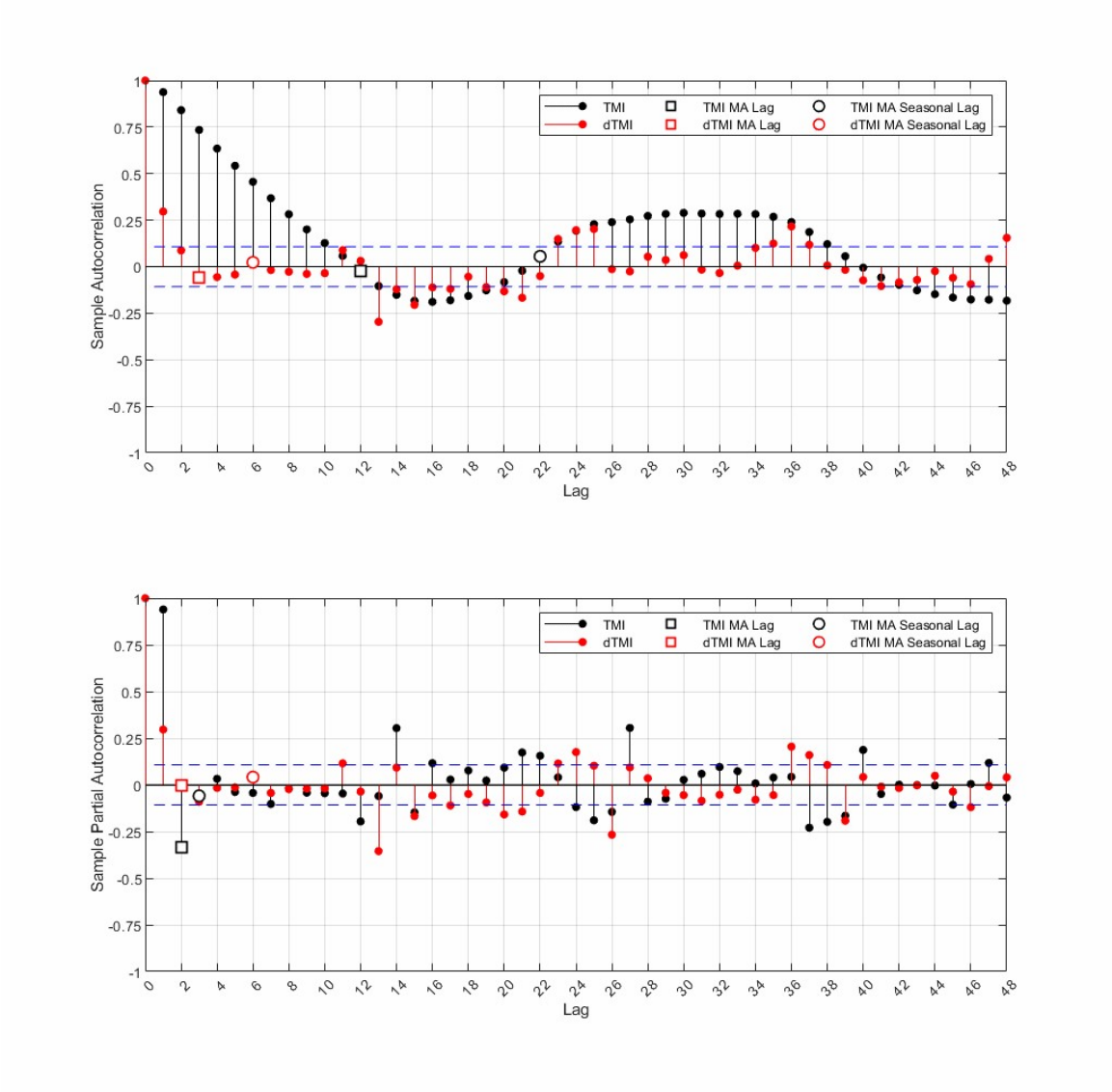

Figure D-52 ACF and PACF for *TMI* and *dTMI* for NOAA Station USW00013960 from 09/1988 to 09/2022

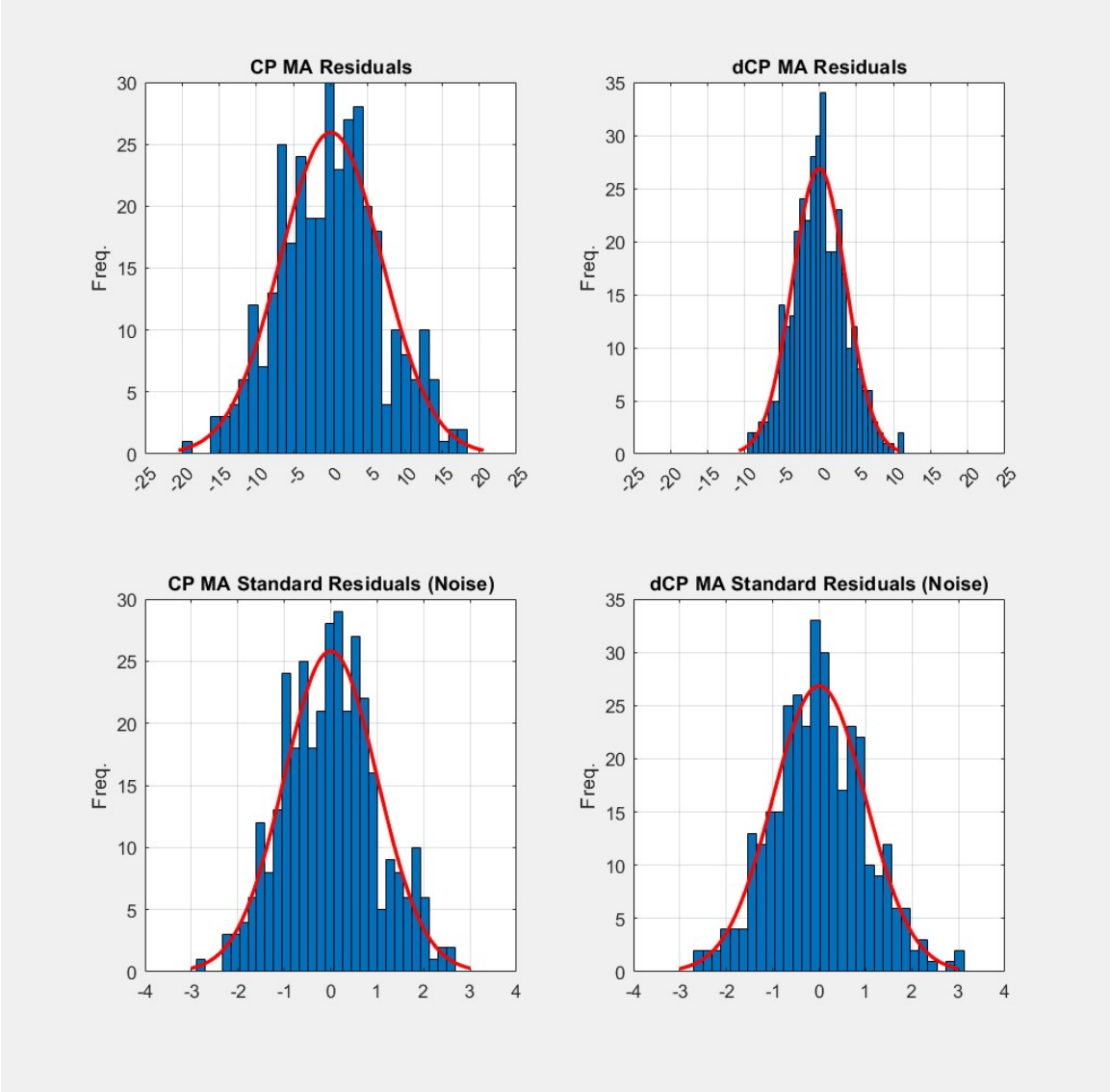

Figure D-53 Histograms for Decomposed *TMI* and *dTMI* for NOAA Station USW00013960 from 09/1988 to 09/2022

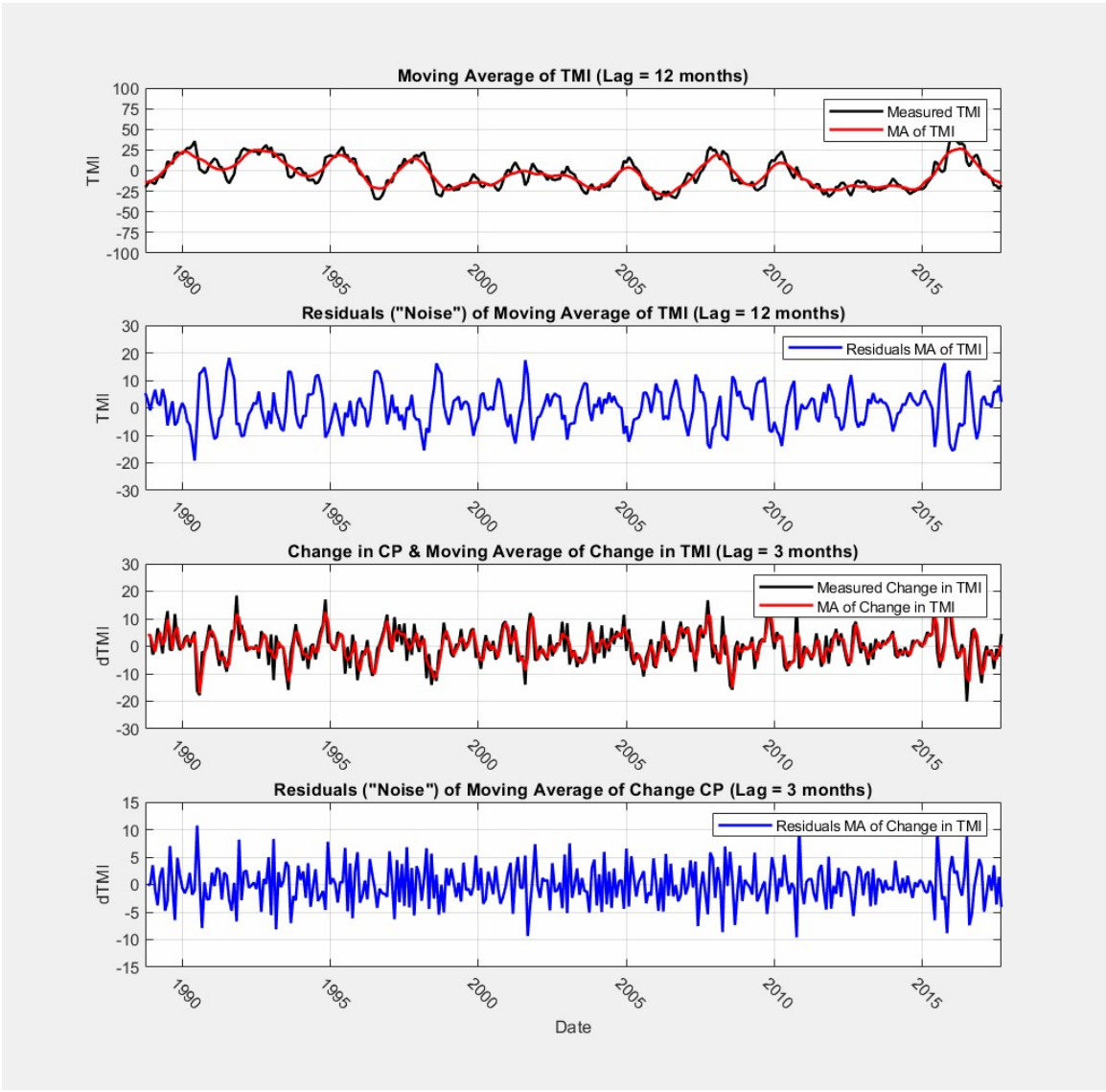

Figure D-54 Time Series Decomposition Using 1st differenced Moving Average for NOAA Station USW00013960 from 09/1988 to 09/2022

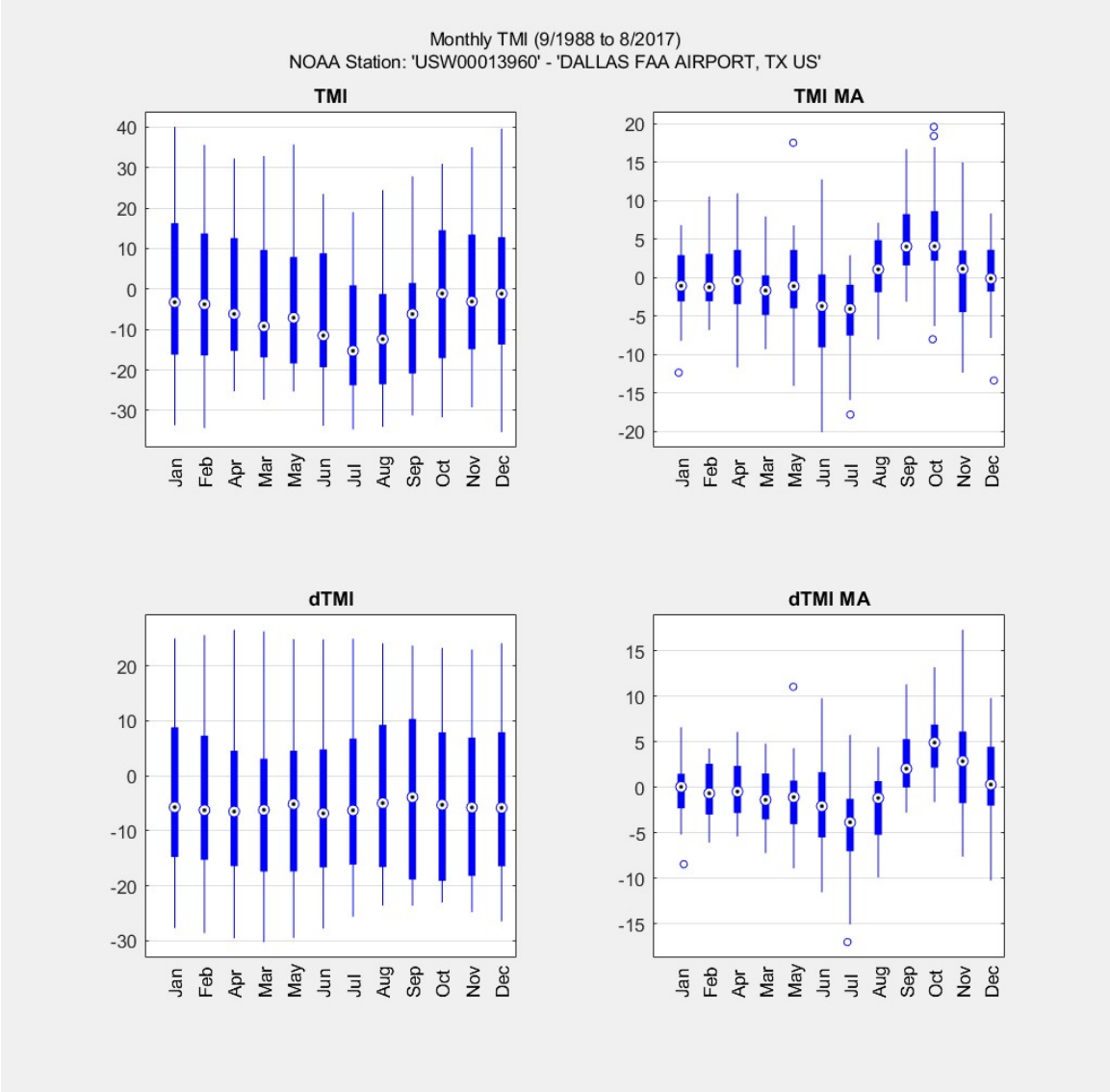

Figure D-55 Box Plots for Monthly Parameterized TMI and dTMI for Decomposed TMI and dTMI for NOAA Station USW00013960 from 09/1988 to 09/2022

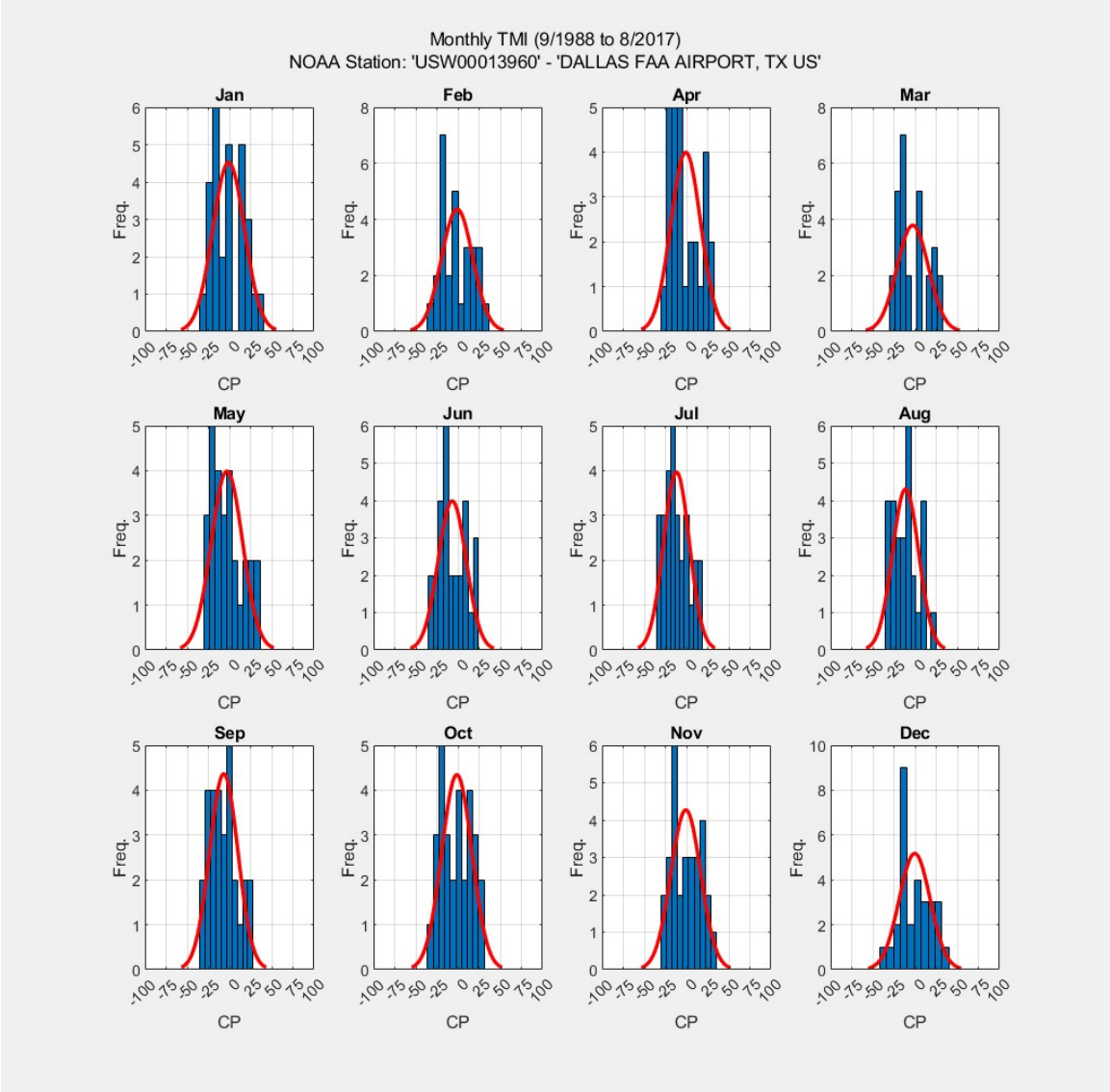

Figure D-56 Histograms for Monthly Parameterized *TMI* for NOAA Station USW00013960 from 09/1988 to 03/2022

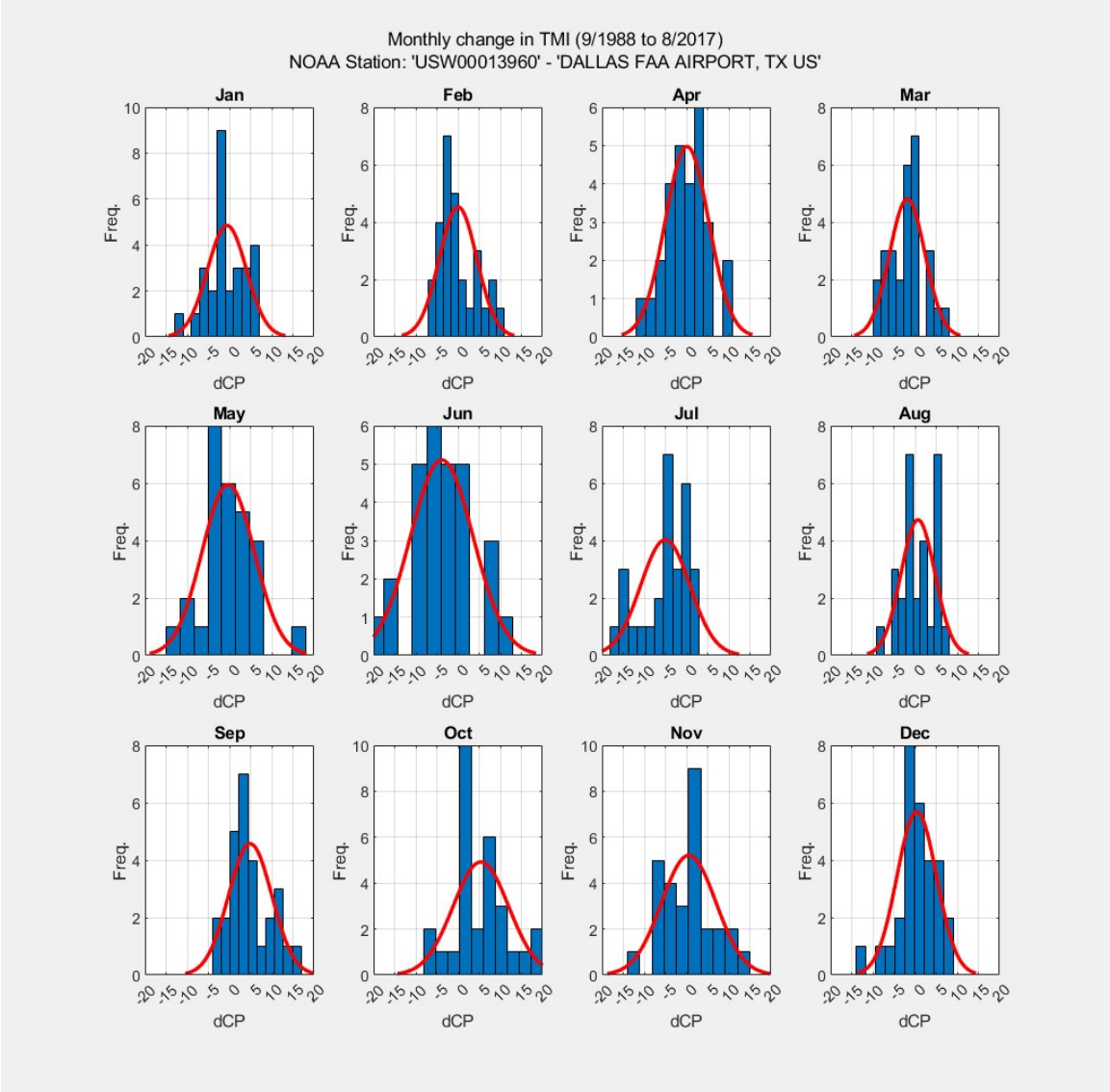

Figure D-57 Histograms for Monthly Parameterized *dTMI* for NOAA Station USW00013960 from 09/1988 to 03/2022

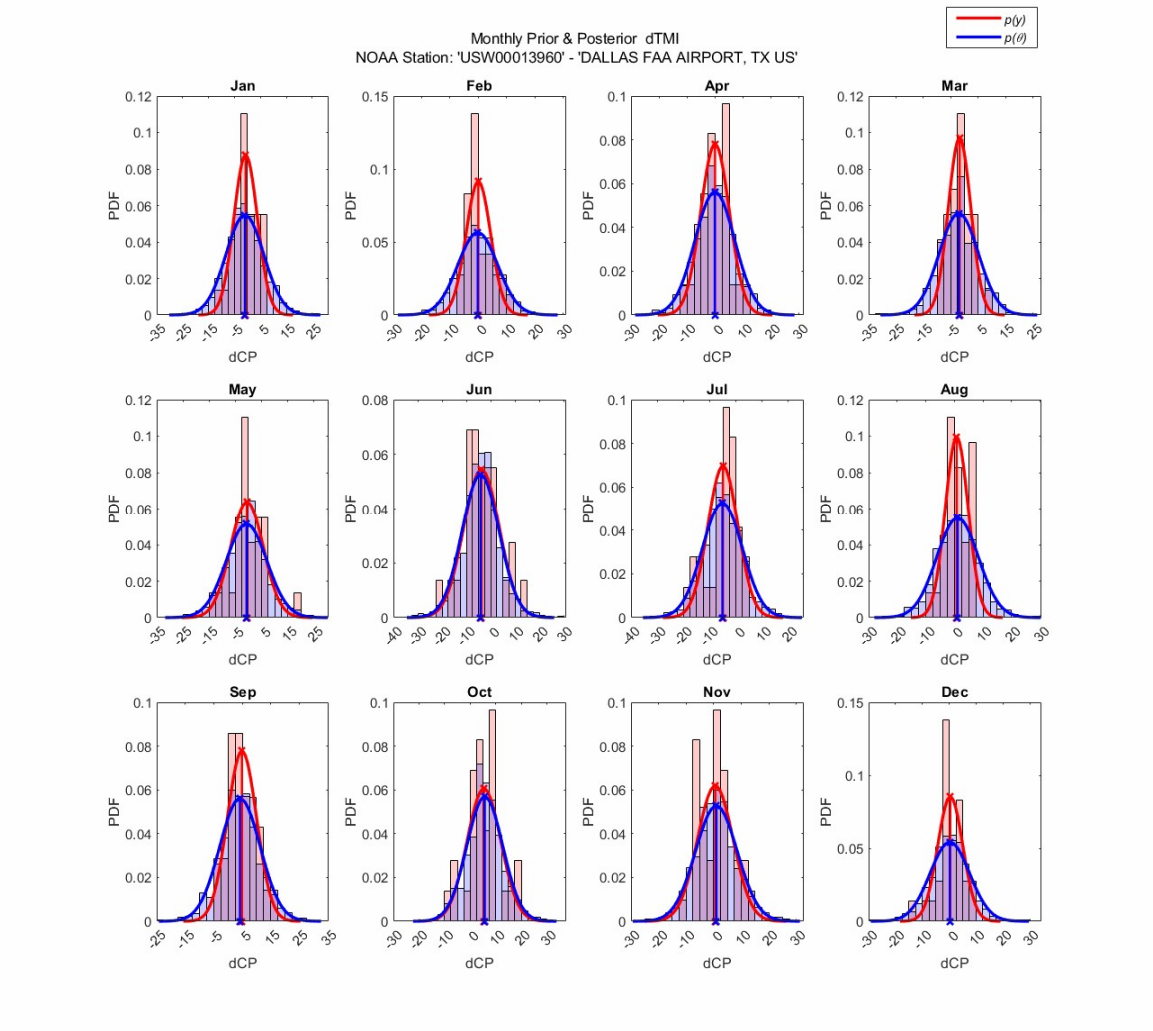

Figure D-58 Histograms of Prior and Posterior (forecasted) *dTMI* for NOAA Station USW00013960 from 09/1988 to 09/2022.

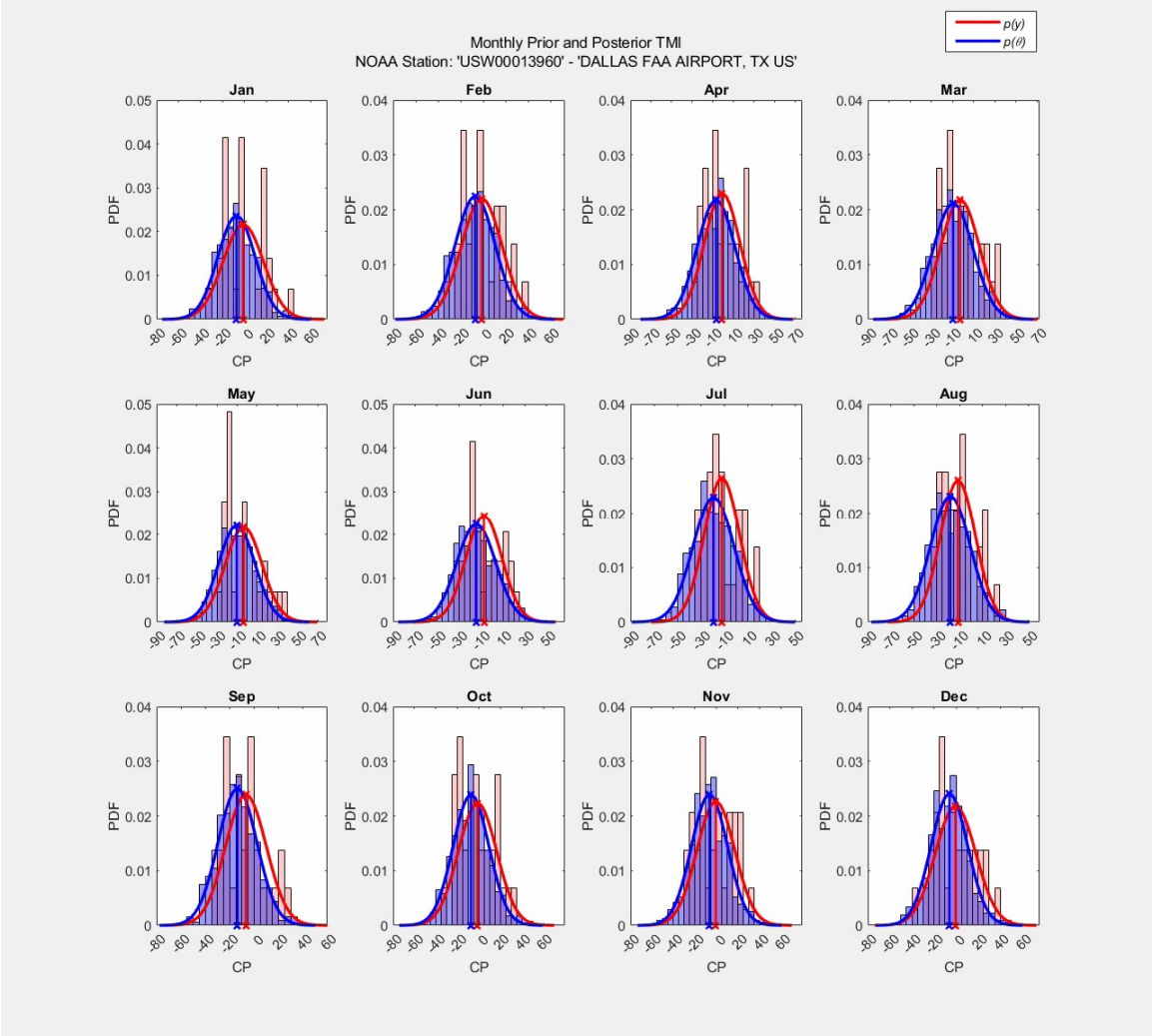

Figure D-59 Histograms of Prior and Posterior (forecasted) *TMI* for NOAA Station USW00013960 from 09/1988 to 09/2022

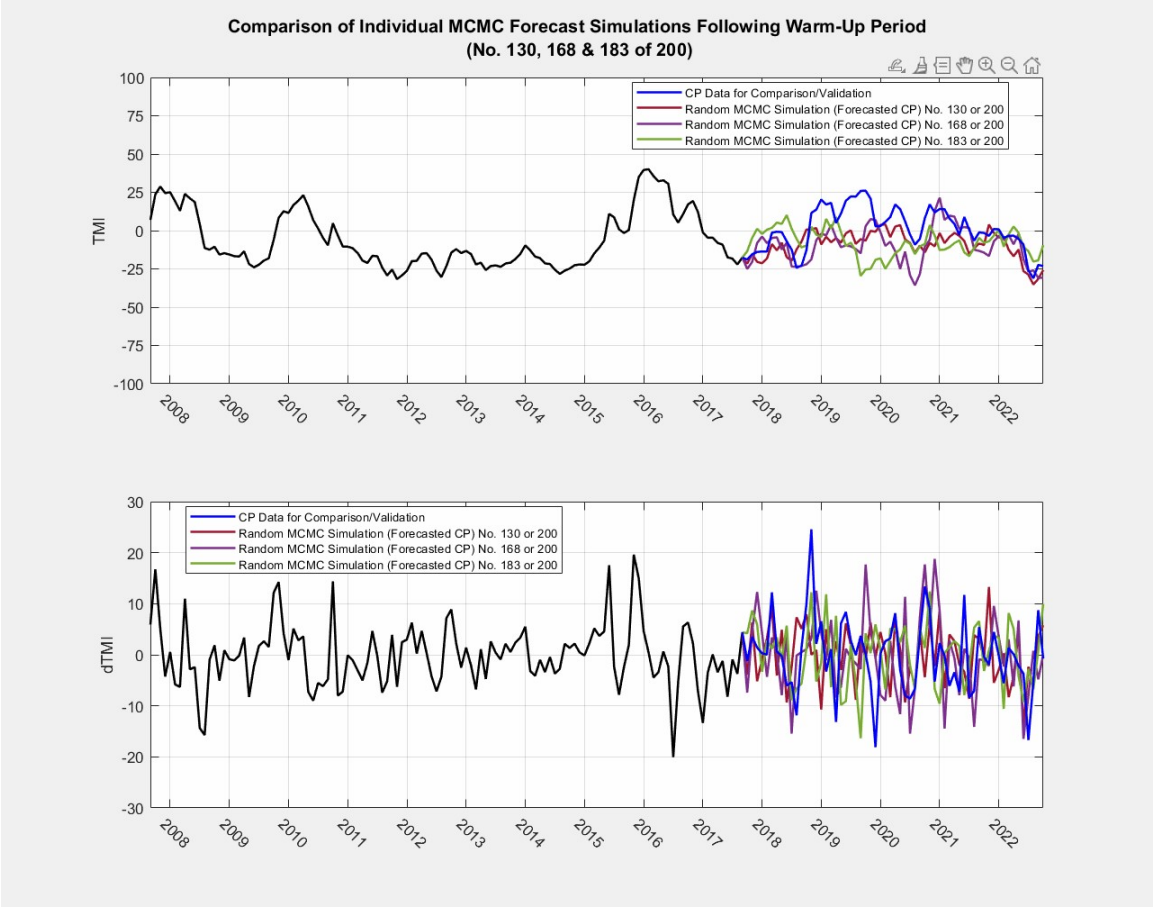

Figure D-60 Example of Single Simulation Results of *dTMI* and *TMI* for NOAA Station USW00013960 from 09/1988 to 09/2022.

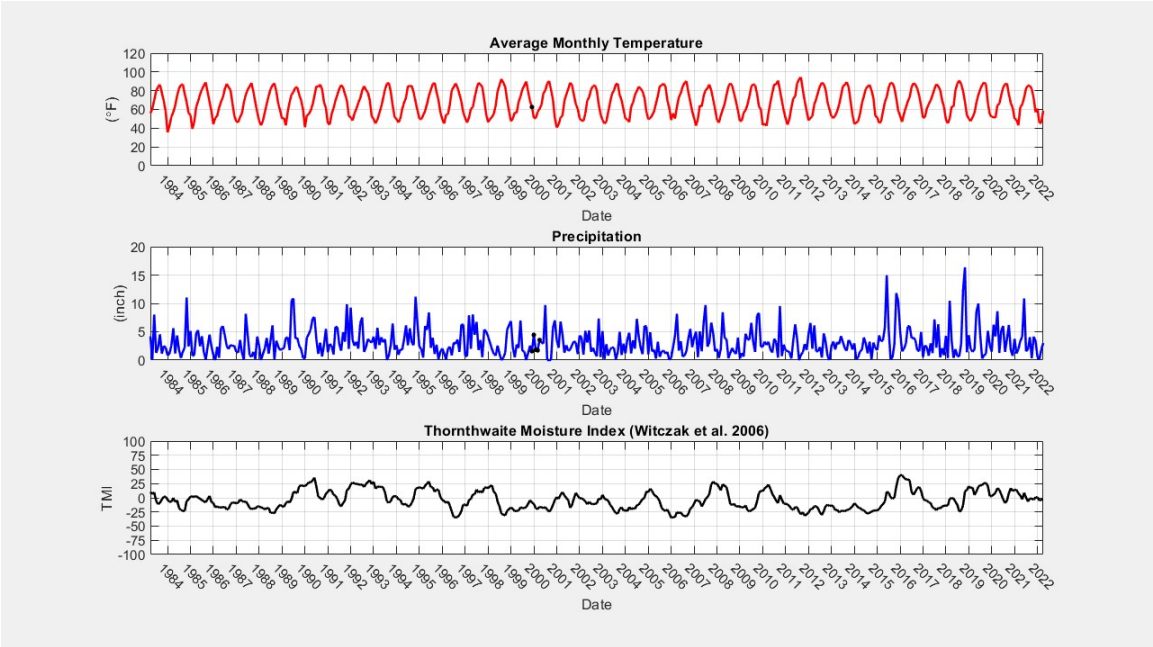

Figure D-61 NOAA Station USW00013960 Climate Data Extract and Calculated *TMI* from 03/1983 to 03/2022

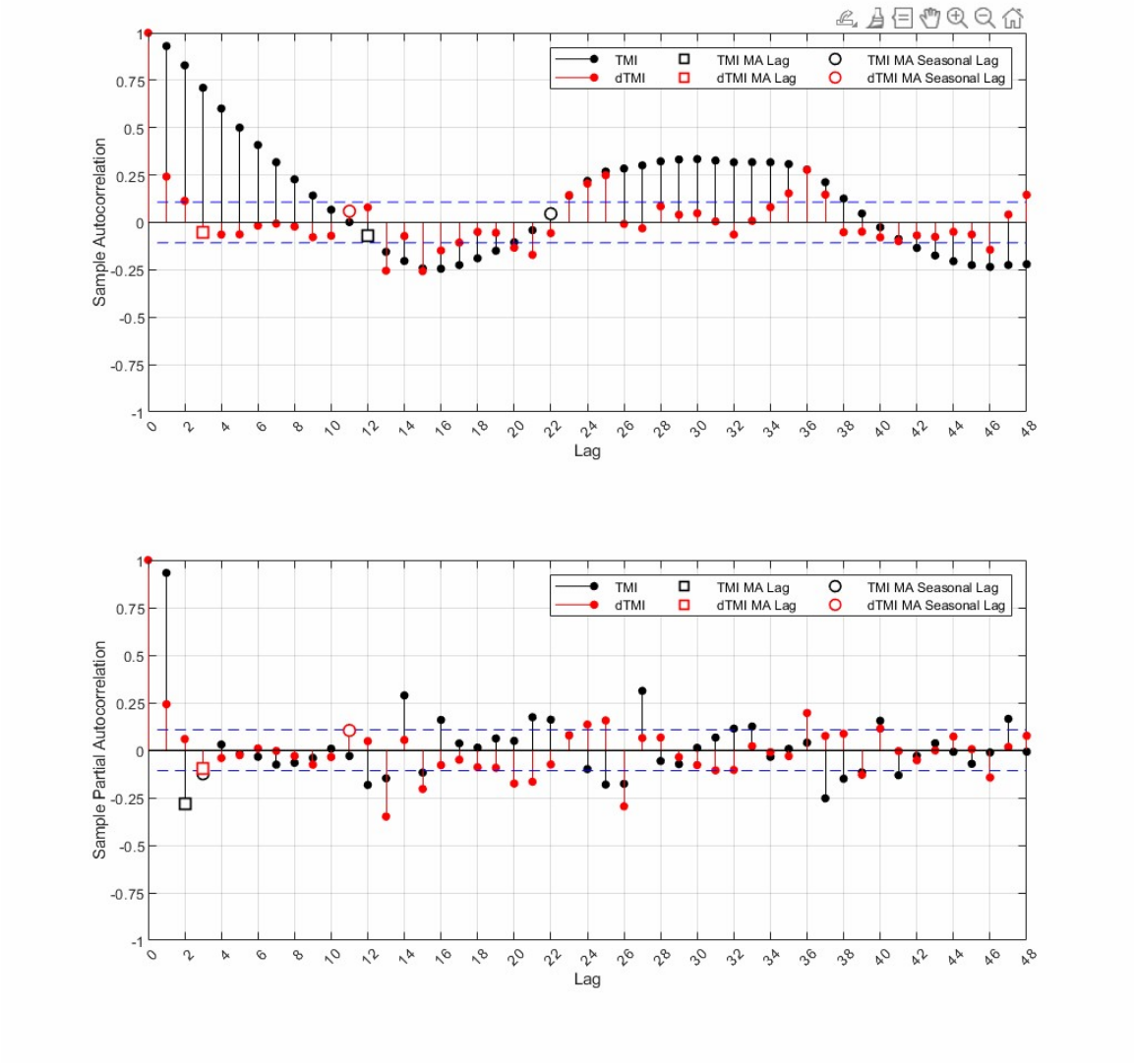

Figure D-62 ACF and PACF for *TMI* and *dTMI* for NOAA Station USW00013960 from 03/1982 to 03/2022

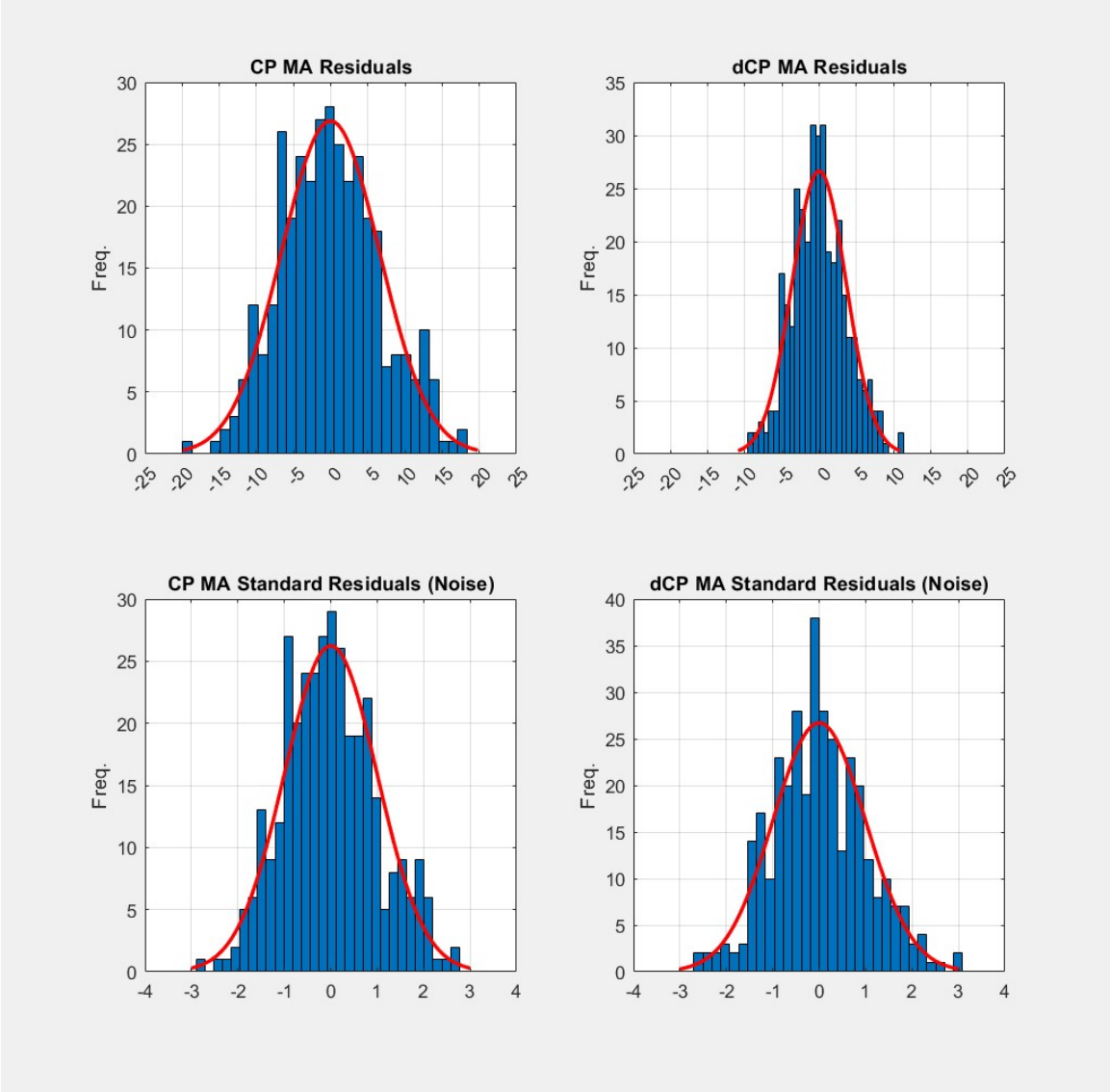

Figure D-63 Histograms for Decomposed *TMI* and *dTMI* for NOAA Station USW00013960 from 03/1982 to 03/2022

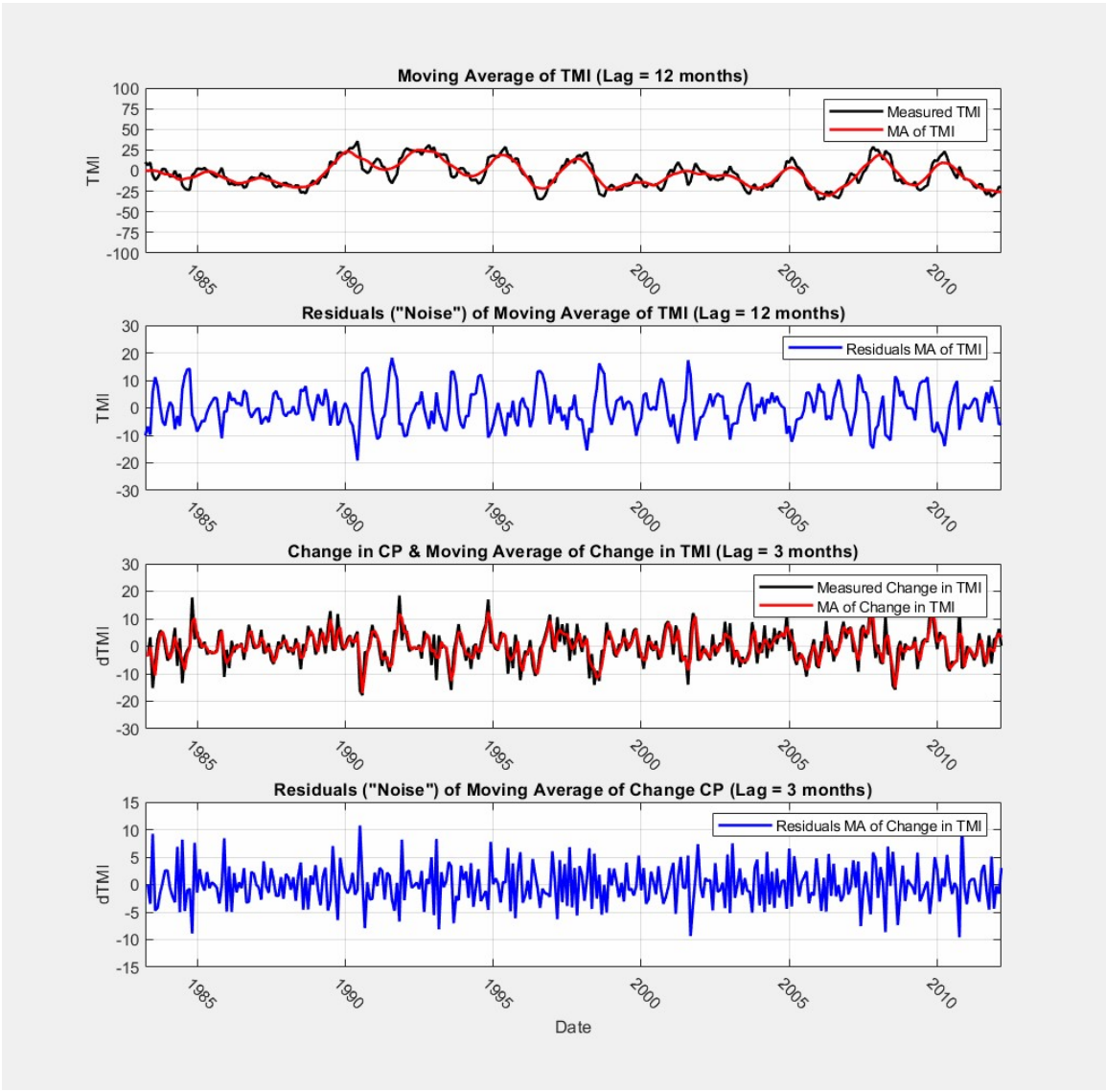

Figure D-64 Time Series Decomposition Using 1st differenced Moving Average for NOAA Station USW00013960 from 03/1982 to 03/2022

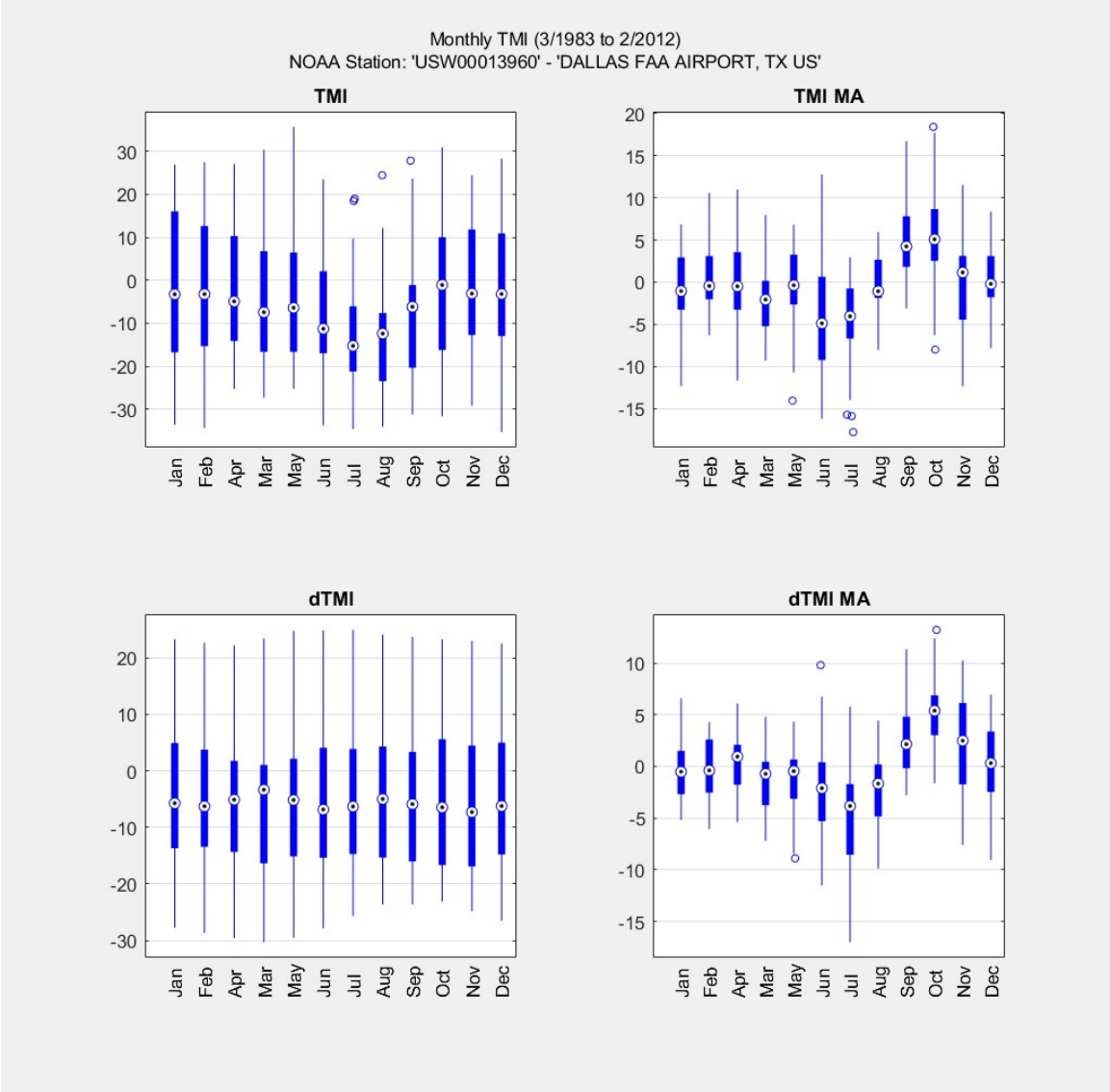

Figure D-65 Box Plots for Monthly Parameterized TMI and dTMI for Decomposed TMI and dTMI for NOAA Station USW00013960 from 03/1982 to 03/2022

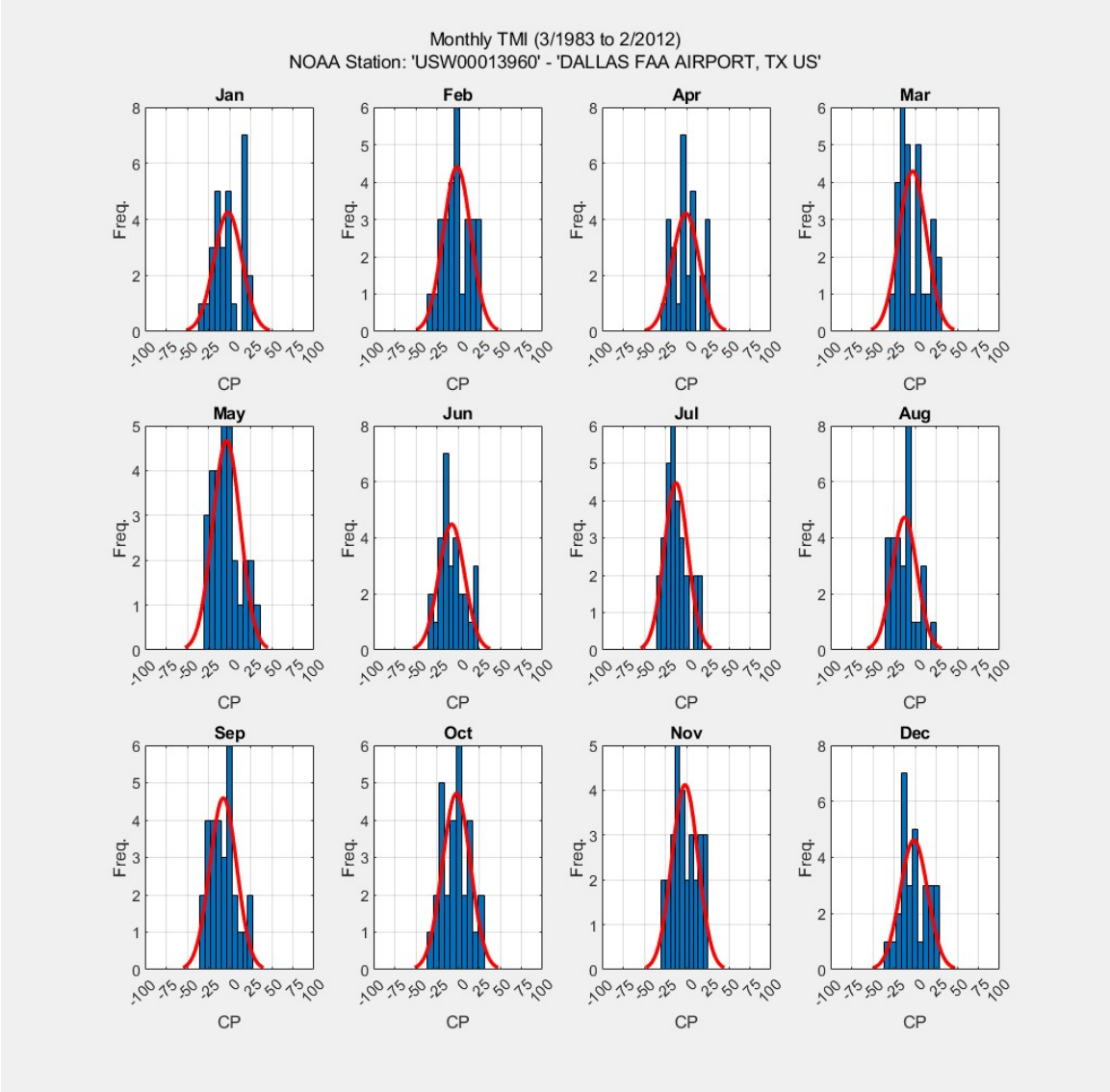

Figure D-66 Histograms for Monthly Parameterized *TMI* for NOAA Station USW00013960 from 03/1982 to 03/2022

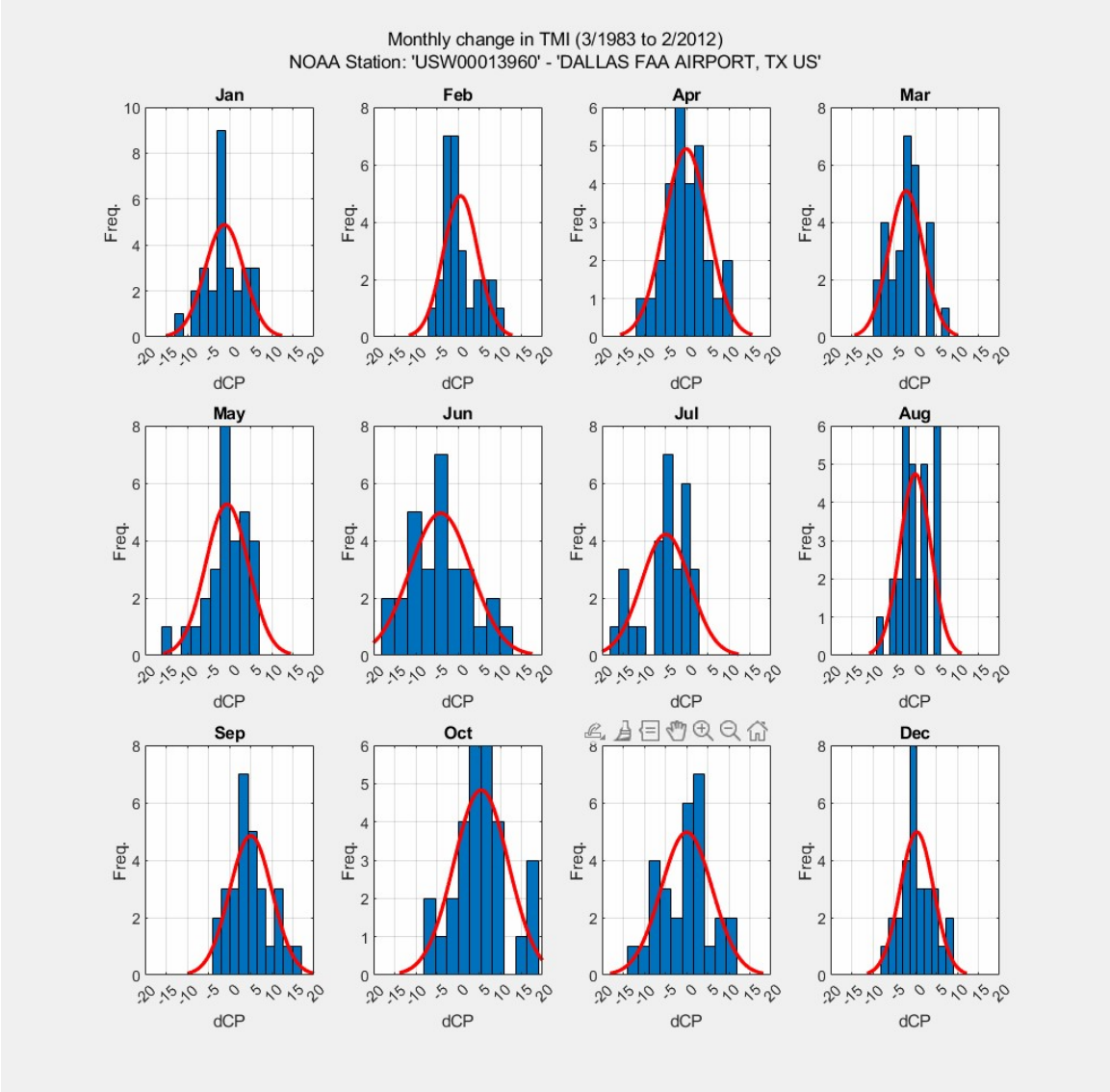

Figure D-67 Histograms for Monthly Parameterized *dTMI* for NOAA Station USW00013960 from 03/1982 to 03/2022

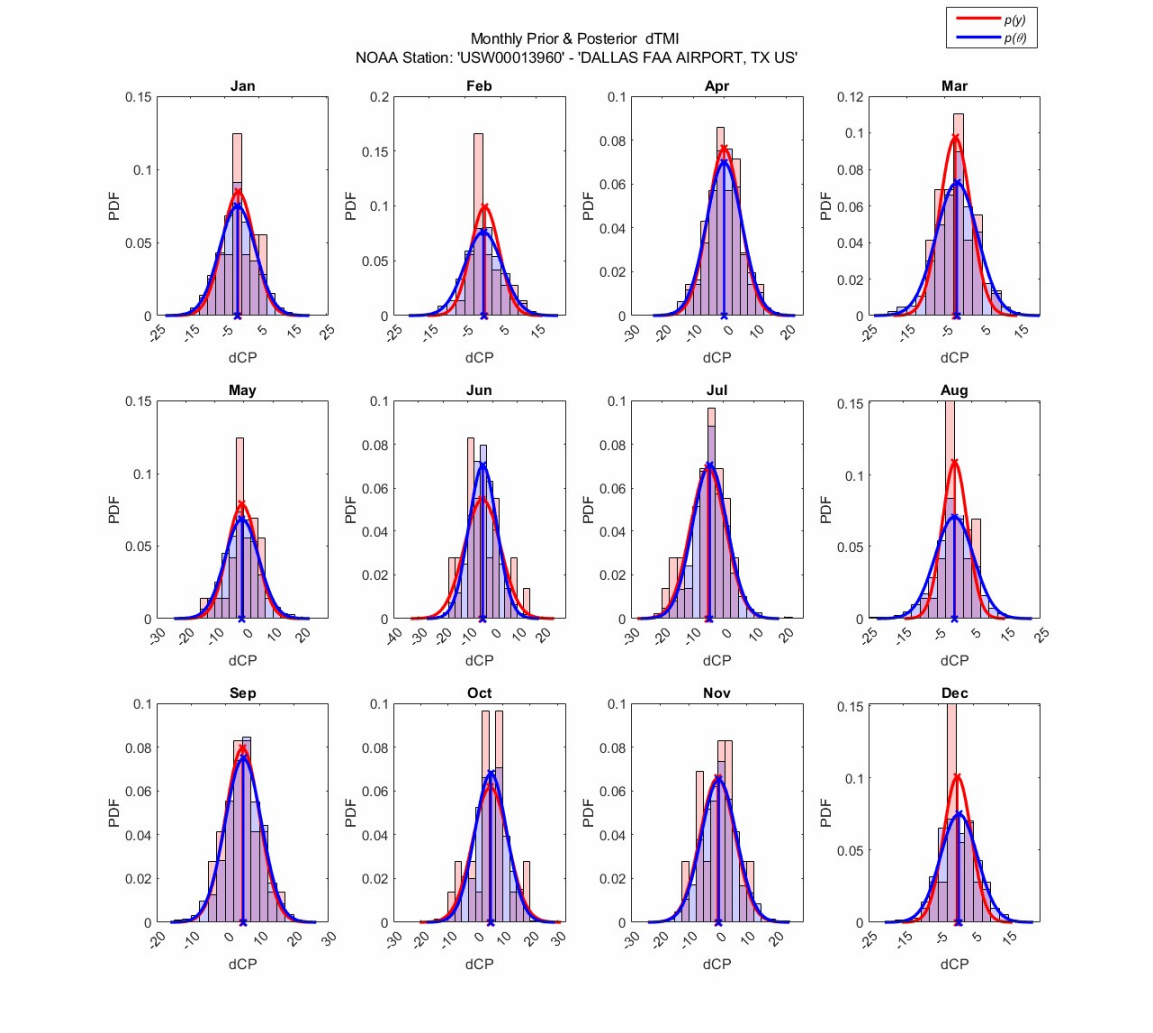

Figure D-68 Histograms of Prior and Posterior (forecasted) *dTMI* for NOAA Station USW00013960 from 03/1982 to 03/2022

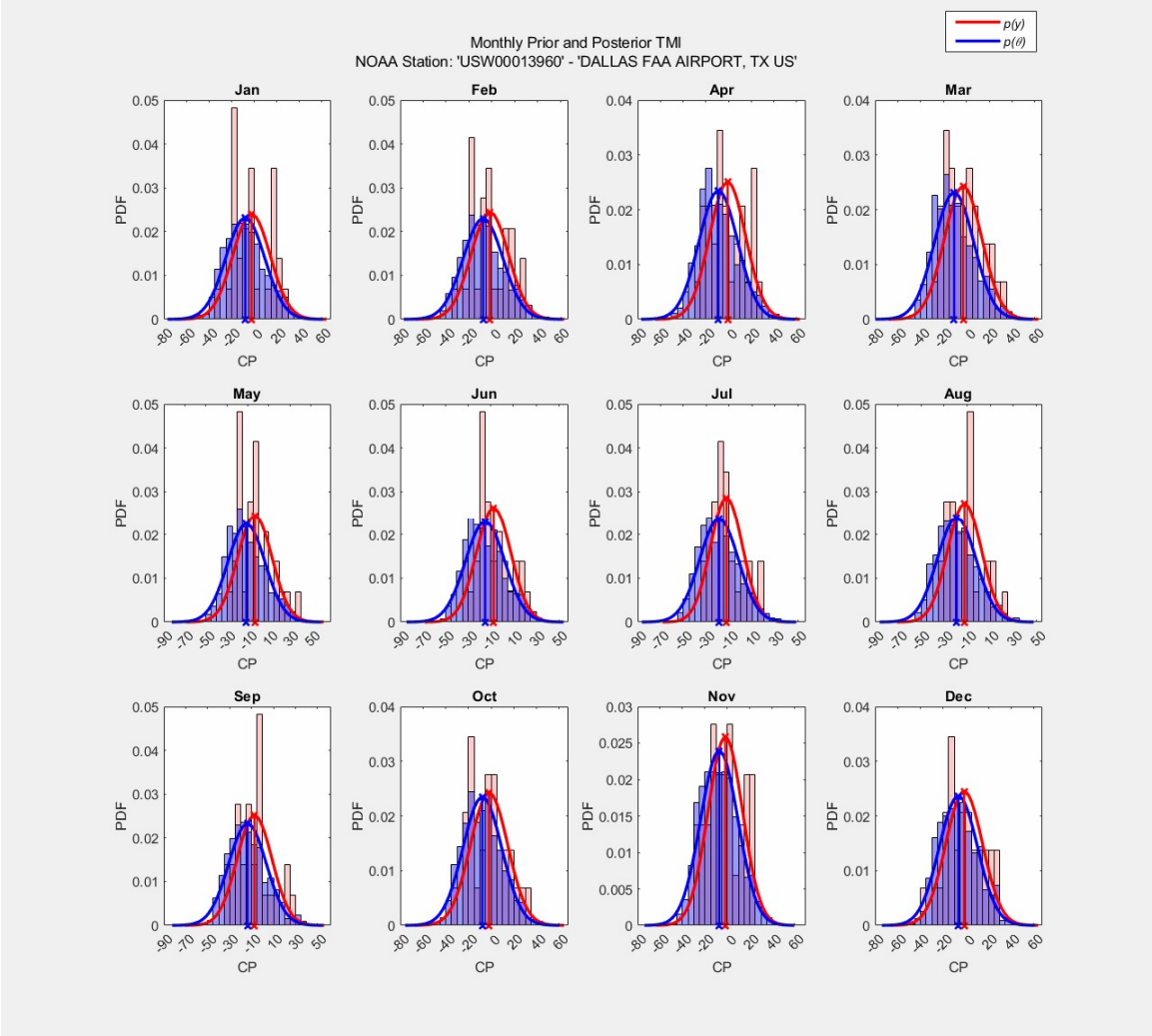

Figure D-69 Histograms of Prior and Posterior (forecasted) *TMI* for NOAA Station USW00013960 from 03/1982 to 03/2022

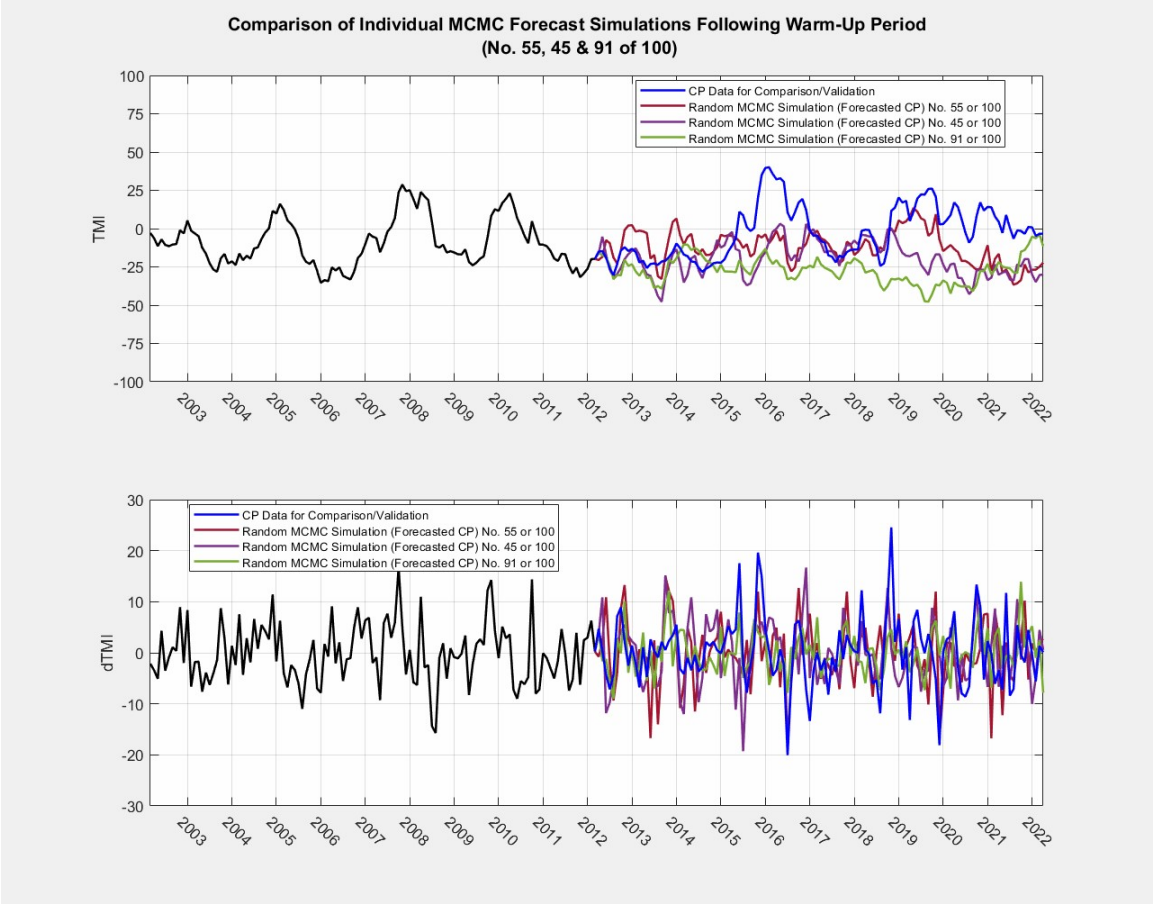

Figure D-70 Example of Single Simulation Results of *dTMI* and *TMI* for NOAA Station USW00013960 from 03/1982 to 03/2022.

APPENDIX F

STOCHASTIC SHRINK-SWELL ANALYSIS OUTPUT

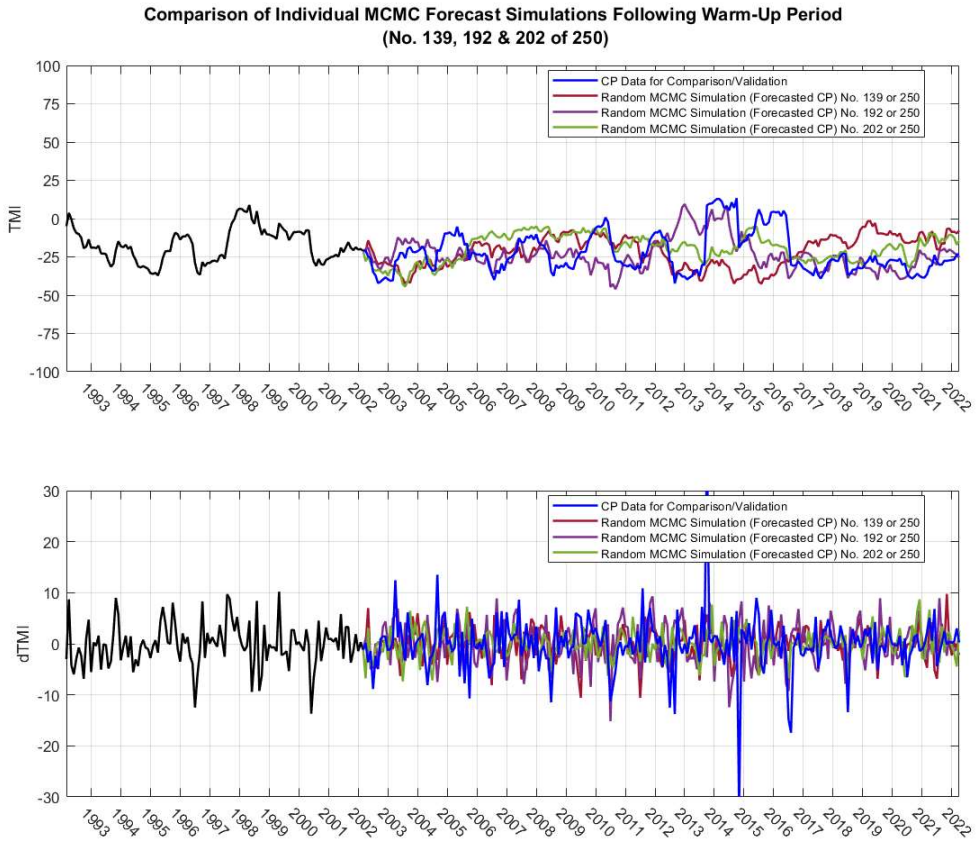

Figure D-71 Example of Single Simulation Results of *dTMI* and *TMI* for NOAA Station USW00023062 from 03/1988 to 03/2022.

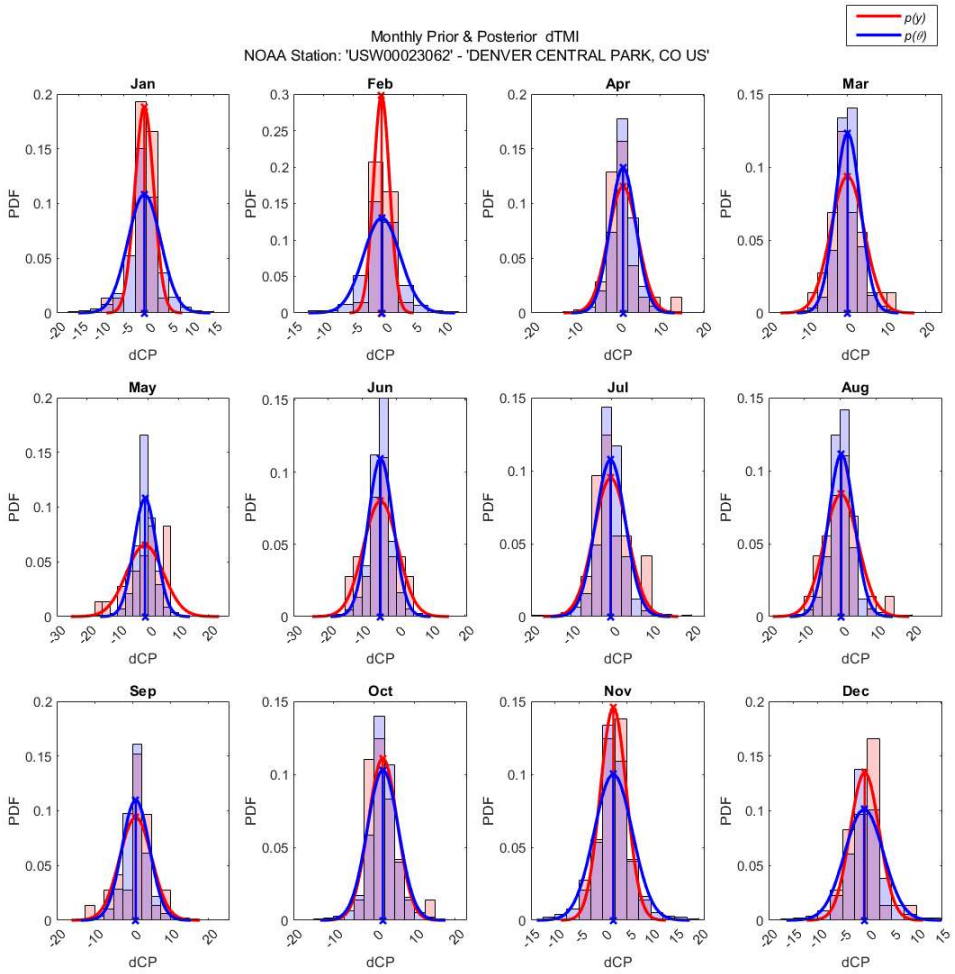

Figure D-72 Histograms of Prior and Posterior (forecasted) dTMI for NOAA Station USW00023062 from 03/1988 to 03/2022

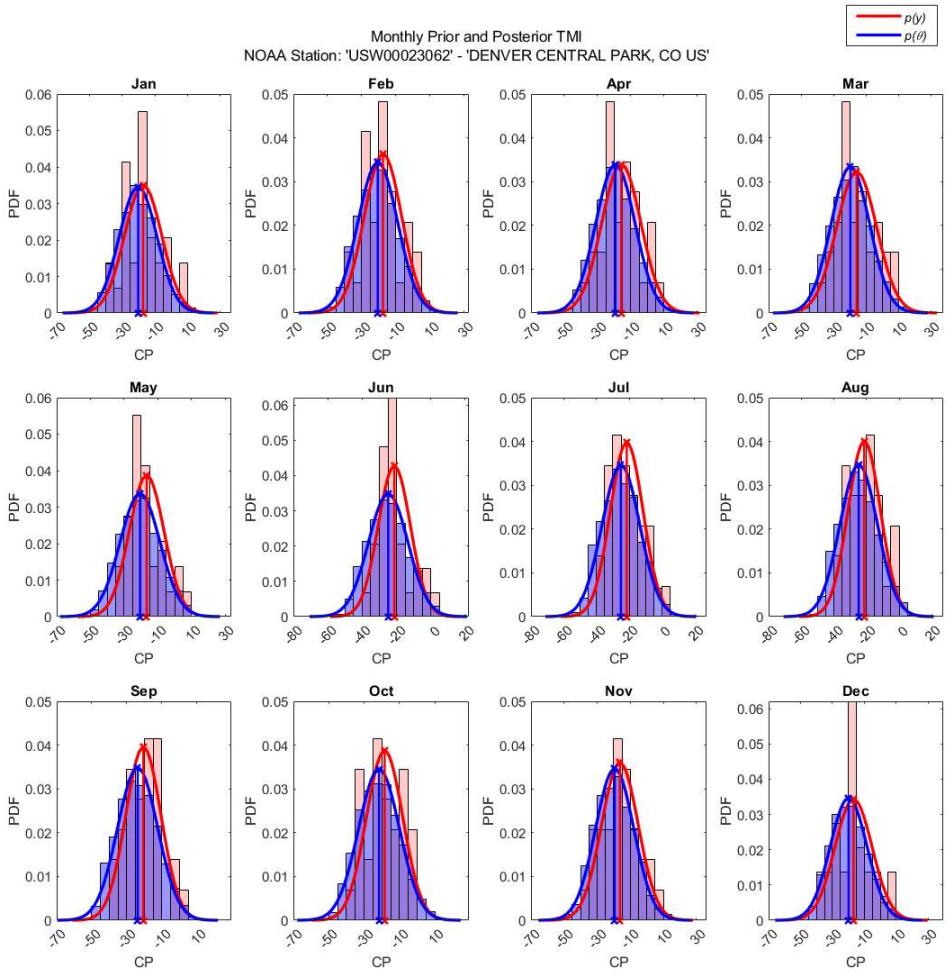

Figure D-73 Histograms of Prior and Posterior (forecasted) TMI for NOAA Station USW00023062 from 03/1988 to 03/2022.

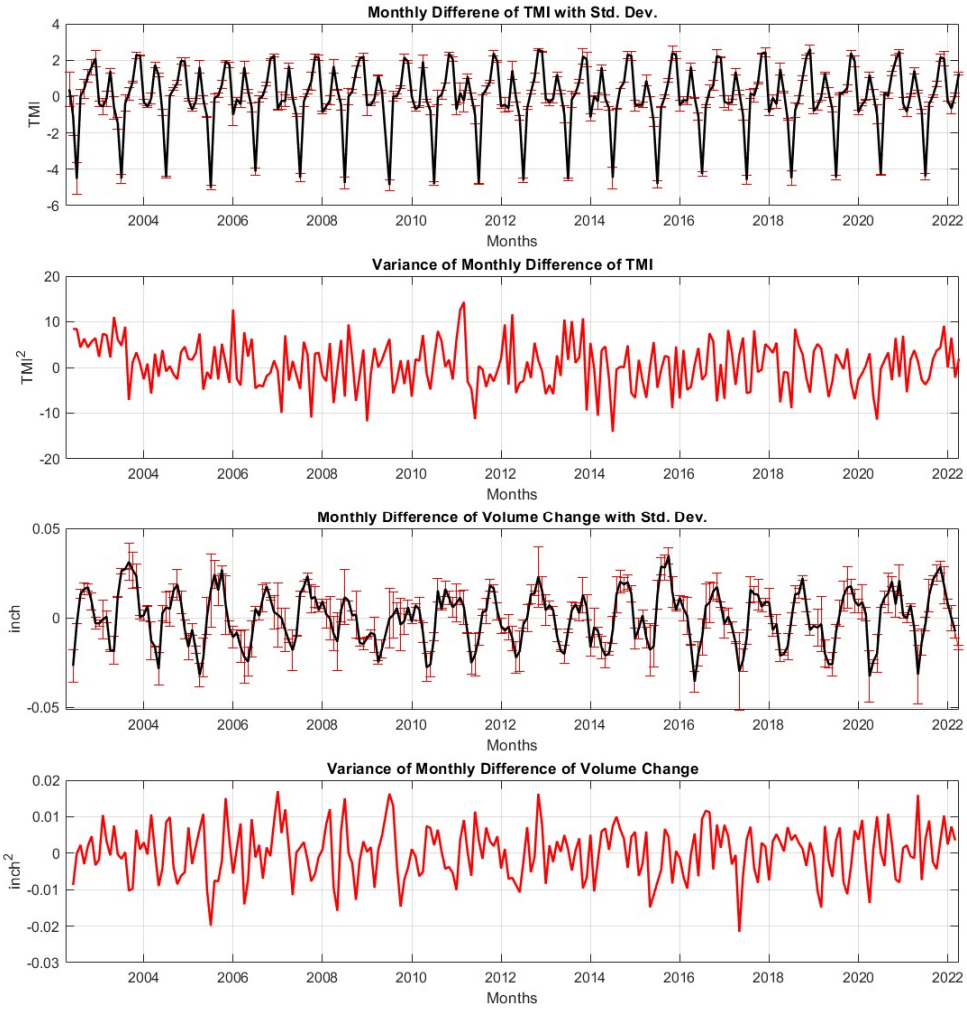

Figure D-74 Example Results of the Stochastic Shrink-Swell Analysis for the Monthly Difference in TMI (*dTMI*) and Monthly Difference in Volume Change for the Denver Study Site from 03/2002 to 03/2022

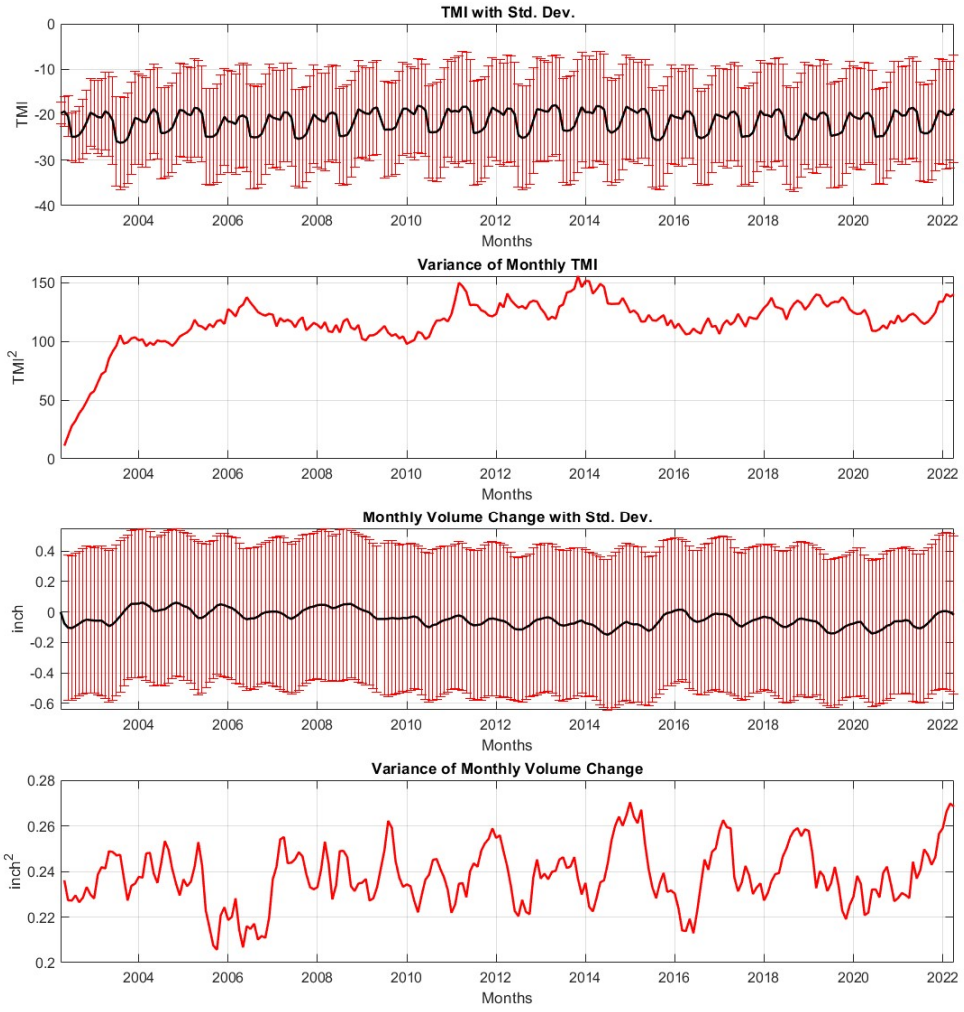

Figure D-75 Example Results of the Stochastic Shrink-Swell Analysis for the Monthly TMI and Monthly Volume Change for the Denver Study Site from 03/2002 to 03/2022